



HAL
open science

Durability of composite materials made from mineral matrices and vegetal fibers (TRM)

Mirna Zaydan

► **To cite this version:**

Mirna Zaydan. Durability of composite materials made from mineral matrices and vegetal fibers (TRM). Civil Engineering. Université de Lyon, 2022. English. NNT : 2022LYSE1151 . tel-04221572

HAL Id: tel-04221572

<https://theses.hal.science/tel-04221572v1>

Submitted on 28 Sep 2023

HAL is a multi-disciplinary open access archive for the deposit and dissemination of scientific research documents, whether they are published or not. The documents may come from teaching and research institutions in France or abroad, or from public or private research centers.

L'archive ouverte pluridisciplinaire **HAL**, est destinée au dépôt et à la diffusion de documents scientifiques de niveau recherche, publiés ou non, émanant des établissements d'enseignement et de recherche français ou étrangers, des laboratoires publics ou privés.



N° d'ordre : 2022LYSE1151

THESE de DOCTORAT DE L'UNIVERSITE DE LYON

opérée au sein de

l'Université Claude Bernard Lyon 1

Ecole Doctorale MEGA ED 162

(Mécanique, Energétique, Génie civil, Acoustique)

Spécialité de doctorat : Génie Civil

Discipline : Matériaux et structures

Soutenue publiquement le 18/07/2022, par :

Mirna ZAYDAN

Durability of composite materials made from mineral matrices and vegetal fibers (TRM)

Devant le jury composé de :

MICELLI Francesco	Professeur Associé	Université du Salento Lecce (Italie)	Rapporteur
OLIVEIRA Daniel	Professeur Associé	Université de Minho Guimares (Portugal)	Rapporteur
BIGAUD David	Professeur des universités	Université d'Angers EA 7315 - LARIS	Examineur
JACQUELIN Eric	Professeur des universités	Université Lyon 1 UMRT 9406 - LBMC	Président
MAGNIONT Camille	Professeure des universités	IUT de Tarbes LMDC	Examinatrice
CURTIL Laurence	Professeure des universités	Université Lyon 1 EA 7427 - LMC2	Directrice de thèse
MICHEL Marie	Maitre de conférences	Université Lyon 1 EA 7427 - LMC2	Co-Directrice de thèse
CAGGEGI Carmelo	Maitre de conférences (HDR)	Université Lyon 1 EA 7427 - LMC2	Co-Directeur de thèse

Acknowledgements

The research studies presented in this thesis were carried out within the “Laboratoire des Matériaux Composites pour la Construction” (LMC²) of the university Claude Bernard Lyon 1. First, I want to thank its former director Mr. Emmanuel Ferrier and its current director Mr. Aron Gabor, for welcoming me and letting me pursue my PhD research within the laboratory.

I would like to express my deepest gratitude and appreciation to the director of my thesis Prof. Laurence Curtil. Without her, none of this work would be possible. She helped me a lot with the funding scholarship of my PhD and she was very nice to me along these years. She was not only my mentor but like a mother for me. Her encouragements, her confidence in me, her understanding and her availability helped me go through each step of this work.

I am also extremely grateful to my supervisors Prof. Marie Michel and Prof. Carmelo Caggegi for guiding me and supporting me throughout these years. Their personal investment, their valuable advices and their suggestions contributed immensely to the proper completion of this work.

I am very grateful for the members of my PhD jury who honored me by accepting to judge my work and to be present for my thesis defense. I would like to thank Mr. Francesco Micelli and Mr. Daniel Oliveira for accepting to be principal reviewers for this manuscript. I also thank the examiners, Prof. David Bigaud, Prof. Eric Jacquelin and Prof. Camille Magniont. I am honored that they have agreed to dedicate their time and their expertise to review my work.

I would like to thank all the permanent staff of the laboratory LMC² for the enjoyable moments that we shared. A big thank you to the research technicians Emmanuel Janin and Norbert Cottet for their technical support, their humor and their sympathy. I would also like to thank the former and the current PhD students for the warm atmosphere they have created, for all the laughs and giggles. Special thanks to Mohamed and Duc Man who were always there when I needed help. A special thank you also to Roufaida and Hassan for their encouragements and for the wonderful coffee breaks that we have shared.

I warmly thank my parents Zeina and Ziad for their continuous encouragements and for everything they have done to me since I was a little baby. Without them, I would have never been where I am now. I am equally indebted to my sisters Sherihan, Sara and Ranya for their moral support and for loving me and being always my best friends. Very special and warm thanks to my nephew Omar and my nieces Rana and Maryam for the lovely video call breaks that we have shared and that helped me continue living abroad. I also thank dearly my in-laws Majeda and Marwan for their help together with my parents, in taking care of my daughter and looking after her while I was busy with writing this report.

Finally, I send all my thoughts and my thanks to my small family: my husband Issam who supported me, helped me, and who always believed in me. Your love, your support and your patience have been the light that enlightened my life. My little princess Mila, you greatly contributed to this work through your love, the adorable and amazing moments that I felt with you and through your patience when I was busy especially towards the end of this thesis. You were and will always be my first and last thought of every day; this thesis and my entire life is dedicated to you.

About the author

Mirna Zaydan was born in Lebanon, in 1991. She received her diploma in Civil engineering from the Lebanese University – Faculty of Engineering, Tripoli in 2014. She received her Master’s degree in “Highway Transportation and Traffic Engineering” from the Lebanese University – Faculty of Engineering, Hadath, Lebanon in 2015. Then she worked in construction in a civil engineering office and as a lecturer in “reinforced concrete” at the National Pedagogical Institute of Technical Education IPNET, Tripoli, Lebanon, from 2015 to 2017. In 2018, she received her second Master’s degree in “Materials and Structures for Sustainable Construction” from the University Claude Bernard Lyon 1, France.

In October 2018, she started a PhD thesis at the University Claude Bernard Lyon 1, France, at the “Laboratoire des Matériaux Composites pour la Construction” (LMC²) – doctoral school in Mechanic, Energetic, Civil Engineering and Acoustic (ED 162, MEGA). Her research studies deal with composites materials for strengthening existing civil engineering structures. She published some of the achieved results in International Journals and presented her work in National and International Conferences. She also had the opportunity of teaching in the same university in parallel with her thesis.

English abstract

In recent years, the use of textile-reinforced mortar (TRM) composites have gained a great interest worldwide. It is considered one of the most innovative and effective techniques for the rehabilitation and seismic retrofitting for existing civil engineering structures. In order to reduce the environmental impacts of these composites, TRM made from natural fiber textile instead of high strength synthetic fibers are lately being investigated by the scientific community. However, few studies in the literature address the durability issues of these fibers when used in such composite.

With the aim of realizing an eco-sustainable rehabilitation or repair interventions, the work of this thesis will focus on the durability of TRMs made from plant fiber textiles (hemp and flax) embedded in mineral matrices (ettringitic and natural hydraulic lime matrices). The thesis studied the effectiveness of these types of composites in the short term as well as the durability of the plant fibers in the alkaline environments of the mineral matrices. Prior to addressing the issue of the composite characterization, the adopted yarns and mortars were physically and mechanically characterized. Then, durability tests on hemp, flax and bio-resin-coated hemp yarns were carried out through different accelerated aging protocols and by using an Arrhenius approach. Then, tensile tests on hemp and bio-resin-coated hemp TRMs were carried out at different curing ages to qualify the composite materials and to evaluate the efficacy of using the Arrhenius approach to predict the service life of such composites. Consequently, on the substrate scale, shear bond tests were carried out on concrete elements and brick-masonry elements reinforced with bio-resin-coated hemp TRMs employing ettringitic and natural hydraulic lime matrix respectively, in order to assess the quality of the textile-matrix and the matrix-substrate bonds behaviors. Finally, this study yielded promising experimental results that showed a technical solution for the use of plant fiber textiles in TRM composites to improve the textile-matrix bond, and outlined the aspects on which it is necessary to act to increase their efficiency and their long-term durability.

Keywords: TRM, plant fibers, hemp, flax, bio-resin, tensile test, shear bond test, durability, Arrhenius approach, textile-matrix bond.

French abstract

Au cours des dernières années, l'utilisation des matériaux composites TRM (Textile Reinforced Mortar) a suscité un grand intérêt dans le monde entier. Elle est considérée comme l'une des techniques les plus innovantes et les plus efficaces pour la réhabilitation et le renforcement parasismique des ouvrages de génie civil existants. Afin de réduire les impacts environnementaux de ces composites, la fabrication de TRM à partir de textiles à base de fibres naturelles au lieu de fibres synthétiques à haute résistance a été récemment explorée par la communauté scientifique. Cependant, peu d'études dans la littérature abordent les problèmes de durabilité de ces fibres lorsqu'elles sont utilisées dans un tel type de composite.

Dans le but de réaliser des interventions de réhabilitation ou de réparation éco-durables, les travaux de cette thèse ont porté sur la durabilité des TRM à base de textiles de fibres végétales (chanvre et lin) incorporés dans des matrices minérales (matrice ettringitique et matrice de chaux hydraulique naturelle). La thèse a étudié l'efficacité de ces types de composites à court terme ainsi que la durabilité des fibres végétales dans les milieux alcalins des matrices minérales. Avant d'aborder le problème de la caractérisation des composites, les fils et les mortiers utilisés ont été caractérisés physiquement et mécaniquement. Ensuite, des tests de durabilité sur des fils de chanvre, de lin et de chanvre imprégné par une résine bio ont été réalisés selon différents protocoles de vieillissement accéléré et selon une approche Arrhenius. Puis, des tests de traction sur des systèmes de TRM à base de fibres de chanvre imprégnés ou non par une résine bio ont été effectués à différentes échéances pour qualifier les matériaux composites et évaluer l'efficacité de l'utilisation de l'approche Arrhenius afin de prévoir la durée de vie de ces types de composites. Ainsi, à l'échelle du support, des essais d'adhérence en cisaillement ont été réalisés sur des éléments en béton et des éléments en maçonnerie renforcés par des TRM à base de fils de chanvre imprégnés par la résine bio et incorporés dans une matrice ettringitique et une matrice à base de chaux hydraulique naturelle, respectivement, afin d'évaluer la qualité de la liaison matrice-textile ainsi que les liaisons matrice-substrat. Enfin, cette étude a délivré des résultats expérimentaux prometteurs qui ont montré une solution technique pour l'utilisation de textiles en fibres végétales dans les composites TRM afin d'améliorer la liaison textile-matrice, et elle permet de préciser les aspects sur lesquels il faut agir pour augmenter leur efficacité et leur durabilité à long terme.

Mots clés: TRM, fibres végétales, chanvre, lin, résine bio, test de traction, test d'adhérence, durabilité, approche Arrhenius, liaison textile-matrice.

Table of contents

General Introduction	25
1.1 Motivation	25
1.2 Contents and structure of the thesis.....	27
Chapter 1 A review on the durability of composite systems made from mineral matrices and different types of textile (TRM).....	29
1.1 Introduction	29
1.2 Textile fibers used in textile reinforced mortar (TRM).....	29
1.2.1 Carbon fiber	30
1.2.1.1 Generality	30
1.2.1.2 Advantages and disadvantages of carbon fibers.....	31
1.2.2 Glass fiber	31
1.2.2.1 Generality	31
1.2.2.2 Advantages and disadvantages of glass fibers.....	32
1.2.3 Basalt fibers	33
1.2.3.1 Generality	33
1.2.3.2 Advantages and disadvantages of basalt fibers	35
1.2.4 Vegetal fibers	37
1.2.4.1 Generality	37
1.2.4.2 Microstructure and biochemical composition of plant-based fiber cell wall ..	39
1.2.4.3 Morphological properties of plant fibers	41
1.2.4.4 Hemp fibers	42
1.2.4.4.1 Generality.....	42
1.2.4.4.2 Manufacturing process	43
1.2.4.5 Flax fibers	44
1.2.4.5.1 Generality.....	44
1.2.4.5.2 Manufacturing process	44
1.2.4.6 Jute fibers.....	45
1.2.4.6.1 Generality.....	45
1.2.4.6.2 Manufacturing process	46
1.2.4.7 Sisal fibers	46

1.2.4.7.1	Generality.....	46
1.2.4.7.2	Manufacturing process	47
1.2.4.8	Advantages and disadvantages of vegetal fibers	47
1.2.5	Comparison between natural fibers, carbon and glass fibers.....	49
1.2.5.1	Comparison of the mechanical properties of plant fibers with those of synthetic fibers	49
1.2.5.2	Comparison of the price of vegetal fibers with that of synthetic fibers	50
1.2.6	Environmental impact of fibers	51
1.2.6.1	Environmental impact of plant fibers	51
1.2.6.2	Environmental impact of basalt fibers.....	55
1.2.7	Summary of textile fibers properties.....	57
1.3	Textile Reinforced Mortar (TRM)	58
1.3.1	Behavior of natural fibers when used in TRM.....	58
1.3.1.1	Degradation mechanisms of basalt fibers in the matrix of cement composite	58
1.3.1.2	Degradation mechanisms of plant-based fibers in the matrix of cement composites.....	60
1.3.1.2.1	Alkaline degradation (hydrolysis)	60
1.3.1.2.2	Mineralization.....	62
1.3.2	Enhancement of the properties of fiber reinforced cement composites.....	63
1.3.2.1	Cement matrix modification	63
1.3.2.2	Fiber pre-treatment	69
1.3.2.3	Combination of cement matrix modification and fiber pre-treatment.....	71
1.3.2.4	Accelerated carbonation curing	73
1.3.3	Mechanical characterization of plant based fiber reinforced cement composites ..	74
1.3.3.1	Tensile behavior of natural fibers	74
1.3.3.2	Tensile behavior of the composite.....	76
1.3.3.3	Flexural behavior of the composite	79
1.3.3.4	Comparison between tensile and flexural behavior.....	80
1.3.3.5	Pull-out behavior of the composite.....	81
1.3.4	Durability tests	82
1.3.4.1	Accelerated aging methods for fiber reinforced cement composites	83
1.3.4.2	Accelerated aging methods for fibers	84

1.4	Conclusions	86
1.5	Aims of the thesis	87
Chapter 2 Materials characterization		89
2.1	Introduction	89
2.2	Matrices characterization: ettringitic matrix (E) and natural hydraulic lime matrix (L)	89
2.2.1	Formulation.....	89
2.2.2	Preparation	91
2.2.3	Consistency test	91
2.2.3.1	Procedure	92
2.2.3.2	Results	93
2.2.4	Setting time test.....	94
2.2.4.1	Procedure	95
2.2.4.2	Results	96
2.2.5	Mechanical properties	97
2.2.5.1	Three-point flexural strength.....	98
2.2.5.2	Compressive strength	99
2.2.5.3	Results	100
2.3	Yarns characterization: Hemp (H), Flax (F) and Bio-resin-coated hemp (HC).....	100
2.3.1	Physical characterization	104
2.3.1.1	Cross-sectional area.....	104
2.3.1.2	Linear density, density and moisture content	107
2.3.1.3	Water absorption and water desorption	110
2.3.2	Mechanical characterization	112
2.3.2.1	Tensile test setup	112
2.3.2.2	Tensile test results	116
2.4	Synthesis of materials' properties	120
Chapter 3 Durability of vegetal yarns in accelerated aging solutions and in ettringitic and lime matrices.....		122
3.1	Introduction	122
3.2	Accelerated aging of hemp and flax yarns	122
3.2.1	Specimens preparation	124

3.2.2	Tensile test setup.....	125
3.2.3	Results of tensile test on the aged H and F yarns	126
3.2.3.1	Influence of the temperature on the behavior of the yarns over time.....	127
3.2.3.1.1	Hemp in R solutions	127
3.2.3.1.2	Hemp in E solutions	130
3.2.3.1.3	Hemp in L solutions.....	132
3.2.3.1.4	Flax in E solution	135
3.2.3.1.5	Flax in L solution.....	137
3.2.3.2	Influence of the pH on the tensile behavior of the yarns over time.....	139
3.2.3.2.1	Hemp at 23°C.....	139
3.2.3.2.2	Hemp at 40°C.....	141
3.2.3.2.3	Hemp at 60°C.....	143
3.2.3.2.4	Flax at 23°C	145
3.2.3.2.5	Flax at 60°C	147
3.2.3.3	Influence of the yarn's type on the tensile behavior over time	149
3.2.3.3.1	In solution E-23	149
3.2.3.3.2	In solution E-60	151
3.2.3.3.3	In solution L-23	153
3.2.3.3.4	In solution L-60	155
3.2.3.4	Summary.....	157
3.3	Natural aging of hemp yarn in the matrix of TRM	162
3.3.1	Specimens preparation	162
3.3.1.1	Textile weaving	162
3.3.2	Mortar casting	163
3.3.2.1	Preparation of the mold	163
3.3.2.2	Fabrication of TRM's specimens	164
3.3.2.3	Demolding of TRM's specimens.....	165
3.3.3	Tensile test setup.....	165
3.3.4	Results of tensile test on hemp TRM's	167
3.3.4.1	H-E and H-L series	169
3.3.4.2	Comparisons between the results of TRM and the results of the durability of yarns in alkaline solutions.....	175

3.4	Conclusions	177
Chapter 4 Durability of bio-resin-coated hemp yarns in accelerated aging solutions and in ettringitic and lime matrices..... 180		
4.1	Introduction	180
4.2	Accelerated aging of bio-resin-coated hemp yarns	180
4.2.1	Specimens preparation	180
4.2.2	Tensile test setup.....	181
4.2.3	Results of tensile test on the aged HC yarns.....	181
4.2.3.1	Influence of the temperature on the behavior of HC yarns over time	182
4.2.3.1.1	In E solutions.....	182
4.2.3.1.2	In L solutions	185
4.2.3.2	Influence of the pH on the tensile behavior of HC yarns over time	187
4.2.3.2.1	At 23°C	187
4.2.3.2.2	At 40°C	189
4.2.3.2.3	At 60°C	191
4.2.3.3	Influence of the bio-resin coating on the tensile behavior of hemp yarns over time	193
4.2.3.3.1	In solution E-23	193
4.2.3.3.2	In solution E-40	195
4.2.3.3.3	In solution E-60	197
4.2.3.3.4	In solution L-23	199
4.2.3.3.5	In solution L-40	201
4.2.3.3.6	In solution L-60	203
4.3	Natural aging of bio-resin-coated hemp yarn in the matrix of TRM	205
4.3.1	Specimens preparation	205
4.3.2	Tensile test setup.....	206
4.3.3	Results of tensile test on bio-resin-coated hemp TRMs	207
4.3.3.1	HC-E TRM series	211
4.3.3.2	HC-L TRM series	216
4.3.3.3	Effect of the resin coating on the tensile response of TRM	220
4.3.3.4	Effect of the matrix on the tensile response of HC-TRM.....	222
4.4	Comparisons between the results of TRM and the results of the durability of yarns ..	225

4.5	Perspectives on the prediction of the durability of HC TRM in the long term	227
4.6	Conclusions	230
Chapter 5 Shear-bond test on bio-resin-coated hemp TRM applied to different substrates		232
5.1	Introduction	232
5.2	Experimental procedure	232
5.2.1	Specimens preparation	232
5.2.1.1	Substrates preparation.....	232
5.2.1.2	Reinforcement of the walls with TRM.....	233
5.2.2	Shear bond test setup	234
5.3	Results and discussions	236
5.3.1	CS-E-HC and MS-L-HC series.....	238
5.3.2	Shear bond test, direct tensile test and guidelines.....	242
5.4	Conclusions	243
Conclusions and perspectives		245
Scientific publications.....		250
References.....		251
Appendix A: Mechanical grip system of hemp and flax yarns.....		266
Appendix B: Detailed results of all the tensile test series of hemp yarns (H)		268
Appendix C: Detailed results of all the tensile test series of Flax yarns (F).....		289
Appendix D: Synthesis of the residual tensile properties of hemp (H) and flax (F) yarns after exposure to aging in different environments		305
Appendix E: Fore-displacement curves for all the tested specimens of the tensile test series of H-E and H-L hemp TRM		310
Appendix F: Detailed results of all the tensile test series of bio-resin-coated hemp yarns (HC).....		315
Appendix G: Synthesis of the residual tensile properties of bio-resin-coated hemp yarns (HC) after exposure to aging in different environments		329

List of figures

Figure 1- 1 : Carbon fibers [24].	30
Figure 1- 2: a) E- glass fibers [31] and AR-glass fibers [32].	31
Figure 1- 3 : Basalt rock (left) [46] and basalt fibers (right) [47].	34
Figure 1- 4: world production of plant fibers (Kt) in 2013. These data is obtained from the Food and Agriculture Organisation (FAO) [60], [61] and from Saneco for flax fibers [62].	37
Figure 1- 5: Production of flax fibers in Europe in 2014 (Kt)[37], [62].	38
Figure 1- 6: world cultivation of hemp in 2016 [63].	38
Figure 1- 7: Evolution of European hemp cultivation from 1993 till 2017 [64].	39
Figure 1- 8 : Microstructure, schematic diagram and molecular structures of natural fiber cell wall [66].	40
Figure 1- 9 : Hemp plant (left) [78] and hemp fibers (right) [79].	42
Figure 1- 10 : Flax plant (left) [84] and flax fibers (right) [85].	44
Figure 1- 11 : Jute plant (left) [90] and jute fibers (right) [91].	45
Figure 1- 12 : Sisal plant (left) [95] and sisal fibers (right) [96].	47
Figure 1- 13: commercial prices of E-glass fibers and some vegetal fibers (2004-2014). The main origin of these prices is the database of food and agriculture organization (FAO) [60]. The prices of flax fibers are provided by Saneco [104],prices of bamboo [105] Kenaf [105] wood [106] and hemp [107] fibers are found in the literature. These prices are compared to those of E-glass fibers [37], AR-glass [38], Basalt fibers [45], and carbon fibers [27].	50
Figure 1- 14 : Energy required to produce 1 kg of natural fibers (flax and hemp) compared with glass and carbon fibers (MJ).	53
Figure 1- 15: comparison of environmental impact between flax fibers and glass fibers production [28].	53
Figure 1- 16 : Carbon footprint of natural fibers (flax and hemp) compared with glass and carbon fibers Kg CO ₂ eq/t.	54
Figure 1- 17: comparison of the environmental impact between basalt fibers and glass fibers production [40].	55
Figure 1- 18: environmental impact of the production of 1 Kg of basalt fibers by 3 different scenarios (Russia, Iceland 1 and Iceland 2) [43].	56
Figure 1- 19:comparison of environmental impact between basalt (Russia and Iceland), glass and carbon fibers production [43].	56
Figure 1- 20 : formation of corrosion at the surface of a basalt fiber after immersion in NaOH solution over 8 (a), 16 (b), 32 (c), and 64 (d) days at ambient temperature [55].	59
Figure 1- 21 : SEM images for basalt fiber in cement paste at 7 days (left) and 28 days (right) [120].	59
Figure 1- 22 : Diagrammatic sketch of natural fiber's alkaline degradation process [66].	60
Figure 1- 23 : Diagrammatic sketch of microstructure of cellulose micro-fibrils [122].	61
Figure 1- 24 : chemical structure of cellulose [123].	61
Figure 1- 25 : Schematic diagram of alkali degradation of cellulose [124].	62

Figure 1- 26 : The effect of the wetting and drying cycles on the sisal fiber microstructure : (a) reference, (b) fiber extracted from a PC-MK matrix, (c and d) fiber extracted from a PC matrix [121].	65
Figure 1- 27 : The effect of the wetting and drying cycles on the sisal fiber surface:: (a) reference, (b) fiber extracted from a PC-MK matrix, (c and d) fiber extracted from a PC matrix [121].	65
Figure 1- 28 : Durability of different natural fiber-reinforced cement mortar after different cycles of wetting and drying estimated by the residual post-cracking flexural strength (study of Wei et al. 2016 [128]).	66
Figure 1- 29 : durability of single natural fibers imbedded in different cement mortars estimated by the residual tensile strength (study of Wei et al. 2016 [128]).	67
Figure 1- 30 : SEM images of uncoated (a) and ZrO ₂ -coated (b) basalt fibers in cement matrix after 30 days [55].	71
Figure 1- 31 : Influence of different fiber treatments on the tensile properties of sisal fibers (study of Ferreira et al. 2015 [136]).	72
Figure 1- 32 : (a) Micrograph showing the fiber matrix interface of polymer modified sisal fiber and (b) a schematic model used to explain the fiber–polymer–concrete interfacial bonding (study of Ferreira et al. 2015 [136]).	73
Figure 1- 33 : Examples of flax fiber curves, showing the strain at which deformation becomes linear again [139].	75
Figure 1- 34 : Examples of hemp fiber curves, showing the strain at which deformation becomes linear again [139].	75
Figure 1- 35 : Examples of ramie fiber curves, showing the strain at which deformation becomes linear again [139].	75
Figure 1- 36 : Typical stress-strain response curve of TRM systems under tensile loading[142].	76
Figure 1- 37 : stress-strain curves of representative composite specimens reinforced with one (F-1S), two (F-2S), and three layers (F-3S) of flax fabrics [143].	77
Figure 1- 38 : stress-strain curves of representative composite specimens reinforced with one (S-1S), two (S-2S), and three layers (S-3S) of sisal fabrics [143].	78
Figure 1- 39 : Typical failure modes of FRCM materials tested in tension. (a) Failure mode A, (b) Failure mode B, (c) Failure mode C, (d) Failure mode D [3].	79
Figure 1- 40 : Representative curve and cracking phases of flax nonwoven fabric reinforced cement composite obtained under flexural stress: (A) first crack; (B) generation of new cracks; (C) increase of crack length [146].	80
Figure 1- 41 : Comparison of flexural vs. tensile response [147].	81
Figure 1- 42 : cracking maps of two composites from the same plate tested under tensile (a) and bending (b) tests [146].	81
Figure 1- 43 : Double-sided pull-out test setup with load application grips and crack width sensors [131].	82
Figure 1- 44 : Typical load-deformation curve of TRM under double-sided pullout test [131].	82

Figure 1- 45 : (a) fiber strands wrapped by aluminum paper and banded by copper wire at the ends, (b) after being wiped by epoxy resin; (c) sketch and typical dimensions of the embedded fiber strands specimen [151].	86
Figure 2- 46 : Flow Table for consistency determination (dimensions in mm) [158].	92
Figure 2- 47 : Flow Table test.	92
Figure 2- 48 : Influence of the amount of superplasticizer on the consistency of the ettringitic matrix over time.	93
Figure 2- 49 : Influence of the amount of retarder on the consistency of the ettringitic matrix over time.	94
Figure 2- 50 : Vicat apparatus for setting time determination: a) Side mold in upright position for initial time setting; b) Front view with mold inverted for final setting time determination (1: mold; 2: correcting weights; 3: base-plate; 4: container. [159].	95
Figure 2- 51 : Vicat test.	96
Figure 2- 52 : Position of the needle vs. time.	97
Figure 2- 53 : schematics of flexural test setup [156].	98
Figure 2- 54 : 3-point bending test setup on a 40 mm x 40 mm x 160 mm matrix specimen.	98
Figure 2- 55 :Schematics of compression test setup.	99
Figure 2- 56 : Compression test setup on a 40 mm x 40 mm x 160 mm matrix specimen.....	99
Figure 2- 57: a) Coil of hemp, b) hemp yarn, c) coil of flax and d) flax yarn.	101
Figure 2- 58 : a) Manual coating of the hemp yarns by the bio-resin, b) drying of the coated yarns and c) coated hemp yarn (HC).	101
Figure 2- 59 : bio-sourced resin formulations proposed by Viretto & Galy 2018 [160].	103
Figure 2- 60 : Stress-strain curves obtained for the different flax fiber composites tested in 3-point bending [163].	104
Figure 2- 61 : Schematic representation of the principle of X-ray tomography [166].	105
Figure 2- 62 : Schematic representation of the reconstruction process [166].	105
Figure 2- 63 : Samples of the studied yarns: a) hemp (H), b) flax (F) and c) bio-resin-coated hemp (HC).	106
Figure 2- 64 : a) Scan of the hemp yarn by X-ray tomography, b) cross section of the fiber and c) 3D view of the hemp yarn reconstructed by “FIJI-ImageJ” software.	106
Figure 2- 65: a) Scan of the flax yarn by X-ray tomography, b) cross section of the fiber and c) 3D view of the flax yarn reconstructed by “FIJI-ImageJ” software.	107
Figure 2- 66: a) Scan of the bio-resin-coated hemp yarn by X-ray tomography, b) porosity, c) cross section of the hemp yarn separated from the coating and d) 3D view of HC yarn reconstructed by “FIJI-ImageJ” software.	107
Figure 2- 67 : water absorption of hemp, flax and bio-resin-coated hemp yarns in function of time.	111
Figure 2- 68 : water desorption of hemp, flax and bio-resin-coated hemp yarns in function of time.	111

Figure 2- 69 : a) NaOH solution (pH 10.5) + hemp yarns, b) NaOH solution (pH 12.5) + hemp yarns, c) hemp yarn, d) hemp yarn after immersion in NaOH (pH 10.5) and e) hemp yarn after immersion in NaOH (pH 12.5).	112
Figure 2- 70 : Different views for the yarns' mechanical grip system.	113
Figure 2- 71 : 3D mesh of the mechanical grip system.	114
Figure 2- 72 : 3D and profile drawings of the yarns' mechanical grip system.....	114
Figure 2- 73 : Fiberglass composite tabs glued to the both ends of the bio-resin-coated hemp yarns.	115
Figure 2- 74 : Tensile tests on the yarns: a), b) & c) test setup for hemp, flax and bio-resin-coated hemp yarns, respectively, d), e) & f) failure hemp, flax and bio-resin-coated hemp yarns, respectively.	116
Figure 2- 75 : Stress-strain curves of hemp yarns (H) tested in tension.	117
Figure 2- 76 : Stress-strain curves of flax yarns (F) tested in tension.	118
Figure 2- 77 : Stress-strain curves of bio-resin coated hemp yarns (HC) tested in tension.....	118
Figure 3- 78 : graphic representation of the days of accelerated aging with respect to the years of service life of the yarns.	124
Figure 3- 79 : Accelerated aging of yarns at T=23°C.....	125
Figure 3- 80 : Accelerated aging of yarns at T=40°C or 60°C.	125
Figure 3- 81 : Drying of the hemp and flax yarns after removal from the aging solutions.	125
Figure 3- 82 : Minimum, maximum and average stress-strain curves obtained by the six tested specimens of series H-0.	127
Figure 3- 83 : Influence over time of the temperature on the average tensile strength of hemp yarns (H) immersed in R solution (normalized residual values).	128
Figure 3- 84 : Influence over time of the temperature on the average tensile modulus of hemp yarns (H) immersed in R solution (normalized residual values).	128
Figure 3- 85 : Influence over time of the temperature on the average ultimate tensile strain of hemp yarns (H) immersed in R solution (normalized residual values).	129
Figure 3- 86 : Influence over time of the temperature on the average tensile strength of hemp yarns (H) immersed in E solution (normalized residual values).	131
Figure 3- 87 : Influence over time of the temperature on the average tensile modulus of hemp yarns (H) immersed in E solution (normalized residual values).	131
Figure 3- 88 : Influence over time of the temperature on the average ultimate tensile strain of hemp yarns (H) immersed in E solution (normalized residual values).....	132
Figure 3- 89 : Influence over time of the temperature on the average tensile strength of hemp yarns (H) immersed in L solution (normalized residual values).	133
Figure 3- 90 : Influence over time of the temperature on the average tensile modulus of hemp yarns (H) immersed in L solution (normalized residual values).	133
Figure 3- 91 : Influence over time of the temperature on the average ultimate tensile strain of hemp yarns (H) immersed in L solution (normalized residual values).....	134

Figure 3- 92 : Influence over time of the temperature on the average tensile strength of flax yarns (F) immersed in E solution (normalized residual values).....	135
Figure 3- 93 : Influence over time of the temperature on the average tensile modulus of flax yarns (F) immersed in E solution (normalized residual values).....	136
Figure 3- 94 : Influence over time of the temperature on the average ultimate tensile strain of flax yarns (F) immersed in E solution (normalized residual values).	136
Figure 3- 95 : Influence over time of the temperature on the average tensile strength of flax yarns (F) immersed in L solution (normalized residual values).....	138
Figure 3- 96 : Influence over time of the temperature on the average tensile modulus of flax yarns (F) immersed in L solution (normalized residual values).....	138
Figure 3- 97 : Influence over time of the temperature on the average ultimate tensile strain of flax yarns (F) immersed in L solution (normalized residual values).	139
Figure 3- 98 : Influence over time of the pH on the average tensile strength of hemp yarn (H) at 23°C (normalized residual values).....	140
Figure 3- 99 : Influence over time of the pH on the average tensile modulus of hemp yarn (H) at 23°C (normalized residual values).....	140
Figure 3- 100 : Influence over time of the pH on the average ultimate tensile strain of hemp yarn (H) at 23°C (normalized residual values).	141
Figure 3- 101 : Influence over time of the pH on the average tensile strength of hemp yarn (H) at 40°C (normalized residual values).....	142
Figure 3- 102 : Influence over time of the pH on the average tensile modulus of hemp yarn (H) at 40°C (normalized residual values).....	142
Figure 3- 103 : Influence over time of the pH on the average ultimate tensile strain of hemp yarn (H) at 40°C (normalized residual values).	143
Figure 3- 104 : Influence over time of the pH on the average tensile strength of hemp yarn (H) at 60°C (normalized residual values).....	144
Figure 3- 105 : Influence over time of the pH on the average tensile modulus of hemp yarn (H) at 60°C (normalized residual values).....	144
Figure 3- 106 : Influence over time of the pH on the average ultimate tensile strain of hemp yarn (H) at 60°C (normalized residual values).	145
Figure 3- 107 : Influence over time of the pH on the average tensile strength of flax yarn (F) at 23°C (normalized residual values).....	146
Figure 3- 108 : Influence over time of the pH on the average tensile modulus of flax yarn (F) at 23°C (normalized residual values).....	146
Figure 3- 109 : Influence over time of the pH on the average ultimate tensile strain of flax yarn (F) at 23°C (normalized residual values).....	147
Figure 3- 110 : Influence over time of the pH on the average tensile strength of flax yarn (F) at 60°C (normalized residual values).....	148
Figure 3- 111 : Influence over time of the pH on the average tensile modulus of flax yarn (F) at 60°C (normalized residual values).....	148

Figure 3- 112 : Influence over time of the pH on the average ultimate tensile strain of flax yarn (F) at 60°C (normalized residual values).....	149
Figure 3- 113 : Influence of the yarn's type on the average tensile strength over time in E-23 solution.....	150
Figure 3- 114 : Influence of the yarn's type on the average tensile modulus over time in E-23 solution.....	150
Figure 3- 115 : Influence of the yarn's type on the average ultimate tensile strain over time in E-23 solution.....	151
Figure 3- 116 : Influence of the yarn's type on the average tensile strength over time in E-60 solution.....	152
Figure 3- 117 : Influence of the yarn's type on the average tensile modulus over time in E-60 solution.....	152
Figure 3- 118 : Influence of the yarn's type on the average ultimate tensile strain over time in E-60 solution.....	153
Figure 3- 119 : Influence of the yarn's type on the average tensile strength over time in L-23 solution.....	154
Figure 3- 120 : Influence of the yarn's type on the average tensile modulus over time in L-23 solution.....	154
Figure 3- 121 : Influence of the yarn's type on the average ultimate tensile strain over time in L-23 solution.....	155
Figure 3- 122 : Influence of the yarn's type on the average tensile strength over time in L-60 solution.....	156
Figure 3- 123 : Influence of the yarn's type on the average tensile modulus over time in L-60 solution.....	156
Figure 3- 124 : Influence of the yarn's type on the average ultimate tensile strain over time in L-60 solution.....	157
Figure 3- 125 : Textile weaving technic: a) spinning of the yarn, b) sewing of the yarns intersections, c) cutting the textile specimen, d) Final textile specimen obtained.....	163
Figure 3- 126 : Geometric characteristics of hemp textile (dimensions are in mm).....	163
Figure 3- 127 : The steps for manufacturing TRM's specimens: a) Screwing the PVC bars of the first mold layer, b) Oiling the mold compartments, c) Pouring and leveling the first matrix layer, d) Placing the textile and screwing the PVC bars of the second layer of the mold, e) Pouring and leveling the second matrix layer and f) Covering the mold with a plastic film.....	164
Figure 3- 128 : Specimens of TRM after demolding.....	165
Figure 3- 129 : Geometric characteristics of the specimens for the tensile test: a) lateral and b) front views (dimensions are in mm).	166
Figure 3- 130 : Preparation of a TRM specimen for the direct tensile test: gluing of aluminum tabs.	167
Figure 3- 131 : Experimental setup of the tensile test.	167
Figure 3- 132 : Typical stress-strain curve of TRM subjected to tensile load [179].	168

Figure 3- 133 : Typical failure modes of TRM materials tested in tension. (a) Failure mode A, (b) Failure mode B, (c) Failure mode C, (d) Failure mode D [3] [144].	168
Figure 3- 134 : Force-displacement curves for the specimens of H-E-28d series.	170
Figure 3- 135: Typical stress-strain curve of natural fibers TRM tested in tension in this study.	170
Figure 3- 136 : Failure mode C recorded for all the series of H-E and H-L TRM.	174
Figure 4- 137 : Drying of bio-resin-coated hemp yarns after removal from aging solutions.	181
Figure 4- 138 : Minimum, maximum and average stress-strain curves obtained by the six tested specimens of series HC-0.	182
Figure 4- 139 : Influence over time of the temperature on the average tensile strength of bio-resin-coated hemp yarns (HC) immersed in E solution (normalized residual values).	183
Figure 4- 140 : Influence over time of the temperature on the average tensile modulus of bio-resin-coated hemp yarns (HC) immersed in E solution (normalized residual values).	184
Figure 4- 141 : Influence over time of the temperature on the average ultimate tensile strain of bio-resin-coated hemp yarns (HC) immersed in E solution (normalized residual values).	184
Figure 4- 142 : Influence over time of the temperature on the average tensile strength of bio-resin-coated hemp yarns (HC) immersed in L solution (normalized residual values).	186
Figure 4- 143 : Influence over time of the temperature on the average tensile modulus of bio-resin-coated hemp yarns (HC) immersed in L solution (normalized residual values).	186
Figure 4- 144 : Influence over time of the temperature on the average ultimate tensile strain of bio-resin-coated hemp yarns (HC) immersed in L solution (normalized residual values).	187
Figure 4- 145 : Influence over time of the pH on the average tensile strength of bio-resin-coated hemp yarns (HC) at 23°C (normalized residual values).	188
Figure 4- 146 : Influence over time of the pH on the average tensile modulus of bio-resin-coated hemp yarns (HC) at 23°C (normalized residual values).	188
Figure 4- 147 : Influence over time of the pH on the average ultimate tensile strain of bio-resin-coated hemp yarns (HC) at 23°C (normalized residual values).	189
Figure 4- 148 : Influence over time of the pH on the average tensile strength of bio-resin-coated hemp yarns (HC) at 40°C (normalized residual values).	190
Figure 4- 149 : Influence over time of the pH on the average tensile modulus of bio-resin-coated hemp yarns (HC) at 40°C (normalized residual values).	190
Figure 4- 150 : Influence over time of the pH on the average ultimate tensile strain of bio-resin-coated hemp yarns (HC) at 40°C (normalized residual values).	191
Figure 4- 151 : Influence over time of the pH on the average tensile strength of bio-resin-coated hemp yarns (HC) at 60°C (normalized residual values).	192
Figure 4- 152 : Influence over time of the pH on the average tensile modulus of bio-resin-coated hemp yarns (HC) at 60°C (normalized residual values).	192
Figure 4- 153 : Influence over time of the pH on the average ultimate tensile strain of bio-resin-coated hemp yarns (HC) at 60°C (normalized residual values).	193

Figure 4- 154 : Influence over time of the bio-resin coating on the average tensile strength of hemp yarns in E-23 solution.	194
Figure 4- 155 : Influence over time of the bio-resin coating on the average tensile modulus of hemp yarns in E-23 solution.	194
Figure 4- 156 : Influence over time of the bio-resin coating on the average ultimate tensile strain of hemp yarns in E-23 solution.	195
Figure 4- 157 : Influence over time of the bio-resin coating on the average tensile strength of hemp yarns in E-40 solution.	196
Figure 4- 158 : Influence over time of the bio-resin coating on the average tensile modulus of hemp yarns in E-40 solution.	196
Figure 4- 159 : Influence over time of the bio-resin coating on the average ultimate tensile strain of hemp yarns in E-40 solution.	197
Figure 4- 160 : Influence over time of the bio-resin coating on the average tensile strength of hemp yarns in E-60 solution.	198
Figure 4- 161 : Influence over time of the bio-resin coating on the average tensile modulus of hemp yarns in E-60 solution.	198
Figure 4- 162 : Influence over time of the bio-resin coating on the average ultimate tensile strain of hemp yarns in E-60 solution.	199
Figure 4- 163 : Influence over time of the bio-resin coating on the average tensile strength of hemp yarns in L-23 solution.	200
Figure 4- 164 : Influence over time of the bio-resin coating on the average tensile modulus of hemp yarns in L-23 solution.	200
Figure 4- 165 : Influence over time of the bio-resin coating on the average ultimate tensile strain of hemp yarns in L-23 solution.	201
Figure 4- 166 : Influence over time of the bio-resin coating on the average tensile strength of hemp yarns in L-40 solution.	202
Figure 4- 167 : Influence over time of the bio-resin coating on the average tensile modulus of hemp yarns in L-40 solution.	202
Figure 4- 168 : Influence over time of the bio-resin coating on the average ultimate tensile strain of hemp yarns in L-40 solution.	203
Figure 4- 169 : Influence over time of the bio-resin coating on the average tensile strength of hemp yarns in L-60 solution.	204
Figure 4- 170 : Influence over time of the bio-resin coating on the average tensile modulus of hemp yarns in L-60 solution.	204
Figure 4- 171 : Influence over time of the bio-resin coating on the average ultimate tensile strain of hemp yarns in L-60 solution.	205
Figure 4- 172 : manual coating of the hemp textile by the bio-sourced resin.	206
Figure 4- 173 : Force-displacement curves for the specimens of HC-E-28d series.	213
Figure 4- 174 : Force-displacement curves for the specimens of HC-E-2m series.	214
Figure 4- 175 : Force-displacement curves for the specimens of HC-E-3m series.	214

Figure 4- 176 : Failure mode B recorded in: a) HC-E-28d-1 specimen (multiple cracking behavior + rupture of the yarns), and b) HC-E-3m-2 specimen (only one cracking behavior + rupture of the yarns).....	215
Figure 4- 177 : Comparison between stress-strain responses of representative specimens of HC-E series with a representative coated-hemp yarn specimen (HC).	215
Figure 4- 178 : Stress-strain curves for the specimens of B-E-2y series.	216
Figure 4- 179 : Force-displacement curves for the specimens of HC-L-28d series.	218
Figure 4- 180 : Force-displacement curves for the specimens of HC-L-2m series.	218
Figure 4- 181 : Force-displacement curves for the specimens of HC-L-3m series.	219
Figure 4- 182 : Failure mode B recorded in all the HC-L series, a) multiple stress behavior during stage II, and b) the rupture of the yarns at the end of stage III.	219
Figure 4- 183 : Comparison between stress-strain responses of representative specimens of HC-L series with a representative coated-hemp yarn specimen (HC).	220
Figure 4- 184: Comparison between Force-displacement responses of representative specimen of H-E TRM series with a representative specimen of HC-E TRM series tested at 28 days of curing.	221
Figure 4- 185: Comparison between Force-displacement responses of representative specimen of H-L TRM series with a representative specimen of HC-L TRM series tested at 28 days of curing.	221
Figure 4- 186 : Comparison between stress-strain responses of representative specimens of HC-E TRM and HC-L TRM series tested at 28 days with a representative coated-hemp yarn specimen (HC).	223
Figure 4- 187 : Comparison between stress-strain responses of representative specimens of HC-E TRM and HC-L TRM series tested at 2 months with a representative coated-hemp yarn specimen (HC).	224
Figure 4- 188 : Comparison between stress-strain responses of representative specimens of HC-E TRM and HC-L TRM series tested at 3 months with a representative coated-hemp yarn specimen (HC).	224
Figure 4- 189 : Prediction of the durability of HC yarns in the ettringitic matrix E up to 60 years of service life (normalized residual values).	228
Figure 4- 190 : Prediction of the durability of HC yarns in the natural hydraulic lime matrix L up to 60 years of service life (normalized residual values).	229
Figure 4- 191 : Clear representation of the prediction of the durability of HC yarns in both matrices E and L up to 1.5 years of service life (normalized residual values).	229
Figure 5- 192 : Steps of the construction of a masonry wall: a) Water saturation of the bricks before using; b) Spreading of the mortar joint on the brick; c) putting a wood piece of 1 cm thick between two bricks; d) putting another brick on the layer of mortar; e) Applying some blows of the hammer; f) Final state of the walls.....	233

Figure 5- 193 : Steps of reinforcement of a concrete wall by a TRM system: a) Introduction of the first layer of the matrix; b) Application of the textile; c) Introduction of the second layer of the matrix; d) Covering the wall with a plastic film.	234
Figure 5- 194 : Geometric characteristics of the specimens for the shear bond test: a) front view of CS-HC-E specimens, b) lateral view of CS-HC-E specimens, c) front view of MS-HC-L specimens and d) lateral view of MS-HC-L specimens (dimensions are in mm).	235
Figure 5- 195 : Experimental setup of the shear bond test.	236
Figure 5- 196 : Failure modes related to the shear bond test [185].	237
Figure 5- 197 : Force-displacement curves for the specimens of CS-E-HC series.	239
Figure 5- 198 : Stress-slip curves for the specimens of CS-E-HC series.	239
Figure 5- 199 : Force-displacement curves for the specimens of MS-L-HC series.	240
Figure 5- 200 : Stress-slip curves for the specimens of MS-L-HC series.	240
Figure 5- 201 : Failure mode recorded in all the specimens of CS-E-HC series: a) Mode F b) uncracked ettringitic matrix for all the specimens tested.	241
Figure 5- 202 : Failure mode recorded in all the specimens of MS-L-HC series: a) Mode F b) uncracked natural hydraulic lime matrix for all the specimens tested.	241
Figure 5- 203 : Application of the procedure suggested in the Italian guidelines [191] for the qualification of the TRM systems to the experimental results of HC-E TRM.	243
Figure 5- 204 : Application of the procedure suggested in the Italian guidelines [191] for the qualification of the TRM systems to the experimental results of HC-L TRM.	243

List of tables

Table 1- 1 : Types of glass fibers [36].	32
Table 1- 2: Chemical composition of basalt and E-glass fibers [42].	35
Table 1- 3: Mechanical properties of basalt and E-glass fibers [42].	35
Table 1- 4: Chemical composition of some plant fibers [37], [71].	41
Table 1- 5: morphological properties of elementary lignocellulosic fibers [37].	42
Table 1- 6: mechanical properties of some plant fibers[37], basalt [42], E-glass and carbon fibers[102], AR-glass fibers [32] [103].	49
Table 1- 7: comparison of environmental impact between hemp fibers and glass fibers production [112].	54
Table 1- 8: life cycle assessment of hemp fiber and glass fiber production [112].	54
Table 1- 9: mechanical, physio-chemical, economic properties and environmental impact of some fibers.	57
Table 1- 10: technical characteristics of some fibers.	57
Table 2- 11 : Ettringitic matrix compositions.	90
Table 2- 12 : Consistency test of the ettringitic matrix (E) and lime matrix (L).	93
Table 2- 13 : Setting time test of the Ettringitic matrix (E).	96

Table 2- 14 : Flexural and compressive strengths at 28 days, on Ettringitic matrix (E) and Natural Hydraulic Lime matrix (L).....	100
Table 2- 15 : Properties of DGEBA 50% bio based epoxy formulation proposed by Viretto & Galy 2018 [160].....	102
Table 2- 16 : Properties of both bio based epoxy formulations proposed by Viretto & Galy 2018 [160].....	103
Table 2- 17 : Average value of the effective cross-sectional area of the yarns.	106
Table 2- 18: Weight, linear density, moisture content, and density of hemp yarns.....	108
Table 2- 19: Weight, linear density, moisture content, and density of flax yarns.	109
Table 2- 20 : Weight, and density of bio-resin-coated hemp yarns.....	109
Table 2- 21 : Water absorption and desorption of hemp, flax and bio-resin-coated hemp yarns.	111
Table 2- 22 : Mechanical properties of the Duralium AU4G.	113
Table 2- 23 : Tensile test results of hemp, flax and bio-resin-coated hemp yarns.	119
Table 2- 24: Properties of the Ettringitic matrix (E) and the Natural Hydraulic Lime matrix (L).	120
Table 2- 25 : Single yarn properties of hemp, flax and bio-resin-coated hemp.....	120
Table 3- 26 : Experimental plan for the accelerated aging of H and F yarns.	123
Table 3- 27 : Correlation between accelerated aging and service life of the yarns.	124
Table 3- 28 : Summary of the accelerated aging results on hemp and flax yarns.	158
Table 3- 29 : Influence of the temperature of the aging solution on hemp yarns.	159
Table 3- 30 : Influence of the pH of the aging solution on hemp yarns.	160
Table 3- 31 : Influence of the temperature of the aging solution on flax yarns.....	160
Table 3- 32 : Influence of the pH of the aging solution on flax yarns.....	161
Table 3- 33 : Influence of yarn's type on the period of occurrence of the different processes. .	162
Table 3- 34 : Tensile test series.....	165
Table 3- 35 : Mechanical characteristics of the EPONAL 380 resin after curing for 7 days at 20°C [178].....	166
Table 3- 36 : Tensile properties of H-TRM at the end of stage I.....	172
Table 3- 37 : Tensile properties of H-TRM at the end of stage II.	173
Table 3- 38: Predicted service life of hemp yarns calculated from accelerated days of exposure by using equation (1) and the real service of TRM.	176
Table 3- 39: Comparison of results between H-E-23 yarns and H-E TRM.....	177
Table 3- 40: Comparison of results between H-L-23 yarns and H-L TRM.....	177
Table 4- 41 : Experimental plan for the accelerated aging of HC yarns.....	180
Table 4- 42 : Tensile test series.....	206
Table 4- 43 : Tensile properties at the end of stage I for all the tested TRM configurations.	208
Table 4- 44 : Tensile properties at the end of stage II for all the tested TRM configurations...	209
Table 4- 45 : Tensile properties at the end of stage III and rupture modes for all the tested TRM configurations.	210

Table 4- 46: Correlation between accelerated aging and service life of HC yarns.....	225
Table 4- 47 : Comparison of results between HC-E-23 yarns and HC-E TRM (specimens with multiple cracking behavior).	225
Table 4- 48 : Comparison of results between HC-E-23 yarns and HC-E TRM (specimens with only one cracking).....	226
Table 4- 49 : Comparison of results between HC-L-23 yarns and HC-L TRM.	226
Table 4- 50: Correlation between accelerated aging and service life of the yarns.	228
Table 5- 51 : Shear bond test series.	235
Table 5- 52 : Experimental results for all the specimens tested in shear-bond test.	237

General Introduction

1.1 Motivation

In the field of civil engineering, the majority of the building stock is designed based on an empirical approach, due to the lack of designing standards and codes for other design issues at the time. However, these structures are permanently exposed to several factors that can reduce their service life. These factors are of various origins, such as natural aging, excessive vertical loads, structure exploitation change, errors of designing or implementation, accidental horizontal forces such as seismic loads, wind loads or movement of the ground. For this reason, structural reinforcement and repair of structures and built heritage are often considered, in order to extend their service life and increase their bearing capacity.

During the last five decades, the use of composite materials for rehabilitation and reinforcement of civil engineering structures has aroused a great interest, due to the fact that they allow the extension of the structure service life and prevent its demolition through providing tensile strength to the elements, modifying the mechanical behavior and the collapse mechanisms of the structure and increasing the structure displacement capacity [1].

Fiber reinforced polymer FRP was the most common type of composites used to reinforce civil engineering structures. They consist of continuous fibers bonded by an organic matrix based on epoxy resin. About 10 years ago inorganic matrix composites (Textile Reinforced Mortar TRM) began to be produced. TRM consists of an open textile grid imbedded in an inorganic matrix. The textile used in TRM is often made of glass, carbon, polyparaphenylene benzobisoxazole (PBO), aramid or basalt fibers [2].

These composite materials have shown significant improvements in case of the rehabilitation of masonry structures which suffer from several deficiencies such as low ductility, low mechanical properties (in particular, poor tensile strength), as well as weak connections between structural elements. Those deficiencies make the masonry structures vulnerable against out-of-plane loads and make fragile their collapse mechanism [1]. They have been also employed for the reinforcement and seismic upgrading of reinforced concrete (RC) structures, such as the confinement of RC columns to increase the rupture strength and the ductility, or the reinforcement of RC beams and RC slabs in the tension zone in order to exploit the high tensile strength of the composite materials.

The use of TRMs in place of FRPs for the reinforcement of civil engineering structures has shown several advantages in terms of fire and heat resistance and vapor permeability (breathability). These are very important characteristics in the field of the rehabilitation of historic monuments [3]. In addition, the use of organic binder (resin) has several drawbacks such as: 1) poor behavior of the resin at temperatures higher than that of the glass transition; 2) high cost of epoxy; 3) potential risks for workers; 4) difficulty of applying FRP on wet surfaces or at low temperatures; 5) lack of vapor permeability; 6) incompatibility of epoxy resins with certain substrate materials

such as clay for example and 7) difficulty of carrying out an assessment of the damage suffered by the masonry behind the FRP after an earthquake. The use of inorganic matrices (such as cement or lime based matrices) instead of organic ones is a solution for these problems [4].

TRM is considered as a technical solution with many advantages. First of all, it is compatible with traditional inorganic (brick/mortar cement) substrates, because it does not require prior preparation of the substrate which causes the degradation of the materials and the loss of the building's value. Furthermore, the inorganic matrix could be adopted by taking into account its adaptability with the existing structure, for example a matrix based on hydraulic lime is recommended in the case of masonry substrates and a cementitious matrix is more suitable in the case of concrete substrates. In several technical contexts the TRM solution is also reversible, this means that after a certain period, it can be easily removed and a new reinforcement can be applied. In addition, TRM is characterized by its light weight, so it limits the addition of overloads to the structure [5].

The lack of standards for the evaluation of the mechanical properties of the materials used in TRM and the identification of design procedures has encouraged the creation of several research groups, including the RILEM Technical committee "Composites for Sustainable Strengthening of Masonry" (TC 250 CSM) and the international code council evaluation services (ICC-ES). These research groups aimed at assessing the mechanical properties of different TRM materials applied to masonry substrates and developing effective test procedures. Direct tensile tests were performed on composite samples to assess their tensile strength and shear bond tests were performed on masonry substrates reinforced with TRM to assess the bonding capacity between the TRM and the masonry [6] [7] [8] [9].

It should be noted that there exists several acronyms for TRM, according to the US standard the acronym that identifies this composite material is FRCM (Fabric Reinforced Cementitious Matrix) [10]. In the literature, they have used different acronyms such as: TRC (Textile Reinforced concrete) [11], MBC (Mineral Based Composites) [12], CMG (Cementitious Matrix- Grid system) [13], IMG (Inorganic Matrix Grid system) [14], or FRC (Fiber Reinforced Cement) [15]. In the rest of this project, we will use the acronym TRM, because it is more generic and it describes all types of mortar.

Currently, the major environmental concerns and the awareness of industrial pollution have encouraged the construction and manufacturing industries to look for innovative, reliable and sustainable materials that can replace conventional synthetic fibers (glass, carbon, etc.) as reinforcements for composite materials. Considerable efforts were dedicated to the use of natural fibers as reinforcement for inorganic matrix composites. The main reasons for selecting natural fibers are: they have low cost, low density, and are recyclable and biodegradable, unlike synthetic fibers that are expensive to manufacture, have high density, are not renewable and cannot be thermally recycled by incineration [16]. According to "RILEM TRC report 36" [17], there are three categories of natural fibers: mineral fibers such as basalt and Asbestos, vegetable fibers such as flax, hemp, jute and sisal, and animal fibers such as mohair and silk. As for the mechanical

properties, some natural fibers such as basalt, flax, hemp are able to present tensile strengths comparable to those presented by synthetic fibers [18], [19]. Moreover, the low to moderate stiffness of plant fibers make them more suitable and more mechanically compatible with the masonry substrate that presents low to moderate stiffness [20]. In civil engineering applications, the plant fibers mostly analyzed and studied as reinforced fibers are bast fibers (jute, flax and hemp), even if to a lesser extent, also seed (coir) and leaf fibers (sisal).

However, despite the several advantages of natural fibers, their use in mineral matrix composite materials is limited by the relatively low resistance to degradation in alkaline environments [21]. Therefore, durability studies of mineral matrix and natural fiber composite materials are required in order to characterize their long-term behavior before using them in the large-scale rehabilitation of structures. Currently, only a few studies, in the literature address the durability of TRM systems, and especially those employing natural fibers.

1.2 Contents and structure of the thesis

The thesis consists on the experimental analysis of mechanical performances of hemp and flax TRM reinforced systems during time. The study will be carried out at different scales of study. From a small scale of investigation aimed at analyzing the physical, mechanical properties and durability of flax and hemp fibers, passing through the assessment of the mechanical response and durability of TRM composites, up to the study of concrete and masonry specimens externally strengthened by bio-resin-coated hemp TRMs. The thesis provides a comprehensive identification of the behavior of different topologies of plant based composites. Each chapter deals with a different scale of investigation; a critical analysis comparing the results at different scales is proposed as well. Finally, some modifications of the TRM components, aimed at improving the performance of the reinforcement, are experienced as conclusion of the work. The structure of the thesis, with the main contents and outcomes of each section, are reported as follow:

- Chapter 1 presents the state of the art review concerning the topic of interest. Specifically, the main research outcomes available in the literature are presented with respect to the use of TRM composites as reinforcement systems in civil engineering, and more specifically with respect to the use of plant fibers in TRM systems. Their strong and their weak points as well as the available solutions and techniques used to improve their behavior.
- Chapter 2 provides the main physical and mechanical properties of the ettringitic matrix and the natural hydraulic lime matrix adopted in the research as well as of the hemp, flax and bio-resin-coated hemp yarns.
- Chapter 3 reports the outcome of the investigation of the durability performance of hemp and flax yarns subjected to different aging protocols, which reproduces the alkaline environment of the matrix as well as the durability of hemp textile TRM systems. And a comparison between the results of accelerated aging on hemp yarns and the natural aging of these yarns imbedded in the real matrix of the TRM, followed by a conclusion concerning the aging protocols.

- Chapter 4 comprises the application of bio-resin-coating aimed at improving the mechanical performance of hemp yarns and hemp TRMs. It also reports the outcome of the investigation of the durability performance of bio-resin-coated hemp yarns subjected to different aging protocols, which reproduces the alkaline environment of the matrix as well as the durability of bio-resin-coated hemp textile TRM systems. The chapter also concerns a comparison between the results of accelerated aging on bio-resin-coated hemp yarns and the natural aging of these yarns imbedded in the real matrix of the TRM. The results of accelerated aging on coated and uncoated hemp yarns will be discussed and followed by a conclusion on the aging protocols and on the role of the bio-resin coating.

- Chapter 5 deals with the assessment of the bond properties between bio-resin-coated hemp TRMs and concrete and masonry substrates as well as between bio-resin-coated hemp textile and ettringitic and natural hydraulic lime mortar by means of single lap shear tests. The results of the experimental study were discussed and compared with similar studies available in the literature.

- In the end, we close the thesis by the main outcomes and the perspectives of the research study.

Chapter 1 A review on the durability of composite systems made from mineral matrices and different types of textile (TRM)

1.1 Introduction

The objective of this chapter is to make the state of the art of textile reinforced mortar. This work comprises two themes. The first one addresses the definition of the different fibers used as reinforcement in TRM systems, their origins, their manufacturing processes, their world productions, their biochemical compositions, as well as their mechanical properties and their impacts on the environment and then the comparison of natural fibers with synthetic fibers. The second one is concerned about the behavior of natural fibers such as hemp, flax and basalt when used in TRM systems, the various methods used to improve the properties of TRM with natural fibers and in particular the fiber-matrix bond, the different tests carried out in the literature to characterize the mechanical behavior of TRMs with natural fibers. And, finally, the durability studies found in the literature and applied to this type of TRM using different aging protocols.

1.2 Textile fibers used in textile reinforced mortar (TRM)

The fiber is the smallest unit contained in the textile, its diameter varies between 5 and 30 μm . The mechanical behavior of TRM is largely influenced by the mechanical, physical and chemical properties of the fibers used in their manufacturing process, as well as by their quantity and arrangement. Therefore, to ensure an effective reinforcement, it is necessary to choose a fiber of strong tenacity, high deformation at break, a modulus of elasticity much larger than that of the mineral matrix to avoid the appearance of cracks that reduces the rigidity of the TRM. In addition to that, the fibers must have a low relaxation under the effect of permanent loads, a good adhesion to the matrix, a low price, and the possibility of ease of handling in the textile manufacturing machines [17].

According to « RILEM TRC report 36 » [17], the fibers can be divided into four different categories, as follow:

- 1- Natural fibers:
 - Mineral fibers: Basalt and Asbestos
 - Vegetal fibers: Flax, hemp ...
 - Animal fibers: mohair, silk ...
- 2- Man-made fibers:
 - Inorganic fibers: Basalt, glass alkali-resistant (glass-AR), & glass-Z.

- Synthetic polymer fibers: Aramid, carbon, Acrylic, polyethylene, polypropylene, polyvinyl alcohol.
- 3- Ceramic fibers
- 4- Metallic fibers

In the following sub paragraphs, we focus on three textile fibers: carbon (1.2.1), glass (1.2.2) and basalt (1.2.3), which are the most commonly used as reinforcement in textile reinforced mortar (TRM), and some vegetal fibers (1.2.4), that interest us in this study, who aims to find natural replacements for the synthetic fibers in the domain of the reinforcement and rehabilitation of existing structures. Then, we compare the mechanical properties, the price (1.2.5) and the environmental impacts (1.2.6) between natural and synthetic fibers Finally, we end with a summary of the properties of textile fibers (1.2.7).

1.2.1 Carbon fiber

1.2.1.1 Generality

Carbon fibers (Figure 1- 1) are the most widely used reinforcements in the composite materials because they have the highest specific modulus and highest specific strength of all reinforcing fibers. In addition to these, carbon fibers are ideal for the use where there are critical requirements such as: high strength, high modulus, low weight, outstanding corrosion and fatigue characteristics, resistance to high temperature, high damping. Moreover, they offer good electrical conductivity, thermal conductivity, and low linear coefficient of thermal expansion [22]. Carbon fibers are used in several fields like: aviation and aerospace, industrial workwear, defense and law enforcement, transportation and furnishings, cable insulation, marine applications, engineering and textile applications, biomedical applications, sports and leisure goods, musical instruments and Hi-Fi, etc. [23].



Figure 1- 1 : Carbon fibers [24].

1.2.1.2 Advantages and disadvantages of carbon fibers

The advantages of the use of carbon fibers in textile-reinforced mortar are the followings [25] [26]:

- They have very good mechanical characteristics, they offer the high specific strength (3,000 - 5,000 MPa) and high specific modulus (200 - 250 GPa) of all reinforcing materials;
- They have very good resistance to alkaline environment of cement matrix;
- They have excellent temperature resistance;
- They are very insensitive to creep, dilatation and X-rays;

Despite the above-mentioned advantages of carbon fibers, they still have some disadvantages, which are:

- They have a very high cost (10,000 - 30,000 \$/ton) [27];
- They are excellent conductors of electricity, so knitting or carbon weaving machines must be insulated, which can increase the cost and the time of production [25] [26];
- During production, they consume a large amount of energy (290 MJ/Kg) [28];
- During production, they emit large amounts of greenhouse gas (about 29,500 kg CO₂ eq/t) [29];
- They present a risk of human toxicity;
- They aren't recyclable or renewable materials.

1.2.2 Glass fiber

1.2.2.1 Generality

Glass is used in different sectors; the four major ones among them are container glass, flat glass, glass fiber and specialty glass. Container glass is used in the kitchen for storing food and beverages. Flat glass is mostly used for windows fabrication. Glass fiber is used in two different applications: either for textile glass fiber which is used as reinforcing materials for composites, or for glass wool which is used as insulation materials for construction. Specialty glass includes a wide variety of products such as cookware, television tubes, etc. [30].



Figure 1- 2: a) E- glass fibers [31] and AR-glass fibers [32].

Table 1- 1 presents the different types of glass fibers available in the market, with their compositions, characteristics and applications. In this study, we are concerned about the continuous filament glass fiber (Figure 1- 2) used for manufacturing of textile reinforced composites. In general, the most widely used type of glass fiber is the electrical glass (E-glass), it represents more than 98% of the textile glass fiber market [33]. The composition of E-glass, for general application, is specified by the American Society for Testing and Materials (ASTM) and it contains the following: 52 - 62 wt% SiO₂, 16 - 25 wt% CaO, 12 - 16 wt% Al₂O₃, 0 - 10 wt% B₂O₃, 0 - 5 wt% MgO, and 0 - 20 wt% others [34]. But we should note that in case of composites made from Inorganic matrices, it is necessary for the glass fibers to resist strongly alkaline environments. Thus, in order to improve some properties like corrosion resistance and mechanical properties, new types of glass fiber are produced such as the alkali-resistant glass (AR-glass) fiber. The presence of ZrO₂ (1% - 18%) and the high content of alkali oxides Na₂O + K₂O (11% - 21%) and TiO₂ (0% - 12%) enhance the resistance of these fibers against alkaline environment and make them suitable reinforcements for cement and concrete matrices [35].

Table 1- 1 : Types of glass fibers [36].

Type	Manufacturing	Composition	Characteristics	Application
A-glass	Produced from cullet glass (often bottle) to fiber	Alkali-lime with little or no boron oxide	Not very resistant to alkali	When alkali resistance is not a requirement
AR-glass			Resistant to alkali	When alkali-resistance is required
C-glass (T-glass)	From used glass staple fibers	Alkali-lime with high boron oxide content	Resistant to chemical attack and most acids which dissolve E-glass	When higher chemical resistance to acid is required, for example for glass staple fibers
D-glass			Borosilicate	High dielectric constant
E-glass		Alumino-borosilicate with less than 1 wt% alkali oxides	Not chloride-ion resistant; E-glass surface is soluble	Mainly for glass-reinforced plastics; originally for electrical applications
E-CR-glass		Alumino-lime silicate with less than 1 wt% alkali oxides	High acid resistance	When high acid resistance is required
R-glass		Alumino silicate without MgO or CaO	Good mechanical properties	With high mechanical requirements
S-glass		Alumino silicate without CaO but with high MgO content	Highest tensile strength among all types of fiber	Aircraft components and missile casings, when high tensile strength required

1.2.2.2 Advantages and disadvantages of glass fibers

The advantages of the use of glass fibers in textile-reinforced mortar are the followings:

- They have good mechanical properties; they offer high specific strength (1,000 - 1,500 MPa) and high specific modulus (72 - 73 GPa);
- They have good electrical insulation properties;
- They can resist at high temperatures;

- E-glass and AR-glass have low costs (1,400 - 2,850 [37] and 3,300 - 3,600 \$/ton [38], respectively), comparing to carbon fibers (10,000 - 30,000 \$/ton) [27].

Glass fibers present also some disadvantages, which are the following:

- They have low resistance to alkaline and acidic environments;
- During production, they consume a large amount of energy (50 MJ/Kg) [28];
- During production, they emit large amount of greenhouse gas (about 1,700 - 2,200 kg CO₂ eq/t) [39];
- They present a risk of human toxicity [40], [28];
- During the production of E-glass fibers, there is significant consumption of water (360 - 960 gallons/ton) [33];
- The furnaces used in the glass industry need to be replaced every 5 - 15 years, as the refractory material deteriorates over time due to the high temperature, and building a furnace may cost 20 million dollars [34].

1.2.3 Basalt fibers

1.2.3.1 Generality

Basalt is a term commonly used to refer to a variety of volcanic rocks resulting from the solidification of lava flow from volcanoes. The melting temperature of basalt rocks (Figure 1- 3) is between 1350 and 1700 °C [41]. The color of basalt varies from brown and gray to dull green depending on its chemical composition [42]. We can find basalt rock in most countries around the world and it is directly suitable for fiber fabrication. It is mainly known for its resistance to high temperatures, its rigidity and its durability. Its chemical composition is too close to that of glass. The main components of basalt are SiO₂, Al₂O₃, Fe₂O₃, FeO, CaO et MgO [42]. Basalt materials are classified, according to their amount of SiO₂, into three categories: alkaline basalts (up to 42% in SiO₂), slightly acidic basalts (43 to 46% in SiO₂) and acidic basalts (more than 46% in SiO₂) [42]. Acidic basalt rocks are the most suitable for the production of basalt fibers [41].

Basalt fiber was originally produced in the Soviet Union during the 1960s to 1980s. Today, the production of basalt fibers is mainly located in Russia and China, with basalt mines located mainly in Ukraine [43], [44]. Few producers are located in West Europe [44]. Basalt rocks up to 200 meters of thickness have been discovered in countries of East Asia. Furthermore, Russia has huge stocks of basalt. There are significant fields of basalt rocks in the Urals, Kamchatka, the Far East, Sakhalin, the Kola Peninsula, north west of Siberia and the Transcaucasian region [41]. The cost of basalt fibers depends on the quality, the type of raw materials used, the production process and the characteristics of the final product. The price of one kg of continuous basalt fibers is around 2.5 \$ [45].

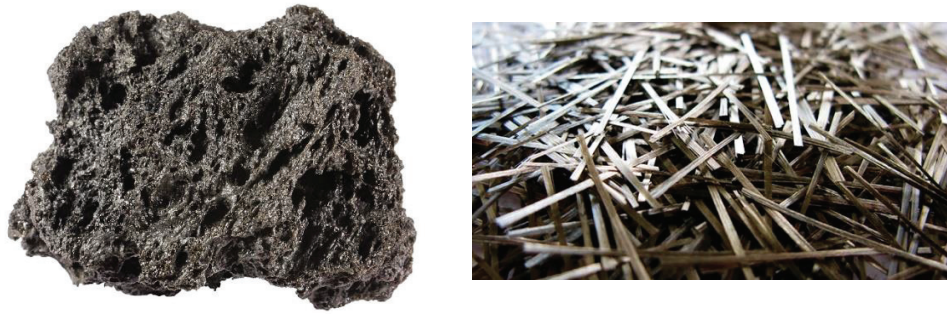


Figure 1- 3 : Basalt rock (left) [46] and basalt fibers (right) [47].

As basalt stone comes from nature, manufacturers of basalt fibers have less direct control over the purity and consistency of raw basalt stone. So the chemical composition of basalt can differ considerably from one spot to another [41]. However, the mechanical properties of basalt fibers depend on its chemical composition. In 2012, Deák et Czigány [42] studied the chemical composition and mechanical properties of different basalt fibers and E-glass fibers. The different fibers studied are: short basalt fibers "SB" manufactured by melt blowing technology by Toplan Ltd. (Hungary), continuous basalt fibers 'CB1', 'CB2' and 'CB3' obtained from three different manufacturers which are respectively Kamenny Vek Co. (Russia), D.S.E Group (Israel) and Technobasalt Co. (Ukraine) and E-glass fibers obtained from Skoplast Ltd. (Slovakia).

Table 1- 2 presents the chemical composition of the different fibers studied, and Table 1- 3 shows their mechanical properties. The main conclusions that they found are: SiO_2 is the basic component of basalt and E-glass. Its proportion is relatively uniform, between 50 and 56% by mass (m%) of continuous basalt fibers. Short basalt fibers have a lower SiO_2 content, while the proportion of SiO_2 in E-glass fibers exceed 58%. E-glass has a more regular chemical composition than basalt fibers. Some components, rarely present in E-glass fibers, are found in large quantities in basalt, for example Fe_2O_3 , K_2O , MgO , Na_2O and TiO_2 . These components determine the differences between basalt and glass fibers. The high heat resistance and the dark color of basalt fiber is mainly due to the Fe proportion. In Table 1- 3, the tensile strength of short basalt fibers is considerably lower than that of continuous basalt fibers and E-glass fibers. The elastic modulus and the diameter of short basalt fibers is also relatively low with high dispersion. The geometric and mechanical properties of continuous basalt fibers and E-glass fibers are similar in terms of diameter, tensile strength and modulus of elasticity (Table 1- 3). They concluded that continuous basalt fibers are competitive with E-glass fibers and short basalt fibers are poorer in terms of quality and mechanical properties.

In 2001, Gur'ev et al. [48] explained that the difference between short basalt fibers and continuous basalt fibers is mainly due to technological reasons. The technology of continuous basalt fiber production is characterized by long stages of melting and glazing, degassing, homogenization and melt cooling which together with the spinneret fibrillation method ensure uniformity diameter and physicochemical properties. On the other hand, short basalt fibers are produced by a technology

in which the time required for the process of melting and fiberizing is not sufficient to equalize its chemical composition by thermal diffusion and to stabilize the process of glazing, fibrillation and homogenization. The inhomogeneity of the melt is apparently the main cause of the irregular diameters of the fibers and the formation of fiber heads.

Table 1- 2: Chemical composition of basalt and E-glass fibers [42].

Element	Oxide	SB		CB1		CB2		CB3		GF	
		Element	Oxide	Element	Oxide	Element	Oxide	Element	Oxide	Element	Oxide
m%	m%	m%	m%	m%	m%	m%	m%	m%	m%	m%	m%
Al	Al ₂ O ₃	9.17	17.35	8.20	15.44	6.49	14.21	9.51	17.97	6.30	11.86
Si	SiO ₂	19.76	42.43	26.04	55.69	24.95	53.36	23.66	50.62	27.24	58.25
Ca	CaO	6.35	8.88	5.31	7.43	5.54	7.74	6.32	8.85	15.05	21.09
Fe	Fe ₂ O ₃	8.17	11.68	7.55	10.80	7.68	10.98	7.77	11.11	0.21	0.30
K	K ₂ O	1.94	2.33	1.25	1.51	0.88	1.06	1.43	1.73	0.36	0.43
Mg	MgO	5.70	9.45	2.45	4.06	3.22	5.35	3.13	5.19	0.32	0.54
Na	Na ₂ O	2.81	3.67	1.78	2.40	2.81	3.79	1.76	2.38	0.22	0.30
Ti	TiO ₂	1.53	2.55	0.74	1.23	1.04	1.73	0.66	1.10	0.25	0.41

Table 1- 3: Mechanical properties of basalt and E-glass fibers [42].

Marking	Diameter	Cross-section	Maximum force	Extension at failure	Tensile strength	Breaking strain	Elastic modulus	Density
	D _{av} [μm]	A _f [μm ²]	F _{fs} [N]	Δl _{fs} [mm]	σ _{fs} [MPa]	ε _{fs} [%]	E _f [GPa]	ρ [g/cm ³]
SB	10.3 ± 3.1	90.2 ± 56.7	0.05 ± 0.04	0.32 ± 0.12	602 ± 295	1.29 ± 0.48	48.2 ± 20.6	2.66
CB1	14.2 ± 1.4	160.2 ± 30.3	0.32 ± 0.09	0.89 ± 0.22	2016 ± 434	3.56 ± 0.89	61.9 ± 3.5	2.56
CB2	12.7 ± 1.5	128.1 ± 31.5	0.21 ± 0.07	0.68 ± 0.17	1608 ± 350	2.72 ± 0.67	62.0 ± 3.6	2.64
CB3	14.1 ± 2.9	163.5 ± 63.3	0.30 ± 0.13	0.87 ± 0.18	1811 ± 331	3.47 ± 0.70	53.2 ± 7.4	2.63
GF	16.8 ± 1.6	223.4 ± 42.0	0.32 ± 0.08	0.68 ± 0.22	1472 ± 395	2.71 ± 0.86	57.0 ± 3.0	2.61

1.2.3.2 Advantages and disadvantages of basalt fibers

Basalt fiber has several advantages that make it a good alternative to fiberglass for the reinforcement of composite materials. These advantages are:

- Basalt fiber is an eco-compatible material; it is very easy to recycle compared to glass fiber, for example. In fact, during the recycling of a composite material and especially during the incineration step glass fibers melt and stick inside the incineration chamber. This results in an expensive cleaning effort and significant downtime. While, basalt fiber has a melting point of around 1400 °C, which means that after incineration of a composite material containing basalt fibers, only unmelted basalt remains, fully usable and removable from the incinerator [49];
- The total energy required to produce 1 kg of basalt fibers is 4.96 kWh [49], which is equal to about 18 MJ, and which is equivalent to about 2/5 and 1/15 respectively of the energy

consumed by the production of 1 kg of glass fibers (50 MJ) and 1 kg of carbon fibers (about 290 MJ);

- The cost of basalt fibers produced using the industrial new technologies is equal and even lower than the cost of glass fibers [41];
- Even though the production process of basalt fiber is very similar to that of glass fiber, but it does not require additives and requires less energy with advantages in terms of environmental impact, economy and maintenance [50];
- The temperature of use of products made from basalt fibers (from - 260 °C to 700 °C) is significantly higher than that of products made from glass fibers (from - 60 °C to 250 °C) [49];
- Basalt fibers have excellent thermal properties compared to E-glass fibers and can easily withstand temperatures of 1100 - 1200 °C for hours without any physical damage [41].
- In corrosive environments, basalt fiber is considered an alternative to glass fiber, even if their corrosion mechanisms are similar, but the degradation of E-glass fiber is more severe than that of basalt fiber [50];
- Several authors have shown that the properties of continuous basalt fibers are comparable or better than those of glass fibers in terms of tensile strength and modulus of elasticity and that it is possible to consider them as alternatives to glass fibers as reinforcements in composite materials [42], [51];
- Basalt fiber is a poor conductor of electricity [50];
- Basalt fiber has no risk of toxicity for human. Kogan et al. [52] forced rats to inhale air containing asbestos fibers and basalt fibers for 6 months. In the case of asbestos fibers at a dose of 1.7 g.kg⁻¹ (referring to the body weight of the rat), a third of the animals died, while a dose of 2.7 g.kg⁻¹ killed all rats. In the case of basalt fiber, all animals survived even when the dose reached the concentration of 10 g.kg⁻¹.

However, the disadvantages of basalt fibers are:

- Basalt fiber is rigid and brittle so that it requires special care [53];
- In alkaline environments, basalt fibers are unstable. In 2005, Sim et al. [54] showed that basalt fiber produced in Russia has a tensile strength of less than 1000 MPa, which is about 30% of that of carbon fiber and 60% of that of high strength glass fiber (S-Glass). When these three types of fibers were immersed in an alkaline solution, the basalt fiber and the glass fiber have lost their volume and strength, producing a reaction product on the surface. While the strength of carbon fiber is not altered. Under accelerated aging conditions, basalt fiber and glass fiber experience a reduction in strength of 13.3% and 16.2%, respectively, for an exposure time of 4000 hours, but the reduction kinetics were slower for basalt fiber than for glass fiber. But when the fibers are exposed to a high temperature above 600 °C, only the basalt fiber has maintained its volumetric integrity and 90% of its strength [54]. It is therefore necessary to carry out a specific coating for the textile reinforcement, before using it in the composite TRM, to protect it against the alkalinity of the mortar.

Furthermore, in 2013, Rybin et al. [55] have shown that the zirconia coating slows down the corrosion of basalt fibers in an alkaline solution.

1.2.4 Vegetal fibers

1.2.4.1 Generality

Vegetal fibers are defined as those obtained from the various organs of the plant. They are classified according to their origin; there are bast fibers, seed fibers, leaf fibers and wood fibers. Bast fibers are collected from the inner bark or liber surrounding the stem of the plant, such as banana, flax, hemp, jute, kenaf, ramie, etc. they have a higher tensile strength than the other fibers. They are used in the industries of durable yarn, fabric, packaging and paper [56]. The seed fibers are manufactured from the seeds of the plant, such as cotton, coconut, palm oil, kapok, etc. they are used in clothing, upholstery, cordage, fabrics, mats, and brushes [57] [56]. The leaf fibers are collected from the leaves of the plant such as sisal, banana, abaca, etc... They are used in the fabrication of rope, twine and woven fabrics [58] [56]. The wood fibers are derived from bamboo or sugar cane (bagasse), they are relatively short and inflexible, but they are usually strong and perform better in cement environment [59].

Figure 1- 4 shows the production of some plant fibers in 2013 all around the world. One can notice that plant fibers are produced in different countries, but Asia is the principal producers of these fibers except for the flax and hemp fibers which are produced mainly in Europe (> 100 Kt) and sisal fibers which are produced mainly in South America (> 100 Kt).

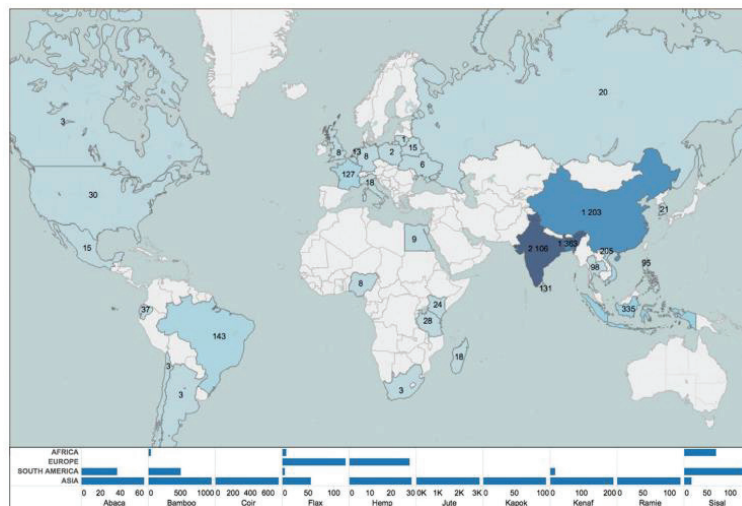


Figure 1- 4: world production of plant fibers (Kt) in 2013. These data is obtained from the Food and Agriculture Organisation (FAO) [60], [61] and from Saneco for flax fibers [62].

We can also notice that in Europe, the production of flax and hemp fibers is the most representative, this because the cultivation of their plants needs a mild climate like that of Europe.

Figure 1- 5 shows the distribution of flax fibers production in Europe in 2014, we can notice that France produces the greater quantity of flax fibers (104 Kt).

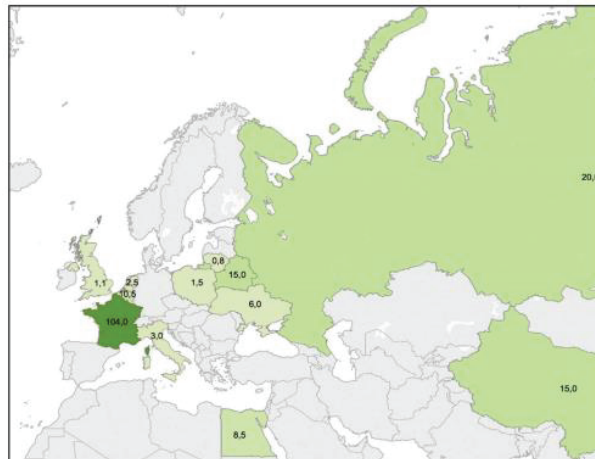


Figure 1- 5: Production of flax fibers in Europe in 2014 (Kt)[37], [62].

Figure 1- 6 shows the world distribution of the countries who cultivate hemp fibers and the countries who consume them in 2016 [63]. We can notice that hemp is cultivated mainly in China (45,000 ha), and then in Europe (33,000 ha).

From Figure 1- 7 [64], we can notice that France is the European leader of the hemp cultivation, it occupies more than half the total surface of cultivation (> 16,000 ha in 2016).



Figure 1- 6: world cultivation of hemp in 2016 [63].

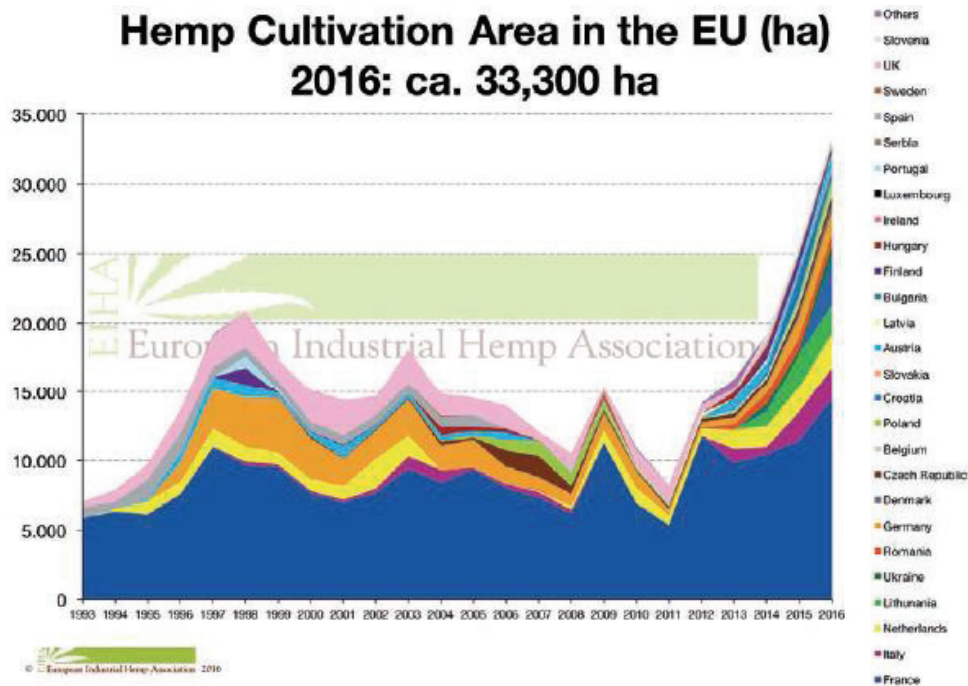


Figure 1- 7: Evolution of European hemp cultivation from 1993 till 2017 [64].

In the following paragraphs, we show the microstructure, the biochemical composition (1.2.4.2) and the morphological properties (1.2.4.3) of plant-based fiber. Then we talk in details about four different vegetal fibers that begin to be investigated in the last years in the domain of civil engineering: hemp (1.2.4.4), flax (1.2.4.5), jute (1.2.4.6) and sisal (1.2.4.7). And finally, we resume the advantages and the disadvantages (1.2.4.8) of plant fibers.

1.2.4.2 Microstructure and biochemical composition of plant-based fiber cell wall

There are three distinct layers from outside to inside of a natural fibril as shown in Figure 1- 8: (i) the middle lamella containing pectin, hemicellulose and lignin; (ii) the primary cell wall containing hemicellulose and cellulose; and (iii) the secondary cell (S1, S2, and S3) walls consisting mainly of cellulose. One single natural fiber is composed of several of these elementary fibrils (typically 10 - 40), bound together with the pectin substance in the middle lamella [65].

The lignin protects the fiber against microbial or chemical degradation of the polysaccharides. Together with the hemicellulose, they make the fiber more stable by binding and fixing the cellulose micro-fibrils. Lignin and hemicellulose are both sensitive to alkaline environment because of their amorphous characteristic. Cellulose is not homogeneous, it consists of both crystalline and amorphous regions. In alkaline environment, the crystalline regions of the cellulose provide its strength because of their good stability compared to the amorphous regions [66].

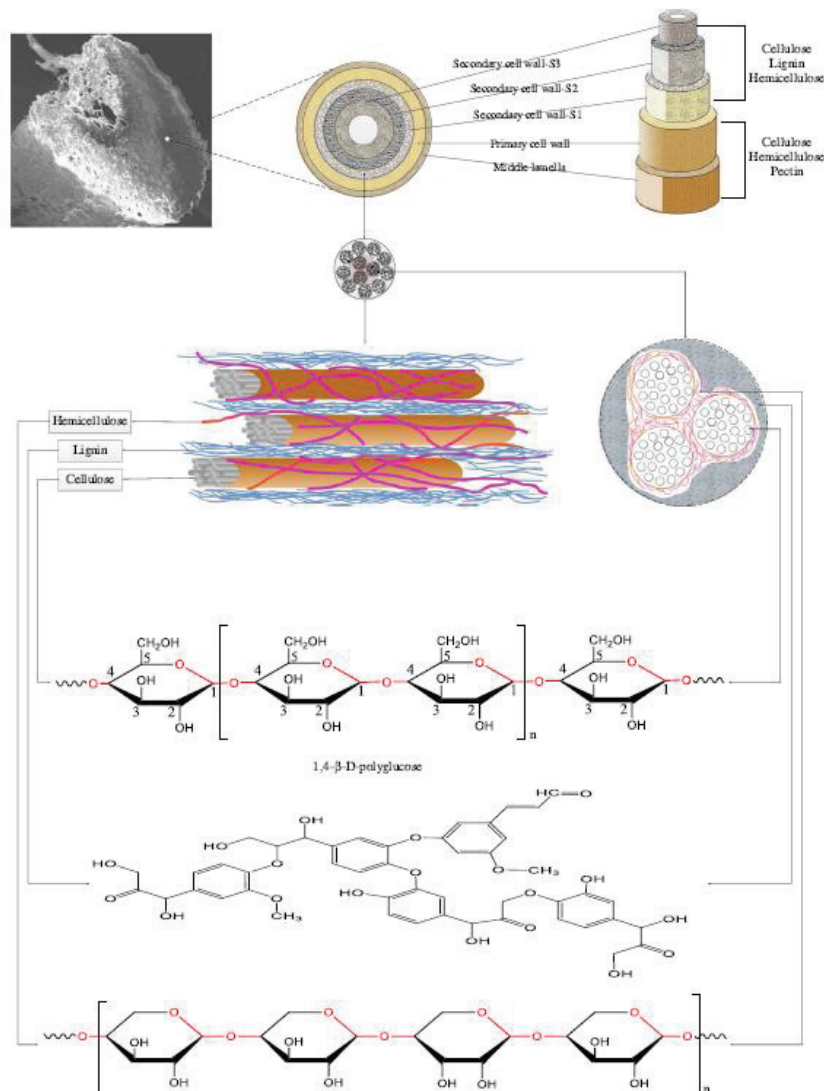


Figure 1- 8 : Microstructure, schematic diagram and molecular structures of natural fiber cell wall [66].

Cellulose is a linear polymer made of glucose subunits linked by β -1,4 bonds, and the basic repeating unit is cellobiose. Cellulose's stiffness and durability are supported by their formation of rigid, insoluble microfibrils chains, integrated by the numerous intra- and intermolecular hydrogen bonds. The high tensile strength of cellulose enables plant cells to withstand osmotic pressure and is responsible for the resistance of plants to mechanical stress [67]. Based on the work of various scientists, the Young's modulus of crystalline cellulose converges to 134 - 136 GPa [68]. The weak mechanical properties of the other components (2 GPa for the stiffness of the hemicelluloses in dry atmosphere (relative humidity = 12%) and 0.2 GPa in ambient atmosphere) allow them to marginally influence these vegetal fibers [69]. The distinct layers of the cell wall structure are the cause of the low density and the excellent mechanical properties of natural fiber, but they also are the cause of the poor resistance of these fibers in the alkaline environment [70].

Table 1- 4 shows the chemical composition of some bast fibers [37], [71]. The proportion of different chemical compositions depends on the age, the growth conditions, the source and the extraction method of the fiber [72]. Some authors have observed the impact of the proportion of cellulose on the mechanical properties [73]. It appears that the fibers which contain the highest level of cellulose, such as flax (60 - 81%), hemp (70 - 92%) or ramie (68 - 76%), have the highest mechanical properties, the tensile strength is between 595 and 1,510 MPa for flax fibers, between 285 and 889 MPa for hemp fibers and between 560 and 900 MPa for ramie fibers. However, this is not always true because cotton, rich in cellulose (82.7 - 98%), has very low tensile properties (287 - 800 MPa). Therefore, the cellulose proportion is not the only responsible for the mechanical capacity of the plant cell wall.

Table 1- 4: Chemical composition of some plant fibers [37], [71].

Fiber type	Cellulose (%)	Hemicellulose (%)	Lignin (%)	Pectin (%)
Banana	60-65	6-19	5-10	3-5
Flax	60-81	14-19	2-3	0.9
Hemp	70-92	18-22	3-5	0.9
Jute	51-84	12-20	5-13	0.2
Kenaf	44-57	21	15-19	2
Ramie	68-76	13-15	0.6-1	1.9-2
Sisal	52.8-65	19.3	11.1-13.5	10-14
Cotton	82.7-98	4-5.7	0.7	4

1.2.4.3 Morphological properties of plant fibers

Table 1- 5 combines data found in the literature concerning the morphology of some plant fibers used in bio composites: length, diameter, density and angle of the cellulose microfibrils with respect to the longitudinal axis of the fiber (microfibril angle MFA) [37]. These latter are difficult to observe because of their Nano metric size. However, atomic force microscopy (AFM) [74] or electron microscopy [75] in some cases allow the visualization of this orientation. But we should note that, it is difficult with these methods to obtain exact values of the angles, in particular with AFM, because of the lack of reference to the axis of the fiber, due to the high amplification of the studied areas. The use of X-Ray Diffraction XRD helps to better understand crystal and molecular orientation and to obtain the appropriate MFA values. By coupling the XRD with the tensile test, it is possible to evaluate the impact of the amorphous part and the crystalline part of fibers on the mechanical measurement [37].

The values of Table 1- 5 correspond to elementary fibers. We note that the morphological properties of plant fibers are very variable. This affects the mechanical performance of the composite comprising these fibers. Length, diameter and MFA vary a lot from fiber to fiber and even for fibers of the same type. The difference in length is very large in the case of cotton, flax,

hemp and ramie. However, the densities are very similar for all types of fiber and for fibers of the same type.

Table 1- 5: morphological properties of elementary lignocellulosic fibers [37].

Fiber type	Length (mm)	Diameter (μm)	MFA ($^\circ$)	Density (g/cm^3)
Abaca	2 - 12	6 - 53	5 - 17	1.5
Alfa	2 - 5	5 - 10	-	1.4
Bamboo	0.5 - 5	5 - 40	8 - 10.7	1.15 - 1.41
Coir	0.28 - 1.1	5.6 - 19.5	30 - 49	1.15 - 1.3
Cotton	10 - 60	12 - 38	20 - 30	1.5 - 1.6
Flax	6 - 80	12.4 - 23.9	8.3 - 11	1.53 - 1.54
Hemp	5 - 55	10.9 - 42.0	11	1.4 - 1.6
Jute	1 - 6	15 - 35	7 - 12	1.38 - 1.4
Kapok	7 - 35	8 - 35	5	1.3
Kenaf	2.1 - 2.7	2.1 - 36	9 - 15	1.45
Ramie	120 - 150	10 - 50	7.5	1.5
Sisal	0.5 - 0.8	10 - 20	20	1.45

1.2.4.4 Hemp fibers

1.2.4.4.1 Generality

The hemp plant, *Cannabis sativa* L. (Figure 1- 9) belongs to the family of fast growing Cannabaceae: it reaches an average length of 3 meters in 4 to 5 months. The average diameter of its stem varies from 1 to 3 cm. However, the morphological characteristics (height, diameter, ramification...) are very dependent on the species, the density of the seedling and the environmental conditions. 30% of the constituents of its stem are fibers rich in cellulose grouped together in fibrous bundles and having a support function. These fibers with exceptional properties are used in the industries [76]. The industrial hemp is identified from recreational hemp (Marijuana) by the amount of delta-9-tetrahydrocannabinol (THC) that it contains. Normally, industrial hemp produced for seed or fiber contains a negligible amount of THC, it is less than 0.2% [64]. Industrial hemp is used in several fields such as: construction, thermal and acoustic insulation, textiles, cosmetics and pharmacology, human and animal alimentation, in addition, it is also used as a fuel or biofuel [77].



Figure 1- 9 : Hemp plant (left) [78] and hemp fibers (right) [79].

1.2.4.4.2 Manufacturing process

The steps of the fabrication of hemp yarns are the following:

a) Harvesting, separation and retting of stems:

First, the plants are cut and the stems are separated from the seeds. Then the stems are usually laid on the ground and left for retting for several weeks [80]. Retting is a rotting process in which the pectin that binds the fibers together decomposes when it is in contact with light and air, giving the long bast fibers [81]. To speed up the process, retting can be done in water tanks, or in ice and snow, this technique produces finer fibers having a lighter color. However, this method has disappeared in Europe because it causes a large amount of water pollution [80]. Currently, the retting process can be accelerated by chemical and enzymatic technics. Depending on weather conditions, the retting time can vary from one to several weeks [81].

b) Fibers decortication:

Decortication is the process of extracting the ligneous heart from the stem. It can be done by two different methods: either immediately after retting, where the wet fibers are peeled from the heart and then dried, or by drying the stems before beating them with a special machine that breaks the ligneous heart and separates it from the fibers [81].

c) Fibers treatment:

In this step, the fibers are gathered in packs, collected and taken from the fields to pass to the spinning process, which is often done without treatment of the fibers. To soften the fibers and improve their elasticity, some producers have proposed chemical or mechanical treatment processes such as soaking the fibers in a boiling solution of soap and soda ash, and then washing these fibers with water, and soaking them in dilute acetic acid, then washing again with water, drying and combing [81].

d) Lignin extraction from fibers:

The roughness of the hemp fiber results from the lignin, which occupy a proportion of 8 to 10% of its dry weight. So, to soften the fiber and make it more flexible, lignin must be extracted. In order to extract the lignin from the hemp fiber without altering its resistance, researchers developed a new technique, in the mid-1980s, which allows extracting the lignin by enzymatic and microbial ways: first, the hemp fiber is treated by the protease enzyme, which digests the protein and reduces the concentration of nitrogen in the stems. Then, a species of fungus that feeds on lignin called *Bjerkandera* is installed on the fibers [81].

e) Fibers spinning:

In order to obtain long continuous yarns, the fibers are twisted together and then they are often coated with wax or a similar agent to produce a water-resistant and a more durable yarn [81].

1.2.4.5 Flax fibers

1.2.4.5.1 Generality

The flax plant, *Linum usitatissimum* L. (Figure 1- 10) belongs to the family of fast-growing Linaceae: it reaches an average length of 80 cm to 1 m in 3 to 4 months [82]. 80% of the world production of flax fiber is of European origin and France is the world leader. Flax plant is cultivated in the countries having temperate or hot weather [83]. In France, cultivation of flax currently takes place in the North, Picardy, Normandy, Brittany and Anjou. The most favorable climate is temperate and slightly humid. Flax requires rich and loose soil [82]. While 90% of European flax is used in the textile market (60% for clothing, 15% for household linen, 15% for furniture and lifestyle), 10% is used in technical outlets: green building, insulation, automobile industry, sports equipment, surgery and health, boating, stationery.... The technical linen fabric in industry, combined with resins, results in "high performance" composite products, such as: window frames (resistance and insulation), sports equipment: helmets, tennis rackets (vibration absorption), automobile, with mirrors and door reinforcements (lightness and rigidity), and eco-construction with chipboards, insulation wool, under roof screen... (acoustic and thermal properties) [83].



Figure 1- 10 : Flax plant (left) [84] and flax fibers (right) [85].

1.2.4.5.2 Manufacturing process

The steps of the fabrication of flax yarns are the following:

a) Uprooting and retting of stems:

First, the plants are uprooted and not mowed. Then, they are placed on the ground in swaths (a row of flax stems with a width of 1 m), and left for retting under the alternation of rain and sun, which allows the transformation of the plant into fibers. This process eliminates the pectose that binds the textile fibers to the woody part of the plant, by reacting with the microorganisms and bacteria present in the soil. These microorganisms secrete enzymes that accelerate the breakdown of pectin in the plant [83], [86]. In addition, the alternation of humid and moderate weather promotes the development of microorganisms (fungi, bacteria) secreting degrading enzymes such as polygalacturonases and xylanases.

b) Fibers scutching:

The flax fibers are contained in the outer layer of the stem. The scutching is a mechanical process that transforms the plant into fiber. It includes four steps: ginning, stretching, grinding and threshing. At the end, two categories of fibers are obtained: long fiber (long strand) and short fiber (tows) [83], [86].

c) Fibers combing:

The combing process prepares the fibers for spinning. In this step, the fibers are calibrated and stretched in the form of soft, lustrous ribbons ready to be spun [83].

d) Fibers spinning:

The spinning transforms the fibers into yarn. It includes different operations: regularization, stretching and twisting. To produce fine yarns (used in clothing, household linen, etc.), spinning is done on wet fibers, by immersion of fibers in water at 60 ° C. However, to produce more rustic and thicker yarns (used in decoration, ropes, etc.), spinning is done on dry fibers [83].

1.2.4.6 Jute fibers**1.2.4.6.1 Generality**

Jute plant (Figure 1- 11), *Corchorus capsularis* (white)/ *olitorius* (dark), belongs to the family of Malvaceae. It grows in tropical lowland areas with humidity of 60 % to 90 % [87]. The jute plant grows up to 3-3.7 m long [88]. Major parts of West Bengal and Bangladesh are involved in Jute cultivation. Jute is also cultivated in many other countries like China, Thailand, Myanmar, Nepal and Bhutan. Jute cultivation requires a warm and wet climate and huge rainfalls (5-8 cm weekly). Jute fibers lie beneath the bark and surround the woody central part of the stem. Jute is harvested between 120 days to 150 days from sowing when the flowers have shed. Early harvesting gives good healthy fibers [89]. Jute fiber is also called the golden fiber for its color. It is used in several fields like: culinary uses, sackcloth, containers for planting young trees, ropes, yarn and twine, hessian, sacking, carpet backing cloth, curtains, chair coverings, cosmetics, medicine, paints, home furnishing, canvas, handicrafts, wall hangings, home textiles, high performance technical textiles, geotextile, composites etc. [88], [89].



Figure 1- 11 : Jute plant (left) [90] and jute fibers (right) [91].

1.2.4.6.2 Manufacturing process

Jute fiber is manufactured following the next steps:

a) Retting:

The bundles of jute plant are placed side by side in retting water, then, they are covered with water-hyacinth or any other weed that does not release tannin and iron, and they are kept emerged (at least 10 cm below the surface of water) with bamboo-crating. Retting is best done in slow moving large volume of clean water. The optimum temperature is around 34 °C. Retting is considered complete once the fiber comes out easily from the wood on pressure from the thumb and fingers [92].

b) Extraction of fibers:

To extract the fiber from the stem, there are two methods: the single plant extraction method and the beat-break-jerk method. In the former, the stripping starts from the bottom, the fiber is slipped out free from the stem up to 8 - 10 cm, then gripped and pulled out slowly from the rest of the stem. Finally, the extracted fiber is washed in clean water. In the latter, a bundle of retted stems is gently beaten at the base with a mallet, then the woody core is broken and the bundles are twisted at the middle, the fiber is gripped where the bundle is broken and shook vigorously in water. The broken sticks slip out and water wrung out of the fiber. Finally, the fiber is washed in clean water, rung and eventually spread to dry, preferably in shade or mild sun. The beat-break-jerk method results in entangled fiber which affect the fiber quality while the single plant extraction method results in a better quality of fiber, this is why it is recommended [92].

1.2.4.7 Sisal fibers

1.2.4.7.1 Generality

Sisal plant, *Agave sisalana* (Figure 1- 12), belongs to the family of Asparagaceae. This plant is native to Mexico but, it is widely cultivated in many other countries such as Angola, Brazil, China, Cuba, Haiti, Indonesia, Kenya, Madagascar, Mozambique, South Africa, Tanzania and Thailand [93]. The leaves of sisal grow up to 1m to 1.5m long, and 10cm to 15cm wide. The fibers are longitudinally embedded in the leaves and are more abundant near the leaf surface. The flowering period of the sisal plant is up to 10 - 12 years but, the first cut of sisal leaves can be 2 - 2.5 years after planting. Sisal produces throughout its entire life from 180 to 240 leaves depending on the location, altitude, level of rainfall and variety of plant [94]. Most types of soil are suitable for sisal cultivation except clay and very moist and saline soils [93]. Sisal fiber is used in several fields like: binder twines, cordage, naturel carpets, cores of elevator ropes, polishing cloth for a wide range of metal surfaces such as stainless steel cutlery and car body parts, plastic and paper products, automobile industry, commercial aircraft, road construction, domestic furniture, and composite material etc. [93] [94].



Figure 1- 12 : Sisal plant (left) [95] and sisal fibers (right) [96].

1.2.4.7.2 Manufacturing process

Sisal fiber is manufactured following the next steps [97]:

a) Decortication or retting:

After the leaves are cut, they are decorticated in a duration less than 48 hours in order to avoid damaging problems during the cleaning process once they become dry. Sisal fiber is usually obtained, from the leaves of the plant, by machine decortications in which the leaf is crushed between rollers and then mechanically scraped [93], [94], [97]. During decortications 15 to 20% of the total leaf fiber is lost [97].

The fiber can also be obtained from the leaves by retting. The leaves are immersed in water for about one week, after which the leaves are beaten on a stone to remove the remaining extraneous matter, and fiber is separated [97].

b) Drying:

After decortication or retting, the fiber is washed, and dried, either in the sun or in drying machines and this gives the fiber a more uniform quality. This process also combs out the shorter fiber strands/strings of 7.5 to 12.5 cm in length. It is important to note that the excessive drying of the fibers in the sun may lead to deterioration in color [97].

c) Brushing:

Once the fibers are dried, they are collected into hanks to be brushed mechanically. The role of this process is to straighten the tangled, wavy fibers and to polish them [97].

1.2.4.8 Advantages and disadvantages of vegetal fibers

Vegetal fibers present many advantages:

- The rigidity of plant fiber in tension as in bending, its resistance to rupture, torsion, and compression make it useful in the design and manufacture of composite materials as an alternative to glass fiber [98];
- They have low densities compared with synthetic fibers [99];

- They have low costs compared with synthetic fibers [99];
- Their plants does not need any irrigation, they have deep roots, which allow it to resist the dryness [16], [64];
- Its cultivation does not need any herbicides, fungicides or insecticides [97], [16], [64], except for some types it may needs little amounts of fertilizers or pesticides [88], [89];
- Its cultivation does not need any genetically modified organism (GMO) and it results in high biomass [16], [64];
- It is 100% eco-responsible: 1 hectare of flax absorbs 3.7 tons of CO₂ [99], 1 hectare of hemp or jute plants absorbs about 15 tons of CO₂ [16], [64], [88], [89];
- In crop rotations, the hemp and flax plants are considered as an excellent starter crop because they leave an optimal soil quality with enriched fertility, which increases to 5 to 10% the yield of the following crops [88], [89];
- Plant fibers are renewable and available materials [16], [64], [93];
- They are 100 % biodegradable and recyclable [88], [89], [93];
- They are environmentally friendly [88], [89], [94];
- Their organic wastes and leaf residues resulted from processing are used to generate bioenergy, produce animal feed, fertilizer and ecological housing material [93];
- No skin irritation during their manufacture. [88], [89];
- All the processes used to transform the plant into fiber: scutching, combing, spinning, weaving, are mechanical (no chemistry) [99].

Despite all the above-mentioned advantages of vegetal fibers, there are many reasons that could limit their use in the domain of reinforcement:

- These fibers have poor resistance to alkaline environment which make their lifetimes much shorter than the AR-glass fibers [21];
- The coating of these fibers with the resin increases their costs and presents a risk of toxicity [100];
- Their physical and mechanical properties vary depending on weather conditions during growth [16], [56], [101].;
- They have poor fire resistance, they degrade from about 200 °C [56], [101];
- They cannot be stored for an extended period of time due to the possibility of degradation [56];
- They can suffer mechanical damage during harvesting [101];
- They are extracted from the stem of the plant by retting, but it is difficult to determine the right time to complete the process and excessive retting can reduce the properties of the fibers [101];
- They have an irregular cross section with a central void (lumen), which makes the determination of their mechanical properties more complex than that of a full circular glass fiber [101];

- They are hydrophilic because they contain a high content of hydroxyl ions in cellulose, so their volumes are unstable [56].

1.2.5 Comparison between natural fibers, carbon and glass fibers

1.2.5.1 Comparison of the mechanical properties of plant fibers with those of synthetic fibers

Table 1- 6: mechanical properties of some plant fibers[37], basalt [42], E-glass and carbon fibers[102], AR-glass fibers [32] [103].

Fiber type	Elementary fiber or bundle	Diameter (μm)	Young Modulus (GPa)	Tensile strength (MPa)	Deformation (%)
E-glass		5.0-24.0	72-73	1100-1500	1.8
AR-glass		13 \pm 2	72-80.4	1700	2.3
Carbon		5.0-8.0	200-250	3000-5000	2.5-3.5
Basalt		12.7-17	53-73	1811-2450	2.72-4.45
Abaca	bundle	179-230	17.1-18.4	755-798	8.8-6.2
Alfa	Elementary and bundle	24.3	31.0-71.0	679-1480	2.4-2.8
Bamboo	Elementary	13.4	32.0-43.7	1200-1610	3.8-5.8
Coir	bundle	100-460	3.39-17.3	131-343	3.7-44.7
Cotton	Elementary		5.5-13.0	287-800	3-10
Flax	Elementary	12.4-23.9	37.2-75.1	595-1510	1.6-3.6
Hemp	Elementary and bundle	10.9-42.0	14.44-44.5	285-889	0.8-3.3
Jute	bundle	60-110	10-31.2	114-629	1.5-1.8
Kapok	Elementary	23.6	1.7-4.0	45-93	1.2-4.0
Kenaf	Elementary	13.3	19	983	4.5
Ramie	Elementary	34-50	24.5-65	560-900	1.2-2.5
Sisal	bundle	25-252	9-25	347-577	2.3-5.45

Table 1- 6 contains the results of tensile tests carried out, in the literature, on E-glass and carbon fibers [102] and on several plant fibers [37], [101]. We note that among plant fibers, bamboo has the greatest tensile strength (1,200 - 1,610 MPa), then come the flax (595 - 1,510 MPa) and the alpha (679 - 1,480 MPa). These resistances are very close to those of E-glass fibers (1,100 – 1,500 MPa) but they are less than the resistance of basalt fibers (1,811 - 2,450 MPa), and less than half the tensile strength of carbon fibers (3,000 - 5,000 MPa).

We also notice that the Young's modulus of flax (37.2 - 75.1 GPa) and Alfa fibers (31.0 - 71.0 GPa) can sometimes reach that of E-glass (72 - 73 GPa) and basalt (53 - 73 GPa) fibers, but they are very small compared to those of carbon fibers (200 - 250 GPa). In the domain of strengthening of historical masonry buildings which constituted the greatest part of the building stock in Europe, fibers with lower stiffness such as plant fibers are preferred more than the use of high stiffness fibers because historical masonry is characterized by moderate compressive and shear strengths,

very low tensile strength and low to moderate stiffness. Therefore, a suitable strengthening system for masonry structures should possess a similar stiffness for mechanical compatibility with the substrate, while exhibiting enough tensile capacity [20].

As we have seen, the mechanical properties of plant fibers differ greatly from one type to another and sometimes within the same type. These properties mainly depend on the cellulose content, the degree of cellulose polymerization and the angle of the microfibrils (MFA). In general, the high cellulose content and the low MFA results in higher tensile strengths [56]. Flax and hemp, having an MFA of between 8 and 11 ° (Table 1- 5) and a cellulose content of between 60 and 92% (Table 1- 4) have good mechanical properties (Table 1- 6), while sisal, which has an MFA of 20 ° (Table 1- 5) and a cellulose content of 52.8 and 65% (Table 1- 4), has lower strength and stiffness (Table 1- 6).

1.2.5.2 Comparison of the price of vegetal fibers with that of synthetic fibers

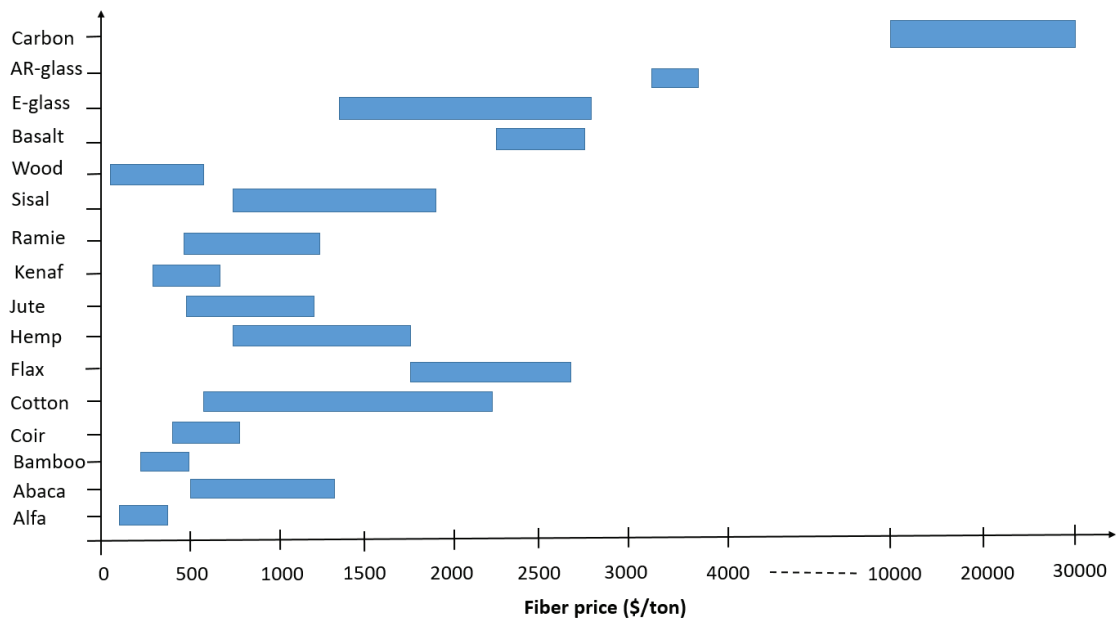


Figure 1- 13: commercial prices of E-glass fibers and some vegetal fibers (2004-2014). The main origin of these prices is the database of food and agriculture organization (FAO) [60]. The prices of flax fibers are provided by Saneco [104], prices of bamboo [105] Kenaf [105] wood [106] and hemp [107] fibers are found in the literature. These prices are compared to those of E-glass fibers [37], AR-glass [38], Basalt fibers [45], and carbon fibers [27].

Figure 1- 13 shows the commercial prices of E-glass, Basalt, carbon fibers and some vegetal fibers. We can notice that the price of plant fibers is unstable, it is not a constant value but a wide range of values. Some of them, like alpha and bamboo, are available at very low prices and are very competitive compared to glass fiber. The others present significantly higher prices. This is generally the case of long fibers such as flax or hemp. These differences are due to the differences in the quality of the fibers linked to cultivation, harvesting and manufacturing conditions or to their mechanical strengths. Furthermore, the variation in supply and demand sometimes causes differences in prices [37]. We can also notice that all the plant fibers in this Figure are cheaper

than E-glass, basalt and AR-glass fibers except flax fibers (1,700 - 2,700 \$/ton) [104], which cost roughly the same price as E-glass (1,400 -2,850 \$/ton) [37], and basalt fibers 2,500 \$/ton [45]. And for sure the carbon fibers are the most expensive among all the fibers, its price varies between 10,000 and 30,000 \$/ton [27].

1.2.6 Environmental impact of fibers

1.2.6.1 Environmental impact of plant fibers

In the domain of plant fibers production, several factors can affect the amount of fossil energy sources replaced or retained, such as the cultivation parameters (water requirement, pesticide requirement), biomass yield, retting method and fiber extraction method. These parameters can be very dependent on the geographical location and climatic conditions. The water dependence of plants is not the same for all types. Kenaf cultivation needs around 450 mm of water from annual precipitation [108], while the need of water is 800 - 1,000 mm for cotton [109] and 150 - 250 mm for flax [110]. Flax and hemp fields do not need irrigation, annual rainfall is sufficient. However, this is not the case for kenaf and cotton. About 53% of the world's cotton area is irrigated and it is mainly located in dry regions: Egypt, Uzbekistan and the Chinese province of Xinjiang are fully irrigated, while in Pakistan and northern India, the Irrigation provides most of the cultivation water. As a result, in Pakistan already 31% of all irrigation water is extracted from groundwater and in China the intensive use of pure water caused a drop in the groundwater level. Thus, due to this overconsumption of water, cotton cultivation has led to ecological disasters such as the disappearance of the Aral Sea and Chad Lake [37]. To produce 1 kg of cotton fiber, 7,000 to 29,000 liters of water are needed [109], while the water need is between 600 and 1,000 L for 1 kg of scutched flax fibers [110], and it is totally supplied by the precipitation. Therefore, it is very important to choose the appropriate cultivation region, taking into account both the local climate and the plant needs.

Experimental flax cultivation have been carried out in arid regions of Spain; their environmental analysis shows that 71% of their energy needs were used for irrigation, while this is not the case in other regions located in France or Belgium [111].

The Life Cycle Assessment (LCA) is a tool designed to evaluate the environmental impacts of a given method, process or product (PRé Consultants, 2014). The data provided by LCA can be used to improve a given process or method. Common impact categories evaluated with LCA include global warming, acidification, eutrophication, ozone depletion, photochemical production, and many other indicators. However, the impacts mentioned above are grouped into three main damage assessment criteria: effects on human health, ecosystem and resources [112]. LCA is a relatively new technique used in the field of natural fibers composites. Therefore, a good assessment of the fundamental properties of the entire material life cycle is desired. In fact, the evaluation of the stages of the raw material production, the processing of the material and the final fabrication of the composite, as well as the paths for the end of the material's life, are becoming more and more necessary to decide or not the 'green quote' for a specific material.

In 2004, Joshi et al. [113] conducted comparative life cycle assessment studies to conclude that from an environmental point of view the use of natural fibers in composites is better than the use of glass fibers. The key factors in the environmental benefit of natural fibers are:

- Natural fibers production has lower environmental impacts compared to the production of glass fibers; Natural fiber cultivation depends mainly on solar energy, and fiber production and extraction use small quantities of fossil fuel energy. On the other hand, glass production and glass fiber production are both energy intensive processes depending mainly on fossil fuels;
- Natural fiber composites have a higher fiber content for equivalent performance, thus reducing the content of polymer, which is more polluting;
- End-of-life incineration of natural fibers theoretically results in no net addition to CO₂ emissions, because plants, from which natural fibers are obtained, sequester atmospheric carbon di-oxide during their growth, which is released during the combustion of natural fibers.

However, the conclusions are distorted by two warnings:

- The use of fertilizers in the cultivation of plant fibers leads to an increase in the emissions of nitrates and phosphates, which can lead to an increase in eutrophication in local water;
- The environmental superiority of composites based on plant fibers can be rejected if the service life is significantly reduced compared to composites based on glass fibers. Therefore, it is very important to study the durability of these composites before using them in the reinforcement of historical structures for example.

According to Shahzad et al. [114] the energy required to produce 1 kg of hemp fibers is 3.4 MJ (Figure 1- 14), which is equivalent to approximately 2/25 and 2/145, respectively, of the energy consumed by the production of 1 kg of glass fibers (50 MJ [28]) and 1 kg of carbon fibers (approximately 290 MJ/kg [28]).

In 2011, Le Duigou et al. [28] showed that, for all environmental impact indicators (except land use), flax fibers perform much better than glass fibers (Figure 1- 15). The energy needed to produce 1 kg of scutched flax fiber is 1/5 (or about 10 MJ/kg) of the energy needed for glass fibers (about 50 MJ/kg) and about 1/30 of the energy needed for carbon fibers (about 290 MJ/kg). Therefore, as the energy required to produce 1 kg of polymer (between 80 and 120 MJ/kg for most technical plastics) is quite high, flax fibers can reduce the energy requirement of polymer composites, which is not the case for glass or carbon fibers (Figure 1- 14).

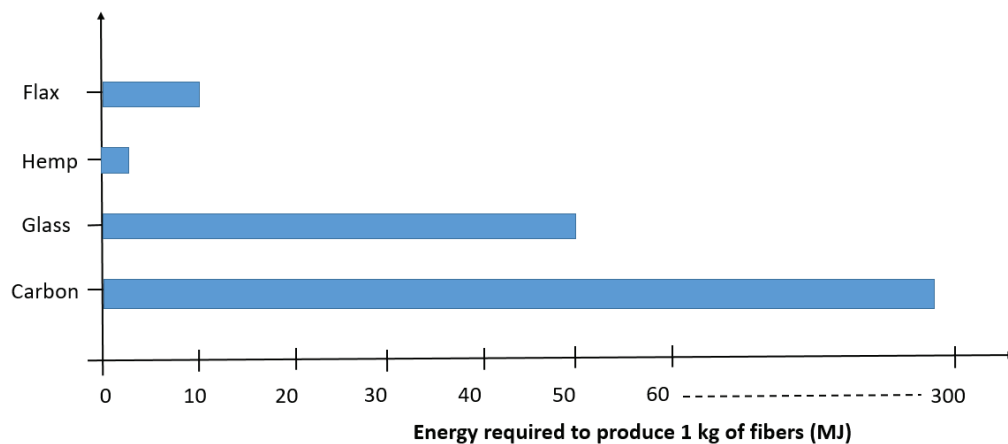


Figure 1- 14 : Energy required to produce 1 kg of natural fibers (flax and hemp) compared with glass and carbon fibers (MJ).

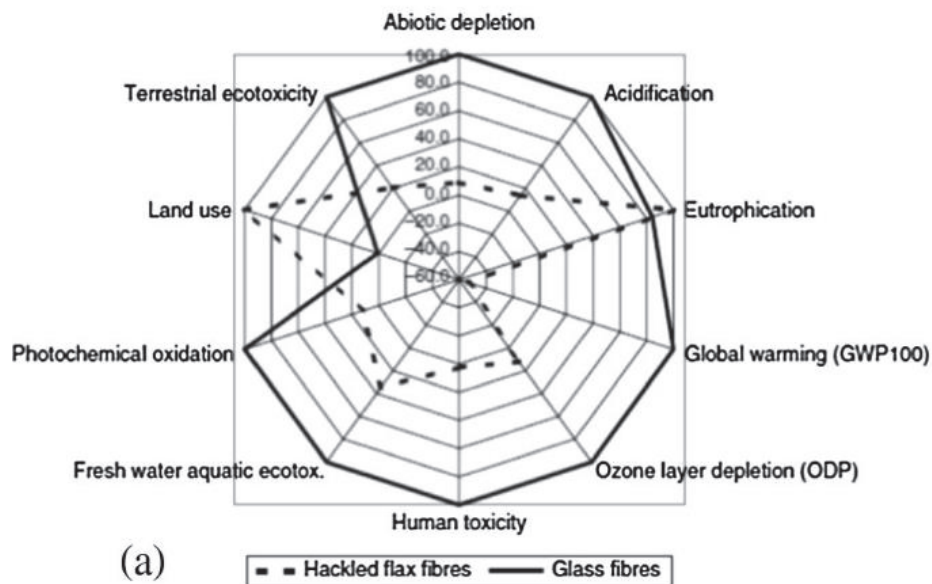


Figure 1- 15: comparison of environmental impact between flax fibers and glass fibers production [28].

In 2017, George et al. [112] evaluated the environmental impact of hemp fibers and compared it to that of glass fibers. The cultivation, extraction and processing of hemp fibers are taken into account in this study. The main environmental impacts are summarized in Table 1- 7. They found that the production of glass fiber has a greater environmental impact in most of the subcategories. In particular, there is high risk of human toxicity caused by the spinning and the extraction of these fibers. The demand for fossil fuel resources is greater in the production of glass fibers than that of hemp fibers. So based on these results, they concluded that the production of glass fibers has a greater environmental, human and ecosystem impact. Table 1- 8 resumes the four main indicators, which allow to evaluate all processes or products. The production of glass fibers requires fewer resources, while the production of hemp fibers requires a lot of soil and water for growth.

Nevertheless, the global warming potential of all types of hemp fiber studied is significantly lower than that of glass fiber production. These numbers reflect the motivation to use natural fibers to strengthen composites, assuming that the properties of the materials produced are comparable.

Table 1- 7: comparison of environmental impact between hemp fibers and glass fibers production [112].

Impact category ^a	Units	Hemp fibre treatment			Glass fibre
		A2S	A3TS	Mercerization	
Climate change	DALY ^b	5.67E-6	5.61E-6	3.38E-6	4.76E-5
Ozone depletion	DALY	1.82E-9	1.39E-9	1.88E-9	2.19E-9
Human toxicity	DALY	1.24E-6	1.60E-9	7.68E-7	1.39E-4
Terrestrial acidification	Species.yr	2.08E-10	2.42E-10	8.56E-11	2.64E-9
Freshwater eutrophication	Species.yr	4.94E-11	6.34E-11	6.00E-11	1.38E-10
Marine ecotoxicity	Species.yr	7.80E-12	9.71E-12	4.83E-12	2.23E-8
Fossil depletion	\$	0.32	0.20	0.10	0.74

^a These categories were selected because they accounted for greater than 90 % of the impact.

^b Disability adjusted life year: a measurement used to assess a specific process or product on human health (quantify the burden of human disease resulting from environmental pollution and attribute it to the life cycle of products or services).

Table 1- 8: life cycle assessment of hemp fiber and glass fiber production [112].

Item	Units	Hemp fibre treatment			Glass fibre
		A2S	A3TS	Mercerization	
Human health	DALY	9.54E-6	1.02E-5	1.92E-5	4.72E-3
Ecosystem Quality	Species.yr	9.96E-8	3.53E-8	6.66E-8	1.40E-3
Resources	\$	0.17	0.23	0.41	2.72E-3
GWP ^a	kg CO ₂ eq	4.09	4.04	8.50	14.20

^a Global warming potential (Characterization method: IPCC GWP 100a).

According to Barth & Carus [39], the production of one ton of glass fibers emits between 1,700 and 2,200 kg of CO₂ equivalent, while the emission of CO₂ equivalent emitted by the production of one ton of hemp is between 670 and 800 kg and in case of flax fibers and it is about 780 kg. according to Das [29], the production of 1 kg of carbon fibers emits 29.5 kg of CO₂ equivalent, so the emission of CO₂ equivalent emitted by the production of one ton of carbon fibers is 29,500 kg. These data are summarized in Figure 1- 16.

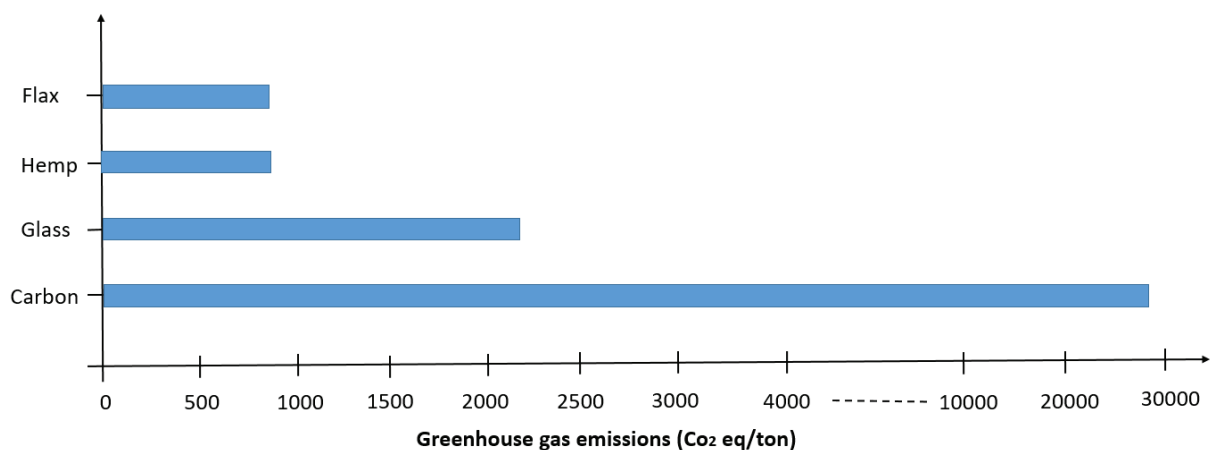


Figure 1- 16 : Carbon footprint of natural fibers (flax and hemp) compared with glass and carbon fibers Kg CO₂ eq/t.

In addition, in the end-of-life phase of a product, natural fiber composites have advantages over glass fiber composites. Several recycling options could be applied. When a thermoplastic matrix is used, end-of-life composites, as well as production waste, can be crushed, granulated and reused in injection molding processes [115]. Thus, composites made from natural fibers could be composted. Defoirdt et al. [116] have shown that flax-epoxy composites are attacked by several types of fungi, which is a necessary condition for composting. In good humidity conditions, flax fibers act as a nutrient source for fungi. When no other recycling option is available, composites can be incinerated to recover the significant amount of energy stored in the polymer matrix. However, during the combustion of glass composites, a glass residue containing ashes requires additional works. During the combustion of natural fibers composites, the fibers also burn, without any residue, and significantly increase the calorific value of the waste. The process is also (almost) CO₂ neutral, because during its growth, the natural fibers have absorbed large amounts of CO₂ [117].

1.2.6.2 Environmental impact of basalt fibers

At the end of 2011, Kammeny Vek finalized a project with the contribution of various European partners and research institutes in the field of life cycle assessment (LCA). The aim of this project was to perform a life cycle assessment (LCA) of basalt fiber textiles and their glass fiber textiles alternatives. The results of this study, in Figure 1- 17, show that basalt fibers and textiles perform significantly better in the main environmental impact categories compared to glass fibers. Especially in the toxicity categories (human, pure water, etc.), basalt fibers show significantly better results than glass fibers [40].

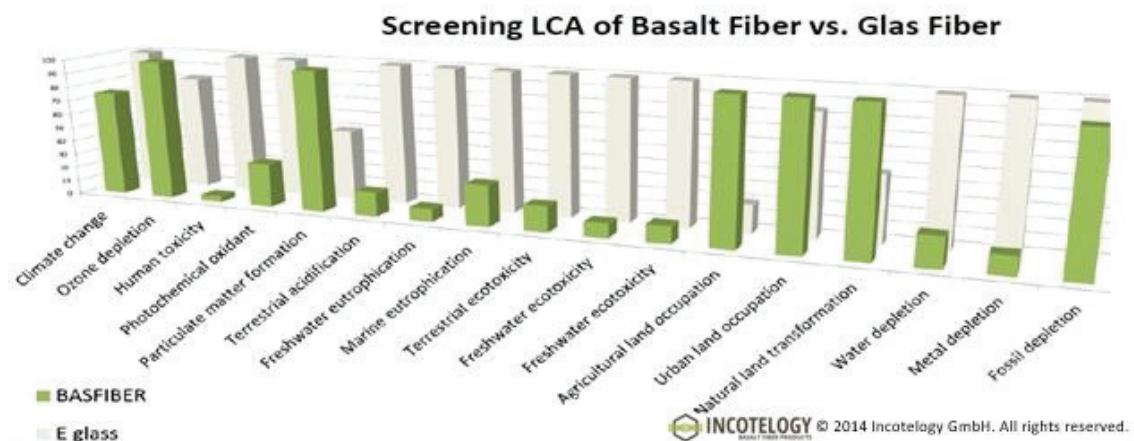


Figure 1- 17: comparison of the environmental impact between basalt fibers and glass fibers production [40].

In 2016, Azrague et al. [43] carried out a life cycle analysis (LCA) to evaluate the environmental impact of three scenarios for the production of continuous basalt fibers: the Russian scenario (raw material from Ukraine, energy input for the furnace: electricity + gas), the Iceland scenario 1 (raw material from the Iceland quarry, energy input for the furnace: electricity only) and the Iceland scenario 2 (raw material from the Iceland quarry, input energy for the furnace: electricity + gas).

*Comparative LCA –
Energy and site production*

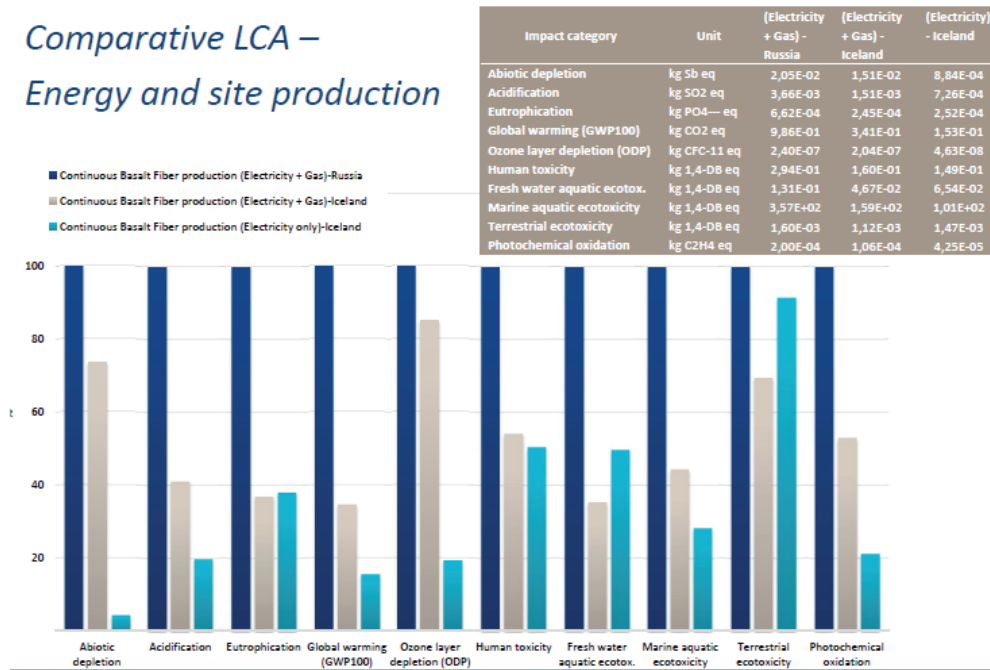


Figure 1- 18: environmental impact of the production of 1 Kg of basalt fibers by 3 different scenarios (Russia, Iceland 1 and Iceland 2) [43].

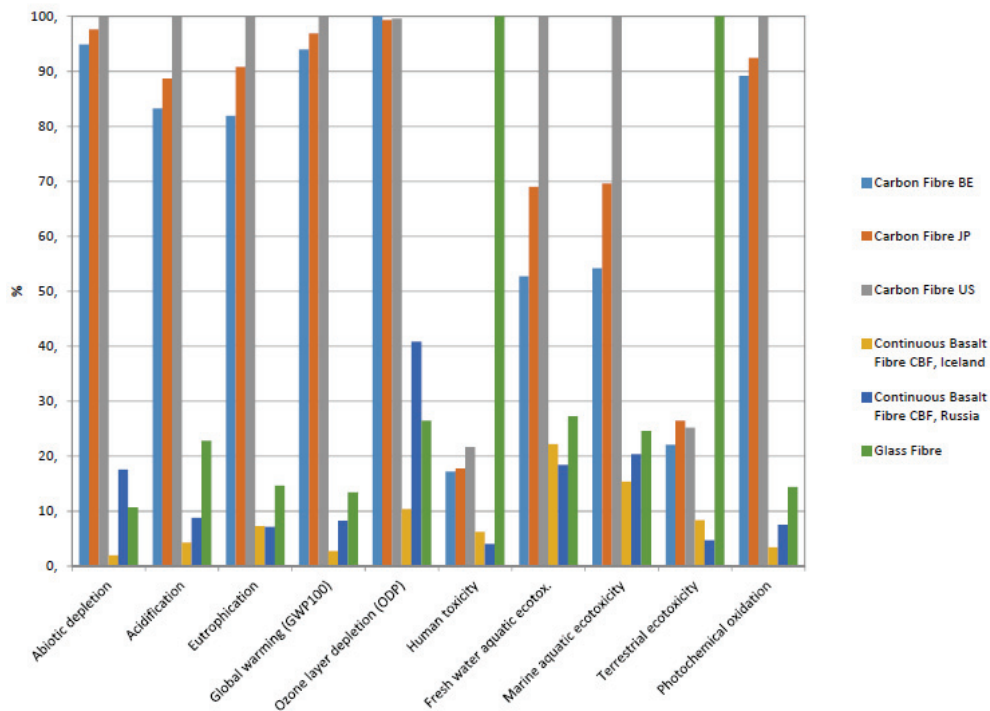


Figure 1- 19: comparison of environmental impact between basalt (Russia and Iceland), glass and carbon fibers production [43].

The results of this study are shown in Figure 1- 18. They found that Icelandic production based 100% on electricity could lead to a 68% reduction in greenhouse gas (GHG) emissions compared to Russian production. In both cases, the energy consumption of the furnaces is considered the factor that contributes the most to GHG emissions. The reduction in the energy consumption of the furnace depends on many parameters, such as the type of furnace, its operation, the composition and size of the basalt fracture, the size of the furnace and the production rate of continuous basalt fibers. Then, they compared the environmental impact of producing continuous basalt fibers with that of producing glass and carbon fibers. The results of this comparison are shown in Figure 1- 19. They found that for most environmental indicators, carbon fiber, followed by glass fiber, is much less environmentally friendly than continuous basalt fiber, including those produced in Russia.

1.2.7 Summary of textile fibers properties

Table 1- 9 summarizes the mechanical, physio-chemical and economical properties as well as the environmental impact of flax, hemp, basalt, E-glass and carbon fibers. Furthermore, the technical characteristics of these fibers are summarized in Table 1- 10.

Table 1- 9: mechanical, physio-chemical, economic properties and environmental impact of some fibers.

Fibres	Flax	Hemp	Basalt	E-glass	AR-glass	Carbon
Resistance to alkaline environments	Low	Low	Low	Low	High	Excellent
Resistance to acidic environments	Low	Low	Excellent	Low		Excellent
Temperature resistance	Low	Low	Excellent	Medium		Excellent
Recyclability	+	+	+	-	-	-
Energy consumed during productions (MJ/kg)	10	3.4	18	50		290
GHG emission (kg CO ₂ eq/t)	780	670-800	153-986	1700-2200		29500
Human toxicity	-	-	-	+	+	+
Cost \$/ton	1700-2700	700-1700	2500	1400-2850	3300-3600	10000-30000

Table 1- 10: technical characteristics of some fibers.

Fibres	Flax	Hemp	Basalt	E-glass	AR-glass	Carbon
Tensile strength (MPa)	595-1510	285-889	1811-2450	1100-1500	1700	3000-5000
Young modulus (GPa)	37.2-75.1	14.44-44.5	53-73	72-73	72-80.4	200-250
Density (g/cm ³)	1.53-1.54	1.4-1.6	2.56-2.63	2.6	2.7	1.8
Diameter (µm)	12.4-23.9	10.9-42.0	12.7-17	5.0-24.0	13 ± 2	5.0-8.0
Deformation (%)	1.6-3.6	0.8-3.3	2.72-4.45	1.8	2.3	1.8

1.3 Textile Reinforced Mortar (TRM)

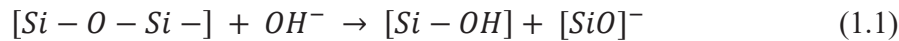
Textile reinforced mortar (TRM) is one of the various composite materials used for the rehabilitation and the reinforcement of masonry structures. It consists of a textile fiber grid imbedded in a mineral matrix. The role of the textile grid is to ensure good mechanical strength of the composite. While the mineral matrix is frequently manufactured with cement-based or lime-based mortar, or with a geopolymer, its role is to protect the textile, to ensure the cohesion between the composite and the substrate and to transfer the efforts from the substrate to the textile [3].

In this study, we focus on the use of natural fibers in TRM, in order to realize an eco-sustainable rehabilitation or repair interventions. So that, in the following paragraphs we talk about the degradation mechanism of basalt and plant fibers when used in TRM (1.3.1) and the different solutions used in the literature in order to enhance the properties of the TRM and enhance its long term behavior (1.3.2). In addition, we show the different mechanical characterization methods used in the literature to characterize the TRM (1.3.3) and the durability tests done on the TRM in order to predict its long-term behavior (1.3.4).

1.3.1 Behavior of natural fibers when used in TRM

1.3.1.1 Degradation mechanisms of basalt fibers in the matrix of cement composite

In alkaline environment, the basalt fiber is subjected to a corrosion, which is mainly governed by the reaction between the OH^- ions and the Si-O-Si resulting in the breakdown of silicon linkage. The rate of this corrosion depends on the chemical composition of the fiber, the alkalinity of the solution as well as on time and temperature [118]. The equation of the corrosion reaction is the following [119]:



When basalt fibers were immersed in alkaline solutions (NaOH, $Ca(OH)_2$, and their combinations with chloride or sulphate ions), initially, they lost their original texture and create fiber balls by sticking together after soaking in alkaline ions. Sometimes after 62 days of immersion in high alkaline solution, the fibers separate from the sticky balls, split into many strands and some of them become powder [119].

Figure 1- 20 shows scanning electron microscope (SEM) images for basalt fibers exposed to alkali solution for different time. It can be noticed that, after 8 days of immersion, a corrosion layer is present in the surface of the fiber. After 16 days and more this corrosion shell appears as it is formed of two sublayers. With increasing immersion time, the thickness of the corrosion shell increases [55]. This corrosion shell consists of the reaction products due to the dissolving of SiO_2 -network [118].

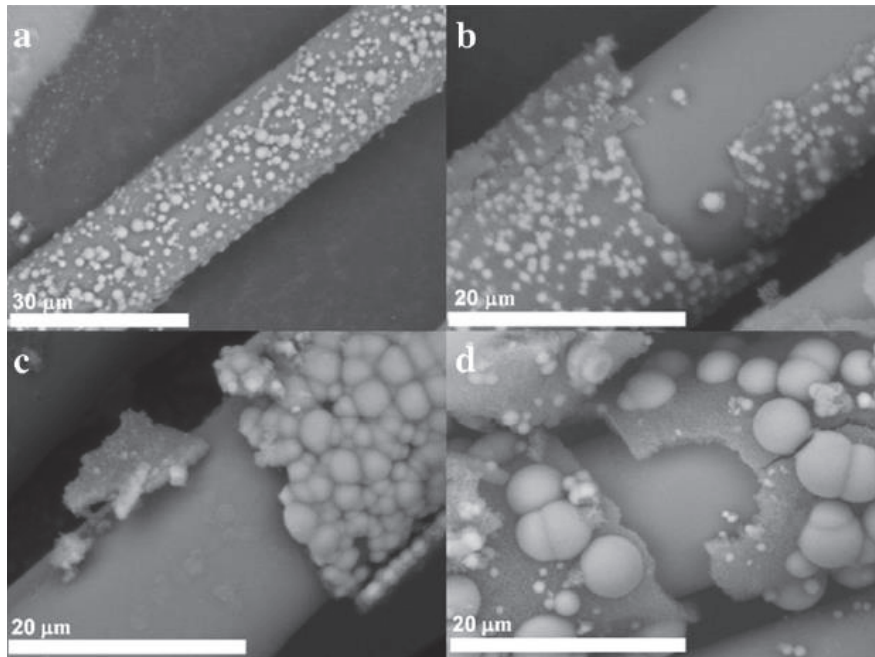


Figure 1- 20 : formation of corrosion at the surface of a basalt fiber after immersion in NaOH solution over 8 (a), 16 (b), 32 (c), and 64 (d) days at ambient temperature [55].

A second degradation mechanism can occur in the fiber reinforced cement composite which is the de-bonding between the fibers and the matrix. Figure 1- 21 shows SEM images for basalt fiber embedded in cement matrix at 7 and 28 days of curing. We can see that after 7 days, the surface of the fiber is covered with densely hydrated cement matrix which implies a good fiber-matrix bond. However, after 28 days, there is a space between fiber and matrix and the interface layer of the matrix is able to be detached from the fiber. This implies a poor fiber-matrix bond which may result in the de-bonding in long term [120]. Moreover, the precipitation of the hydration products between the fibers of the yarn may reduce their flexibility.

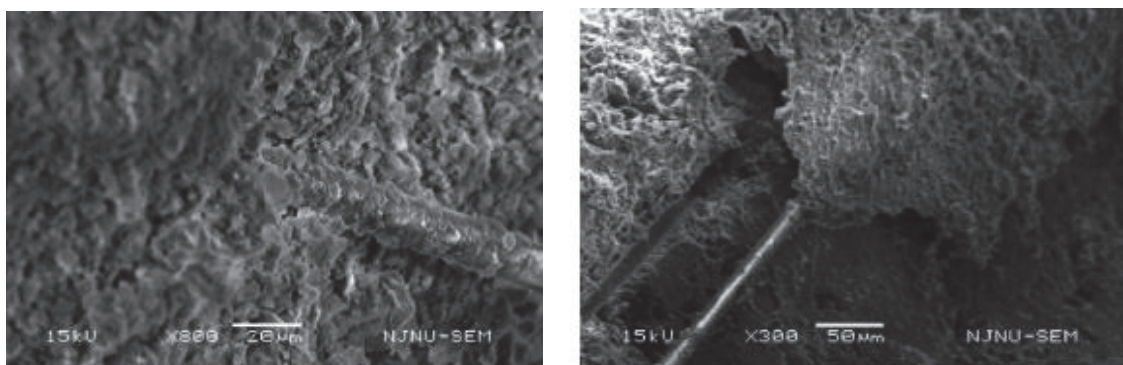


Figure 1- 21 : SEM images for basalt fiber in cement paste at 7 days (left) and 28 days (right) [120].

1.3.1.2 Degradation mechanisms of plant-based fibers in the matrix of cement composites

In the literature, two degradation mechanisms for cellulosic fibers in cement were proposed [121] and quantified by directly investigating the fiber's component change, degradation of tensile strength and crystallization indices [66]: alkaline hydrolysis and mineralization.

1.3.1.2.1 Alkaline degradation (hydrolysis)

The alkaline degradation of natural fiber in a cement matrix, due to the high alkalinity of cement solid phase and pore solution comprises four steps as shown in Figure 1- 22. (i) degradation of lignin and part of hemicellulose, which leads to the exposure of holocellulose in the pore solution and solid phase of the matrix; (ii) in this step, degradation occurs mainly on hemicellulose, which causes the decrease of integrity and stability of the cell wall of natural fiber; (iii) After the degradation of lignin, hemicellulose and intramolecular hydrogen bonding, no binding remains for cellulose micro-fibrils, and as a result cellulose fibers disperse in the pore solution of the matrix, which in turn, accelerates the degradation of cellulose; (iv) The last step is the failure of cellulose micro-fibrils, which is caused by alkaline hydrolysis of amorphous regions containing non-reducing end, and leads to the complete degradation of natural fiber. As the degradation proceeds, the hydration products, such as C-S-H and soluble portlandite, gradually infiltrate into the cell, which in turn leads to mineralization and embrittlement of the natural fiber [66]. The rate of degradation depends on the crystallinity and fibrillar morphology of the cellulose contained in these fibers. Hence, degradation rate is slower the higher the crystallinity of cellulose.

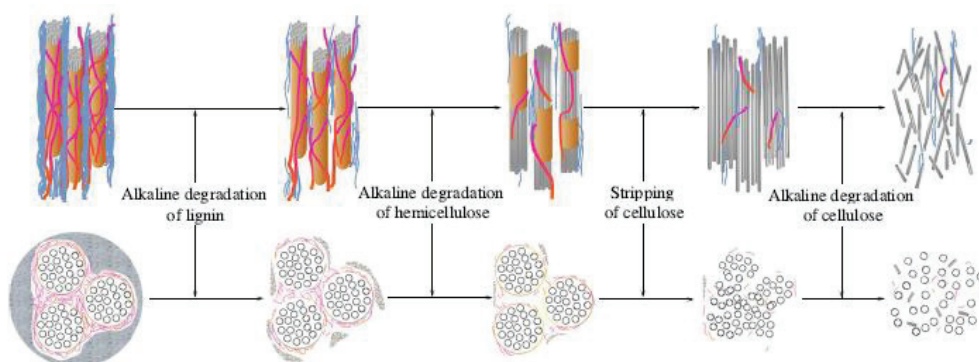


Figure 1- 22 : Diagrammatic sketch of natural fiber's alkaline degradation process [66].

The microfibrillic and chemical structures of cellulose are shown in Figure 1- 23 and Figure 1- 24, respectively. We can see that in amorphous regions, cellulose molecules have a non-reducing end and a reducing one, along with repeating glucose units. The reducing and non-reducing ends feature are C4-OH and C1-OH, respectively [122].

The reducing end is a latent aldehyde, like an aldehyde function, responding to both reduction and oxidation processes and it plays a key role in the alkaline degradation of cellulose. In alkaline environment, it undergoes a peeling-off reaction in which it splits off from the cellulose chain, resulting in soluble degradation products such as isosaccharinic acid (ISA) [123].

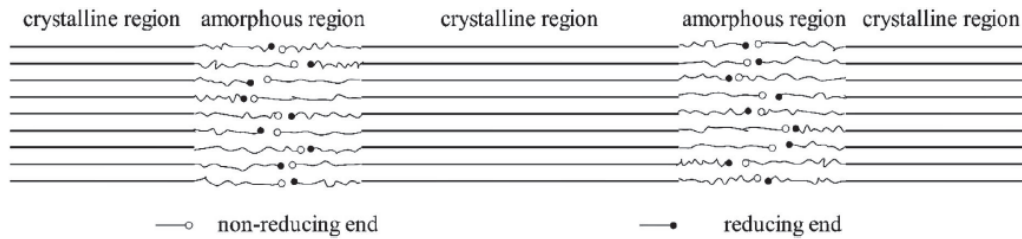


Figure 1- 23 : Diagrammatic sketch of microstructure of cellulose micro-fibrils [122].

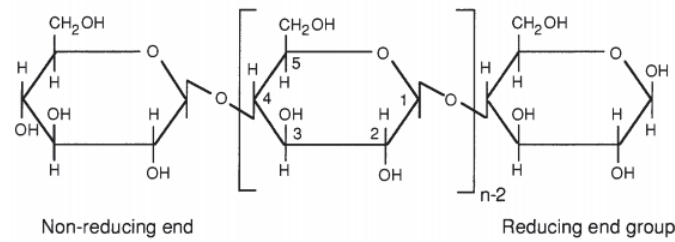


Figure 1- 24 : chemical structure of cellulose [123].

Figure 1- 25 shows the four processes of the degradation of cellulose under alkaline conditions, which are: peeling-off reaction, chemical stopping reaction, physical stopping reaction, and alkaline hydrolysis [124]. The peeling-off reaction is an endwise degradation process by which a reducing end group is split off from the cellulose chain, resulting in soluble degradation products such as ISA. This reaction is controlled by two competing reactions: a progressive shortening of the cellulose molecule in which glucose units are progressively eliminated from the cellulose molecule (starting at the reducing end group) and a stopping reaction. The stopping reaction can be subdivided into a chemical and a physical stopping reaction. The former is the transformation of reducing end group into a stable metasaccharinic acid end group, which terminate the depolymerization. The latter implies that a reducing end group reaches the crystalline region of the cellulose and is no longer accessible to alkali [123]. Alkaline hydrolysis is accompanied by the cleavage of glycosidic bonds in cellulose, and leads to a production of new reducing end groups, which create favorable conditions for the above three decomposition mechanisms. In principle this would enable complete degradation of the cellulose [125]. In fact, the shorter a cellulosic chain is, the smaller the number of glycosidic bond is, and the less energy it needs to decompose thermally [126].

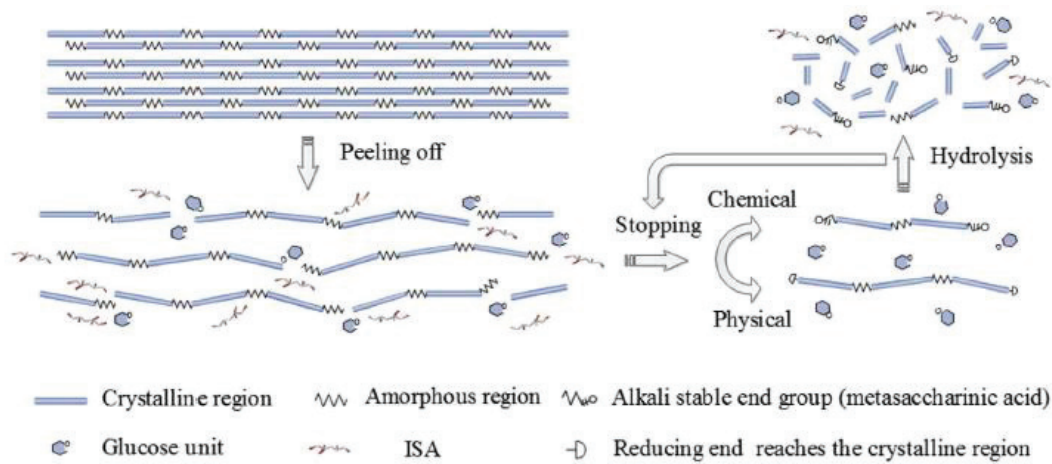


Figure 1- 25 : Schematic diagram of alkali degradation of cellulose [124].

1.3.1.2.2 Mineralization

Cell wall mineralization is also an important degradation mechanism which leads to the fiber embrittlement (increase in fiber tensile modulus) and the reduction of strength and strain capacity [66], [127]. Two mineralization mechanisms are proposed by Wei and Meyer: the CH-mineralization and the self-mineralization.

CH-mineralization

The migration of cement hydration products (calcium hydroxide) to lumens and to the middle lamella, combined with the volume variation of the natural fibers due to their high water absorption cause the CH-mineralization of these fibers. This phenomenon produces a significant increase in the stiffness of the fiber. Furthermore, the crystallization of CH in cell walls, through nucleation and growth processes causes the damage of the bonding between the various components, the corrosion of the cellulose micro-fibrils, the increase of the brittleness and the reduction of the strength of the vegetal fiber [66], [127].

Self-mineralization

The hydrolysis of amorphous phases of vegetal fibers causes their self-mineralization. Unlike CH-mineralization, a slight hydrolysis of lignin and hemicellulose has no effect on Young's modulus of the fiber. However when the crystallinity index exceeds 0.80, the fiber's Young modulus increases causing a significant reduction in the fiber deformability. This indicates that Young's modulus of natural fiber mainly depends on the cellulose, which is the primary structural component of cell walls. However, lignin and hemicellulose within the fiber cell wall act as a barrier to pore solution ingress/egress and by their very presence prevent precipitation of mineral based phases within the fiber cell wall, thereby minimizing fiber mineralization. In order to restrain the degradation of natural fiber in the cement matrix, both amorphous components (lignin,

hemicellulose) and cellulose should be protected by reducing the OH^- concentration of pore solution [66], [127].

1.3.2 Enhancement of the properties of fiber reinforced cement composites

The mechanical compatibility between the textile and the matrix is an essential parameter to ensure the transfer of stresses from the structure to the textile; it depends on the capacity of the mortar to impregnate the fibers of the yarn, the fiber-matrix bond, the fiber-fiber bond and the arrangement of the fibers in the textile.

In the literature, they used four strategies to improve the resistance and the durability of fibers in the alkaline environment of the cement matrix and in the different weathering conditions. One possibility is to modify the composition of the matrix in order to reduce or remove the alkaline compounds. The second way is to modify the fibers with chemical or physical treatments to increase their stability in the cementitious matrix. The third way is the combination of cement matrix modification with fiber pre-treatment and the fourth way is the accelerated carbonation curing.

Pre-treatment of natural fiber may require more effort, can increase cost, and need to consider the compatibility between modifying agents and the cement matrix, as well as its effect on the interfacial properties of fiber-cement. Therefore it is more logical to improve the initial mechanical properties and durability of natural fiber-reinforced cement composites through modifying the hydration of cement [127], [128].

1.3.2.1 Cement matrix modification

Some studies reported the effect of modifying the cement matrix using pozzolanic materials to reduce the matrix alkalinity. Other studies modified the matrix using additives in order to refine the porous structure of the matrix and limit the water absorption capacity of the composite.

There are several pozzolanic additions to reduce the alkalinity of the matrix, such as microsilica or silica fume, metakaolin, blast furnace slag or fly ash among others. Depending on the reactivity, it will modify the matrix in different manners.

In 2003, Toledo Filho et al. [129] studied the durability effect of partial replacement of ordinary Portland cement (OPC) by 10 wt.% undensified silica fume and 40 wt.% blast-furnace slag. Specimens were subjected to three different aging conditions: immersion in water, wetting and drying cycles and exposition to natural weather. They found that the presence of undensified silica fume in the matrix is an effective means of slowing down the strength loss and embrittlement of the vegetal fiber reinforced cement composite. However, the specimens made with blast-furnace slag showed a strong deterioration with time.

In 2010, Toledo Filho et al. [130] demonstrated that the use of matrix where the Portland cement is replaced by 20 wt.% and 30 wt.% with crushed waste calcined clay bricks and metakaolin,

respectively, results in a $Ca(OH)_2$ free matrix that promotes an adequate environment in which sisal fiber reinforcement did not suffer any process of mineralization.

In 2013, Melo Filho et al. [121] studied continuous sisal fiber cement composites using two different matrices: one with 50 % partial cement replacement by metakaolin (PC-MK) and the other composed by ordinary Portland cement only (PC). The two composites were subjected to 5, 10, 15, 20 and 25 wetting and drying cycles and then tested under a four points bending load configuration. Furthermore, PC-MK composites were tested under bending load at ages ranging from 28 days to 5 years. The thermogravimetric analysis indicated that the Portland cement replacement by 50 % of amorphous metakaolin lead to a significant reduce of the calcium hydroxide formation: no sign of calcium hydroxide was detected at 28 days. Flexural tests performed after the accelerated aging cycles showed that the PC composite system completely loses its ductility and strength after 25 cycles of wetting and drying. It was observed that the accelerated aging process is more severe in the first 10 cycles for the PC composite. The residual mechanical parameters after 25 cycles were the same as those observed in unreinforced matrices. The fracture process changed from a multiple to a single cracking formation after 20 cycles. However, for the PC-MK systems the mechanical performance was slightly affected by the aging cycles. The cracking pattern has not been altered during the aging cycles and the crack spacing remained constant to around 19 mm. A small reduction in strength and toughness was noticed during the first 10 cycles. They related this phenomenon to a fatigue in the fiber matrix-interface due to the volumetric changes of the sisal fiber with wetting and drying cycles. PC-MK composites tested after curing ages ranging from 28 days to 5 years showed a progressive increase in the post cracking stiffness resulting in a decrease of toughness and cracking density. Microstructural observation suggested that the sisal fibers undergo a mineralization process when used in Portland cement matrices. The cell walls of the fibers were damaged after the wetting and drying cycles while no signs of fiber degradation were noticed for sisal fibers exposed to the aging process in PC-MK composites (Figure 1- 26). No sign of calcium hydroxide was found in the fiber surface extracted from the PC-MK composites, while on the fiber's surface extracted from the PC matrix, a high concentration of hydration products including calcium hydroxide crystals was observed (Figure 1- 27). Thermogravimetric analysis (TGA) performed in the sisal fibers revealed that both lignin and hemicellulose are degraded when the fiber is exposed, in both matrices, to cycles. For the PC matrix, a 15 % weight loss was observed in the peak of cellulose while in the PC-MK matrix, a loss of 5 % was noticed. The author's hypothesis is that cellulose is also being degraded in fibers used for reinforcing the PC matrix.

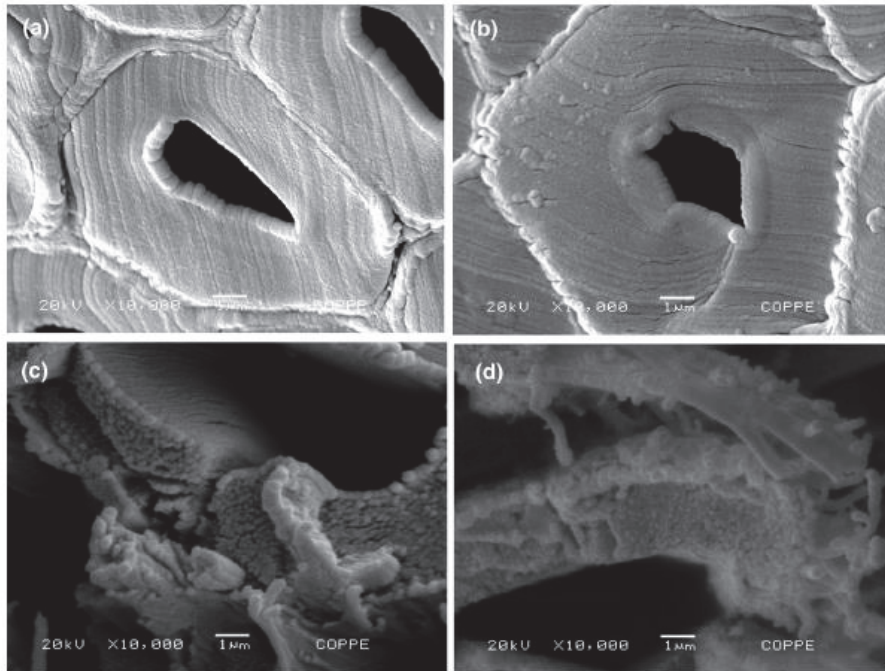


Figure 1- 26 : The effect of the wetting and drying cycles on the sisal fiber microstructure : (a) reference, (b) fiber extracted from a PC-MK matrix, (c and d) fiber extracted from a PC matrix [121].

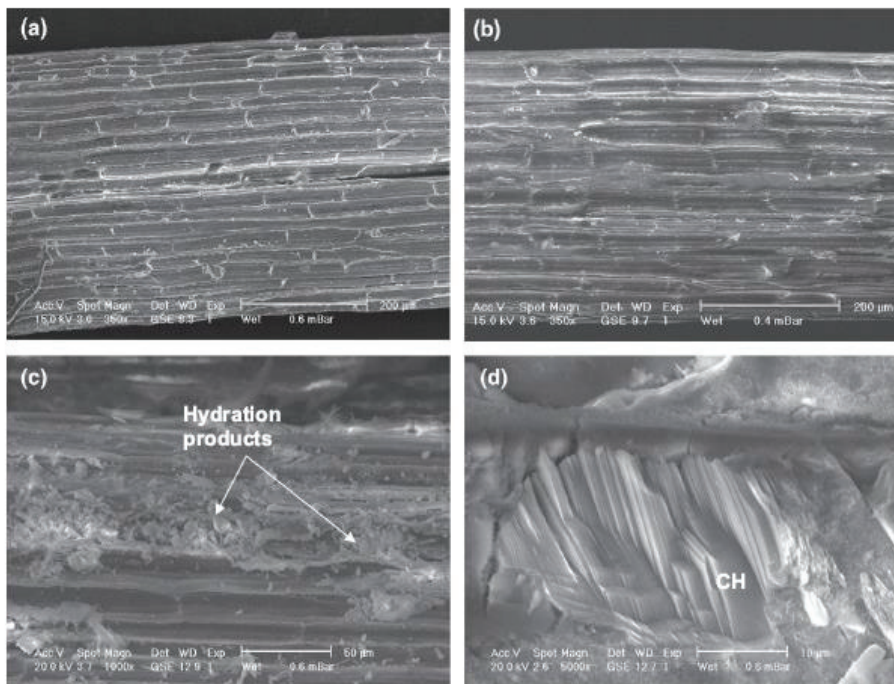


Figure 1- 27 : The effect of the wetting and drying cycles on the sisal fiber surface: (a) reference, (b) fiber extracted from a PC-MK matrix, (c and d) fiber extracted from a PC matrix [121].

Similarly, in 2015, Wei et al. [66] found that by replacing 30 wt.% cement by metakaolin, the durability of sisal fiber reinforced cement based composites subjected to wetting and drying cycles was effectively improved. Therefore controlling the PH value of the pore solution at a relatively low level is an effective way to mitigate degradation of natural reinforcements.

In 2016, Wei et al. [128] studied the influence of cement hydration on the durability of natural fiber-reinforced cement composites and the deterioration of embedded fibers by testing composites made with pure cement matrix (PC) and blends with cement substitutions by Metakaolin MK, Rice husk ash RHA, silica fume SA and fly ashes FA at 30 wt.% (MK30), 20 wt.% (RHA20), 10 wt.% (SF10), and 30 wt.% (FA30) levels, respectively. Owing to the high Al_2O_3 and SiO_2 content, and their large particle surface area, MK and SF showed higher pozzolanic activities and better modification effects than RHA and FA in improving the degree of cement hydration and $Ca(OH)_2$ consumption. Also, cement substitution resulted in increases of interfacial bond properties between natural fiber and cement matrices: the porosity and thickness of the transition zone were reduced by reducing $Ca(OH)_2$, ettringite and forming more C-S-H on the natural fiber surface. As a result, the initial flexural properties of natural fiber-reinforced cement composites were improved significantly before aging (Figure 1- 28). Furthermore, after different cycles of wetting and drying, significant increase in durability of natural fiber-reinforced cement composites was achieved by cement substitution. The worst and best durability, determined by means of post-cracking flexural strength and toughness, were yielded by neat PC and MK30, which showed the lowest and the highest degree of cement hydration, respectively. SF, RHA and FA also showed acceptable effects in mitigating deterioration of the composites (Figure 1- 28).

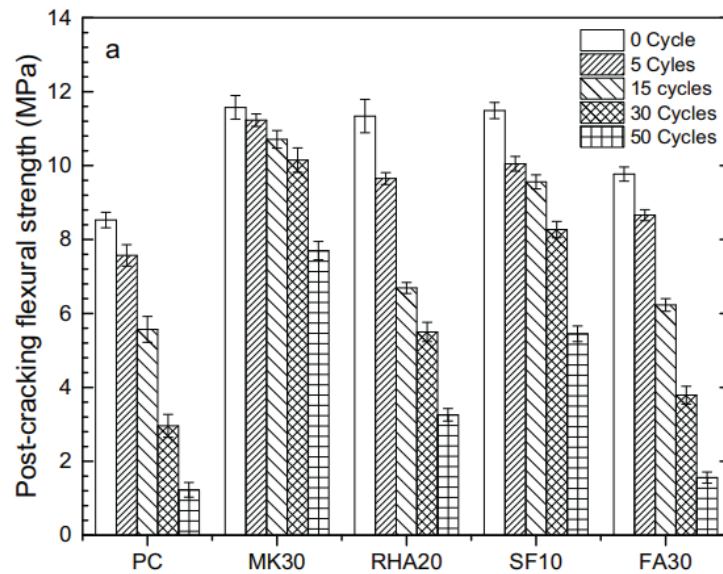


Figure 1- 28 : Durability of different natural fiber-reinforced cement mortar after different cycles of wetting and drying estimated by the residual post-cracking flexural strength (study of Wei et al. 2016 [128]).

The degradation of the embedded natural fiber was effectively mitigated by modifying the cement matrix. After wetting and drying cycles, the tensile strength of natural fibers imbedded with the modified cement matrices were much higher than of the fiber in neat PC (Figure 1- 29). The Young's modulus was also decreased. The results of TGA, XRD and microstructure analysis indicated that the alkaline hydrolysis of amorphous components of natural fiber, the mineralization of fiber cell walls and the stripping of cellulose micro-fibrils were mitigated in the modified cement matrices, especially MK30 and SF10. They concluded that the durability of natural fiber-reinforced cement composites strongly depends on the cement matrix composition.

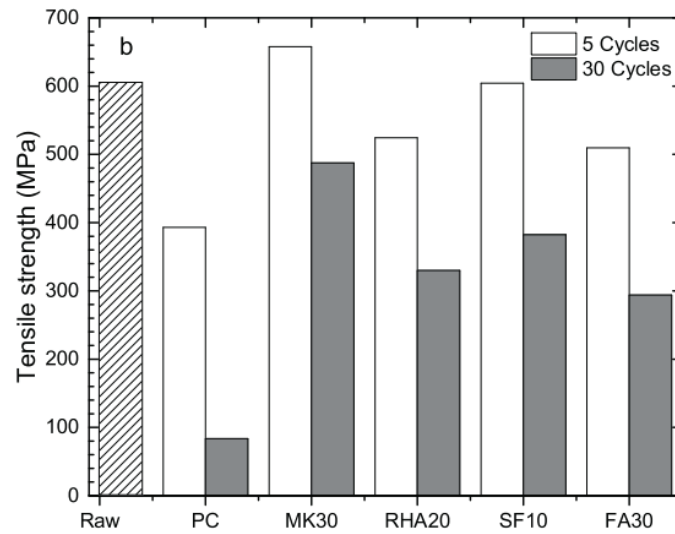
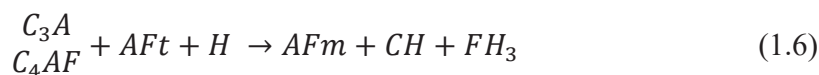
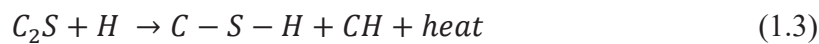
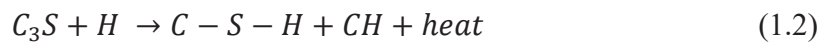


Figure 1- 29 : durability of single natural fibers imbedded in different cement mortars estimated by the residual tensile strength (study of Wei et al. 2016 [128]).

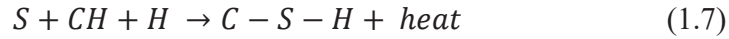
The reduction of alkalinity in a matrix with a blend of Portland cement and pozzolanic material can be explained due to the secondary pozzolanic reaction which causes a lowering of the calcium hydroxide content. The main reactions of hydration for Portland cement are based on the mineral compounds of the clinker. They can be written as [121], [128], [130]:



Where: $C = CaO$, $S = SiO_2$, $F = Fe_2O_3$, $A = Al_2O_3$, $N = Na_2O$, $K = K_2O$, $\bar{S} = SO_3$ and $H = H_2O$. $C - S - H$ represents calcium silicate hydrate, where the symbol ‘-’ indicates no

exact stoichiometric proportions; CH represents calcium hydroxide, or $Ca(OH)_2$; Aft is the abbreviation of ettringite $Ca_6Al_2(SO_4)_3(OH)_{12} \cdot 26H_2O$, and AFm is the abbreviation of monosulfate $Ca_4Al_2O_6SO_4 \cdot 14H_2O$.

When the amorphous silica (pozzolans) are added to the Portland cement, they react with calcium hydroxide forming C-S-H in an exothermic reaction as shown in the following equation:



The amplified precipitation of $Ca(OH)_2$ between filaments reduces the slip of the filaments in the vicinity of cracks, and leads to their failure at smaller crack widths. Moreover, the straining of the filaments causes local spalling in and on the shells as well as the splitting of the $Ca(OH)_2$ crystals. The wedged crystals at the surface of the filaments act as notches, leading to their premature failure. However, the stratum of fine $C - S - H$ phases leads to good and flawless fiber-matrix bond and allow the partial de-bonding and the slipping of the filaments in the vicinity of the matrix cracks, leading to the overall ductile behavior of the crack-bridging yarn [131].

The secondary pozzolanic reaction impose an additional transformation of the hydration products. However, as the pozzolanic material contains a significant portion of Al_2O_3 , the components dissolving from the metakaolin and water form a secondary C-S-A-H gel that includes the contributions of both pozzolanic and PC hydration reactions [121], [128], [130].

In 2017, Wei et al. [127] studied the influence of a coupled substitution of metakaolin and montmorillonite in Portland cement on degradation of natural fiber. Degradation of sisal fiber in cement matrices was investigated indirectly by testing the flexural behavior of sisal fiber-reinforced cement mortar beams, and directly by investigating uniaxial tensile properties, thermal decomposition behavior, crystallinity indices, and microstructures of the embedded fibers by means of uniaxial tension tests, TGA, XRD and SEM, respectively. Due to the high amount of aluminate, the incorporation of metakaolin mitigates the fiber degradation more effectively at early age, while the high amounts of silicon minerals promote the complementary effect of montmorillonite on reducing alkalinity of the matrix for a long-term and the deterioration of sisal fiber at a later stage was hence mitigated. The combination of these two clay minerals validates their synergistic effect on enhancing hydration of cement and mitigating fiber degradation at different stages of aging. The authors observed a disagreement between durability of sisal fiber-reinforced cement composites and degradation of the embedded fibers. This might be attributed to the fact that flexural properties of fiber-reinforced composites are influenced by at least three factors: strength of the matrix, interfacial bonding properties between fiber and matrix, and fiber strength. At a high cement substitution level (50 %), the degradation of sisal fiber was mitigated most significantly. However, both strength of cement blends and interfacial bonding strength between sisal fiber and the cement matrix are greater at a cement substitution level of 30 %.

In 2018, Wei [124] investigated, experimentally, the aging kinetic of cellulose exposing to pore solutions of cementitious materials and he developed a model for service-life prediction of

cellulose in cement. According to the model, he found that the time needed to complete degradation of cellulose in the sisal fiber was extended by 13.7 times by incorporating 30 wt% metakaolin. This model was in good agreement with the experimental observations.

In 2014, Chafei et al. [132] studied the effect of the addition of latex adhesion promoter (BARRALATEX 30T) to the matrix of a flax reinforced cementitious composite after 7, 14, 28 and 90 days of aging. They noticed a better workability for composite prepared with latex admixture which is assigned to the plasticizing effect of the latex, but the initial setting time did not change. Furthermore, the addition of latex adhesion promoter showed a better fiber-matrix interface adhesion.

1.3.2.2 Fiber pre-treatment

There are various processes for fiber pre-treatment such as silane treatment, alkali treatment, polymer coating, hornification, ZrO_2 treatment etc.... The objective of these treatments is to reduce the capacity of the fibers in absorbing water which will consequently limit their mineralization and thus improve their bond to the matrix.

In 2003, Toledo Filho et al. [129] studied the durability effect of treatment of sisal fiber with slurried silica fume prior to being incorporated in the OPC matrix. Specimens were subjected to three different aging conditions: immersion in water, wetting and drying cycles and exposition to natural weather. They found that this treatment is an effective method to improve the strength and toughness of composites with time. They explained that by the presence of silica fume at the fiber-matrix interface which creates a zone of low PH around the fibers and then, it reduces the alkaline attack and the transport of calcium products to the vegetal fibers.

In 2011, Claramunt et al. [133] studied the influence of prior hornification of softwood kraft pulp and cotton linters fibers on the mechanical performance and durability of the cement mortar composites. The hornification of the fibers was achieved by four drying and rewetting cycles. The mechanical performance of the composites was tested via both flexural and compression test, after 28 days of curing and after four wet-dry aging cycles. They found improvements in both flexural and compressive strength, for composites reinforced with both treated kraft pulp and treated cotton linters fibers, in both unaged and aged conditions, with respect to the composites reinforced with untreated fibers.

In 2016, Alves Fideli et al. [134] studied the effect of styrene butadiene polymer coating of jute textile on the bonding behavior of these fibers with a cementitious matrix, by means of double-sided pull-out tests before and after accelerated aging. They found that the OPC composite system yielded better results for specimens with coated fabric.

In 2017, Afroz et al. [119] compared the long-term behavior of modified and non-modified basalt fibers in different alkaline solutions. The modification of basalt fibers was done by using a silane (SiH_4) surface coating agent. They found that the silane modified basalt fiber is more stable in

alkaline media than the non-modified one, and thus, they have long term suitable properties to be used as reinforcement in fiber reinforced concrete even in severe environment.

In 2014, Chafei et al. [132] studied the effect of the NaOH-treated flax fabrics in a cementitious composite after 7, 14, 28 and 90 days of aging. They found that the treatment with sodium hydroxide reduces the initial setting time of the cement composite from 12 to 7 hours, because it dissolves the pectins and impurities from the fiber surface. These latter disturb the hydration reaction of the cement due to the chelating effect of pectins (1 - 3 wt%) on the Ca_2^+ ions released during the hydration of cement and responsible for the formation of the silico-calcium gel. Also the NaOH-treatment slightly improves the workability of the cement composite. Furthermore, it makes the fiber surface rougher, which would improve the fiber-matrix adhesion.

In 2018, Boulos et al. [135] compared the durability of flax fabrics in a cementitious matrix and the evolution of the fiber-matrix interface throughout 90 days of aging. Three conditions of flax fabrics were used, including untreated, pre-treated (acetone treatment followed by alkali treatment (NaOH)) and ZrO_2 -treated fabrics. From the tensile tests conducted on fabrics, they found that the pre-treated fabrics performed greater elongation and tensile load in comparison with the untreated ones. The pre-treatment (acetone and NaOH) performed on flax fabrics removes extractives such as wax and oil, and amorphous components such as pectin, lignin and hemicellulose which provides the micro-fibrils with a greater freedom of movement. The ZrO_2 -treated fabrics exhibited less elongation and a greater loading capacity than pre-treated fabrics. This is due to the presence of the ZrO_2 coating on fibers surface which restricts the movement of micro-fibrils and rigidifies the fibers on one hand; on the other, it reinforces micro-fibrils by blunting cracks and defects present on their surface. From the tensile tests conducted on composites after 28 days of curing, they found that composites demonstrating numerous fragmentations reflected a strong fiber-cement matrix bonding, which was the case for pre-treated and ZrO_2 -treated specimens. However, the greater number of cracks and lower crack spacing observed particularly on the ZrO_2 -treated specimen in comparison with the pre-treated one suggest the stronger adhesion of the ZrO_2 -treated fibers to the cementitious matrix. From the study of the mechanical properties of the different specimens after 1, 3, 7, 14, 21, 28, 60 and 90 days, they found that ZrO_2 -treated fabric reinforced cementitious composites exhibited greater mechanical performance than untreated and pre-treated specimens. This was due to the improved durability of the ZrO_2 -treated fabrics in the cement paste and their stronger adhesion to the matrix. Furthermore, in 2013, Rybin et al. [55] proved that the coating of the basalt fiber with ZrO_2 improves its corrosion resistance in alkali media. Figure 1-30 shows SEM images of uncoated and ZrO_2 -coated basalt fibers after 30 days of embedment in cement matrix. From this Figure, we can notice the formation of the corrosion shell in a great extent for the uncoated basalt fiber compared the ZrO_2 -coated one.

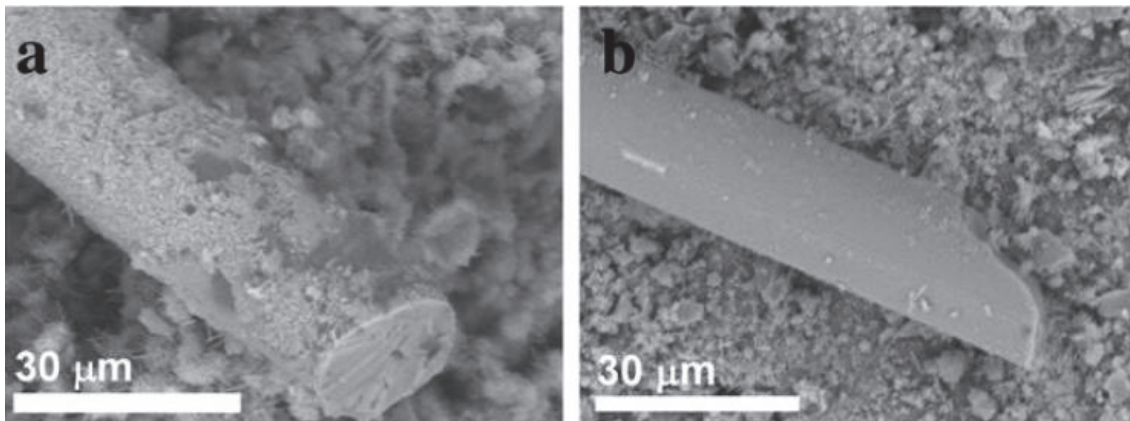


Figure 1- 30 : SEM images of uncoated (a) and ZrO_2 -coated (b) basalt fibers in cement matrix after 30 days [55].

1.3.2.3 Combination of cement matrix modification and fiber pre-treatment

In 2003, Toledo Filho et al. [129] studied the durability effect of the immersion of the aligned long sisal fibers in a silica fume slurry prior to their addition to a matrix in which 40 % by weight of cement was replaced with blast-furnace slag. Specimens were subjected to three different aging conditions: immersion in water, wetting and drying cycles and exposition to natural weather. They found an enhancement in the durability of vegetal fiber reinforced cement composite, which was attributed to the treatment of fibers with silica fume slurry.

In 2014, Chafei et al. [132] studied the durability effect of the treatment of flax fibers with NaOH solution prior to their addition to a matrix containing latex adhesion promoter (BARRALATEX 30T). Composite specimens were subjected to three points bending tests after 7, 14, 28 and 90 days of aging. They found that this method improves flexural strength of the cement composites, but this increase in strength was lower than that of the composite made with latex adhesion promoter only. So, they concluded that the composite made with latex adhesion promoter only is more efficient and there is no synergic effect between the sodium hydroxide treatment and the latex adhesion promoter.

In 2015, Ferreira et al. [136] studied four different treatments of sisal fibers. They studied the effect of these treatments on their physical and mechanical properties and on the fiber-matrix interface behavior with a cement based matrix. The binder of the matrix was composed of 30 % of Portland cement, 30 % of metakaolin and 40 % of fly ash. The treatments used were: hornification, alkali treatment with calcium hydroxide, polymer impregnation with styrene butadiene and a combination of hornification and polymer impregnation. All treatments have led to an improvement in tensile strength of sisal fibers (Figure 1- 31) and to an enhancement of fiber-matrix bond:

- The alkali treatment removes the non-cellulosic materials and impurities so the fibrils become more capable of rearranging themselves along the directions of tensile deformation

since the interfibrillar region occurs to be less dense and less rigid due to the removal of hemicelluloses.

- The cycles of wetting and drying, in the hornification treatment, change the microstructure of vegetal fibers, which modifies the polymeric structure of the fiber-cells resulting in higher tensile strength and strain.
- During the polymer treatment, the fiber absorbs the solution, allowing the penetration of the polymer between the fiber cells and the internal walls of the lumen. After drying, the polymer becomes more rigid making the fiber structure rigid and dense.
- The hybrid (polymer + hornification) treatment showed the same increase in tensile strength when compared to polymer treatment. However, the hybrid treatment has led to the highest improvement in fiber-matrix bond. This result was due to the dimensional stability promoted by hornification and the chemical interaction between the polymer coating and the Portland cement of the matrix. The main constituent of a sisal fiber is cellulose which contains a large number of intra and inter-molecular bonded hydroxyl groups. During polymer modification, the cellulose eventually reacts with the carboxylic acid group of the polymer latex (carboxylated styrene butadiene copolymer) to form a linkage. Another part of this co-polymer forms bond with calcium ion of the hydrated cement. Thus the polymer forms a bridge between the fiber surface and cement matrix (Figure 1- 32).

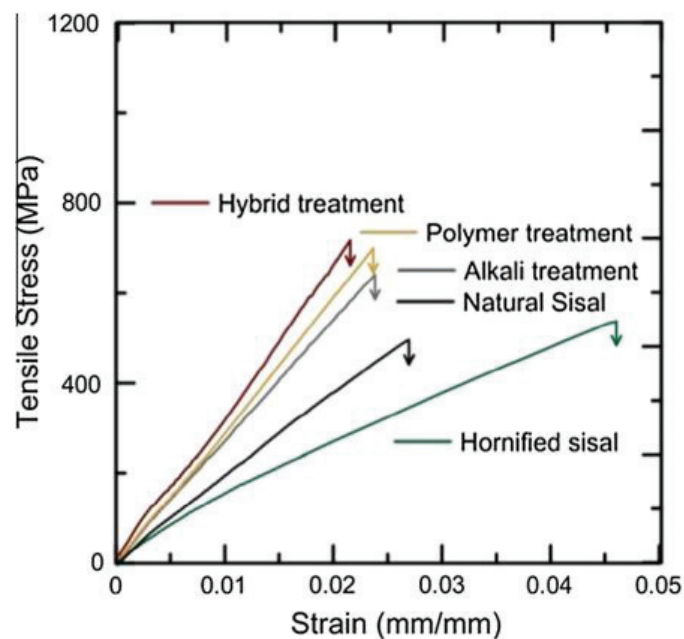


Figure 1- 31 : Influence of different fiber treatments on the tensile properties of sisal fibers (study of Ferreira et al. 2015 [136]).

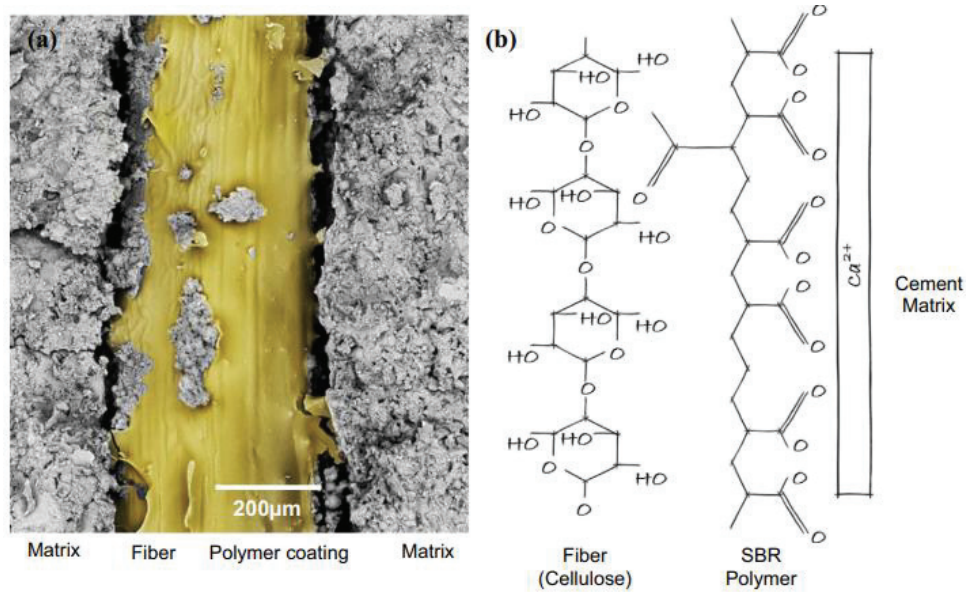


Figure 1- 32 : (a) Micrograph showing the fiber matrix interface of polymer modified sisal fiber and (b) a schematic model used to explain the fiber–polymer–concrete interfacial bonding (study of Ferreira et al. 2015 [136]).

In 2016, Alves Fidelis et al. [134] studied the effect of styrene butadiene polymer coating of jute textile on the bonding behavior of these fibers with a cementitious matrix made with 50 % partial cement replacement by metakaolin, by means of double-sided pull-out tests before and after accelerated aging. They found that, compared to the results of the polymer coating of the fiber only and the presence of metakaolin in the matrix, the polymer coating combined with a matrix containing metakaolin produced the best bonding properties between fabric and matrix. The metakaolin consumed the calcium hydroxide, reducing alkalinity in the pore solution, hence avoiding the fiber degradation. Moreover, the metakaolin was also beneficial in protecting the polymer from reaction with $Ca(OH)_2$.

1.3.2.4 Accelerated carbonation curing

A cementitious composite is usually subjected to the CO_2 of the atmosphere. When the CO_2 enters the unsaturated pores of the cementitious matrix. Then, the aqueous phase in the pores dissolves the CO_2 and transforms it into a carbonic acid (H_2CO_3). This latter is afterward, dissociated into ions HCO_3^- and CO_3^{2-} . Similarly, the calcium hydroxide dissolves in Ca^{2+} and OH^- ions, resulting in the formation of calcium carbonate ($CaCO_3$). This process is known as carbonation. It reduces the alkalinity of the matrix and thus improves the durability of the vegetal fiber reinforced cement composite [137]. Moreover, the accelerated carbonation may have potential for the treatment of wastes and contaminated soils and for the sequestration of CO_2 which is an important greenhouse gas [138].

In 2003, Toledo Filho et al. [129] studied the effect of early cure in CO_2 rich environment on the durability of vegetal fiber reinforced cement composites. Samples were demolded one day after casting, conditioned in a CO_2 incubator, immediately, in order to accelerate and achieve a high

depth of carbonation and then aged under water or exposed to cycles of wetting and drying or to the natural weather. Flexural tests were carried out before and after 6 and 12 months ageing. They found that the early cure in a CO₂-rich environment is a promising alternative to increase the durability of vegetal fiber reinforced cement composites with aging.

In 2013, Almeida et al. [137] studied the effect of accelerated carbonation curing at early stage on the durability of eucalyptus cellulosic pulp reinforced cement based composite. Non-carbonated curing composite (NCC) and accelerated carbonation curing composite (ACC) at early stage (after two days of controlled curing) were subjected to four-points bending tests after 28 days of controlled curing without aging, after 200 and 400 soaking and drying cycles, and after one year of natural weathering. For the ACC composite, the mechanical properties were better at 28 days, and these properties were maintained after accelerated and natural aging, indicating their improved durability. Furthermore, the carbonation curing at early stages decreases the $Ca(OH)_2$ content forming a higher precipitation of CaCO₃ which is a more stable and denser product, resulting in a lower PH value, lower porosity and a denser matrix. Therefore, this process improves the fiber-matrix bonding, the mechanical properties and the durability of vegetal fiber-reinforced cement composite.

1.3.3 Mechanical characterization of plant based fiber reinforced cement composites

First, the use of TRM in the strengthening and rehabilitation of civil engineering structures must be preceded by mechanical characterization. In the following sub-paragraphs, we show some of the mechanical tests used in the literature to characterize the fibers and the TRM.

1.3.3.1 Tensile behavior of natural fibers

In fact, the stress-strain curve of natural fibers subjected to tensile tests is not linear. It can be divided into three parts: (i) the first part is linear, it is associated with a global loading of the fiber, through the deformation of each cell wall (elongation of the cellulosic micro-fibrils and the amorphous region); (ii) the second part is non-linear, it represents the elasto-visco-plastic deformation of the fiber, especially of the thickest cell wall (S₂). This deformation is involved in the alignment of the micro-fibrils with tensile axis, which in turn causes the re-arrangement of the amorphous part of the wall; (iii) the final part is linear, it corresponds to the elastic behavior of the aligned micro-fibrils subjected to a tensile load [139]. The following Figures (Figure 1- 33, Figure 1- 34, and Figure 1- 35) show many examples of stress-strain curves of flax, hemp and ramie fibers respectively.

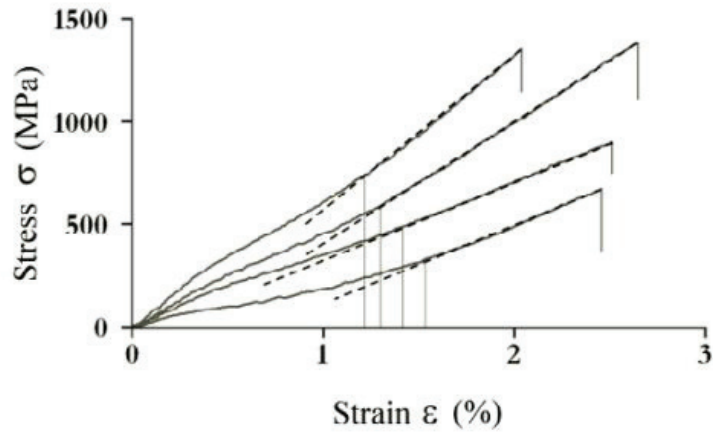


Figure 1- 33 : Examples of flax fiber curves, showing the strain at which deformation becomes linear again [139].

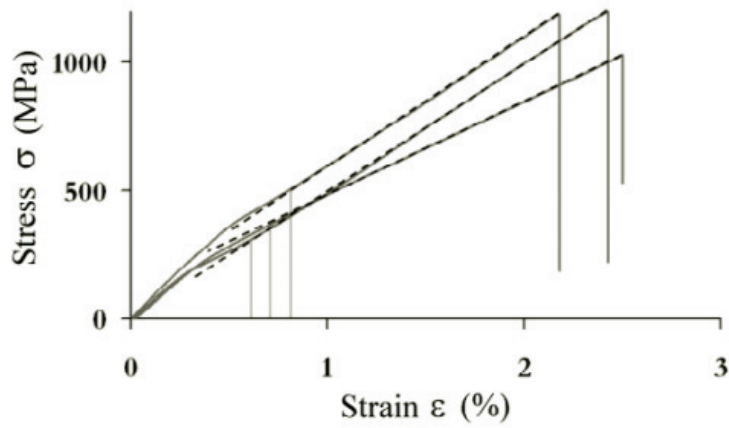


Figure 1- 34 : Examples of hemp fiber curves, showing the strain at which deformation becomes linear again [139].

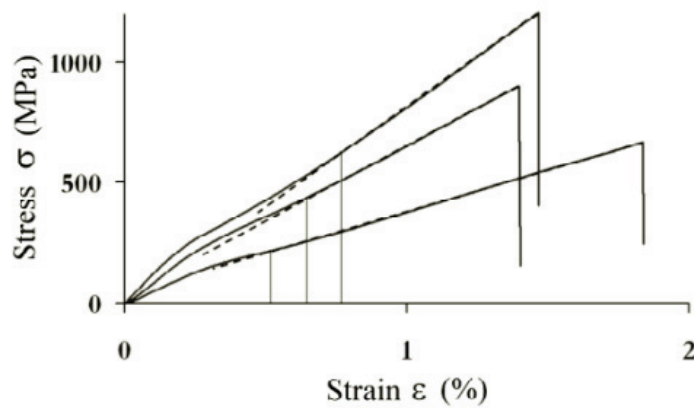


Figure 1- 35 : Examples of ramie fiber curves, showing the strain at which deformation becomes linear again [139].

1.3.3.2 Tensile behavior of the composite

The tensile behavior of textile reinforced mortar has been investigated, by many studies in the literature, via a tensile test which consists in placing the test specimen in a testing machine and subjecting it to loading until it fractures. The tensile force is recorded as a function of the increase in gauge length. During the application of tension, the elongation of the gauge section is recorded against the applied force. Tensile properties of composites are determined based on tensile strength and modulus. The tensile strength depends on how well the stress can be transferred from the broken to the surviving fibers through shear in the matrix at the interface and the amount of the stress can withstand before failure occurred [140]. Generally, load-bearing behavior is evaluated by means of bending or tensile tests. In ceramic and porous materials, the former are easier to perform. However, stress-strain curves obtained by means of uniaxial tensile tests provide more detailed information about the properties and real behavior of this kind of composite material [141].

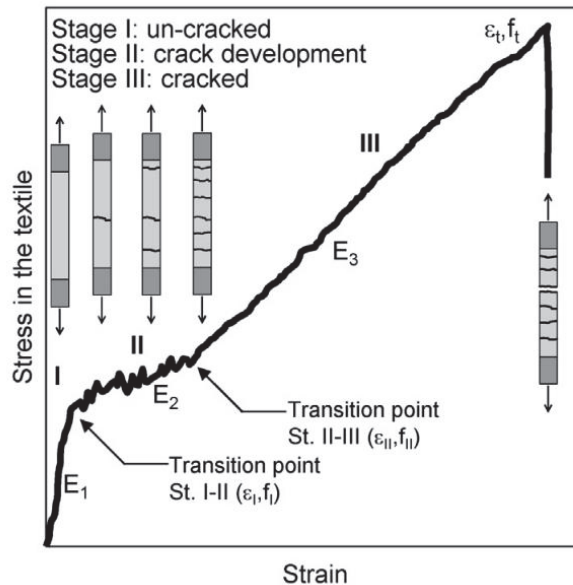


Figure 1- 36 : Typical stress-strain response curve of TRM systems under tensile loading[142].

In the literature, we find that the stress-strain curve of TRMs made with basalt, carbon, glass, or steel textile is not linear. It is composed of three stages (Figure 1- 36): (I) pre-cracking, (II) crack development and (III) post-cracking stages: in the first stage, the matrix and the fibers behave together without any cracks and the response is linear. When the load exceeds the tensile strength of the matrix, a first crack appears identifying the transition to the second stage where the matrix transfers the load progressively to the textile and the cracks develop progressively and the rigidity decreases. These cracks are identified in the stress-strain curve as a sudden drop in the tensile strength. With the increase of the tensile force, new cracks appear in the specimen, due to the bond between rovings and mortar, forces are initiated again in the matrix. When the tensile strength of the cementitious mortar is reached once more, a new crack is formed. As soon as the number of

cracks stabilizes, an increase in the stiffness occurs identifying the transition to the third stage where the response is linear again and the tensile load is almost entirely transferred to the textile. In this stage, a widening of cracks occurs caused by the additional imposed strain and the tensile behavior of the TRM mainly depends on the mechanical properties of the textile. Finally, the failure usually occurs in the textile, when the tensile load exceeds its tensile strength, taking place in one roving/cord and suddenly propagating to the other ones [141], [142].

The tensile behavior of the TRMs made with vegetal fibers is investigated in the literature by few authors. Some of them [100], [135] have found that these TRM have the same typical stress-strain curve of those made with non-vegetal fibers. Others like Cevallos et al. [143] have found some differences in the behavior of the two systems (vegetal and non-vegetal TRMs). These researchers have studied the tensile behavior of three TRM systems composed of flax, sisal and glass fabrics strips, respectively, embedded in a natural hydraulic lime (NHL) grouting mix. The stress-strain curves of representative composite specimens reinforced with flax and sisal are presented in Figure 1- 37 and Figure 1- 38, respectively. These two composite systems exhibited a similar behavior during the two first stages, but the first stage was less visible than that of TRM with non-vegetal fabrics. This behavior was due to the high ductility of the flax and sisal fabrics. Also in the third stage, they observed a multiple cracking formation, which resulted in significant reductions in strength. Therefore, they concluded that the contribution of the matrix to the mechanical behavior in the third stage should not be neglected in the composites made with vegetal fibers with high ductility, contrary to what is assumed in conventional models.

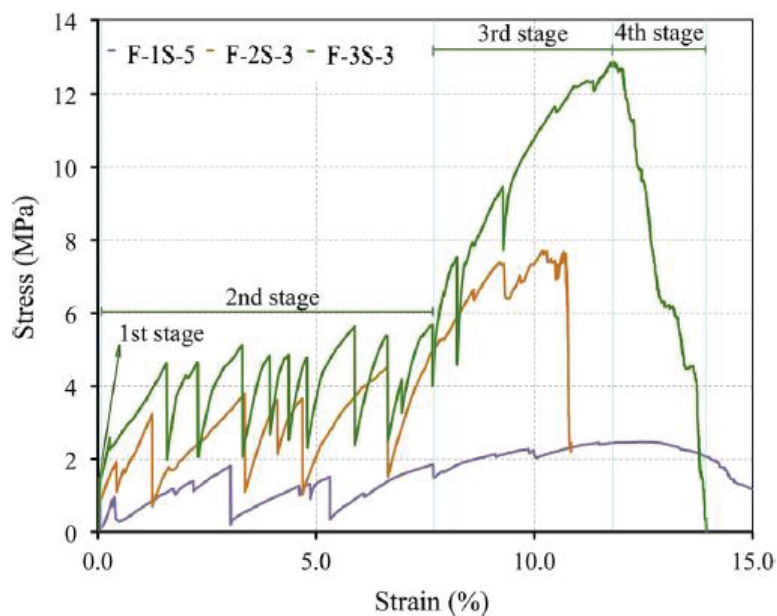


Figure 1- 37 : stress-strain curves of representative composite specimens reinforced with one (F-1S), two (F-2S), and three layers (F-3S) of flax fabrics [143].

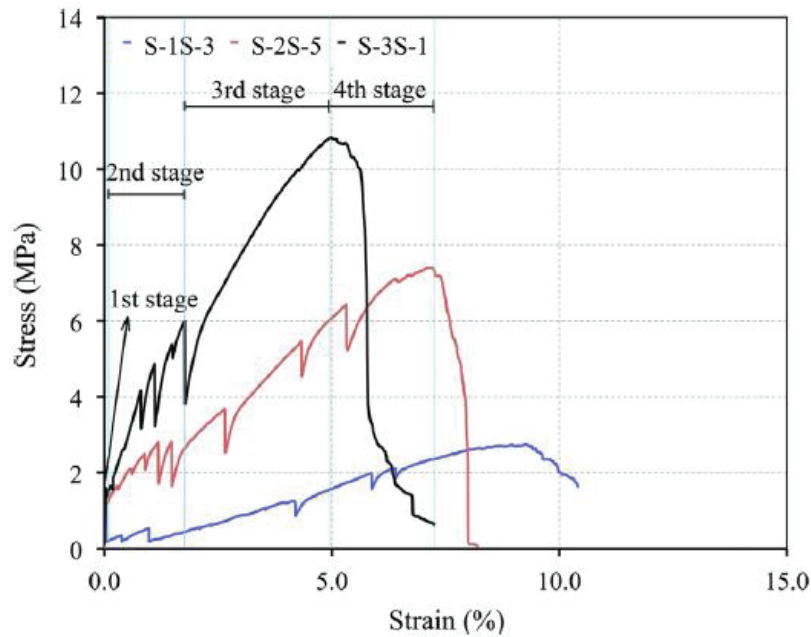


Figure 1- 38 : stress-strain curves of representative composite specimens reinforced with one (S-1S), two (S-2S), and three layers (S-3S) of sisal fabrics [143].

In addition, many researchers [3], [6], [144] have explained the typical failure modes of the TRM behavior in tension which are presented in Figure 1- 39. The failure mode A occurs at the clamps, the failure mode B is characterized by the cracking of the matrix and the tensile rupture of the fibers, the failure mode C occurs by the cracking of the matrix and the slippage of fibers, and finally, the failure mode D which is the detachment of the two mortar layers from the textile. The occurrence of a certain failure mode among the other ones strongly depends on the transversal stress applied to the ends of the specimen by the clamping devices and the fibers-matrix and fiber-fiber bond performances [3]. It is important to understand that the tensile strength of the TRM depends mainly on the tensile strength of the fibers which are capable to withstand the load transmitted to them by the matrix. Therefore, the transmission of matrix-mesh stresses is one of the main requirements to be considered, which depends on the geometric adaptability of the mesh and its chemical stability (durability) within the matrix [145]. If the matrix can penetrate between the fibers and fills the voids among them, it acts as a binder, increasing the adhesion of the fibers to the matrix and binding the fibers strongly together. A good fiber-matrix bond leads to a great number of cracks with a low crack width, and increases the maximum tensile strength of fabric reinforced cementitious composites [135]. In this case, the failure occurs by the rupture of the fibers after exhaustion (Mode B). However, when the fiber-matrix bond is not sufficient, the failure occurs by slippage of the fibers within the matrix at a value of load smaller than the tensile strength of the fibers (Mode C), or by detachment of the two layers of the matrix from the textile (Mode D). In certain cases, some fibers slip within the matrix and the others rupture (Mode B+C). It is also important to note that in some cases if the fiber-matrix bond is very strong, the fibers may rupture before they can contribute to the resistance in the post-cracking phase.

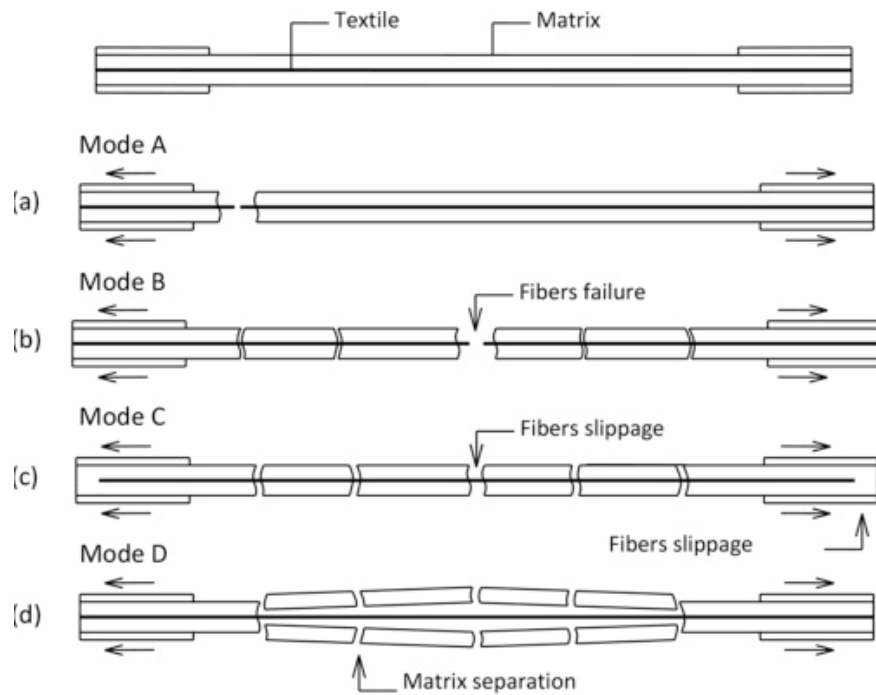


Figure 1- 39 : Typical failure modes of FRCM materials tested in tension. (a) Failure mode A, (b) Failure mode B, (c) Failure mode C, (d) Failure mode D [3].

1.3.3.3 Flexural behavior of the composite

According to Claramunt et al. [133] the most useful tests for showing the reinforcing effects of the fibers with respect to the matrix in cementitious composites are the bending tests.

Taken from [146], Figure 1- 40 shows the typical bending stress vs. mid span deflection curves and the cracking phases obtained under flexural configuration. In the initial phase, the response was linear and the curve had a high slope until the first crack appeared (zone A). In this zone, the composite works by maintaining compatibility of deformation, i.e., the fibers and the matrix deform exactly the same length, so the resulting stress depends on the amount of material and its modulus of elasticity. After the formation of the first crack, the zone B begins characterized by a multiple cracking formation in the composite. In this zone, the material works without compatibility of deformation since the matrix absorbs most of the compression forces on the upper part of the specimen and the fibers absorb most of the tensile forces on the nether part of the specimen. Under these conditions, the stress transfer mechanism is achieved by the fibers-matrix adhesion in the zones between cracks. If there is a low fiber-matrix adhesion, once the first crack appears there is a debonding of the fibers and fracture of the composite. If the adhesion between the two phases is very high, the nether part can deform as long as fibers do not break, opening evenly distributed numerous cracks. Finally, after the formation of all the cracks, the behavior of the material is defined by a widening of the cracks characterized by a smoothing of the curve (zone C).

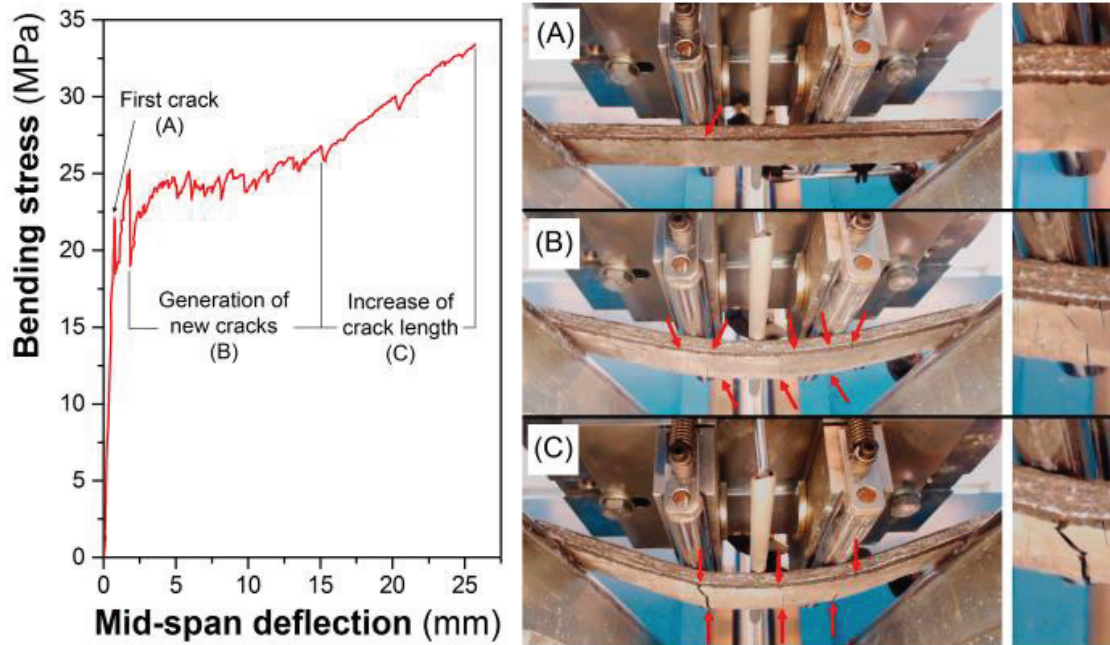


Figure 1- 40 : Representative curve and cracking phases of flax nonwoven fabric reinforced cement composite obtained under flexural stress: (A) first crack; (B) generation of new cracks; (C) increase of crack length [146].

1.3.3.4 Comparison between tensile and flexural behavior

The following parameters could be obtained from the curves of both tensile and flexural tests [146]:

- The limit of proportionality (LOP) (in some cases it is named bend over point BOP for tensile test), is defined as the stress value at the upper point before the appearance of the first crack;
- The modulus of rupture (MOR) (in some cases it is ultimate tensile strength UTS for tensile test), corresponds to the maximum stress supported by the material, reached either by breaking or by obtaining a displacement of more than 10% of the separation between the span supports;
- The modulus of stiffness for each zone or E_{zone} , calculated as the relationship between the stress and strain between two points on the stress-strain curve;
- The specific energy absorbed by the material during the test or toughness is calculated as the area under the curve force versus displacement from the starting to the value of the ordinate corresponding to a reduction higher than 40% of the MOR or a span higher than 10%, divided by the areal cross section of the specimen.

In 2009, Silva et al. [147] have compared the tensile and flexural response of sisal fiber reinforced cement composite. As it can be seen in Figure 1- 41, they found that under bending, loads associated with the formation of the first crack occur at stress levels twice as those observed for

the direct tension tests, while the values of toughness obtained in case of tensile tests were almost twice as those obtained in case of bending tests. They have also found that the values reported for MOR was approximately two times greater than that of the UTS, and the saturation crack spacing under flexural loads was twice as large as that of tensile loads. These results are consistent with the study of Claramunt et al. 2017 [146]. Furthermore, the latter remarked a cracking pattern which is irregular, and partially followed the tensile direction (Figure 1- 42). They related this irregularity to the anisotropic distribution of the fibers on the nonwoven specimen.

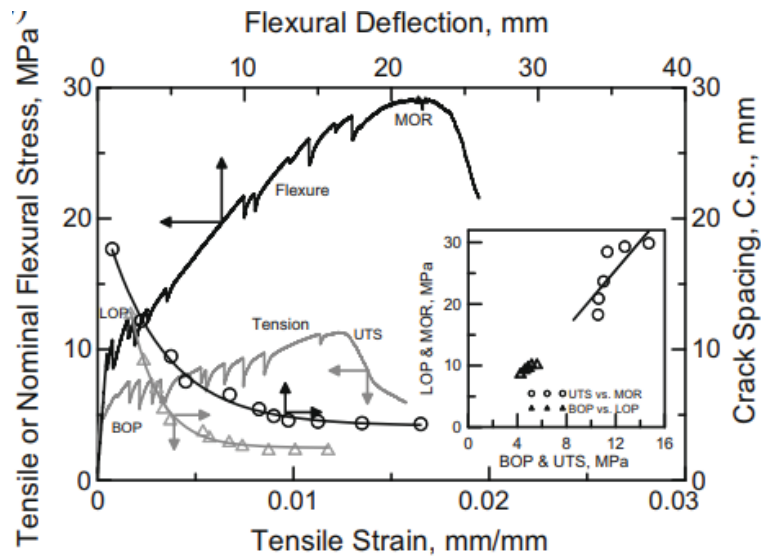


Figure 1- 41 : Comparison of flexural vs. tensile response [147].



Figure 1- 42 : cracking maps of two composites from the same plate tested under tensile (a) and bending (b) tests [146].

1.3.3.5 Pull-out behavior of the composite

The typical load-deformation curve under double-sided pullout test (Figure 1- 43) is shown in Figure 1- 44. This curve is composed of three zones depending on the degree of deformation. Zone I represents the behavior of the un-cracked specimen until the occurrence of the first crack. Zone II is characterized by a snap-back which is a sudden drop in load happening because the specimen contains an amount of fiber less than the critical one. If the fiber-matrix bond is very strong, the specimen fails in zone II. Finally, the third zone (III) represents the typical multifilament yarn pullout while a deformation hardening can be observed. In this zone, the filaments of the yarn are

stretched in different manners during crack opening. Once the load reaches the maximum pullout load, F_{max} , a complete failure of the filaments occurs and the specimen behavior is characterized by a pronounced softening [131], [134].

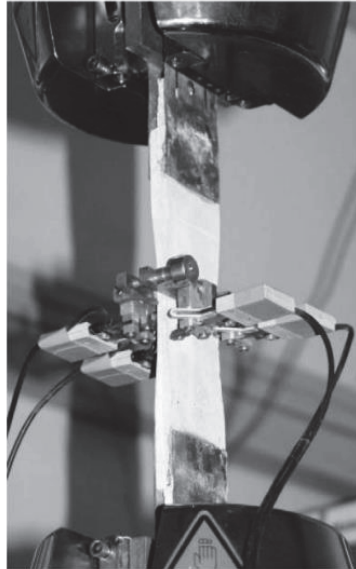


Figure 1- 43 : Double-sided pull-out test setup with load application grips and crack width sensors [131].

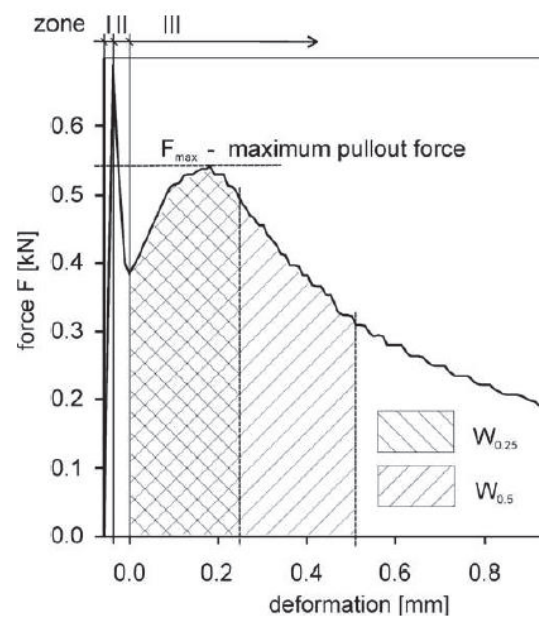


Figure 1- 44 : Typical load-deformation curve of TRM under double-sided pullout test [131].

1.3.4 Durability tests

The durability in structural design, is the ability of the tested materials to maintain the mechanical properties after a well-defined period of exposure in a certain aggressive environment [148]. The

durability of the textile reinforced mortar is evaluated by the changes in its mechanical performance after aging which depends on the durability of the fibers, the durability of the matrix itself and the durability of the matrix-fiber interface. The studies in scientific literature report different durability tests in order to evaluate the long term performance of TRM: either by the accelerated aging of TRM, or by the accelerated aging of textile fibers in simulated matrix environments or by natural aging.

1.3.4.1 Accelerated aging methods for fiber reinforced cement composites

In 1999, MacVicar et al. [149] used two different accelerated aging methods to simulate the possible aging mechanisms for which the material may experience under service conditions.

The first method consists of 2-days cycles which include:

- 16 hours of immersion of the specimens in distilled water at 20 °C,
- 1 hour in a forced draft oven at 80 °C,
- 5 minutes full vacuum,
- 7 hours in a 0.124 MPa CO₂ environment at 20 °C,
- And 8 hours in a forced draft oven at 80 °C.

The second method consists of 3-days cycles which include:

- 24 hours of immersion of the specimens in distilled water at 20 °C,
- 24 hours of freezing at -17 °C,
- 2 hours of thawing at 20 °C,
- And 22 hours in a forced draft oven at 80 °C.

For the first and the second method, physical and mechanical property tests were conducted on specimens after 0, 1, 4, 9, 16, 25, 36 aging cycles, and after 0, 3, 7, 14, 21 aging cycles, respectively. Finally, they compared both methods to the natural aging for 5 years in roofing. They found that the first method of accelerated aging seems to be more suitable for the simulation of the natural aging than the second method.

In 2009, Toledo Filho et al. [130] studied the durability of sisal fiber-cement mortar laminates (SFRML) based on the flexural strength and toughness obtained before and after 0, 25, 50, 75, 100 cycles of wetting and drying and on observations of the fibers in a scanning electron microscope (SEM). In 2010, the same research group [150] also studied the durability of the same composite through its immersion in hot water at 60 °C for 6 months. The obtained results were in accordance with those of wetting and drying cycles [130].

In 2014, Wei et al. [151] studied the effect of seven accelerated aging conditions on the durability of sisal fiber-reinforced cement composites. The specimens were treated in two static accelerated aging conditions, namely hot-dry (oven with circulating air environment) and hot-soak (tap water), at 50, 70 and 90 °C (D50, D70, D90, S50, S70 and S90), and a dynamic wetting and drying (W&D)

where the specimens were submerged in sealed tap water at 70 °C and then oven dried in a circulating air environment at 70 °C alternately. The durability of sisal fiber-reinforced cement composites was determined by testing degradation of the flexural properties of the samples subjected to the static aggressive conditions. Flexural testing results indicate that the most effective static approach for accelerating the degradation of natural fiber in cement composites is to soak the samples or change the humidity at 70 °C and higher temperature. The W&D treatment has a more aggressive effect on strength and toughness decline of the samples.

In 2016, Alves Fidelis et al. [134] carried out an accelerated aging on specimens of polymer coated and uncoated jute fabric reinforced cement composite. First they demolded the specimens one day after fabrication, then they immersed them in water at 20 °C for 28 days and, finally, they subjected them to a temperature of 40 °C and a relative humidity of 99 % over 28, 56, 90, 180, and 365 days. They observed an improvement of the textile-matrix bond and a reduction in the fiber degradation in case of coated fabrics.

In 2018, De Munck et al. [152] studied the durability of AR-glass textile reinforced mortar by subjecting specimens to three different aging protocols based on the European standard NBN EN 12467. The first protocol consists of 100 freeze (-20 °C)-thaw (20 °C) cycles (FT), the second one consists of 50 heat (60°C)-rain (water bath) cycles (HR), and the third is a combination of the first two protocols. They found that HR cycles deteriorate the structural behavior more than FT cycles. They explained this by the fact that after subjection to HR cycles a greater amount of the matrix penetrate in the fiber bundle and densify near the fibers. Moreover, the heat lead to further hydration of cement particles and a precipitation of the hydration products between the filaments of the yarn, which can result in notching the fibers and an embrittlement of the cementitious composite.

1.3.4.2 Accelerated aging methods for fibers

In the literature, two methods of fiber aging are found: either by immersion in NaOH solutions or simulated cementitious environments, or by aging in the cement matrix and then carrying the extraction carefully for testing.

In 2017, Micelli and Aiello [148] studied the durability of different types of fibers by exposing them to four different aging protocols in alkaline solutions. The first environment is representative of lime mortar, which is an aqueous solution of distilled water containing 0.16 % $Ca(OH)_2$ by weight. The second one is representative of Portland cement mortar, which is a solution of distilled water containing 0.16 % $Ca(OH)_2$ + 1 % $NaOH$ + 1.4 % KOH by weight. The other two environments are not directly related to applications of composite materials in civil structure, they are taken as reference. The first one is composed of water with 0.2 % KOH , and the second contains 5 % $NaOH$. In order to accelerate the diffusion process of the aggressive fluids (alkaline ions) inside the fibrous material, they used different temperatures which are estimated based on the following equation found in [153]:

$$\frac{N}{C} = 0.098 \cdot e^{(0.0558T)} \quad (1.8)$$

Where: N = age in natural days, T = conditioning temperature in °F, and C = days of accelerated exposure at temperature T .

It is important to note that, it is impossible to find a solution which can be representative of all the possible combinations of inorganic matrix and its admixture, so in order to simulate the behavior over time of the fibers in cementitious matrices as closely as possible to the real behavior, Litherland et al. [153] in 1981, developed the ‘strand-in-cement test’ (SIC test), which was then, improved by Wei et al. [151] in 2014. As can be seen in Figure 1- 45, this test consists of wiping a strand of natural fiber with epoxy resin except the middle part (50 mm) which should be wrapped using aluminum foil until the hardening of the epoxy resin. Afterwards, the middle part of the strand should be wrapped with a wire mesh prior to the casting of a block of cementitious paste around it. The wire mesh allows the contact between the matrix and the surface of the fibers and help in removing the cement block later. The edge of the cementitious block should be filled by plasticene to prevent its corrosion. Then, the specimens were treated in two static accelerated aging conditions, namely hot-dry (oven with circulating air environment) and hot-soak (tap water), at 50, 70 and 90 °C (D50, D70, D90, S50, S70 and S90), and a dynamic wetting and drying (W&D) where the specimens were submerged in sealed tap water at 70 °C and then oven dried in a circulating air environment at 70 °C alternately. And finally, the block of cement was removed carefully and the strand was then subjected to tensile test, analysis of the degree of crystallization (X-ray diffraction XRD), thermal analysis (thermogravimetric analysis TGA and derivative thermogravimetry analysis DTG), and microanalysis (scanning electron microscope SEM) [151]. The deterioration of sisal fiber was determined by investigating the degradation of tensile properties, crystallization degree, thermal decomposition, and surface topography of the raw and embedded fibers. They found that the W&D treatment has a more accelerating effect on both the alkali hydrolysis of fiber’s amorphous components and the mineralization of fiber cell wall indicated by the high crystallinity indices and minimum content of cellulose. This study provided a direction for future work that the fiber degradation will be determined after being treated by wetting and drying cycles as accelerated aging conditions.

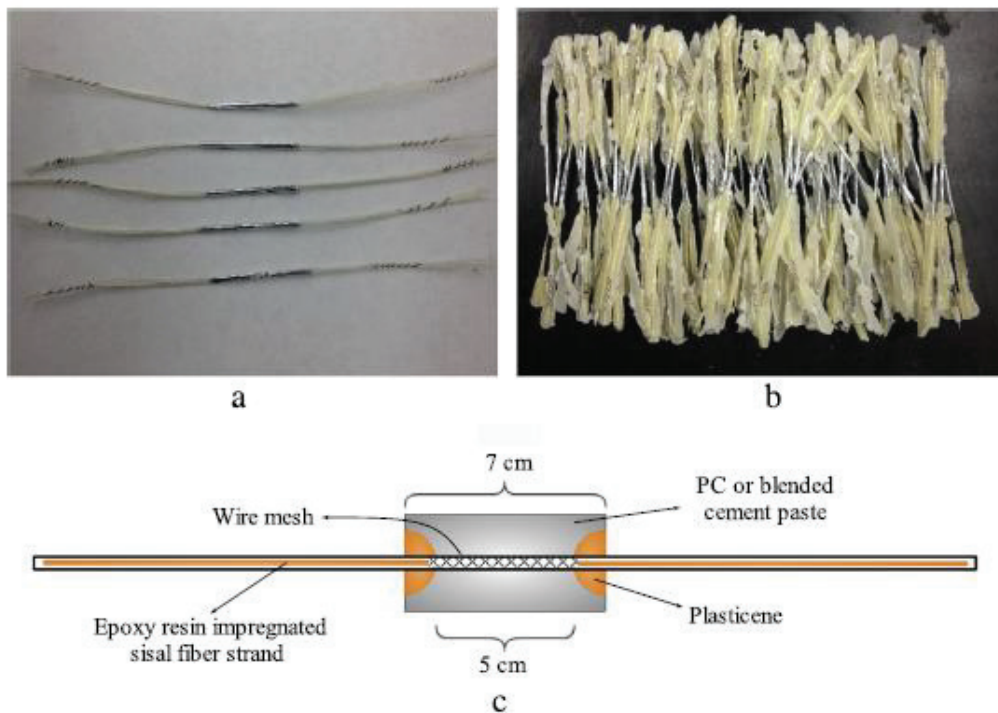


Figure 1- 45 : (a) fiber strands wrapped by aluminum paper and banded by copper wire at the ends, (b) after being wiped by epoxy resin; (c) sketch and typical dimensions of the embedded fiber strands specimen [151].

1.4 Conclusions

The state of the art review emphasizes the importance of the use of innovative and environmentally friendly techniques in the domain of rehabilitation and seismic strengthening of existing structures. It is essentially focused on the use of plant fibers instead of manmade synthetic fibers in the fabrication of textile reinforced mortar systems (TRM), the advantages and the disadvantages of this substitution as well as the durability issues and the long term performance of plant fibers when imbedded in the alkaline environment of the inorganic matrix of TRM and the solutions for this problem addressed and studied in the literature.

In the first part some synthetic fibers commonly used in the fabrication of TRM are presented with their advantages and disadvantages. In addition, some plant fibers mostly used in the civil engineering field are presented and their environmental benefits are discussed. These subsections are followed by a comparison between plant natural fibers and synthetic fibers from different point of views: mechanical behavior, costs and environmental impact.

In the second part, the degradation mechanisms of natural fibers when imbedded in the alkaline environment of the inorganic matrix is discussed in details followed by a presentation of the different solutions used in the literature to prevent this degradation from occurring or to extend the service life of natural based TRM systems such as cement matrix modifications, fiber pre-treatment, combination of the both and accelerated carbonation curing. Furthermore, some of the

mechanical tests used in the literature to characterize the fibers and the TRM as well as the characterization of the fiber-matrix bond are presented. At the end of this part, the durability tests through different accelerated aging protocols already investigated by different researchers in the literature on TRM systems and fibers are presented and discussed.

From these two complementary parts of the state of the art review, one can conclude that all the advantageous characteristics of plant fibers (good mechanical properties, low costs, low environmental impacts, reduced thickness and low weight, non-abrasiveness to the working tools, non-irritation to the skin, less health risk, reduced water requirement in their culture step, renewability and biodegradability...) drew the attention on their use in the retrofitting of the historical and heritage structures. However, the experimental results, in some cases encourage to invest further efforts to improve the performance and to shed light on several aspects still unclear, especially the durability issues. It is important to spend more energy in improving the available treatments already existent, and eventually develop new green ones. Finally, it is necessary to enrich the knowledge with respect to the long-term efficiency of the application of Natural TRMs reinforcement through durability tests and service life prediction methods.

1.5 Aims of the thesis

In the light of what it was presented in the state of the art review, several outstanding issues still remain unsolved concerning the use of plant fibers as reinforcement in TRM systems. It is necessary, on the basis of the potential exhibited by such systems, and on the basis of their limitations with respect to conventional reinforcement systems, to intensify experimental analysis in order to have a more robust scientific background. In this context, the present thesis aims at providing a comprehensive investigation of a plant fiber and plant fiber-based TRM systems. Specifically, hemp and flax yarns were adopted not only from their low environmental impacts and their low costs, but also because of their good mechanical properties as it is seen in the literature, making them suitable to reinforce structural elements. The overall interest of the work is to provide, by means of experimental investigations, a detailed analysis concerning the durability of hemp and flax fibers subjected to alkaline solutions as well as the durability of TRM specimens made from hemp textile and bio-resin-coated hemp textile. The comprehensive characterization carried out in the study moves from the physical and mechanical investigation of the employed plant fibers, to the investigations of TRM specimens and finally to the analysis of the bond behavior between substrates and TRM systems through shear bond tests. In order to respect the consistency between existing and reinforcing materials, two different types of matrix were adopted: the ettringitic matrix and the natural hydraulic lime matrix. The first matrix is recommended in case of reinforcement of concrete structures, while the second matrix is more appropriate in case of reinforcement of masonry structures. In order to get a deep understanding of the overall mechanical behavior, the investigation starts from detailed scales of analysis.

- At the smallest scale of analysis, a physical and mechanical characterization of the adopted matrices and plant fibers is presented aiming at providing the necessary information to

evaluate the mechanical behavior on greater scales of analysis, and to compare the adopted materials with each others.

- Durability tests on the employed hemp and flax yarns is proposed with the aim of defining to what extent it can be both mechanically and chemically suitable as reinforcement in inorganic matrices. Both mechanical and durability tests provide more information on such aspect and represent the basis from which possible necessary improvement solutions may be properly conceived.
- Bio-resin coating of hemp yarns, is proposed as a solution for enhancing their durability in alkaline environments of inorganic matrices, improving the textile-matrix bond behavior and optimizing the mechanical behavior of the composite. Durability and mechanical tests on bio-resin-coated hemp yarns provide more information on the suitability of such reinforcement for the use in TRM applications.
- Mechanical and durability tests on the composite scale of analysis were planned with the aim of qualifying the material according to standardized procedures, and of comparing its performance with the performance of yarns subjected to accelerated aging protocols. At this scale of investigation too, the analysis of results provides both potential aspects and limitations of the system as well as of the aging protocols adopted.
- The global mechanical response of concrete and masonry elements strengthened with TRM composites aims at characterizing the bond between the bio-resin-coated hemp TRMs and the substrate as well as the bond between the bio-resin-coated hemp textile and the corresponding matrix. Such investigation is necessary because it provides information on the TRM when their applied to the substrate. A further objective of the present study consists of taking advantage of the adopted multi-scale approach of the analysis to define the connection between the mechanical performance assessed on the material scale of investigation and the global response of the structural elements. Therefore, in a global perspective, the comprehensive characterization herein proposed has the aim of investigating the efficiency of a bio-resin-coated hemp TRM composite as external strengthening of concrete and masonry elements, by highlighting both the potentials and the limitations, with respect to a mechanical point of view. Moreover, to move a step further than a mechanical characterization for its own sake, the study aims to preliminary investigate technical solutions, i.e. fiber coating and mortar types.

Chapter 2 Materials characterization

2.1 Introduction

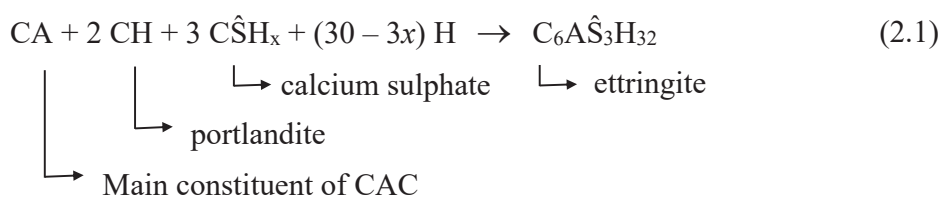
Prior to addressing the investigation of TRMs characterized by natural fibers, and to studying its influence on structural elements, it is necessary to characterize the materials used to manufacture it. Such step, conducted at the constituent “materials” scale of analysis, is of fundamental importance for the interpretation of the mechanical behavior at greater scales of analysis. This chapter presents the different materials used in this study as well as the experimental techniques implemented to characterize their physical and mechanical properties. The first part concerns the physical and mechanical properties of the two matrices used: the ettringitic mortar (E) and the hydraulic lime mortar (L). The second one presents the physical and mechanical properties of the different yarns used: the hemp (H), the flax (F) and the bio-resin-coated hemp (HC).

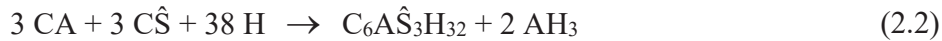
2.2 Matrices characterization: ettringitic matrix (E) and natural hydraulic lime matrix (L)

In the domain of the reinforcement of existing structures, it is required to use materials that is consistent as possible with the existing materials. For example, in the case of masonry structure, the use of TRM made from hydraulic lime-based mortar is recommended, while in the case of reinforced concrete structure, the use of cement-based matrix is more appropriate. For this reason, two different matrices are used in this study: a specific matrix developed at LMC² laboratory, based on an ettringitic binder (E) and a commercialized natural hydraulic lime matrix (L). At first, the consistency and the setting time for five different compositions of E matrix are studied to finally choose the one that is most suitable for manufacturing TRM composites and then the flexural and the compressive strength of the two matrices E and L are determined.

2.2.1 Formulation

The formulation of the ettringitic matrix used in this study is based on the international patent WO 2015/158891 A1 [154]. We should note that, in this international patent, the objective was to strengthen water tanks so that there was a water repellent agent in the composition of the mortar. However, in our study we did not use this agent in order to assure a good breathability for the structure. In particular, this matrix comprises an ettringitic binder, a granular skeleton, and several additives. The ettringitic binder is a binder whose main hydrate formed is ettringite (equations (2.1) and (2.2)). It consists of aluminous cement (CAC), calcium sulphate and Portland cement.





In the case of TRM characterization and use, thin elements with a large surface are manufactured, so the phenomenon of water evaporation is significant and can cause cracking. For this reason, an ettringitic binder is used. Indeed, unlike Portland cement, the ettringitic binder does not have a dormant period, which allows it to harden and quickly rise in resistance. Since the time of hydration decreases, this limits the evaporation of the water, which in turn limits shrinkage and thus the formation of cracks on the surface of the matrix. However, this quick reaction does not allow enough time to apply the matrix before it begins to set, so that we can use a setting modifier agent, and more precisely a setting retarder.

The granular skeleton used consists of milled silica and calcareous filler. The additives include a rheology agent, an adhesion reinforcing agent, a viscosity agent, and a resin. The rheology agent, a superplasticizer, improves the fluidity of the mineral matrix. The adhesion reinforcing agent increases the adhesion of the matrix to the support and it allows the matrix to stick to the textile. The viscosity agent improves the stability thereof. The resin gives flexibility to the matrix at the time of drying, that is to say when the shrinkage phenomenon is the most important. That makes it possible to increase the life of the concrete after drying. Table 2- 11 presents the five different compositions of ettringitic matrix characterized at first in order to choose only one composition among them to use later in the TRM.

Table 2- 11 : Ettringitic matrix compositions.

Components (g)		Designation of compositions				
		Compo 1 SP R	Compo 2 0.5SP R	Compo 3 0.25SP R	Compo 4 0.25SP 1.38R	Compo 5 0.25SP 2R
Ettringitic Binder		273.0	273.0	273.0	273.0	273.0
Granular Skeleton		633.0	633.0	633.0	633.0	633.0
Additives	Resin	90.8	90.8	90.8	90.8	90.8
	Adhesion reinforcing agent	0.5	0.5	0.5	0.5	0.5
	Viscosity agent	0.4	0.4	0.4	0.4	0.4
	Superplasticizer (SP)	2.3	1.2	0.6	0.6	0.6
Total of solid components (S)		1000.0	998.9	998.3	998.3	998.3
Liquid components	Setting retarder (R)	36.0	36.0	36.0	50.0	72.0
	Water	200.0	200.0	200.0	186.0	164.0
Total of liquid components (L)		236.0	236.0	236.0	236.0	236.0
L/S ratio		0.236	0.236	0.236	0.236	0.236

All the compositions have the same quantity of binder and granular skeleton, but they differ either by the quantity of superplasticizer or by the quantity of setting retarder. Since the setting retarder used here is in liquid form, then the increase in the amount of retarder, leads to a decrease in the

amount of water used in the reference composition (Compo 1), in order to have the same liquid to solid ratio (L/S) for all the studied compositions. The purpose was to find a matrix with a fluid consistency to facilitate the preparation of the TRM plates and to allow a good penetration of the matrix between the yarns of the textile as well as between the filaments of the same yarn. In addition, the pot-life of the matrix should be greater than the time needed to prepare the TRM plates.

The natural hydraulic lime matrix (L) used in this study is a commercial matrix labelled **GeoCalce® F Antisismico** commercialized by the Italian company “KERAKOLL S.p.a” [155]. It is recommended for operations on highly breathable walls and concrete structures, and ideal for use in GreenBuilding and Historical Restoration. It contains raw materials of only natural origin and recycled minerals. It has a low CO₂ emission and very low volatile organic compound emissions. It provides natural ventilation to improve indoor air quality, natural bacteriostatic and fungistatic effect. Furthermore, it is recyclable as an inert material at the end of its life. The mortar was produced by mixing an amount of water equal to 530 ml with 2.5 Kg of the pre-mixed formula of binder and aggregates, as recommended by the manufacturer [155].

2.2.2 Preparation

To prepare the matrix, the following steps are followed:

- The powder components of the matrix are weighed, to an accuracy of ± 0.001 g;
- The water and the setting retarder (water only in case of L matrix) together in the same beaker are weighed, to an accuracy of ± 0.1 g;
- The powder components are placed into the bowl of the mixer and mixed first at low speed (140 ± 5 rpm according to standard NF EN 196-1 [156]) for 30 s;
- After 30 s, about 3/4 of the amount of water and retarder (water only in case of L matrix) are added regularly (or until we obtain a dough that looks like bread dough) for the next 10 to 15 s without stopping the mixer;
- After 30 s of mixing, the remaining quantity of liquid is added and mixed for an additional 30 s;
- Then, the mixer is stopped and the mortar adhering to the walls and bottom part of the bowl are removed by means of a rubber or plastic scraper and placed in the middle of the bowl;
- Afterwards the mixer is started at low speed for a further 30 s;
- Finally, the mixer is switched to fast speed (285 ± 10 rpm according to standard NF EN 196-1 [156]) for a further 60 s.

2.2.3 Consistency test

The presence of the superplasticizer in the mass of the hydraulic binder increases the fluidity of the matrix after mixing. It is therefore necessary to know the consistency of the fresh matrix in order to determine if it is suitable for vertical or horizontal application. The test was carried out according to the standard NF EN 413-2:2017 [157], using the flow Table described in EN 459-2:2012 [158] (Figure 2- 46) which gives the flow diameter.

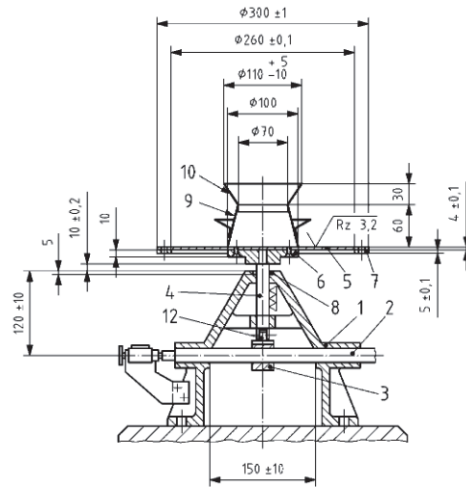


Figure 2- 46 : Flow Table for consistency determination (dimensions in mm) [158].

2.2.3.1 Procedure

The flow Table and the cone are cleaned and lightly moistened. Then, the cone is placed in the center of the flow Table. It is filled uniformly with the fresh mortar immediately after its mixing. The voids in the paste are removed by a gently tapping the slightly overfilled mold against the ball of the hand. The excess is removed by a gentle sowing action with a straight-edged held at an angle of about 45 degrees. Note that the test was performed statically: no vibration or shock is applied to the matrix. After 10 to 15 s, the cone is lifted slowly and vertically from the Table. The diameter of mortar spread is measured with a caliber in two directions at right angles to one another (Figure 2- 47). The mean value of these measurements gives the flow diameter. This procedure is repeated, every 15 minutes, for a duration of one hour.



Figure 2- 47 : Flow Table test.

2.2.3.2 Results

The flow diameter for all the ettringitic matrix compositions tested as well as for the natural hydraulic lime matrix (L) at different time intervals is shown in Table 2- 12. Figure 2- 48 presents the influence of the amount of superplasticizer on the consistency of the ettringitic matrix (E) over the time. Figure 2- 49 presents the influence of the amount of retarder on the consistency of the ettringitic matrix (E) over time.

Table 2- 12 : Consistency test of the ettringitic matrix (E) and lime matrix (L).

Time (min)	Flow diameter (cm)					Lime matrix (L)
	E: Compo 1 SP R	E: Compo 2 0.5SP R	E: Compo 3 0.25SP R	E: Compo 4 0.25SP 1.38R	E: Compo 5 0.25SP 2R	
0	20	18	14	15	17.5	8
15	19.5	18.5	12	15	15.5	8
30	19.5	18	10.5	13	15	8
45	19.5	15	-	12.5	13.5	8
60	18	15	-	10	12	8

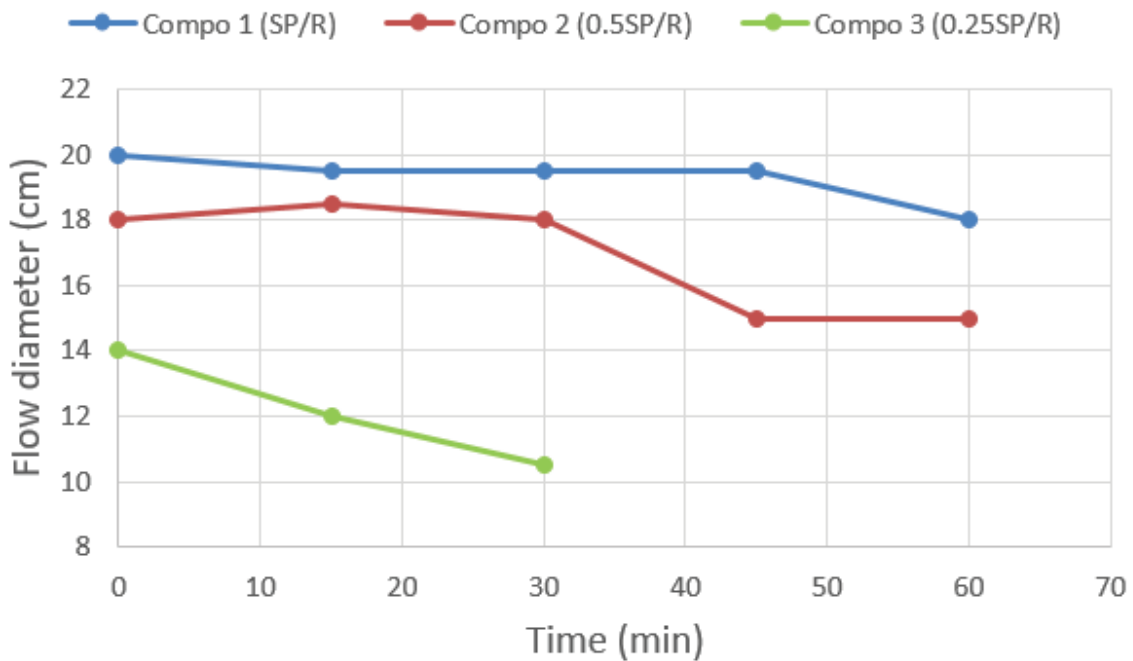


Figure 2- 48 : Influence of the amount of superplasticizer on the consistency of the ettringitic matrix over time.

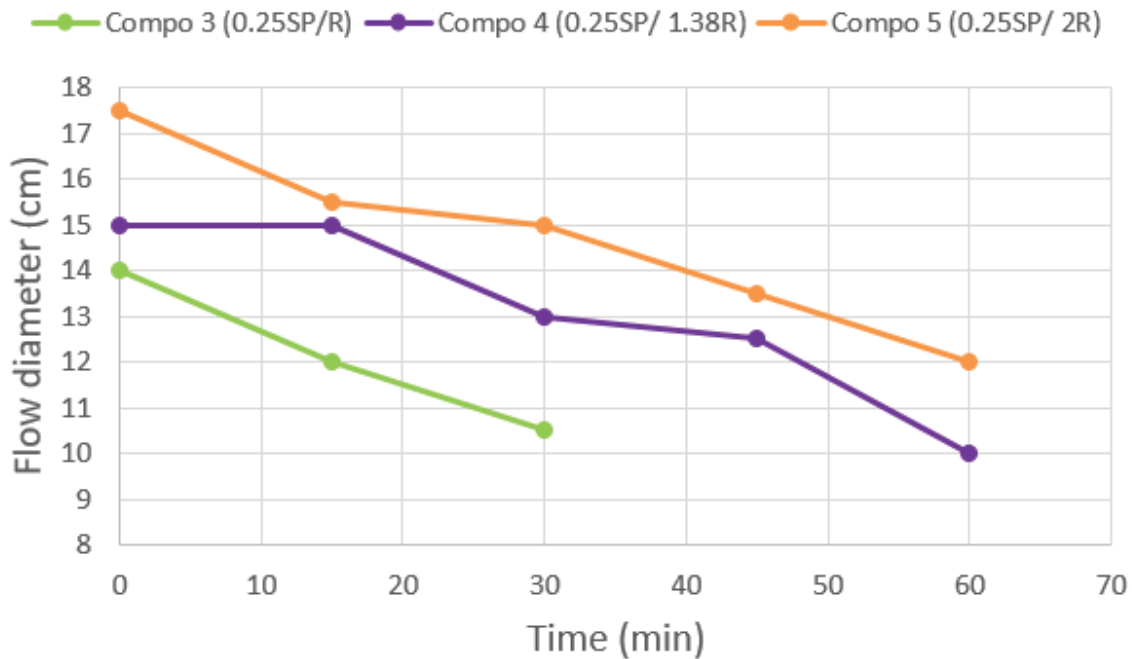


Figure 2- 49 : Influence of the amount of retarder on the consistency of the ettringitic matrix over time.

From Figure 2- 48, it can be noted that the decrease in the amount of superplasticizer reduces the fluidity of the matrix from the first moments, thus it reduces its workability. Furthermore, the loss in workability is more rapid when the reduction in the amount of superplasticizer is more significant.

From Figure 2- 49, it can be noted that the increase in the amount of setting retarder increases the fluidity of the matrix from the first moments. However, it has no effects on the evolution of workability over time of the matrix since the reduction in flow diameter after 60 minutes is the same (5 cm) for compo 4 and compo 5.

2.2.4 Setting time test

It is necessary to know the setting time of the binder in order to evaluate the effect of the setting retarder on the progression of the hydration reaction. The test was carried out according to the standard NF EN 196-3 [159], using the Vicat apparatus (Figure 2- 50) which gives two practical references: the beginning of setting and the end of setting. The test consists in following the transformation of state of a viscous material, easy to work in the state of a hardened material (more difficult or impossible to work).

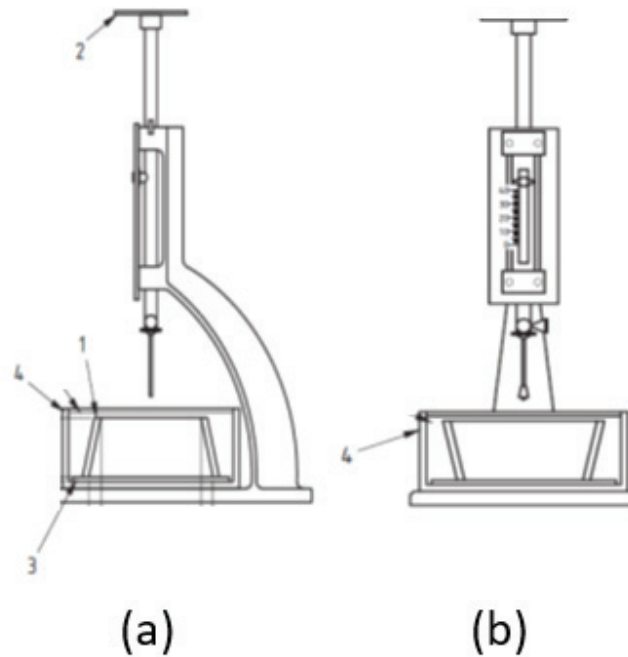


Figure 2- 50 : Vicat apparatus for setting time determination: a) Side mold in upright position for initial time setting; b) Front view with mold inverted for final setting time determination (1: mold; 2: correcting weights; 3: base-plate; 4: container. [159].

2.2.4.1 Procedure

The paste is transferred, immediately after the mixing, to the lightly oiled Vicat mold, which has previously been placed on a lightly oiled base-plate. The voids in the paste are removed by gently tapping the slightly overfilled mold against the ball of the hand. The excess is removed by a gentle sowing motion with a straight-edged implement in such a way as to leave the paste filling the mold and having a smooth upper surface. Then, the mold and the base-plate are transferred under the needle of the Vicat apparatus (Figure 2- 51). The needle is lowered gently until it is in contact with the paste. It is paused in that position for between 1 s and 2 s in order to avoid initial velocity or forced acceleration of the moving parts. Then the moving parts are quickly released and the needle is allowed to penetrate vertically into the paste. The scale is read when penetration has ceased, or 30 s after the release of the needle, whichever is the earlier. The scale reading, which indicates the distance between the end of the needle and the base-plate, is recorded, together with the time from zero. The penetration on the same specimen is repeated, every 15 minutes, at conveniently spaced positions, not less than 8 mm from the rim of the mold or 5 mm from each other and at least 10 mm from the last penetration position. The Vicat needle is cleaned immediately after each penetration. This procedure is stopped when the Vicat needle no longer enters the mold.

The initial setting time is determined as the time elapsed between ‘zero time’ and the time at which the distance between the Vicat needle and the base-plate is (6 ± 3) mm, measured to the nearest minute. Then, when the needle penetrates only 5 mm into the specimen, the filled mold is inverted on its base-plate to calculate the final setting time. The mold and the base-plate are transferred

under the needle of the Vicat apparatus, the same procedure already done for the determination of the initial setting time is repeated, and it is stopped when the Vicat needle no longer enters the mold. The final setting time is the elapsed time, measured from zero to that at which the needle first penetrates only 0.5 mm into the specimen, to the nearest 15 min.



Figure 2- 51 : Vicat test.

2.2.4.2 Results

Table 2- 13 presents the initial setting time, the final setting time and the total setting time for different compositions of the ettringitic matrix (E) as well as for the natural hydraulic lime matrix (L). Figure 2- 52 presents the position of the needle as a function of the time for the different compositions of the ettringitic matrix.

Table 2- 13 : Setting time test of the Ettringitic matrix (E).

	Compo 1 SP R	Compo 3 0.25SP R	Compo 4 0.25SP 1.38R	Compo 5 0.25SP 2R	Lime matrix (L)
Initial setting start time	5 h 45 min	1 h 45 min	1 h 50 min	1 h 50 min	24 h
Final setting time	6 h 10 min	2 h	2 h 20 min	2 h 50 min	28 h 50 min
Total setting time	25 min	15 min	30 min	1 h	4 h 50 min

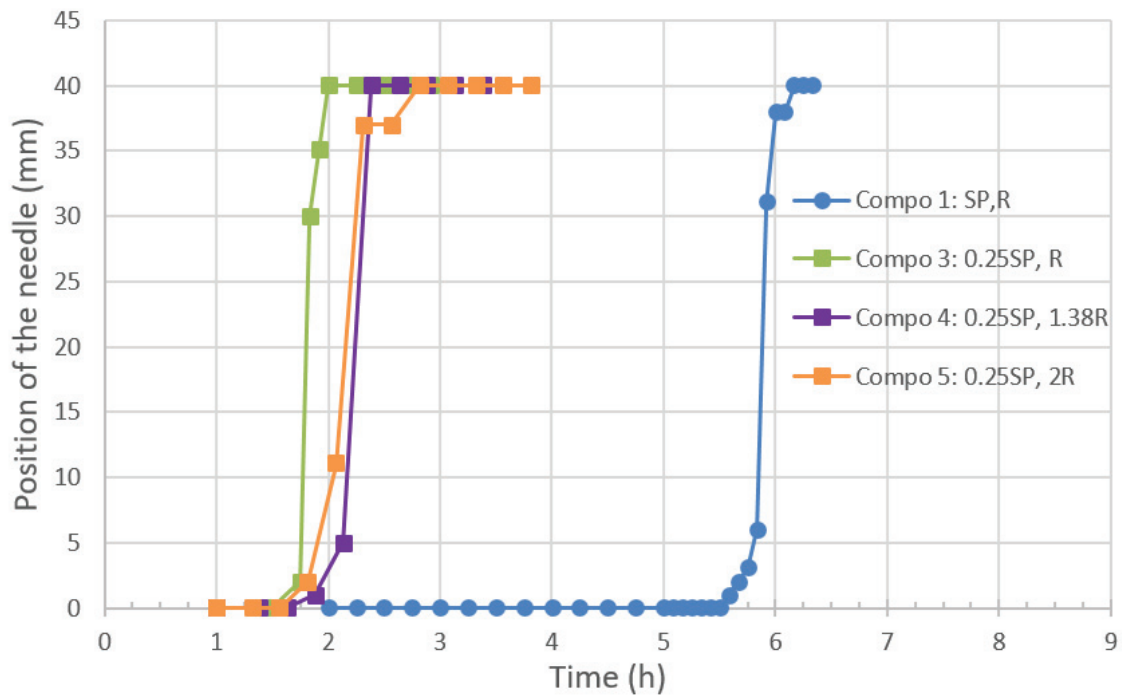


Figure 2- 52 : Position of the needle vs. time.

From Table 2- 13 and Figure 2- 52, it can be noted that the reduction in the amount of superplasticizer accelerate the initial setting time (compo 1 and compo 3) and the increase in the amount of setting retarder increases the total setting time by increasing the final setting time without affecting the initial setting time (compo 3, compo 4 and compo 5).

After these tests, we chose to use, in this project, the composition 5 of the matrix E, so that we reduce the amount of superplasticizer, which is expensive, and we increase the amount of retarder, which is not expensive. In addition, we preferred the initial spread of 17.5 cm, which is a little fluid, it facilitates the preparation of the composite plates and allows the matrix to penetrate well between the yarns. After 60 minutes, this spread will be 12 cm but that does not bother us since we manufacture small quantities, thus we do not need a lot of time to finish casting the matrix. We cast 2,5 kg of matrix which is the maximum quantity that we can put in the mixer. This quantity allows us to manufacture three plates of TRM in maximum half an hour. On the other hand, to use this matrix on an industrial scale, we can adjust its spreading so that it becomes applicable on a vertical support, and the initial setting time can also be adjusted so that it becomes applicable in large quantities at a time.

2.2.5 Mechanical properties

The mechanical characterization of the two matrices E and L was carried out according to the French standard NF EN 196-1 [156]. From each matrix, six specimens of 40 mm × 40 mm × 160 mm were prepared using polystyrene molds. Then, they are demolded after 72 hours and kept in plastic films for 7 days, then in the open air for 21 days. At the age of 28 days, they were subjected

to flexural and compressive tests. Before testing, the specimens were weighed in order to calculate the average density of the matrix.

2.2.5.1 Three-point flexural strength

The Perrier test apparatus for the determination of the flexural strength (Figure 2- 53, Figure 2- 54) is characterized by two steel supporting rollers of (10.0 ± 0.5) mm diameter, spaced 106.7 mm from each other, and a loading roller, made of steel, of the same diameter, equidistant from the first two. The length of these rollers must be between 45 mm and 50 mm. The loading device is shown in Figure 2- 53. One of the supporting rollers and the loading roller shall be capable of tilting slightly to allow a uniform distribution of the load over the width of the specimen without subjecting it to any torsional stresses [156].

The specimen was placed in the apparatus (Figure 2- 54), its lateral face was on the support rollers and its longitudinal axis perpendicular to the supports. The load was set at 0 N, then the machine was started. The load increased steadily at a rate of (50 ± 10) N/s until rupture and the specimen broke in two half-prisms.

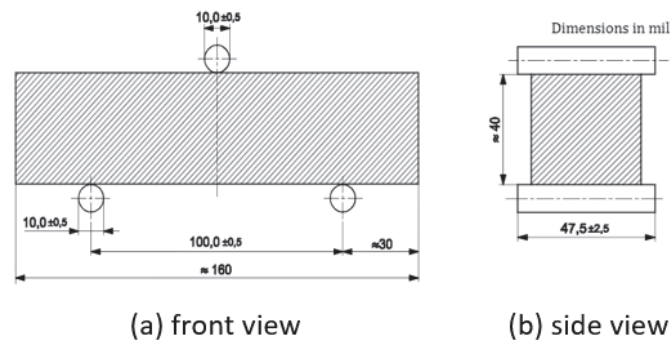


Figure 2- 53 : schematics of flexural test setup [156].



Figure 2- 54 : 3-point bending test setup on a 40 mm x 40 mm x 160 mm matrix specimen.

According to standard NF EN 196-1 [156], the flexural strength is calculated by the following equation:

$$\sigma = \frac{3}{2} \frac{F \cdot L}{b \cdot h^2} \quad (2.3)$$

Where:

- F : The load applied to the middle of the specimen at fracture, in Newtons;
- L : The distance between the supports = 106.7 mm ;
- b : The side of the square section of the specimen = 40 mm ;
- h : The height of the square section of the specimen = 40 mm.

2.2.5.2 Compressive strength

The compression test was carried out, at the age of 28 days, on the two halves of the specimen broken by the three-point bending test using the Cyber Tronic machine (Figure 2- 55, Figure 2- 56). This machine is provided with steel platens that shall be at least 10 mm thick, (40.0 ± 0.1) mm wide and (40.0 ± 0.1) mm long. The specimen half was centered to the platens of the machine within ± 0,5 mm, and longitudinally such that the end face of the prism overhangs the auxiliary platens by about 10 mm (Figure 2- 55, Figure 2- 56). The oil valve was closed and the load was increased regularly at a rate of 1.5 MPa/s until fracture. Finally, the compressive strength was displayed on the screen.

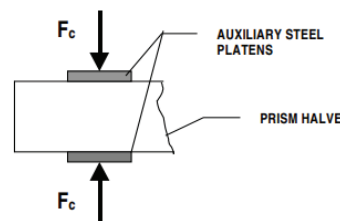


Figure 2- 55 :Schematics of compression test setup.

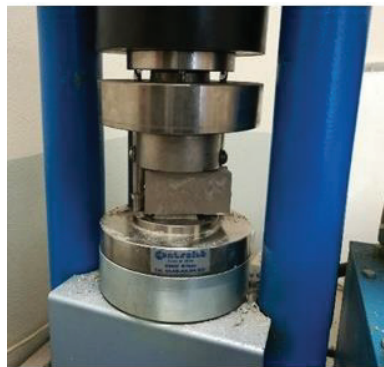


Figure 2- 56 : Compression test setup on a 40 mm x 40 mm x 160 mm matrix specimen.

2.2.5.3 Results

Table 2- 14 presents the density, the flexural strength, and the compressive strength for the ettringitic matrix (E) and the natural hydraulic lime matrix (L). One can notice that E matrix is more resistant in bending and in compression than L matrix.

Table 2- 14 : Flexural and compressive strengths at 28 days, on Ettringitic matrix (E) and Natural Hydraulic Lime matrix (L).

Specimen number	Ettringitic matrix (E)			Natural hydraulic lime matrix (L)		
	Density (g/cm ³)	Flexural strength (MPa)	Compressive strength (MPa)	Density (g/cm ³)	Flexural strength (MPa)	Compressive strength (MPa)
1	1.683	3.6	10.7	1.768	2.8	7.6
2	1.671	4.1	12.2	1.766	2.8	7.7
3	1.666	4.4	11.8	1.743	3.1	7.7
4	1.671	5.0	12.1	1.789	2.8	7.9
5	1.658	5.2	12.4	1.792	2.7	7.7
6	1.652	4.1	11.5	1.798	2.9	8.2
Average	1.667	4.4	11.8	1.776	2.8	7.8
Std. dev.	0.01	0.59	0.62	0.02	0.14	0.24
CoV (%)	0.6	13.4	5.3	1.1	5.0	3.1

2.3 Yarns characterization: Hemp (H), Flax (F) and Bio-resin-coated hemp (HC)

Three types of yarn are used in this study: the hemp yarn (H), the flax yarn (F) and the bio-resin-coated hemp yarn (HC). The hemp yarns (H) were manufactured and supplied in form of coils (Figure 2- 57a) by Stabilimento Militare Produzione Cordami (Agenzia Industrie Difesa, Italy). A single yarn consists of three set of filaments, twisted together without any coating (Figure 2- 57b). The flax yarns (F) are also supplied in form of coils (Figure 2- 57c). A single yarn consists of several filaments assembled next to each other without twisting or coating (Figure 2- 57d). The bio-resin-coated hemp yarns (HC) are manufactured in our laboratory by using the dry hemp yarns and coating them manually. The yarns were immersed in the resin bucket, then they are quickly taken off and the excess of resin were removed from the surface of the yarn by wringing it out manually. Then the yarns were left to dry at ambient temperature. Wooden bars and plastic clamps were used in order to obtain a straight yarn after the cure of the resin (Figure 2- 58).

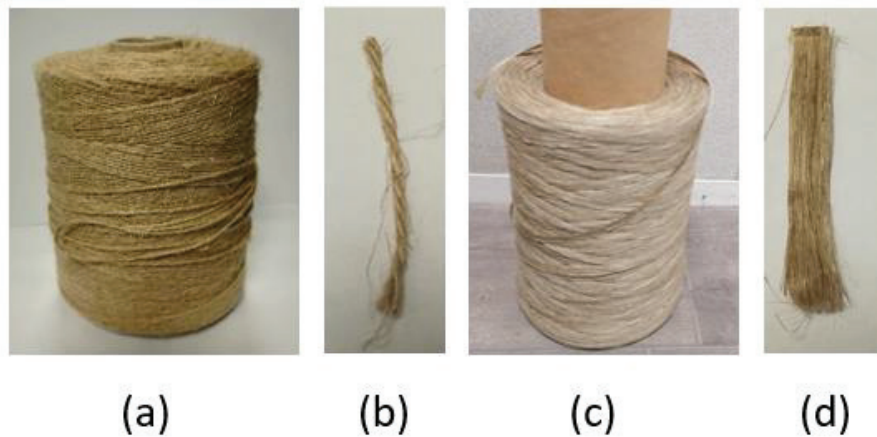


Figure 2- 57: a) Coil of hemp, b) hemp yarn, c) coil of flax and d) flax yarn.

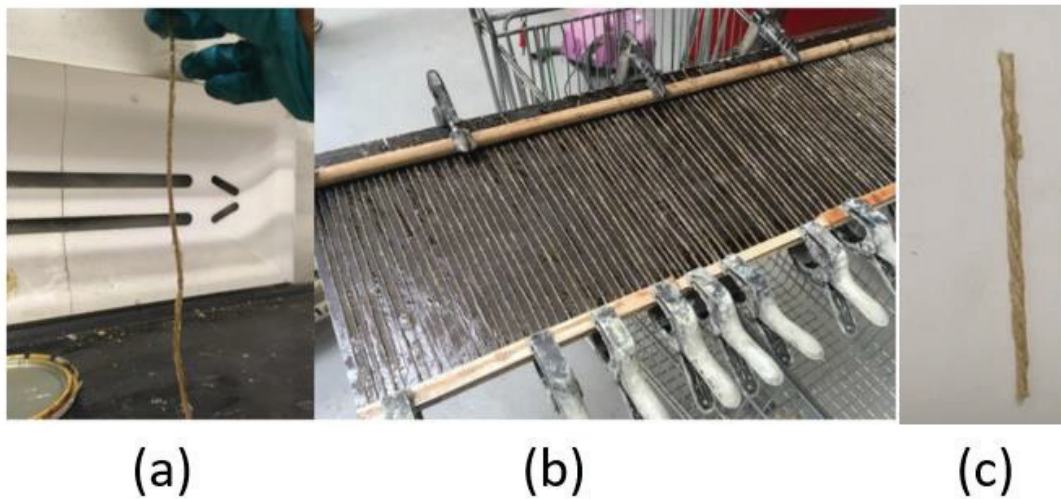


Figure 2- 58 : a) Manual coating of the hemp yarns by the bio-resin, b) drying of the coated yarns and c) coated hemp yarn (HC).

The bio-resin used to coat the hemp yarns is the epoxy resin DGEBA 50% bio based developed by Viretto & Galy 2018 [160]. A first step consisted in establishing specifications based on the characteristics of the reference petro-based epoxy system Foreva Epx TFC, which is already commonly used on site and considered to be efficient and reliable. The Foreva TFC® process is a reinforcement solution for civil engineering structures or buildings marketed by Freyssinet, a company specializing in structural rehabilitation and reinforcement. This process has a technical opinion established by the CCFAT (Commission Chargée de Formuler les Avis Techniques) whose secretariat is provided by the CSTB (Centre Technique du Bâtiment) (CCFAT 2017 [161]). The objective here is to define specifications making it possible to guarantee optimal conditions for the implementation of the composite on structures by manual stratification and a level of performance adapted to structural reinforcement applications and at the same time this system should be innovative with a reduced environmental footprint.

The development of this epoxy bio-resin for the use in the external reinforcement of a damaged structure was based on the strict requirements provided in (Viretto & Galy 2018 [160]) such as:

- Its viscosity must be compatible with a hand lay-up process;
- Its reactivity which means the pot-life also must be compatible with a hand lay-up process;
- Its curing must be at ambient temperature in a reasonable time;
- It must have a glassy network after curing;
- It must have a high modulus after curing;
- It must have a low water absorption after curing;
- It must withstand severe conditions of outdoor processing.

A characterization campaign of the Foreva Epx TFC system carried out at the INSA-IMP laboratory [160] made it possible to define target values which will then be valuable in guiding the work of formulating the bio-sourced resin in the next step. These target values are listed in Table 2- 15.

Table 2- 15 : Properties of DGEBA 50% bio based epoxy formulation proposed by Viretto & Galy 2018 [160].

Properties	Characteristics	Value	Method
Reactivity	Pot life at 25°C	60 min	Provided by Freyssinet
	Gel times at 40°C	80 min	Rotational rheometer
	Peak maximum temperature T _{pic}	117°C	DSC analysis at 10°C/min
Thermo-mechanical properties	Glass transition temperature T _g	>50°C	DSC analysis at 10°C/min
	Main transition temperature T _α	>59°C	DMA
	Storage modulus E' at 20°C (GPa)	3.8 GPa	DMA
Water absorption	Water absorption at 24°C	<6%	Gravimetric analysis

An experimental campaign was then carried out in order to find a bio-based formulation proposing bio-sourced alternatives approaching the specifications of the petro-sourced reference [162] from 18 bio-sourced epoxy monomers existing on the market. (bisphenol A, sorbitol, glycerol, isosorbide, succinic acid or cardanol type) and 3 bio-sourced diamine hardeners (phenalkamine and priamine type).

At the end of this work, it was possible to propose a 100% bio-sourced epoxy formulation free of CMR compounds (sorbitol/phenalkamine system) as well as a partially bio-sourced alternative formulation (bio-DGEBA/phenalkamine system) with properties conforming to the specifications. These systems are shown in Figure 2- 59. Their compositions and characteristics are detailed in Table 2- 16 [160].

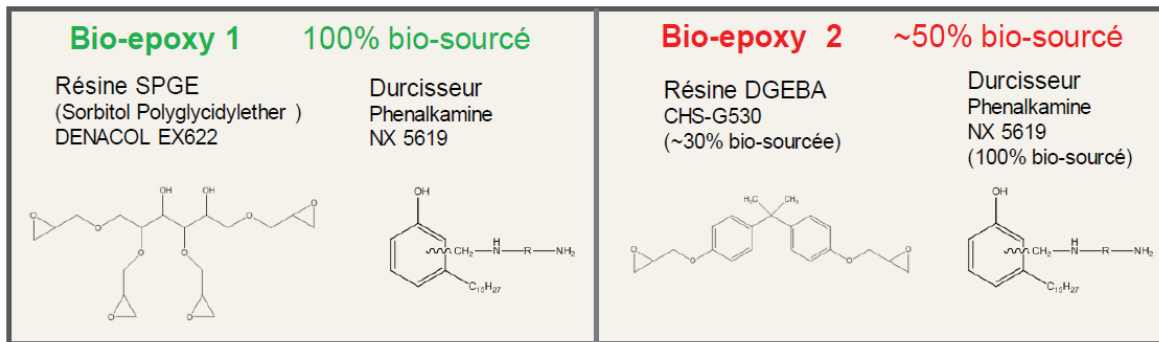


Figure 2- 59 : bio-sourced resin formulations proposed by Viretto & Galy 2018 [160].

Table 2- 16 : Properties of both bio based epoxy formulations proposed by Viretto & Galy 2018 [160].

Properties	SPGE 100% bio based	DGEBA 50% bio based
Pot-life at 40°C (min)	55	90
Gel times at 40°C (min)	57	140
Peak maximum temperature Tpic (°C)	108	119
Glass transition temperature Tg (°C)	40	54
Main transition temperature Tα (°C)	46	61
Storage modulus E' at 20°C (GPa)	1.88	2.78
Water absorption at room temperature (%)	4.8	0.88

A complementary study was conducted by the LTDS (École centrale de Lyon) on composite laminates made from the 2 bio-sourced epoxy formulations previously identified by the IMP laboratory and flax fabrics [163]. An additional laminate was also produced by impregnating flax fabrics with Foreva Epc TFC resin, for comparison. Figure 2- 60 presents the stress-strain curves recorded for the different materials tested by the 3-point bending test. One can notice that the composite with a partially bio-sourced matrix (DGEBA/phenalkamine formulation) has a significantly higher bending capacity than that of the composite with a 100% bio-sourced matrix (SPGE/phenalkamine formulation), even higher than that of the laminate with Foreva Epx TFC. Furthermore, a scanning electron microscopy (SEM) observation has shown that for the composites with SPGE/phenalkamine matrix the flax fibers are poorly impregnated by the matrix, thus these composites suffers from poorly fiber/matrix adhesion. This same defects was observed in case of composites with Foreva Epx TFC matrix, which is not surprising since this resin is optimized for the impregnation of carbon fibers and not for flax ones. However, the composites with DGEBA/phénalkamine matrix presented better fiber-matrix adhesion.

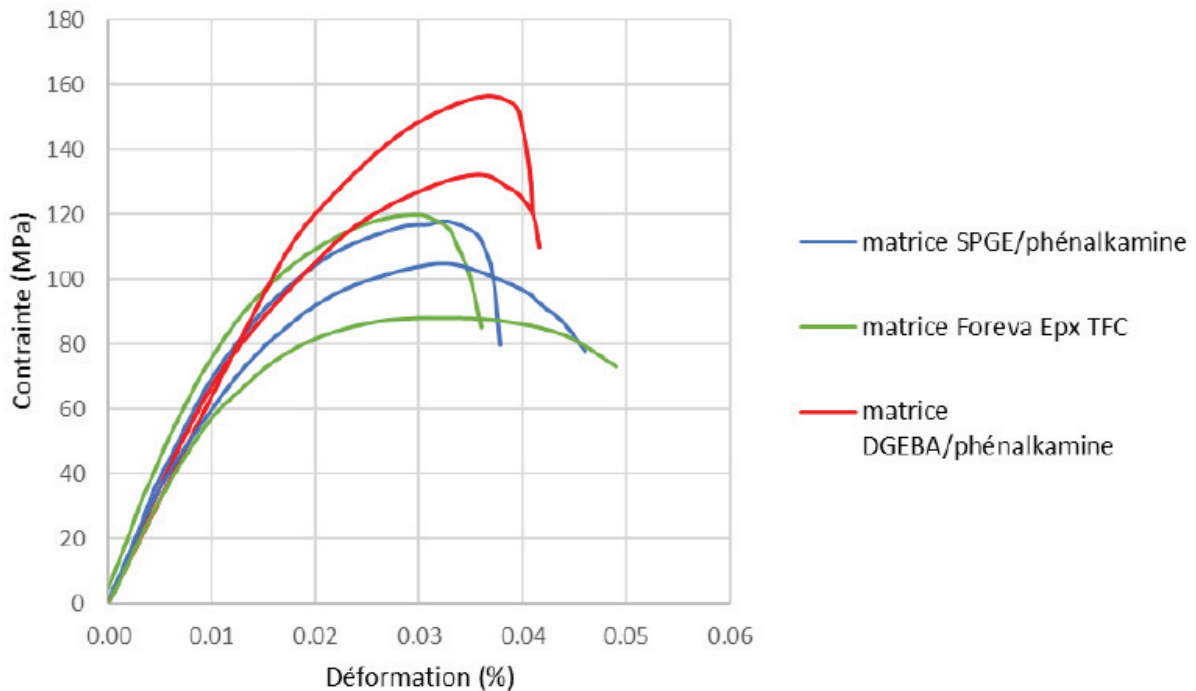


Figure 2- 60 : Stress-strain curves obtained for the different flax fiber composites tested in 3-point bending [163].

These results lead to the conclusion that the partially bio-sourced epoxy formulation (DGEBA/phenalkamine) is better suited to the impregnation of vegetal fibers than the 100% bio-sourced formulation. Therefore in our durability study, we preferred the use of the DGEBA/phenalkamine formulation which makes it possible to optimize the performance of the hemp fibers and to avoid manufacturing defects which would be detrimental to long-term resistance. In addition, this formulation presented lower water absorption capacity and higher glass transition temperature (Table 2- 16), which constitutes a probable advantage in terms of durability. This formulation being partially bio-sourced, it also respects the principal context of the project which is to offer a reinforcing composite system with a reduced environmental footprint. This matrix is characterized in tension by Chlela [164], it has a tensile strength of (44 ± 6) MPa and a tensile modulus of (2.8 ± 0.3) GPa.

The three yarns adopted in this study were characterized physically and mechanically, the results are shown in the following sub-paragraphs.

2.3.1 Physical characterization

2.3.1.1 Cross-sectional area

The yarns' cross-sectional areas had been determined by the X-ray tomography. This technique allows access to the internal vision of an object in a non-destructive and a non-invasive way. It has a similar principle as the technique used in medicine allowing a vision inside the patient body. They both consist of exposing the object to collimated X-rays, generated by the X-ray tube, numerous times under different angles and the detector converts the X-rays into digital radiographs

(2D images (Figure 2- 61)). Then, these radiographs can be reconstructed by means of a reconstruction software algorithm to obtain the 3D volume of the object (Figure 2- 62) [165] [166]. However, lab-scale devices are based on the rotation of the sample (Figure 2- 61) instead of the synchronous rotation of the source and detector used in medicine. This imaging technique is based on the property of X-rays to cross the material and to be absorbed according to the nature and density of the constituents they encounter. Thus, it provides a volume image of the distribution of linear X-ray absorption coefficient (μ) [167].

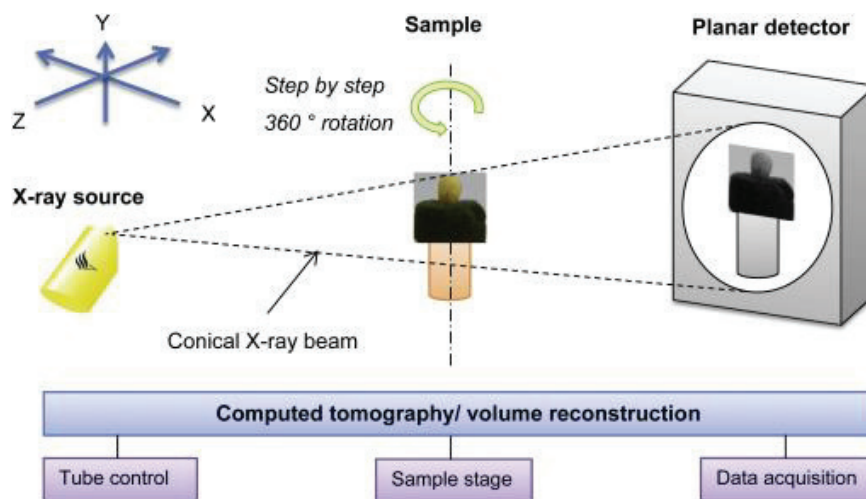


Figure 2- 61 : Schematic representation of the principle of X-ray tomography [166].

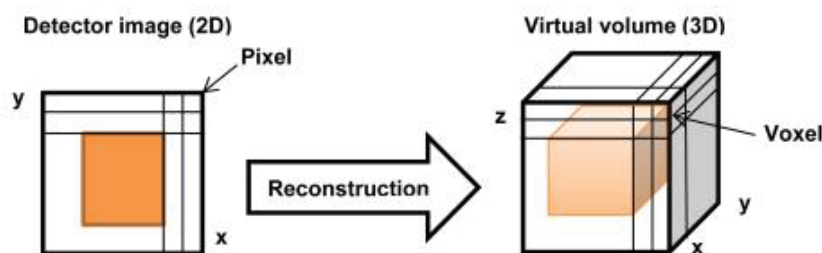


Figure 2- 62 : Schematic representation of the reconstruction process [166].

For this study, samples of hemp (H), flax (F) and bio-resin-coated hemp yarns (HC) (Figure 2- 63) were scanned by X-ray tomography (Figure 2- 64a, Figure 2- 65a, and Figure 2- 66a). Then, the images were processed with the “FIJI-ImageJ” software by adjusting the contrast and brightness (histogram stretch) and making a thresholding to separate the different phases (yarn and void for H and F, and yarn, resin and void for HC). Finally, the cross-sectional area of the yarn is determined by averaging the ratios of the number of pixels of yarn over the number of pixels of the entire surface of each Figure. Table 2- 17 contains the average value of the cross-sectional A_f of each yarn. Furthermore, the percentage of resin in the bio-resin-coated hemp yarn (HC) is

determined by averaging the ratios of the number of pixels of resin over the number of pixels of the entire surface of the coated yarn. It is equal to 71 %.

Table 2- 17 : Average value of the effective cross-sectional area of the yarns.

Yarns	Cross-sectional area A_f (mm ²)	Standard deviation (mm ²)	Coefficient of variation (CoV%)
Hemp (H)	0.751	0.002	0.26
Flax (F)	0.861	0.002	0.23
Bio-resin-coated hemp (HC)	3.278	0.036	1.1

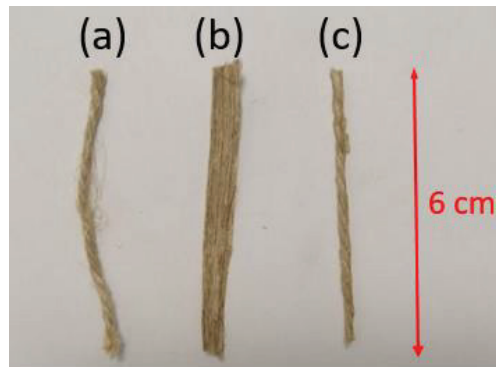


Figure 2- 63 : Samples of the studied yarns: a) hemp (H), b) flax (F) and c) bio-resin-coated hemp (HC).

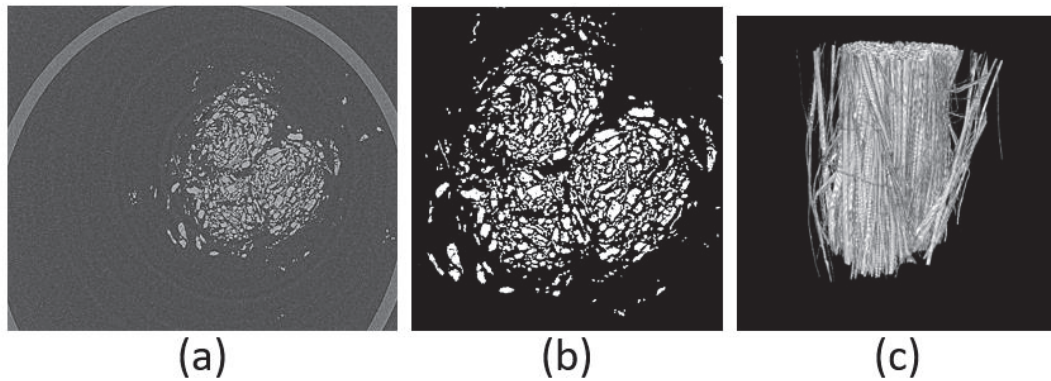


Figure 2- 64 : a) Scan of the hemp yarn by X-ray tomography, b) cross section of the fiber and c) 3D view of the hemp yarn reconstructed by "FIJI-ImageJ" software.

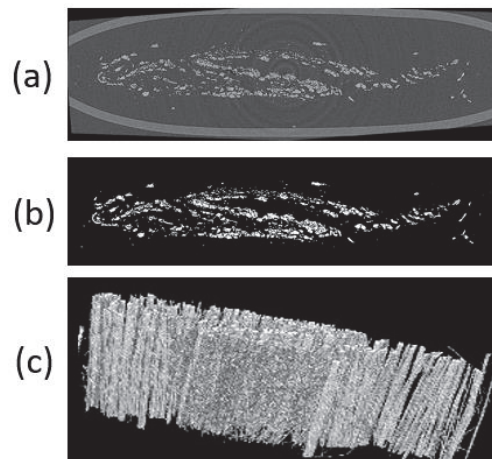


Figure 2- 65: a) Scan of the flax yarn by X-ray tomography, b) cross section of the fiber and c) 3D view of the flax yarn reconstructed by "FIJI-ImageJ" software.

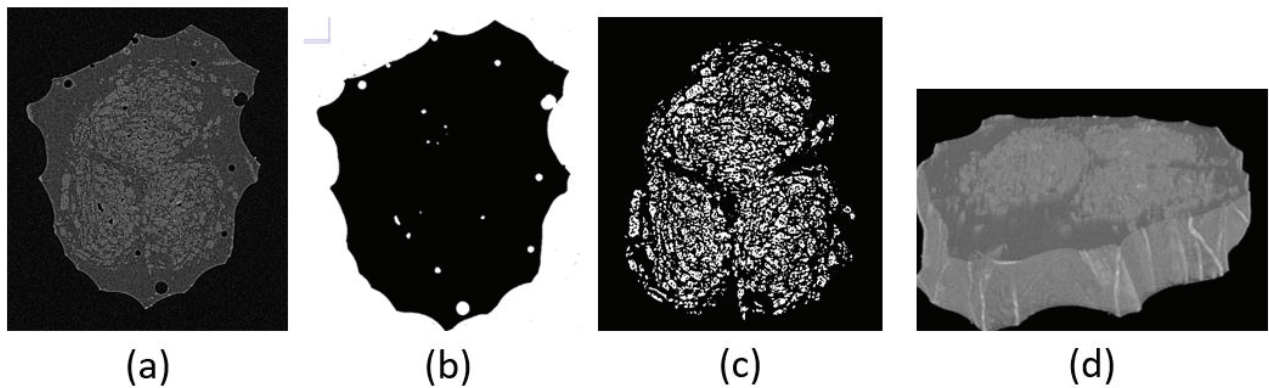


Figure 2- 66: a) Scan of the bio-resin-coated hemp yarn by X-ray tomography, b) porosity, c) cross section of the hemp yarn separated from the coating and d) 3D view of HC yarn reconstructed by "FIJI-ImageJ" software.

2.3.1.2 Linear density, density and moisture content

The standard NF EN ISO 1889:2009 [168] specifies a method for the determination of the linear density of glass-fiber, carbon-fiber, aramid-fiber and any other reinforcement-fiber yarns. It is also applicable to all types of yarn. It consists of cutting specimens from the yarn to a specified length and weighing them, then calculating the mass per unit length. The unit generally used is the Tex, which corresponds to one gram per kilometer of yarn.

Six specimens of 1 m of hemp and flax yarns were cut and weighed, to an accuracy of ± 0.001 g. Then they were dried in an oven at 110 °C for 2 hours. After drying, the specimens were placed in a desiccator to cool down. After cooling down, the specimens were weighed again, to the same accuracy.

Table 2- 18 and Table 2- 19 present the weight before and after drying, the linear density and the moisture content for all the specimens tested as well as the average linear density and the average moisture content, for hemp and flax yarns, respectively. As we can see, the hemp and flax yarns

have an average linear density of 1200 Tex and 1194 Tex, respectively, and they contain a 5.75 % and 5.45 % by mass of moisture, respectively.

The linear density of the yarns was calculated using the following equation:

$$Tt = \frac{1000 \times Wd}{L} \quad (2.4)$$

Where: Tt = the linear density of the yarn;

Wd = the residual weight of the specimen after drying and cooling;

L = the length, in meters, of the specimen.

The moisture content of the yarns is the average of weight loss ratio, it was calculated as follows:

$$w = 100 \% \times \frac{Wi - Wd}{Wi} \quad (2.5)$$

Where: w = the moisture content in percent;

Wi = the initial mass, in grams, of the dry specimen;

Wd = the residual weight of the specimen after drying and cooling.

The yarn density was obtained by dividing the linear density by the cross-sectional area of the yarn. It is equal to 1.598 g/cm³ and 1.386 g/cm³ for hemp and flax yarns respectively.

Table 2- 18: Weight, linear density, moisture content, and density of **hemp** yarns.

Specimen	Initial weight W_i (g)	Residual weight W_d (g)	Linear density (tex)	Moisture content w (%)	Density (g/cm ³)
1	1.339	1.264	1264	5.6	1.683
2	1.337	1.258	1258	5.9	1.675
3	1.195	1.126	1126	5.8	1.499
4	1.173	1.105	1105	5.8	1.471
5	1.240	1.169	1169	5.7	1.557
6	1.355	1.278	1278	5.7	1.702
Average			1200	5.8	1.598
Standard deviation			76.2	0.11	0.1
CoV (%)			6.35	1.83	6.35

Table 2- 19: Weight, linear density, moisture content, and density of flax yarns.

Specimen	Initial weight W_i (g)	Residual weight W_d (g)	Linear density (Tex)	Moisture content w (%)	Density (g/cm^3)
1	1.320	1.247	1247	5.5	1.448
2	1.303	1.232	1232	5.5	1.431
3	1.233	1.166	1166	5.4	1.354
4	1.276	1.206	1206	5.5	1.401
5	1.178	1.114	1114	5.4	1.294
6	1.265	1.197	1197	5.4	1.390
Average			1194	5.5	1.386
Standard deviation			48.1	0.05	0.56
CoV (%)			4.03	0.96	4.03

In addition, 24 specimens of 25 cm of hemp yarns were cut and weighed to an accuracy of ± 0.001 g, then they were coated by a bio-sourced resin and left to dry for 24 hours. After drying, the resin-coated hemp yarns were weighed to an accuracy of ± 0.001 g. Table 2- 20 presents the maximum, minimum and average of: the weight of the yarns before and after coating, the percentage of the bio-sourced resin needed to coat the hemp yarns, and the density of the resin-coated hemp yarns. As we can see, the resin-coated hemp yarns have a density of 5 g/cm^3 .

The percentage of the resin in the yarns is calculated as follows:

$$R = 100 \% \times \frac{W_{ac} - W_{bc}}{W_{ac}} \quad (2.6)$$

Where: R = the resin content in percent; W_{bc} = the mass, in grams, of the yarn before coating; and

W_{ac} = the mass, in grams, of the yarn after coating.

The average percentage of resin contained in the bio-resin-coated hemp yarn calculated by means of weights is 64 % (Table 2- 20). This value could be considered very close to the value obtained by X-ray tomography (71 %), since the coating of the yarns is manually done, so the quantities of the resin added to each yarn are not perfectly similar.

Table 2- 20 : Weight, and density of bio-resin-coated hemp yarns.

Specimen	Weight before coating W_{bc} (g)	Weight after coating W_{ac} (g)	Weight of the bio-sourced resin R (%)	Density g/cm^3
maximum	0.431	1.486	80.0	7.350
minimum	0.331	0.768	56.9	3.783
Average	0.388	1.097	64.0	5.402
Std. dev.	0.06	0.20	4.2	0.981
CoV (%)	15.6	18.2	6.6	18.2

2.3.1.3 Water absorption and water desorption

The mechanical performance and the durability of the natural fiber reinforced cementitious composites are affected by the capacity of the fibers to absorb water. When fibers are imbedded in the fresh cement matrix, they absorb water from it, so they undergo a volume expansion. Afterwards, during the hardening time, the fibers reject some of the already absorbed water in the fiber-matrix interface forming an alkaline pore solution, which leads to the early deterioration of natural fiber [66].

Specimens of hemp, flax and bio-resin-coated hemp yarns were immersed in two different NaOH solutions: one having a pH 10.5 and the other having a pH 12.5 at ambient temperature 23 °C. The yarns were weighed before immersion and after 24, 40, 48, 64, 72, 88, 96, and 112 hours of immersion when they reached a moisture absorption balance. The water absorption percentage was calculated as follows:

$$wa = 100 \% \times \frac{M1 - M0}{M0} \quad (2.7)$$

Where: wa = the water absorption in percent;

$M0$ = the mass, in grams, of the specimen before immersion in the NaOH solution;

$M1$ = the mass, in grams, of the specimen at the moisture absorption balance.

After taking masses ($M1$) up to 112 hours, the yarns were subjected to drying in the laboratory conditions. They were weighed after 24 and 30 hours of drying when their masses stabilize.

The water desorption percentage was calculated as follows:

$$wd = 100 \% \times \frac{M2 - M0}{M0} \quad (2.8)$$

Where: wd = the water desorption in percent;

$M0$ = the mass, in grams, of the specimen before immersion in the NaOH solution;

$M2$ = the mass, in grams, of the specimen after complete desorption.

Figure 2- 67 and Figure 2- 68 present the water absorption and the water desorption of the different yarns, respectively, in function of time. Table 2- 21 presents the total water absorption and water desorption capacity of the different yarns.

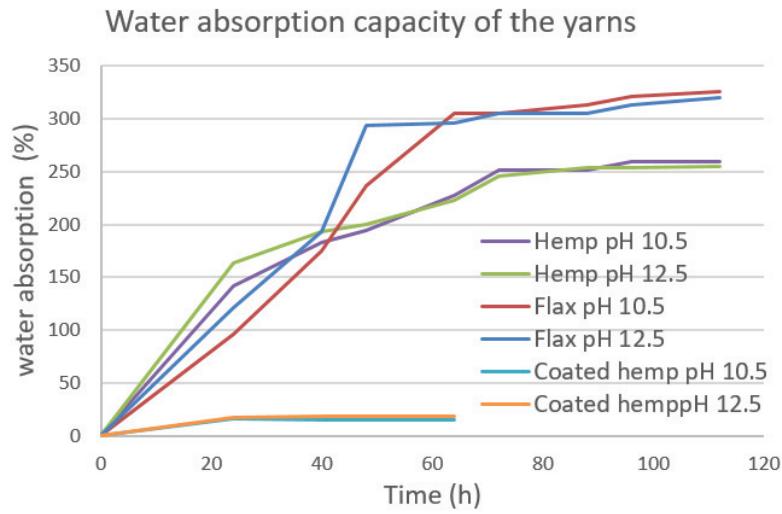


Figure 2- 67 : water absorption of hemp, flax and bio-resin-coated hemp yarns in function of time.

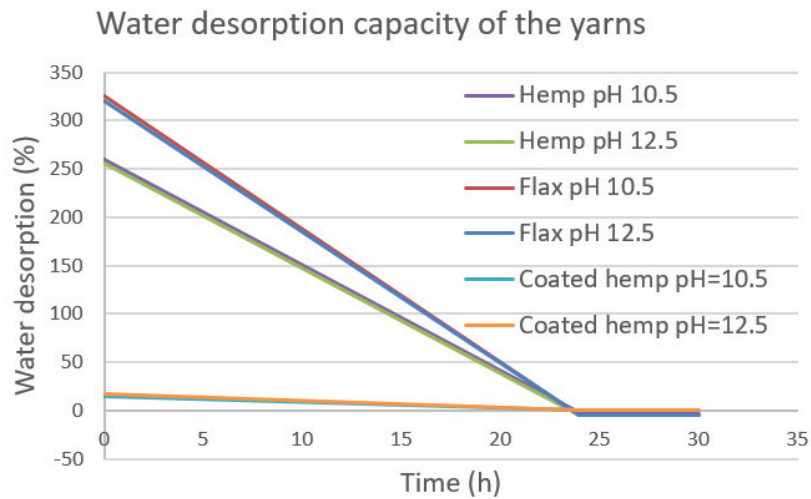


Figure 2- 68 : water desorption of hemp, flax and bio-resin-coated hemp yarns in function of time.

Table 2- 21 : Water absorption and desorption of hemp, flax and bio-resin-coated hemp yarns.

	Water absorption (%)	Water desorption (%)
H (pH 10.5)	260.2	-3.1
H (pH 12.5)	255.4	-4.6
F (pH 10.5)	325.6	-4.1
F (pH 12.5)	320.7	-5.0
HC (pH 10.5)	15.9	-0.1
HC (pH 12.5)	17.5	-0.1

From Table 2- 21, we can notice that the flax yarns have the greater water absorption capacity between all the yarns tested, but the capacity of hemp (H) yarns to absorb water is much greater than that of coated hemp yarns (HC). Thus, the resin coating of the hemp fibers largely reduces their ability to absorb water, so that it expected to be a good protection for the fibers against the degradation when they are subjected to the alkaline environments of the matrices. We can also notice that the water desorption is negative, which means that, after a cycle of immersion and drying, the yarns' masses did not return to their original values, but they were reduced. This can be explained by the fact that, the alkali-treatment of natural fibers for short periods, also called mercerization, removes extractives such as wax and oil, and amorphous substances such as pectin, lignin and hemicellulose from the surface of the fiber. This leads to the development of rough surface topography and that results in better fiber-matrix interface adhesion and an increase in mechanical properties. This was proved by many researchers [135], [132] [19], [169]. In addition, the color change of the uncoated hemp yarns after immersion in NaOH solution as well as the color change of the solution itself prove this hypothesis (Figure 2- 69). In case of coated hemp yarns the water desorption is almost zero, it is probably due to the presence of resin, which prevents the phenomenon of mercerization from occurring.

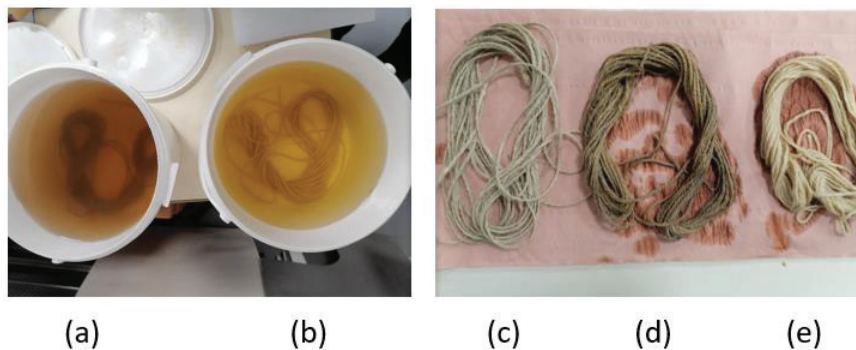


Figure 2- 69 : a) NaOH solution (pH 10.5) + hemp yarns, b) NaOH solution (pH 12.5) + hemp yarns, c) hemp yarn, d) hemp yarn after immersion in NaOH (pH 10.5) and e) hemp yarn after immersion in NaOH (pH 12.5).

2.3.2 Mechanical characterization

To define their mechanical characteristics, single hemp (H), flax (F) and bio-resin-coated hemp (HC) yarns were subjected to tensile tests. The test set up and the results are shown in the following two sub-paragraphs.

2.3.2.1 Tensile test setup

In order to avoid the concentration of stress, which causes the failure at the clamp of hemp and flax yarns tested in tension, a new mechanical grip system (Figure 2- 70) has been developed and designed by using a Finites Elements Method (FEM) analysis ('SALOME MECA' software, Figure 2- 71). The yarn was wound 2 times in the middle of the horizontal cylinder and then attached to the end. This cylinder has the shape of a sandglass to facilitate the positioning of the yarn in its middle which will be superimposed with the axis of the rod where the tensile load will be applied (Figure 2- 72).

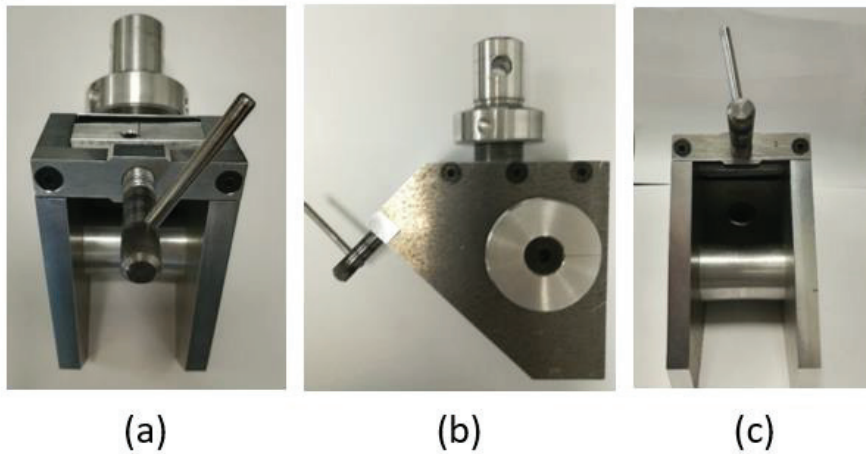


Figure 2- 70 : Different views for the yarns' mechanical grip system.

The material used to make this system is the Duralium AU4G whose properties are presented in Table 2- 22.

Table 2- 22 : Mechanical properties of the Duralium AU4G.

Duralium AU4G	
Young's modulus (MPa)	72500
Poisson's ratio	0.33
Shear modulus (MPa)	27200
Density (kg/m ³)	2790
Coefficient of thermal expansion (/K)	22.9 E ⁻⁶
Elastic limit (MPa)	380
Thermal conductivity (W/m.K)	134

The 3D mesh of the element (Figure 2- 71) is characterized by the following properties:

- It is subdivided in 26471 tetrahedrons.
- The function shape of the elements is linear (4 nodes each).

The boundary conditions are described as follows:

- A surface load L_s [MPa] is applied on the top of the vertical cylinder on the direction Z (Figure 2- 71). The stress L_s is equal to the maximum capacity of the Universal machine increased by 25 % ($65 \times 1.25 = 81.25$ kN) divided by the surface of application ($\frac{\pi \times 30^2}{4}$ mm²).

$$L_s = \frac{81250}{\frac{\pi \times 30^2}{4}} = 114.9 \text{ MPa.} \quad (2.9)$$

- The displacements in the middle of the horizontal cylinder are blocked (DX=DY=DZ=0).

The maximum stress value considered admissible in this design study is the yield stress of Duralium AU4G (380 MPa). The Von Mises and the Tresca stresses were smaller than the yield stress in all the regions of the mechanical grip system. Thus, we can conclude that this configuration of the grip system is sufficiently rigid to avoid the yielding of the metal material. Note that before this configuration, we have tried many ones with lower cylinder diameter that didn't verify the Von Mises and the Tresca stresses. More details of the final geometry configuration of the grip system are shown in Appendix A.

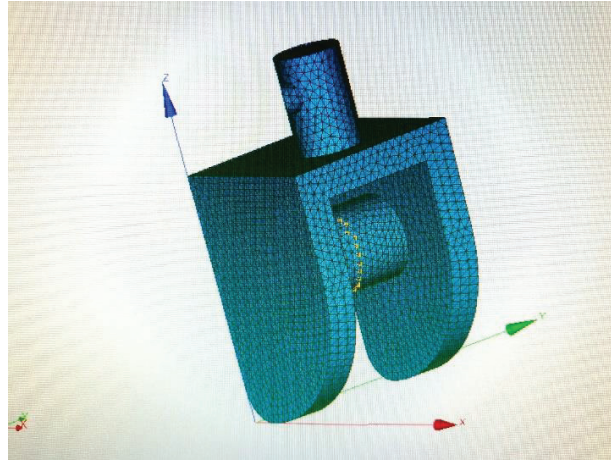


Figure 2- 71 : 3D mesh of the mechanical grip system.

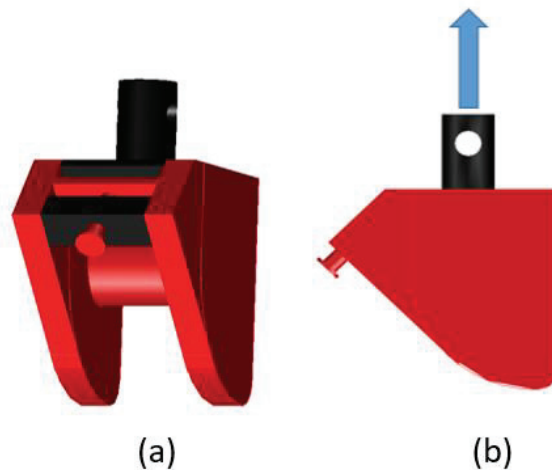


Figure 2- 72 : 3D and profile drawings of the yarns' mechanical grip system.

Unlike hemp and flax yarns, the bio-resin-coated hemp yarns are more rigid, so they cannot be wound on the cylinder of this grip system. For this reason, fiberglass composite boards are manufactured by our laboratory and then cut into small tabs (1 mm × 50 mm × 25 mm) which are glued to both ends of the specimen using a resin epoxy SC980 (Figure 2- 73). The role of the tabs

is to ensure a uniform distribution of the stress and avoid damaging the yarns in the fixing zone before reaching its tensile strength.



Figure 2- 73 : Fiberglass composite tabs glued to the both ends of the bio-resin-coated hemp yarns.

Because of the lack of standards for testing vegetal yarns, Hemp (H) and Flax (F) yarns are tested in tension according to ISO 2062:2009 standard [170], which can be used for all types of yarns, except glass, elastomeric, aramid, high molecular polyethylene (HMPE), ultra-high molecular polyethylene (UHMPE), ceramic and carbon yarns and polyolefin tape. The tests were conducted with a gauge length of 250 mm and a loading rate of 250 mm/min, in a universal testing machine Zwick of 50 kN capacity in displacement control. Similarly, there is no standards for testing resin coated vegetal yarns so bio-resin-coated hemp yarns (HC) are tested according to ISO 10618:2005 standard [171] which is dedicated for resin-coated carbon fibers. The tests were conducted with a gauge length of 150 mm and a loading rate of 5 mm/min. To ensure alignment of the fibers and to have them straight enough, preload of 6 N was applied to all the tested yarns. The test setups for all the yarns as well as their failure modes are shown in Figure 2- 74.

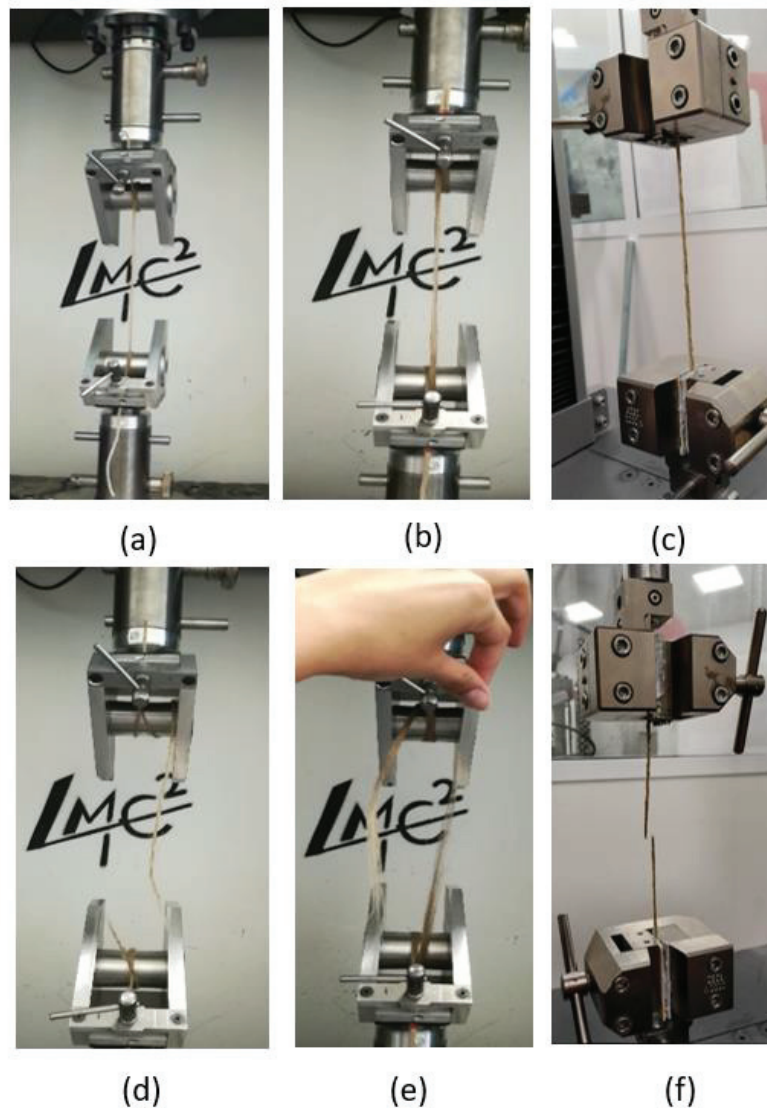


Figure 2- 74 : Tensile tests on the yarns: a), b) & c) test setup for hemp, flax and bio-resin-coated hemp yarns, respectively, d), e) & f) failure hemp, flax and bio-resin-coated hemp yarns, respectively.

2.3.2.2 Tensile test results

Figure 2- 75, Figure 2- 76 and Figure 2- 77 present the stress-strain curves for hemp, flax and bio-resin-coated hemp yarns, respectively. Table 2- 23 presents the maximum tensile load F_{\max} , the maximum tensile strength σ_{\max} , the maximum displacement U_{\max} , and the Young's modulus E for the different yarns tested. The stress σ refers to the ratio between the tensile load and the cross-sectional area of the yarn. The strain ε is the ratio between the global displacement of the cross head and the gauge length of the yarn. The elastic modulus refers to the slope of the stress-strain curve. It is calculated from the branch of the curve situated between 70 % and 90 % of the maximum tensile strength, which corresponds to a fairly linear behavior.

From Figure 2- 75 and Figure 2- 76, we can notice that the behavior in tension of hemp (H) and flax (F) yarns is not linear, but it is constituted from two branches: the first branch is non-linear; it is probably due to the realignment of the single fiber, which constitutes each filament of the yarn. The second branch is almost linear up to the rupture of the yarn. However, from Figure 2- 77, we can notice that the behavior of the bio-resin-coated hemp yarns (HC) is linear up to the rupture of the yarn. This small branch which appears at the beginning of each curve (at $\varepsilon < 0.1\%$) having different slope than the rest of the curve is also obtained in the study of Chlela [164] and it was also attributed to the reorientation of the single fibers which constitute each filaments of the yarn. Furthermore, the tensile strength of the bio-resin-coated hemp yarns (HC) is approximately 48 % lower than that of the uncoated ones (H), but their Young's modulus is 2.3 times higher than that of uncoated yarns (Table 2- 23). This is because of the penetration of the resin between the filaments of the hemp yarn, so it sticks them together, making the structure of the yarn stiffer and denser resulting in a reduction of the tensile strength as well as the tensile elongation of the fiber. Moreover, we should note that the tensile rupture of the fibers was far from the anchorage system, which indicated a proper gripping system. The coefficient of variation (CoV%) was between 3.8 % and 16.20 % which can be considered within an acceptable range of experimental error especially in case of plant yarns which properties vary within a large range depending on several factors such as the weather conditions during the growth of the plant, the harvesting process, and the retting process...

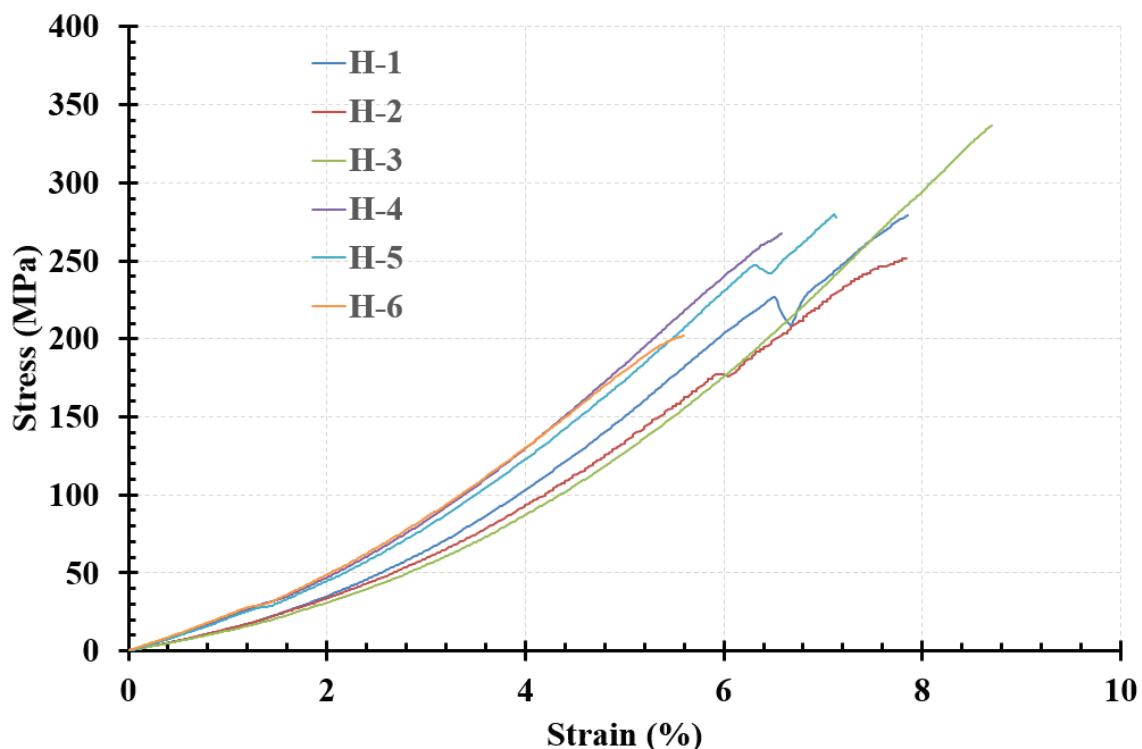


Figure 2- 75 : Stress-strain curves of hemp yarns (H) tested in tension.

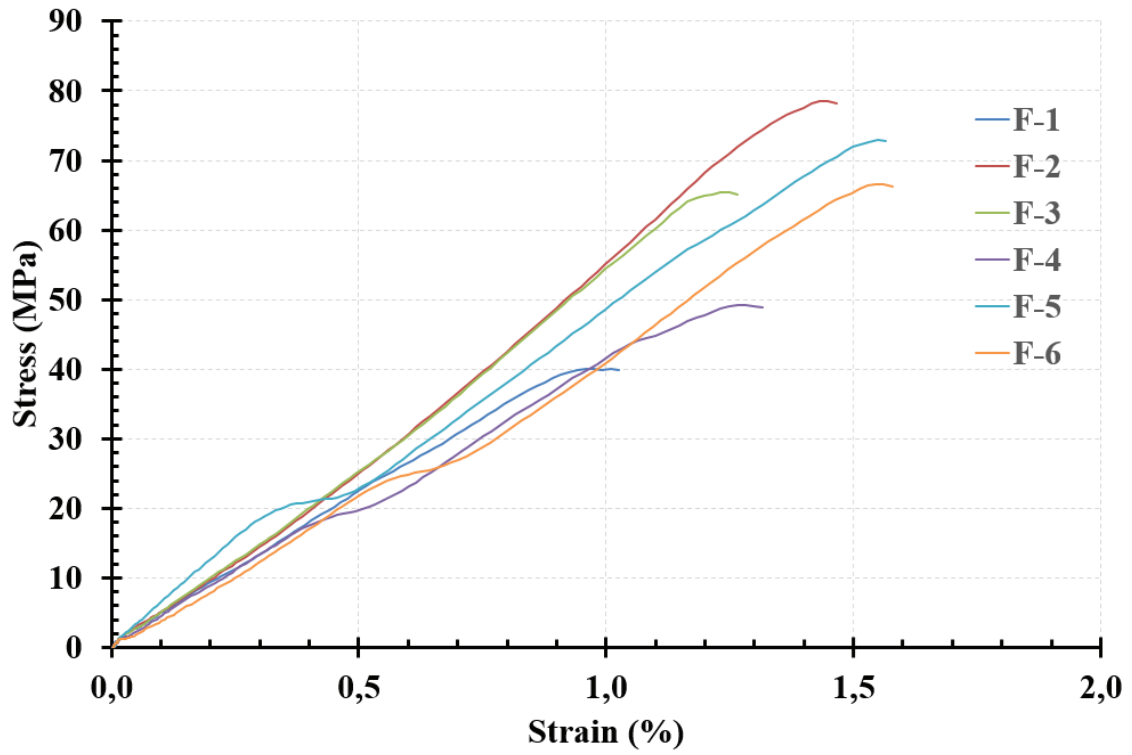


Figure 2- 76 : Stress-strain curves of flax yarns (F) tested in tension.

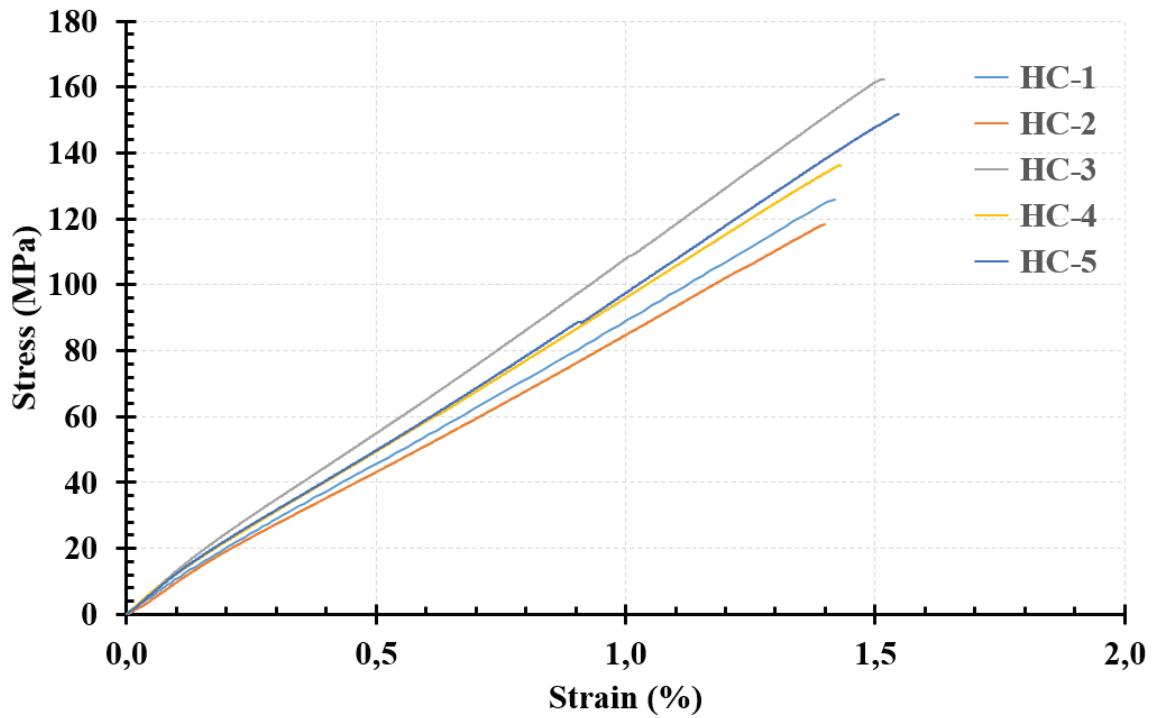


Figure 2- 77 : Stress-strain curves of bio-resin coated hemp yarns (HC) tested in tension.

Table 2- 23 : Tensile test results of hemp, flax and bio-resin-coated hemp yarns.

yarns	Specimen	F _{max} (N)	σ _{max} (MPa)	U _{max} (mm)	ε (%)	E (MPa)
H	1	209.7	279.2	19.6	7.9	4.3
	2	189.0	251.7	19.5	7.8	3.6
	3	252.5	336.3	21.8	8.7	4.4
	4	200.7	267.2	16.5	6.6	4.8
	5	210.0	279.6	17.8	7.1	4.3
	6	151.8	202.1	14.0	5.6	4.1
	Average	202.3	269.3	18.2	7.3	4.2
	Std. dev.	32.78	43.64	2.73	1.09	0.39
	CoV (%)	16.2	16.2	15.0	15.0	9.2
F	1	67.7	78.6	3.6	1.5	6.0
	2	56.3	65.4	3.1	1.2	5.4
	3	42.4	49.2	3.2	1.3	4.7
	4	62.8	73.0	3.9	1.6	5.2
	5	57.4	66.6	3.9	1.6	5.0
	Average	57.3	66.6	3.5	1.4	5.3
	Std. dev.	9.51	11.05	0.37	0.15	0.49
	CoV (%)	16.6	16.6	10.4	10.4	9.3
HC	1	412.8	125.9	2.1	1.4	8.9
	2	388.1	118.4	2.1	1.4	8.7
	3	532.0	162.3	2.3	1.5	11.1
	4	445.5	135.9	2.1	1.4	9.4
	5	497.9	151.9	2.3	1.5	10.1
	Average	455.3	138.9	2.2	1.4	9.7
	Std. dev.	59.41	18.12	0.08	0.05	0.97
	CoV (%)	13.0	13.0	3.8	3.8	10.1

2.4 Synthesis of materials' properties

Table 2- 24 resumes all the studied properties of both matrices used: the ettringitic matrix (E) and the natural hydraulic lime matrix (L).

Table 2- 24: Properties of the Ettringitic matrix (E) and the Natural Hydraulic Lime matrix (L).

	Ettringitic matrix (E)		Natural hydraulic lime matrix (L)	
	Mean	CoV (%)	Mean	CoV (%)
Compression strength (MPa)	11.8	5.3	7.8	3.1
Flexural strength (MPa)	4.4	13.4	2.8	5.0
Density (g/cm ³)	1.667	0.6	1.776	0.1
Initial flow diameter (cm)	17.5	-	8	-
Flow diameter after 1 hour of casting (cm)	12	-	8	-
Setting start time	1 h 50 min	-	24 h	-
Setting end time	2 h 50 min	-	28 h 50 min	-
Total setting time	1 h	-	4 h 50 min	-

Table 2- 25 resumes all the studied properties of the single hemp (H), flax (F) and bio-resin-coated hemp (HC) yarns.

Table 2- 25 : Single yarn properties of hemp, flax and bio-resin-coated hemp.

	Hemp (H)		Flax (F)		Bio-resin-coated hemp (HC)	
	Mean	CoV (%)	Mean	CoV (%)	Mean	CoV (%)
Area A _f (mm ²)	0.751	0.26	0.861	0.23	3.278	1.1
Linear density (Tex)	1200.0	6.4	1193.7	4.0	1200.0	6.4
Moisture content (%)	5.8	1.8	5.5	1.0	-	-
Water absorption (%)	pH 10.5	260	-	326	-	15.9
	pH 12.5	255	-	321	-	17.5
Water desorption (%)	pH 10.5	-3.1	-	-4.1	-	-0.1
	pH 12.5	-4.6	-	-5.0	-	-0.1
Density (g/cm ³)	1.6	6.4	1.4	4.0	5.0	18.2
Young's modulus (GPa)	4.2	9.2	5.1	11.1	9.7	10.1
Strain to failure (%)	7.3	15.0	1.4	15.7	1.4	3.8
Tensile strength (MPa)	269.3	16.2	62.1	23.6	138.8	13.0

After the physical and the mechanical characterizations of the adopted materials carried out in the present chapter, in the following three chapters, these materials are used and investigated as follow:

- In chapter 3, durability tests are carried out on the hemp (H) and the flax (F) yarns through assessing their tensile behavior after being subjected to different accelerated aging protocols. Then hemp TRM systems employing the ettringitic matrix (E) and the natural hydraulic lime matrix (L) are investigated through tensile tests at different curing ages;
- In chapter 4, durability tests on the bio-resin-coated hemp (HC) yarns through assessing their tensile behavior after being subjected to same aging protocols as used for uncoated hemp yarns. Then HC TRM systems employing E matrix and L matrix are investigated through tensile tests at different curing ages;
- In chapter 5, the bond behavior between the HC yarns and both matrices E and L, are investigated through shear bond tests on concrete and masonry elements strengthened with HC-E and HC-L TRM systems, respectively.

Chapter 3 Durability of vegetal yarns in accelerated aging solutions and in ettringitic and lime matrices

3.1 Introduction

The use of plant fibers in mineral matrices gives rise to several problems in terms of durability. The two main aging effects that arise in such alkaline environments are the alkaline hydrolysis and the mineralization process of fibers constituents. The aim of this chapter is to study the durability of hemp (H) and flax (F) yarns, by means of an experimental research intended at determining the tensile behavior of the yarns when subjected to various accelerated aging protocols. In order to reproduce the environment of the matrices used, the accelerated aging of yarns was done by immersing them in alkaline solutions having the same pH of the ettringitic (E) and hydraulic lime (L) matrices and different temperatures were used in order to accelerate the aging process. Furthermore, TRMs made from hemp textile were manufactured and tested in tension at different ages and the results were compared with the results of the accelerated aging of hemp yarns. Hemp yarns are chosen for this investigation because they are more resistant in tension than flax yarns as we have seen in chapter 2, and because they are twisted and they are easier to be weaved as a textile grid.

3.2 Accelerated aging of hemp and flax yarns

The purpose of the accelerated aging of the yarns is to reproduce an environment that could be as representative as possible of the matrix environment, and to accelerate the degradation mechanism of the fibers in a way to predict the behavior of yarns imbedded in the alkaline matrix of the TRM for a long period. Since there is a lack of standards in this field, the aging protocols have been defined to reproduce the alkalinity of the ettringitic (E) and hydraulic lime (L) matrices. Three different solutions were prepared:

- A solution of distilled water with pH 7, which is a reference solution chosen to evaluate the effect of the alkalinity of the solution on the yarn,
- A solution of sodium hydroxide with pH 10.5, which corresponds to the pH of E matrix,
- A solution of sodium hydroxide with pH 12.5, which corresponds to the pH of L matrix.

In addition, three different temperatures were selected:

- A temperature of 23°C,
- A temperature of 40°C,
- A temperature of 60°C.

The temperatures of 40°C and 60°C are used in order to accelerate the diffusion process of the alkaline ions inside the specimens, so that it accelerates the degradation of the yarn.

The yarns were subjected to tensile test after 7, 14, 28, 42, 60, 74, 90 days of immersion in the different water solutions/temperatures (even more than 90 when it is necessary). The experimental plan for the accelerated aging of the different yarns is summarized in Table 3- 26.

Table 3- 26 : Experimental plan for the accelerated aging of H and F yarns.

Solutions	(R-23)	(R-60)	(E-23)	(E-40)	(E-60)	(L-23)	(L-40)	(L-60)
Yarns	Distilled water pH 7 T = 23 °C	Distilled water pH 7 T = 60 °C	NaOH pH 10.5 T = 23 °C	NaOH pH 10.5 T = 40 °C	NaOH pH 10.5 T = 60 °C	NaOH pH 12.5 T = 23 °C	NaOH pH 12.5 T = 40 °C	NaOH pH 12.5 T = 60 °C
(H)	✓	✓	✓	✓	✓	✓	✓	✓
(F)			✓ +		✓	✓ +		✓

Aging durations

✓ :7, 14, 28, 42, 60, 74, 90 days

+ :More than 90 days

The choice of temperatures and aging durations is based on the equation (3.1) below found in Litherland et al.1981 [153] and used by Micelli and Aiello in 2019 [148]. This formula correlates the real life of the yarns and the duration of accelerated aging at a given temperature.

$$\frac{N}{C} = 0.098. e^{(0.0558T)} \tag{3.1}$$

Where:

N = age in natural days;

T = conditioning temperatures in °F;

C = days of accelerated exposure at temperature T.

The application of this formula in our case, gives us that an accelerated aging period of 90 days at 23°C corresponds to 1.5 years in real life, at 40°C it corresponds to 47 years and at 60°C it corresponds to 60 years (Table 3- 27, Figure 3- 78).

Table 3- 27 : Correlation between accelerated aging and service life of the yarns.

	T = 23°C	T = 40°C	T = 60°C
Days of accelerated exposure	Years of service life	Years of service life	Years of service life
0	0,0	0,0	0,0
7	0,1	3,7	4,6
14	0,2	7,3	9,3
28	0,5	14,7	18,6
42	0,7	22,0	27,9
60	1,0	31,4	39,8
74	1,2	38,8	49,1
90	1,5	47,2	59,7

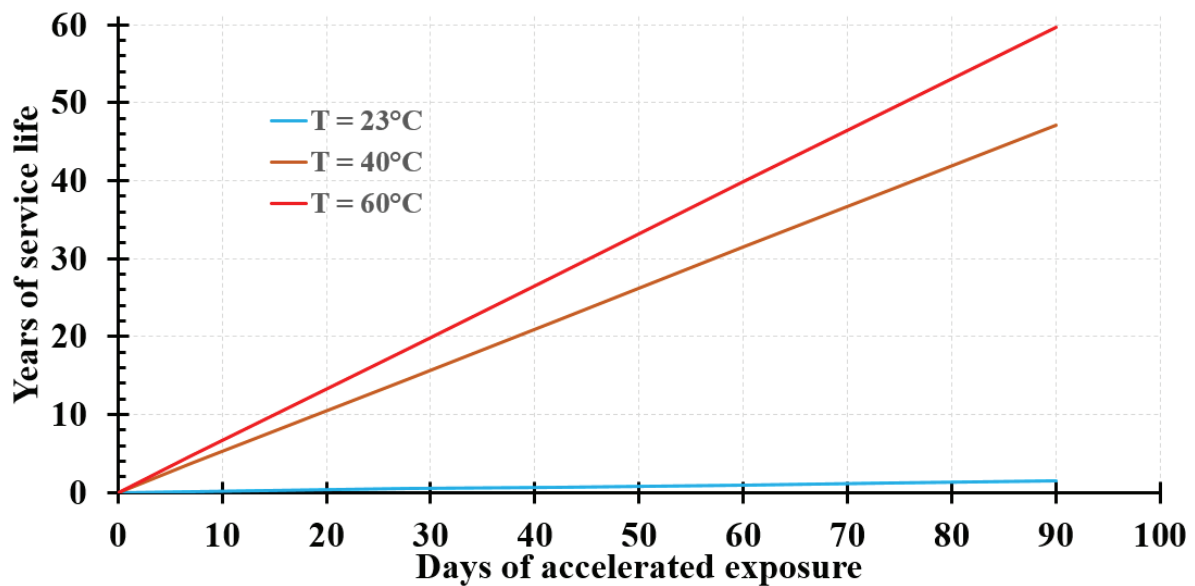


Figure 3- 78 : graphic representation of the days of accelerated aging with respect to the years of service life of the yarns.

3.2.1 Specimens preparation

The yarns were cut and immersed in the different solutions, already, prepared in plastic boxes. The specimens at 23°C are left in a controlled room temperature of 23°C (Figure 3- 79) and the ones at 40°C and 60°C, are placed in a heating chamber (Figure 3- 80).



Figure 3- 79 : Accelerated aging of yarns at $T=23^{\circ}\text{C}$.



Figure 3- 80 : Accelerated aging of yarns at $T=40^{\circ}\text{C}$ or 60°C .

After removal from the aging solution, the samples were dried in ambient conditions for 24 hours before being tested. They were weaved between two nails placed on a wooden frame as shown in Figure 3- 81.



Figure 3- 81 : Drying of the hemp and flax yarns after removal from the aging solutions.

3.2.2 Tensile test setup

Similarly to the tensile test setup used in chapter 2, Hemp (H) and Flax (F) yarns are tested in tension according to ISO 2062:2009 [170] with a gauge length of 250 mm and a loading rate of 250 mm/min, in a universal testing machine Zwick of 50 kN capacity in displacement control. To ensure alignment of the fibers and to have them straight enough, preloads of 6 N were applied to all the tested yarns. Each series was characterized by six specimens. The mechanical behavior of

yarns obtained in chapter 2 without aging was considered as a reference for the durability evaluation of aged yarns.

In the following, the name of each specimen consists of five acronyms separated by “-”: the first acronym refers to the nature of the yarn tested, it is either H (Hemp) or F (Flax). The second one refers to the pH value of the aging solution, it is either R (Reference) for pH 7, or E (Ettringitic matrix) for pH 10.5 or L (Lime matrix) for pH 12.5. The third one refers to the temperature of the aging solution; it is either 23, or 40 or 60°C. The fourth one refers to the duration of the aging, it contains a number and a letter which is either d (days) or m (months), and the fifth and last acronym refers to the specimen number in the tested series.

3.2.3 Results of tensile test on the aged H and F yarns

The results obtained by the tensile test on the aged H and F yarns revealed different behaviors due to several factors such as the material type, the exposure environment and the exposure period. First, the results of each series of yarns tested is analyzed by calculating the tensile strength σ_{\max} , the ultimate tensile strain ε_{\max} and the tensile modulus E. These results are available, in form of Tables for each series tested, in appendix B (hemp yarns) and appendix C (flax yarns). Then, a minimum curve, a maximum curve and an average stress-strain curve for each series are drawn as shown in Figure 3- 82. In order to not encumber the report, only the curves for the series H-0 are shown as an example. The stress σ refers to the ratio between the tensile load and the cross-sectional area of the yarn (0.751 mm² for H and 0.861 mm² for F). The strain ε is the ratio between the global displacement of the cross head and the gauge length of the yarn (250 mm). The elastic modulus E refers to the slope of the branch of stress-strain curve situated between 70 % and 90 % of the maximum tensile strength. Therefore, in order to better understand which are the factors that influenced the variation in mechanical properties of the different yarns after different exposure periods, the results are summarized in terms of Tables that present the tensile strength σ_{\max} , the elastic modulus E and the ultimate tensile strain ε_{\max} in the different environments at different exposure periods. These Tables are available in appendix D. In the following, in order to better understand the influence of the temperature and the alkalinity of the matrix on the tensile properties of hemp and flax yarns, the results are reported in terms of diagrams that show normalized residual values of tensile strength, Young's modulus and ultimate tensile strain in the different environments at different exposure periods. The normalized value is the ratio between the value at a given period of aging with respect to that of the same yarn but before aging. Only for the diagram that compare hemp with flax yarns the real values of σ_{\max} , ε_{\max} and E are presented.

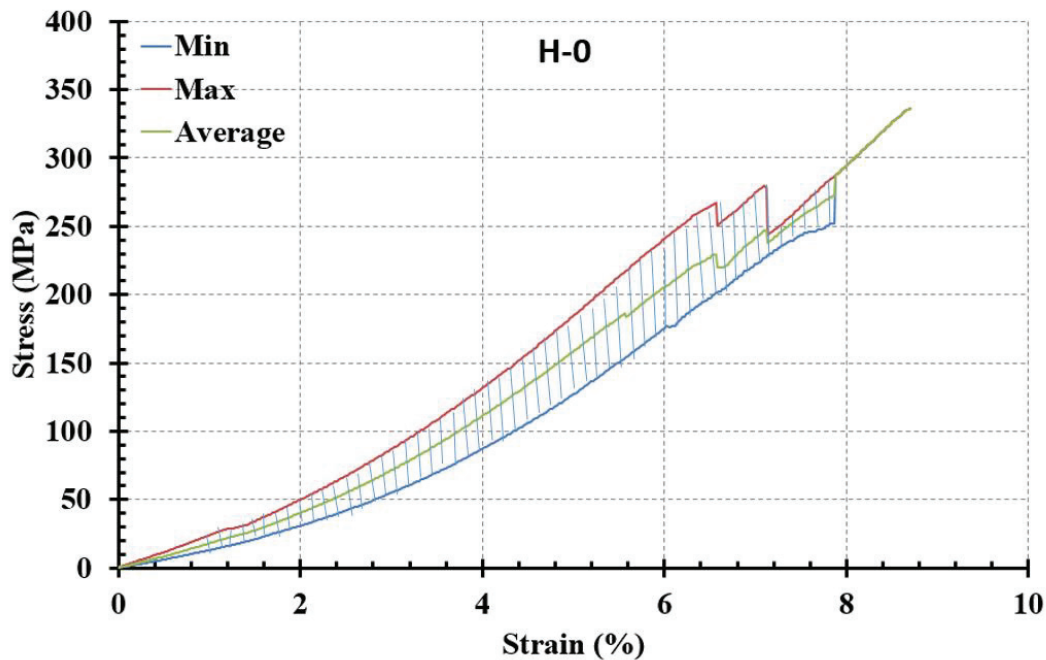


Figure 3- 82 : Minimum, maximum and average stress-strain curves obtained by the six tested specimens of series H-0.

3.2.3.1 Influence of the temperature on the behavior of the yarns over time

3.2.3.1.1 Hemp in R solutions

Figure 3- 83, Figure 3- 84 and Figure 3- 85 present the influence over time of the temperature on the average tensile strength, the average tensile modulus and the average ultimate tensile strain respectively, of hemp yarns subjected to aging in the reference solution (R). One can notice that the immersion of hemp yarns in solution R-23 up to 14 days leads to an increase of 38 % in their average tensile strength, 62 % in their average tensile modulus and 14% in their average tensile strain. Afterwards, the average tensile strength and the average tensile modulus of hemp yarns start to decrease progressively to retain only 28 % and 62 % of their initial values respectively, after 90 days of immersion. The average tensile strain continue increasing after 14 days of immersion to reach its maximum value (+ 31 %) after 42 days of immersion and then it starts to decrease progressively to retain only 58 % of its initial value, after 90 days of immersion. The immersion of hemp yarns in R-60 solution up to 7 days leads to an increase of 39 % in their average tensile strength, 45 % in their average tensile modulus and 27 % in their average tensile strain. Afterwards, the average tensile strength, the average tensile modulus and the average tensile strain of hemp yarns start to decrease progressively to retain 75 %, 110 % and 100 % of their initial values respectively, after 90 days of immersion.

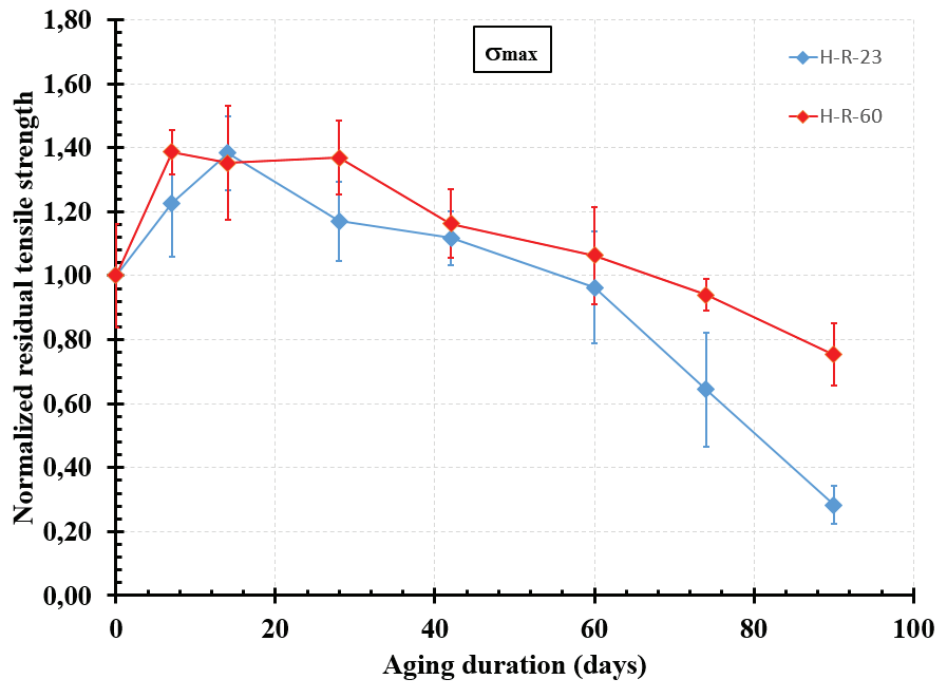


Figure 3- 83 : Influence over time of the temperature on the average tensile strength of hemp yarns (H) immersed in R solution (normalized residual values).

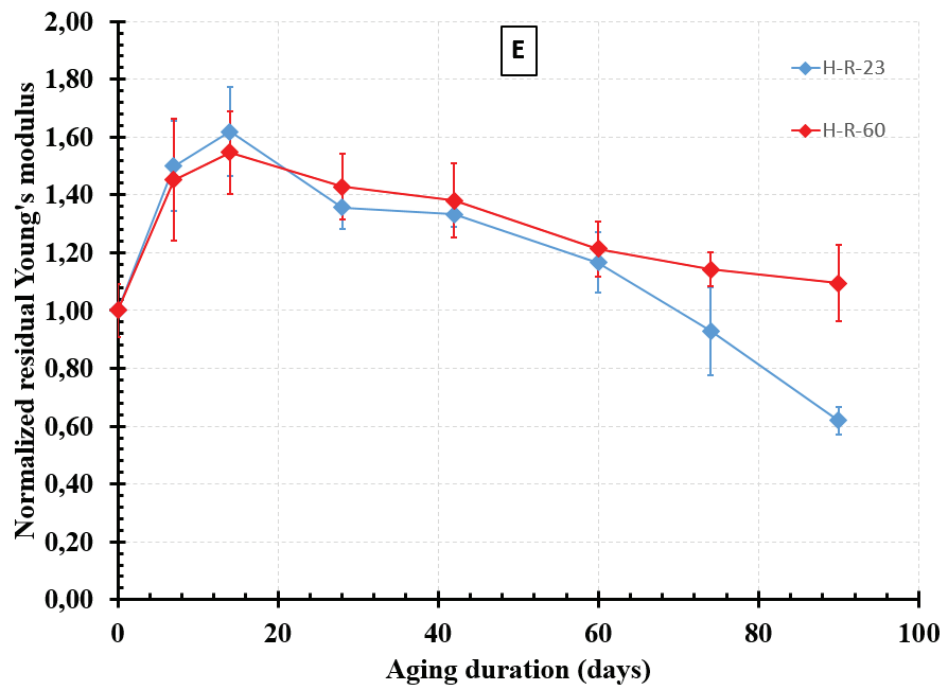


Figure 3- 84 : Influence over time of the temperature on the average tensile modulus of hemp yarns (H) immersed in R solution (normalized residual values).

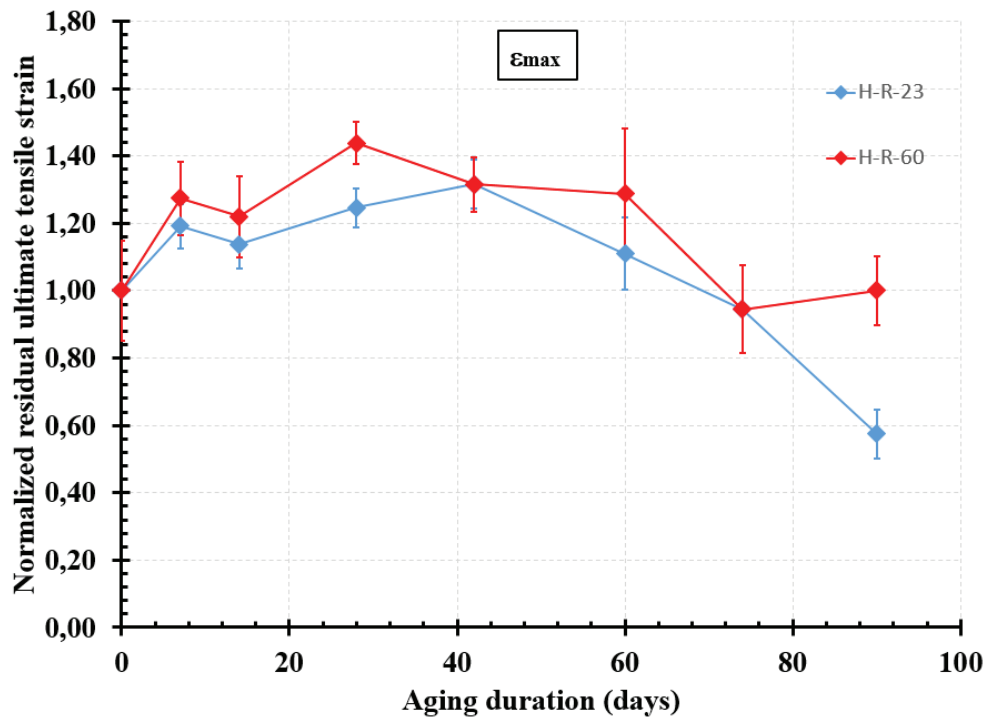


Figure 3- 85 : Influence over time of the temperature on the average ultimate tensile strain of hemp yarns (H) immersed in R solution (normalized residual values).

One can conclude that, in a first step of aging, the R solutions, having a pH 7 have beneficial effect on hemp yarn, enhancing their tensile properties. This phenomenon could be considered as the retting process [172] which is applied to the hemp fiber during the manufacturing process as we have already seen in chapter 1. The retting is a rotting process in which the pectin that binds the fibers together decomposes when it is in contact with light and air, giving the long bast fibers. In other words, it is a process resting on the (random) action of microorganisms to remove non-cellulosic components from natural fibers and separate fibers from the plant stem structure to obtain cellulose-rich fibers with higher tensile properties. Sometimes to speed up the process, retting can be done in water tanks, this technique produces finer fibers having a lighter color. However when the retting time increases, the risk of damage to the cellulosic fibers increases due to the persistent fungal growth and proliferation of a wide range of bacteria of which some may produce cellulolytic enzymes [172]. This is exactly what we observed in this study, when the retting time exceeded 14 days, the tensile strength and modulus of hemp yarns started to decrease progressively. This decrease in tensile properties was more severe when the yarns was immersed in water tanks at 23°C (R-23). So, the temperature of 60°C did not accelerated the aging of yarns as it was expected, but it played beneficial role for hemp yarns by slowing down the aging process as we have seen for solution R-60.

3.2.3.1.2 Hemp in E solutions

Figure 3- 86, Figure 3- 87 and Figure 3- 88 present the influence over time of the temperature on the average tensile strength, the average tensile modulus and the average ultimate tensile strain respectively, of hemp yarns subjected to aging in the ettringitic matrix solution (E). One can notice that the immersion of hemp yarns in solution E-23 up to 60 days leads to an increase of 17 % in their average tensile strength, 36 % in their average tensile modulus and 22 % in their average tensile strain. Afterwards, the average tensile strength, average tensile modulus and average tensile strain of hemp yarns starts to decrease progressively to retain only 5 %, 7 % and 26 % of their initial values respectively, after 90 days of immersion. The immersion of hemp yarns in solution E-40 leads to progressive decrease in their tensile characteristics until 90 days of immersion where they retain only 13 % of their average tensile strength, 38 % of their average tensile modulus and 37 % of their average tensile strain. The immersion of hemp yarns in solution E-60 up to 7 days leads to an increase of 25 % in their average tensile strength, 26 % in their average tensile modulus and 42 % in their average tensile strain. Afterwards, the average tensile strength, average tensile modulus and average tensile strain of hemp yarns start to decrease progressively to retain only 18 %, 31 % and 85 % of their initial values respectively, after 90 days of immersion.

One can conclude that, in a first step of aging, the E solutions, having a pH 10.5 at 23 and 60°C have beneficial effect on hemp yarns. This can be explained by the fact that the alkaline solution removes the non-cellulosic or in other words the amorphous components such as pectin, lignin and hemicellulose materials and impurities such as wax and oil so the fibrils become more capable of rearranging themselves along the directions of tensile deformation and become more rigid. Furthermore, this leads to an increase in the crystallinity index of the fiber, which leads to a better packing of cellulose chains and better tensile strength and modulus. This process is called mercerization in Bledzki & Gassan 1999 [173] and Kalia et al. 2009 [19]. However, we have noticed that, once the immersion period exceeds a certain value of time, the yarns undergo a progressive damage, which leads to their complete degradation. This period differs from an environment to the other. In addition, this period maybe shorter are greater depending on the method of treatment of the yarns during their manufacturing process. As we have already seen in chapter 1, sometimes during the manufacture of hemp yarns, in order to soften the fibers and improve their elasticity, they are subjected to chemical or mechanical treatment processes such as soaking the fibers in a boiling solution of soap and soda ash, and then washing these fibers with water, and soaking them in dilute acetic acid, then washing again with water, drying and combing [81]. In addition, as we all know that the soap is considered as alkaline solution since it contains NaOH.

Furthermore, since after 90 days of immersion, the hemp yarns are completely damaged in solutions E-23, E-40 and E-60 having same pH but different temperatures, and since the average tensile strengths of hemp yarns, are greater at 60°C than at 40°C at all the studied durations. We can conclude that the temperature did not play an accelerating role for the diffusion of the aggressive fluid inside the hemp yarns.

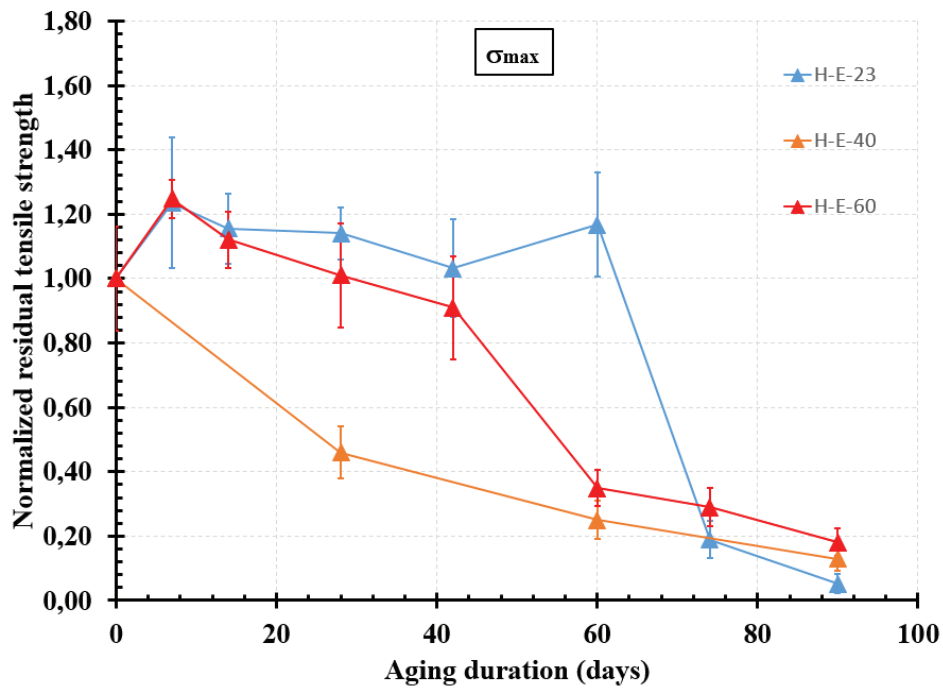


Figure 3- 86 : Influence over time of the temperature on the average tensile strength of hemp yarns (H) immersed in E solution (normalized residual values).

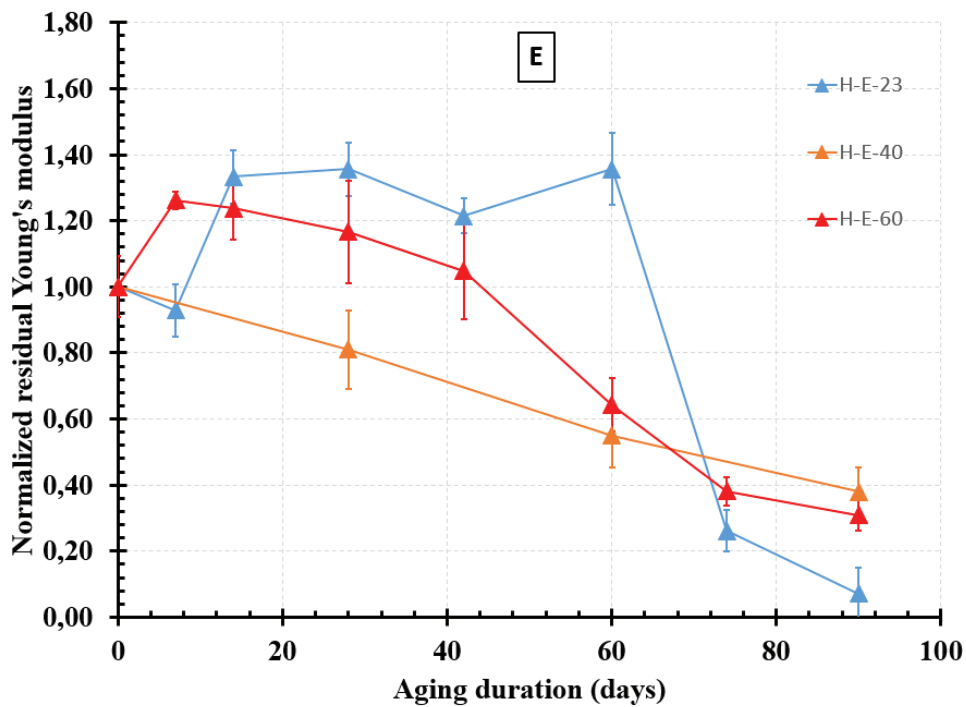


Figure 3- 87 : Influence over time of the temperature on the average tensile modulus of hemp yarns (H) immersed in E solution (normalized residual values).

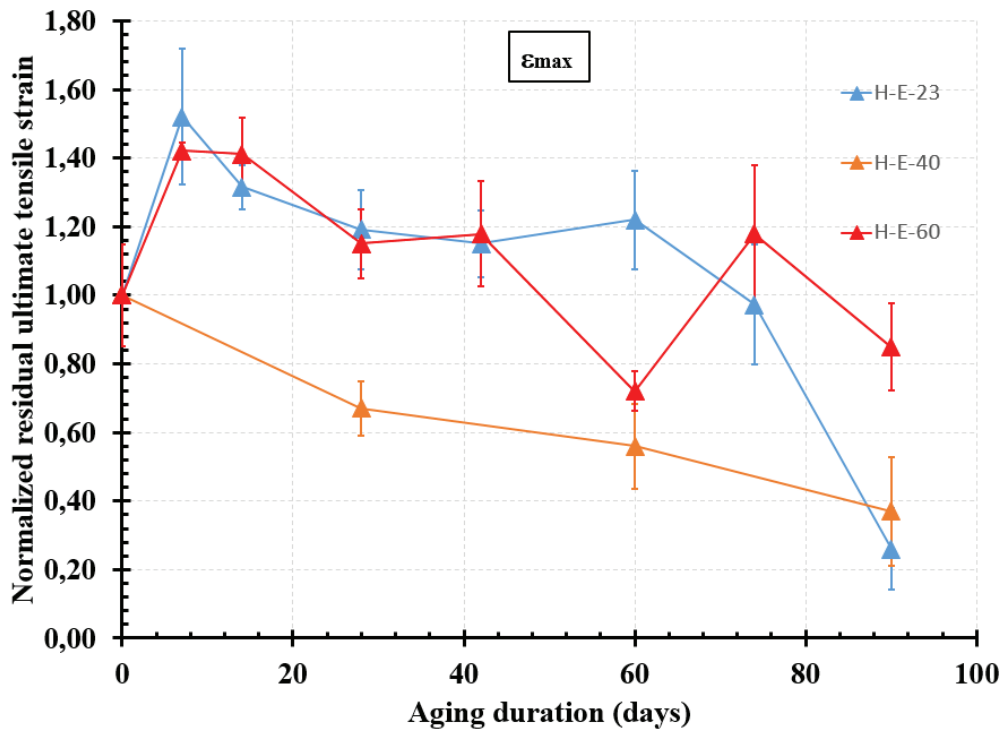


Figure 3- 88 : Influence over time of the temperature on the average ultimate tensile strain of hemp yarns (H) immersed in E solution (normalized residual values).

3.2.3.1.3 Hemp in L solutions

Figure 3- 89, Figure 3- 90 and Figure 3- 91 present the influence over time of the temperature on the average tensile strength, the average tensile modulus and the average ultimate tensile strain respectively, of hemp yarns subjected to aging in the natural hydraulic lime matrix solution (L). One can notice that the immersion of hemp yarns in solution L-23 up to 28 days leads to an increase of 28 % in their average tensile strength, 24 % in their average tensile modulus and 48 % in their average tensile strain. Afterwards, the average tensile strength, average tensile modulus and average tensile strain of hemp yarns start to decrease progressively to retain only 2 %, 12 % and 14 % of their initial values respectively, after 90 days of immersion. The immersion of hemp yarns in solution L-40 up to 28 days leads to an increase of 18 % in their average tensile strength, 43 % in their average tensile modulus and 18 % in their average tensile strain. After 90 days of immersion, the hemp yarns can retain 100 % of their average tensile strength, 124 % of their average tensile modulus and 115 % of their average tensile strain. The immersion of hemp yarns in solution L-60 up to 14 days leads to an increase of 24 % in their average tensile strength, 29 % in their average tensile modulus and 48 % in their average tensile strain. Afterwards, the average tensile strength, average tensile modulus and average tensile strain of hemp yarns start to decrease progressively, but they did not undergo a sharp decrease, as it is the case in solution L-23 because they could retain 102 % and 131 % and 115 % of their initial values respectively, after 90 days of immersion. It is worth reminding that the scattering of the results and the re-increase of the tensile properties after a decrease as it is the case in solution L-60 (a new increase in the tensile properties

appeared at 90 days) is considered normal because plant fibers are inhomogeneous by their own nature, their properties vary within a large range depending on several factors such as the weather conditions during the growth of the plant, the harvesting process, and the retting process...

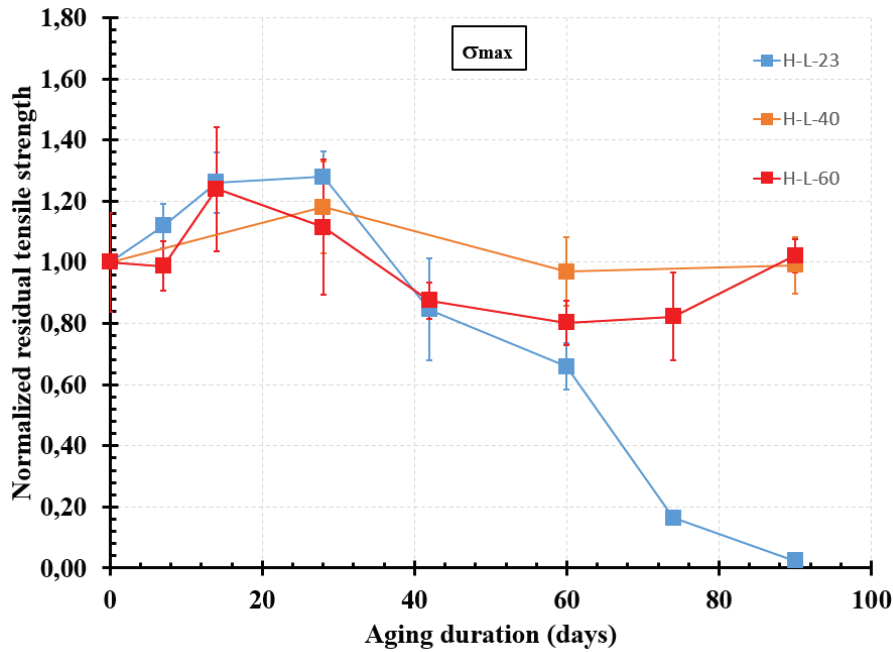


Figure 3- 89 : Influence over time of the temperature on the average tensile strength of hemp yarns (H) immersed in L solution (normalized residual values).

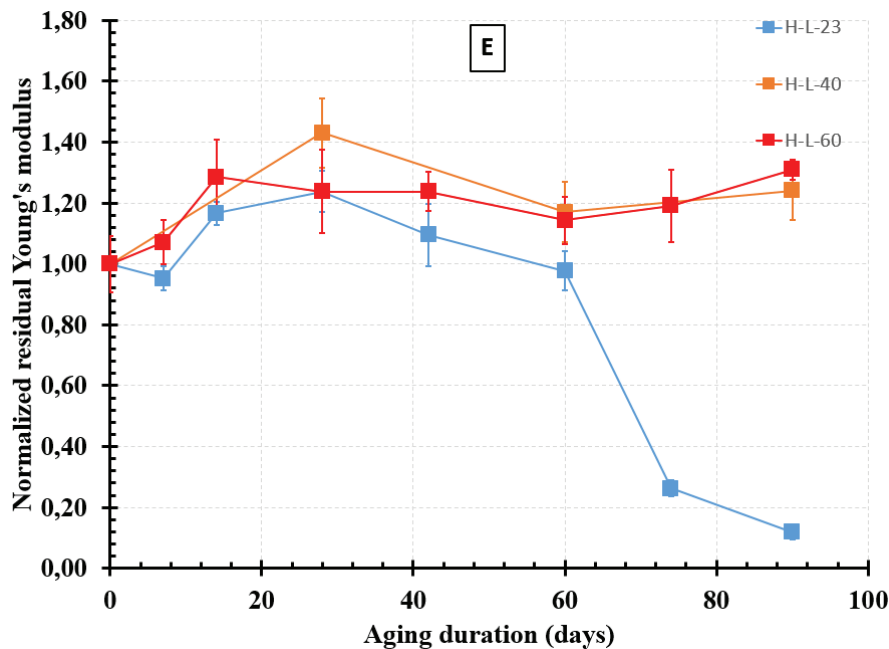


Figure 3- 90 : Influence over time of the temperature on the average tensile modulus of hemp yarns (H) immersed in L solution (normalized residual values).

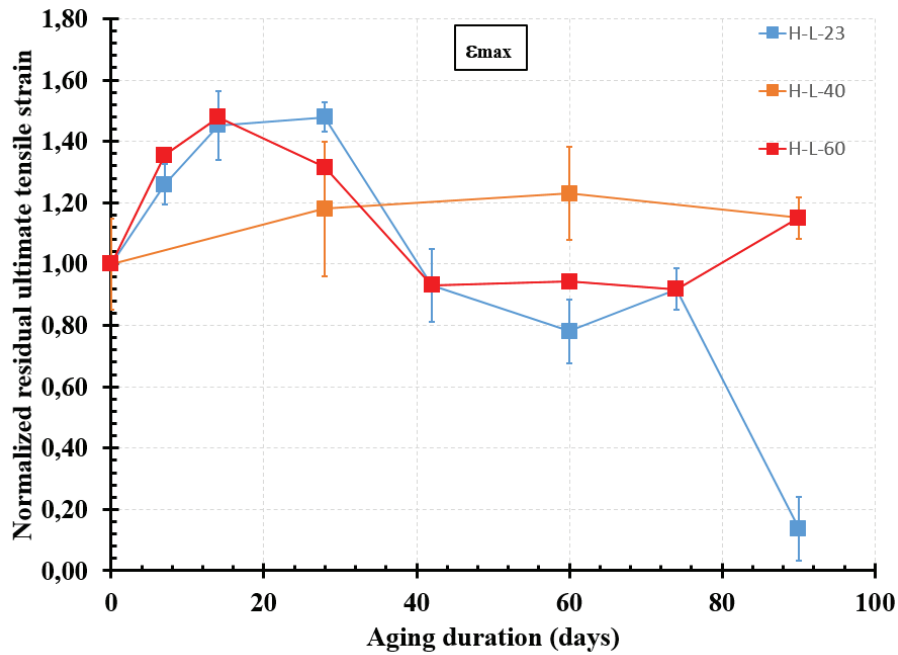


Figure 3- 91 : Influence over time of the temperature on the average ultimate tensile strain of hemp yarns (H) immersed in L solution (normalized residual values).

We can conclude that, in a first step of aging, the L solutions, having a pH 12.5 have beneficial effect on hemp yarn, allowing them to undergo the process of mercerization [19]. Then at 23°C, as we have seen before in case of E-solutions, once the immersion period exceeds a certain value of time, the yarns undergo a progressive damage, which leads to their complete degradation after 90 days of aging. However, at 40 and 60°C, the yarns still have good tensile strength and properties after 90 days of aging. These are the only alkaline environment, which has beneficial effect on the hemp yarns for allowing them to retain good tensile properties. Thus, the heating up to 60°C along with pH 12.5 did not damage the fiber as it was expected but they played beneficial role for hemp yarns by slowing down the aging process. This process could also be considered as a mechanical treatment of the fibers in hot solution of soap already seen in chapter 1, in order to soften the fibers and improve their elasticity [81]. Maybe the curing of natural hydraulic lime matrix (pH 12.5) at 40 and 60°C have beneficial effects on the hemp yarns by retarding their degradation thus improving the mechanical performance of H-L TRM. Further experimental and analytical work is needed on real H-L TRM specimens cured at 40 and 60°C to verify this hypothesis. This is found to be true for other types of yarn. For example, in the study of Estevan et al. 2022 [174], a TRM made from polymer-coated alkali resistant (AR) glass fiber meshes imbedded in a ready-mixed mortar made from natural hydraulic lime, reactive inorganic compounds, natural sand, special admixtures and micro-fibers have been subjected to temperatures of 20, 100, 200, 400 and 600 °C, for one hour. Then they were cooled slowly for 24 hours, and they were tested in tension. They observed a clear improvement in the behavior of these composite subjected to temperature up to 200 °C. They attributed this improvement to two reasons: (i) during the cooling process that

follows the thermal treatment, a shrinkage of the mortar matrix occurs that improves the adhesion with the fibers, an effect that is increased as the water contained in the material evaporates. (ii) at these temperature levels it has been found that some polymers with which the meshes are coated change from viscoelastic to plastic state with heat, recovering their original state upon cooling, a process that improves the adhesion between the fibers and the matrix.

3.2.3.1.4 Flax in E solution

Figure 3- 92, Figure 3- 93 and Figure 3- 94 present the influence over time of the temperature on the average tensile strength, the average tensile modulus and the average ultimate tensile strain respectively, of flax yarns subjected to aging in the ettringitic matrix solution (E). One can notice that the immersion of flax yarns in solution E-23 up to 60 days leads to an increase of 40 % in their average tensile strength and 85 % in their average tensile strain. Then, after 90 days of immersion, the flax yarns can retain about 90 % of their initial average tensile strength, 72 % of their initial average tensile modulus and 114 % of their initial average tensile strain. However, when flax yarns are subjected to E-60 solution, the average tensile strength and modulus start to decrease immediately and progressively to retain only 28 % and 28 % of their initial values respectively, after 90 days of immersion. While the average tensile strain increases from the beginning to reach its maximum value (+ 114 %) after 74 days of immersion. This increase in tensile strain along with the decrease in tensile strength and modulus is the result of the plasticization effect of the water within the fiber, which weakens intermolecular bonding such as Van der Waals forces, reduces fiber crystallinity, but increases the mobility of macromolecular chains, the plasticity and the flexibility of the fiber [175].

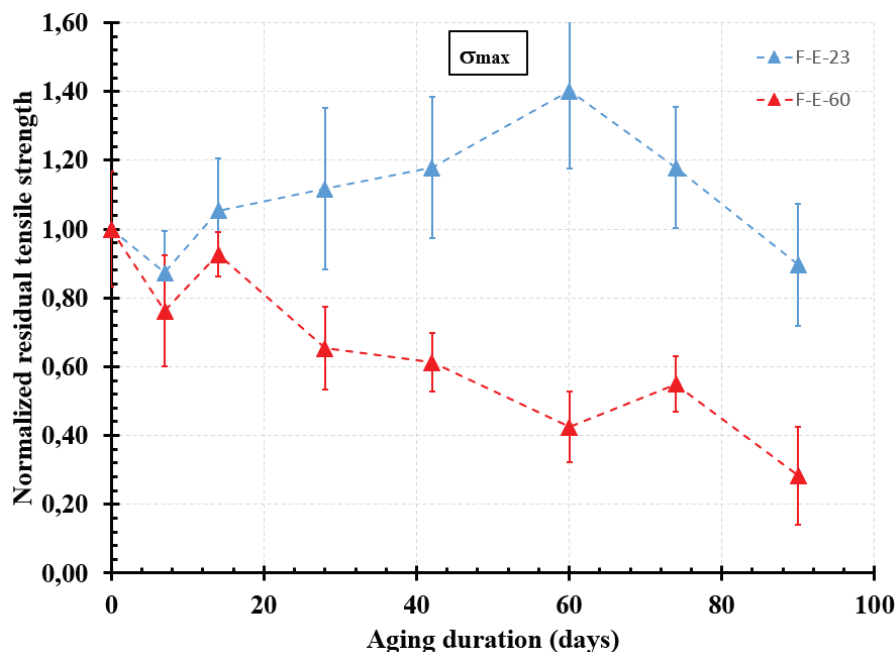


Figure 3- 92 : Influence over time of the temperature on the average tensile strength of flax yarns (F) immersed in E solution (normalized residual values).

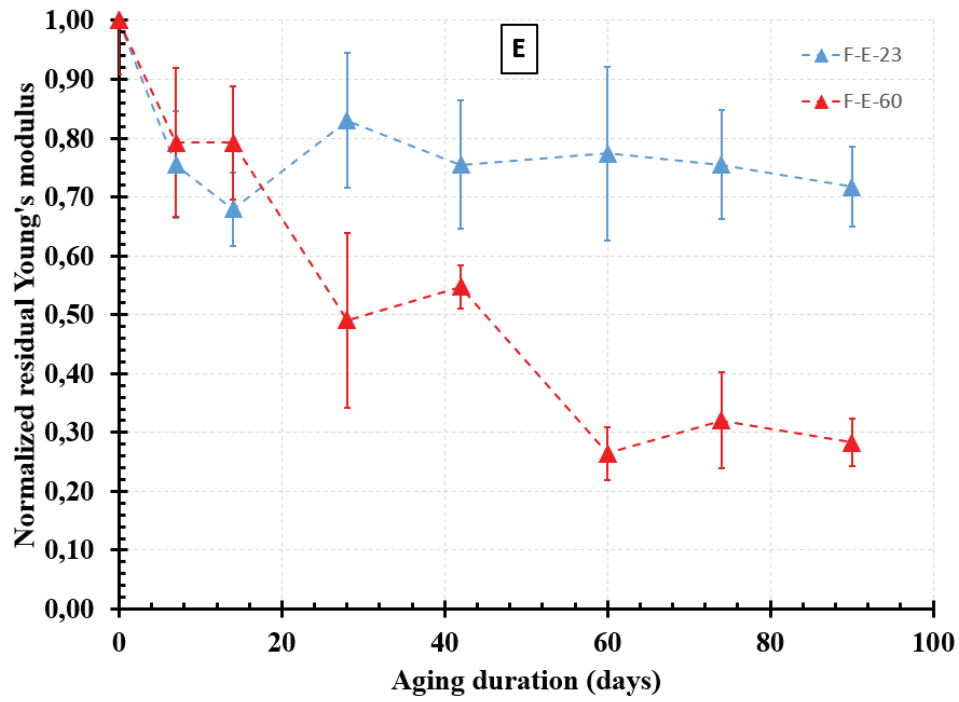


Figure 3- 93 : Influence over time of the temperature on the average tensile modulus of flax yarns (F) immersed in E solution (normalized residual values).

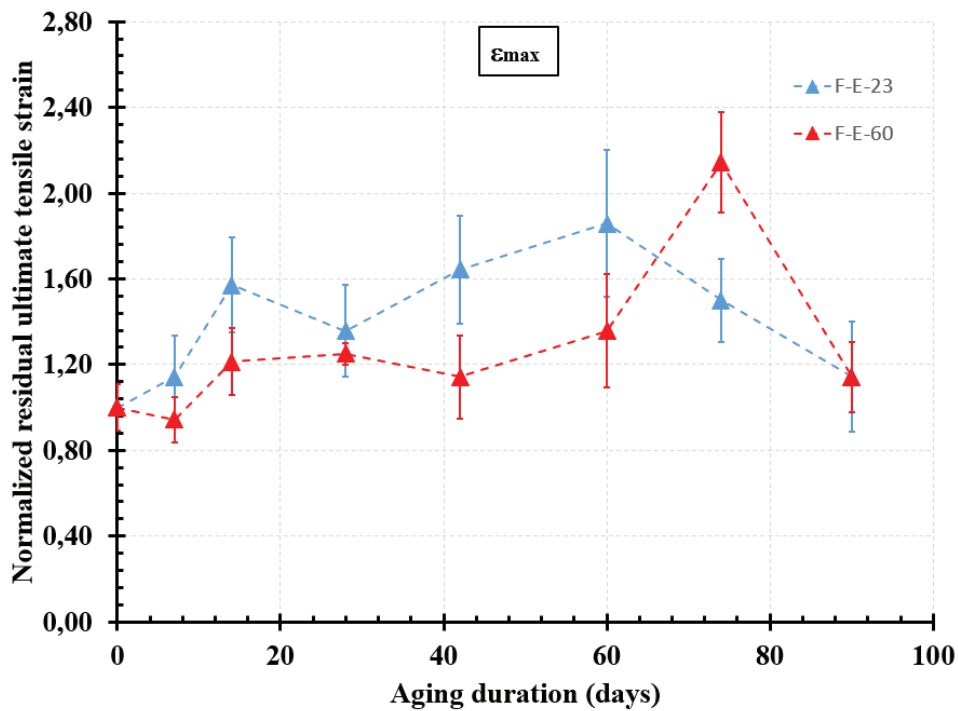


Figure 3- 94 : Influence over time of the temperature on the average ultimate tensile strain of flax yarns (F) immersed in E solution (normalized residual values).

One can conclude that, in a first step of aging in E solution at 23°C, the flax yarns undergo a mercerization process [19] and reach their best tensile properties after 60 days of immersion . Then, when the aging process continue, they could retain good properties after 90 days of immersion. However, the same did not happen at a temperature of 60°C, where the yarns immediately undergo a progressive decrease in their tensile properties without undergoing a mercerization process and the E-60 solution was the most severe environment on flax yarns. Thus, we can conclude that, unlike for hemp yarns, the temperature of 60°C along with the pH 10.5 did not allow the occurring of the mercerization process but from the first time they played an accelerating role for the diffusion of the aggressive fluid inside the flax yarns, thus accelerating the aging of the yarns by reducing their tensile strength and modulus and increasing their elongation.

3.2.3.1.5 Flax in L solution

Figure 3- 95, Figure 3- 96 and Figure 3- 97 present the influence over time of the temperature on the average tensile strength, the average tensile modulus and the average ultimate tensile strain respectively, of flax yarns subjected to aging in the natural hydraulic lime matrix solution (L). One can notice that the immersion of flax yarns in solution L-23 up to 74 days leads to an increase of 22 % in their average tensile strength and 71 % in their average tensile strain. Then, after 90 days of immersion, the flax yarns can retain about 88 % of their initial average tensile strength, 60 % of their initial average tensile modulus and 185 % of their average ultimate tensile strain. This increase in tensile strain along with the decrease in tensile strength and modulus is the result of the plasticization effect of the water within the fiber [175]. However, when flax yarns are subjected to L-60 solution, the average tensile strength and modulus start to decrease immediately and progressively, but they can retain about 80 % of their initial average tensile strength, 47 % of their initial average modulus, after 90 days of immersion. Furthermore, they undergo the plasticization process by having an increase of 150 % of their initial tensile strain after 90 days of immersion.

One can conclude that, in a first step of aging in L solution at 23°C, the flax yarns undergo a mercerization process [19] and reach their best tensile properties after 74 days of immersion. Then, when the aging process continue, they undergo the plasticization process [175] by having a decrease in their tensile strength and modulus and an increase in their tensile strain. However, at a temperature of 60°C, when the yarns did not undergo the mercerization process, they immediately undergo a progressive decrease in their tensile strength and modulus. But they undergo the plasticization process. Thus, we can conclude that the temperature of 60°C did not allow the occurring of the mercerization process. One can also notice that, after 90 days of immersion the flax yarns have comparative tensile properties in both solutions (L-23 and L-60). So we can conclude that the temperature did not play an accelerating role for the diffusion of the aggressive fluid inside the flax yarns when they are immersed in L solution (pH 12.5), which is not the case when flax yarns where immersed in E solution (pH 10.5).

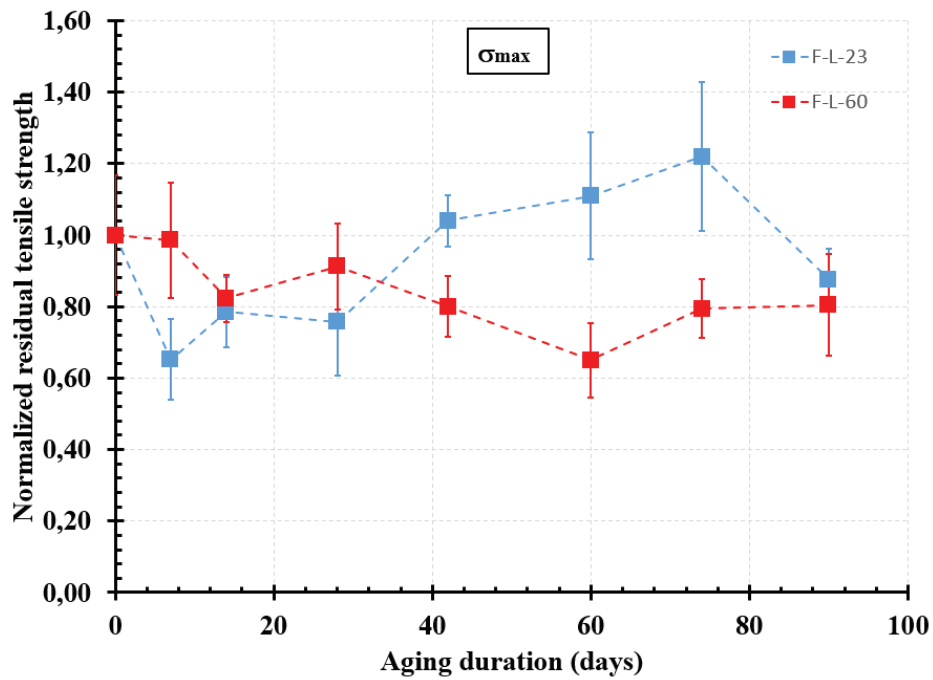


Figure 3- 95 : Influence over time of the temperature on the average tensile strength of flax yarns (F) immersed in L solution (normalized residual values).

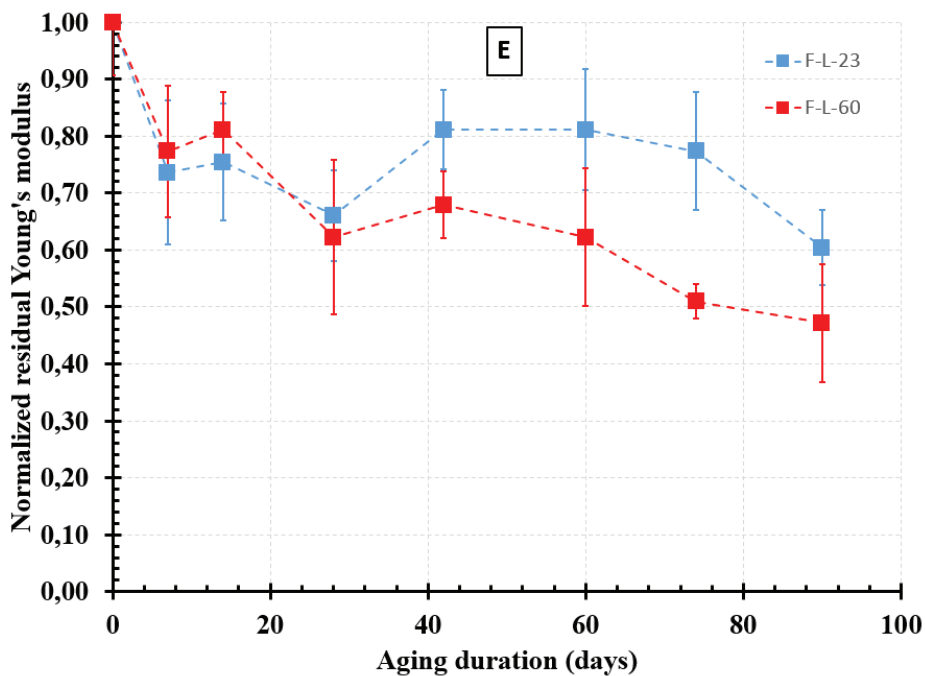


Figure 3- 96 : Influence over time of the temperature on the average tensile modulus of flax yarns (F) immersed in L solution (normalized residual values).

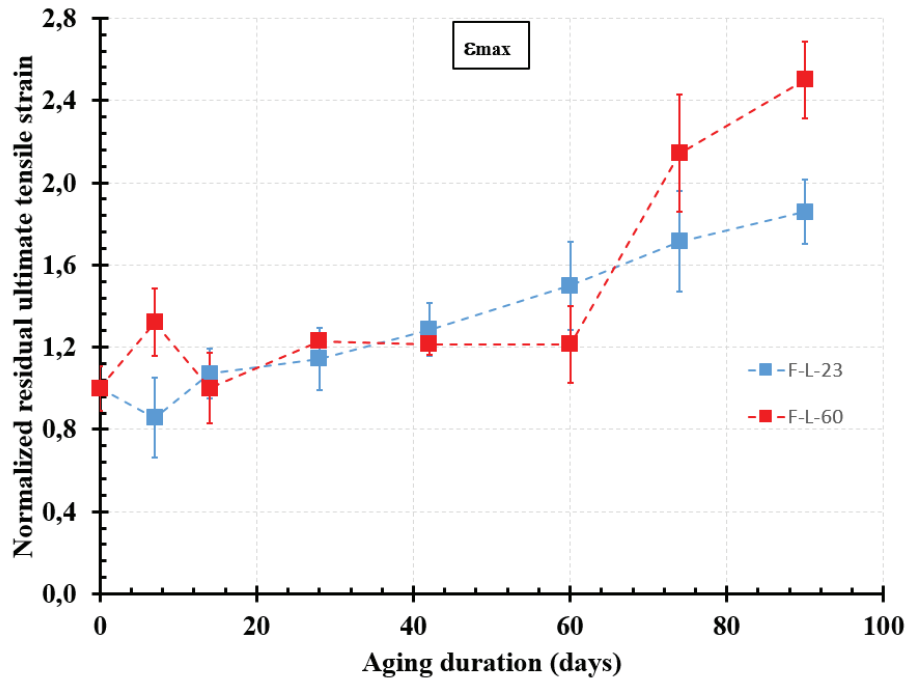


Figure 3- 97 : Influence over time of the temperature on the average ultimate tensile strain of flax yarns (F) immersed in L solution (normalized residual values).

3.2.3.2 Influence of the pH on the tensile behavior of the yarns over time

3.2.3.2.1 Hemp at 23°C

Figure 3- 98, Figure 3- 99 and Figure 3- 100 present the influence over time of the pH on the average tensile strength, the average tensile modulus and the average ultimate tensile strain respectively, of hemp yarns subjected to aging at 23°C. One can notice that, at 23°C in all the studied solutions, the hemp yarns undergo first an increase in their average tensile properties; this process is called retting [172] when the yarns are subjected to water and mercerization [173], [19] when they are subjected to NaOH solutions. Then, they undergo a sharp decrease in their average tensile properties after 90 days of immersion, leading to their complete damage. So we can conclude that not only the alkaline solutions leads to the degradation of the natural fibers, but also these fibers lose their tensile characteristics when they are subjected to distilled water only. Thus at 23°C, the degree of alkalinity of the matrix did not have a big influence on the period at which the yarns degrades completely. However, it influences the period at which the mercerization process stops and the decrease in the tensile properties starts. For pH 10.5, it is 60 days and for pH 12.5, it is 28 days. Therefore, we can conclude that, at 23°C the mercerization process is faster when the pH is greater.

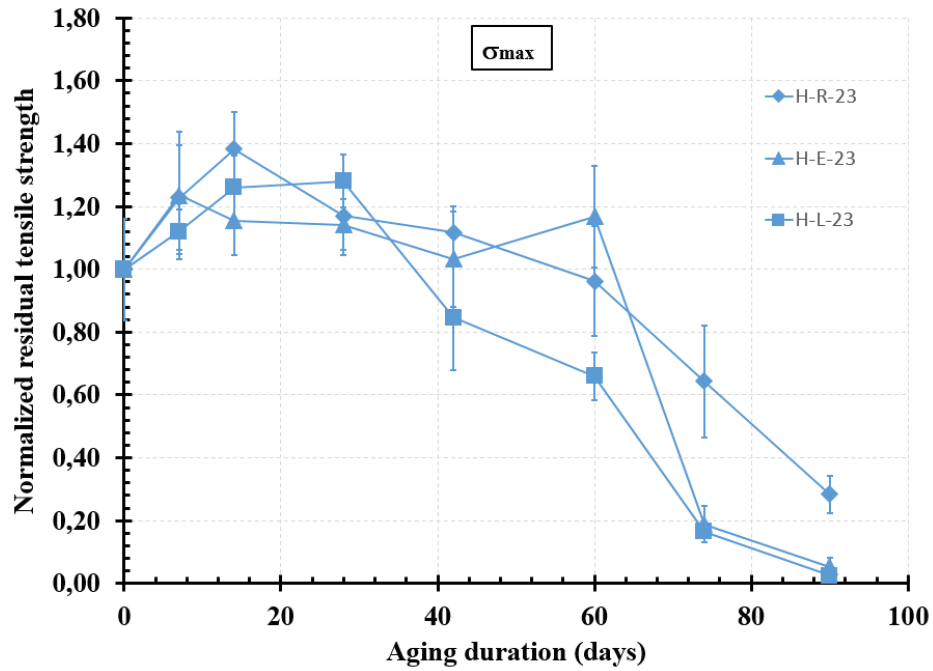


Figure 3- 98 : Influence over time of the pH on the average tensile strength of hemp yarn (H) at 23°C (normalized residual values).

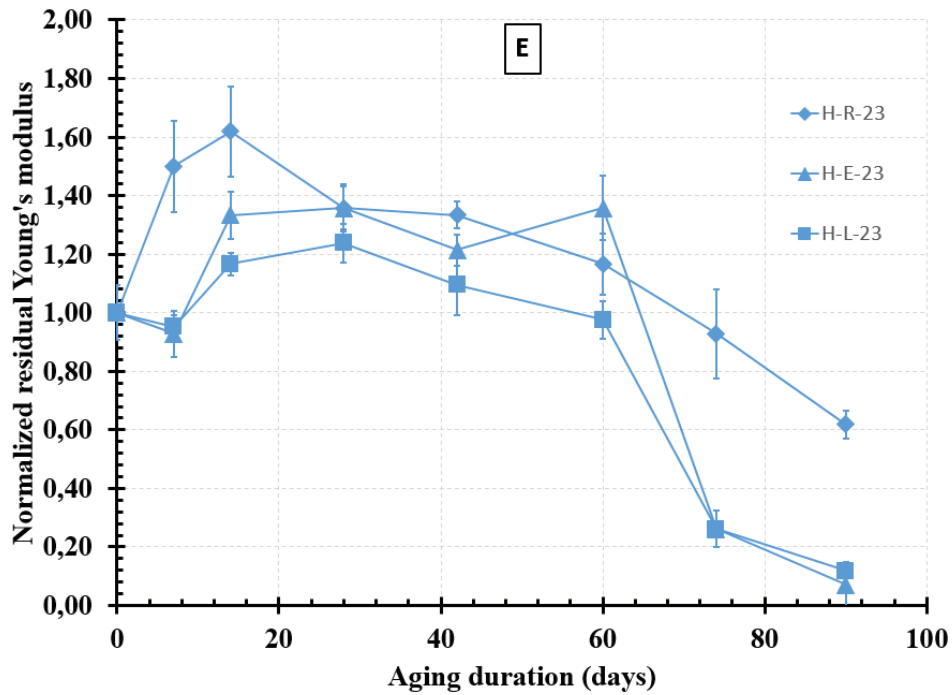


Figure 3- 99 : Influence over time of the pH on the average tensile modulus of hemp yarn (H) at 23°C (normalized residual values).

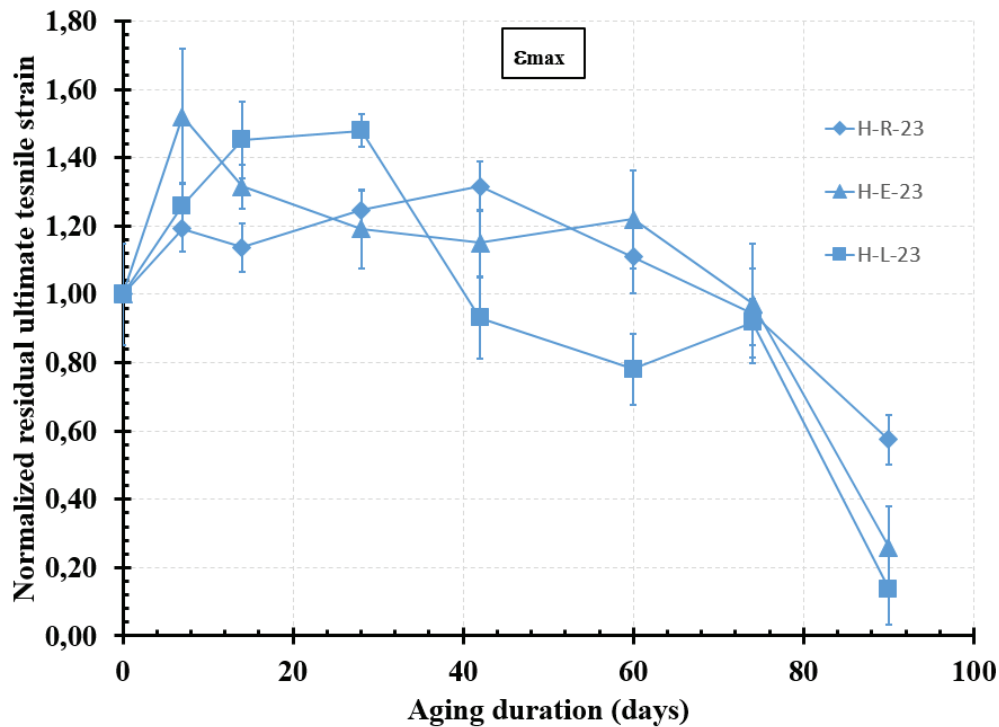


Figure 3- 100 : Influence over time of the pH on the average ultimate tensile strain of hemp yarn (H) at 23°C (normalized residual values).

3.2.3.2.2 Hemp at 40°C

Figure 3- 101, Figure 3- 102 and Figure 3- 103 present the influence over time of the pH on the average tensile strength, the average tensile modulus and the average ultimate tensile strain respectively, of hemp yarns subjected to aging at 40°C. One can notice that at 40°C, when hemp yarns are immersed in solution E, they undergo a sharp decrease in their average tensile properties after 90 days of immersion, leading to their complete damage. However, when hemp yarns are immersed in L solution, they first undergo the mercerization process at 28 days and then they can retain good tensile properties after 90 days of immersion. Thus at 40°C, the degree of alkalinity of the matrix influences the period at which the yarns degrade completely. Therefore, we can conclude that, at 40°C the degradation process is slower when the pH is greater. We cannot conclude about the period at which the mercerization process stops and the decrease in the tensile properties starts, since we do not have data between 0 and 28 days.

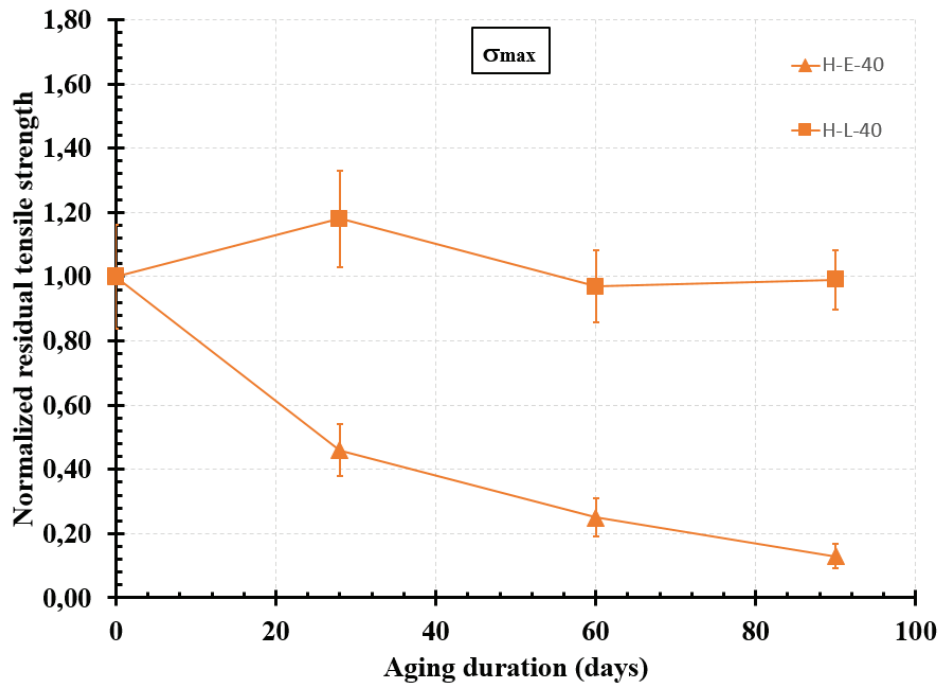


Figure 3- 101 : Influence over time of the pH on the average tensile strength of hemp yarn (H) at 40°C (normalized residual values).

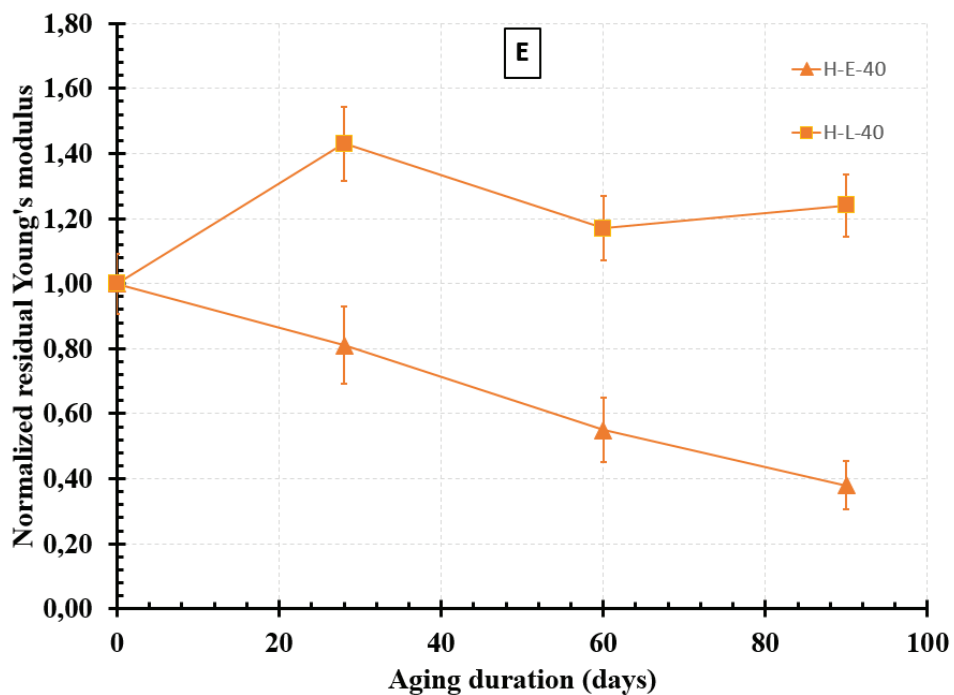


Figure 3- 102 : Influence over time of the pH on the average tensile modulus of hemp yarn (H) at 40°C (normalized residual values).

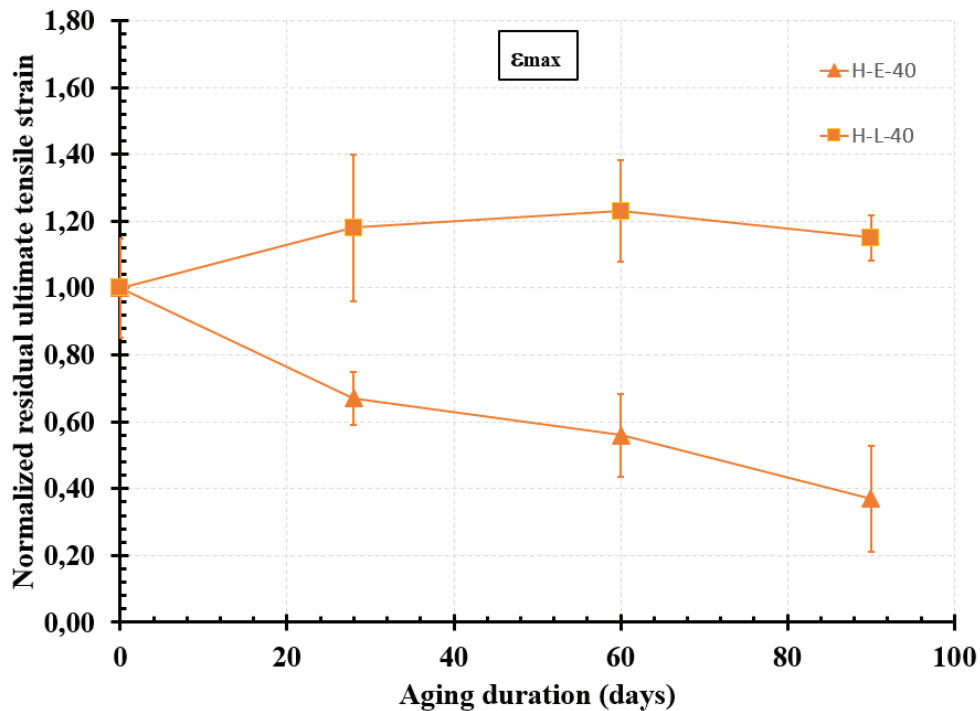


Figure 3- 103 : Influence over time of the pH on the average ultimate tensile strain of hemp yarn (H) at 40°C (normalized residual values).

3.2.3.2.3 Hemp at 60°C

Figure 3- 104, Figure 3- 105 and Figure 3- 106 present the influence over time of the pH on the average tensile strength, the average tensile modulus and the average ultimate tensile strain respectively, of hemp yarns subjected to aging at 60°C. One can notice that at 60°C, when hemp yarns are immersed in solution E, they undergo first a mercerization process after 7 days, and then they undergo a sharp decrease in their average tensile strength and modulus after 90 days of immersion, leading to their complete damage. However, when hemp yarns are immersed in R solution, they undergo the retting process after 28 days and L solutions, they undergo the mercerization process after 14. Then, in both solution R and L, they retain good tensile properties after 90 days of immersion. Thus, at 60°C the degree of alkalinity of the matrix influences the period at which the mercerization process stops and the decrease in the tensile properties starts. For pH 10.5, it is 7 days and for pH 12.5, it is 14 days. Therefore, we can conclude that, at 60°C the mercerization process is slower when the pH is greater. It also influences the period at which the yarns degrade completely. For pH 10.5, it is 90 days, and for pH 7 and 12.5, it is not attained yet, so it is greater than 90 days.

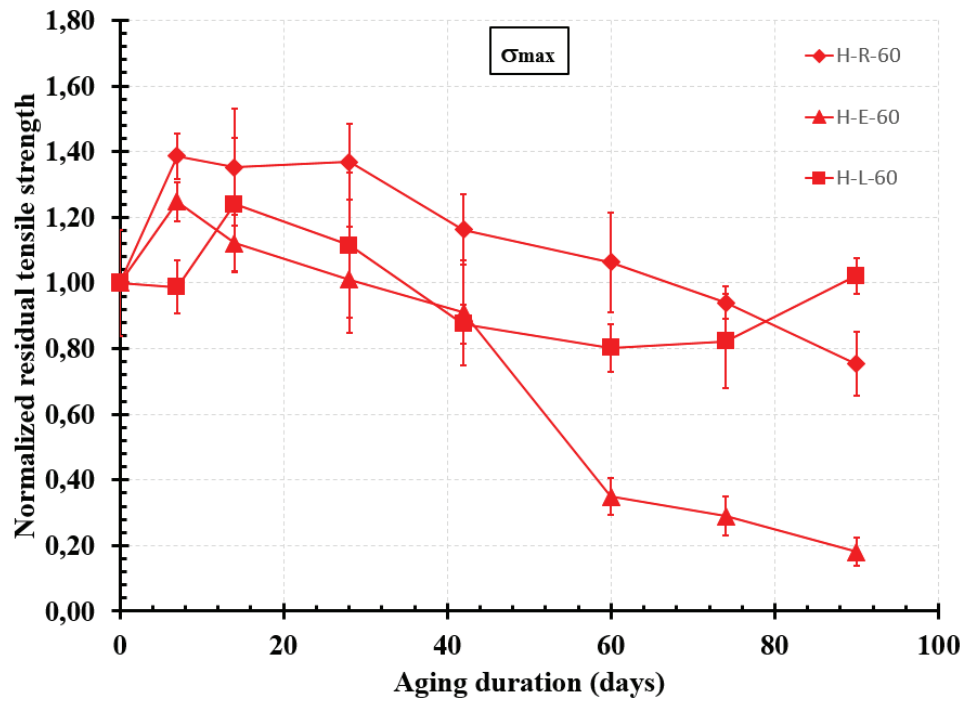


Figure 3- 104 : Influence over time of the pH on the average tensile strength of hemp yarn (H) at 60°C (normalized residual values).

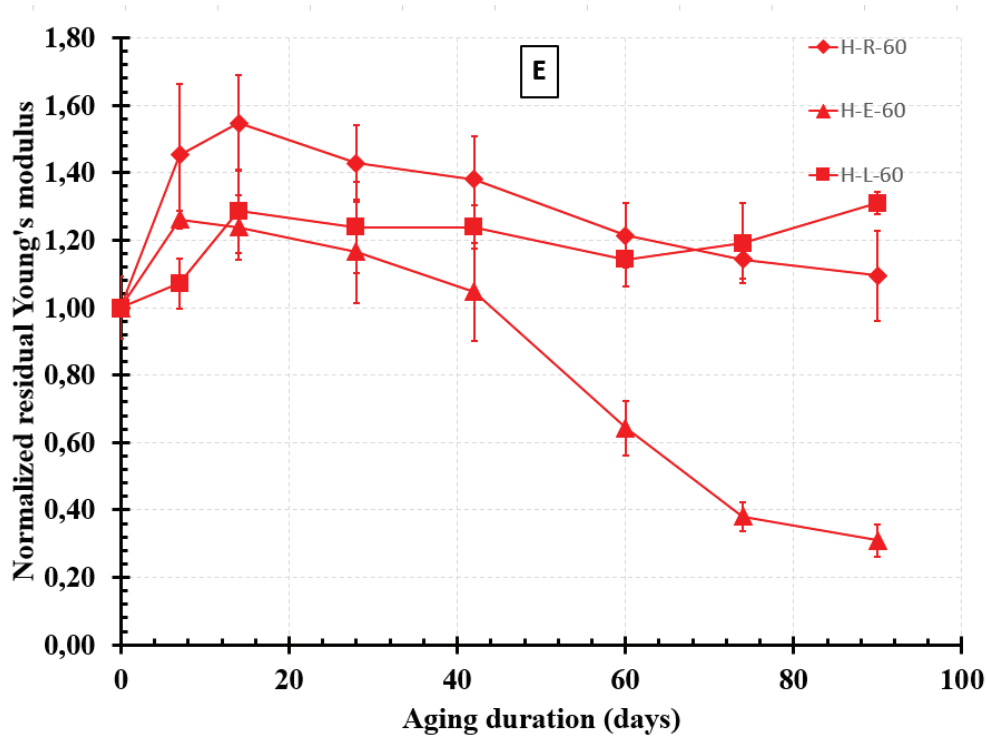


Figure 3- 105 : Influence over time of the pH on the average tensile modulus of hemp yarn (H) at 60°C (normalized residual values).

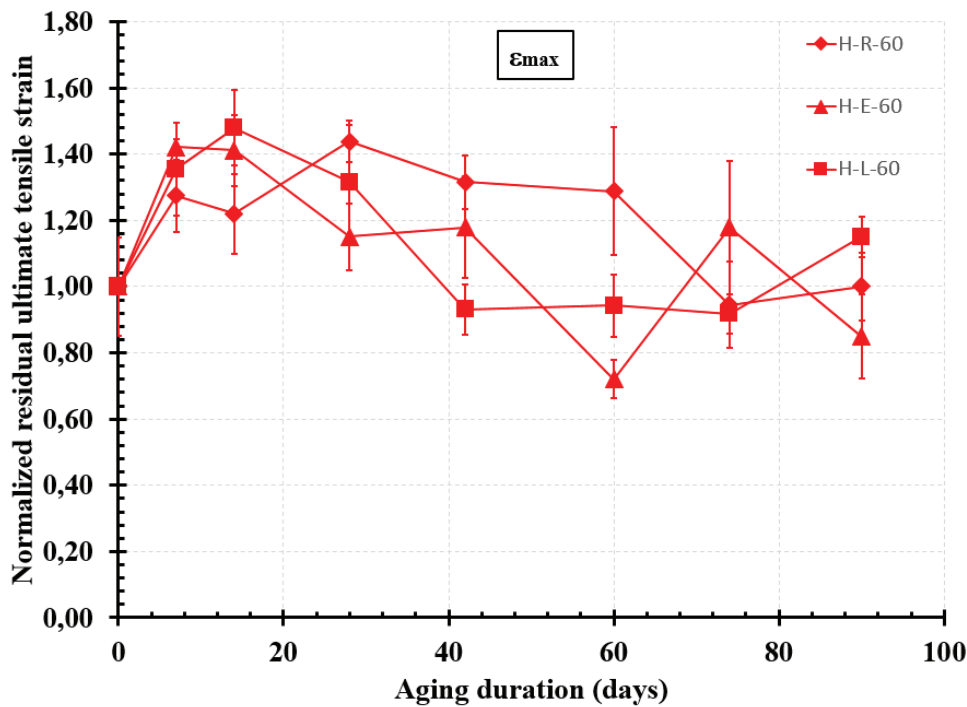


Figure 3- 106 : Influence over time of the pH on the average ultimate tensile strain of hemp yarn (H) at 60°C (normalized residual values).

3.2.3.2.4 Flax at 23°C

Figure 3- 107, Figure 3- 108 and Figure 3- 109 present the influence over time of the pH on the average tensile strength, the average tensile modulus and the average ultimate tensile strain respectively, of flax yarns subjected to aging at 23°C. One can notice that, at 23°C when flax yarns are immersed in solution E and L, their average tensile properties increase progressively to undergo a mercerization process after 60 and 74 days respectively. Then, after 210 days of immersion, they undergo a small decrease in their average tensile strength and modulus but an increase in their average ultimate tensile strain. This could be related to the plasticization effect of the water within the fiber [175]. Thus at 23°C, the degree of alkalinity of the matrix did not influence the degradation of flax yarns, since there is no big difference in tensile properties between the yarns subjected to pH 10.5 and the others subjected to pH 12.5. However, the pH influences the period at which the mercerization process stops and the decrease in the tensile properties starts. For pH 10.5, it is 60 days and for pH 12.5, it is 74 days. Therefore, we can conclude that, at 23°C the mercerization process of flax yarns is slower when the pH is greater.

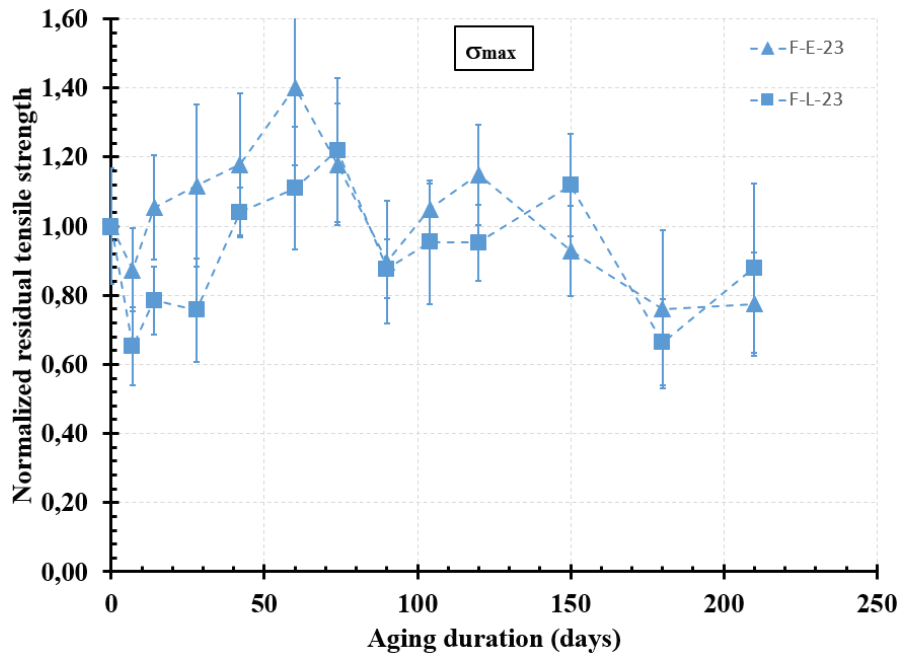


Figure 3- 107 : Influence over time of the pH on the average tensile strength of flax yarn (F) at 23°C (normalized residual values).

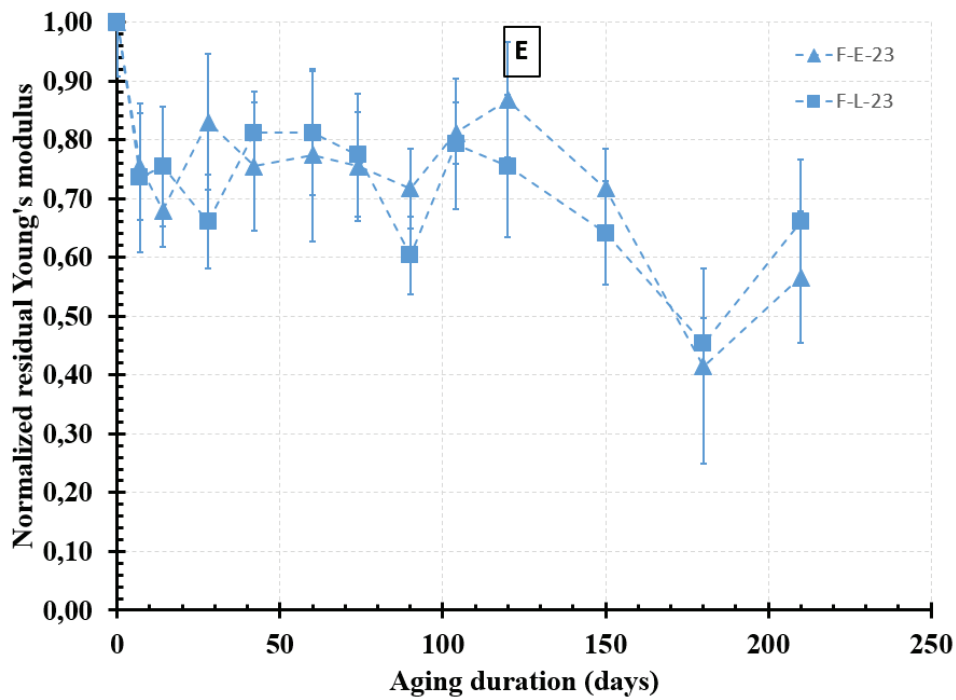


Figure 3- 108 : Influence over time of the pH on the average tensile modulus of flax yarn (F) at 23°C (normalized residual values).

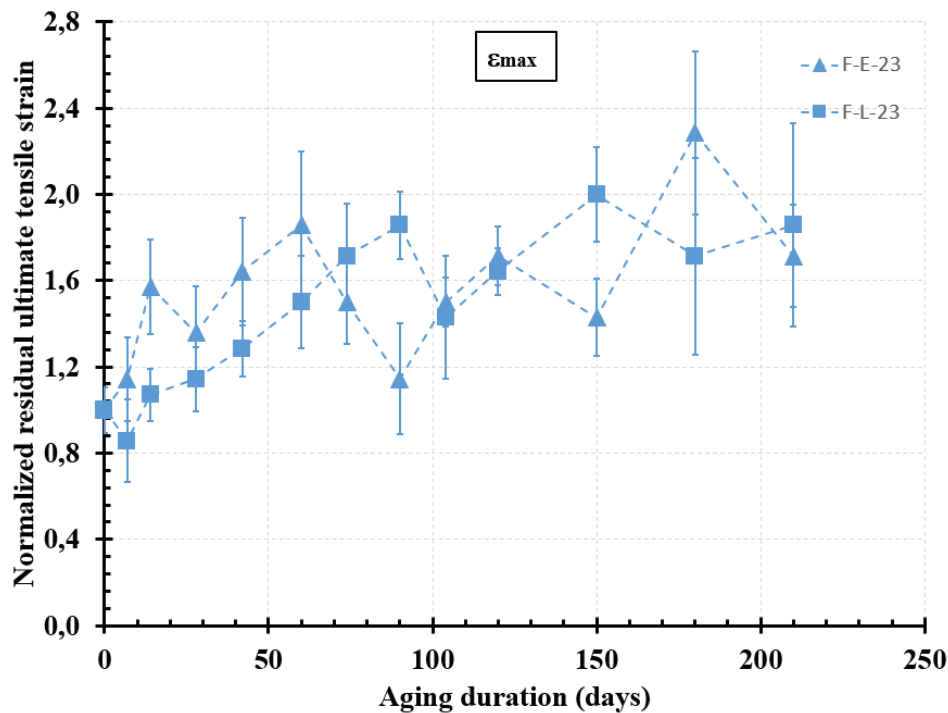


Figure 3- 109 : Influence over time of the pH on the average ultimate tensile strain of flax yarn (F) at 23°C (normalized residual values).

3.2.3.2.5 Flax at 60°C

Figure 3- 110, Figure 3- 111 and Figure 3- 112 present the influence over time of the pH on the average tensile strength, the average tensile modulus and the average ultimate tensile strain respectively, of flax yarns subjected to aging at 60°C. One can notice that, at 60°C there is no occurring of the mercerization process neither in E nor in L solutions. Then, after 90 days of immersion in E and L solutions, the yarns undergo a decrease in their average tensile properties. Furthermore, the increase in strain in both solutions along with the decrease in average tensile strength and modulus, indicates the occurrence of the plasticization process [175]. Since after 90 days of immersion, flax yarns subjected to solution L-60 have tensile properties greater than those subjected to E-60, we can conclude that at 60°C, the degradation process of flax fibers is slower when the alkalinity of the matrix is greater. Same explanation as in case of hemp yarns in solutions L-40 and L-60 (3.2.3.1.3) can be employed here: maybe the curing of natural hydraulic lime matrix (pH 12.5) at 60°C have beneficial effects on the flax yarns by retarding their degradation thus improving the mechanical performance of F-L TRM. Also, further experimental and analytical work is needed on real F-L TRM specimens cured at 60°C to verify this hypothesis.

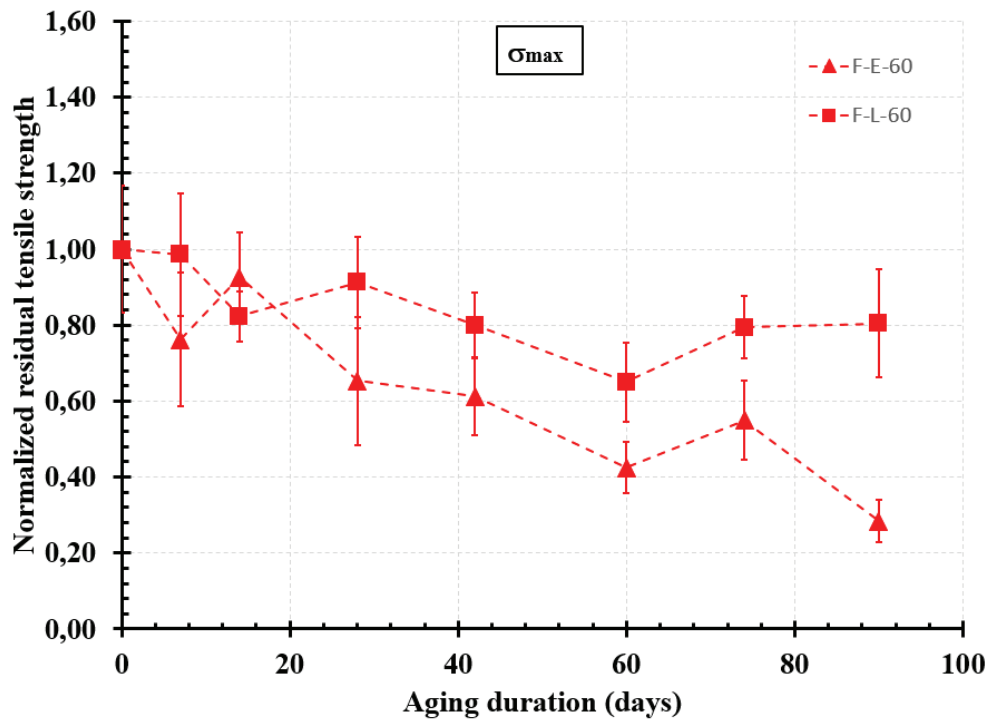


Figure 3- 110 : Influence over time of the pH on the average tensile strength of flax yarn (F) at 60°C (normalized residual values).

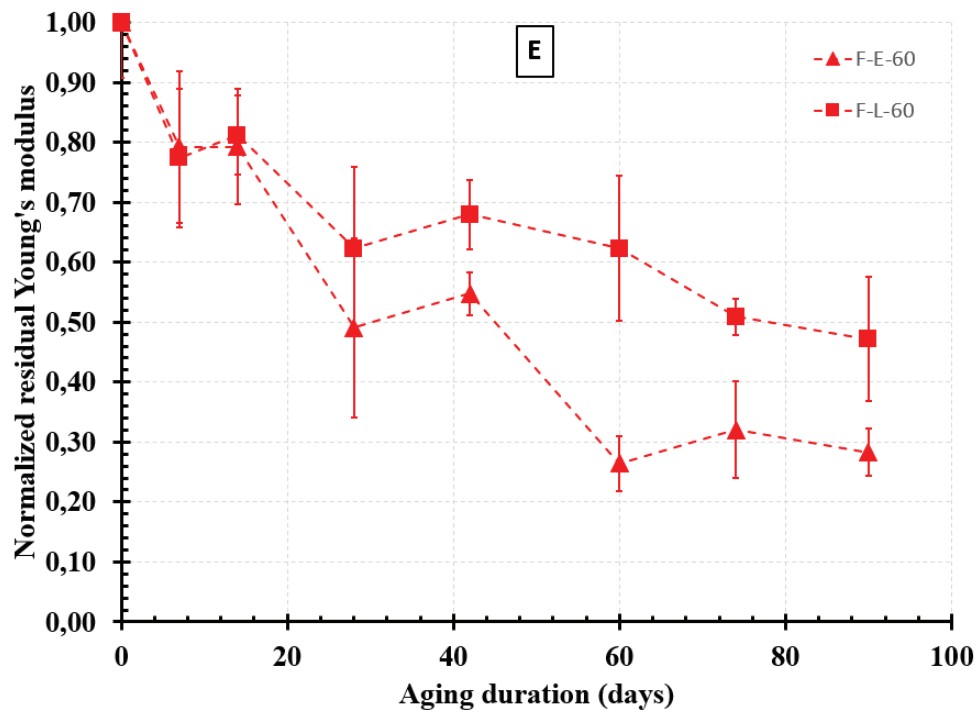


Figure 3- 111 : Influence over time of the pH on the average tensile modulus of flax yarn (F) at 60°C (normalized residual values).

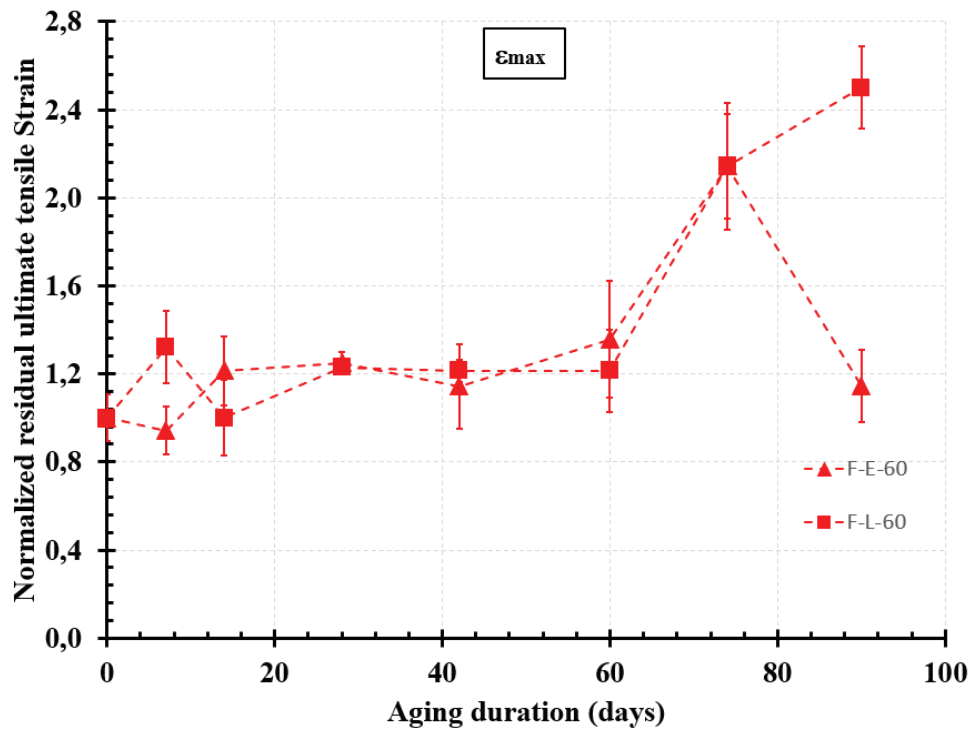


Figure 3- 112 : Influence over time of the pH on the average ultimate tensile strain of flax yarn (F) at 60°C (normalized residual values).

3.2.3.3 Influence of the yarn's type on the tensile behavior over time

3.2.3.3.1 In solution E-23

Figure 3- 113, Figure 3- 114 and Figure 3- 115 present the influence of the yarn's type on the average tensile strength, the average tensile modulus and the average ultimate tensile strain respectively, when the yarns are immersed in solution E-23. At first, as we have also mentioned in chapter 2, without aging (at 0 days), hemp yarns are 4 times more resistant in tension than flax yarns. However, after aging in solution E-23, we can notice that, hemp yarns undergo a sharp decrease in their average tensile properties leading to their complete degradation after 90 days of immersion. While flax yarns retain tensile properties that are very close to their initial ones after 90 days of immersion. Therefore, we can conclude that, flax yarns are more resistant to E-23 solution than hemp yarns. Furthermore, both types of yarns undergo a mercerization process after 60 days of immersion. However, only flax yarns undergo the plasticization process while hemp yarn do not.

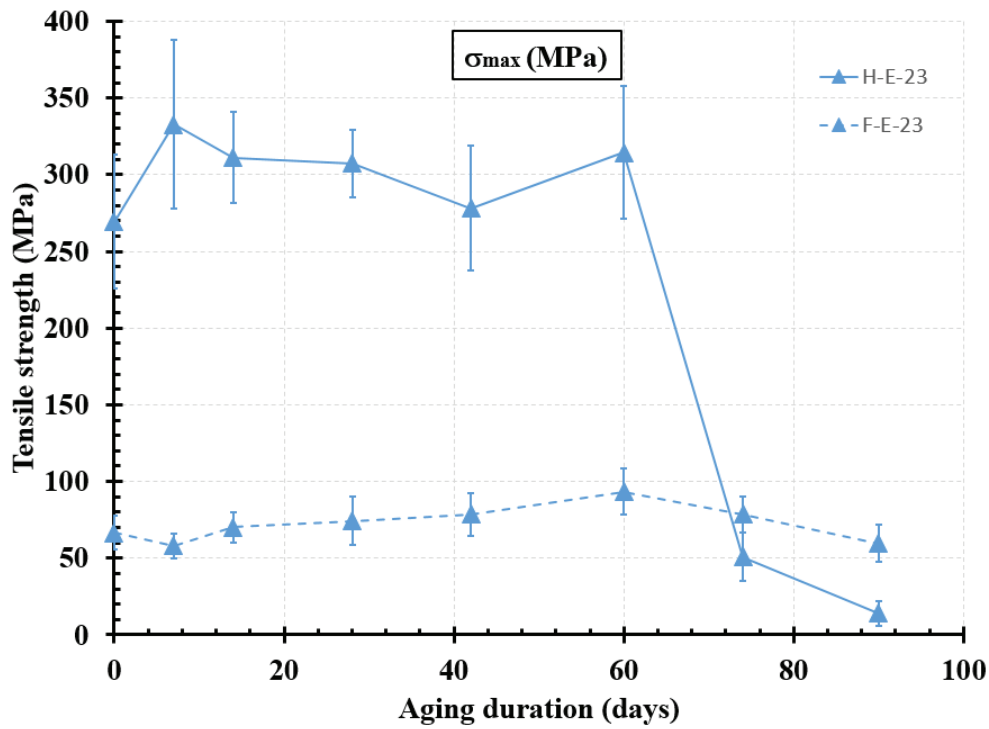


Figure 3- 113 : Influence of the yarn's type on the average tensile strength over time in E-23 solution.

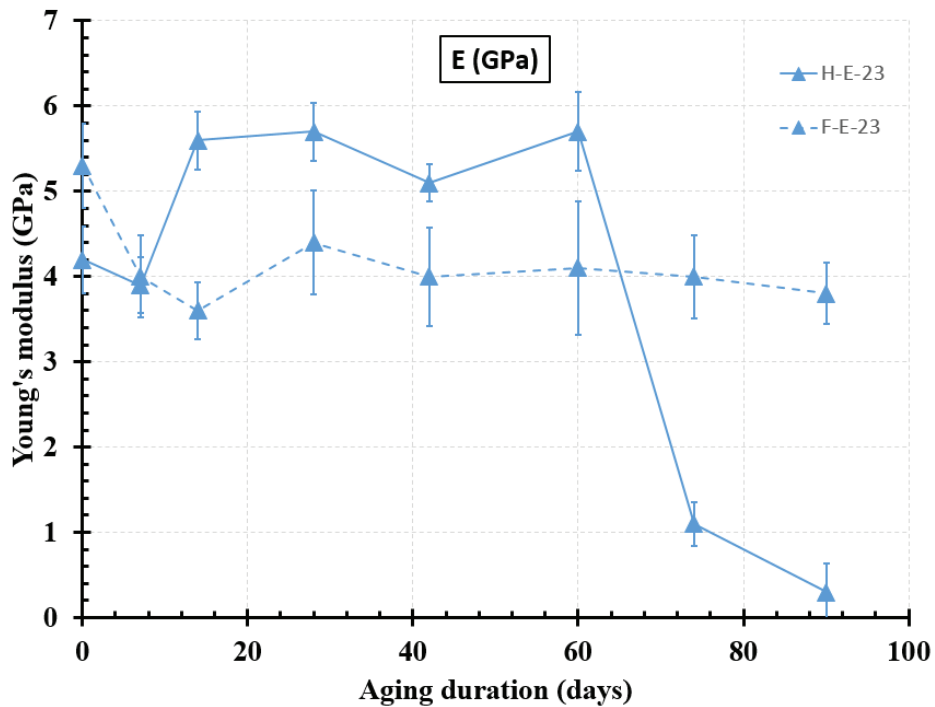


Figure 3- 114 : Influence of the yarn's type on the average tensile modulus over time in E-23 solution.

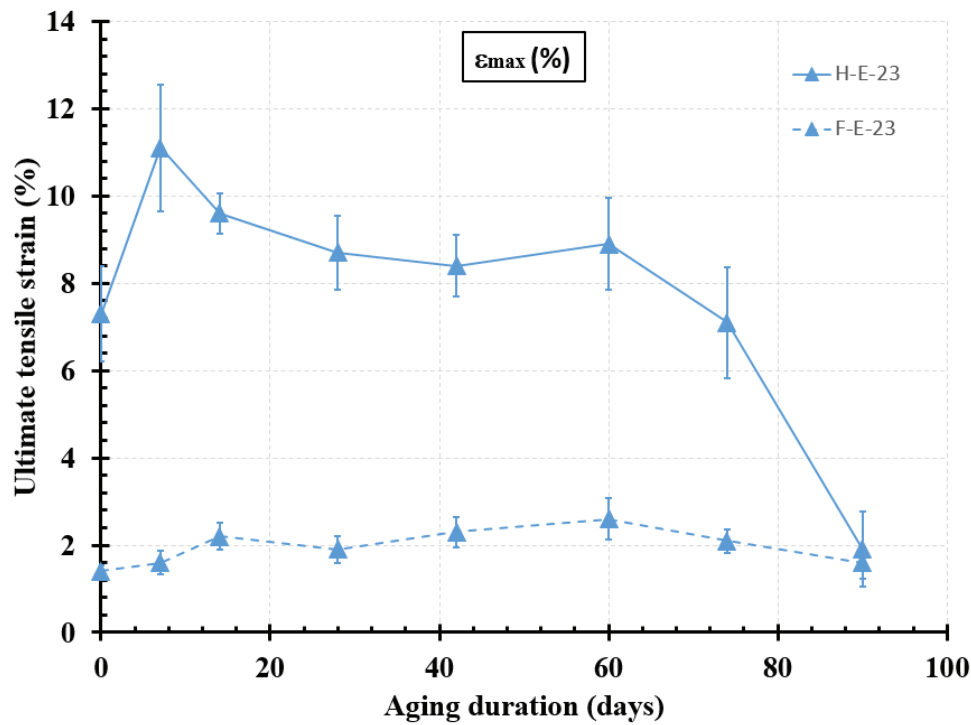


Figure 3- 115 : Influence of the yarn's type on the average ultimate tensile strain over time in E-23 solution.

3.2.3.3.2 In solution E-60

Figure 3- 116, Figure 3- 117 and Figure 3- 118 present the influence of the yarn's type on the average tensile strength, the average tensile modulus and the average ultimate tensile strain respectively, when the yarns are immersed in solution E-60. One can notice that in solution E-60, both types of yarn undergo a sharp decrease in their average tensile properties after 90 days of immersion (a decrease of 82 % and 72 % in the average tensile strength for hemp and flax yarns respectively). Thus, E-60 solution have the same effect on the aging of hemp and flax yarns. Furthermore, hemp yarns undergo a mercerization process while flax yarns do not. However, flax yarns undergo the plasticization process while hemp yarn do not.

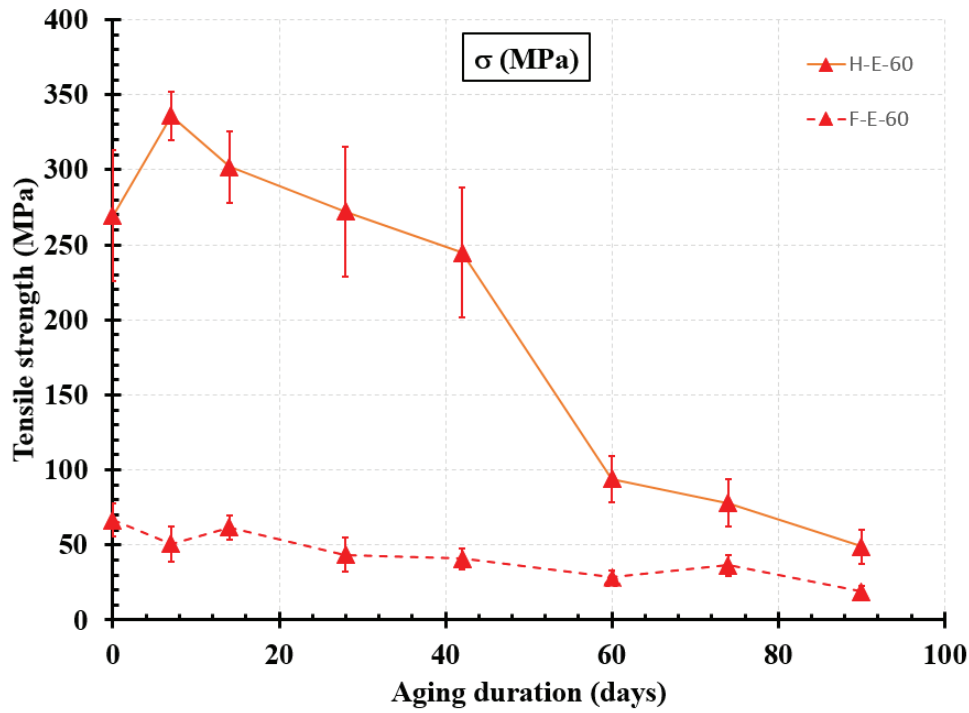


Figure 3- 116 : Influence of the yarn's type on the average tensile strength over time in E-60 solution.

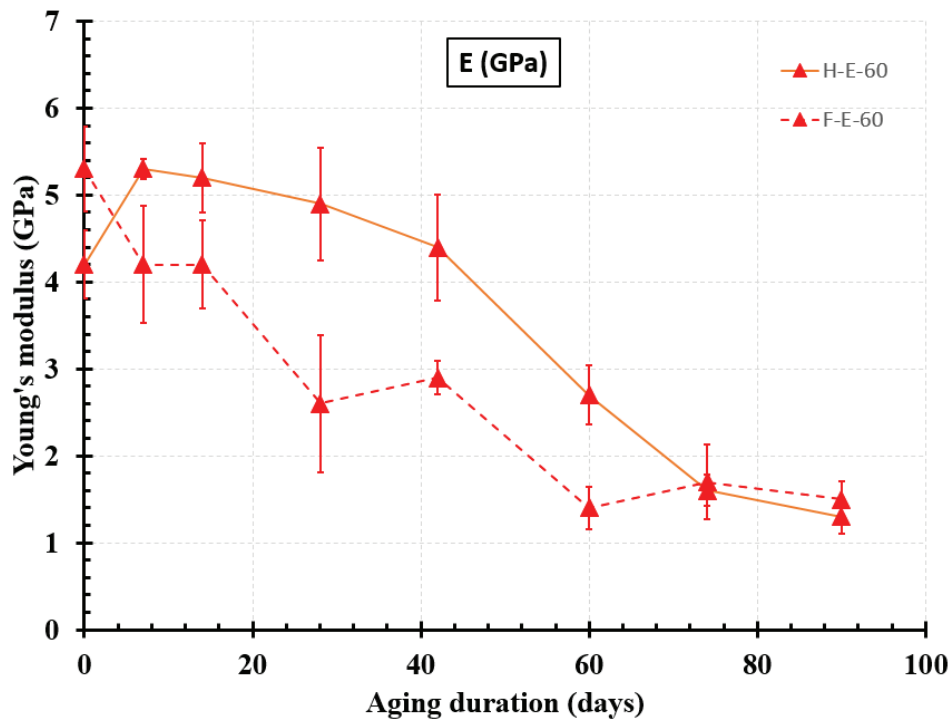


Figure 3- 117 : Influence of the yarn's type on the average tensile modulus over time in E-60 solution.

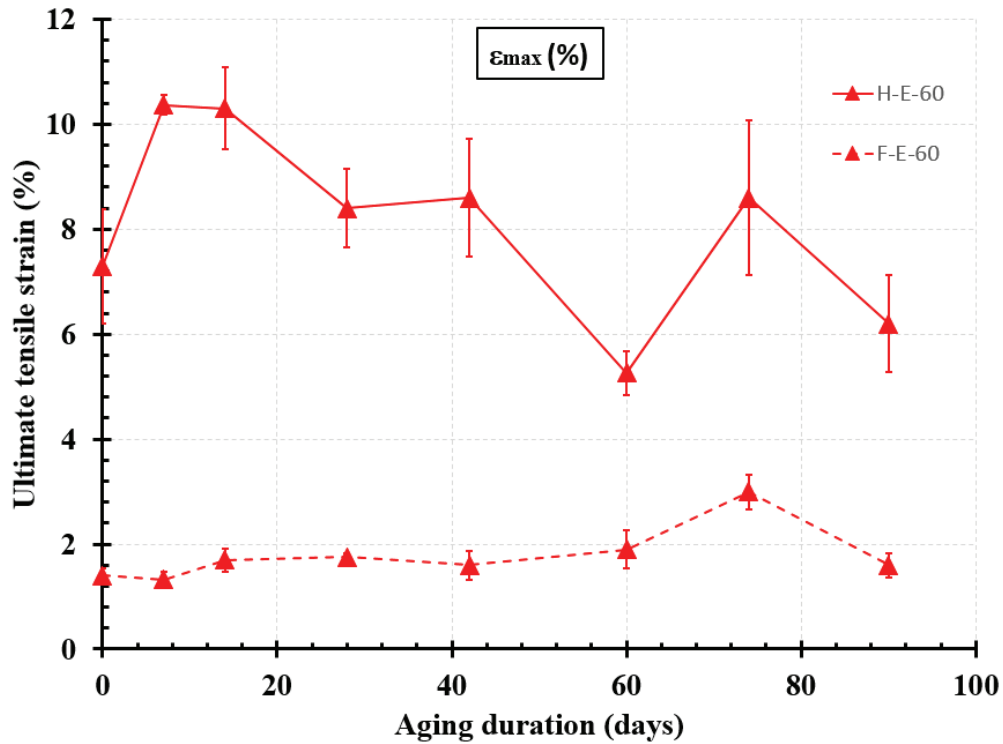


Figure 3- 118 : Influence of the yarn's type on the average ultimate tensile strain over time in E-60 solution.

3.2.3.3.3 In solution L-23

Figure 3- 119, Figure 3- 120 and Figure 3- 121 present the influence of the yarn's type on the average tensile strength, the average tensile modulus and the average ultimate tensile strain respectively, when the yarns are immersed in solution L-23. One can notice that, hemp yarns undergo a sharp decrease in their average tensile properties leading to their complete degradation after 90 days of immersion. While flax yarns retain average tensile properties that are very close to their initial ones after 90 days of immersion. Therefore, we can conclude that flax yarns are more resistant to L-23 solution than hemp yarns. Furthermore, hemp and flax yarns undergo a mercerization process after 28 and 74 days, respectively. However, only flax yarns undergo the plasticization process while hemp yarn do not.

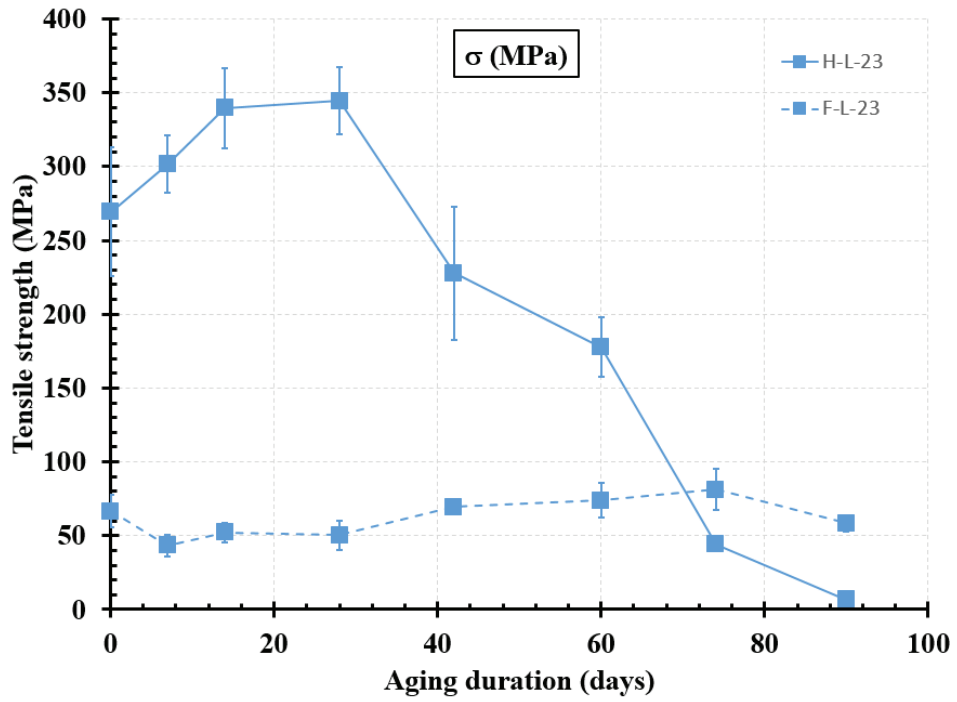


Figure 3- 119 : Influence of the yarn's type on the average tensile strength over time in L-23 solution.

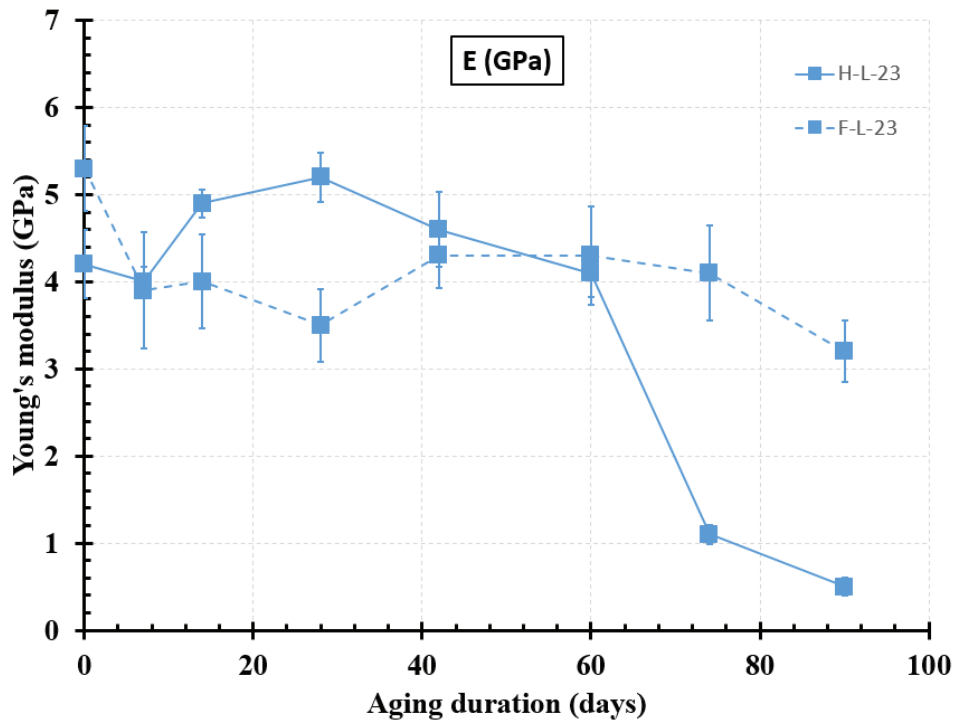


Figure 3- 120 : Influence of the yarn's type on the average tensile modulus over time in L-23 solution.

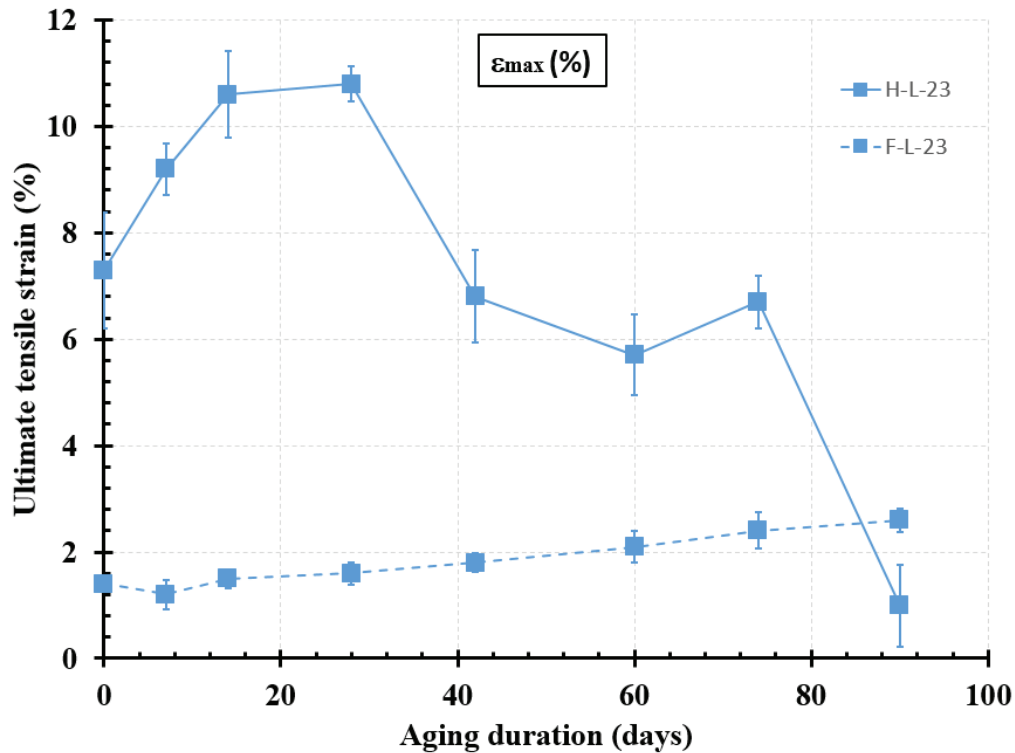


Figure 3- 121 : Influence of the yarn's type on the average ultimate tensile strain over time in L-23 solution.

3.2.3.3.4 In solution L-60

Figure 3- 122, Figure 3- 123 and Figure 3- 124 present the influence of the yarn's type on the average tensile strength, the average tensile modulus and the average ultimate tensile strain respectively, when the yarns are immersed in solution L-60. One can notice that in L-60 solution, both types of yarn could retain average tensile properties that are very close to their initial ones after 90 days of immersion. Thus, both types of yarn could resist to solution L-60 up to 90 days of immersion. In other words, at 60°C, the degradation process of natural fibers is slower when the alkalinity of the matrix is greater. Furthermore, hemp yarns undergo a mercerization process while flax yarns do not. However, flax yarns undergo the plasticization process while hemp yarn do not.

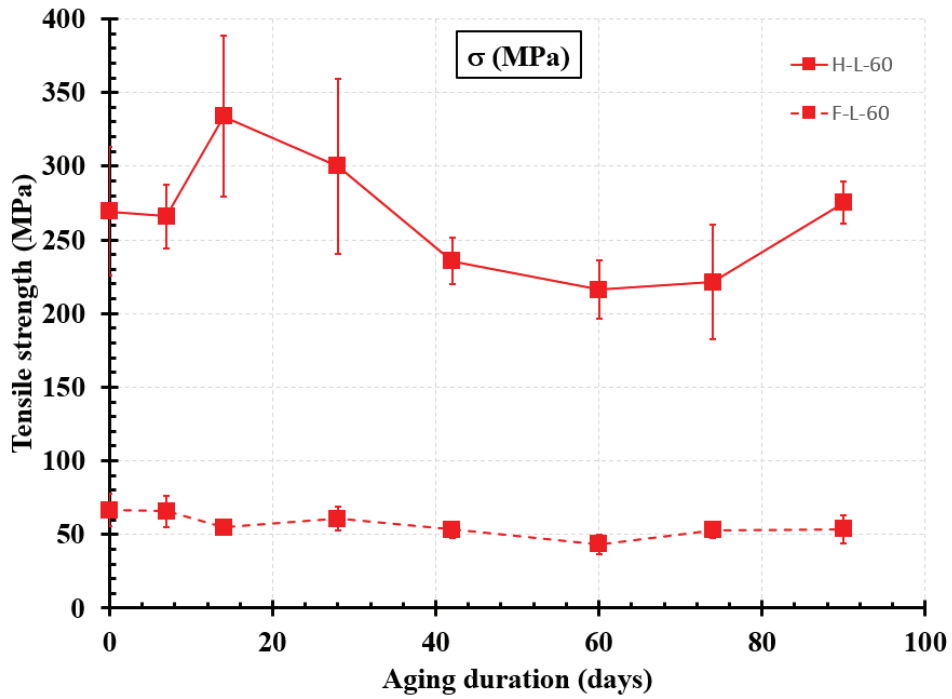


Figure 3- 122 : Influence of the yarn's type on the average tensile strength over time in L-60 solution.

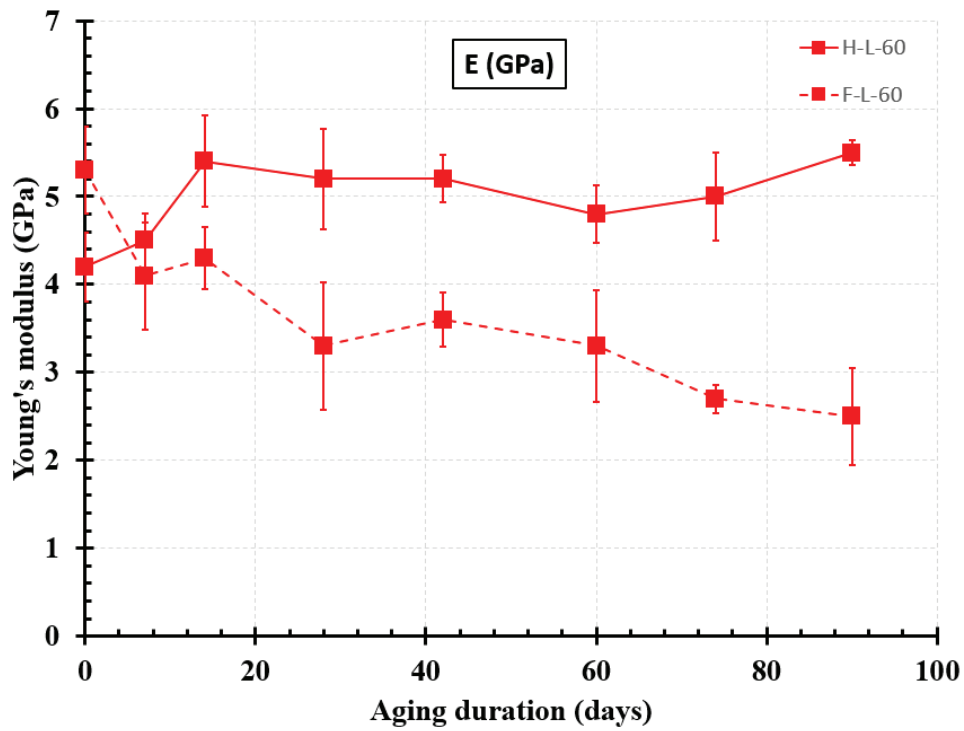


Figure 3- 123 : Influence of the yarn's type on the average tensile modulus over time in L-60 solution.

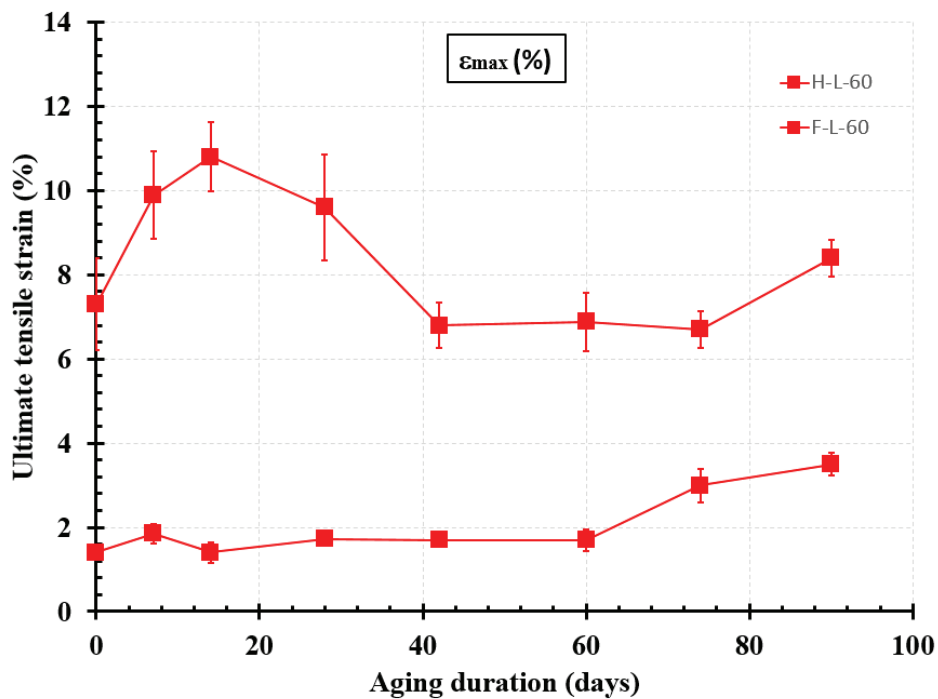


Figure 3- 124 : Influence of the yarn's type on the average ultimate tensile strain over time in L-60 solution.

3.2.3.4 Summary

Table 3- 28 summarizes the results of the accelerated aging of hemp and flax yarns in the different solutions, more specifically it presents the duration at which the different processes (retting, mercerization, plasticization, 20 % damage and 50 % damage) occur on hemp and flax yarns. NA in Table 3- 28 means that the results are not available and the '-' means that the process is not observed. As a reminder, the retting is a rotting process in which the pectin that binds the fibers together decomposes when it is in contact with light and air or when the fiber are immersed in water, giving the long bast fibers. In other words, it is a process resting on the (random) action of microorganisms to remove non-cellulosic components from natural fibers and separate fibers from the plant stem structure so as to obtain cellulose-rich fibers with higher tensile properties [172]. The mercerization is a process done in alkaline solution to remove the non-cellulosic components and impurities so the fibrils become more capable of rearranging themselves along the directions of tensile deformation resulting in better tensile strength and modulus [173], [19]. However, excessive retting or mercerization could damage the natural fiber. The plasticization effect of the water weakens intermolecular bonding such as Van der Waals forces and reduces fiber crystallinity, but increases the mobility of macromolecular chains, the plasticity and the flexibility of the fiber, this result in an increase in the ultimate tensile strain of the fiber along with a decrease in tensile strength and modulus [175]. In this study, we suppose that the plasticization process starts when the loss in tensile strength exceeds 20 % and the gain in ultimate tensile strain exceeds 20 %. Furthermore, we define two damage phases, the first one is when the loss in tensile strength

exceeds 20 % and the second one is when it exceeds 50%. The ages at which these damages occur are obtained from the normalized residual stress σ_{max} curves by extrapolation.

Table 3- 28 : Summary of the accelerated aging results on hemp and flax yarns.

		Retting (in water)	Mercerization (in NaOH)	Plasticization (σ_{max} loss > 20 % & ϵ_{max} gain > 20 %)	20 % of damage (σ_{max} loss)	50 % of damage (σ_{max} loss)
Hemp	H-R-23	14 d	-	-	58 d	80 d
	H-R-60	7 d	-	-	86 d	> 90 d
	H-E-23	-	60 d	-	66 d	70 d
	H-E-40	-	NA	-	11 d	26 d
	H-E-60	-	7 d	-	46 d	56 d
	H-L-23	-	28 d	-	46 d	65 d
	H-L-40	-	28 d	-	> 90 d	> 90 d
	H-L-60	-	14 d	-	> 90 d	> 90 d
Flax	F-E-23	-	60 d	180 d	170 d	> 210 d
	F-E-60	-	-	28 d	6 d	52 d
	F-L-23	-	74 d	180 d	5 d	> 210 d
	F-L-60	-	-	60 d	42 d	> 90 d











From the results (Table 3- 28), we can conclude the following:




Influence of the temperature on hemp yarns:

- The temperature speed up the retting process for hemp yarns;
- The temperature speed up the mercerization process for hemp yarns in both solutions E (pH 10.5) and L (pH 12.5);
- No plasticization process for hemp yarns in all the solutions tested;
- In solution E (pH 10.5), the temperature speed up both the 20 % and the 50 % damage of hemp yarns;
- In solution R (pH 7) and solution L (pH 12.5), the temperature slow down both the 20 % and the 50 % damage of hemp yarns.

The conclusions are summarized in schematic way in Table 3- 29.

Table 3- 29 : Influence of the temperature of the aging solution on hemp yarns.

Hemp yarns (H)					
T (°C) 	Retting	Mercerization	Plasticization	> 20 % Damage	> 50 % Damage
R (pH 7)			No occurrence		
E (pH 10.5)			No occurrence		
L (pH 12.5)			No occurrence		










 = increase,  = faster,  = slower.




Influence of the degree of alkalinity of the matrix on hemp yarns:

- At 23°C, the degree of alkalinity of the matrix speed up the mercerization process of hemp yarns;
- At 23°C, the degree of alkalinity of the matrix (pH) speed up both the 20 % and the 50 % damage of hemp yarns;
- At 40°C, We cannot conclude about the period at which the mercerization process stops and the decrease in the tensile properties of hemp yarns starts, since we do not have data between 0 and 28 days;
- At 40°C, the degree of alkalinity of the matrix slow down both the 20 % and the 50 % damage of hemp yarns. This means that the ettringitic environment produced higher strength loss than the lime environment at 40°C.
- At 60°C, the degree of alkalinity of the matrix slow down the mercerization process of hemp yarns;
- At 60°C, the degree of alkalinity of the matrix slow down both the 20 % and the 50 % damage of hemp yarns. This means that the ettringitic environment produced higher strength loss than the lime environment at 60°C.

The conclusions are summarized in schematic way in Table 3- 30.

Table 3- 30 : Influence of the pH of the aging solution on hemp yarns.

Hemp yarns (H)				
pH 	Mercerization	Plasticization	> 20 % Damage	> 50 % Damage
T = 23 °C		No occurrence		
T = 40 °C	No data	No occurrence		
T = 60 °C		No occurrence		







 = increase,  = faster,  = slower.




Influence of the temperature on flax yarns:

- No mercerization process for flax yarns at 60°C, it is only at 23°C;
- The temperature speed up the plasticization process for flax yarns in both solutions E (pH 10.5) and L (pH 12.5);
- In E solution (pH 10.5), the temperature speed up both the 20 % and the 50 % damage of flax yarns;
- In solution L (pH 12.5), the temperature slow down the 20 % damage, but we cannot conclude about the 50 % damage because in both solution E and L, it is not attained yet, and no data available between 90 and 210 days for F-L-60 series.

These conclusions are summarized in schematic way in Table 3- 31.

Table 3- 31 : Influence of the temperature of the aging solution on flax yarns.

Flax yarns (F)				
T (°C) 	Mercerization	Plasticization	> 20 % Damage	> 50 % Damage
E (pH 10.5)	No occurrence at 60 °			
L (pH 12.5)	No occurrence at 60 °			No loss yet







 = increase,  = faster,  = slower.




Influence of the degree of alkalinity of the matrix on flax yarns:

- At 23°C the degree of alkalinity of the matrix slow down the mercerization process of flax yarns;
- At 23°C, the degree of alkalinity of the matrix did not influence the plasticization period of flax yarns, it is 180 days in both solutions E and L;
- At 23°C, the degree of alkalinity of the matrix speed up the 20 % damage, but we cannot conclude about the 50 % damage because in both solution E and L, the tensile strength loss of the yarns is lower than 50 % at 210 days;
- At 60°C, no mercerization process for flax yarns, in both solution E and L;
- At 60°C, the degree of alkalinity of the matrix slow down the plasticization process of flax yarns;
- At 60°C, the degree of alkalinity of the matrix slow down both the 20 % and the 50 % damage of flax yarns.

These conclusions are summarized in schematic way in Table 3- 32.

Table 3- 32 : Influence of the pH of the aging solution on flax yarns.

Flax yarns (F)				
pH 	Mercerization	Plasticization	> 20 % Damage	> 50 % Damage
T = 23 °C		No influence		No loss yet
T = 60 °C	No occurrence			


 = increase,  = faster,  = slower.


Influence of yarn’s type on the period of occurrence of the different processes:

- In E-23, the mercerization process occurs at the same time for both flax and hemp yarns;
- In E-23, both 20 % and 50 % damage occurs first for hemp yarns;
- In E-60, the 20 % damage occurs first for flax yarns, while the 50 % damage occurs at the same time for both flax and hemp yarns;
- In L-23, the mercerization process occurs first for hemp yarns;
- In L-23, the 20 % damage occurs first for flax yarns, while the 50 % damage occurs first for hemp yarns;
- In L-60, the 20 % damage occurs first for flax yarns, while the 50 % damage occurs at the same time for both flax and hemp yarns.

These conclusions are summarized in schematic way in Table 3- 33.

Table 3- 33 : Influence of yarn's type on the period of occurrence of the different processes.

	Mercerization	Plasticization	> 20 % Damage	> 50 % Damage
E-23	Same speed	No occurrence for hemp	Hemp	Hemp
E-60	No occurrence for flax	No occurrence for hemp	Flax	Same speed
L-23	Hemp	No occurrence for hemp	Flax	Hemp
L-60	No occurrence for flax	No occurrence for hemp	Flax	Same speed

 = faster.

3.3 Natural aging of hemp yarn in the matrix of TRM

In this section, hemp textile imbedded in real ettringitic and lime matrices in form of TRM plates are investigated in tension in order to compare the real service life of the yarns with the accelerated one and verifying the validity of the correlation formula. Hemp yarns are chosen for this investigation because they are more resistant in tension than flax yarns as we have seen in chapter 2, and they are twisted and easier to be weaved as a textile grid.

3.3.1 Specimens preparation

The preparation of hemp TRM's plates consists of two steps: the textile weaving and the mortar casting. The specimen preparation details were defined by Rilem Technical Committee 250 CSM [3].

3.3.1.1 Textile weaving

The textile used is not a commercial product, but it is a handmade textile, which is, weaved (in weft and warp directions) from the dry hemp yarns received in form of coil, using a technics elaborated especially for this work. It consists of several pulleys placed on a wooden support. Two pulleys, instead of one, were used for each end to adjust the spacing between the yarns. The hemp yarn is spun around the pulleys first longitudinally and then transversely (Figure 3- 125a). The intersections of the longitudinal yarns with the transverse yarns are sewn by hand using a thread and a needle (Figure 3- 125b). Finally, the edges are cut (Figure 3- 125c), to obtain the sample of the textile ready to be used in TRM (Figure 3- 125d). The geometric configuration of hemp textile is shown in Figure 3- 126. Its length is 600 mm and it has a 20 mm x 20 mm bi-directional mesh. The choice of hemp coils as well as the mesh size of hemp textile is based on the study of Menna et al. 2015 [176]. They used the same hemp yarns (same manufacturer) with the same mesh configuration, but impregnated with a low viscosity epoxy resin, to reinforce both a natural hydraulic lime mortar and a pozzolanic mortar. In the study of Menna et al, these systems were

employed to strengthen tuff and brick masonry panels. These latter were then subjected to diagonal compression tests. In the study, the hemp TRM exhibited good mechanical performances; for this reason, we adopt the same kind of textile grid geometry. The cross-sectional area of the textile is (3.004 mm^2), it is equal to the number of yarns (4 yarns) multiplied by the cross-sectional area of the yarn (0.751 mm^2) already determined in chapter 2 (Table 2- 25).

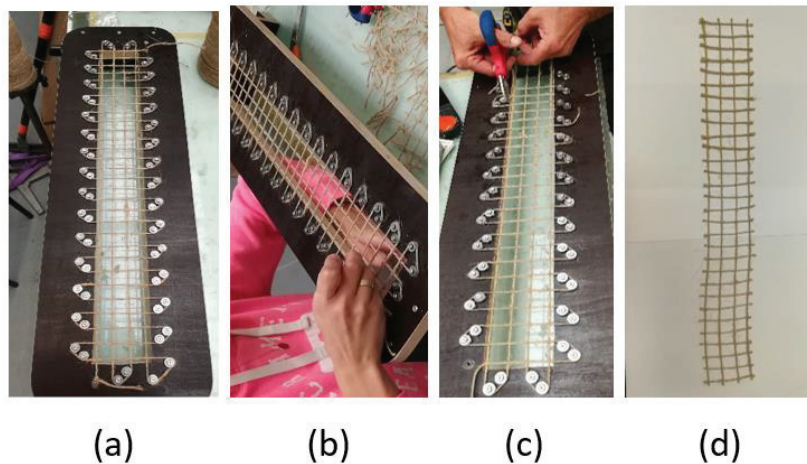


Figure 3- 125 : Textile weaving technic: a) spinning of the yarn, b) sewing of the yarns intersections, c) cutting the textile specimen, d) Final textile specimen obtained.

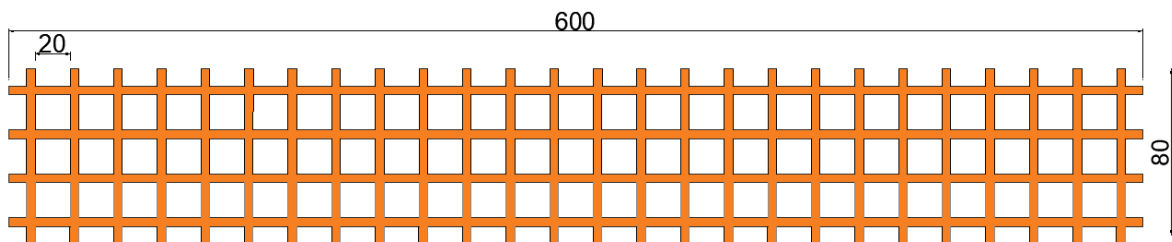


Figure 3- 126 : Geometric characteristics of hemp textile (dimensions are in mm).

3.3.2 Mortar casting

3.3.2.1 Preparation of the mold

A mold of 600 mm x 690 mm was prepared (Figure 3- 127a) to make six TRM's specimens of 600 mm x 80 mm x 10 mm. The steps of the mold preparation are as follows:

- In a 5 mm thick PVC board, 14 bars (7 for the first layer and 7 for the second) of length 600 mm and width 30 mm and 4 bars (2 for the first layer and 2 for the second) of length 690 mm and width 30 mm were cut;
- On a CTBX wooden support, the PVC bars of the first layer were screwed: 7 bars of length 600 mm spaced 80 mm and 2 bars of 690 mm perpendicular to the latter at their two ends respectively;
- The screws were covered with tape so that they cannot be filled with mortar;

- The remaining bars were screwed in the same manner over the bars of the first layer but after molding of the first matrix layer and placing the textile.

3.3.2.2 Fabrication of TRM's specimens

The TRM's specimens were prepared by following the next steps:

- The mold was cleaned well by using the compressed air (Figure 3- 127a);
- Using a brush, the mold was oiled to avoid the sticking of the TRM plates to its bottom, then the excess quantity of oil was wiped with paper towels (Figure 3- 127b);
- The first layer of the matrix was poured, directly from the mixing bowl, in each compartment of the mold, using an appropriate spoon, and making sure to ensure a surplus;
- The excess mortar was removed, immediately, by means of a metal ruler (Figure 3- 127c);
- The textile grid was put on the first layer of the matrix and a low hand pressure was applied to ensure better textile impregnation by the matrix (Figure 3- 127d);
- The second layer of PVC bars is screwed on top of the first one; so that we obtain a thickness of 10 mm. Then the screws are covered with Scotch tape;
- The second layer of the matrix was poured in each compartment of the mold, making sure to ensure a surplus;
- The leveling operation, already done for the first layer of the matrix, was now repeated, making sure to obtain a smooth surface (Figure 3- 127e);
- The mold was covered with a plastic film so that the water does not evaporate during the hydration of the mortar (Figure 3- 127f).

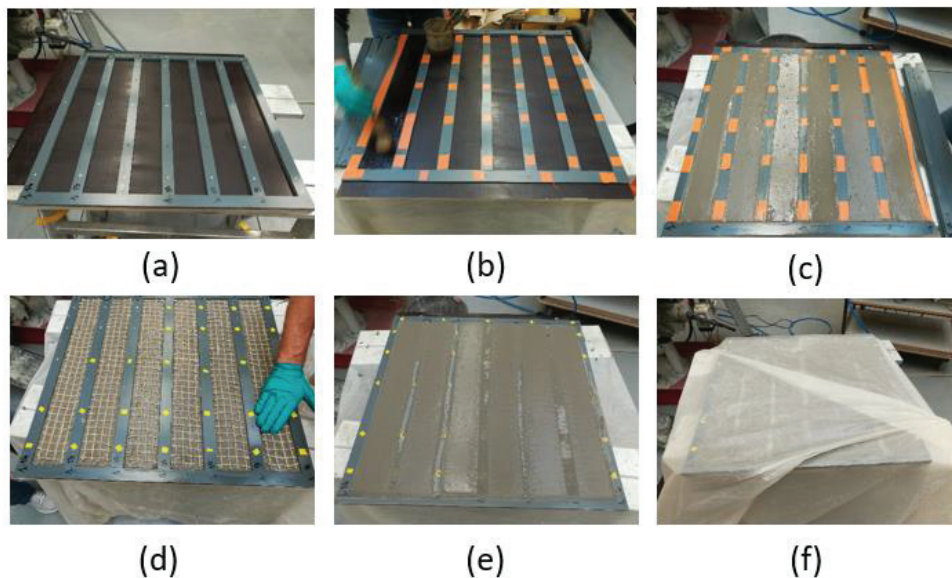


Figure 3- 127 : The steps for manufacturing TRM's specimens: a) Screwing the PVC bars of the first mold layer, b) Oiling the mold compartments, c) Pouring and leveling the first matrix layer, d) Placing the textile and screwing the PVC bars of the second layer of the mold, e) Pouring and leveling the second matrix layer and f) Covering the mold with a plastic film.

3.3.2.3 Demolding of TRM's specimens

The TRM's specimens were demolded after 72 hours, taking care not to damage them. After demolding, all the specimens were kept in a plastic film for 4 days, then in the open air for 21 days. As shown in Figure 3- 128, the specimens were stored vertically on a wooden shelf, separated by clues to assure a same space between all the specimens. This space allows a direct contact of the specimens with the air from both sides.

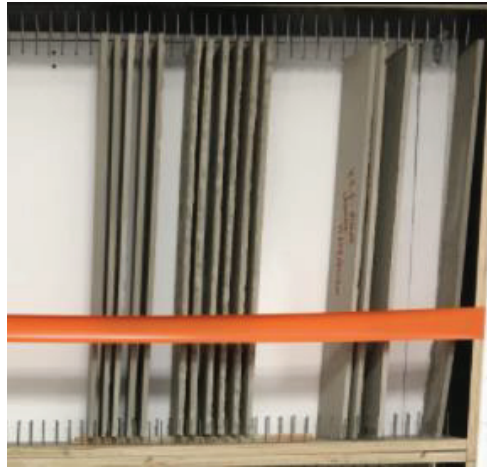


Figure 3- 128 : Specimens of TRM after demolding.

3.3.3 Tensile test setup

Two reinforcement configurations were taken into account in this study: the first one labelled H-E consisted of hemp textile (H) imbedded in Ettringitic mortar (E). The second one labelled H-L consisted of hemp textile (H) imbedded in Natural Hydraulic Lime mortar (L). These two TRM systems were tested in tension at different curing times (Table 3- 34).

Table 3- 34 : Tensile test series.

TRM systems	Series name	Number of specimens	Curing time
H-E	H-E-28d	5	28 days
	H-E-2m	5	2 months
	H-E-3m	3	3 months
	H-E-1y	6	1 year
	H-E-1.5y	3	1.5 years
	H-E-2y	3	2 years
H-L	H-L-28d	3	28 days
	H-L-2m	5	2 months
	H-L-3m	2	3 months
	H-L-1y	4	1 year
	H-L-1.5y	4	1.5 years

The tensile tests were carried out, by using a clevis type setup system [3], [177] (Figure 3- 129, Figure 3- 131). Three days before the test, aluminum tabs measuring 120 mm x 80 mm x 4 mm are glued to the ends of each plate at a 7 cm length and on both sides (Figure 3- 129) using EPONAL 380 epoxy glue, the characteristics of this latter provided by the company were summarized in Table 3- 35 [178]. To ensure a good adherence to the composite, the tabs are clamped using plastic clamps for two days (Figure 3- 130). The role of the tabs is to ensure a uniform distribution of the stress in the fixing zone and to limit the damage of the matrix. Furthermore, the tabs have a hole that allows the use of a clevis articulation to fix the specimen in the testing machine (Figure 3- 129b).

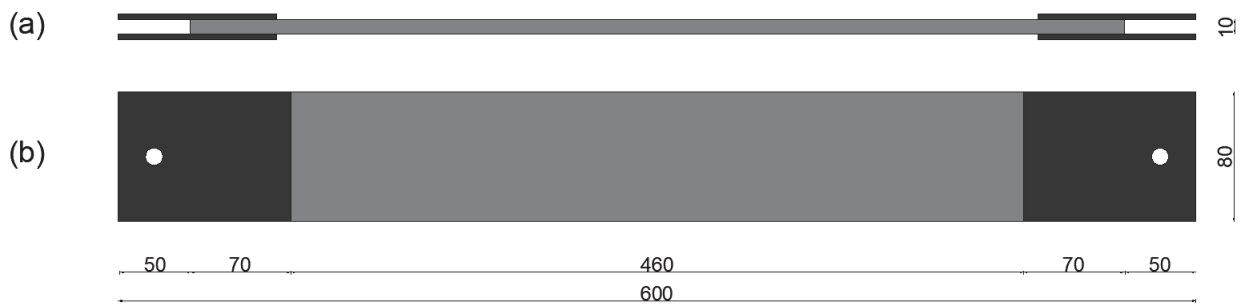


Figure 3- 129 : Geometric characteristics of the specimens for the tensile test: a) lateral and b) front views (dimensions are in mm).

Table 3- 35 : Mechanical characteristics of the EPONAL 380 resin after curing for 7 days at 20°C [178].

EPONAL 380	
Tensile strength	29.5 ± 1.0 MPa
Compressive strength	83 ± 1.6 MPa
Flexural strength	48 ± 4 MPa
Elongation at break	0.65 ± 0.1 %
Tensile elastic module in tension	4940 ± 170 MPa
Compressive elastic module	4200 ± 150 MPa
Flexural elastic module	5050 ± 450 MPa

Tensile tests were carried out in universal testing machine Zwick of 50 kN capacity in displacement control with a loading rate of 0.3 mm/min (Figure 3- 131). The load applied to the specimen and the displacement of the cross-head were recorded by the machine.



Figure 3- 130 : Preparation of a TRM specimen for the direct tensile test: gluing of aluminum tabs.

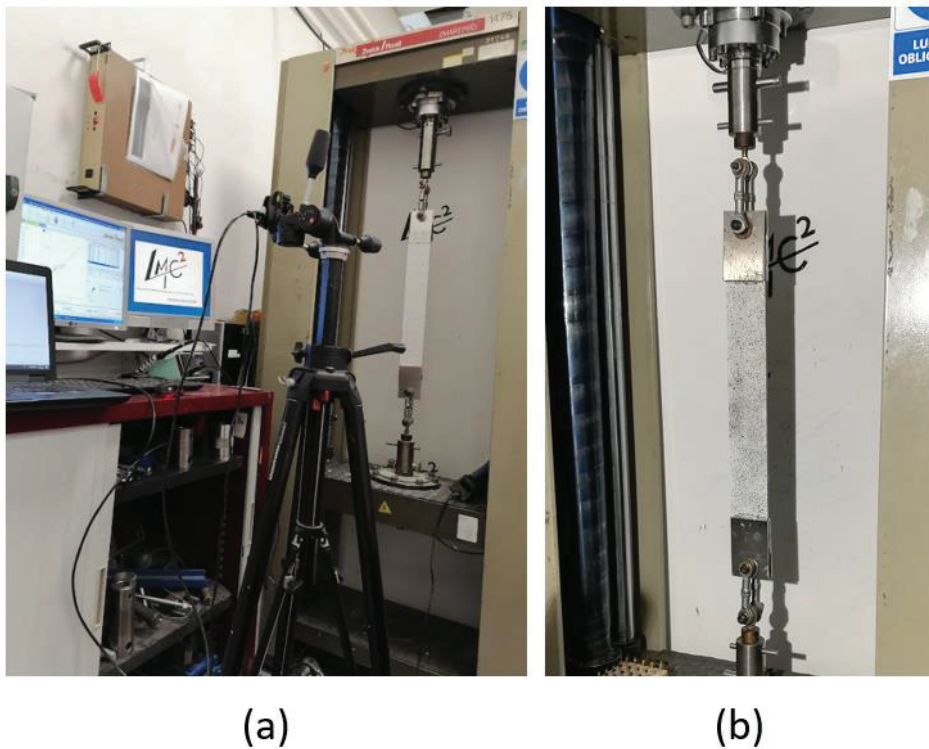


Figure 3- 131 : Experimental setup of the tensile test.

3.3.4 Results of tensile test on hemp TRM's

The results obtained by the tensile test on the different TRM systems are reported in terms of force-displacement curves (F-d) and failure modes. Figure 3- 132 presents the typical tensile behavior of TRM found in the literature [179]. The tensile stresses at the end of each stage are named σ_1 , σ_2 and σ_{max} , respectively. The corresponding strains are named ϵ_1 , ϵ_2 and ϵ_{max} , respectively. The failure modes observed will be evaluated in the context of the typical failure modes of TRM subjected to tension defined in the literature (Figure 3- 133).

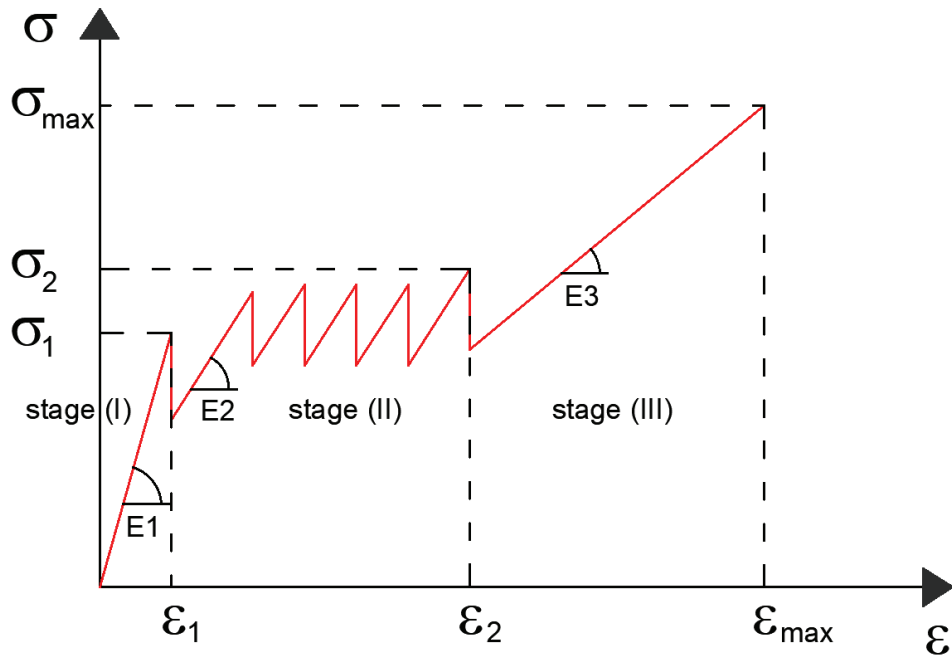


Figure 3- 132 : Typical stress-strain curve of TRM subjected to tensile load [179].

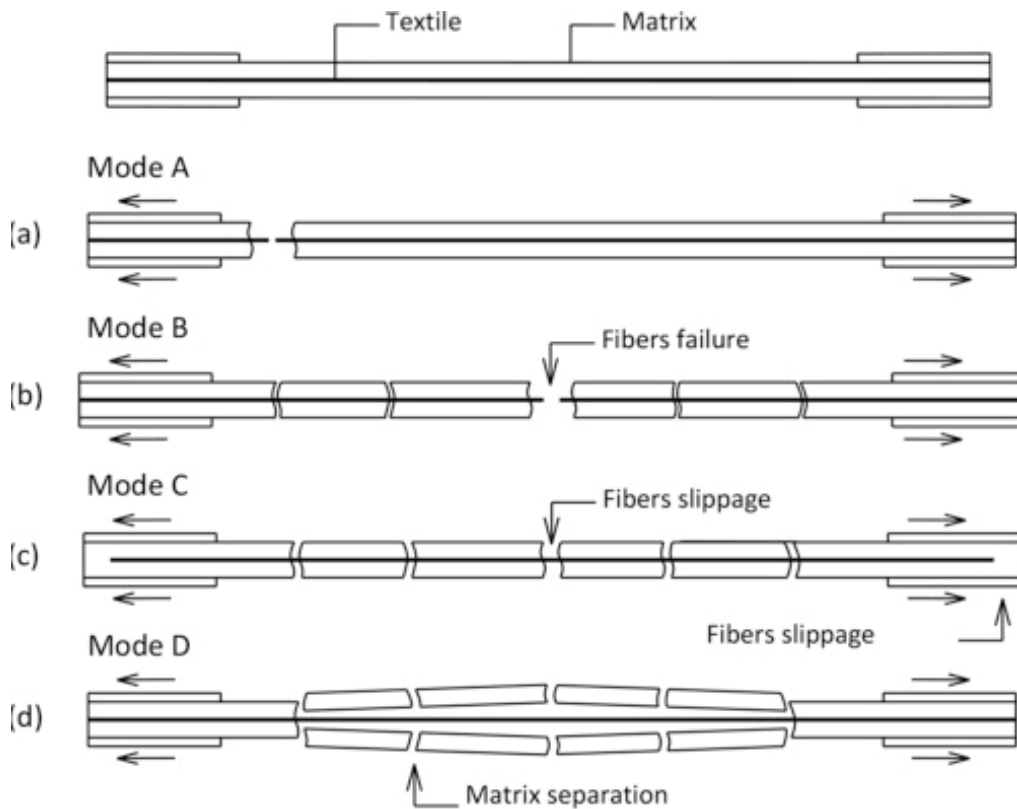


Figure 3- 133 : Typical failure modes of TRM materials tested in tension. (a) Failure mode A, (b) Failure mode B, (c) Failure mode C, (d) Failure mode D [3] [144].

3.3.4.1 H-E and H-L series

Figure 3- 134 presents the force-displacement curves of the specimens of H-E-28d TRM series. The curves for the specimens of all the other series exhibited similar behavior, so in order to not encumber the reports these curves are placed in appendix E. Comparing the tensile behavior of these TRM series with the typical tensile behavior described in the literature (Figure 3- 132); we find that, these TRM exhibited a very different tensile behavior. It is characterized by a first elastic stage, which represents the behavior of the uncracked specimen. After the peak load, a new stage begins when the first and only crack occurs, with a sharp snap-back behavior characterized by a sudden drop in load until it reaches zero. This behavior may be due to the low initial stiffness of hemp fibers when subjected to tensile loading conditions. Then, the load increases announcing the beginning of the post peak stage II, until it reaches a second peak load and then starts to decrease and the test ended by the slippage of the textile within the matrix. This behavior can be due to the large water absorption capacity of hemp yarns (it is about 260 % as we have seen in chapter 2), which causes their swelling during the hydration of the matrix and their retracting after drying of the system. This in turn causes the formation of pores at the interface textile-matrix allowing the slippage of the textile with the matrix. In addition when the vegetal fibers are wet they lose stiffness and gain ductility in other word their ultimate tensile strength increases and becomes greater than that of the matrix, which may leads to changes in the contact pressure across the interface and weakens the fiber-matrix bond [59]. It may also be due to the clevis type system used to apply the tension at the end of the TRM specimens, which cannot grip uniformly all the surface at both extremities of the specimen. For this reason, a new typical stress-strain curve is designed to analyze the TRM with natural fibers tested in this study. This curve is shown in Figure 3- 135.

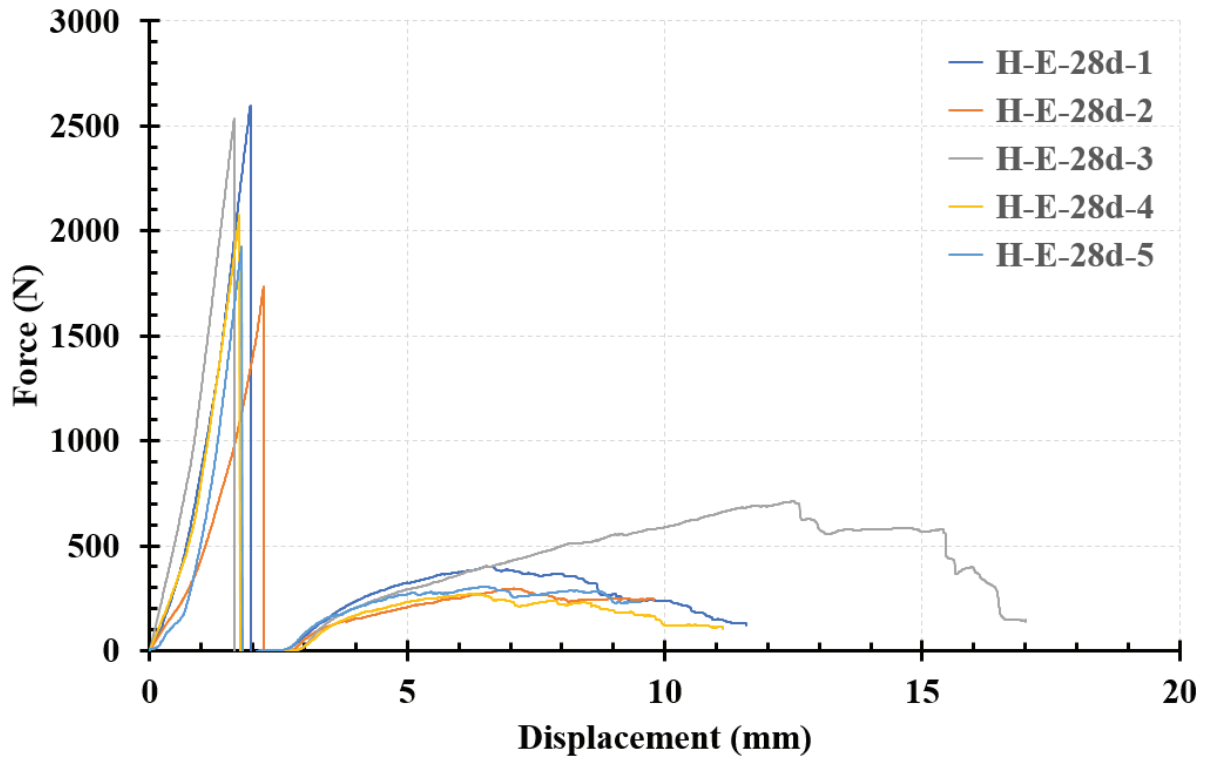


Figure 3- 134 : Force-displacement curves for the specimens of H-E-28d series.

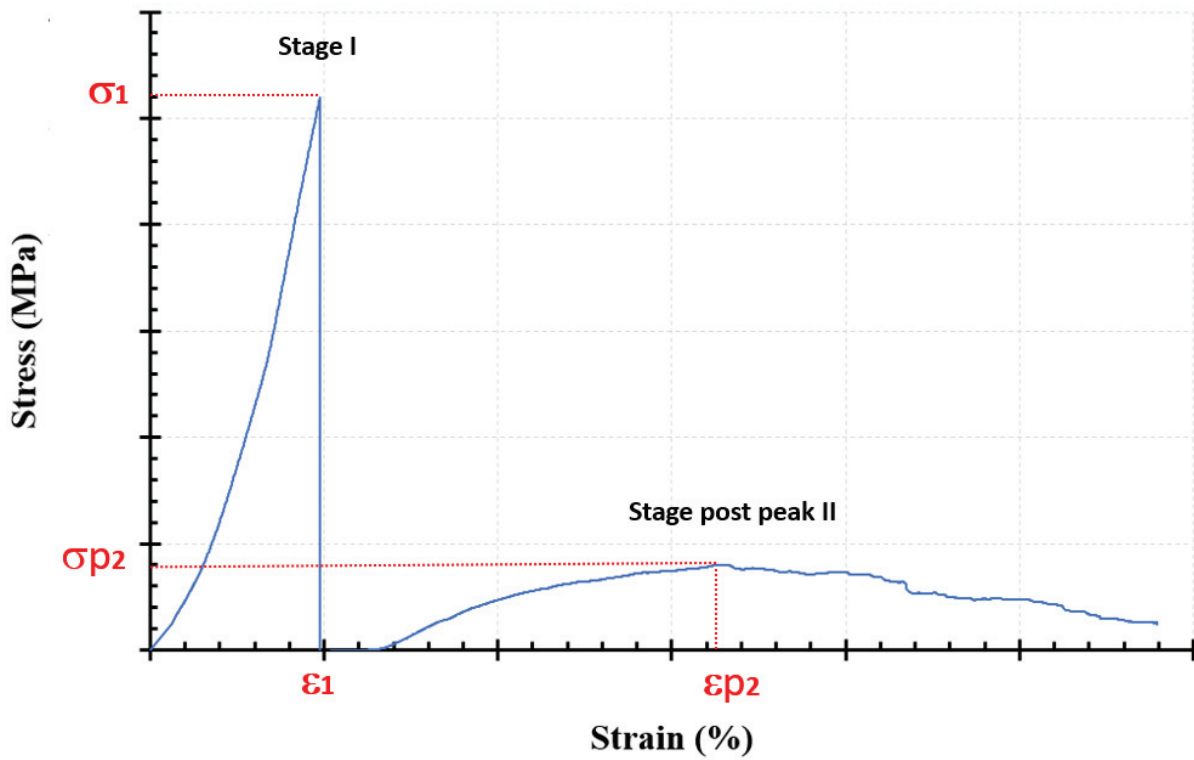


Figure 3- 135: Typical stress-strain curve of natural fibers TRM tested in tension in this study.

Table 3- 36 and

Table 3- 37 summarizes the tensile properties at the end of stage I and stage II respectively, for all the tested H-TRM configurations. The stress σ_c is the ratio between the maximum tensile load at the end of the first stage and the cross-sectional area of the composite ($A_c = 10 \text{ mm} \times 80 \text{ mm}$). The stresses σ_1 and σ_2 refer to the ratio between the maximum tensile load in stage I and stage II respectively, and the cross-sectional area of the textile ($A_t = 3.004 \text{ mm}^2$). The strain ε_1 and ε_2 refer to the ratio between the global displacement of the cross head U_1 and U_2 respectively, which correspond to σ_1 and σ_2 respectively, and the gauge length of the specimen (460 mm). The elastic modulus E refers to the slope of the second phase of the F-d curve multiplied by the cross-sectional area of the textile ($A_t = 3.004 \text{ mm}^2$) and divided by the gauge length of the specimen (460 mm). Regarding the strength evaluation, it is suggested to use the average first cracking stress σ_c , which take into account the total cross-sectional area of the composites in the first phase, namely before the mortar cracking, in order to more realistically include the contribution of the mortar; while in the second, we refer to σ_2 which take into account the cross-area of the textile reinforcement alone.

Table 3- 36 : Tensile properties of H-TRM at the end of stage I.

		Stage I				
	series/ nb of specimens	F_1 (N)	$\sigma_1 = F_1 / A_t$ (MPa)	$\sigma_c = F_1 / A_c$ (MPa)	U_1 (mm)	ε_1 (%)
HE-TRM	H-E-28d/5	2161.7	720.6	2.7	1.9	0.3
	CoV (%)	15.0	15.0	15.0	10.5	10.5
	H-E-2m/5	1867.2	622.4	2.3	2.0	0.4
	CoV (%)	35.8	35.8	35.8	11.3	11.3
	H-E-3m/3	3182.4	1060.8	4	2.1	0.5
	CoV (%)	23.0	23.0	23.0	6.0	6.0
	H-E-1y/6	2073,7	690.3	2.6	0.8	0.2
	CoV (%)	24.3	24.3	24.3	49.9	49.9
	H-E-1.5y/3	1077.8	358.8	1.3	0.6	0.1
	CoV (%)	25.3	25.3	25.3	27.2	27.2
	H-E-2y/3	2331.8	776.2	2.9	0.9	0.2
	CoV (%)	3.4	3.4	3.4	22.0	22.0
HL-TRM	H-L-28d/3	887.7	295.5	1.1	0.9	0.2
	CoV (%)	11.9	11.9	11.9	16.6	16.6
	H-L-2m/5	534.3	177.9	0.7	0.1	0.03
	CoV (%)	12.0	12.0	12.0	43.9	43.9
	H-L-3m/2	1022.8	340.5	1.4	1.0	0.2
	CoV (%)	6.2	6.2	6.2	3.3	3.3
	H-L-1y/4	588.0	195.7	0.7	0.4	0.1
	CoV (%)	20.6	20.6	20.6	13.9	13.9
	H-L-1.5y/4	269.9	89.8	0.3	0.5	0.1
	CoV (%)	9.3	9.3	9.3	29.3	29.3

Table 3- 37 : Tensile properties of H-TRM at the end of stage II.

		Stage II					
	series/ nb of specimens	F ₂ (N)	σ _{p2} (MPa)	U ₂ (mm)	ε _{p2} (%)	E (GPa)	Rupture mode
HE-TRM	H-E-28d/5	379.4	126.3	7.7	1.7	8.9	C
	CoV (%)	43.3	43.3	28.3	28.3	9.4	
	H-E-2m/5	490.3	163.4	12.6	2.7	8.8	C
	CoV (%)	37.8	37.8	31.4	31.4	17.5	
	H-E-3m/3	325.8	108.6	7.7	1.7	8.9	C
	CoV (%)	50.2	50.2	34.7	34.7	14.0	
	H-E-1y/6	265.3	88.3	5.0	1.1	9.1	C
	CoV (%)	36.8	36.8	34.0	34.0	22.0	
	H-E-1.5y/3	375.8	125.1	7.8	1.7	8.7	C
	CoV (%)	45.2	45.2	25.7	25.7	18.2	
	H-E-2y/3	525.2	174.8	5.0	1.1	16.6	C
	CoV (%)	0.6	0.6	7.4	7.4	13.0	
HL-TRM	H-L-28d/3	401.1	133.5	13.6	2.9	6.5	C
	CoV (%)	2.0	2.0	5.5	5.5	14.2	
	H-L-2m/5	208.4	69.4	9.0	2.0	3.2	C
	CoV (%)	28.0	28.0	4.0	4.0	22.6	
	H-L-3m/2	225.0	74.9	10.9	2.4	5.1	C
	CoV (%)	22.4	22.4	1.2	1.2	24.7	
	H-L-1y/4	205.5	68.4	9.6	2.1	3.5	C
	CoV (%)	30.0	30.0	3.0	3.0	20.8	
H-L-1.5y/4	196.4	65.4	11.2	2.4	3.7	C	
CoV (%)	25.5	25.5	18.8	18.8	29.2		

Figure 3- 136 presents the failure which generally occurred by slippage of the yarns inside the mortar matrix without reaching their tensile strength nor their rupture (failure mode C), which resulted in a last branch with a gentle slope in which it was not possible to establish a specific point of failure in all cases.



Figure 3- 136 : Failure mode C recorded for all the series of H-E and H-L TRM.

The average first cracking stress σ_c of the first stage, the average tensile strength σ_{p2} and the average tensile modulus E of the third stage are the key characteristics of the response of these composites and therefore will be analyzed and discussed hereafter:

- The flexural tensile strength of the ettringitic mortar (4.4 MPa) was not reached in almost all the cases. For H-E TRM, the obtained σ_c values are about 61 % for H-E-28d, 52 % for H-E-2m, 91 % for H-E-3m, 59 % for H-E-1y, 29 % for H-E-1.5y and 66 % for H-E-2y series (Table 3- 36). Only for H-E-3m series (91 %), the average stress σ_c is very close to the flexural strength of the Ettringitic matrix (E). These percentages are calculated with respect to the flexural tensile strength of the Ettringitic matrix (E) (4.4 MPa), already determined in chapter 2 (Table 2- 24). In case of H-L TRM, The flexural tensile strength of natural hydraulic lime mortar (2.8 MPa) was not reached in all the cases, the obtained σ_c values are about 39 % for H-L-28d, 25 % for H-L-2m, 50 % for H-L-3m, 25 % for H-L-1y and 11 % for H-L-1.5y series (Table 3- 36). These percentages are calculated with respect to the flexural tensile strength the natural hydraulic lime matrix (L) (2.8 MPa). These results are consistent with those reported in Estevan et al. 2022 [7], [174], employing glass, carbon and basalt meshes.
- The tensile strength of hemp yarns (269.3 MPa) was not reached in any case. For H-E TRM, the obtained average stresses σ_{p2} values are about 47 % for H-E-28d, 61 % for H-E-2m, 40 % for H-E-3m, 33 % for H-E-1y, 46 % for H-E-1.5y and 65 % for H-E-2y series (Table 3- 37). In case of H-L TRM series, the obtained average stresses σ_{max} values are about 50 % for H-L-28d, 26 % for H-L-2m, 28 % for H-L-3m, 25 % for H-L-1y and 24 % for H-L-1.5y (Table 3- 37). These percentages are calculated with respect to the tensile strength hemp yarns (269.3 MPa). It should be noted that the underlying factor responsible for reaching the tensile strength of the yarns, is the type of fabric, so that the evolution of this parameter is strongly conditioned by the meshes used. In our case, it is not reached due to the slippage of the yarns within the matrix before reaching their tensile strength and rigidity (Failure mode C). These results are consistent with those reported in other experimental campaigns with glass [7], [174], carbon and basalt meshes [174].

- The tensile modulus of hemp yarns (4.2 GPa) was exceeded in all the case of H-E TRM, the average elastic modulus E obtained are about 212 % for H-E-28d, 210 % for H-E-2m, 212 % for H-E-3m, 217 % for H-E-1y, 207 % for H-E-1.5y and 395 % for H-E-2y series (Table 3- 37). In case of H-L-TRM, The average elastic modulus E obtained are about 155 % for H-L-28d, 76 % H-L-2m, 121 % for H-L-3m, 83 % for H-L-1y and 88 % for H-L-1.5y series (Table 3- 37). These percentages are calculated with respect to the tensile modulus of hemp yarns (4.2 GPa). As we have seen, in case of H-L TRM, the tensile modulus are lower than that of H-E TRM and closer to the tensile modulus of hemp yarns. The increase in stiffness experienced by H-E series was remarkable, with the tensile modulus superior to double the tensile modulus of hemp yarns. This increase has already been reported in some previous investigations [7], [174], [180], where they attributed it to the fact that mortar matrix can provides additional stiffness in certain cases. In addition, sometimes it allows a much more homogeneous distribution of stresses between the fibers with respect to the tensile test of dry meshes, where irregular distributions or stress concentrations may occur in the anchorage zones.

3.3.4.2 Comparisons between the results of TRM and the results of the durability of yarns in alkaline solutions

In this section, the results of tensile tests done on aged hemp yarns are compared with the results of tensile tests done on TRMs made from these yarns referring to equation (1) [153], [148]. As shown in Table 3- 38, the days of accelerated exposure of yarns corresponds to a predicted service life, which do not match exactly the service life obtained by the tested TRMs, for this reason we compare the results of the TRMs at a service life that is as close as possible to the predicted service life of the yarns. This means that TRM at 2 months will be compared with yarns at 7 days, TRM at 3 months will be compared to yarns at 14 days , TRM at 1 year will be compared with yarns at 74 days and TRM at 1.5 year will be compared with yarns at 90 days (Table 3- 38). Only the aging of yarns at 23°C are taken into accounts in this comparison because the smallest period of accelerated exposure 7 days, at 40°C and 60°C corresponds to 3.67 and 4.64 years in predicted service life, respectively (Table 3- 27), and we don't have corresponding results at these ages in the case of TRM. Table 3- 39 and Table 3- 40 presents the average value of the tensile stress and modulus of H-E-23 and H-L-23 yarns respectively, at a given accelerated exposure with the average values of the tensile stress and modulus of the H-E and H-L TRM respectively, tested at the corresponding service life (Table 3- 38). One can notice that, the tensile stress of H yarns did not match the tensile stress of H TRM in any case:

- The tensile stresses of both H-E-23 and H-L-23 yarns at 7 days of accelerated exposure are greater than the tensile stresses of both H-E and H-L TRM respectively at 2 months of service life.
- The tensile stresses of both H-E-23 and H-L-23 yarns at 14 days of accelerated exposure are greater than the tensile stresses of both H-E and H-L TRM respectively at 3 months of service life.

- The tensile stresses of both H-E-23 and H-L-23 yarns at 74 days of accelerated exposure are lower than the tensile stresses of both H-E and H-L TRM respectively at 1 year of service life.
- The tensile stresses of both H-E-23 and H-L-23 yarns at 90 days of accelerated exposure are lower than the tensile stresses of both H-E and H-L TRM respectively at 1.5 year of service life.

These differences in tensile stresses between yarns and TRM are due to two facts:

- The slippage of the textile in both matrices E and L before attaining their tensile strength. This was explained above by two reasons: either the formation of the pores at the interface textile-matrix or the clevis type system used to apply the tensile load at both extremities of the specimen. A special surface treatment or coating of hemp textile is needed before using them in the TRM composites. In addition, further investigations on tensile properties of hemp TRM are needed by using a grip system that allows a uniform clamping at all the surface of both extremities of the TRM specimen.
- The invalidity of the correlation formula in case of aging of dry hemp yarns in L solution (pH 12.5). Before using this formula, it was expected that the temperature accelerates the aging and the degradation of the yarns, but this was not what we observed from the experimental results of aging of hemp yarns in R and L solutions. In these solutions, we have seen that the temperature played a beneficial role by slowing down the aging process. However, in Micelli and Aiello [148]. This formula has proved to be effective for the accelerated aging of glass, carbon, basalt, PBO and steel fibers in solutions having a pH greater than 12.5.

The remarkable differences in tensile modulus between H-E-23 yarns and H-E TRM have been already explained.

Table 3- 38: Predicted service life of hemp yarns calculated from accelerated days of exposure by using equation (1) and the real service of TRM.

H Yarns		H-TRM
Days of accelerated exposure (T=23°C)	Predicted service life (days)	service life obtained by the tested TRM
7	41.2	2 months
14	82.4	3 months
74	435.7	1 year
90	529.9	1.5 year

Table 3- 39: Comparison of results between H-E-23 yarns and H-E TRM.

H-E-23 Yarns			H-E TRM		
Accelerated exposure	σ_{\max} (MPa)	E (GPa)	Service life	σ_{\max} (MPa)	E (GPa)
7 d	332.7	3.9	2 months	163.4	8.8
14 d	311.0	5.6	3 months	108.6	8.9
74 d	50.8	1.1	1 year	88.3	9.1
90 d	14.0	0.3	1.5 year	125.1	8.7

Table 3- 40: Comparison of results between H-L-23 yarns and H-L TRM.

H-L-23 Yarns			H-L TRM		
Accelerated exposure	σ_{\max} (MPa)	E (GPa)	Service life	σ_{\max} (MPa)	E (GPa)
7 d	301.5	4.0	2 months	69.4	3.2
14 d	339.6	4.9	3 months	74.9	5.1
74 d	44.3	1.1	1 year	68.4	3.5
90 d	6.6	0.5	1.5 year	65.4	3.7

3.4 Conclusions

In this chapter, the effect of alkaline solutions reproducing the environments of the ettringitic (E) and the natural hydraulic lime (L) mortars along with the effect of different temperatures on the tensile behavior of hemp (H) and flax (F) yarns were examined. Their residual tensile strengths, tensile modulus and ultimate tensile strains after different exposure periods have been quantified and discussed. In addition, TRMs made from hemp textile (H) and ettringitic (E) and lime (L) matrices are mechanically characterized by means of tensile tests at different service lives. Finally, a comparison between the results of tensile tests on aged H yarns with the results of tensile tests on TRMs made using these yarns was done.

From the results of tensile tests on the aged H yarns, the following main conclusions can be drawn:

- The temperature played an accelerated role for the retting process and the mercerization process of hemp yarns for both pH 10.5 and 12.5;
- The most severe environments on hemp yarns were E-23, E-40, E-60, R-23 and L-23. In these environments, a total strength loss was obtained after 90 days of immersion.
- Only for pH 10.5, the temperature played an accelerated role for both the 20 % damage and the 50 % damage of hemp yarns, while for pH 7 and pH 12.5 it played the role of delaying these damages; so the Arrhenius approach used in the aging protocols of hemp yarns could be valid in case of pH 10.5 but it is not recommended to use for pH 7 and pH 12.5;
- The pH of the solution played an accelerated role for the mercerization process of hemp yarns at 23°C;

- The pH of the solution played an accelerated role for both 20 % damage and the 50 % damage of the hemp yarns at 23°C, while it played the role of delaying both damages at 40°C and 60°C.

From the results of tensile tests on aged F yarns, the following main conclusions can be drawn:

- Flax yarns undergo a mercerization process only at 23°C for both pH 10.5 and 12.5;
- The most severe environment on flax yarn was E-60, which corresponds to a pH of 10.5 and a temperature of 60°C. In this environment, flax yarns lost about 72 % of their tensile strength and modulus after 90 days of immersion.
- The temperature played an accelerated role for the plasticization process of flax yarns for both pH 10.5 and 12.5. It also played an accelerated role for both the 20 % and the 50 % damage of flax yarns for pH 10.5, while it played the role of delaying the damage for pH 12.5.
- The pH of the solution played the role of delaying the mercerization process of flax yarns at 23°C;
- The pH of the solution played the role of delaying the plasticization process of flax yarns at 60°C;
- The pH of the solution played the role of accelerating the damage of flax yarns at 23°C, while it played the role of delaying the damage of flax yarns at 60°C. This was also the case for hemp yarns. Therefore, it seems that a pH of 12.5 along with a temperature of 60°C have beneficial effects on the durability of hemp and flax yarns and not detrimental effects as it was expected. Further durability investigations on vegetal yarns are needed in order to find a more reliable approach which depends not only to the temperature of the aging protocols but also to the pH of the solution;

From the results of tensile tests on the TRMs made from dry hemp textile, the following main conclusions can be drawn:

- The TRMs made from dry hemp textile did not exhibit the same behavior of the typical three stages tensile behavior of TRM systems made from synthetic fibers textile found in the literature. For both kind of matrices E and L, TRMs exhibited a two stages behavior: the first stage is linear up to the rupture of the matrix afterwards a sudden drop in the tensile stress occurs until it reaches zero. Such experimental evidence may be due to the low initial stiffness of hemp fibers when subjected to tensile loading conditions. Then the second stage starts by a new increase of the tensile stress until reaching a new peak load and then decreasing. Finally the tests ended by the textile slippage within the matrix without attaining their tensile strength.
- Dry hemp yarns used in this study, have demonstrated to be not effective to use in TRM strengthening systems employing the ettringitic mortar or the natural hydraulic lime mortar, without any treatment. A special surface treatment or coating of hemp yarns are

needed before their use in the TRM, in order to enhance the textile-matrix bond and thus allowing the tensile properties of the TRM to reach the tensile properties of the yarns.

- Further investigations on tensile properties of hemp TRM by using a grip system that allows a uniform clamping on all the surface of both extremities of the TRM specimen is needed. In addition investigations through X-ray tomography allowing the visualization of the interface textile-matrix is needed in order to evaluate the porosity and the bond behavior of these composites and trying to better understand the causes of the textile slippage.

From the comparison of the results between tensile tests on aged hemp yarns and tensile tests on aged hemp TRM, the following conclusions can be drawn:

- Since the TRM did not reach the tensile properties of the yarns in any case, so we cannot conclude about the durability of hemp TRM investigated in this study, because the durability is evaluated by the changes in the mechanical performance of the system after aging. It depends on the durability of the fibers, the durability of the matrix itself and the durability of the matrix-fiber interface. As we have already mentioned an enhancement of the textile-matrix bond of these TRM in the short-term, is needed in order to prevent slipping of the textile within the matrix and make them reach greater tensile properties. Then, after improving the validity of this enhancement in the short-term, further investigations concerning their durability in the long-term are needed;
- Since the temperature did not play an accelerated role for the damages of the fibrous materials of hemp yarns, and since the tensile properties of H-E TRMs did not match the tensile properties of aged H-E yarns, so it is not recommended to use an Arrhenius approach in the aging protocols for the prediction of the long-term behavior of hemp and flax yarns in alkaline environments. Further investigations are necessary in order to find a new approach that correlate better the duration of accelerated exposure of natural yarns to alkaline ions with the service life of these yarns when embedded in lime and cementitious matrix of a TRM. As we have already mentioned, the correlation formula should also depends on the pH of the aging solution and not only on the temperature of this solution.

Chapter 4 Durability of bio-resin-coated hemp yarns in accelerated aging solutions and in ettringitic and lime matrices

4.1 Introduction

As we have seen in chapter 3, dry hemp yarns (H) encounters durability problems when they are subjected to alkaline solutions. In addition, we have seen that when TRM made from dry hemp textile are tested in tension, the yarns exhibit a slippage within the matrix and could not reach their tensile strength nor their rupture. Thus, in order to improve the durability of hemp yarns in alkaline environments as well as improving the bond between the hemp yarns and the matrix of a TRM specimen, a coating of bio-resin is used to protect the fibers. Thus, the aim of this chapter is to study the durability of the bio-resin-coated hemp yarns (HC), by reporting the results of an experimental research intended at determining the tensile behavior of the yarns when subjected to various ageing protocols already used for hemp yarns (H). Then, TRMs made from bio-resin-coated hemp textile were manufactured and tested in tension at different ages. Finally, the results are compared with those of chapter 3.

4.2 Accelerated aging of bio-resin-coated hemp yarns

The experimental plan for the accelerated aging of the HC yarns is summarized in Table 4- 41. Same aging environments as for hemp yarns are used for bio-resin-coated hemp yarns except the reference solutions (R-23 and R-60). Then, HC yarns were subjected to tensile test after 7, 14, 28, 42, 74, 90 days of accelerated aging.

Table 4- 41 : Experimental plan for the accelerated aging of HC yarns.

Solutions	(R-23)	(R-60)	(E-23)	(E-40)	(E-60)	(L-23)	(L-40)	(L-60)
Yarn	Distilled water pH 7 T = 23 °C	Distilled water pH 7 T = 60 °C	NaOH pH 10.5 T = 23 °C	NaOH pH 10.5 T = 40 °C	NaOH pH 10.5 T = 60 °C	NaOH pH 12.5 T = 23 °C	NaOH pH 12.5 T = 40 °C	NaOH pH 12.5 T = 60 °C
(HC)			✓	✓	✓	✓	✓	✓

Aging durations

✓ : 7, 14, 28, 42, 74, 90 days

✓ : only 28 and 90 days

4.2.1 Specimens preparation

The yarns were cut from the hemp coils, and then they were manually coated in bio-resin (procedure already shown in chapter 2) and after drying of the resin, the bio-resin-coated hemp

yarns (HC) were immersed in the different solutions, already, prepared in plastic bucket. As in case of H yarns, the specimens of HC yarns at 23°C are left in a controlled room temperature of 23°C, and the ones at 40°C and 60°C, are placed in a heating chamber.

After removal from the aging solution, the samples were left to dry on a Table in ambient conditions for 24 hours before being tested (Figure 4- 137).

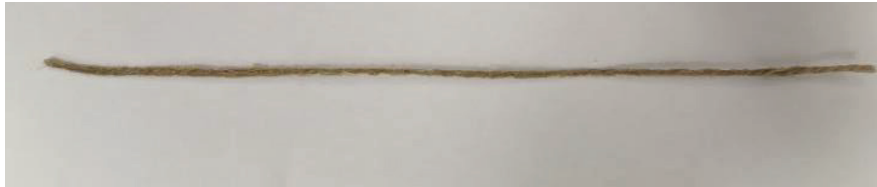


Figure 4- 137 : Drying of bio-resin-coated hemp yarns after removal from aging solutions.

4.2.2 Tensile test setup

Similarly to the tensile test setup used in chapter 2, bio-resin-coated hemp yarns (HC) are tested according to ISO 10618:2005 [171] with a gauge length of 150 mm and a loading rate of 5 mm/min. To ensure alignment of the fibers and to have them straight enough, preloads of 6 N were applied to all the tested yarns. Each series was characterized by six specimens. The mechanical behavior of yarns obtained in chapter 2 without aging was considered as a reference for the durability evaluation of aged yarns.

In the following, the name of each specimen consists of five acronyms separated by “-”: the first acronym refers to the nature of the yarn tested, it is HC (bio-resin-coated hemp). The second one refers to the pH value of the aging solution, it is either E (Ettringitic matrix) for pH 10.5 or L (Lime matrix) for pH 12.5. The third one refers to the temperature of the aging solution; it is either 23, or 40 or 60°C. The fourth one refers to the duration of the aging, it contains a number and a letter which is either d (days) or m (months), and the fifth and last acronym refers to the specimen number in the tested series.

4.2.3 Results of tensile test on the aged HC yarns

First, the results of each series of HC yarns tested is analyzed by calculating the average tensile strength σ_{\max} , the average ultimate tensile strain ε_{\max} and the average tensile modulus E. These results are available, in form of Tables for each series tested, in appendix F. A minimum curve, a maximum curve and an average stress-strain curve for each series are drawn as shown in Figure 4- 138. In order to not encumber the report, only the curves for the series HC-0 are shown as an example. The stress σ refers to the ratio between the tensile load and the cross-sectional area of the yarn (3.278 mm²). The strain ε is the ratio between the global displacement of the cross head and the length of the yarn (150 mm). The elastic modulus E refers to the slope of the branch of stress-strain curve situated between 70 % and 90 % of the maximum tensile strength. Therefore, a Table that summarizes the tensile strength σ_{\max} , the elastic modulus E and the ultimate tensile strain ε_{\max} in the different environments at different exposure periods is available in appendix G.

In the following, in order to better understand the influence of the temperature and the alkalinity of the matrix on the tensile properties of HC yarns, the results are reported in terms of diagrams that show normalized residual values of tensile strength, Young's modulus and ultimate tensile strain in the different environments at different exposure periods. The normalized value is the ratio between the value at a given period of aging with respect to that before aging. Only for the diagram that compare H with HC yarns the real values of σ_{\max} , ε_{\max} and E are presented.

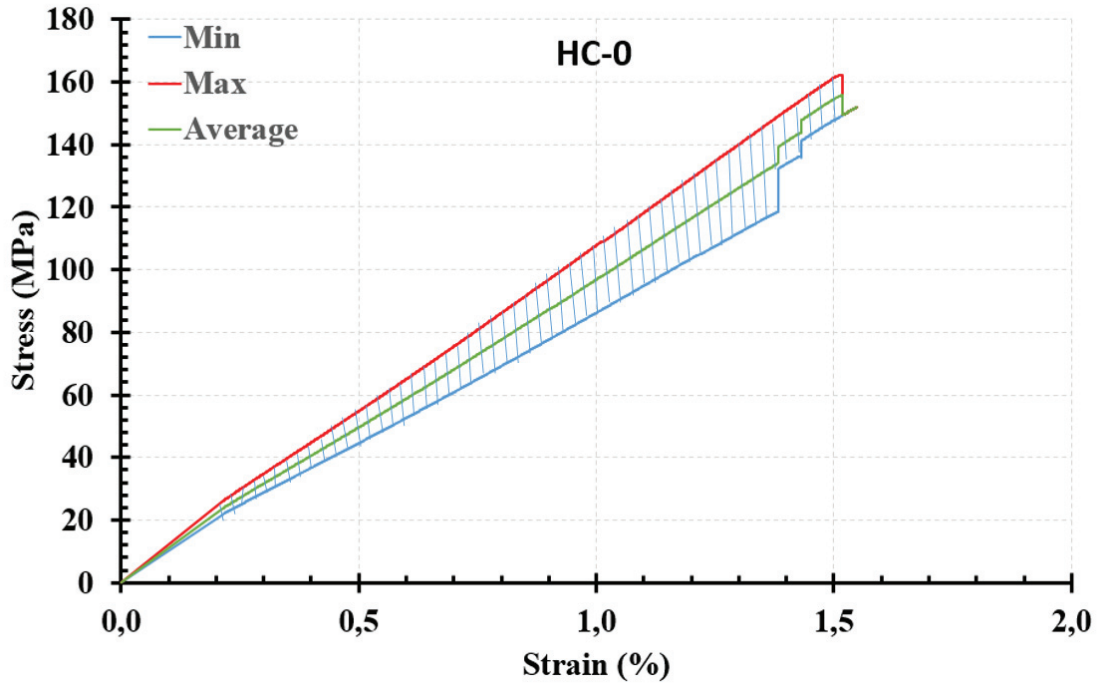


Figure 4- 138 : Minimum, maximum and average stress-strain curves obtained by the six tested specimens of series HC-0.

4.2.3.1 Influence of the temperature on the behavior of HC yarns over time

4.2.3.1.1 In E solutions

Figure 4- 139, Figure 4- 140 and Figure 4- 141 present the influence over time of the temperature on the average tensile strength, the average tensile modulus and the average ultimate tensile strain respectively, of HC yarns subjected to aging in the ettringitic matrix solution (E). One can notice that in solution E and at all the different temperatures 23, 40 and 60°C, there is no significant loss in the average tensile strength of HC yarns. After 90 days of aging, the loss in average σ_{\max} is 8 %, 17 % and 6 % at 23, 40 and 60°C, respectively. Thus, the 20 % damage is not attained in these solutions. Concerning the average tensile modulus, the loss at 23°C is not significant, it is 17 % starting after 42 days of immersion. However, this loss in the average tensile modulus becomes significant with the increase in temperature. It is 32 % at 40°C starting after 28 days (maybe before) and 41 % at 60°C starting after 7 days of immersion. Concerning the average ultimate tensile strain, there is no loss in any case; on the contrary, this parameter encounters a significant increase in solution E, at all the different temperatures. The maximum increase in average ε_{\max} is 64 % at 23°C

after 74 days of immersion, 64 % at 40°C after 28 days of immersion (maybe more increase later between 28 and 90 days), and 121 % at 60°C after 74 days of immersion. We can conclude that in solution E (pH 10.5), the increase in the temperature up to 60°C do not have a significant influence on σ_{\max} but it causes a decrease in E along with an increase in ε_{\max} . This same behavior was observed in the study of Chlela [164] concerning the durability of a composite system made from flax yarns and the same bio-resin used in this study. They related this occurrence to the combined effect of plasticization of the resin network due to the absorbed water, which causes microcracks in the resin and allow the penetration of the aggressive fluids which in turn causes the degradation of the vegetal fibers (hydrolysis of the outer layer of the fibers, debonding at fiber/fiber interfaces, cracking of interfaces between matrix and fiber bundles). It is worth mentioning here that in case of coated hemp yarns, the scattering of the results is due to two reasons: the inhomogeneity of the plant fibers by their own nature and the manual coating of the yarns, which do not assure the same amount of resin for all the specimens.

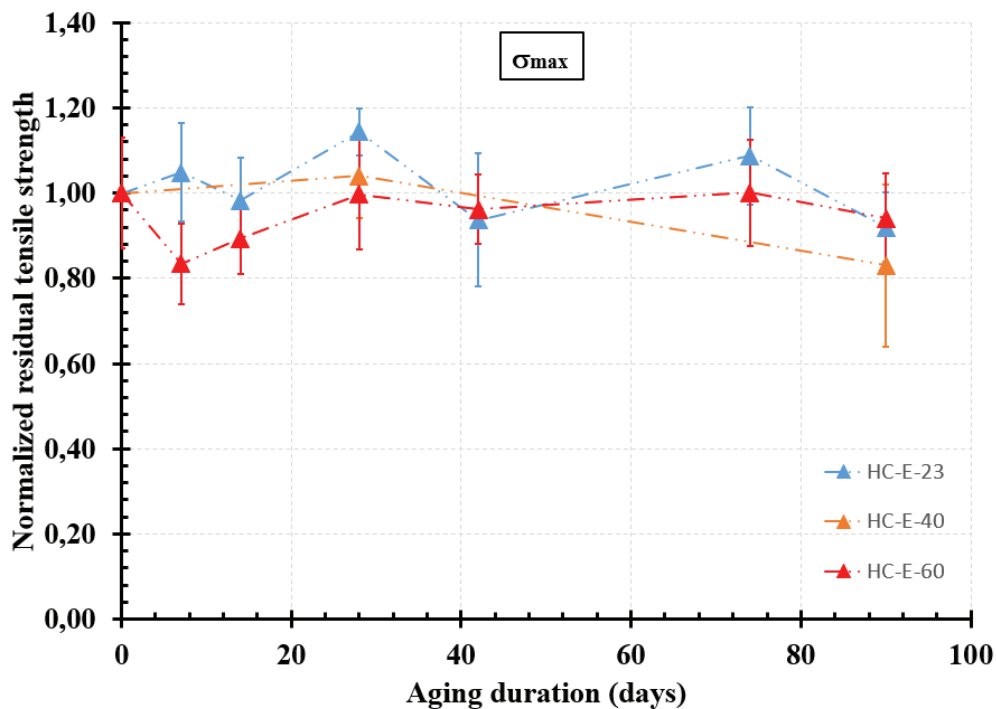


Figure 4- 139 : Influence over time of the temperature on the average tensile strength of bio-resin-coated hemp yarns (HC) immersed in E solution (normalized residual values).

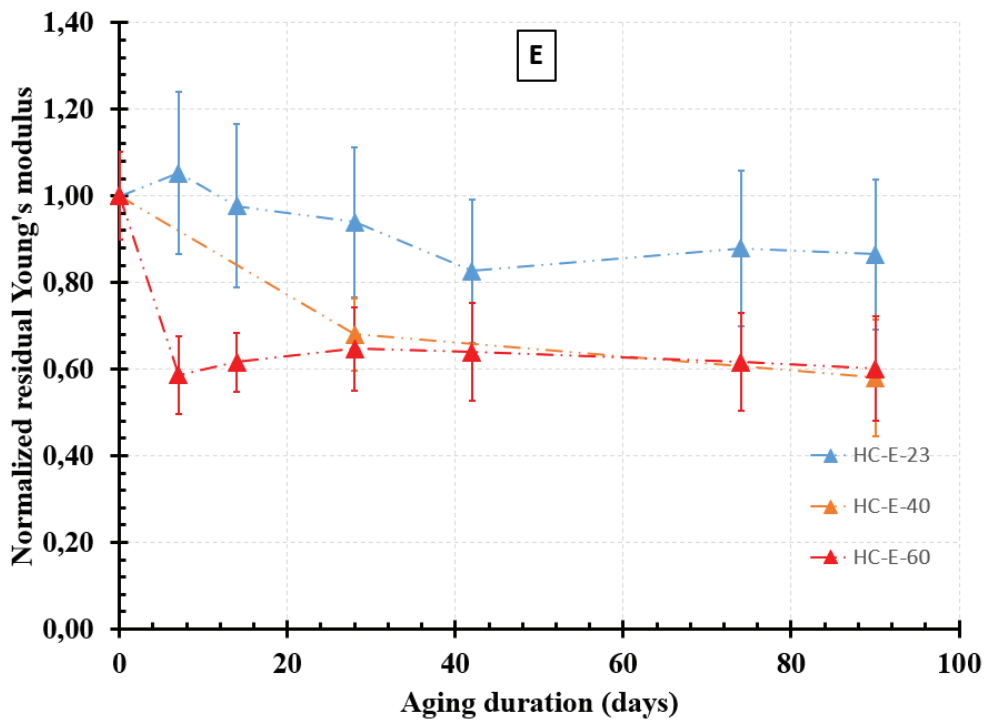


Figure 4- 140 : Influence over time of the temperature on the average tensile modulus of bio-resin-coated hemp yarns (HC) immersed in E solution (normalized residual values).

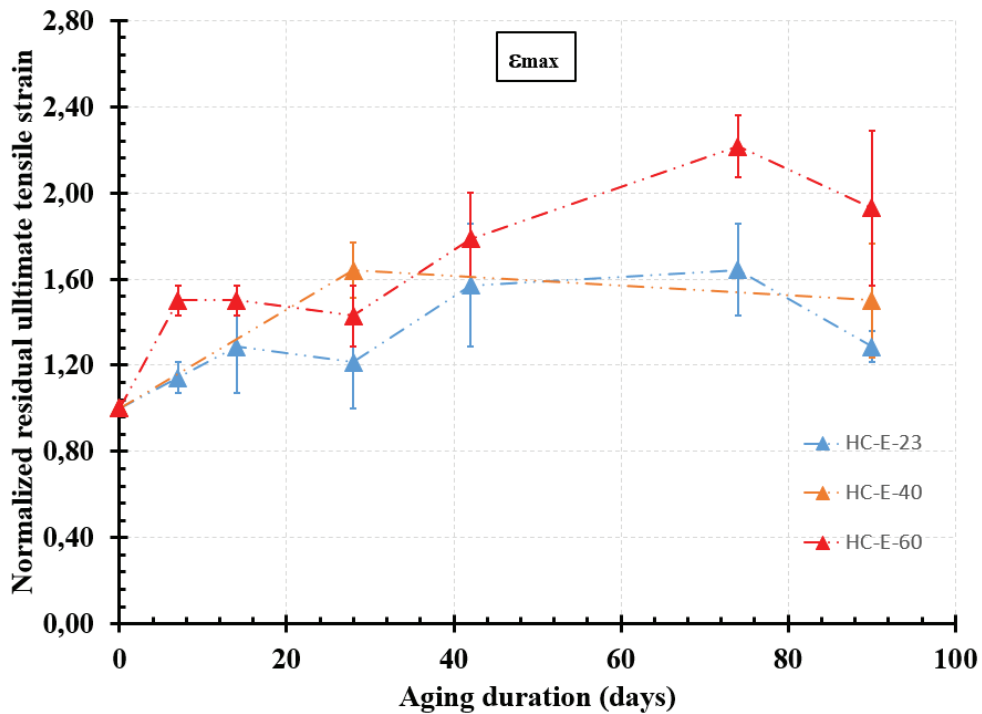


Figure 4- 141 : Influence over time of the temperature on the average ultimate tensile strain of bio-resin-coated hemp yarns (HC) immersed in E solution (normalized residual values).

4.2.3.1.2 In L solutions

Figure 4- 142, Figure 4- 143 and Figure 4- 144 present the influence over time of the temperature on the average tensile strength, the average tensile modulus and the average ultimate tensile strain respectively, of HC yarns subjected to aging in the natural hydraulic lime matrix solution (L). One can notice that in solution L at 23 and 40°C, there is no significant loss in the average tensile strength of HC yarns. After 90 days of immersion, no loss at 23°C and it is only 5 % at 40°C. Thus, the 20 % damage is not attained in these solutions. However, at 60°C, the loss in the average tensile strength of HC yarns is significant; it is 43 % after 90 days of immersion. Concerning the average tensile modulus, the loss at 23°C is not significant, it is 10 % starting after 90 days of immersion. However, it is 42 % at 40°C starting after 28 days of immersion (maybe before) remaining constant after 90 days of immersion. At 60°C, the loss in the average tensile modulus is 33 % starting after 7 days of immersion until reaching 43 % after 90 days of immersion. Concerning the average ultimate tensile strain, there is no loss in any case; on the contrary, this parameter encounters a significant increase in solution E, at all the different temperatures. The maximum increase in ϵ_{\max} is 64 % at 23°C after 74 days of immersion, 79 % at 40°C after 90 days of immersion (maybe more increase later between 28 and 90 days), and 86 % at 60°C after 42 days of immersion. We can conclude that in solution L (pH 12.5), the increase in the temperature of 60°C have a significant influence on the tensile properties of HC yarns allowing the occurrence of the plasticization of the resin network by the water molecules [175], which leads to the decrease in the tensile properties of the resin and making it unable to distribute and share properly the external forces to the fibers, resulting in a macroscopic reduction in the tensile strength of the coated yarn [148]. In addition, the diffusion of the aggressive fluid through the resin matrix may have caused the degradation of hemp fibers (hydrolysis of the outer layer of the fibers, debonding at fiber/fiber interfaces, cracking of interfaces between matrix and fiber bundles) also contributed to this degradation. Both effects resulted in an increase in the average ultimate tensile strain of the fiber along with a decrease in the average tensile strength and modulus.

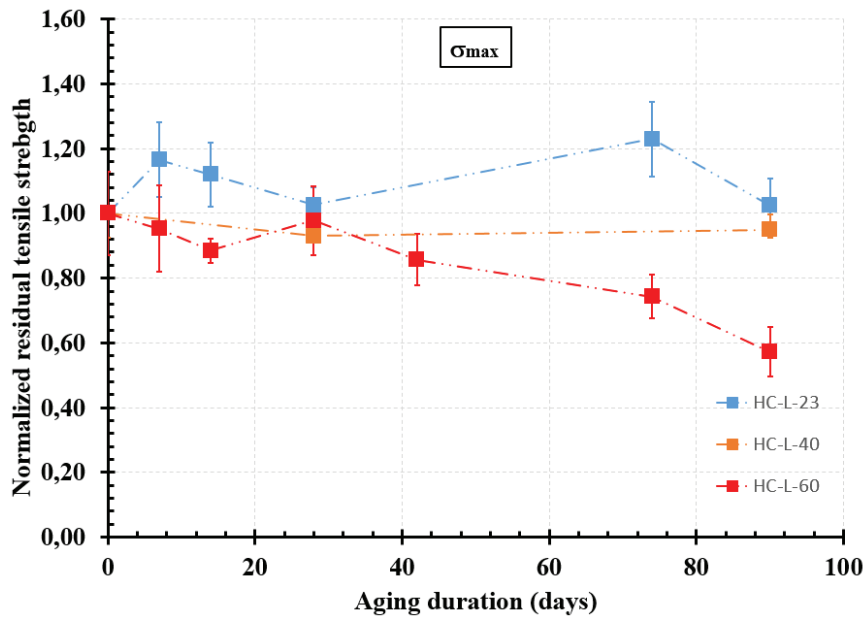


Figure 4- 142 : Influence over time of the temperature on the average tensile strength of bio-resin-coated hemp yarns (HC) immersed in L solution (normalized residual values).

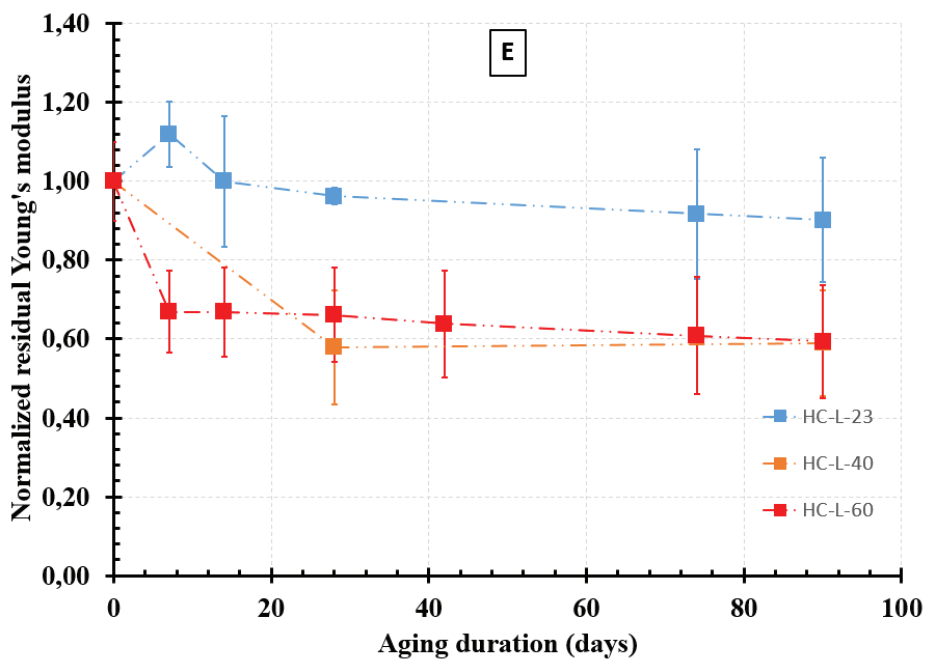


Figure 4- 143 : Influence over time of the temperature on the average tensile modulus of bio-resin-coated hemp yarns (HC) immersed in L solution (normalized residual values).

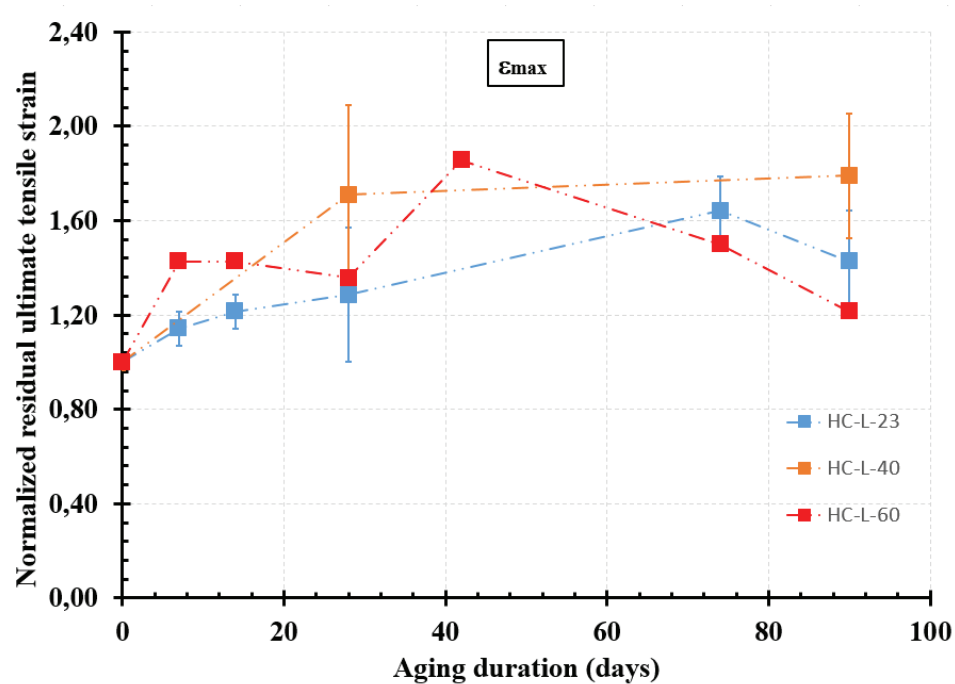


Figure 4- 144 : Influence over time of the temperature on the average ultimate tensile strain of bio-resin-coated hemp yarns (HC) immersed in L solution (normalized residual values).

4.2.3.2 Influence of the pH on the tensile behavior of HC yarns over time

4.2.3.2.1 At 23°C

Figure 4- 145, Figure 4- 146 and Figure 3- 100 present the influence over time of the pH on the average tensile strength, the average tensile modulus and the average ultimate tensile strain respectively, of HC yarns subjected to aging at 23°C. One can notice that, in both solutions E and L, there is no significant loss in the average tensile strength of HC yarns. After 90 days of immersion, the loss in average σ_{\max} is 8 % in solution E and no loss in solution L. Thus, the 20 % damage is not attained in these solutions. Concerning the average tensile modulus, the loss is again not significant in both solution. It is 14 % in solution E and 10 % in solution L after 90 days of immersion. Concerning the average ultimate tensile strain, there is no loss in any case; on the contrary, this parameter encounters a significant increase in both solution E and L. The maximum increase in average ϵ_{\max} is 64 % in both solutions after 74 days of immersion. Furthermore, we can clearly notice that the average values of σ_{\max} , E and ϵ_{\max} for HC yarns are very close for both series HC-E-23 and HC-L-23 at all the exposure periods (Figure 4- 145, Figure 4- 146 and Figure 3- 100). Therefore, we can conclude that, at 23°C, both solutions E and L have same effect on HC yarns maintaining good tensile properties after 90 days of immersion. In other words, the pH variation did not affect the tensile behavior of HC yarns at 23°C.

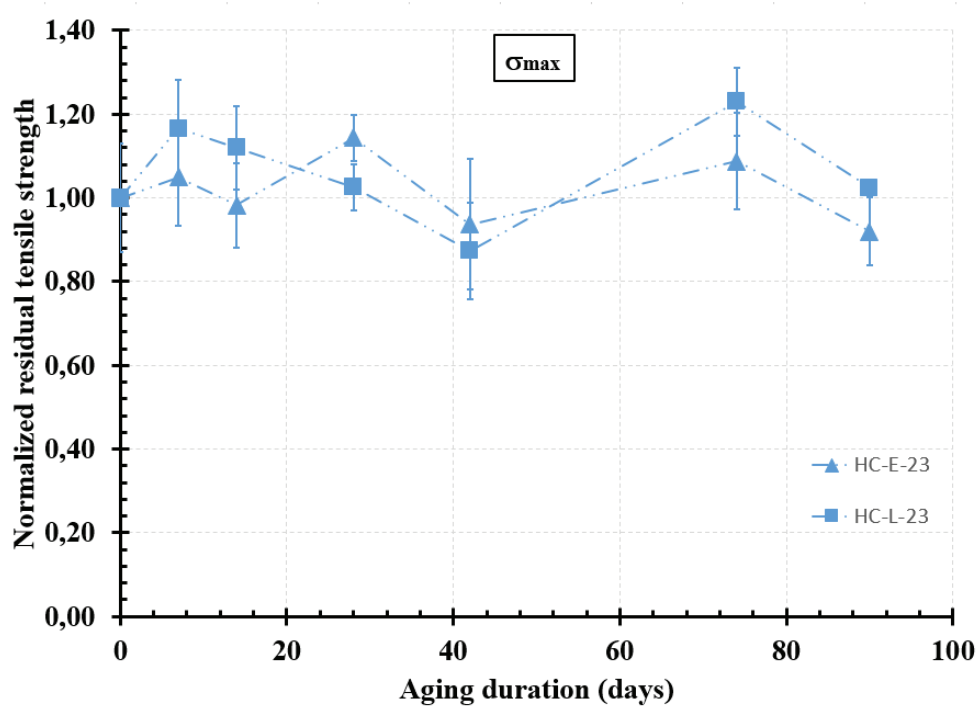


Figure 4- 145 : Influence over time of the pH on the average tensile strength of bio-resin-coated hemp yarns (HC) at 23°C (normalized residual values).

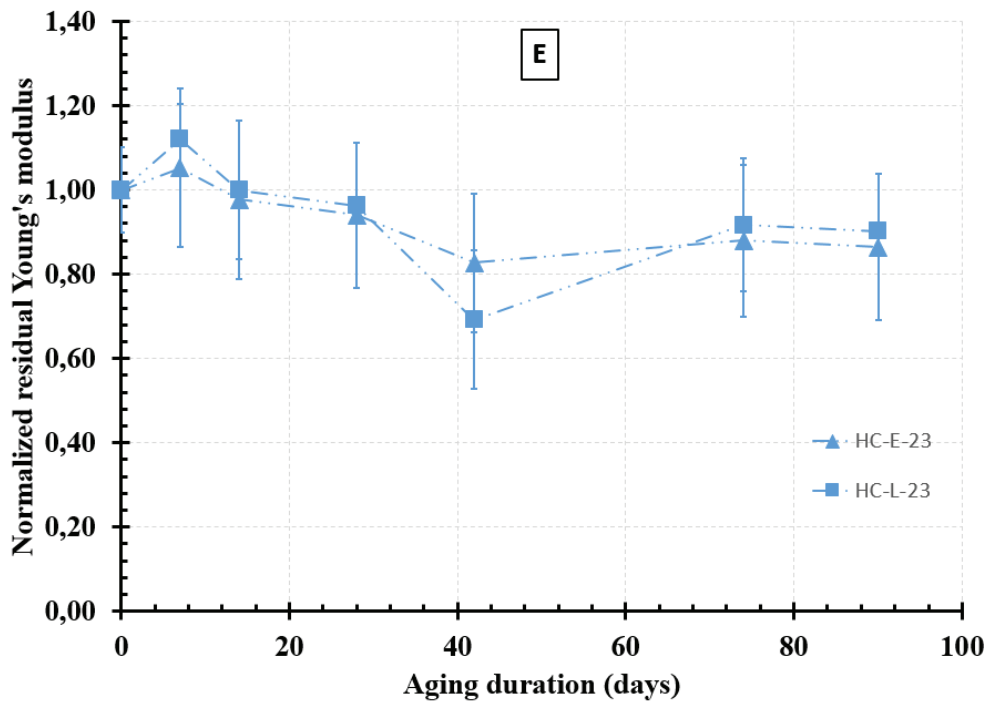


Figure 4- 146 : Influence over time of the pH on the average tensile modulus of bio-resin-coated hemp yarns (HC) at 23°C (normalized residual values).

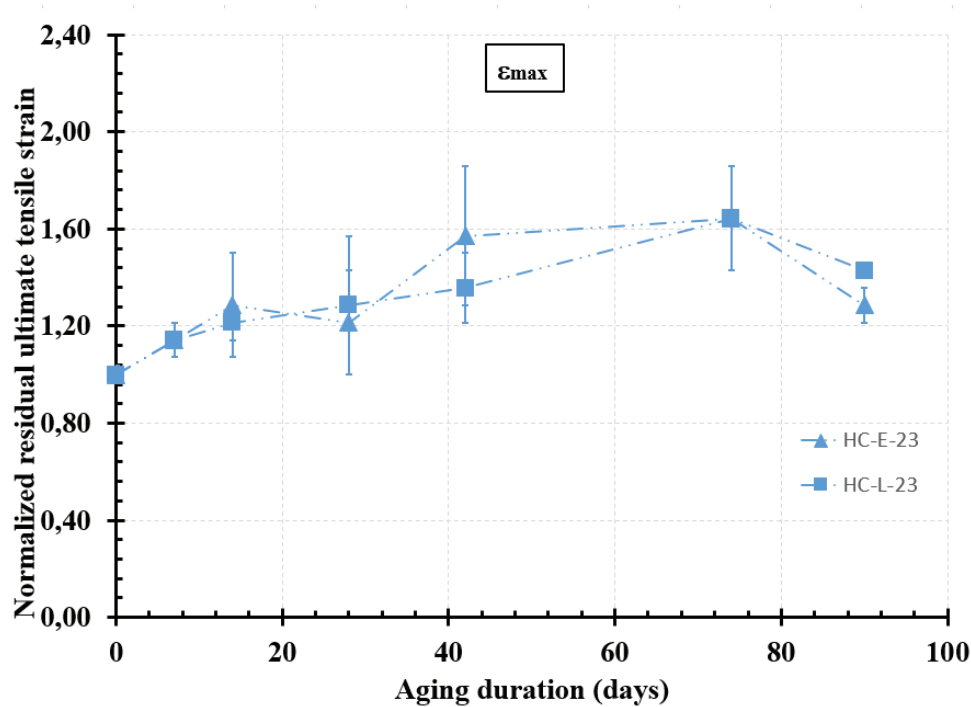


Figure 4- 147 : Influence over time of the pH on the average ultimate tensile strain of bio-resin-coated hemp yarns (HC) at 23°C (normalized residual values).

4.2.3.2.2 At 40°C

Figure 4- 148, Figure 4- 149 and Figure 4- 150 present the influence over time of the pH on the average tensile strength, the average tensile modulus and the average ultimate tensile strain respectively, of HC yarns subjected to aging at 40°C. One can notice that, in both solutions E and L. There is no significant loss in the tensile strength of HC yarns. After 90 days of immersion, the loss in the average σ_{\max} is 17 % in solution E and 5 % in solution L. Thus, the 20 % damage is not attained in these solutions. Concerning the average tensile modulus, the loss is significant in both solution. It is 42 % in solution E and 41 % in solution L after 90 days of immersion. Concerning the average ultimate tensile strain, there is no loss in any case; on the contrary, this parameter encounters a significant increase in both solution E and L. The maximum increase in the average ϵ_{\max} is 64 % in solution E and 71 % in solution L after 28 days of immersion. Furthermore, we can clearly notice that the average values of σ_{\max} , E and ϵ_{\max} for HC yarns are very close for both series HC-E-40 and HC-L-40 at all the exposure periods (Figure 4- 148, Figure 4- 149 and Figure 4- 150). Therefore, we can conclude that, at 40°C, both solutions E and L have same effect on HC yarns maintaining good tensile strength, while decreasing the tensile modulus of about 41-42 % and increasing the ultimate tensile strength of about 50-79 % after 90 days of immersion.

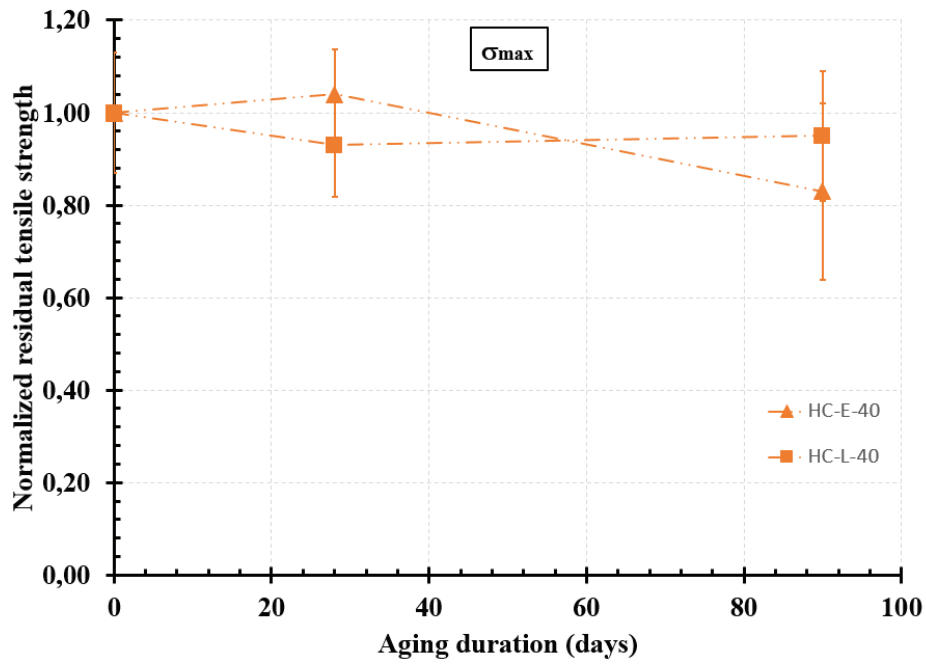


Figure 4- 148 : Influence over time of the pH on the average tensile strength of bio-resin-coated hemp yarns (HC) at 40°C (normalized residual values).

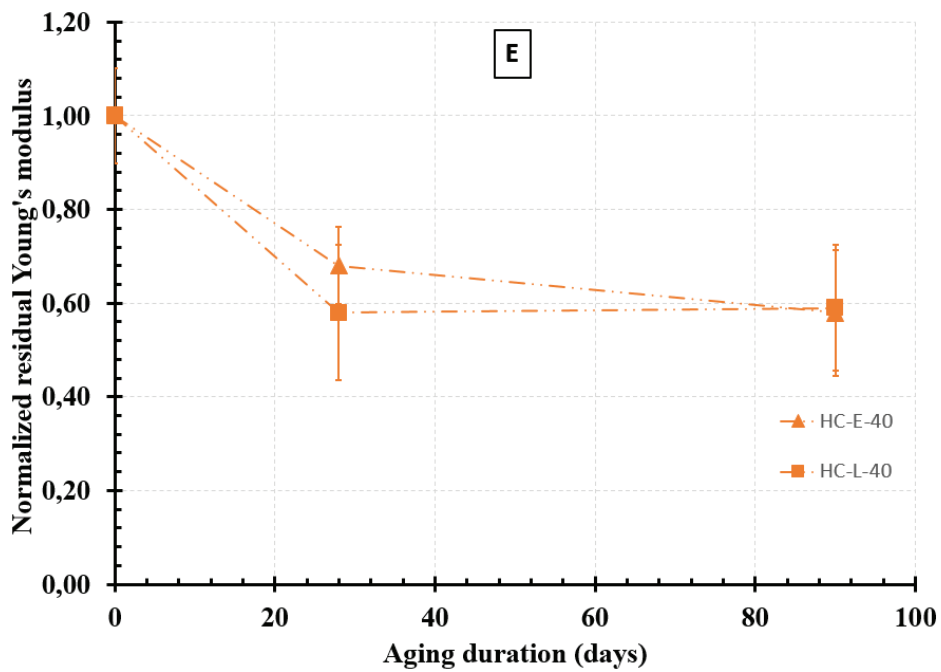


Figure 4- 149 : Influence over time of the pH on the average tensile modulus of bio-resin-coated hemp yarns (HC) at 40°C (normalized residual values).

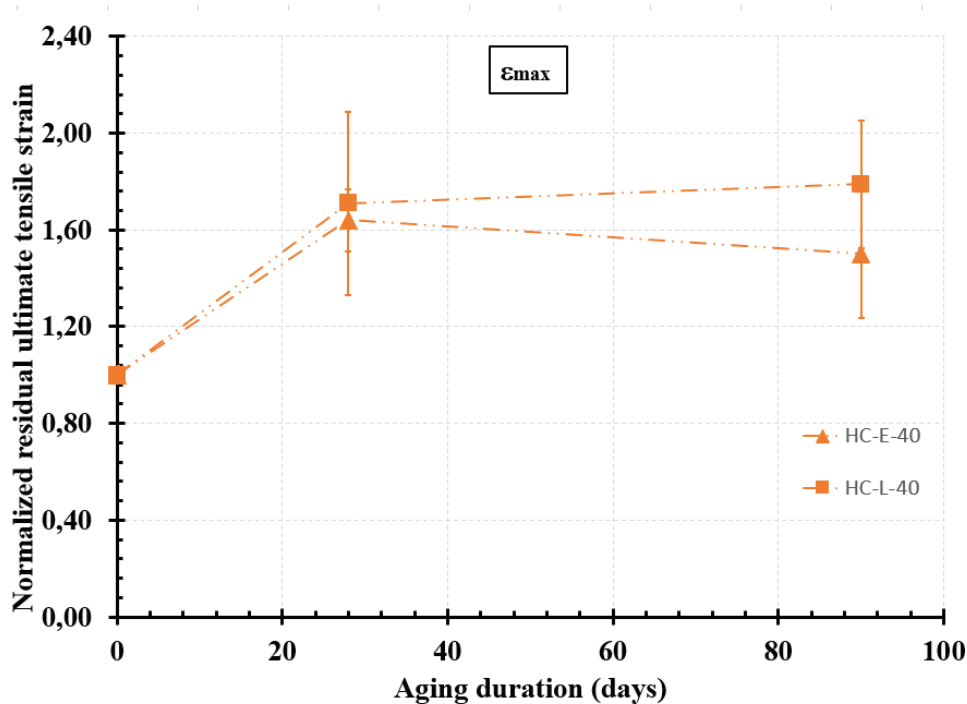


Figure 4- 150 : Influence over time of the pH on the average ultimate tensile strain of bio-resin-coated hemp yarns (HC) at 40°C (normalized residual values).

4.2.3.2.3 At 60°C

Figure 4- 151, Figure 4- 152 and Figure 4- 153 present the influence over time of the pH on the average tensile strength, the average tensile modulus and the average ultimate tensile strain respectively, of HC yarns subjected to aging at 60°C. One can notice that, in solution E, there is no significant loss in the tensile strength of HC yarns. After 90 days of immersion, the loss in the average σ_{max} is 6 % after 90 days of immersion. Thus, the 20 % damage is not attained in this solution. However, in solution L, the loss is significant, it is 43 % after 90 days of immersion. Concerning the average tensile modulus, the loss is significant in both solution. It is 40 % in solution E and 41 % in solution L after 90 days of immersion. Note that, the loss in the average tensile modulus starts immediately after 7 days of immersion and remains constant until 90 days. Concerning the average ultimate tensile strain, there is no loss in any case; on the contrary, this parameter encounters a significant increase in both solution E and L. The maximum increase in the average ϵ_{max} is 121 % in solution E after 74 days of immersion and 86 % in solution L after 42 days of immersion. Therefore, we can conclude that, at 60°C, both solutions E and L have same effect on the tensile modulus (Figure 4- 152) and ultimate tensile strain (Figure 4- 153) of HC yarns but different effect on tensile strength (Figure 4- 151). In addition, the solution L-60 has demonstrated to be the most severe environment on HC yarns. In Micelli and Aiello [148], they explained that sometimes even if the polymeric matrix is not damaged, it may produce a drop in the composite strength if fluid penetration causes micro cracks. In this occurrence, the stiffness of the matrix is reduced and local regions of stress concentration may arise within the composite

structure. At this point, the matrix is not able to distribute and share properly the external forces to the fibers, resulting in a macroscopic reduction of the composite tensile strength.

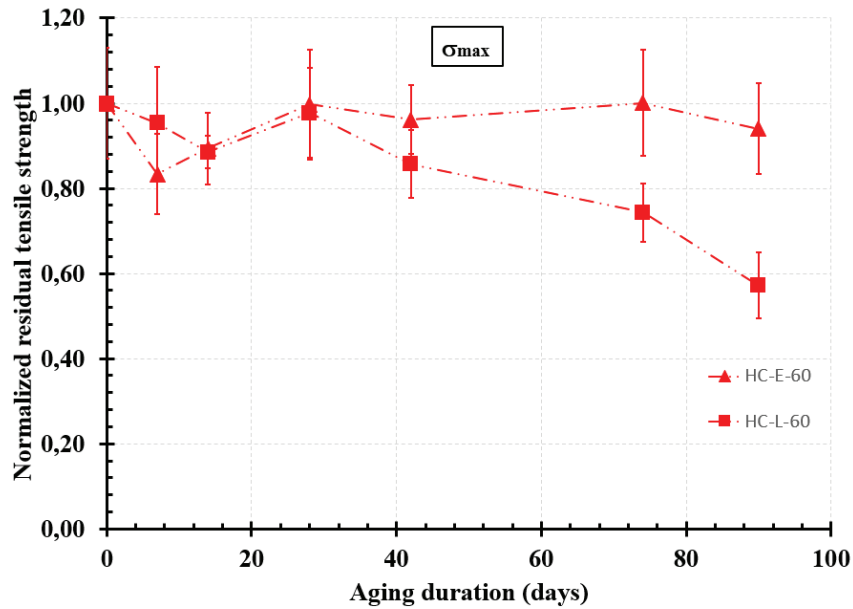


Figure 4- 151 : Influence over time of the pH on the average tensile strength of bio-resin-coated hemp yarns (HC) at 60°C (normalized residual values).

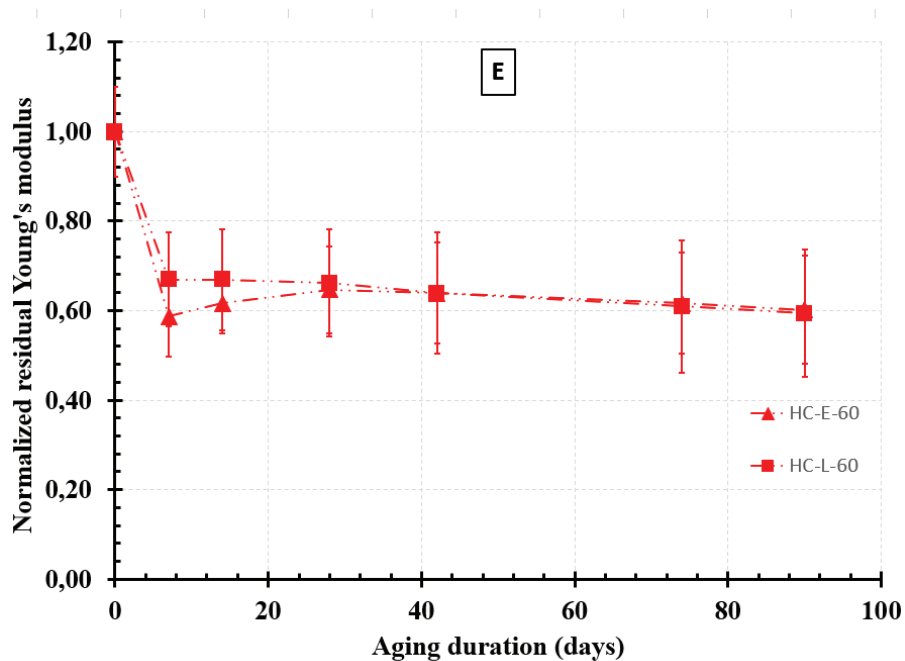


Figure 4- 152 : Influence over time of the pH on the average tensile modulus of bio-resin-coated hemp yarns (HC) at 60°C (normalized residual values).

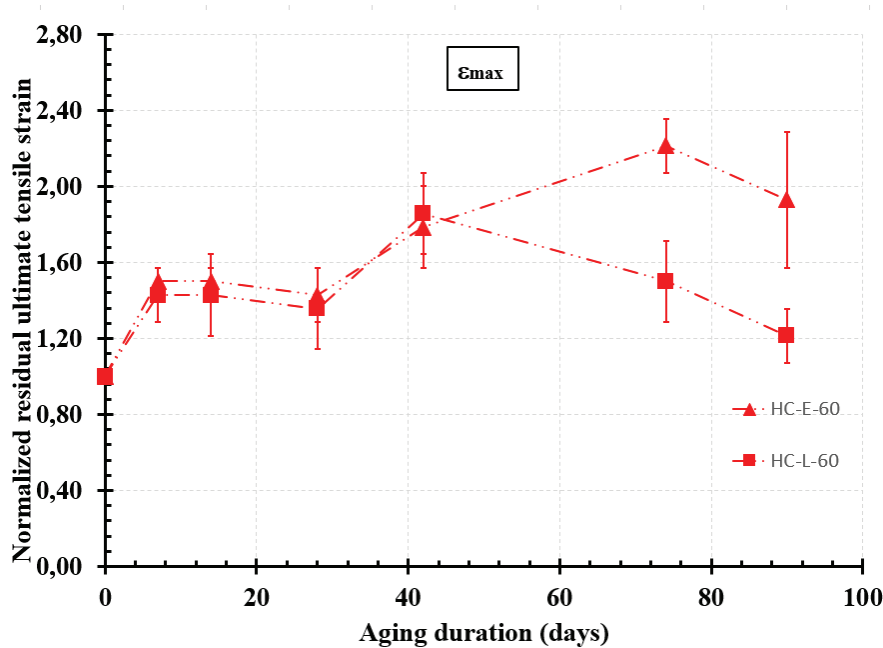


Figure 4- 153 : Influence over time of the pH on the average ultimate tensile strain of bio-resin-coated hemp yarns (HC) at 60°C (normalized residual values).

4.2.3.3 Influence of the bio-resin coating on the tensile behavior of hemp yarns over time

4.2.3.3.1 In solution E-23

Figure 4- 154, Figure 4- 155 and Figure 4- 156 present the influence of the bio-resin coating on the average tensile strength, the average tensile modulus and the average ultimate tensile strain respectively, of hemp yarns immersed in solution E-23. At first, as we have also seen in chapter 2, without aging (at 0 days), the average tensile strength of the bio-resin-coated hemp yarns (HC) is approximately 48 % lower than that of the uncoated ones (H), but their average Young's modulus is 2.3 times higher than that of uncoated yarns. This is because during the resin treatment, the fiber absorbs the solution, allowing the penetration of the polymer between the fiber cells and the internal walls of the lumen. After drying, the polymer becomes more rigid it sticks the fibers together making their structure stiffer and denser resulting in a reduction of the tensile strength as well as the tensile elongation of the fiber. However, after aging in solution E-23, we can notice that, up to 60 days of immersion H yarns undergo a mercerization process while HC yarns do not. Thus, the resin prevented the mercerization process from occurring. Then, H yarns undergo a sharp decrease in the tensile properties leading to their complete degradation after 90 days of immersion. While HC yarns retain tensile properties that are very close to their initial ones after 90 days of immersion.

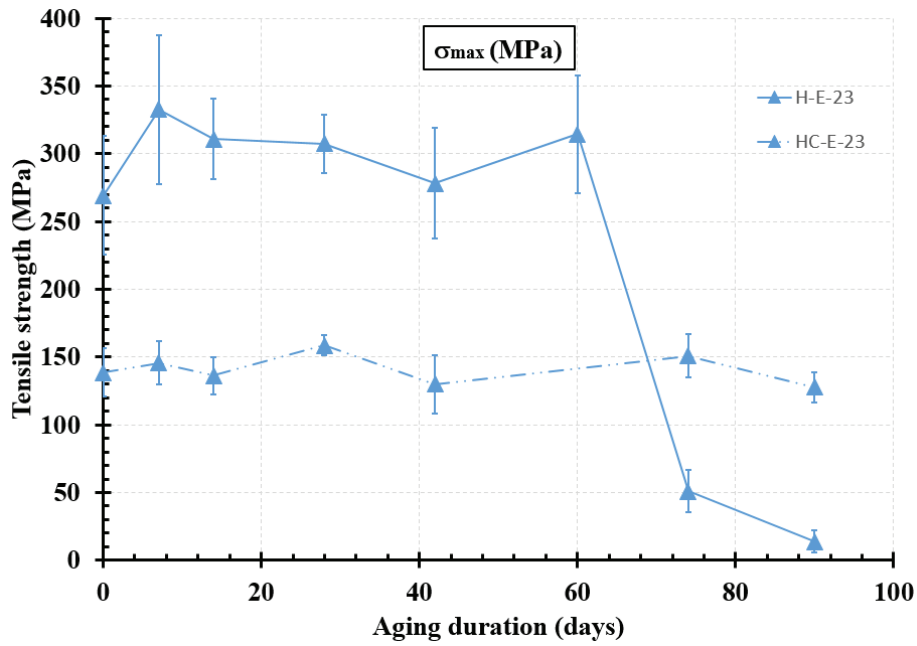


Figure 4- 154 : Influence over time of the bio-resin coating on the average tensile strength of hemp yarns in E-23 solution.

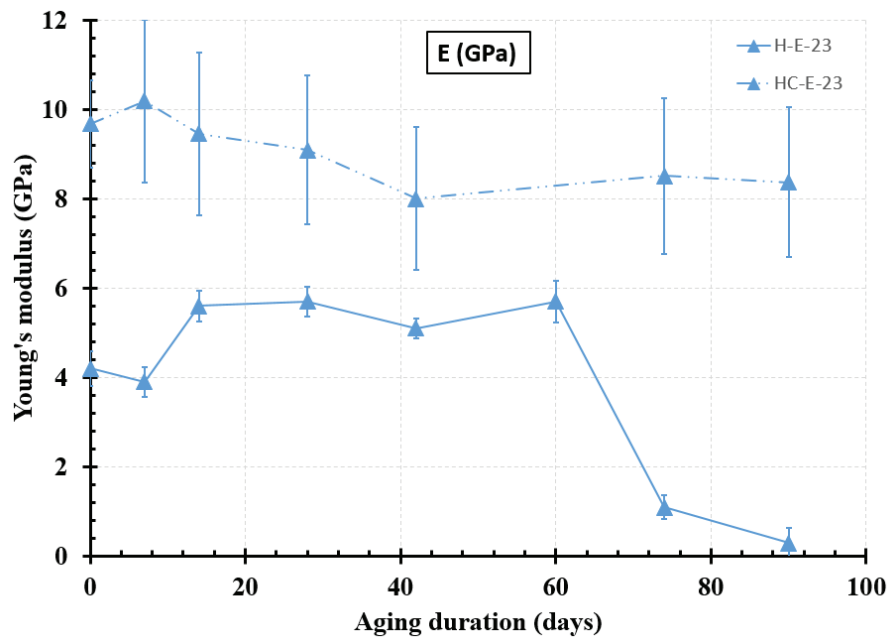


Figure 4- 155 : Influence over time of the bio-resin coating on the average tensile modulus of hemp yarns in E-23 solution.

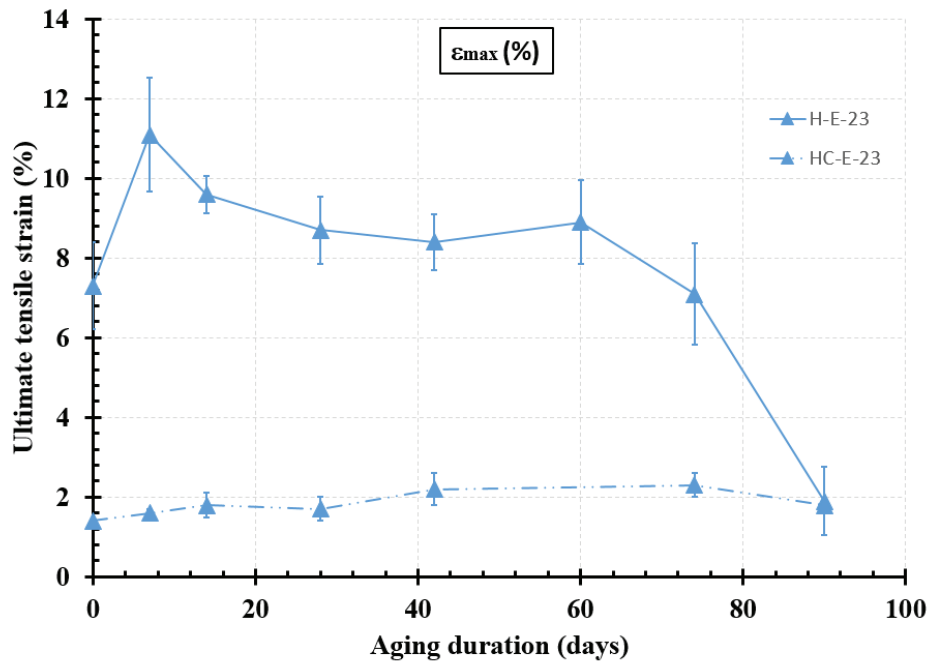


Figure 4- 156 : Influence over time of the bio-resin coating on the average ultimate tensile strain of hemp yarns in E-23 solution.

Therefore, we can conclude that, in addition to enhancing tensile modulus and reducing the water absorption capacity of hemp yarns. The bio-resin coating used in this study has a beneficial effects on their durability by reducing their chemical vulnerability in alkaline environments and preventing the mineralization process and the alkaline hydrolysis process from occurring, which in turns prevents the degradation of the fiber. Moreover, one can clearly notice the decrease of the standards deviation in case of HC yarns when comparing them to those of H yarns (Figure 4- 154, Figure 4- 155 and Figure 4- 156).

4.2.3.3.2 In solution E-40

Figure 4- 157, Figure 4- 158 and Figure 4- 159 present the influence of the bio-resin coating on the average tensile strength, the average tensile modulus and the average ultimate tensile strain respectively, of hemp yarns immersed in solution E-40. One can notice that again in this solution, the bio-resin coating prevented the mercerization process from occurring but protected the hemp yarns without being sensitive to chemical/mechanical degradation.

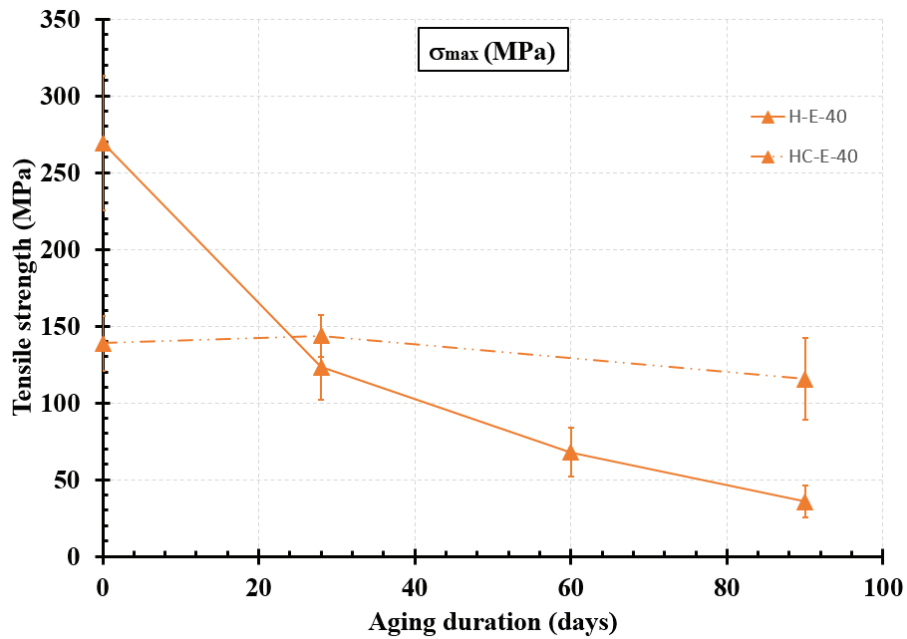


Figure 4- 157 : Influence over time of the bio-resin coating on the average tensile strength of hemp yarns in E-40 solution.

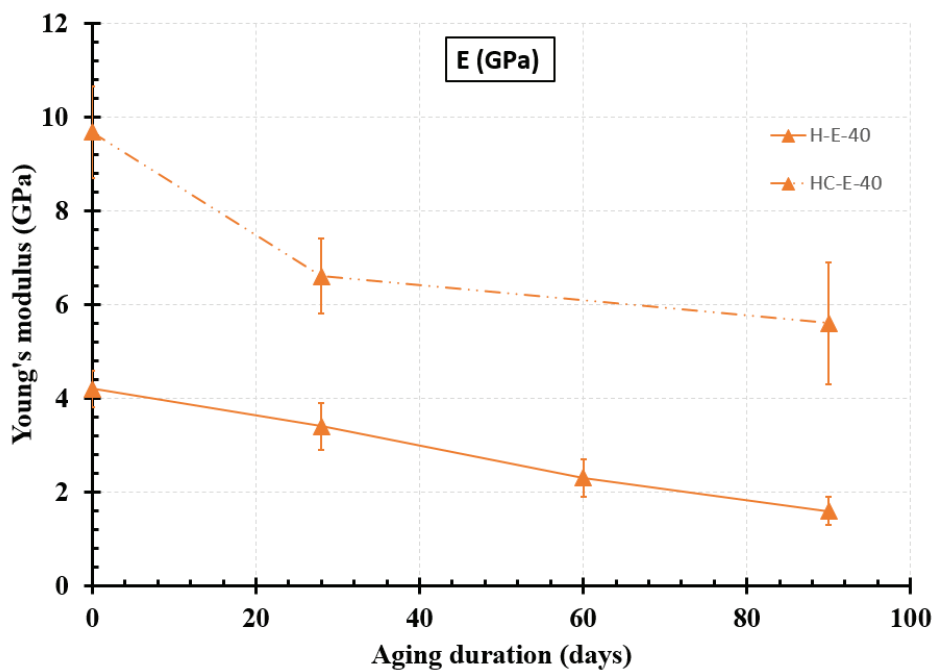


Figure 4- 158 : Influence over time of the bio-resin coating on the average tensile modulus of hemp yarns in E-40 solution.

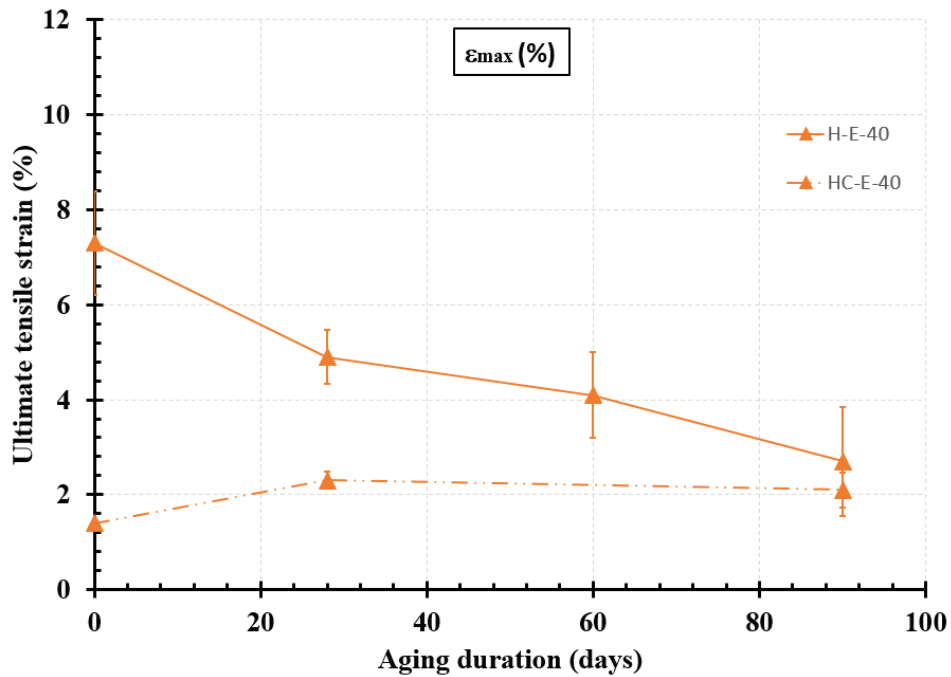


Figure 4- 159 : Influence over time of the bio-resin coating on the average ultimate tensile strain of hemp yarns in E-40 solution.

4.2.3.3.3 In solution E-60

Figure 4- 160, Figure 4- 161 and Figure 4- 162 present the influence of the bio-resin coating on the average tensile strength, the average tensile modulus and the average ultimate tensile strain respectively, of hemp yarns immersed in solution E-60. One can notice that again in this solution, the bio-resin coating prevented the mercerization process from occurring but protected the hemp yarns against the alkaline degradation.

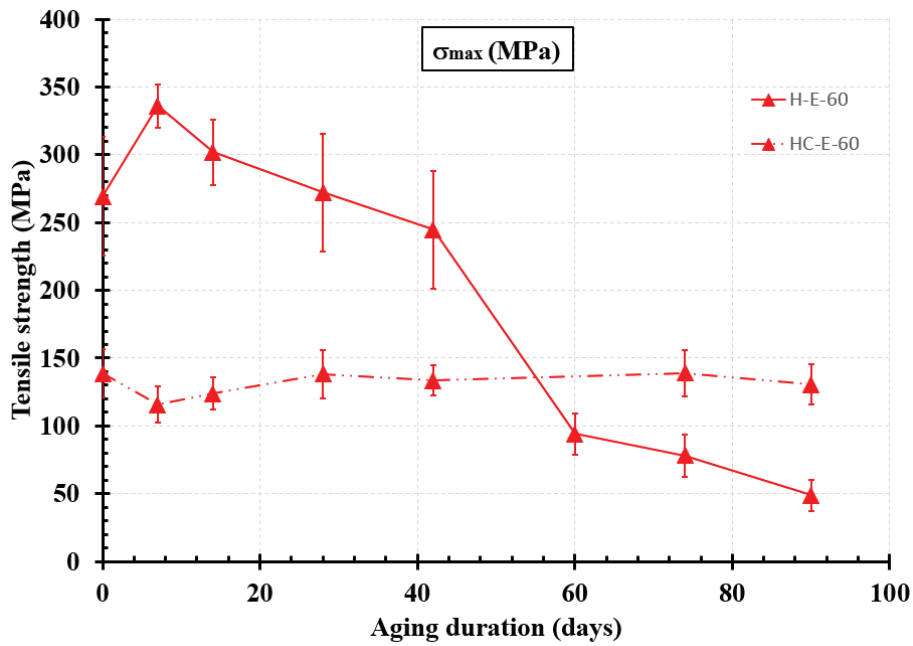


Figure 4- 160 : Influence over time of the bio-resin coating on the average tensile strength of hemp yarns in E-60 solution.

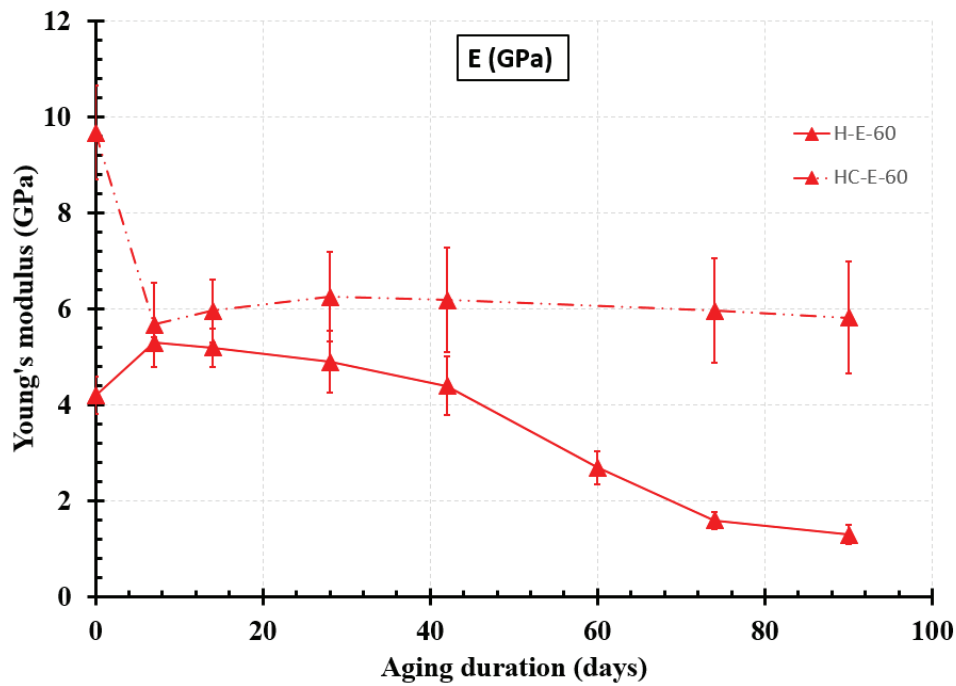


Figure 4- 161 : Influence over time of the bio-resin coating on the average tensile modulus of hemp yarns in E-60 solution.

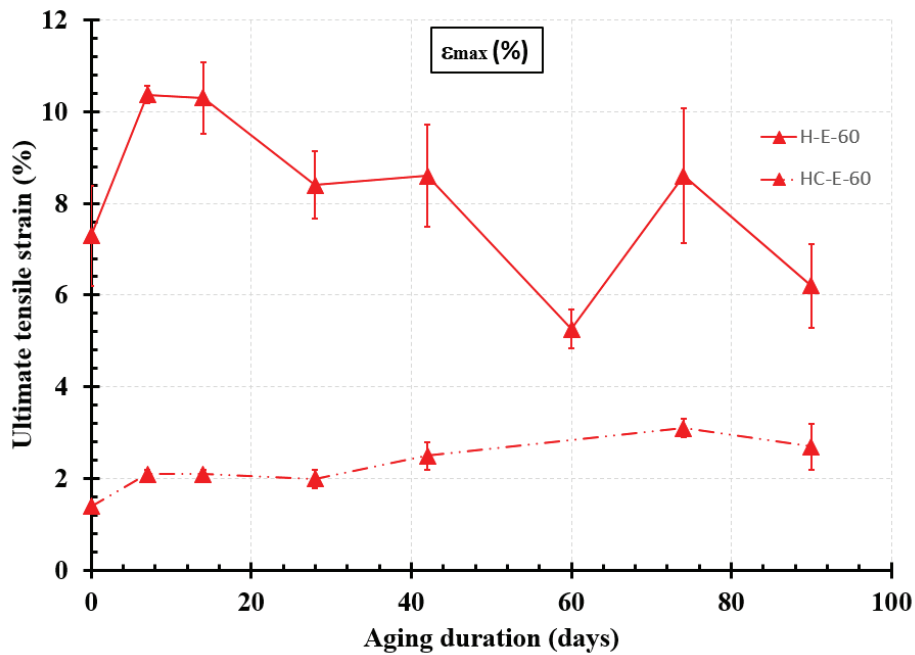


Figure 4- 162 : Influence over time of the bio-resin coating on the average ultimate tensile strain of hemp yarns in E-60 solution.

4.2.3.3.4 In solution L-23

Figure 4- 163, Figure 4- 164 and Figure 4- 165 present the influence of the bio-resin coating on the average tensile strength, the average tensile modulus and the average ultimate tensile strain respectively, of hemp yarns immersed in solution L-23. Also in this solution, the bio-resin coating prevented the mercerization process from occurring and protected the hemp yarns from the alkalinity of the solution.

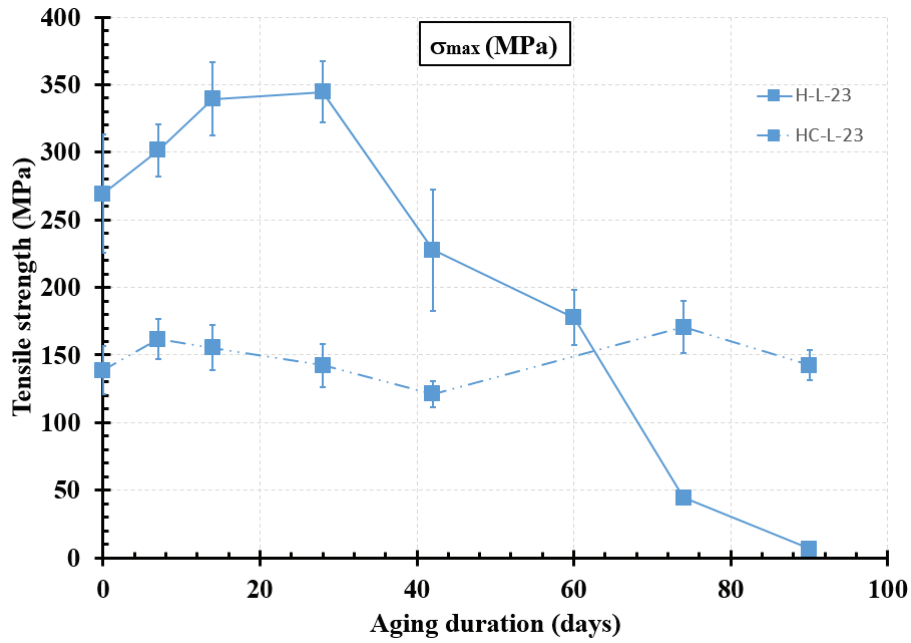


Figure 4- 163 : Influence over time of the bio-resin coating on the average tensile strength of hemp yarns in L-23 solution.

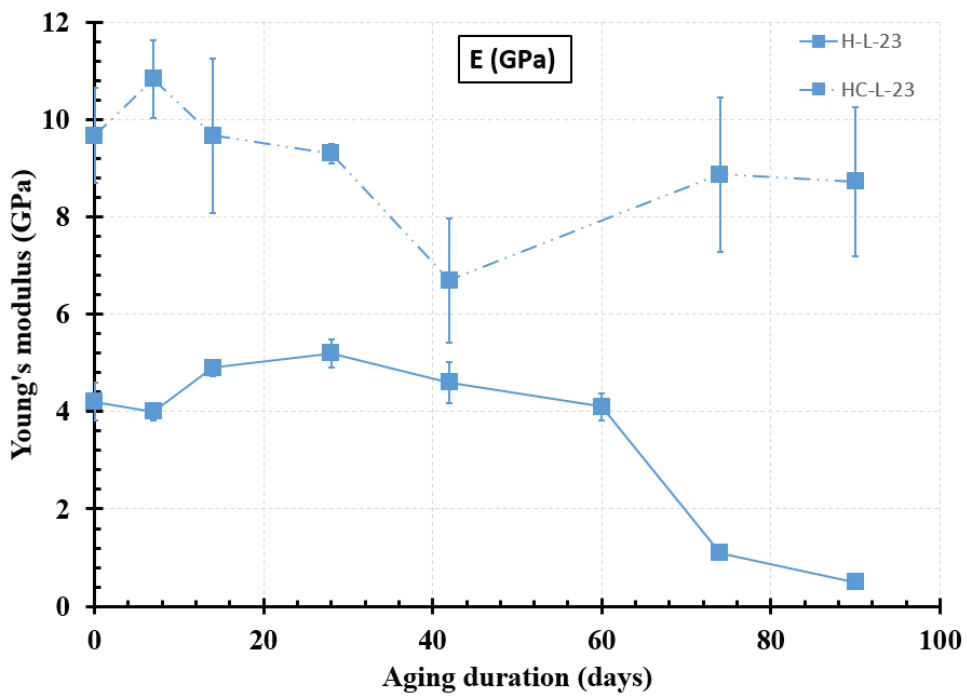


Figure 4- 164 : Influence over time of the bio-resin coating on the average tensile modulus of hemp yarns in L-23 solution.

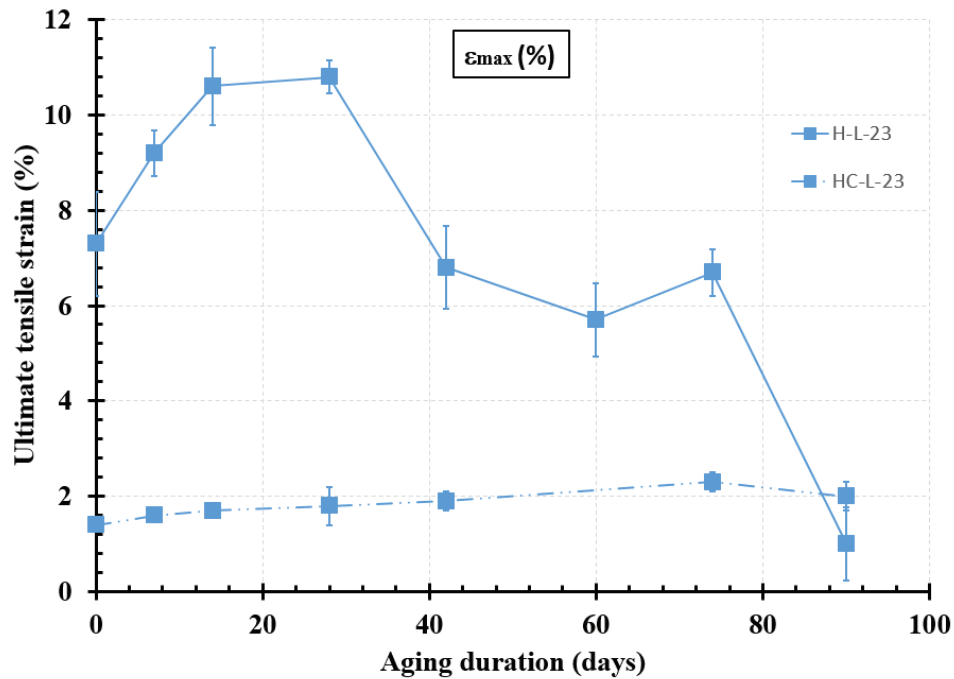


Figure 4- 165 : Influence over time of the bio-resin coating on the average ultimate tensile strain of hemp yarns in L-23 solution.

4.2.3.3.5 In solution L-40

Figure 4- 166, Figure 4- 167 and Figure 4- 168 present the influence of the bio-resin coating on the average tensile strength, the average tensile modulus and the average ultimate tensile strain respectively, of hemp yarns immersed in solution L-40. In this solution, both H and HC yarns do not encounter significant strength losses up to 90 days of immersion. However, one can notice a significant loss in the average tensile modulus of HC yarns starting at 28 days (or maybe before). After this loss, the average tensile modulus of HC yarns remains constant and very close to that of H yarns until 90 days of immersion. Thus, further investigations in this solution at periods greater than 90 days are needed to conclude about the influence of the bio-resin coating on hemp yarns.

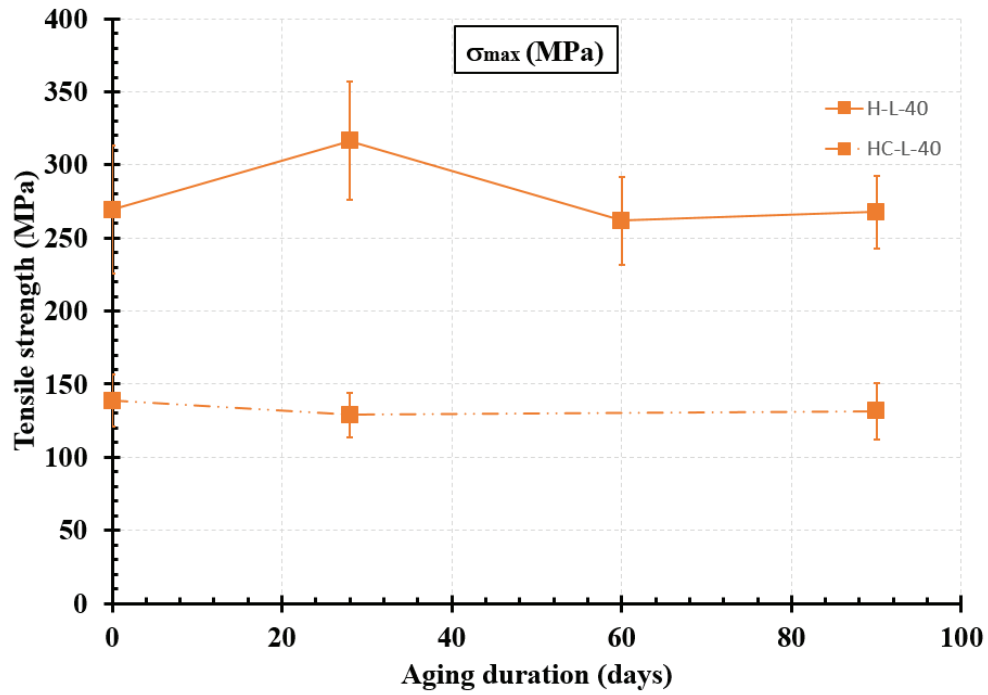


Figure 4- 166 : Influence over time of the bio-resin coating on the average tensile strength of hemp yarns in L-40 solution.

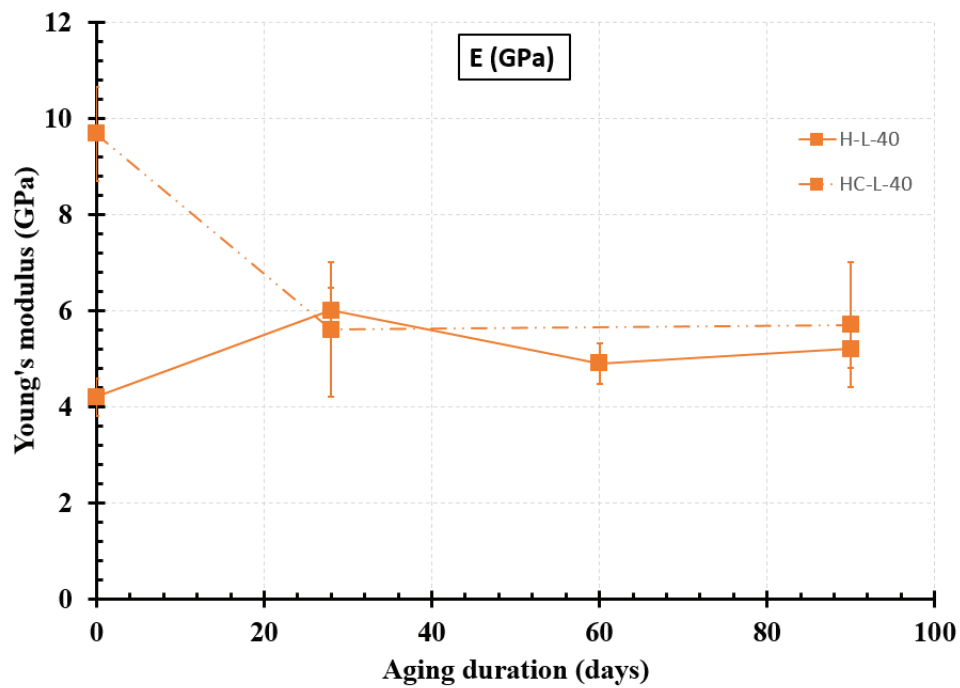


Figure 4- 167 : Influence over time of the bio-resin coating on the average tensile modulus of hemp yarns in L-40 solution.

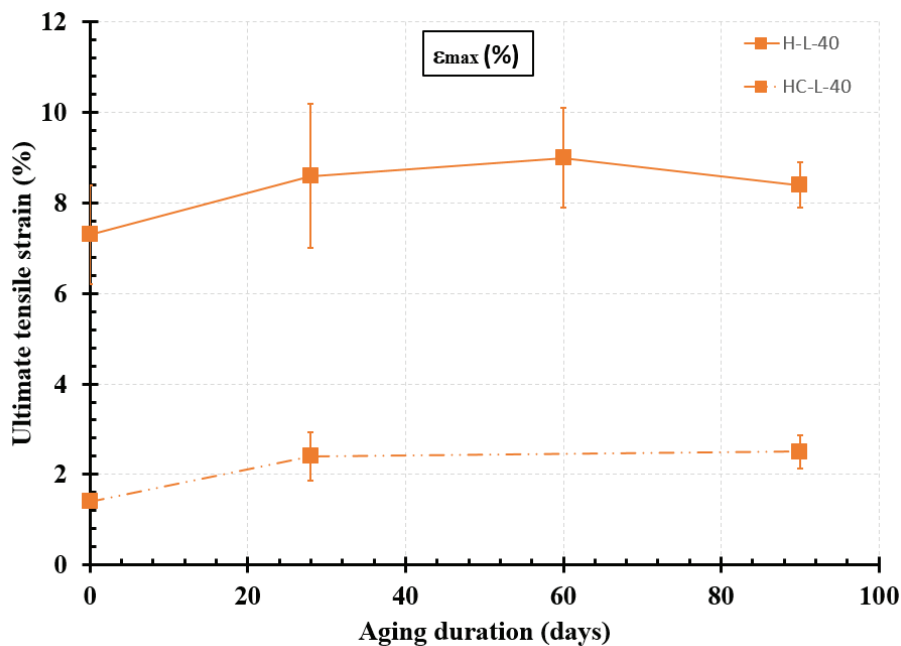


Figure 4- 168 : Influence over time of the bio-resin coating on the average ultimate tensile strain of hemp yarns in L-40 solution.

4.2.3.3.6 In solution L-60

Figure 4- 169, Figure 4- 170 and Figure 4- 171 present the influence of the bio-resin coating on the average tensile strength, the average tensile modulus and the average ultimate tensile strain respectively, of hemp yarns immersed in solution L-60. In this solution, H yarns do not encounter significant loss in their tensile properties up to 90 days of immersion. However, HC yarns lost about 43 % of their average tensile strength and 41 % of their average tensile modulus after 90 days of immersion. This solution has demonstrated to be a beneficial environment for H yarns up to 90 days of immersion, but the most severe environment for HC yarns. This is probably related to the plasticization of the resin network by the water and the penetration of the fluid inside the resin causing micro cracks even if the latter is not damaged, which reduce the stiffness of the resin and making it unable to distribute and share properly the external forces to the fibers, resulting in a macroscopic reduction in the tensile strength of the coated yarn [148].

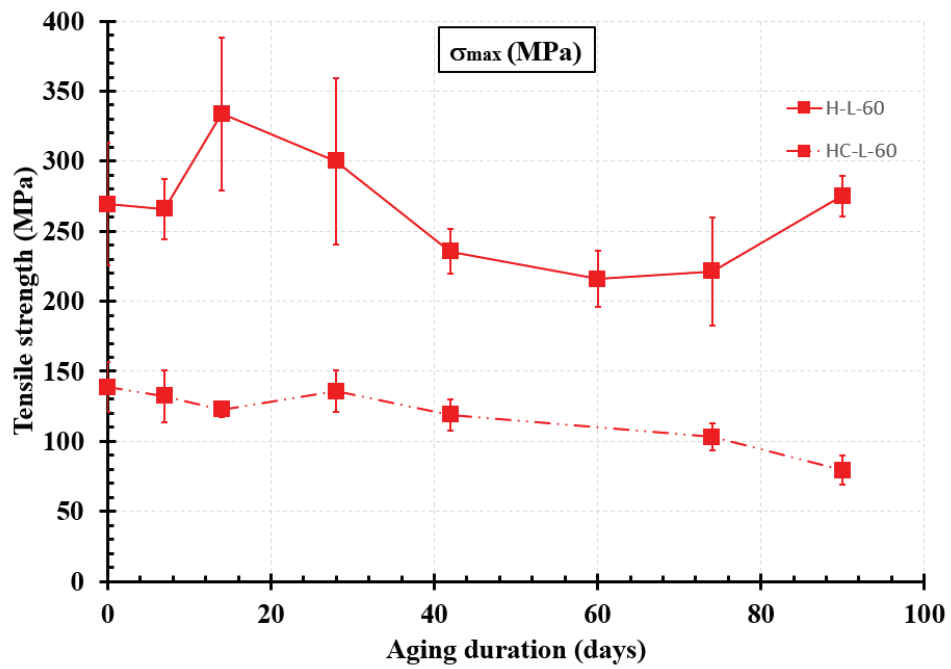


Figure 4- 169 : Influence over time of the bio-resin coating on the average tensile strength of hemp yarns in L-60 solution.

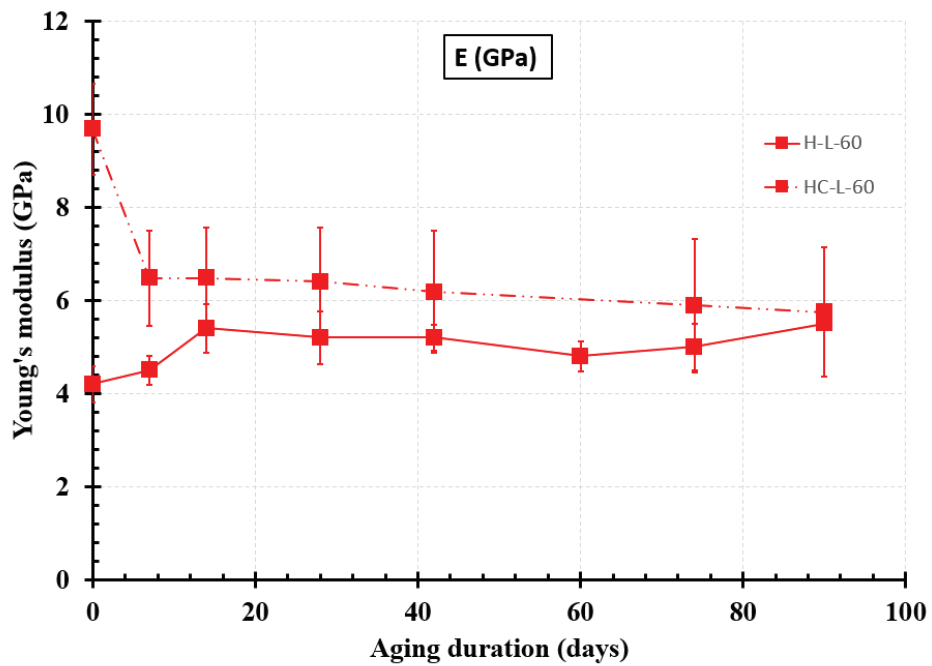


Figure 4- 170 : Influence over time of the bio-resin coating on the average tensile modulus of hemp yarns in L-60 solution.

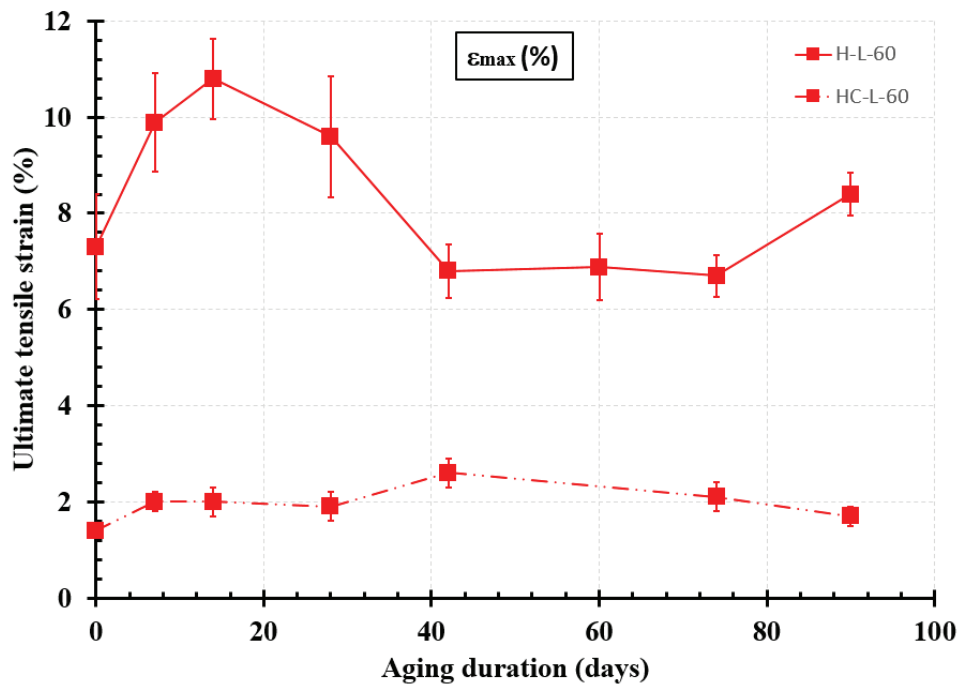


Figure 4- 171 : Influence over time of the bio-resin coating on the average ultimate tensile strain of hemp yarns in L-60 solution.

4.3 Natural aging of bio-resin-coated hemp yarn in the matrix of TRM

In this section bio-resin-coated hemp textile imbedded in real ettringitic and lime matrix in form of TRM plates are investigated in tension in order to compare their behavior with the behavior of TRM plates made from uncoated hemp yarns (chapter 3). Furthermore, the real service life of the yarns will be compared with the accelerated one.

4.3.1 Specimens preparation

The same preparation steps for Hemp TRM (chapter 3) are used here to prepare bio-resin-coated hemp TRM with an additional step, which comes between the textile weaving and the mortar casting. It is the textile coating after the manual weaving of the dry hemp textiles, these latter are immersed in the resin bucket, then they are quickly taken off and the excess of resin were removed from the surface of the textile by wringing it out manually as shown in Figure 4- 172a. Then the coated textile were placed between nails in order to keep them straight and left to dry at ambient temperature as shown in Figure 4- 172b. Finally, after drying they are imbedded in the mortar using the same procedure of hemp TRM (chapter 3). The final HC textile grid have a total cross-sectional area of 13.11 mm².

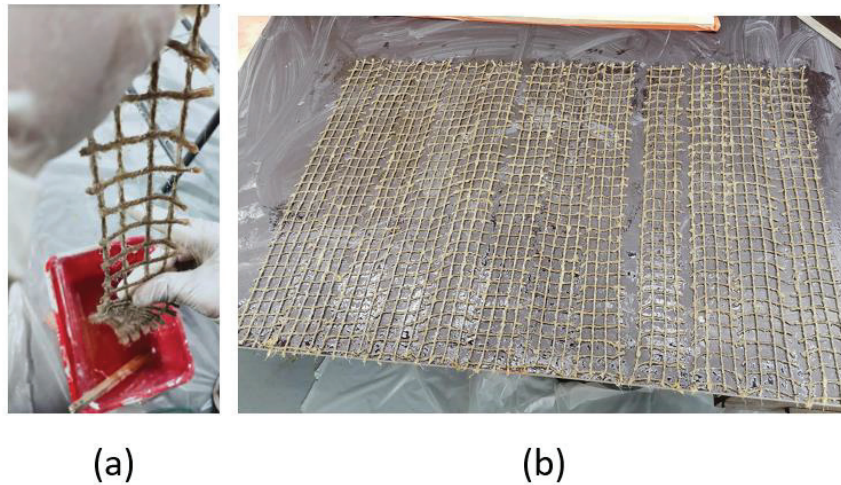


Figure 4- 172 : manual coating of the hemp textile by the bio-sourced resin.

4.3.2 Tensile test setup

Two reinforcement configurations were taken into account in this study: the first one labelled HC-E consisted of bio-resin-coated hemp textile (HC) imbedded in Ettringitic mortar (E). The second one labelled HC-L consisted of bio-resin coated hemp textile (HC) imbedded in Natural Hydraulic Lime mortar (L). These two TRM systems were tested in tensions after 28 days, 2 months and 3 months of curing. Furthermore, for the goal of comparison only, a series of 3 TRM specimens made from the same basalt textile T1 used in Zaydan et al. [179], imbedded in the ettringitic matrix (E) has been tested at the age of 2 years, it is labelled B-E-2y. T1 textile consists of one layer of three basalt yarns with a center to center distance of 25 mm between two yarns in the two orthogonal directions and a free spacing of 20 mm. a total cross-sectional area of 4.83 mm². The tensile strength a single basalt yarn is 1089 MPa and their modulus of elasticity is 56 GPa. Table 4- 42 summarizes the name, the number of specimens and the curing time for each series tested.

Table 4- 42 : Tensile test series.

TRM systems	Series name	Number of specimens	Curing time
HC-E	HC-E-28d	4	28 days
	HC-E-2m	6	2 months
	HC-E-3m	6	3 months
HC-L	HC-L-28d	5	28 days
	HC-L-2m	6	2 months
	HC-L-3m	5	3 months
B-E	B-E-2y	3	2 years

As for Hemp TRM (chapter 3), the tensile tests were carried out by using a clevis type system [181]. The preparation of the specimens for the tensile tests and the tensile test setup are the same as those done before in chapter 3 in the case of hemp TRM.

4.3.3 Results of tensile test on bio-resin-coated hemp TRMs

Table 4- 43, Table 4- 44 and Table 4- 45 summarize the tensile properties at the end of the stages I, II and III respectively, for all the tested TRM configurations. Referring to Figure 3- 132 in chapter 3, the tensile stresses at the end of each stage will be named σ_1 , σ_2 and σ_{\max} , respectively. The corresponding strains will be named ε_1 , ε_2 and ε_{\max} , respectively. The stress σ refers to the ratio between the tensile load and the cross-sectional area of the textile ($A_t = 13.11 \text{ mm}^2$). The stress σ_c is the ratio between the maximum tensile load at the end of the first stage and the cross-sectional area of the composite ($A_c = 10 \text{ mm} \times 80 \text{ mm}$). The strain ε is the ratio between the global displacement of the cross head and the gauge length of the specimen (460 mm). The elastic modulus E refers to the slope of the third phase of the F-d curve multiplied by the cross-sectional area of the textile ($A_t = 13.11 \text{ mm}^2$) and divided by the free length of the specimen (460 mm). The exploitation rate is the ratio between the maximum stress obtained and the tensile strength of HC yarns (138.8 MPa). Furthermore, in the following subparagraphs, the results obtained by the tensile test on the different TRM systems are reported in terms of force-displacement curves (F-d) and failure modes. The failure modes observed will be evaluated in the context of the typical failure modes of TRM subjected to tension defined in the literature (Figure 3- 133 in chapter 3). Regarding the strength evaluation, it is suggested to use the average first cracking stress σ_c , which takes into account the total cross-sectional area of the composites in the first phase, namely before the mortar cracking, in order to more realistically include the contribution of the mortar; while in the second and the third stage we refer to σ_2 and σ_{\max} , respectively, which take into account the cross-sectional area of the textile reinforcement alone.

Table 4- 43 : Tensile properties at the end of stage I for all the tested TRM configurations.

	Stage I					
	series/ nb of specimens	F_1 (N)	$\sigma_t = F_1 / A_t$ (MPa)	$\sigma_c = F_1 / A_C$ (MPa)	U_1 (mm)	ϵ_1 (%)
HCE-TRM	HC-E-28d/4	1332.5	101.6	1.7	1.6	0.3
	CoV (%)	3.9	3.9	3.9	12.7	12.7
	HC-E-2m/3	1687.2	128.7	2.1	1.3	0.3
	CoV (%)	1.1	1.1	1.1	17.8	17.8
	HC-E-2m/3	2612.3	199.2	3.3	2.0	0.4
	CoV (%)	5.1	5.1	5.1	16.6	16.6
	HC-E-3m/2	1259.2	96.1	1.6	0.7	0.2
	CoV (%)	20.1	20.1	20.1	27.3	27.3
	HC-E-3m/4	2053.3	215.0	2.6	1.0	0.2
CoV (%)	35.0	35.0	35.1	38.4	38.4	
HCL-TRM	HC-L-28d/5	416.6	31.8	0.5	0.3	0.1
	CoV (%)	25.2	25.2	25.2	17.2	17.2
	HC-L-2m/6	262.6	20.0	0.3	0.3	0.1
	CoV (%)	35.0	35.0	35.0	37.0	37.0
	HC-L-3m/5	369.7	28,2	0.5	0.4	0.1
	CoV (%)	18.8	18.8	18.8	26.0	26.0
BE-TRM	B-E-2y/3	3666.6	759.1	4.6	1.1	0.2
	CoV (%)	16.1	16.1	16.1	22.3	22.3

Table 4- 44 : Tensile properties at the end of stage II for all the tested TRM configurations.

	Stage II					
	series/ nb of specimens	F2 (N)	σ_2 (MPa)	U ₂ (mm)	ϵ_2 (%)	
HCE-TRM	HC-E-28d/4	1612.5	123.0	4.2	0.9	
	CoV (%)	6.3	6.3	5.2	5.2	
	HC-E-2m/3	1838.6	140.2	6.0	1.3	
	CoV (%)	4.5	4.5	2.9	2.9	
	HC-E-2m/3	No appearance for the stage II in these specimens				
	CoV (%)					
	HC-E-3m/2	1739.5	132.7	1.4	0.3	
	CoV (%)	15.8	15.8	33.1	33.1	
	HC-E-3m/4	No appearance for the stage II in these specimens				
CoV (%)						
HCL-TRM	HC-L-28d/5	1002.9	76.5	4.5	1.0	
	CoV (%)	9.4	9.4	15.3	15.3	
	HC-L-2m/6	600.8	45.8	2.7	0.6	
	CoV (%)	19.1	19.1	24.2	24.2	
	HC-L-3m/5	1031.5	78.7	3.7	0.8	
	CoV (%)	14.2	14.2	21.0	21.0	
BE-TRM	B-E-2y/3	4083.5	845.5	5.9	1.3	
	CoV (%)	11.6	11.6	10.9	10.9	

Table 4- 45 : Tensile properties at the end of stage III and rupture modes for all the tested TRM configurations.

		Stage III						
	series/ nb of specimens	F _{max} (N)	σ_{max} (MPa)	U _{max} (mm)	ϵ_{max} (%)	E (GPa)	Exploitation rate (%)	Rupture mode
HCE-TRM	HC-E-28d/4	1662.8	126.8	4.8	1.0	19.7	91.3	B (all the specimens have multiple cracks in second stage)
	CoV (%)	6.0	6.0	3.4	3.4	26.4		
	HC-E-2m/3	1872.3	142.8	6.5	1.4	20.6	102.8	B (3 specimens with multiple cracks in second stage)
	CoV (%)	4.4	4.4	1.7	1.7	22.3		
	HC-E-2m/3	2393.2	182.5	2.2	0.5	57.5	131.5	B (3 specimens with only one crack in second stage)
	CoV (%)	6.0	6.0	21.0	21.0	13.3		
	HC-E-3m/2	1727.4	131.7	1.7	0.4	54.7	94.8	B (2 specimens with multiple cracks in second stage)
	CoV (%)	3.4	3.4	23.3	23.3	13.6		
	HC-E-3m/4	1834.8	139.9	1.4	0.3	70.4	100.7	B (4 specimens with only one crack in second stage)
CoV (%)	10.7	10.7	17.7	17.7	33.3			
HCL-TRM	HC-L-28d/5	1611.3	122.9	7.5	1.6	8.4	88.5	B (all the specimens have multiple cracks in second stage)
	CoV (%)	12.9	12.9	10.3	10.3	3.1		
	HC-L-2m/6	1551.0	118.3	7.4	1.6	7.2	85.2	B (all the specimens have multiple cracks in second stage)
	CoV (%)	5.5	5.5	10.6	10.6	7.9		
	HC-L-3m/5	1371.0	104.6	5.7	1.2	8.0	75.4	B (all the specimens have multiple cracks in second stage)
	CoV (%)	12.5	12.5	14.7	14.7	15.7		

BE-TRM	B-E-2y/3	4628.3	958.2	8.4	1.8	35.7	88	B (all the specimens have multiple cracks in second stage)
	CoV (%)	5.5	5.5	13.4	13.4	9.8		

4.3.3.1 HC-E TRM series

Figure 4- 173, Figure 4- 174 and Figure 4- 175 show the Force-displacement curves of HC-E composites tested at 28 days, 2 months and 3 months, respectively. Comparing the tensile behavior of these TRM series with the typical tensile behavior described in the literature (Figure 3- 132 in chapter 3), we find that, all the specimens of the HC-E-28d series are characterized by only two stages: the precracking and the cracks propagation stages. Then the rupture of the yarns occurs without a clear observation of the third stage (Figure 4- 173). For HC-E-2m series, half of the specimens have the same behavior of HC-E-28d series specimens, while the other half exhibited only one cracking before the rupture of the yarns (Figure 4- 174, Figure 4- 176). However, in the HC-E-3m series, only two specimens (HC-E-3m-4 and HC-E-3m-6) exhibited a multiple cracking behavior in the second stage of the stress-strain curve (Figure 4- 175, Figure 4- 176).

As shown in Figure 4- 176, the failure of the HC-E TRM was a result of crack widening, leading to the textile rupture, which is called failure mode B. Furthermore, it is worth noting that, for both series HC-E-2m and HC-E-3m, the specimens who have only one cracks in the second stage, have an average F_1 at the end of stage I greater than the average F_{max} . While, the specimens who exhibited multiple cracking behavior have an average F_1 at the end of stage I lower than the average F_{max} (Table 4- 43). It seems that, at the age of 28 days the HC-E TRM presents a good bonding performance between the Ettringitic matrix (E) and the bio-resin-coated hemp yarns (HC). However, beyond this age, the ettringitic reactions make the matrix denser, and the textile-matrix bonding starts to intensify gradually, leading to the brittle failure of the specimens without exhibiting a multiple cracking behavior.

In Zaydan et al. 2021 [179], tensile tests were carried out at the age of 28 days on TRMs made from basalt textile imbedded in this same ettringitic matrix E, two series with two different reinforcement ratio were investigated: 0.54 % (series TT1) and 0.89 % (series TT2). Series TT1 exhibited the same behavior as HC-E-28d (only the precracking and the cracks propagation stages) while series TT2 exhibited well the three stages of the typical tensile behavior of the TRM. However, for all these series the average maximum stress of the composite were very close to the average tensile strength of the yarns. The reinforcement ratio is the ratio of the cross-sectional area of the textile grid over the cross-sectional area of the composite. In our case (HC-E-28d) it is equal to $A_t/A_c = 13.11/800 = 1.64$ %. Furthermore, for B-E-2y series tested in this study at the age of two years with a basalt reinforcement ratio of 0.6 %, the specimens exhibited the same behavior as HC-E-28d, they have only the precracking and the cracks propagation stages (Figure 4- 178). It

seems that there is an interval of reinforcement ratios, when it is respected the TRM with ettringitic matrix could exhibited the typical three stages behavior.

Analyzing the specific values, it can be seen that:

- The flexural tensile strength of the ettringitic mortar (4.4 MPa) was not reached in almost all the cases. For HC-E TRM, the obtained σ_c values are about 39 % for HC-E-28d, 48 % for HC-E-2m (multiple cracks), 75 % for HC-E-2m (only one crack), 36 % for HC-E-3m (multiple cracks), 59 % for HC-E-3m (only one crack) (Table 4- 43). These percentages are calculated with respect to the flexural tensile strength of the Ettringitic matrix (E) (4.4 MPa), already determined in chapter 2 (Table 2- 24). These results are consistent with those reported in Estevan et al. 2022 [7], concerning TRMs employing glass, carbon and basalt meshes and cured at room temperature. However, in case of basalt textile imbedded in ettringitic matrix (Zaydan et al. [179]), the average stresses σ_c were very close to the flexural strength of the matrix. Furthermore, for B-E-2y series tested in this study at the age of two years with a reinforcement ratio of 0.6 %, the average stress σ_c is 4.6 MPa very close to the flexural strength of the ettringitic matrix (4.4 MPa). One can also notice that when the specimens exhibited only one crack behavior the average σ_c is higher than that for the specimens who exhibited multiple cracking behavior.
- The tensile strength of HC yarns (138.9 MPa) was almost reached in all the cases. For HC-E TRM, the obtained average stresses σ_{max} values are about 91 % for HC-E-28d, 103 % for HC-E-2m (multiple cracks), 131 % for HC-E-2m (only one crack), 95 % for HC-E-3m (multiple cracks), 101 % for HC-E-3m (only one crack) (Table 4- 45). These percentages are calculated with respect to the tensile strength of hemp yarns (138.8 MPa). These results are consistent with those reported in Zaydan et al. [179] employing coated basalt textile imbedded in ettringitic mortar. We can conclude that, the ettringitic reactions combined with the resin coating protected the hemp yarns from reactions with NaOH, which reduce the tensile properties of the yarns and leads to their degradation.
- The tensile modulus of HC yarns (9.7 GPa) was exceeded in all the cases of HC-E TRM, the average elastic modulus E obtained are about 203 % for HC-E-28d, 212 % for HC-E-2m (multiple cracks), 593 % for HC-E-2m (only one crack), 564 % for HC-E-3m (multiple cracks), 726 % for HC-E-3m (only one crack) (Table 4- 45). These percentages are calculated with respect to the tensile modulus of HC yarns (9.7 GPa). The increase in stiffness experienced by HC-E TRM series was remarkable. We can also clearly see it from the slopes of the curves in Figure 4- 177, which presents the stress-strain response of three representative specimens for the three series of HC-E TRM tested at different ages with the stress-strain curve of a representative coated-hemp yarn (HC). This increase has already been reported in some previous investigations [7], [174], [180], where they attributed it to the fact that the mortar matrix can provides additional stiffness in certain cases. In addition, sometimes it allows a much more homogeneous distribution of stresses between the fibers with respect to the tensile test of dry meshes, where irregular distributions or stress

concentrations may occur in the anchorage zones. These explanations could be also valid in our case, since the HC-TRM curves did not exhibited the third stage behavior, but they stayed in stage 2 where the rigidity of the TRM refers to the rigidity of the composite and not the rigidity of the textile only.

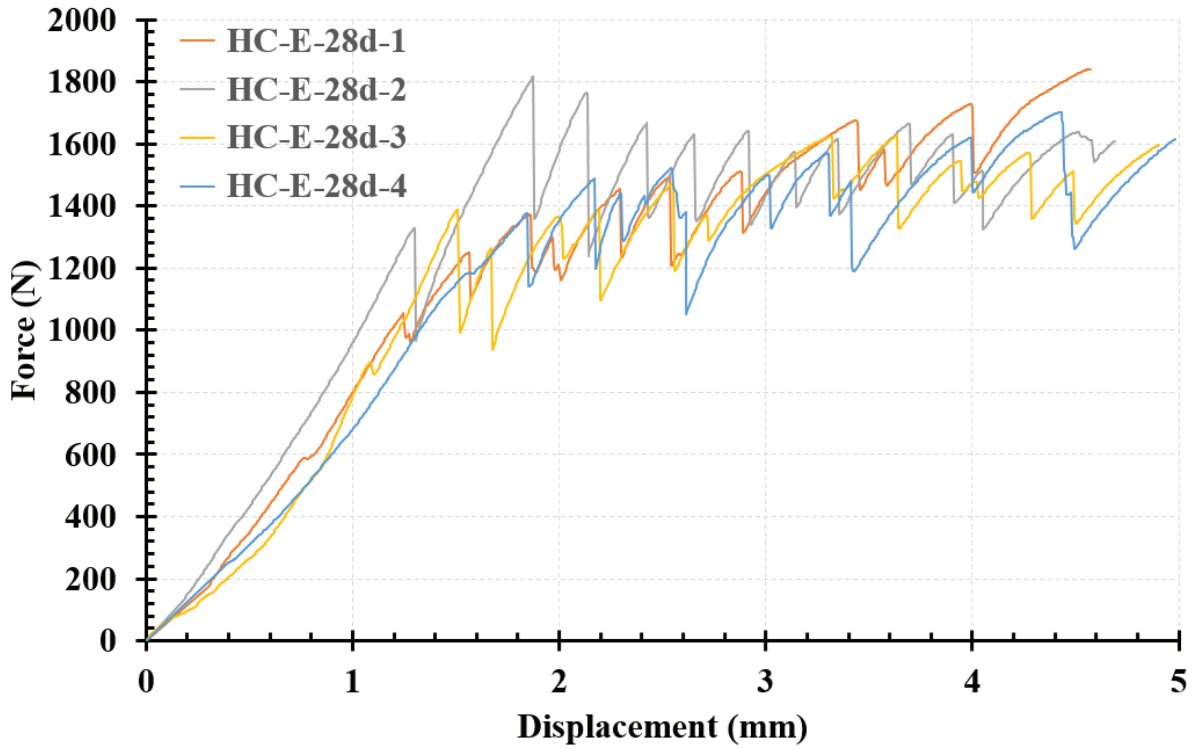


Figure 4- 173 : Force-displacement curves for the specimens of HC-E-28d series.

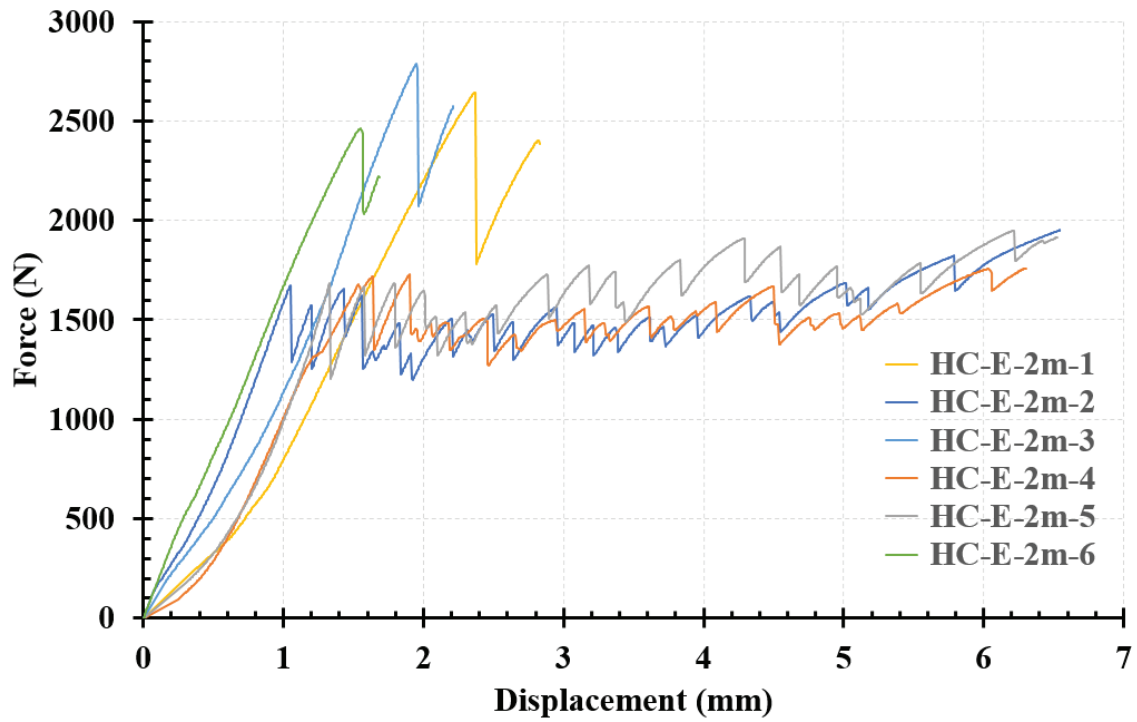


Figure 4- 174 : Force-displacement curves for the specimens of HC-E-2m series.

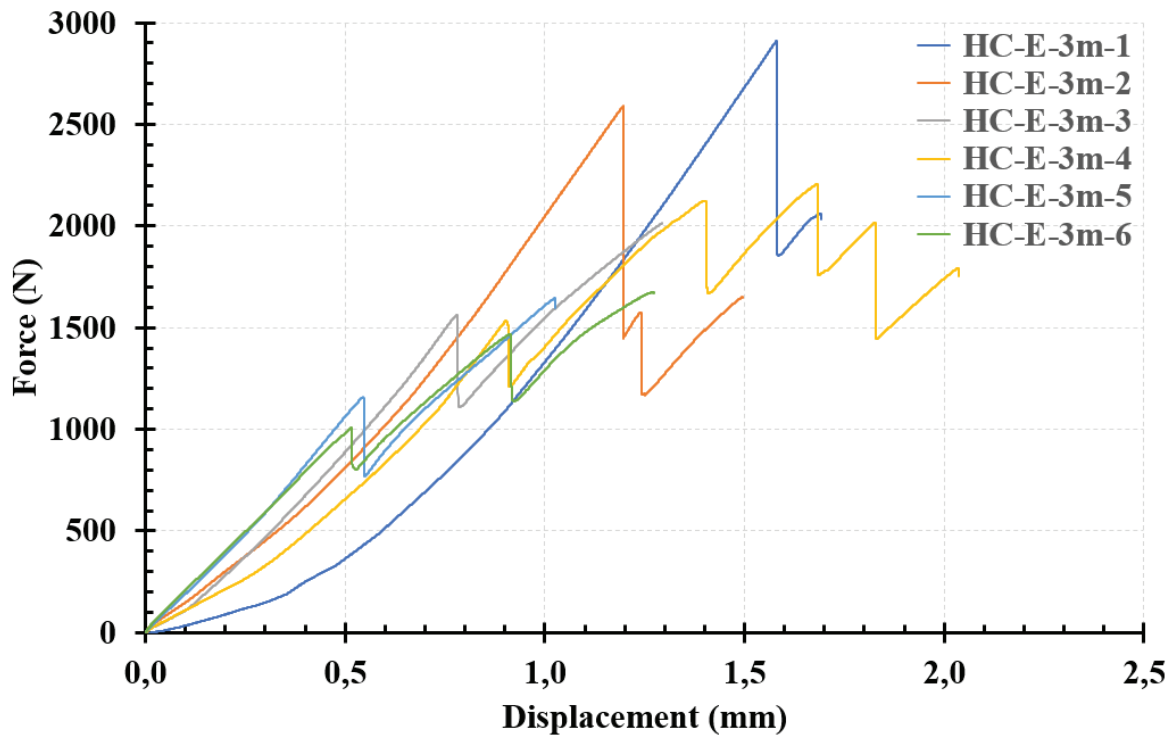


Figure 4- 175 : Force-displacement curves for the specimens of HC-E-3m series.

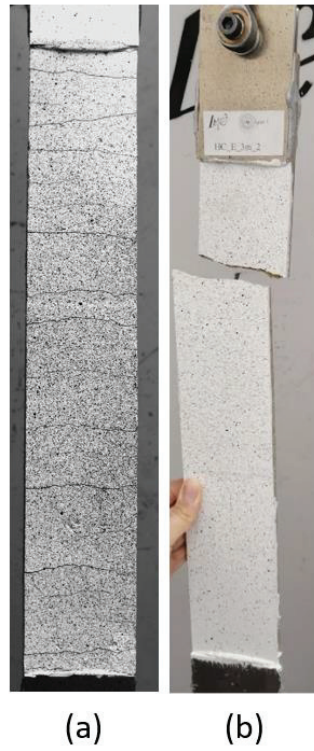


Figure 4- 176 : Failure mode B recorded in: a) HC-E-28d-1 specimen (multiple cracking behavior + rupture of the yarns), and b) HC-E-3m-2 specimen (only one cracking behavior + rupture of the yarns).

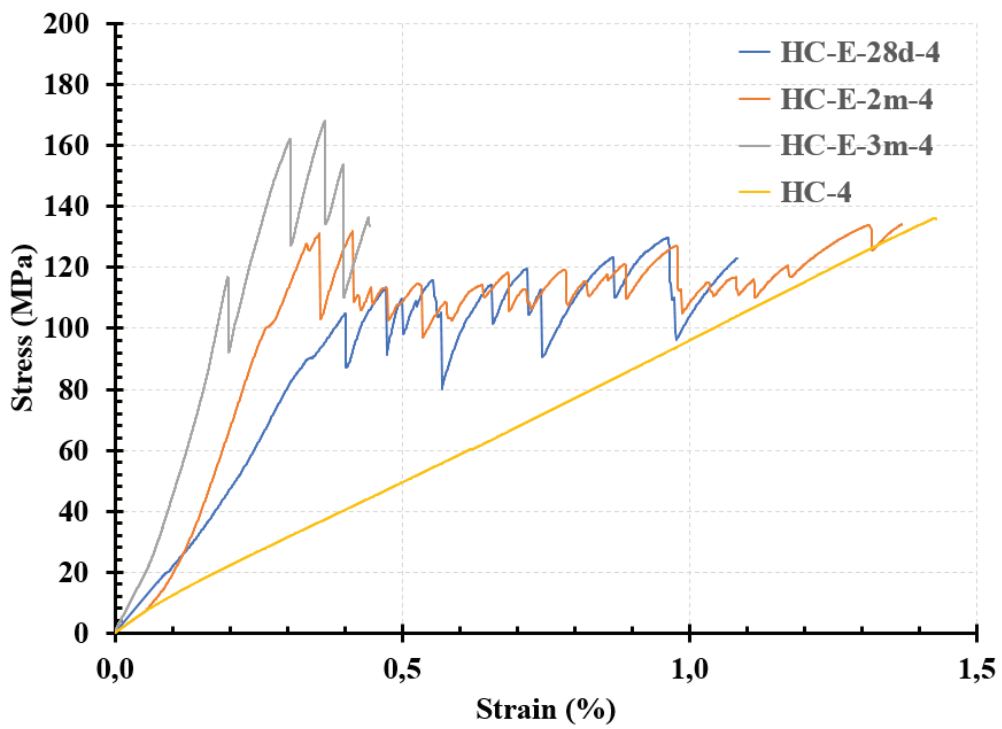


Figure 4- 177 : Comparison between stress-strain responses of representative specimens of HC-E series with a representative coated-hemp yarn specimen (HC).

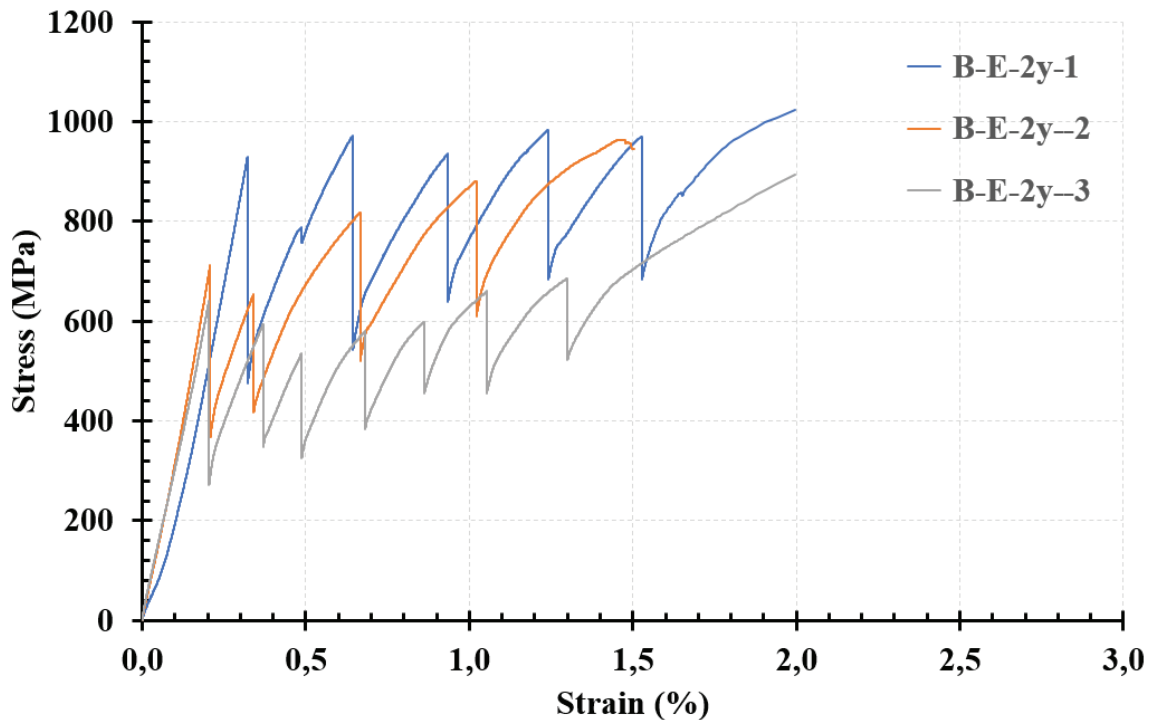


Figure 4- 178 : Stress-strain curves for the specimens of B-E-2y series.

4.3.3.2 HC-L TRM series

Figure 4- 179, Figure 4- 180 and Figure 4- 181 show the stress-strain curves of HC-L composites tested at 28 days, 2 months and 3 months, respectively. These composites exhibited similar behavior as the typical stress-strain behavior of the TRM (Figure 3- 132 in chapter 3), during the first and the second stages. However, the first stage was less visible. After this stage, the tensile behavior was characterized by the formation of multiple cracking in the matrix. However, this multiple cracking behavior did not disappear in the third stage of the curve, as it is the case for the typical tensile behavior of TRM, but we can notice small drops in this stage characterizing the opening of micro-cracks. This same behavior was obtained by O.A. Cevallos and R.S. Olivito 2015 [143], when they tested TRMs made from flax or sisal fabrics imbedded in natural hydraulic lime grouting (NLG) mix with added natural pozzolan and carbonate filler. It is probably due to the ability of the NHL matrix to store energy even when the stiffness of the composite is mainly affected by the stiffness of the natural fabrics. Therefore, the contribution of the matrix to the mechanical behavior in the third stage should not be neglected in these composite systems, contrary to what is assumed in the typical stress-strain models.

Figure 4- 182 presents the failure mode B recorded in all the specimens of HC-L TRM with the formation of many cracks in the second stage. The occurrence of this failure mode among the others reflects the high anchorage ability of the bio-resin-coated hemp textile (HC), which allows a good penetrability of the matrix between the fabric openings. Furthermore, the resin coating played the role of increasing the roughness of the yarn surface preventing the yarn slippage within

the matrix and resulting in a good textile-matrix bond. Moreover, as we have already seen in chapter 2, the resin coating reduces the water absorption capacity of hemp yarns, which prevents their swelling when they are subjected to the hydration products of the matrix and their retraction later after the complete drying. This results in preventing the formation of voids at the fiber-matrix interface thus, enhancing the textile-matrix bond of the composite.

We can also notice that, the cracks are orthogonal to the direction of loading and the number of cracks gradually increases with the loading.

Analyzing the specific values, it can be seen that:

- The flexural tensile strength of the natural hydraulic lime mortar (2.8 MPa) was not reached in almost all the cases. For HC-L TRM, the obtained σ_c values are about 18 % for HC-L-28d, 11 % for HC-L-2m and 18 % for HC-L-3m (Table 4- 43). These percentages are calculated with respect to the flexural tensile strength of the natural hydraulic lime mortar (L) (2.8 MPa), already determined in chapter 2 (Table 2- 24). These results are consistent with the results of HC-E TRM series and with those reported in Estevan et al. 2022 [7], employing glass, carbon and basalt meshes and Zaydan et al. [179] employing basalt mesh.
- The average stresses σ_{max} values obtained are about 88 % for HC-L-28d, 85 % for HC-L-2m and 75 % for HC-L-3m (Table 4- 45). These percentages are calculated with respect to the tensile strength hemp yarns (138.8 MPa). The tensile strength of the composite is about 12–25 % lower than the tensile strength of HC yarns.
- The average elastic modulus E obtained are about 87 % for HC-L-28d, 74 % for HC-L-2m and 82 % for HC-L-3m (Table 4- 45). These percentages are calculated with respect to the tensile modulus of HC yarns (9.7 GPa). The stiffness of this third stage is about 13–26 % lower than the elastic modulus of HC yarns. Hence, the stage III curve could be, approximately, parallel to the stress – strain curve of the HC yarns under pure tensile load. This can be seen from Figure 4- 183, which presents the stress-strain response of three representative specimens for the three series of HC-L tested at different ages with the stress-strain curve of a representative coated-hemp yarn (HC).

These small differences in tensile strength and modulus between HC-L TRM and HC yarns are caused by two complementary factors. This is due to inhomogeneous load distribution between the filaments of the yarns. Furthermore, we should note that these percentages are calculated with respect to the tensile strength of a single yarn not the tensile strength of the textile, which contributed also in this difference. In addition, we should not forget the contribution of the matrix in the mechanical behavior of the composite during the third stage of the stress-strain curve.

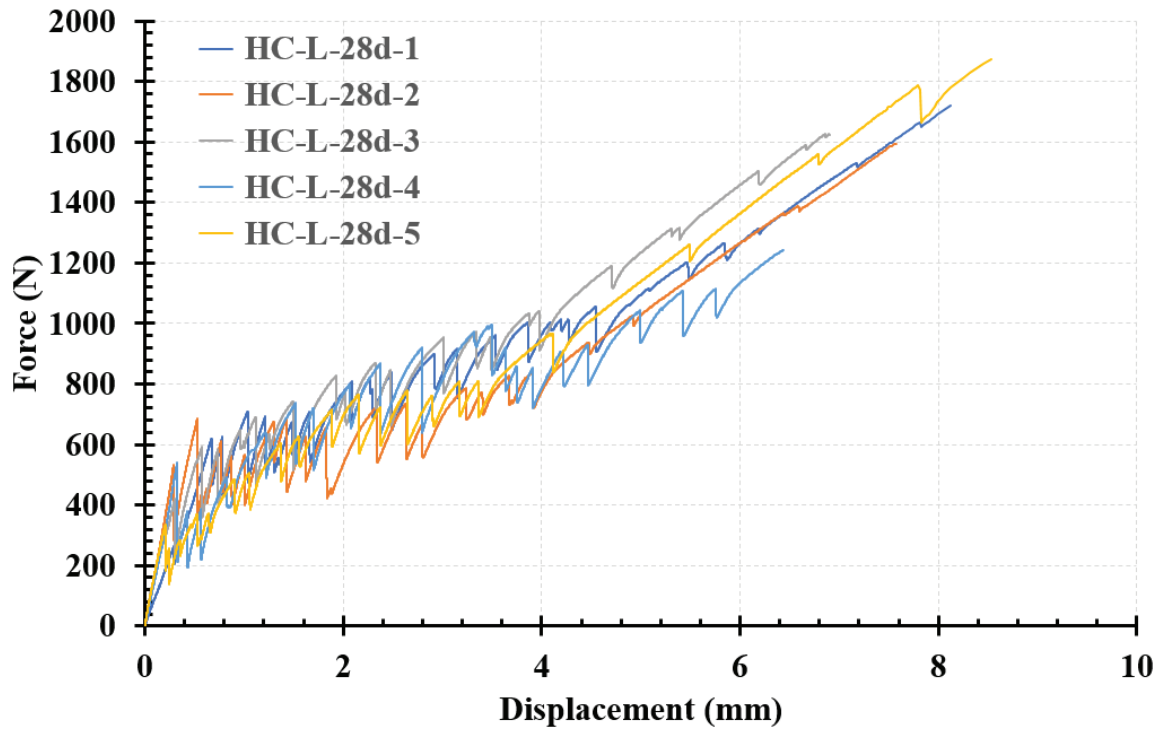


Figure 4- 179 : Force-displacement curves for the specimens of HC-L-28d series.

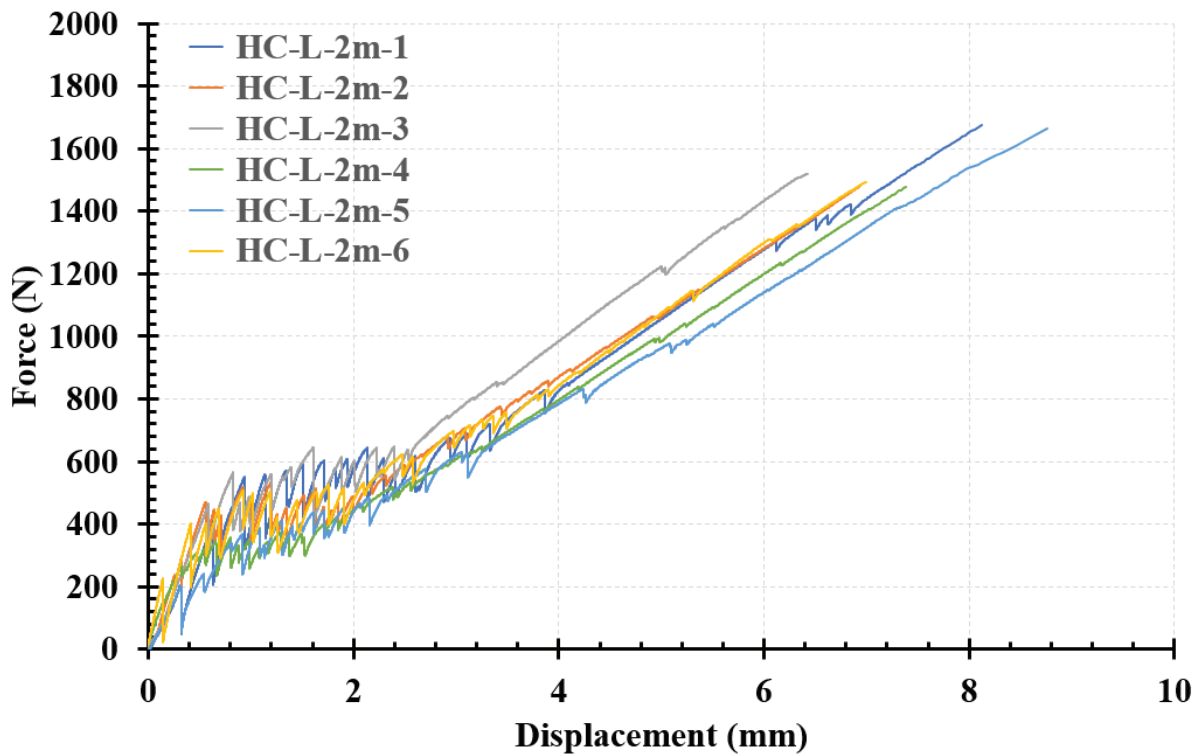


Figure 4- 180 : Force-displacement curves for the specimens of HC-L-2m series.

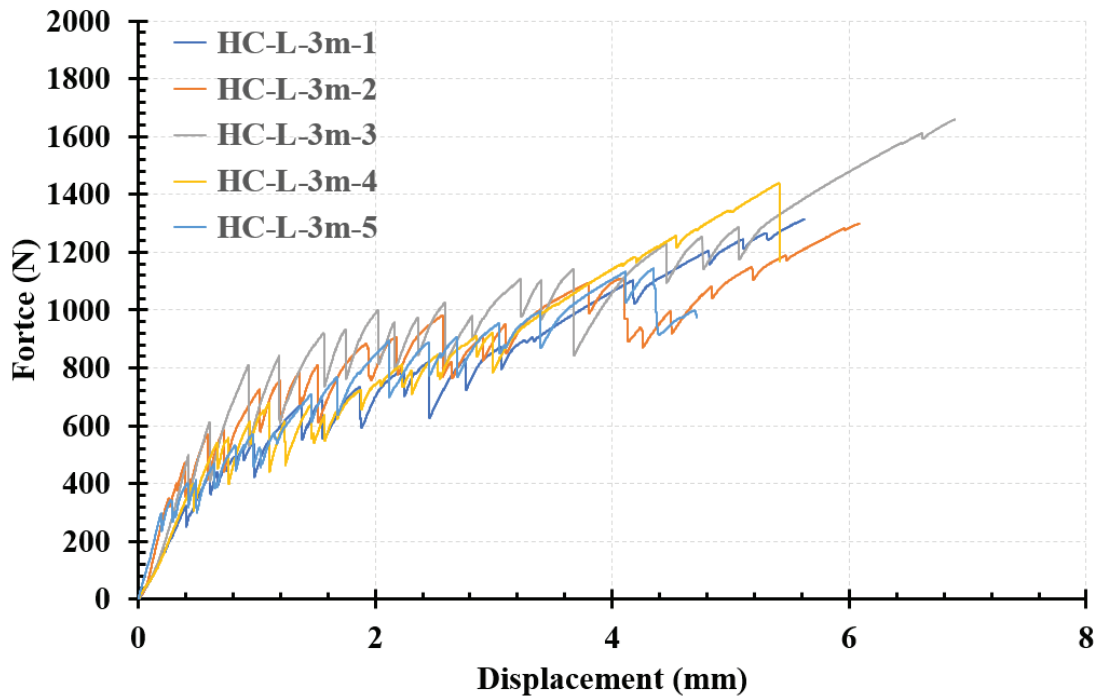


Figure 4- 181 : Force-displacement curves for the specimens of HC-L-3m series.



Figure 4- 182 : Failure mode B recorded in all the HC-L series, a) multiple stress behavior during stage II, and b) the rupture of the yarns at the end of stage III.

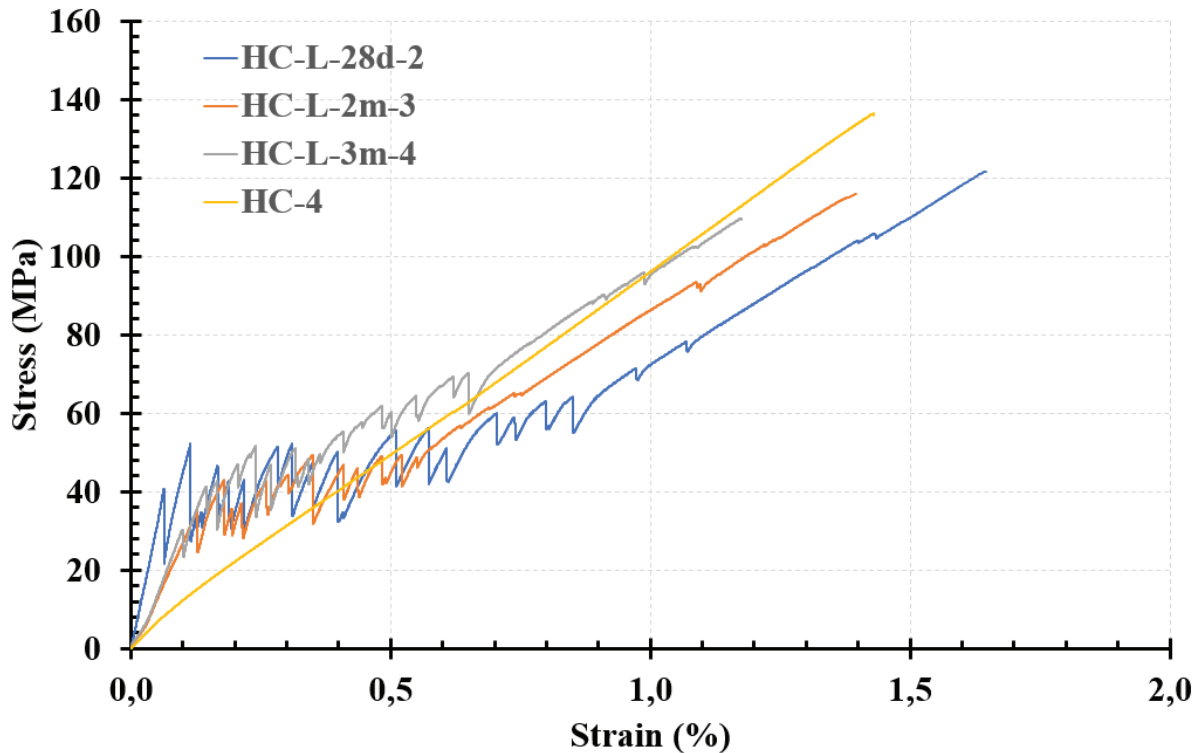


Figure 4- 183 : Comparison between stress-strain responses of representative specimens of HC-L series with a representative coated-hemp yarn specimen (HC).

4.3.3.3 Effect of the resin coating on the tensile response of TRM

Figure 4- 184 compares the force-displacement responses of a representative specimen of H-E TRM series with a representative specimen of HC-E TRM series tested at 28 days of curing. Figure 4- 185 compares the force-displacement responses of a representative specimen of H-L TRM series with a representative specimen of HC-L TRM series tested at 28 days of curing. A marked difference was observed between the behavior of the composites made from dry hemp textile (H) and the others made from bio-resin-coated hemp textile (HC) for both kinds of matrices used: E and L. At first, the stress σ_c at the end of the first stage is greater in case of TRM with dry hemp textile. However, in both case, this stress cannot reach the flexural strength of the matrix. Furthermore, H-TRM are not able to produce multiple cracks, they undergo only one crack in the second stage while all the specimens of HC-TRM series undergo multiple cracks at 28 days. In the third stage, H-TRM suffer from the slippage of the yarns in the matrix before reaching their tensile strength. This is not the case for HC-TRM where the textile reached a value very close to the tensile strength of the yarns and the failure of all the specimens occurs by the textile rupture.

We can conclude that this kind of bio-resin coating increases the roughness of the yarn surface, and decreases the water absorption capacity of the yarns, which decreases their ability to swell and retract, thus preventing the formation of the pores at the fiber-matrix interface and preventing the

elongation of the fibers within the matrix, which in turn protect the fiber-matrix bond and prevent the slippage of the yarns within the matrix.

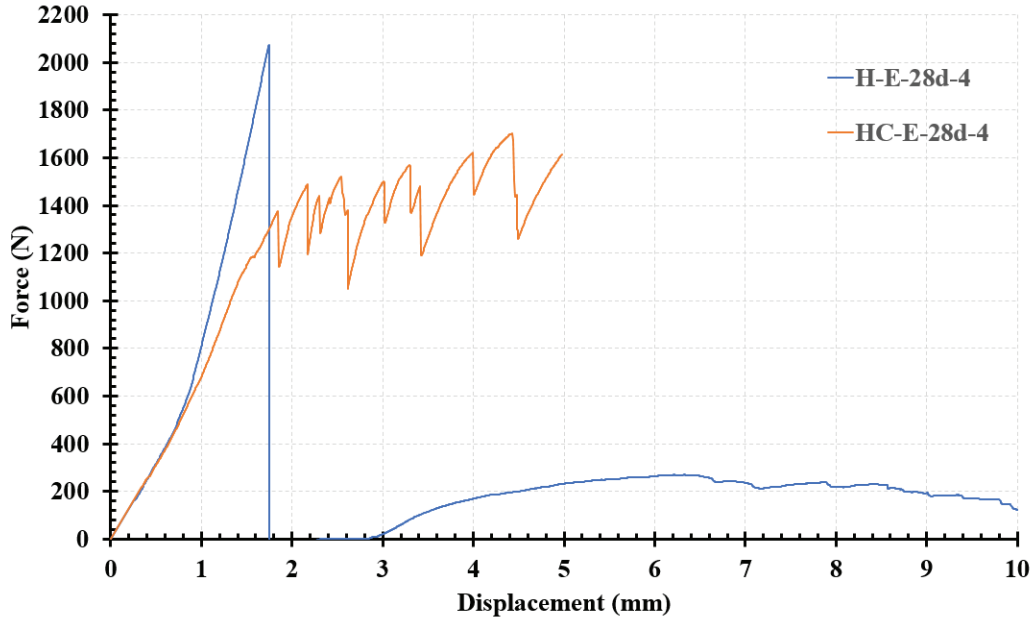


Figure 4- 184: Comparison between Force-displacement responses of representative specimen of H-E TRM series with a representative specimen of HC-E TRM series tested at 28 days of curing.

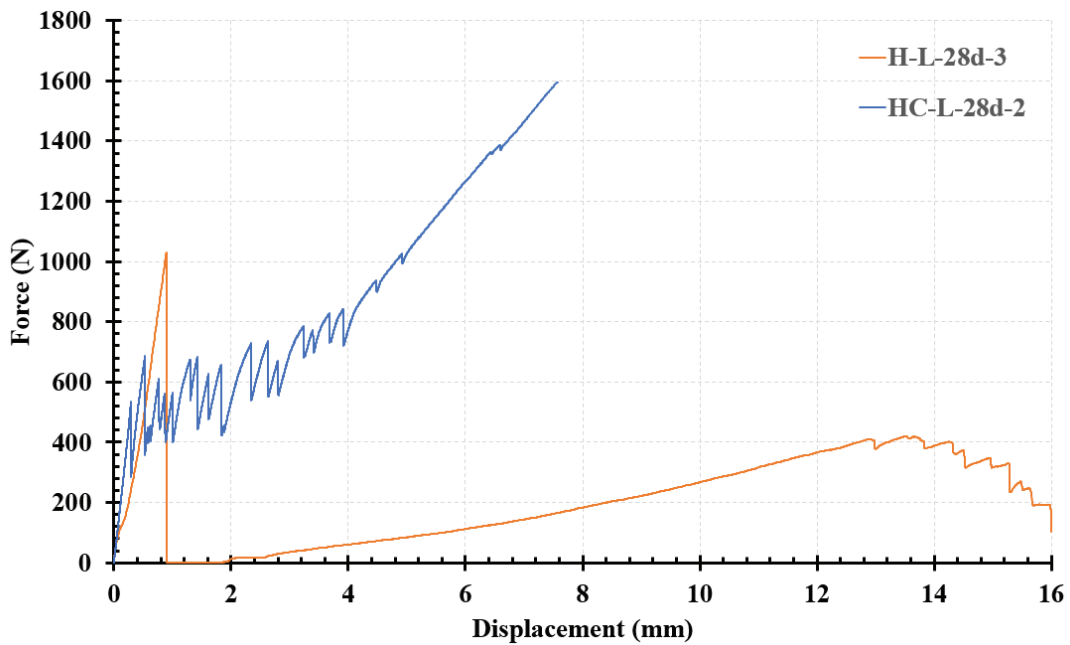


Figure 4- 185: Comparison between Force-displacement responses of representative specimen of H-L TRM series with a representative specimen of HC-L TRM series tested at 28 days of curing.

4.3.3.4 Effect of the matrix on the tensile response of HC-TRM

Figure 4- 186, Figure 4- 187 and Figure 4- 188 compare the stress-strain responses of representative specimens of HC-E and HC-L TRM series tested at 28 days, 2 months and 3 months respectively, with a representative stress-strain curve of coated-hemp yarn specimen (HC).

First from these Figures and from Table 4- 43, we can notice that for HC-E TRMs the first crack occurs at an average σ_c greater than that of HC-L TRMs at all the ages, which is logic because the flexural strength of the ettringitic matrix (4.4 MPa) is greater than the flexural strength of the natural hydraulic lime matrix (2.8 MPa). But in both cases, the average first cracking stress σ_c cannot reach the flexural strength of the matrix. Maybe if the specimens were cured in high humidity conditions we could attain higher σ_c as it is the case in Dalalbashi et al. 2021 [182] who observed that the steel-lime TRMs cannot reach their full mechanical properties under indoor conditions even after 3 years of curing. While the TRM cured under outdoor conditions (high humidity and rain), achieved significantly higher mechanical properties due to a better hydration of the lime mortar in these conditions.

At 28 days, in the second stage, HC-E TRMs exhibited between 9 and 12 cracks which is less than the number of cracks obtained in case of HC-L TRMs (between 17 and 20). The third stage did not appear clearly in case of HC-E TRMs while it can be clearly seen in case of HC-L TRMs. Furthermore, as we have seen before, at the age of 2 and 3 months, not all the specimens of HC-E TRM series have the same behaviors, there are specimens that exhibited only one crack behavior. Moreover, the number of cracks for the specimens who exhibited multiple cracking behavior at 2 months was between 18 and 20 but at 3 months, it has been decreased to 5 cracks maximum. This is not the case for HC-L TRM specimens who exhibited the same multiple cracking behavior with the same number of cracks at the different ages. These numbers of cracks are extracted from the force displacement curves of the specimens of each TRM series, it is equal to the number of drops in the second stage of these curve. In the future, a digital image correlation will be applied on these TRMs to quantify better the number of cracks, to visualize the crack pattern, and to calculate the displacement and the deformation fields.

The average maximum tensile stresses σ_{max} for HC-E TRMs are closer to the tensile strength of the bio-resin-coated hemp yarns (138.9 MPa) than that of HC-L TRMs. The average elastic modulus E of HC-E TRMs are greater than the average elastic modulus of HC yarns (9.7 GPa), while the average elastic modulus E of HC-L TRMs are lower but closer to the average elastic modulus of HC yarns (9.7 GPa). This can be clearly noticed from the slopes of the curves in Figure 4- 186, Figure 4- 187 and Figure 4- 188.

We can conclude that the textile-matrix bonding of HC-E TRM is stronger than that of HC-L TRM. In addition, the ettringitic matrix can provides additional stiffness and allows a much more homogeneous distribution of stresses between the fibers with respect to the tensile test of the yarns, where irregular distributions or stress concentrations may occur in the anchorage zones. Thus, in case of HC-E TRM, the absence of the third stage and the one cracking behavior obtained in some

specimens after 2 and 3 months of curing and the lower number of cracks as well as the lower elongation with respect to HC-L TRM, are due to the high mechanical characteristics of the ettringitic matrix. Contrariwise, in case of HC-L TRM, the natural hydraulic lime matrix caused a small decrease in the stiffness of the composite and small inhomogeneity in the distribution of load between the filaments of the yarns. But even though, the behavior of all the specimens of HC-L-TRM reflected a good and sufficient textile-matrix bonding which allows having the three stages of the typical tensile behavior of TRM at all the ages: 28 days, 2 months and 3 months. Thus, in case of TRMs made from ettringitic matrix, we cannot rely on the results of tensile tests after 28 days of curing, since their behavior changes after this age because of the ettringitic reactions, which did not stop, but they continue. This make the matrix denser, and the textile-matrix bonding starts to intensify gradually, leading to the brittle failure of the specimens without exhibiting a multiple cracking behavior. While for TRMs made from natural hydraulic lime mortars, the tensile test at 28 days could be considered as a reference.

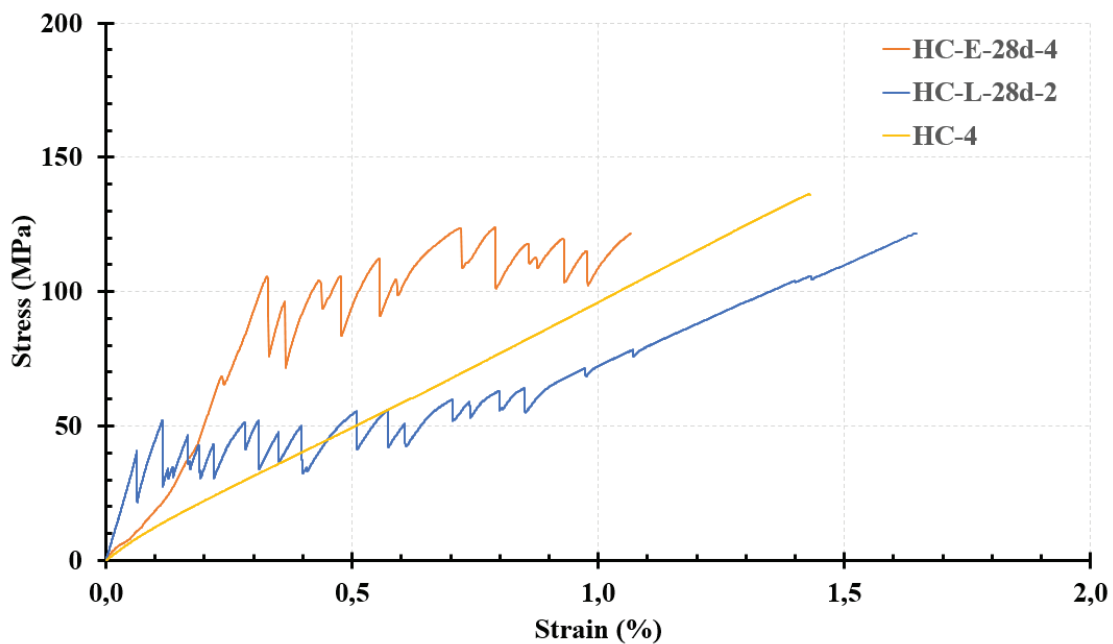


Figure 4- 186 : Comparison between stress-strain responses of representative specimens of HC-E TRM and HC-L TRM series tested at 28 days with a representative coated-hemp yarn specimen (HC).

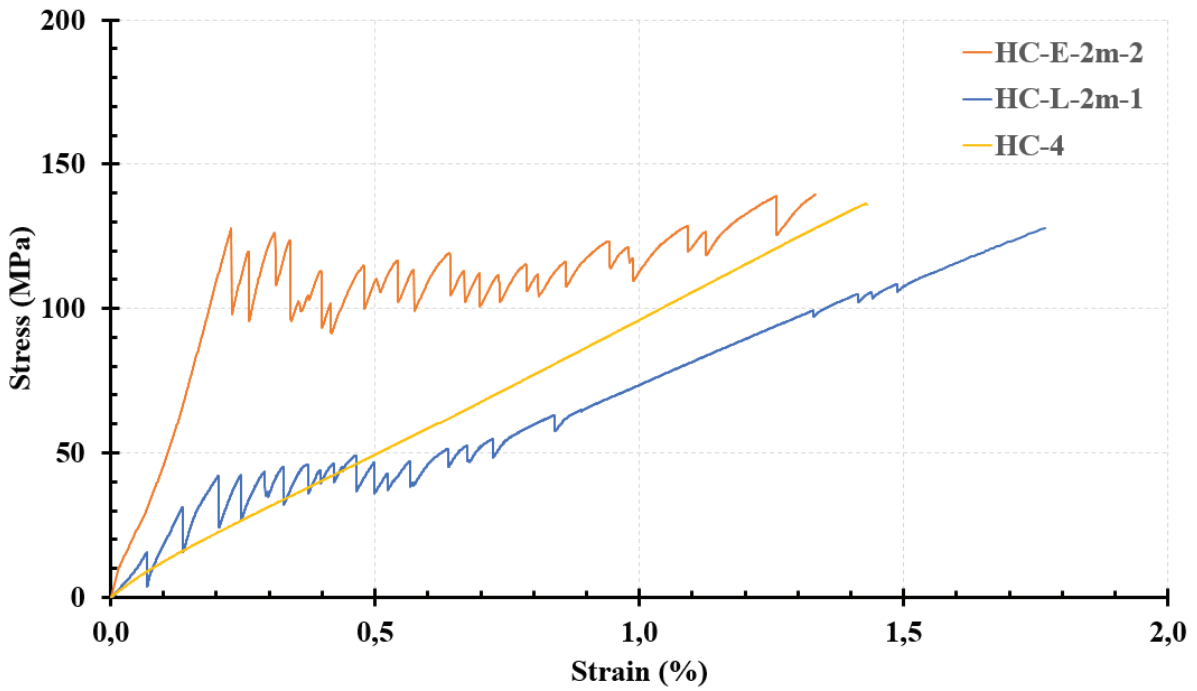


Figure 4- 187 : Comparison between stress-strain responses of representative specimens of HC-E TRM and HC-L TRM series tested at 2 months with a representative coated-hemp yarn specimen (HC).

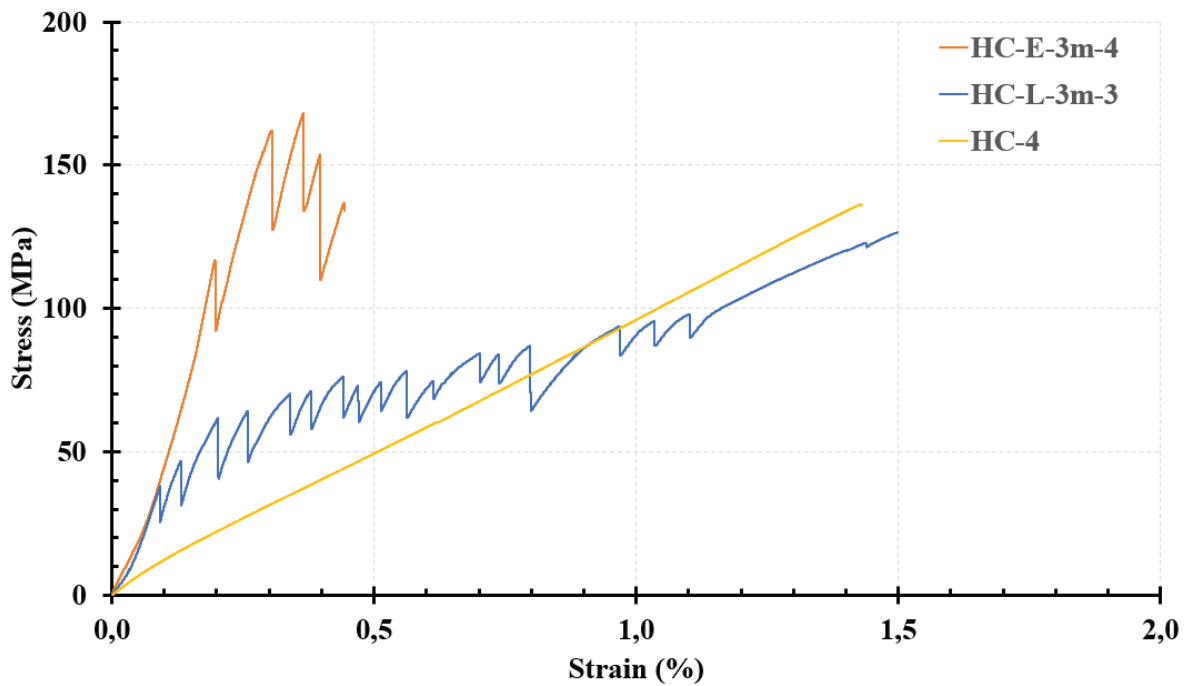


Figure 4- 188 : Comparison between stress-strain responses of representative specimens of HC-E TRM and HC-L TRM series tested at 3 months with a representative coated-hemp yarn specimen (HC).

4.4 Comparisons between the results of TRM and the results of the durability of yarns

In this section, the results of tensile test done on aged HC yarns are compared with the results of tensile tests done on TRMs made from these yarns. Referring to equation (3.1) already used in chapter 3 [153], [148], TRM at 2 months will be compared with yarns at 7 days and TRM at 3 months will be compared to yarns at 14 days (Table 4- 46). Only the aging of yarns at 23°C are taken into accounts in this comparison because the smallest period of accelerated exposure 7 days, at 40°C and 60°C corresponds to 3.67 and 4.64 years in service life, respectively (Table 3- 27 in chapter 3), and we don't have corresponding results at these ages in the case of TRM.

Table 4- 47 and Table 4- 48 present the average values of tensile stress and modulus of HC-E-23 yarns at a given accelerated exposure with the average values of tensile stress and modulus of the HC-E TRM for the specimens that exhibited multiple cracking behavior and the specimens with one crack behavior respectively, tested at the corresponding service life (Table 4- 46). Table 4- 49 presents the average values of tensile stress and modulus of HC-L-23 yarns at a given accelerated exposure with the average values of tensile stress and modulus of the HC-L TRMs, tested at the corresponding service life (Table 4- 46).

Table 4- 46: Correlation between accelerated aging and service life of HC yarns.

HC Yarns		HC-TRMs
Days of accelerated exposure (T=23°C)	Predicted service life (days)	service life obtained by the tested TRM
7	41.2	2 months
14	82.4	3 months

Table 4- 47 : Comparison of results between HC-E-23 yarns and HC-E TRM (specimens with multiple cracking behavior).

HC-E-23 Yarns			HC-E TRMs (multiple cracking behavior)		
Accelerated exposure	σ_{\max} (MPa)	E (GPa)	Service life	σ_{\max} (MPa)	E (GPa)
7 d	145.5	10.2	2 months	142.8	20.6
14 d	136.3	9.5	3 months	131.7	54.7

Table 4- 48 : Comparison of results between HC-E-23 yarns and HC-E TRM (specimens with only one cracking).

HC-E-23 Yarns			HC-E TRMs (one cracking behavior)		
Accelerated exposure	σ_{\max} (MPa)	E (GPa)	Service life	σ_{\max} (MPa)	E (GPa)
7 d	145.5	10.2	2 months	182.5	57.5
14 d	136.3	9.5	3 months	139.9	70.4

Table 4- 49 : Comparison of results between HC-L-23 yarns and HC-L TRM.

HC-L-23 Yarns			HC-L TRMs		
Accelerated exposure	σ_{\max} (MPa)	E (GPa)	Service life	σ_{\max} (MPa)	E (GPa)
7 d	161.8	10.8	2 months	118.3	7.2
14 d	155.4	9.7	3 months	104.6	8.0

From Table 4- 47, one can notice that:

- The maximum tensile strength of HC-E-23-7d series of yarns is very close to that of HC-E-2m series of TRM (specimens with multiple cracks only). While the tensile modulus of the yarns is about half the tensile modulus of the composite.
- the maximum tensile strength of HC-E-23-14d series of yarns is very close to that of HC-E-3m series of TRM (specimens with multiple cracks only). While the tensile modulus of the yarns is lower than the tensile strength of the composite. This difference in stiffness between HC-E TRM and HC yarns is already explained, it is due to the contribution of the ettringitic matrix which can provides additional stiffness as explained before when the behavior of HC-E TRM are compared with the behavior of HC yarns without any aging.

From Table 4- 48, one can notice that:

- The maximum tensile strength of HC-E-23-7d series of yarns is slightly lower than that of HC-E-2m series of TRM (specimens with only one crack). While the tensile modulus of the yarns is lower than the tensile strength of the composite.
- the maximum tensile strength of HC-E-23-14d series of yarns is very close to that of HC-E-3m series of TRM (specimens with only one crack). While the tensile modulus of the yarns is lower than the tensile strength of the composite.

The large differences in tensile modulus between HC-E TRM and HC yarns is already explained, it is due to the fact that the ettringitic matrix provided additional stiffness to the composite who stayed in stage II where the rigidity of the TRM refers to the rigidity of the composite and not the rigidity of the textile only.

From these results, we can conclude that the formula used to correlate the accelerated aging days of HC yarns with the service life of these yarns when imbedded in the ettringitic matrix of the composite could be effective. The accelerated aging protocol in solution E at 23°C has demonstrated to be consistent with the service life since the tensile strengths of HC-E TRM were very close to those of aged HC yarns. Further investigations on HC TRM cured for longer periods are needed in order to compare their results with the results of HC yarns aged at 40°C and 60°C which corresponds to longer service lives.

From Table 4- 49, one can notice that:

- The maximum tensile strength and the tensile modulus of HC-L-2m TRM series are lower than those of HC-L-23-7d series of yarns.
- the maximum tensile strength and the tensile modulus of HC-L-3m series of TRM are lower than those of HC-L-23-14d series of yarns.

From these results we cannot conclude that the accelerated aging protocols in L-23 solution is less severe on HC yarns than their exposure to the L matrix of the HC-TRM, because these differences in tensile strength and modulus between HC-L TRM and HC yarns are already explained. They are probably due to an inhomogeneous load distribution between the filaments of the yarns. In addition we should not forget that the tensile properties of the HC TRM in the third stage depends to the tensile properties of the HC textile made from four yarns. Therefore, an inhomogeneous load distribution between the yarns of the textile could also be a cause.

4.5 Perspectives on the prediction of the durability of HC TRM in the long term

Further investigations on tensile strength of TRMs made from HC fibers imbedded in E and L matrices for long periods are needed to validate the correlation formula. If the latter is validated, we could predict the behavior of HC yarns when imbedded in ettringitic matrix and natural hydraulic lime matrix of a TRM for longer durations. Table 4- 50 reminds the years of service life, which corresponds to each exposure duration at a given temperature. To better illustrates this prediction; the results are reported in terms of diagrams that show residual values of tensile strength with respect to the predicted years of service life and not the exposure duration. Figure 4- 189 and Figure 4- 190 present the residual tensile strength of HC yarns subjected to matrix E and matrix L respectively, with respect to the years of service life calculated through the correlation formula. The representation of the series aged at 23°C is not clear in those two Figures, since the maximum service life duration for these series is 1.5 years very smaller than that of 60°C (60 years), thus those series are presented in Figure 4- 191. One can notice that the HC yarns could maintain their durability in the ettringitic matrix up to 60 years of exposure without a significant loss in their tensile strength (Figure 4- 189). The loss is lower than 20 % in all cases. While in natural hydraulic lime matrix, these yarns started to lose more than 20 % of their tensile strength after 38 years of service life. The loss after 60 years was significant, it is 43 %.

Table 4- 50: Correlation between accelerated aging and service life of the yarns.

	T = 23°C	T = 40°C	T = 60°C
Days of accelerated exposure	Years of service life	Years of service life	Years of service life
0	0,0	0,0	0,0
7	0,1	3,7	4,6
14	0,2	7,3	9,3
28	0,5	14,7	18,6
42	0,7	22,0	27,9
60	1,0	31,4	39,8
74	1,2	38,8	49,1
90	1,5	47,2	59,7

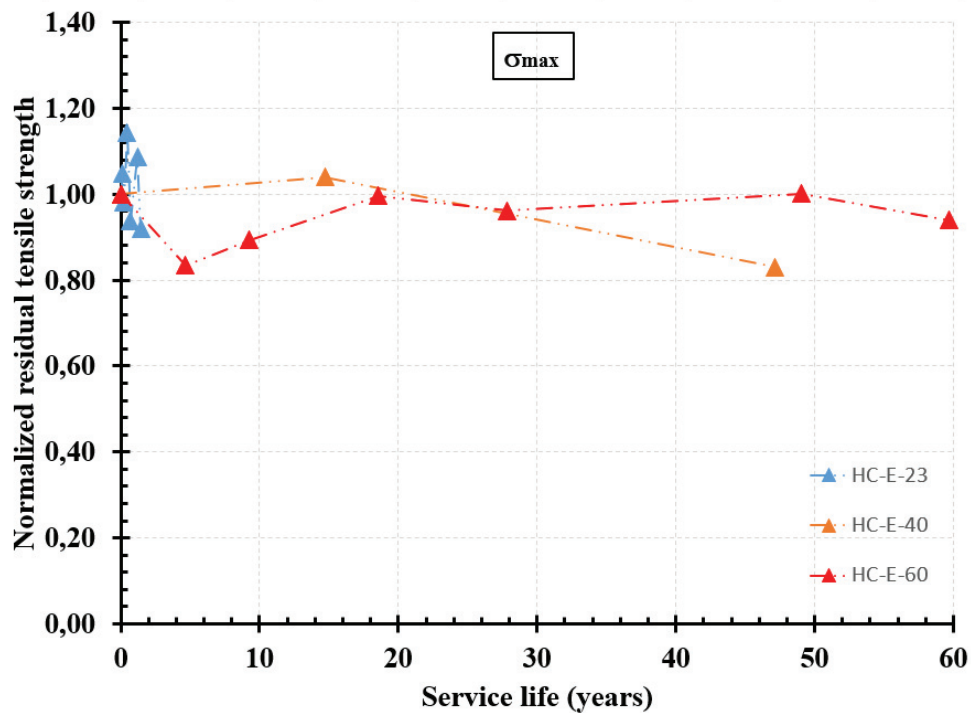


Figure 4- 189 : Prediction of the durability of HC yarns in the ettringitic matrix E up to 60 years of service life (normalized residual values).

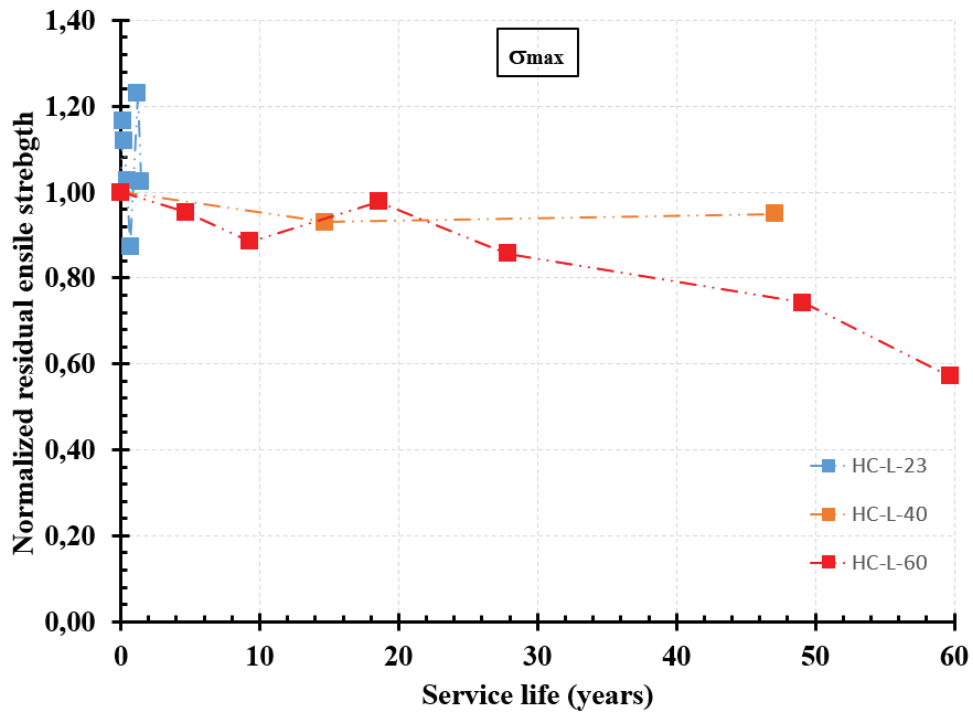


Figure 4- 190 : Prediction of the durability of HC yarns in the natural hydraulic lime matrix L up to 60 years of service life (normalized residual values).

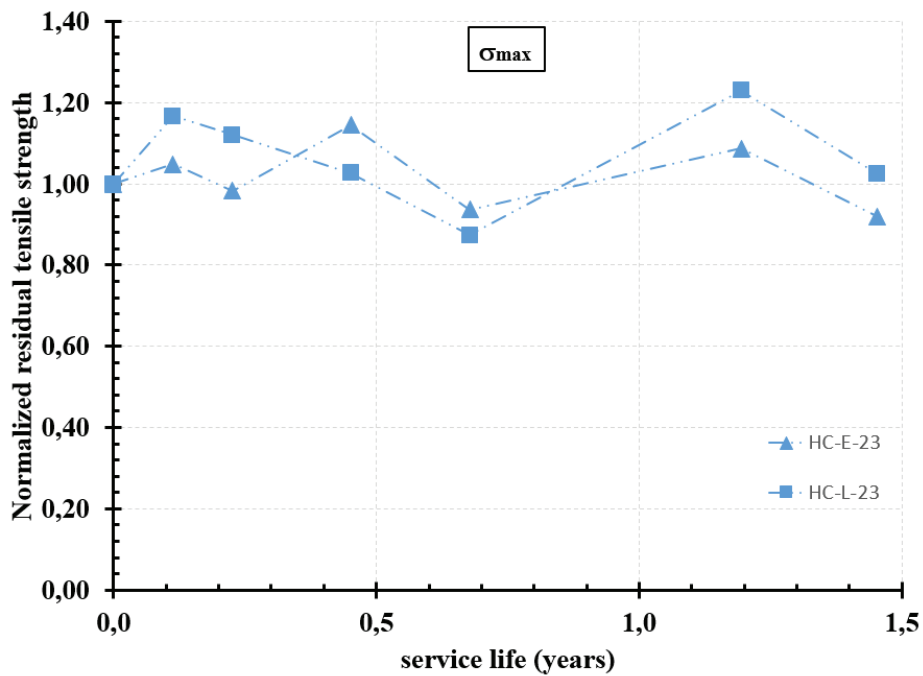


Figure 4- 191 : Clear representation of the prediction of the durability of HC yarns in both matrices E and L up to 1.5 years of service life (normalized residual values).

4.6 Conclusions

In this chapter, the effect of alkaline solutions reproducing the environments of the ettringitic (E) and the natural hydraulic lime (L) mortars along with the effect of different temperatures on the tensile behavior of bio-resin-coated hemp yarns (HC) were examined. The residual tensile strengths, tensile modulus and ultimate tensile strains of HC yarns after different exposure periods have been quantified and discussed. In addition, the effect of the bio-resin coating and the mortar types on the tensile behavior of hemp TRM was also examined through tensile tests at different ages. Finally, a comparison between the results of tensile tests on aged HC yarns with the results of tensile tests on TRMs made using these yarns was done.

From the results of tensile tests on aged HC yarns, the following main conclusions can be drawn:

- For pH 10.5, the temperature did not have any significant influence on the tensile strength of HC yarns, but it caused a decrease in their tensile modulus along with an increase in their elongation.
- For pH 12.5, up to 40°C, the temperature also did not influence the tensile strength of HC yarns, while it decreased their tensile modulus and increased their elongation.
- Both pH used in this study 10.5 and 12.5 had same effects on HC yarns at 23°C and 40°C. At 23°C, they maintain tensile strength and modulus close to the initial ones, but they increase the elongation of these yarns. While at 40°C, they maintain tensile strength close to the initial value, they undergo a decrease in the tensile modulus and an increase in the elongation.
- The most severe environment on HC yarns was L-60, which corresponds to a pH of 12.5 with a temperature of 60°C. In this environment, HC yarns underwent a plasticization process and the temperature accelerated the damage of the yarns, which lost about 43 % of their tensile strength and modulus after 90 days of immersion. This degradation in the tensile properties of hemp yarns is probably due to two reasons: the plasticization of the resin network by the water molecules, which leads to the decrease in the tensile properties of the resin and making it unable to distribute and share properly the external forces to the fibers, resulting in a reduction in the tensile strength of the coated yarn. In addition, the diffusion of the aggressive fluid through the resin matrix may have caused the degradation of hemp fibers (hydrolysis of the outer layer of the fibers, debonding at fiber/fiber interfaces, cracking of interfaces between matrix and fiber bundles) also contributed to this degradation. Both effects resulted in an increase in the average ultimate tensile strain of the fiber along with a decrease in the average tensile strength and modulus.
- The bio-resin coating used in this study offered additional stiffness to the structure of the hemp fibers about 2.3 times higher, by sticking them together and resulted in a decrease in the tensile strength and elongation of these yarns
- A beneficial effect was observed using bio-resin coating. It is the significant improvement that offers concerning the durability of hemp yarns in alkaline solutions. It prevented their

degradation by protecting them and preventing the processes of mineralization and alkaline hydrolysis from occurring in all the solutions except the solution L-60.

From the results of tensile tests on HC TRMs, the following main conclusions can be drawn:

- The resin coating of hemp yarns was also found to be beneficial when these yarns are imbedded in both kinds of matrices used in this study: E and L. it allowed a more uniform distributions of the stress along the fibers and prevented the slippage of the yarns within the matrix, resulting in better textile-matrix bond. It also reduced the water absorption capacity of the fibers, thus enhanced its volumetric stability and prevented the apparition of the porosity at the fiber-matrix interface as well as the fiber elongation within the matrix.
- The matrix type influenced the tensile behavior of TRM. The textile-matrix bond is stronger in case of ettringitic matrix than that of natural hydraulic lime matrix, which prevented the appearance of the stage III in case of HC-E TRM while it can be clearly observed in case of HC-L TRM who proved a sufficient textile-matrix bond. In addition, more uniform distribution of load between the filaments of the yarns was attained in case of ettringitic matrix, contributed to higher tensile properties.
- Special attention needs to be given to the hydration degree of the mortar and its effect on the performance of TRMs. The 28 days curing testing age, as usually used for cementitious mortars, does not seem to be particularly a good reference for ettringitic mortars since different behaviors was observed at 2 and 3 months.
- Further investigations on new formulations of the ettringitic matrix are needed in order to decrease its rigidity, thus allowing more deformability for the TRM, which make them more suitable for the retrofitting of the structures.

From the comparison of the results between tensile tests on aged HC yarns and tensile tests on HC TRMs, the following conclusions can be drawn:

- The accelerated aging protocols at 23°C along with the Arrhenius approach used to predict the service life of the yarns have demonstrated to be useful to predict 3 months, for both kinds of matrix used.
- Based on the Arrhenius approach used, the bio-resin-coated hemp yarns embedded in ettringitic matrix are expected to maintain good tensile properties for at least 60 years of service life, while in natural hydraulic lime matrix a loss in the tensile strength greater than 20% was expected after 38 years and a 43% of loss after 60 years of service life.
- Further investigations on TRMs made from HC textile and ettringitic and natural hydraulic lime matrices for several years are needed in order to validate the use of Arrhenius approach in case of aging protocols employing temperatures of 40 and 60°C.

Chapter 5 Shear-bond test on bio-resin-coated hemp TRM applied to different substrates

5.1 Introduction

According to the Round Robin Test methodology formulated by the RILEM Technical Committee TC 250-CSM [183], it is recommended to test the adhesion between the textile and the matrix as well as between the TRM and the substrate, which allows us to predict the behavior of the TRM when it is used in the large-scale rehabilitation of the structures. For this reason, the aim of this chapter is to characterize the bond performance of bio-resin-coated hemp TRMs applied to two different substrates: concrete and brick masonry elements. In case of concrete substrate, the Ettringitic matrix (E) was used to manufacture the TRM while in case of masonry substrate, the TRM reinforcement system was made from the Natural Hydraulic Lime matrix (L). The first part of this chapter concerns the specimens' preparation, such as substrates' construction, and substrates' reinforcement, as well as the experimental protocol of the shear bond test. Then, the second part presents and discusses the results of shear bond tests. In addition, a comparison between the results of tensile tests done in chapter 4 on the TRM plates with the results of shear bond tests done in this chapter on substrates reinforced with the same TRMs' systems is discussed hereafter.

5.2 Experimental procedure

5.2.1 Specimens preparation

The specimens' preparation for the shear bond test consists of two phases: the substrates' preparation and then the reinforcement of the substrates with TRM.

5.2.1.1 Substrates preparation

The dimensions of the masonry substrates were 315 mm x 250 mm x 120 mm. They consist of five clay bricks of dimensions 250 mm x 120 mm x 55 mm each and four mortar's joint layers of 10 mm thick each. The bricks are characterized by a compressive strength of 14.8 MPa, a tensile strength of 2.5 MPa and a modulus of elasticity of 5760 MPa [184]. The mortar's joint consists of 1 volume of cement, 1 volume of natural hydraulic lime NHL, and 5 volumes of sand. The mechanical properties of the mortar joint were determined through flexural and compressive tests on six prismatic specimens of dimensions 40 mm × 40 mm × 160 mm, after 56 days of curing. The results showed an average flexural strength of 4.8 MPa (CoV 8.6 %) and an average compressive strength of 20.2 MPa (CoV 2.8 %). The steps of construction of masonry walls are presented in Figure 5- 192.

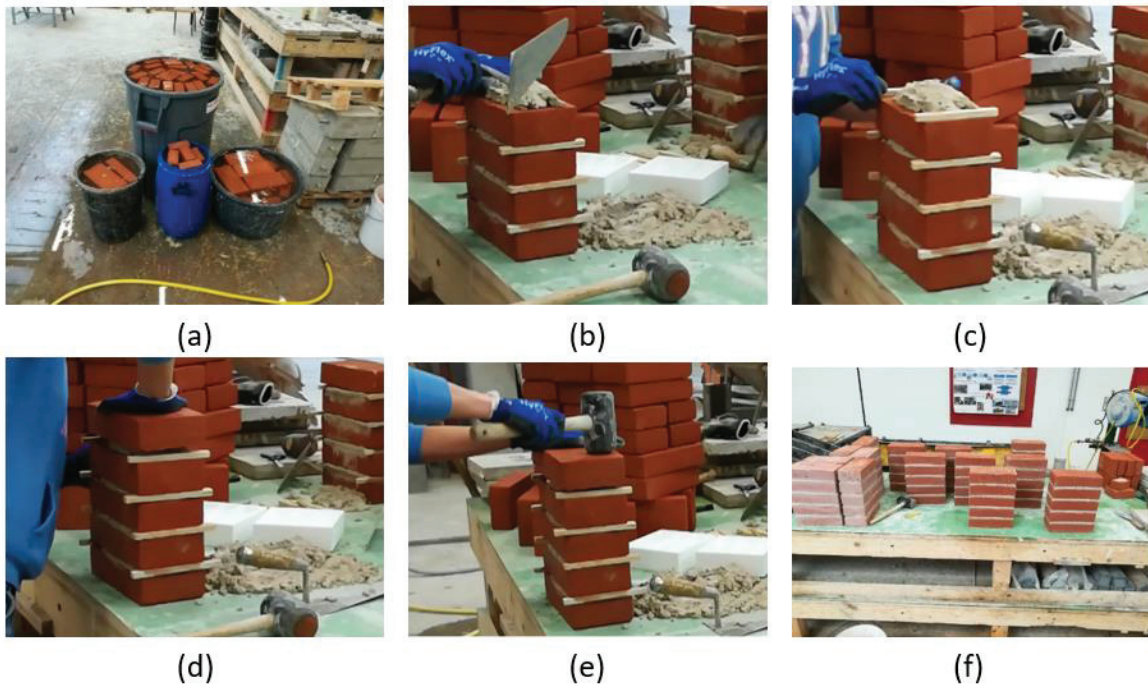


Figure 5- 192 : Steps of the construction of a masonry wall: a) Water saturation of the bricks before using; b) Spreading of the mortar joint on the brick; c) putting a wood piece of 1 cm thick between two bricks; d) putting another brick on the layer of mortar; e) Applying some blows of the hammer; f) Final state of the walls.

The concrete substrates were of same dimensions as the masonry walls 315 mm x 250 mm x 120 mm. The compressive strength of each concrete element was measured directly before its reinforcement with TRM, by means of a sclerometer. The resultant average compressive strength obtained is 28 MPa.

5.2.1.2 Reinforcement of the walls with TRM

The concrete elements were reinforced with HC-E TRM configuration while the brick masonry elements were reinforced with HC-L TRM configuration. The reinforcement of both types of substrate was carried out by applying a system of TRM in their centers having a section of 90 mm x 10 mm, and a length of 260 mm, following the next steps:

- Before beginning, the walls were thoroughly cleaned to remove all traces of mortar and dust and to ensure effective bonding of the composite;
- The region of each wall where the TRM should be applied was manually wet using a wet sponge;
- The first layer of the matrix (5 mm thick) was poured into the mold, using an appropriate trowel, and making sure to ensure a surplus (Figure 5- 193a);
- The excess mortar was removed, immediately, by means of a metal ruler, held almost vertically; but inclined in the direction of the leveling. The ruler was moved slowly, pulled in a cross saw motion, one time in each direction;

- The bars constituting the second layer of the mold are glued on top of the first ones; so that we obtain a total thickness of 10 mm;
- While the mortar was still fresh, the textile grid was put on the first layer of the matrix and a low hand pressure was applied to ensure better textile impregnation by the matrix (Figure 5- 193b);
- The second layer of the matrix (5 mm thick) was poured over the textile grid, making sure to ensure a surplus, and then the surplus was removed by the metal ruler (Figure 5- 193c);
- Finally, the surface was smoothed while still fresh and the TRM was covered with a plastic film so that the water does not evaporate during the hydration of the mortar (Figure 5- 193d).

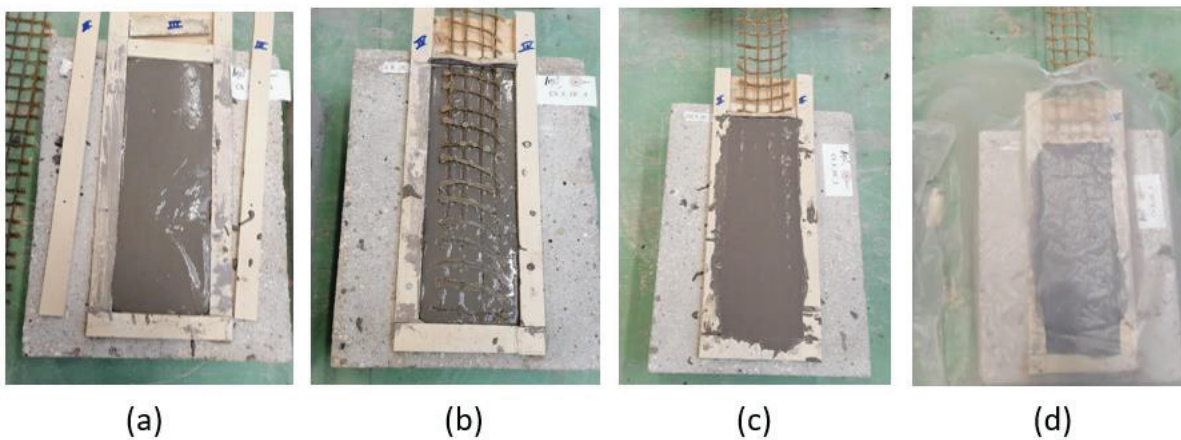


Figure 5- 193 : Steps of reinforcement of a concrete wall by a TRM system: a) Introduction of the first layer of the matrix; b) Application of the textile; c) Introduction of the second layer of the matrix; d) Covering the wall with a plastic film.

The specimens were demolded 72 hours later, kept in plastic film for 4 days, then they were removed from the plastic film and cured for 21 days at ambient temperature (23 ± 2 °C) and relative humidity of 50-60 %. Like that, the total curing days was 28 days.

5.2.2 Shear bond test setup

The shear bond tests were carried out, according to RILEM Technical Committee TC 250 CSM [183]. Based on tensile test results, only two series of specimens characterized by coated hemp were considered:

- CS-HC-E: six concrete substrate (CS) specimens strengthened by the composite in the reinforcement configuration HC-E (Figure 5- 194a, b).
- MS-HC-L: six masonry substrate (MS) specimens characterized by five bricks masonry externally strengthened by the composite in the reinforcement configuration HC-L (Figure 5- 194c, d).

Figure 5- 194 presents the geometrical properties of all the specimens tested. Table 5- 51 summarizes the name, the number of specimens, the number of yarns in the longitudinal direction

and the strengthening ratio of each one of the series. Specifically, the strengthening ratio is equal to the percentage obtained by the ratio between the cross sectional area of the longitudinal yarns (13.112 mm²) over the cross section of the composite (90 mm x 10 mm).

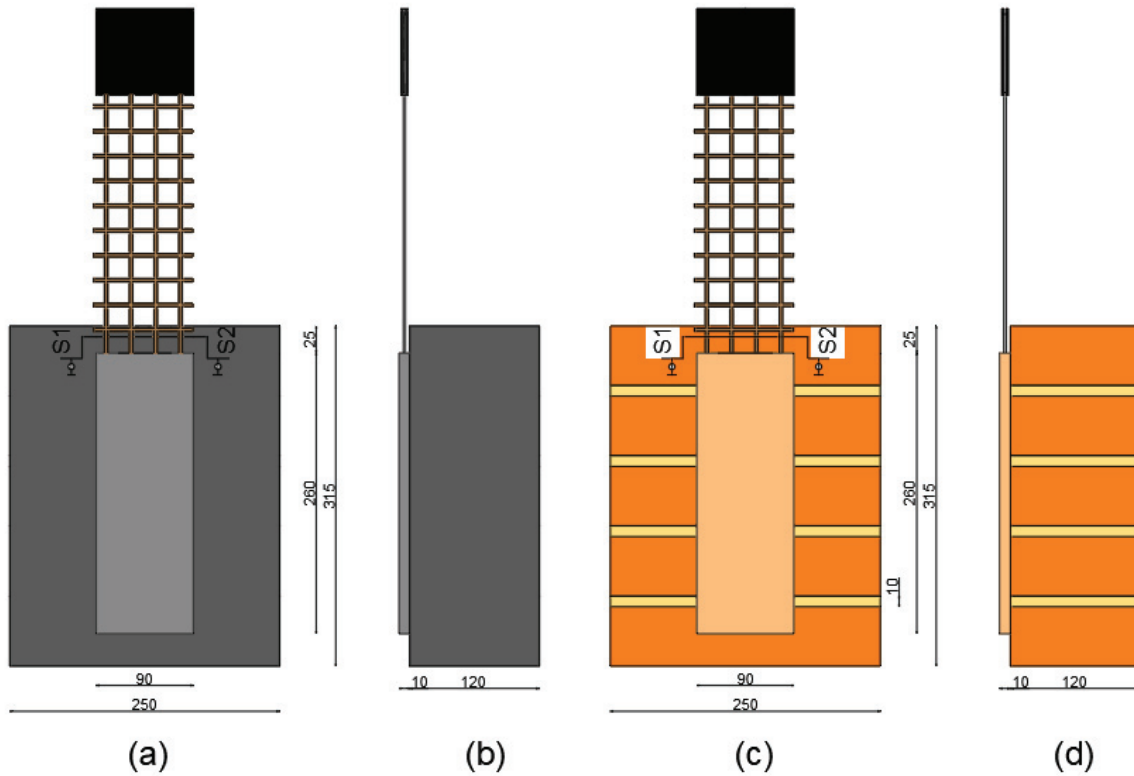


Figure 5- 194 : Geometric characteristics of the specimens for the shear bond test: a) front view of CS-HC-E specimens, b) lateral view of CS-HC-E specimens, c) front view of MS-HC-L specimens and d) lateral view of MS-HC-L specimens (dimensions are in mm).

Table 5- 51 : Shear bond test series.

Series name	Nb. of specimens	Nb. of yarns	Strengthening ratio (%)
CS-HC-E	6	4	1.457
MS-HC-L	6	4	1.457

Shear bond tests were carried out by using a universal testing machine Zwick of 50 kN capacity in displacement control with a loading rate of 0.3 mm/min. the load applied to the specimen and the displacement of the cross-head were recorded by the machine. A steel system, consisting of two metallic plates connected by four threaded rods, locked the wall so that no rotation of the reinforced substrate could occur (Figure 5- 195). The free end of the composite TRM, consisting of longitudinal yarns bonded to steel tabs, was fixed by a mechanical device connected to the cross-head by a hinge so that no bending moments could be transmitted to the TRM system (Figure 5- 194, Figure 5- 195). In order to avoid load eccentricity and, consequently, out-of-plane tensile

stresses (peeling) at the interface between the substrate and the reinforcing system, each specimen was duly placed to ensure that the textile was aligned with the direction of the load, with no eccentricity. Moreover, in order to record possible slipping of the textile within the mortar matrix, an aluminum device, named “ Ω ” for its shape, was bonded to the textile at a distance of 5 mm from the TRM edge and instrumented by two displacement transducers LVDT, S1 and S2 which are also bonded to the masonry substrate. Their role is to monitor any motion of the “ Ω ” plate during the test (Figure 5- 194, Figure 5- 195).

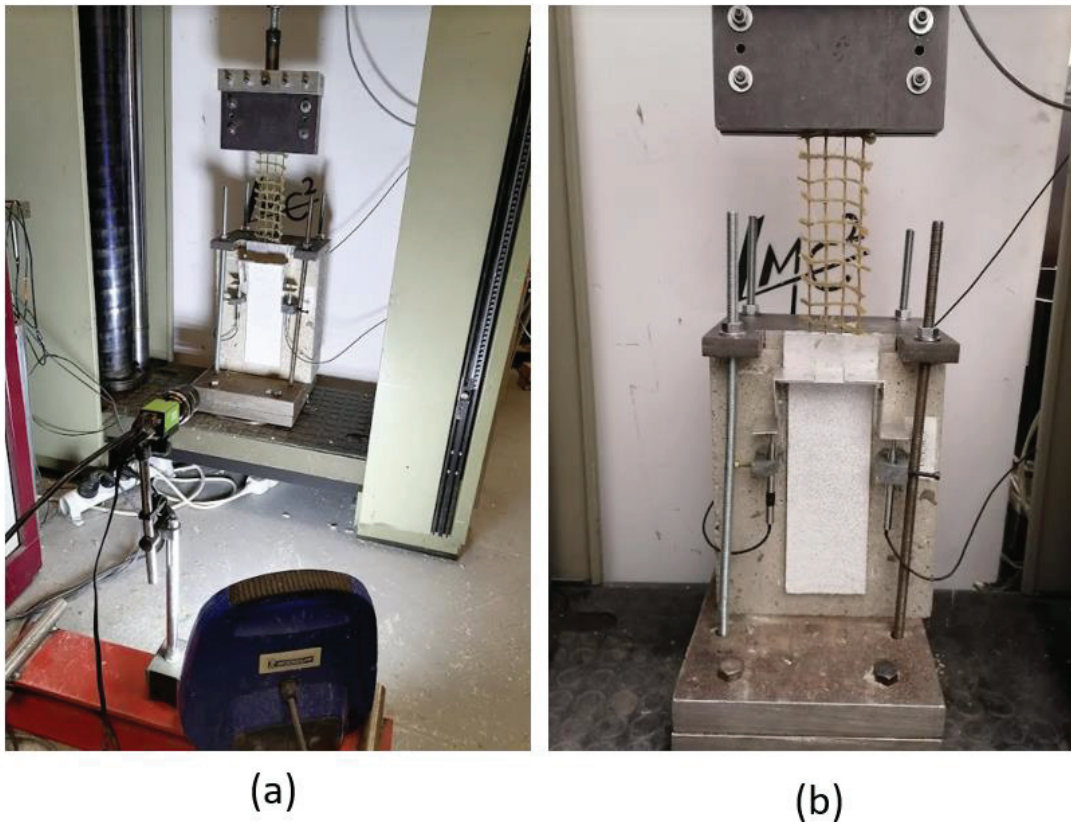


Figure 5- 195 : Experimental setup of the shear bond test.

5.3 Results and discussions

The results obtained by the shear bond test are reported in terms of Force-displacement (F-d) curves, stress-slip curves (σ -s) and failure modes. Furthermore, Table 5- 52 contains the value of the maximum load F_{\max} , the maximum stress σ_{\max} , the corresponding displacement U , the corresponding slip s , the exploitation rate, and the failure mode for each specimen tested. The specimens CS-E-HC-2 and MS-L-HC-4 are not treated because of several problems encountered during their fixing. The stress σ_{\max} is calculated by assuming a uniform distribution of the stress between the fibers; it is equal to the ratio between the force measured and the cross-sectional area of the textile (13.11 mm^2). The displacement U refers to the global displacement of the cross head. The slip s is obtained by averaging the slip values recorded by the two LVDT S1 and S2. The

exploitation rate is the ratio between the maximum stress obtained and the tensile strength of HC yarns (138.8 MPa). The observed failure modes will be evaluated in the context of the typical failure modes relating to the shear bond tests carried out on the TRM-masonry interface (Figure 5- 196) [185]. Mode A is characterized by the debonding of the reinforcement system with cohesive rupture in the substrate. Mode B is characterized by the detachment at the matrix-substrate interface. Mode C is characterized by the debonding at the textile-matrix interface. Mode D is characterized by the sliding of the textile in the matrix. Mode E is characterized by the sliding of the textile and the cracking of the external layer of the mortar. And finally, mode F is characterized by the rupture of the textile in tension out of the bonded area.

Table 5- 52 : Experimental results for all the specimens tested in shear-bond test.

Series	Specimen	F_{max} (N)	σ_{max} (MPa)	U (mm)	Slip at σ_{max} (mm)	Exploitation rate (%)	Failure mode
CS-E-HC	CS-E-HC-1	1371.3	104.6	2.8	0.9	75.3	F
	CS-E-HC-2	-	-	-	-	-	
	CS-E-HC-3	1283.3	97.9	3.5	1.3	70.5	F
	CS-E-HC-4	1406.6	107.3	3.4	1.9	77.2	F
	CS-E-HC-5	1251.9	95.5	3.0	0.8	68.8	F
	CS-E-HC-6	1708.3	130.3	3.8	1.2	93.8	F
	Average	1404.3	107.1	3.3	1.2	77.1	F
	Std. Dev.	162.1	12.4	0.3	0.4	8.9	
	CoV (%)	11.5	11.5	10.4	31.1	11.5	
MS-L-HC	MS-L-HC-1	1401.6	106.9	3.5	0.2	77.0	F
	MS-L-HC-2	1634.1	124.6	4.6		89.7	F
	MS-L-HC-3	1550.8	118.3	3.6	0.9	85.1	F
	MS-L-HC-4	-	-	-	-	-	-
	MS-L-HC-5	1427.4	108.9	3.2	0.5	78.4	F
	MS-L-HC-6	1161.9	88.6	2.7	0.5	63.8	F
	Average	1435.2	109.5	3.5	0.6	78.8	F
	Std. Dev.	160.5	12.2	0.6	0.2	8.8	
	CoV (%)	11.2	11.2	17.7	30.9	11.2	

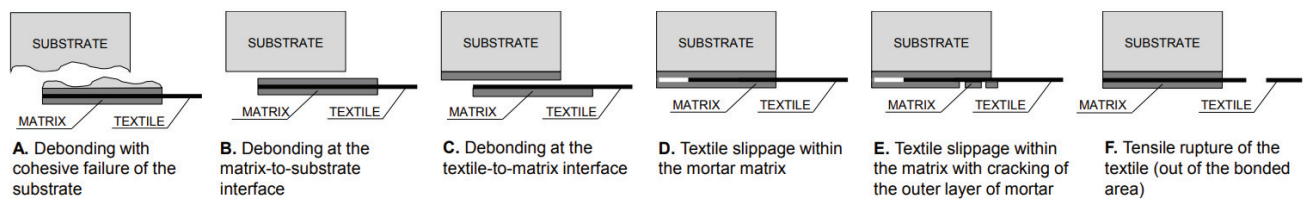


Figure 5- 196 : Failure modes related to the shear bond test [185].

5.3.1 CS-E-HC and MS-L-HC series

Figure 5- 197 and Figure 5- 198 present the force-displacement curves and the stress-slip curves respectively, of the specimens of CS-E-HC series. Figure 5- 199 and Figure 5- 200 present the force-displacement curves and the stress-slip curves respectively, of the specimens of MS-L-HC series. The stress-slip curves of specimens MS-L-HC-1 and MS-L-HC-2 are not plotted because of problems encountered with the fixation of the 'Ω'. Figure 5- 201 and Figure 5- 202 present the failure mode F recorded for all the tested specimens of CS-E-HC and MS-L-HC series, respectively. A tensile rupture of the textile out of the bonded area characterizes this failure mode.

At first, one can notice that the failure of the textile occurred in different levels, characterized by different drops after the peak load of the Force-displacement curves (Figure 5- 197, Figure 5- 199). The drops are related to the progressive tensile failure of the yarns due to an inhomogeneous load distribution. We can also notice that almost all the stress-slip curves plotted show a snap-back behavior after failure (Figure 5- 198, Figure 5- 200). This is probably related to the displacement of the aluminium plate (with an 'Ω' shape) bonded to the textile and directly connected to the LVDT to measure the slip. Since the failure occurred frequently between the load cell and the 'Ω' (Mode F), the self-load of the 'Ω' allows the recording of a snap-back behavior. These load drops and snap-back behaviors after failure were also recorded in Zaydan et al. 2021 [179].

The bond strength resulted thus adequate for HC-TRM composite to attain the yarns rupture, avoiding premature failure due to debonding or sliding. The average exploitation rate is about 77 % and 79 % for CS-E-HC and MS-L-HC, respectively (Table 5- 52). This is due to an inhomogeneous load distribution between the filaments of the yarns. Furthermore, we should note that the exploitation rate is calculated with respect to the tensile strength of a single yarn not the tensile strength of the textile, which contributed also in this difference. We can also notice that the exploitation rate for both series are very close, which is normal since we have seen in Zaydan et al. 2021 [179], that the maximum force obtained during a shear-bond test is proportional to the reinforcement rate used. In other words, the ultimate tensile strength depends mainly on the textile used in the TRM and not on the matrix. In our case, the exploitation rates are close for both series, because they have same reinforcement rates, the only difference between them is the matrix type.

In all the specimens tested, the matrix is neither cracked nor detached from the textile; this failure mode translates a good adhesion between the bio-resin coated hemp textile and the used matrices (Figure 5- 201, Figure 5- 202). Furthermore, the adhesion between the ettringitic matrix and the concrete as well as between the natural hydraulic lime matrix and the masonry is sufficient to avoid the failure mode B (detachment at the matrix-substrate interface).

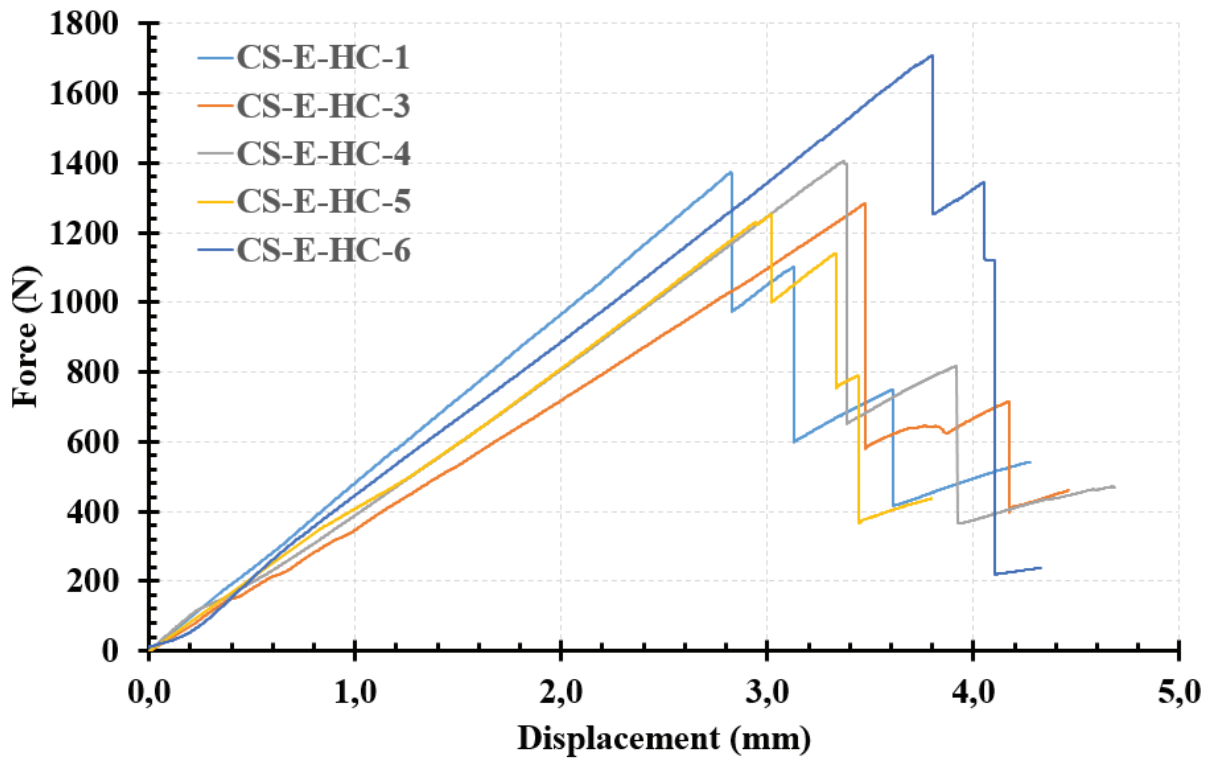


Figure 5- 197 : Force-displacement curves for the specimens of CS-E-HC series.

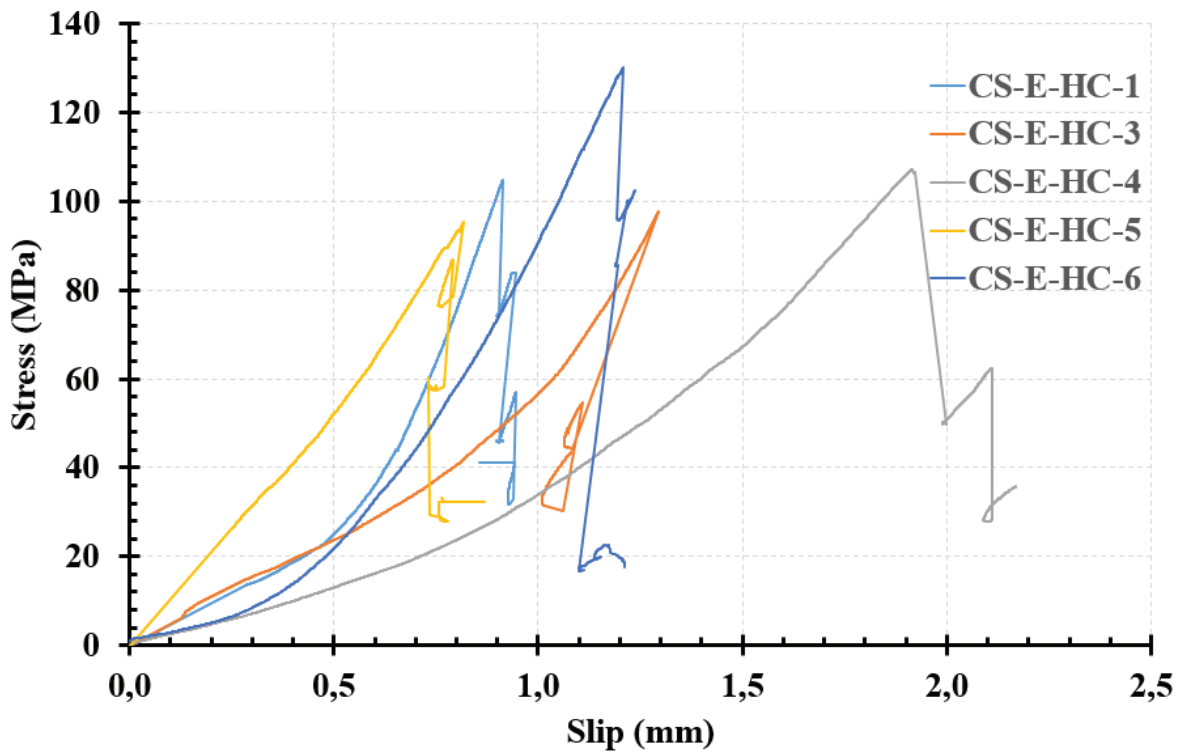


Figure 5- 198 : Stress-slip curves for the specimens of CS-E-HC series.

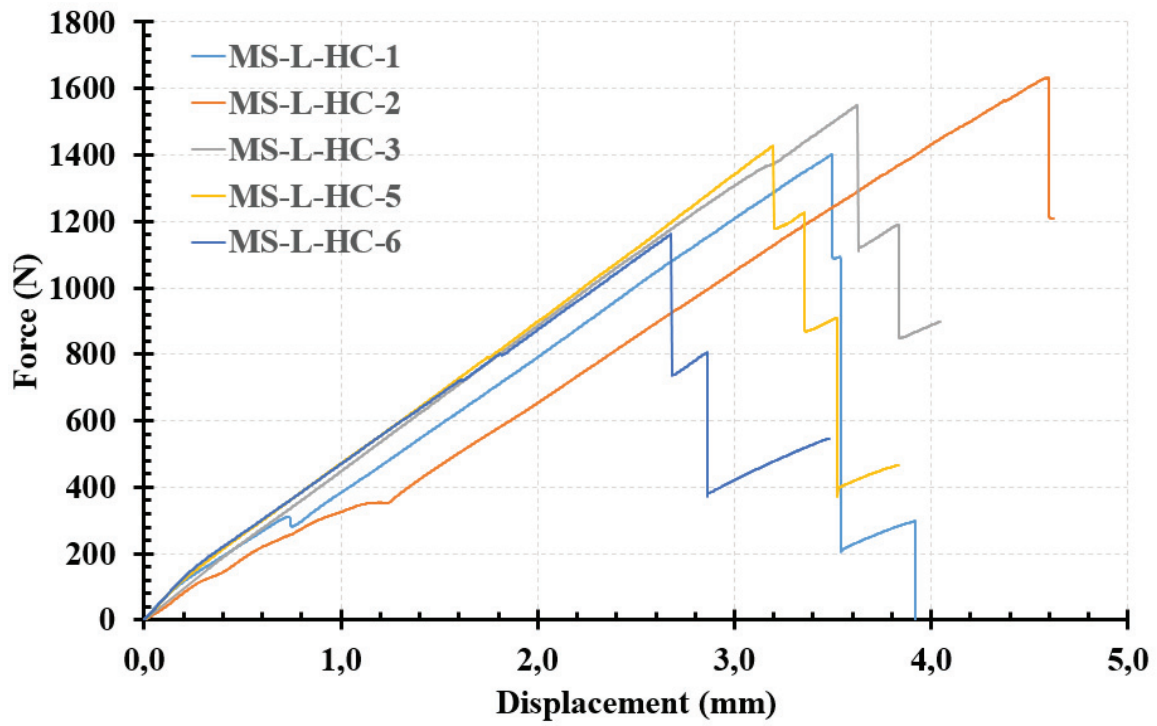


Figure 5- 199 : Force-displacement curves for the specimens of MS-L-HC series.

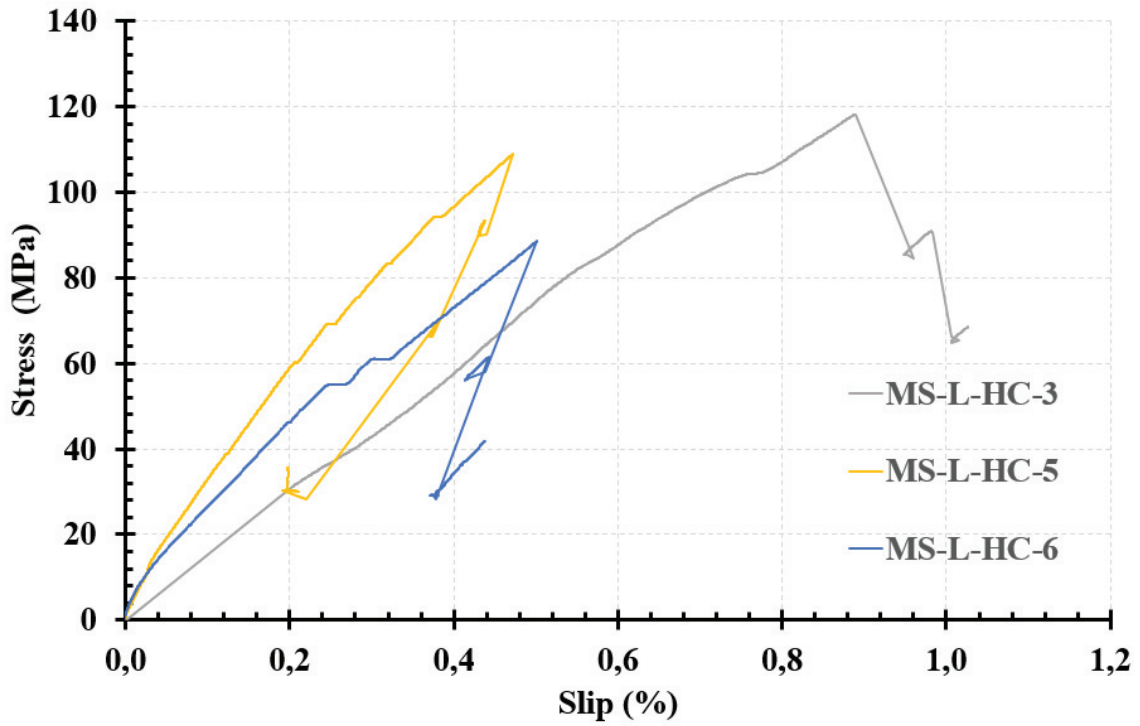


Figure 5- 200 : Stress-slip curves for the specimens of MS-L-HC series.



(a)



(b)

Figure 5- 201 : Failure mode recorded in all the specimens of CS-E-HC series: a) Mode F b) uncracked ettringitic matrix for all the specimens tested.



(a)



(b)

Figure 5- 202 : Failure mode recorded in all the specimens of MS-L-HC series: a) Mode F b) uncracked natural hydraulic lime matrix for all the specimens tested.

5.3.2 Shear bond test, direct tensile test and guidelines

The ratio of the average maximum stress obtained for the shear-bond test (SST) series to the average maximum stress obtained for the tensile test (TT) series is equal to $107.1/126.8 = 0.84$ and $109.5/122.9 = 0.89$ for the E and L series respectively. These ratios indicate that the average maximum stress obtained for the SST series is close to the average maximum stress obtained for the TT series, which is normal since the rupture mode obtained for the two series was the rupture of HC textile, which will take place when the load exceeds the tensile strength of hemp fibers. However, this does not mean that we can characterize a TRM system by applying only one of these two tests. According to Ascione et al. 2015 [185], these two tests are complementary for the qualification of externally bonded TRM systems. They propose to determine the maximum stress and the expected failure modes through shear bond test, seeing that the applied force can be exactly recorded during this test, but the slip measurements may be affected by relatively large scatter. However, they proposed to rely on the tensile tests for the determination of the strain seeing that in this test, the displacements/strains can be measured more precisely. Furthermore, the ministry of public works in Italy published new guideline [186] providing acceptance criteria and design provisions for externally bonded TRM systems, relying on the results obtained recently by many works (Ascione et al. 2015 [185], Bellini et al. 2017 [187], Carozzi et al. 2017 [6], De Santis et al. 2017 [188], Focacci et al. 2017 [189], Valluzzi et al. 2014 [190]). The main features of this guideline have been summarized by Ascione et al. 2018 [191]. In this guideline, the parameters needed to design a TRM system are: the conventional limit stress and conventional limit strain obtained through shear bond test, the slope of the cracked stage and the effective tensile strain obtained through tensile test. The same does not happen in the American guidelines ACI 549.4R-13[192], which do not take into account the results of the debonding test in the acceptance procedure of a TRM system. It only relies on the tensile tests to define the parameters needed, which are: the slope of the cracked stage and the effective tensile strain obtained by dividing the ultimate tensile stress by the slope of the cracked stage.

In our case, we have obtained close maximum stress for tensile and shear bond test because we haven't obtained the failure mode characterized by the detachment of the TRM from the substrate or the detachment at the fiber matrix interface while applying shear bond test. However, in case of the occurrence of these failure modes the maximum stress obtained through shear bond test could be lower than that obtained through tensile test as we can see in Caggegi & al. 2017 [3]. Finally, we can conclude that the application of tensile and shear bond tests are essential for the design of a TRM system and we cannot rely on the results of one of them neglecting the other one. The application of the qualification procedure proposed in the Italian guideline [186] [191], to the TRM systems tested in this study is shown in Figure 5- 203 for HC-E TRM and in Figure 5- 204 for HC-L TRM. For the HC-E TRM the conventional limit stress obtained is equal to 92 MPa and the conventional limit strain is equal to 0.98 %. For the HC-L TRM, the conventional limit stress obtained is equal to 100 MPa and the conventional limit strain is equal to 1.04 %. For these two TRM systems, the mean value of the ultimate tensile strength obtained by tensile tests ($\sigma_{\max} = 126.8$ MPa for HC-E and 122.9 MPa for HC-L (Table 4- 45 in chapter 4)) is higher than 85% of

the ultimate tensile stress of HC yarns ($0.85 \times 138.9 = 118.1$ MPa). It is also higher than 15% of the conventional limit stress ($\sigma_{\text{limit,conv}} = 92$ MPa for HC-E and 100 MPa for HC-L) which is consistent with the recommendations of the Italian guidelines (Figure 5- 203, Figure 5- 204).

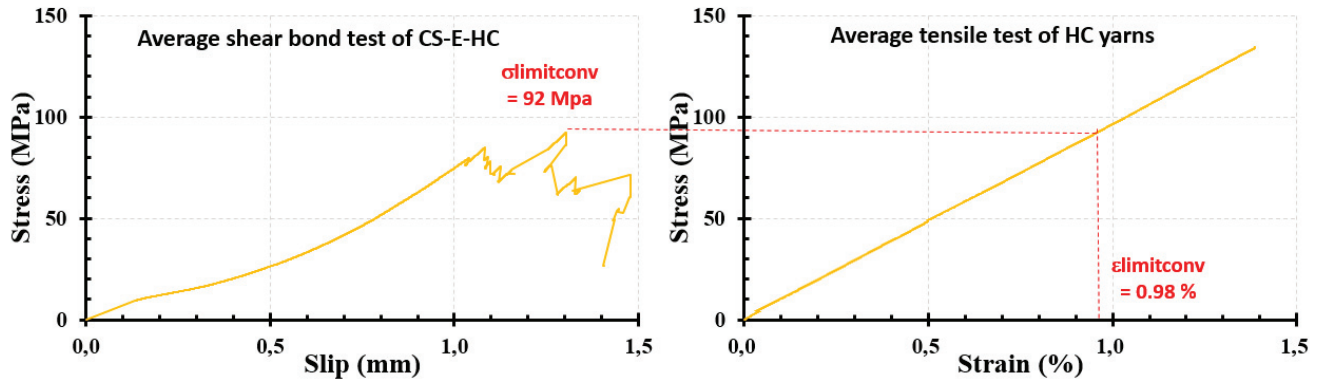


Figure 5- 203 : Application of the procedure suggested in the Italian guidelines [191] for the qualification of the TRM systems to the experimental results of HC-E TRM.

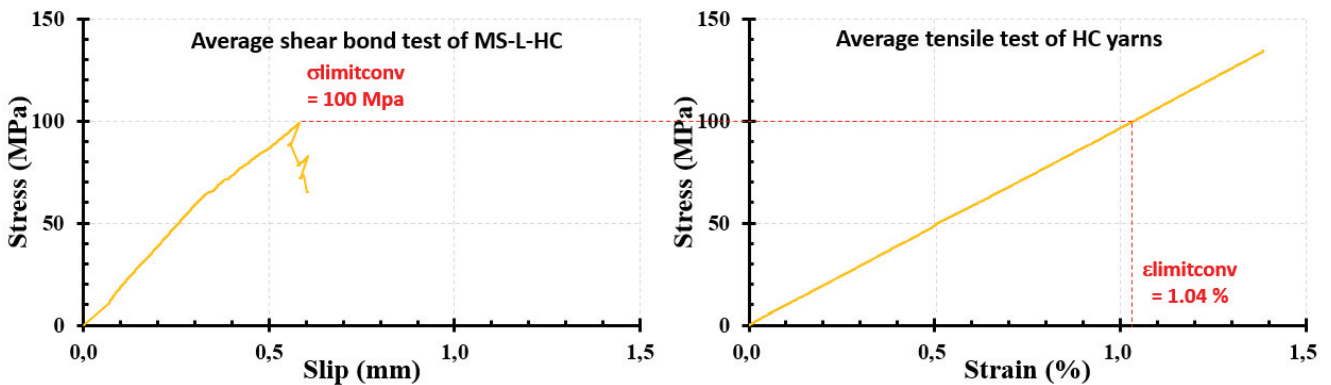


Figure 5- 204 : Application of the procedure suggested in the Italian guidelines [191] for the qualification of the TRM systems to the experimental results of HC-L TRM.

5.4 Conclusions

This chapter aimed at providing an exhaustive mechanical characterization of the bio-resin-coated hemp TRM system under investigation, at the scale of analysis of the substrate. The shear bond performance with concrete and masonry substrates were considered. The concrete substrate were reinforced with a TRM system consisting on HC yarns embedded in ettringitic matrix, while the masonry substrate were reinforced with a TRM system employing HC yarns with natural hydraulic lime matrix. Both composite systems have shown that they could be used for the rehabilitation and the reinforcement of civil engineering structures. The main findings of the experimental analysis are summarized as follows:

- All the tested specimens showed an elastic response of the textile in the free length of the loaded edge ending up in a rupture of the textile in this area. This behavior occurred in both reinforcement configurations, emphasizing that these composite systems are characterized by a good adhesion at the interface between HC textile and both matrices used as well as at the interface between ettringitic matrix and concrete substrate and the interface between natural hydraulic lime matrix and masonry substrate.
- Almost all the specimens tested showed a snap-back behavior in the stress-slip curve, which is probably explained by the displacement of the aluminum plate 'Ω' bonded to the textile where the failure occurred.
- Load drops in the force-displacement curves occurred with a number proportional to the number of yarns composing the textile (four), announcing an inhomogeneous load distribution between the yarns.
- The average maximum stress obtained by the shear bond test was 16 % and 11 % lower than the average maximum stress obtained by the direct tensile for E and L series respectively.
- The bond length of 260 mm resulted thus adequate for HC-TRM composite to attain the yarns rupture, avoiding premature failure due to debonding or sliding. Further investigations considering shorter bond lengths should be carried out to assess the minimum bond length value that permits to fully establish the matrix-fiber stress transfer mechanism and to reach the yarns tensile failure. However, reasonably, the detachment of the mortar from the substrate is not expected, as the yarns slippage occurs.
- By applying the procedure suggested in the Italian guideline to characterize a TRM system, we found that HC-E TRM have a conventional limit stress of 92 MPa, and HC-L TRM have a conventional limit stress of 100 MPa. The test is successfully passed for these two types of TRM. Finally, the use of a TRM made with bio-resin-coated hemp textile embedded in ettringitic matrix for the reinforcement of concrete elements or in natural hydraulic lime matrix for the reinforcement of brick masonry elements have shown to be efficient based on their short-term mechanical behavior. Additional studies are required to investigate their long-term mechanical behavior.

Conclusions and perspectives

This thesis was intended to assess the potential of the use of natural fibers textile especially hemp and flax fibers, as a reinforcement in the TRM composites through durability tests. In order to achieve a deep understanding of the long term mechanical behavior of plant fiber based TRMs, the study started by a comprehensive characterization that consists of assessing the durability of hemp (H), flax (F) and bio-resin-coated hemp (HC) yarns through tensile tests on these yarns after their subjection to different aging protocols, trying to reproduce the environments of both ettringitic (E) and natural hydraulic lime (L) mortar. Different temperatures have been considered based on an Arrhenius approach used to correlate the accelerated exposure periods with the service life. Then, it moved to the investigation at the scale of composite where TRM systems made from hemp and bio-resin-coated hemp textile have been studied at different curing ages through tensile tests. The results of the tensile tests on the accelerated aged yarns have been compared with the results of tensile tests on TRMs made from these yarns. Afterwards, concrete and masonry elements strengthened with TRM systems made from bio-resin-coated hemp textile embedded in ettringitic (E) and natural hydraulic lime (L) mortar respectively have been investigated through shear bond tests to assess the bond behavior at the textile-matrix interface as well as at the matrix-substrate interface. The main outcomes of the research study are discussed hereafter.

As preliminary investigation, the physical and mechanical properties, as well as some durability aspects, of the hemp and flax yarns used in the study were studied. The results demonstrated that the hemp yarns with promising mechanical properties as the yarns employed in this research could be utilized as internal reinforcement for TRM systems. The flax yarns used in the study have shown a tensile strength equivalent to 23 % of the tensile strength of hemp yarns.

In terms of durability, hemp yarns showed a good performance in the short term, exhibiting a retting or a mercerization process, but significant decreases of tensile properties after accelerated aging exposures while flax yarns have shown to be more resistant to alkaline solutions than hemp yarns. Furthermore, the use of Arrhenius approach, which was intended to accelerate the aging process when the temperature increases, have done its job when the pH of the aging solutions was 10.5, but it demonstrated the opposite when aging solutions with a pH of 12.5 were used. Thus, further investigations are needed in order to find an approach that correlates well the accelerated aging protocols of hemp yarns with the service life of TRM made from these yarns by taking into consideration not only the temperature but also the pH of the aging solution.

In addition, hemp TRM employing both kinds of matrix E and L showed a tensile behavior different from the typical three stages tensile behavior of conventional high strength fiber based TRMs found in the literature. It is mainly due to the strengthening ratio of the TRM and to the relation between the mortar and textile grid properties. The stress-strain curves started by an elastic behavior until the rupture of the matrix, which was achieved in all cases before reaching the flexural strength of the matrix. Then a sudden drop in the curve occurred until the stress reached zero, this evidence may be due to the low initial stiffness of hemp yarns when subjected to tensile

loading conditions. Then the curve started to increase non-linearly until it reaches a second peak and it started to decrease. In all cases, the tensile strength of the yarns was not reached and the tensile rupture of the textile was not detected because of the slippage of these latter in both matrices E and L. All the above-mentioned observations highlighted the need of a special treatment or coating for hemp yarns before using them as a reinforcement in TRM systems in order to enhance their durability in alkaline solutions as well as the textile-matrix bond.

In light of the first outcomes presented above, a coating of hemp yarns with a bio-resin has been proposed. At first, in the short term, before being subjected to accelerated aging protocols, HC yarns exhibited a linear elastic tensile behavior up to the rupture. The bio-resin coating played the role of a binder for the filaments, which constituted each yarn, and resulted in a stiffer and more rigid yarn with a reduced tensile strength and tensile elongation.

In terms of durability, the bio-resin-coated hemp yarns (HC) have shown significant improvements when compared with the uncoated hemp yarns. It allowed the hemp yarn to conserve residual tensile properties very close to their initial ones even after 90 days of accelerated exposure periods in almost all the aging solutions except when the pH was 12.5 and the temperature was 60°C. This solution was the most severe environment for HC yarns, in which they lost about 43 % of their tensile strength after 90 days of exposure (Figure conclusion- 1, Figure conclusion- 2). This degradation in the tensile properties of coated hemp yarns is probably due to the plasticization of the resin network by the water molecules, which leads to the decrease in the tensile properties of the resin and making it unable to distribute and share properly the external forces to the fibers.

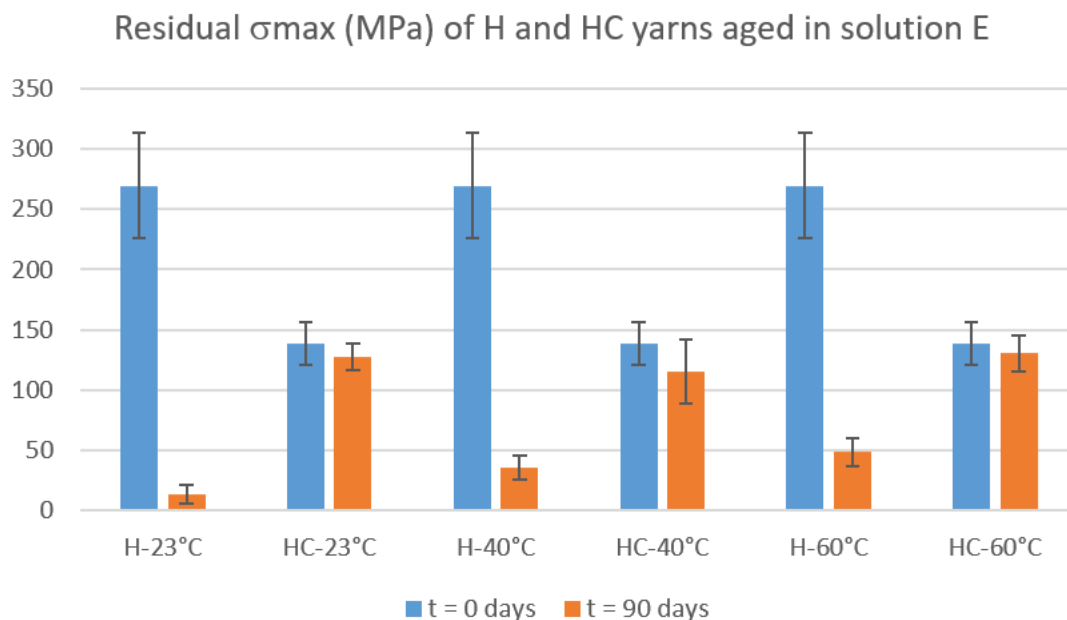


Figure conclusion- 1 : Residual average tensile strength of hemp and bio-resin coated hemp yarns after 90 days of immersion in solution E (pH 10.5).

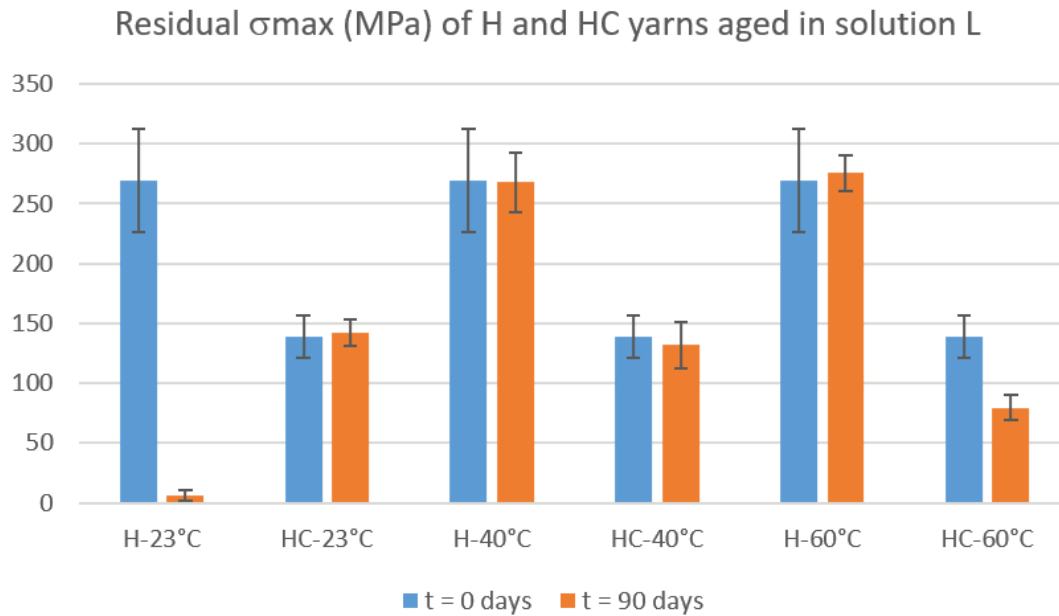


Figure conclusion- 2 : Residual average tensile strength of hemp and bio-resin coated hemp yarns after 90 days of immersion in solution L (pH 12.5).

In light of the encouraging outcomes on the yarn scale of analysis, the study moved to the investigation of tensile behavior of TRMs made from manually weaved and manually coated hemp textile embedded in either ettringitic (E) or natural hydraulic lime (L) matrix. At first, in the short term (after 28 days of curing), the stress-strain curves of HC-E TRM series showed a first linear elastic branch up to the rupture of the matrix. Then multiple drops of the stress occurred announcing the formation of multiple cracks in the ettringitic matrix. Finally, the test ended with the rupture of the textile when the stress exceeded 91% of the tensile strength of HC yarns but without a clear observation of the third stage, which appears in the tensile behavior of conventional high strength fiber, based TRMs. HC-L TRM series exhibited different behavior from HC-E TRM series. It consisted of three stages: the first linear elastic stage which was not clearly observed, and then a second stage with multiple cracking which was clearly observed. Finally, a clear third stage was observed but it wasn't linear, as it is the case in the tensile behavior of conventional high strength fiber, based TRMs, it contained small drops in the stress announcing the formation of micro-cracks in this stage. Thus, the contribution of the natural hydraulic lime matrix in the third stage should not be neglected in these types of composites. Finally, the tests ended with the tensile rupture of the textile when the stress exceeded 88 % of the tensile strength of HC yarns.

When the behavior of HC TRMs was compared to that of H TRM, it was found that the bio-resin coating adopted in this study contributed to significant beneficial improvements in terms of textile-matrix bond for both kinds of matrix adopted: E and L. This was explained by the ability of the resin to create a rough layer on the surface of hemp yarn and to decrease the water absorption capacity of these yarns, which in turn decreases the capacity of these yarns to swell during the

hydration of the mortar and retract after complete drying of the composite. This results in decreasing the porosity at the textile-matrix interface and preventing the elongation of the fibers within the matrix, thus protecting the fiber-matrix bond and preventing the slippage of the yarn within the matrix.

In terms of durability, not all the specimens of HC-E TRM series tested at 2 and 3 months of curing, exhibited the same behavior which was observed after 28 days of curing. However, about half of these specimens exhibited only one crack in the crack propagation stage and then the failure occurred with the rupture of the textile at tensile stresses very close to the tensile strength of HC yarns. This brittle failure of the TRM based on ettringitic matrix was explained by the fact that this matrix presents good bonding to HC yarns up to 28 days of curing, afterwards this bonding becomes stronger because of the ettringitic reactions that did not stop, which made the ettringitic matrix denser. Thus, for composite with ettringitic matrix, the test after 28 curing days could not be a reference as it is usually the case for cementitious mortars. According to HC-L TRM series tested at 2 and 3 months of curing, all the specimens exhibited the same behavior of the specimens tested at day 28 of curing with tensile strength equivalent to 85 % and 75 % of that of HC yarns, respectively.

Unlike what it is the case for H-E and H-L TRMs, the Arrhenius approach used to predict the service life of HC yarns in alkaline environments, from the accelerated exposure periods has been found to be effective to predict 3 months of mechanical properties of these yarns embedded in ettringitic or natural hydraulic lime mortar. Further tests are needed to analyse the behavior of TRM for longer period of aging. If the Arrhenius approach could be validated for this kind of composites, a prediction of long-term behavior of these yarns in both mortars could be carried out. By making this prediction simulation taking into account the results of the thesis, it was found that HC yarns could resist up to 60 years of service life in the ettringitic mortar without any losses in their tensile properties. However, in natural hydraulic lime mortar, a 20 % loss in their tensile properties was expected after 38 years and 43 % after 60 years of service life. Further investigations on HC TRM series cured and stored for periods longer than 3 months, are needed in order to consolidate the use of this approach in case of the prediction of the durability of HC TRM as well as to consolidate the efficiency of the adopted aging protocols.

Based on the satisfactory experimental evidences deriving from the characterization at the composite scale of analysis, the HC-E TRM and the HC-L TRM systems were applied to concrete and masonry elements, respectively. Their bond behaviors were assessed through shear bond test. All the specimens exhibited a promising behavior with a fiber exploitation rate of about 77 % and 79 % for HC-E and HC-L TRMs, respectively. The experimental evidences showed a rupture of the textile out of the bonded area. This behavior emphasized that the system is characterized by a good adhesion at the fiber-matrix interface as well as at both interfaces ettringite-concrete and lime-masonry.

The results of this study, contribute to advanced knowledge about the use of plant fiber textiles as reinforcement in mortar-based composites, and paves the way for further research activities aimed at optimizing the sustainable strengthening system object of study. Many perspectives of the study may be defined:

- Further mechanical investigations aimed at the definition of optimized improvement techniques, such as the use of another textile treatment or coating, the use of optimized fiber reinforcement amounts and textile arrangements or the use of different matrix compositions;
- The immersion of the vegetal yarns in distilled water (retting process) or in alkaline solutions (mercerization process) for a given short period leads to an increase in their tensile properties. But this do not mean that these processes make the vegetal fibers useful as a reinforcement in the textile reinforced mortar systems without any treatment or coating because they cannot ensure a long term service life of the fibers in the alkaline environment of the matrix of a TRM system, thus this cannot ensure a long term reinforcement for the structural element. However, further investigations are needed on hemp yarns subjected to a retting or a mercerization process for a short period in order to enhance their tensile properties and then directly coated after drying in the purpose of protecting them and allowing them to maintain those enhanced properties in the long term.
- More durability studies on HC TRM systems are needed, for instance the natural aging in the outside conditions as well as accelerated aging through different aging protocols by cycles of freeze-thaw and heat-rain, etc. Thus, finding new approaches optimizing the long-term service life prediction of the durability of plant fibers when used in alkaline environments is crucial.
- More investigations concerning the mechanical behavior of high scale structural elements reinforced by the more durable solution defined in this thesis (HC TRM) are needed.
- A life cycle assessment (LCA) of HC-TRM systems is also crucial.

Applying these above-mentioned directives in future research studies, may end up in optimizing the plant based TRM composites, and enriching the scientific literature about them, hence hopefully creating codes and standards concerning their applications in actual civil engineering rehabilitation.

Scientific publications

Journal publication:

A published article in the international journal EJECE

- **M. Zaydan**, C. Caggegi, M. Michel, & L. Curtil, *Experimental analysis on tensile and bond properties of basalt-ettringite TRM for strengthening masonry structures*, European Journal of Environmental and Civil Engineering, 2021. <https://doi.org/10.1080/19648189.2021.1941266>
- Four journal publications are in preparation

Conference Publications:

- **M. Zaydan**, M. Michel, C. Caggegi, & L. Curtil, (2020). *Comportement mécanique et durabilité des fils de lin exposés à l'environnement alcalin d'une matrice ettringitique*. *Academic Journal of Civil Engineering*, 38(1), 237-240, Special issue - RUGC 2020 Marrakech. <https://doi.org/10.26168/ajce.38.1.58>
- **M. Zaydan**, C. Caggegi, M. Michel, & L. Curtil, *Durability of hemp cords exposed to alkaline environment of lime mortar*, Brick and Block masonry, Brick and Block Masonry - From Historical to Sustainable Masonry: Proceedings of the 17th International Brick/Block Masonry Conference (17thIB2MaC 2020), Kraków, Poland (1st ed.). CRC Press. <https://doi.org/10.1201/9781003098508>

References

- [1] S. Casacci, C. Gentilini, A. D. Tommaso, D. V. Oliveira, Shear strengthening of masonry wallettes resorting to structural repointing and FRCM composites, *Construction and Building Materials* 206 (2019) 19-34.
- [2] T. D'antino, C. Carloni, L. H. Sneed, C. Pellegrino, Matrix-fiber bond behavior in PBO FRCM composites: A fracture mechanics approach, *Engineering Fracture Mechanics*, 117 (2014) 94-111.
- [3] C. Caggegi, F. G. Carozzi, S. De Santis, F. Fabbrocino, F. Focacci, Ł. Hojdys, E. Lanoye, L. Zuccarino, Experimental analysis on tensile and bond properties of PBO and aramid fabric reinforced cementitious matrix for strengthening masonry structures, *Composites Part B: Engineering* 127 (2017) 175-195.
- [4] ACI-549.2R-04 Report on Thin Reinforced Cementitious Product 19/05/2004.
- [5] C. G. Papanicolaou, T. C. Triantafillou, K. Karlos, and M. Papathanasiou, Textile-reinforced mortar (TRM) versus FRP as strengthening material of URM walls: in-plane cyclic loading, *Materials and structures* 40 (2017) 1081–1097.
- [6] F. G. Carozzi, A. Bellini, T. D'Antino, G. De Felice, F. Focacci, Ł. Hojdys, L. Laghi, E. Lanoye, F. Micelli, M. Panizza, C. Poggi, Experimental investigation of tensile and bond properties of Carbon-FRCM composites for strengthening masonry elements, *Composites Part B* 128 (2017) 100-119.
- [7] M. Leone, M. A. Aiello, A. Balsamo, F. G. Carozzi, F. Ceroni, M. Corradie, M. Gams, E. Garbin, N. Gattesco, P. Krajewski, C. Mazzotti, D. Oliveira, C. Papanicolaou, G. Ranocchiali, F. Roscini, D. Saenger, Glass fabric reinforced cementitious matrix: Tensile properties and bond performance on masonry substrate, *Composites Part B Engineering* 127 (2017) 196–214.
- [8] G. P. Lignola, C. Caggegi, F. Ceroni, S. De Santis, P. Krajewski, P. B. Lourenço, M. Morganti, C. Papanicolaou, C. Pellegrino, A. Prota, L. Zuccarino, Performance assessment of basalt FRCM for retrofit applications on masonry, *Composites Part B: Engineering* 128 (2017) 1-18.
- [9] S. De Santis, F. Ceroni, G. De Felice, M. Fagone, B. Ghiassi, A. Kwiecień, G. P. Lignola, M. Morganti, M. Santandrea, M. R. Valluzzi, A. Viskovic, Round Robin Test on tensile and bond behaviour of Steel Reinforced Grout systems, *Composites Part B: Engineering* 127 (2017) 100-120.
- [10] M. Ekenel, F. De Caso y Basalo, A. Nanni, Acceptance Criteria for Concrete and Masonry Strengthening Using Fabric-Reinforced Cementitious Matrix (FRCM) and Steel Reinforced Grout (SRG) Composites, *ACI*, 324 (2018) 4.1-4.6.

- [11] A. D'Ambrisi, L. Feo, and F. Focacci, Bond-slip relations for PBO-FRCM materials externally bonded to concrete, *Composites Part B: Engineering* 43 (2012) 2938–2949.
- [12] T. Björn, B. Thomas, Mineral-Based Bonding of Carbon FRP to Strengthen Concrete Structures, *Journal of Composites for Construction* 11 (2007) 120-128.
- [13] A. Prota, G. Marcari, G. Fabbrocino, G. Manfredi, C. Aldea, Experimental In-Plane Behavior of Tuff Masonry Strengthened with Cementitious Matrix–Grid Composites, *Journal of Composites for Construction* 10, No 3 (2006).
- [14] F. Parisi, G. P. Lignola, N. Augenti, A. Prota, G. Manfredi, Nonlinear Behavior of a Masonry Subassemblage Before and After Strengthening with Inorganic Matrix-Grid Composites, *Journal of Composites for Construction* 15 (2011) 821-832.
- [15] H.C. Wu, P. Sun, Fiber Reinforced Cement Based Composite Sheets for Structural Retrofit (2005).
- [16] O. Faruk, A.K. Bledzki, H.P. Fink, M. Sain, Progress report on natural fiber reinforced composites, *Macromolecular Materials and Engineering* 299 (1) (2014) 9-26.
- [17] W. Brameshuber, Report 36: Textile Reinforced Concrete - State-of-the-Art Report of RILEM TC 201-TRC. RILEM Publications, 2006.
- [18] H. Ku, H. Wang, N. Pattarachaiyakoop, M. Trada, A review on the tensile properties of natural fiber reinforced polymer composites, *Composites Part B Engineering* 42(4) (2011) 856-873.
- [19] S. Kalia, B.S. Kaith, I. Kaur, Pretreatments of natural fibers and their application as reinforcing material in polymer composites – a review, *Polymer Engineering and Science* 49 (7) (2009) 1253-1272.
- [20] R. Codispoti, D. V. Oliveira, R. S. Olivito, P. B. Lourenço, R. Figueiro, Mechanical performance of natural fiber-reinforced composites for the strengthening of masonry, *Composites part B: Engineering* 77 (2015) 74-83.
- [21] M. Ardanuy, J. Claramunt, R.D. Toledo Filho, Cellulosic fiber reinforced cement based composites: A review of recent research, *Construction and Building Materials* 79 (2015) 115–128.
- [22] S. Chand, Review carbon fibers for composites, *Journal of Materials Science* 35 (2000) 1303-1313.
- [23] P. Morgan, *Carbon fibers and their composites*, Boca Raton, CRC Press (2005) DOI: <https://doi.org/10.1201/9781420028744>.
- [24] “<https://www.sglcarbon.com/en/carbon-fibers-and-cfrp/>.”

- [25] R. Contamine. Contribution à l'étude du comportement mécanique de composites textile-mortier: application à la réparation et/ou renforcement de poutres en béton armé vis-à-vis de l'effort tranchant. PhD thesis, Université Claude Bernard Lyon 1, 2011.
- [26] O. Homoro. Influence de la pré-imprégnation sur le comportement mécanique des composites verre-matrice ettringitique: Etude expérimentale et numérique. PhD thesis, Université Claude Bernard Lyon 1, 2019.
- [27] <https://docplayer.net/21505588-Carbon-fiber-composites-low-cost-materials-manufacturing-options.html> (accessed on 29/10/2018).
- [28] A. Le Duigou, P. Davies, C. Baley, Environmental impact analysis of the production of flax fibres to be used as composite material reinforcement. *Journal of Biobased Materials and Bioenergy* 5 (1) (2011) 153-165.
- [29] S. Das, Life cycle assessment of carbon fiber-reinforced polymer composites, *The International Journal of Life Cycle Assessment* 16 (2011) 268-282.
- [30] Energy and environmental profile of the U.S. glass industry, April 2002 <https://www.nrel.gov/docs/fy02osti/32135.pdf> (accessed on 14/01/2019).
- [31] <https://worstroom.com/types-of-fiberglass/> (accessed on 14/04/2022).
- [32] <https://www.super-silicon.com/products/ar-glass-fiber/> (accessed on 14/04/2022).
- [33] B. M. Scalet, M. Garcia Munoz, A. Q. Sissa, W. Roudier, L. Delgado Sancho, Best available techniques (BAT) reference document for the manufacture of glass (2013) http://eippcb.jrc.ec.europa.eu/reference/BREF/GLS_Adopted_03_2012.pdf (accessed on 14/01/2019).
- [34] Q. Dai, J. Kelly, J. Sullivan and A. Elgowainy, Life-Cycle Analysis Update of Glass and Glass Fiber for the GREET Model, September 2015, <https://greet.es.anl.gov/publication-glass-fiber-update> (accessed on 14/01/2019).
- [35] Technical paper AGY, High strength glass fibers, <http://pdf.directindustry.com/pdf/agy/high-strength-glass-fibers/50640-395471.html> (accessed on 14/01/2019).
- [36] M. Zhang & J. P. Matinlinna, E-Glass Fiber Reinforced Composites in Dental Applications, *Silicon* 4 (2012) 73–78. DOI 10.1007/s12633-011-9075-x.
- [37] A. Bourmaud, J. Beaugrand, D. U. Shah, V. Placet, C. Baley, Towards the design of high-performance plant fibre composites, *Progress in Materials Science* 97 (2018) 347-408.

- [38] <https://utekcomposites.en.made-in-china.com/product/eSzEFTMhbHcn/China-120GSM-Ar-Glassfiber-Chopped-Strand-Mat-Fiberglass.html> (accessed on 14/04/2022).
- [39] N. de Beus, M. Barth, M. B. Carus, Carbon footprint and sustainability of different natural fibres for biocomposites and insulation material, *Comprehensively revised second edition*, Hürth (Germany), January 2019.
- [40] Life Cycle Assessment (LCA) of Basalt Fibers versus Glass Fibers. <https://basaltfiberworld.wordpress.com/scientifical-research/life-cycle-assessment-lca-of-basalt-fibers-versus-glass-fibers/> (accessed on 25/10/2018).
- [41] K. Singha, A short review on basalt fiber, *International Journal of textile Science*, 1 (4) (2012) 19-28.
- [42] T. Deak and T. Czigan, Chemical composition and mechanical properties of basalt and glass fibers: A comparison, *Textile research journal* 79 (7) (2009) 645-651 DOI: 10.1177/0040517508095597.
- [43] K. Azrague, M. R. Inman, L. I. Alnæs, R. D. Schlanbusch, B. Jóhannesson, T. I. Sigfusson, E. R. Thorhallsson, H. Franzson, A. B. Arnason, S. Vares, Life Cycle Assessment as a tool for resource optimisation of continuous basalt fibre production in Iceland, *ECI Symposium Series*, (2016). https://dc.engconfintl.org/lca_waste/10.
- [44] M. Inman, E. R. Thorhallsson, K. Azrague, A mechanical and environmental assessment and comparison of basalt fibre reinforced polymer (BFRP) rebar and steel rebar in concrete beams, *Energy Procedia* 111 (2017) 31-40.
- [45] B. Wang, Glass Fiber and Basalt Fiber Industries, <https://www.nextbigfuture.com/2010/08/glass-fiber-and-basalt-fiber-industries.html> (accessed on 29/10/2018).
- [46] <https://www.sandatlas.org/basalt/> (accessed on 10/12/2018).
- [47] <http://basalt.today/2017/07/11818/> (accessed on 10/12/2018).
- [48] V. V. Gur'ev, E. I. Neproshin, G. E. Mostovoi, The Effect of Basalt Fiber Production Technology on Mechanical Properties of Fiber, *Glass Ceramics* 58 (2001) 62–65.
- [49] P. De Fazio, Basalt fibra: from earth an ancient material for innovative and modern application, <https://www.enea.it/it/seguici/pubblicazioni/pdf-eai/maggio-giugno-2011/sr-basaltfibra.pdf> (accessed on 22/10/2018).
- [50] V. Fiore, T. Scalici, G. Di Bella, A review on basalt fibre and its composites, *Composites Part B: Engineering* 74 (2015) 74-94.

- [51] E. Quagliarini, F. Monni, S. Lenci, F. Bondioli, Tensile characterization of basalt fibre rods and ropes: a first contribution, *Construction and Building Materials* 34 (2012) 372-380.
- [52] F. M. Kogan, O. V. Nikitina, Solubility of chrysotile asbestos and basalt fibres in relation to their fibrogenic and carcinogenic action. *Environmental Health Perspective* 102 (1994) 205-206.
- [53] T. Czigány, Basalt fiber reinforced hybrid polymer composites, *Materials Science Forum* 473-474 (2005) 59-66.
- [54] J. Sim, C. Park, and D. Y. Moon, Characteristics of basalt fiber as a strengthening material for concrete structures, *Composites Part B: Engineering* 36 (6) (2005) 504–512.
- [55] V. A. Rybin, A. V. Utkin, N. I. Baklanova, Alkali resistance, microstructural and mechanical performance of zirconia-coated basalt fibres. *Cement and Concrete Research* 53 (2013) 1-8.
- [56] A.V. Kiruthika, A review on physico-mechanical properties of bast fibre reinforced polymer composites, *Journal of Building Engineering* 9 (2017) 91–99.
- [57] <https://www.textileschool.com/400/natural-cellulosic-seed-fibres/> (accessed on 27/05/2020).
- [58] <https://www.britannica.com/science/leaf-fiber> (accessed on 27/05/2020).
- [59] F. Micelli, W. V. Mera Ortiz, A. La Tegola, Mechanical properties and durability of natural fiber reinforced mortar, Technical report 2001.
- [60] Food and Agriculture Organisation of the United Nations (FAO). Future fibres. *Futur Fibres*; 2015. <http://www.fao.org/economic/futurefibres/prices/en/> (accessed on 10/10/2018).
- [61] FAO Trade and Market Division. Unlocking the commercial potential of natural fibers; 2012.
- [62] SANECO. Rapport de récolte final; 2014.
- [63] <https://www.hempbassadors.ca/fr/agriculture/> (accessed on 20/05/2022).
- [64] Record cultivation of industrial hemp in Europe 2016, <https://renewable-carbon.eu/news/record-cultivation-of-industrial-hemp-in-europe-in-2016/> (accessed on 20/05/2022).
- [65] C. Baley, F. Busnel, Y. Grohens, O. Sire, Influence of chemical treatments on surface properties and adhesion of flax fibre-polyester resin, 2006, *Composites Part A: Applied Science and Manufacturing* 37 (10) (2006) 1626-1637.

- [66] J. Wei, C. Meyer, Degradation mechanisms of natural fiber in the matrix of cement composites, *Cement and Concrete Research* 73 (2015) 1-16.
- [67] S.G. Bergstrom, H. –E. Gram, Durability of alkali-sensitive fibres in concrete, *International Journal of Cement Composites and Lightweight concrete* 6 (1984) 75-80.
- [68] A. K. Bledzki, A. Jaszkiwicz, Mechanical performance of biocomposites based on PLA and PHBV reinforced with natural fibres – a comparative study to pp, *Composites Science and Technology* 70 (12) (2010) 1687–1696.
- [69] R. Kozłowski, Władysław-Przybylak, A. M Kicińska-Jakubowska, State of art in the research on natural fibres and their properties used in composites. In: Bledzki AK, Sperber VE, editors. *Proc. 7th Glob. WPC Nat. Fibre Compos.*; 2008.
- [70] R.D. Toledo Filho, K. Scrivener, G.L. England, K. Ghavami, Durability of alkali-sensitive sisal and coconut fibres in cement mortar composites, *Cement and Concrete Composites* 22 (2000) 127-143.
- [71] L.Y. Mwaikambo, Review of history, properties, and application of plant fibres, *African Journal of Science and Technology* 7 (2006) 120–133.
- [72] M. Paster, J. Pellegrino, T. Carole, *Industrial Bioproducts: Today and Tomorrow*, Report prepared for the US Department of Energy, Washington, 2003.
- [73] WTY. Tze, S. Wang, TG. Rials, GM. Pharr, SS. Kelley, Nanoindentation of wood cell walls: Continuous stiffness and hardness measurements. *Composites Part A: Applied Science and Manufacturing* 38 (3) 2007 945–953.
- [74] G. Raj. *Interfacial interactions in Flax fibre / PLA biocomposite : from model surfaces to real fibres* PhD thesis. Univ South Britany; 2010.
- [75] H. H. Wang, J. G. Drummond, S. M. Reath, K. Hunt , P. A. Watson, An improved fibril angle measurement method for wood fibres, *Wood Science and Technology* 34 (2001) 493–503.
- [76] <http://www.terresinovia.fr/chanvre/cultiver-du-chanvre/le-chanvre-et-ses-atouts/connaitre-le-chanvre/print.pdf?print=1> (accessed on 19/10/2018).
- [77] <https://www.dressingresponsable.com/les-fibres-textiles-le-chanvre/> (accessed on 19/10/2018).
- [78] <https://wsau.com/news/articles/2018/apr/15/state-still-taking-industrial-hemp-applications/> (accessed on 10/12/2018).
- [79] <http://rovingcrafters.com/2015/07/29/hemp-the-red-headed-stepchild-of-the-fiber-world/> (accessed on 10/12/2018).

- [80] D.E. Akin , G.R. Gamble, W.H. Morrison Iii, L.L. Rigsby, R.B. Dodd, Chemical and structural analysis of fibre and core tissues from flax, *Journal of the Science of Food and Agriculture* 72 (1996) 155-165.
- [81] <https://sensiseeds.com/fr/blog/comment-les-textiles-base-de-chanvre-sont-ils-fabriques/> (accessed on 19/10/2018).
- [82] <http://www.snv.jussieu.fr/bmedia/textiles/06-lin-historique.html> (accessed on 19/10/2018).
- [83] European Linen and Hemp <http://www.mastersoflinen.com/fre/breves> (accessed on 19/10/2018).
- [84] C. King, Optimal seeding practices for flax, April 28, 2017. <https://www.topcropmanager.com/seeding-planting/optimal-seeding-practices-for-flax-20066> (accessed on 10/12/2018).
- [85] Flax fiber royalty-free images. <https://www.shutterstock.com/search/flax+fiber> (accessed on 10/12/2018).
- [86] <http://www.saneco.com/en/flax/> (accessed on 19/10/2018).
- [87] <http://www.fao.org/economic/futurefibres/fibres/jute/en/> (accessed on 10/12/2018).
- [88] Md. Mahbubul Islam and Md. Mujibur Rahman, Advances in Jute and allied fibres post-harvest processing technologies in Bangladesh: Adoption constraints, prospect and future thrust, *Research Web Pub* 12 (2013) 20-30.
- [89] <http://www.jute.com/web/guest/green-jute/agriculture-raw-jute> (accessed on 10/12/2018).
- [90] <https://www.gettyimages.fr/vid%C3%A9os/jute-plant?sort=mostpopular&offlinecontent=include&phrase=jute%20plant> (accessed on 10/12/2018).
- [91] <http://www.wildfibres.co.uk/html/jute.html> (accessed on 10/12/2018).
- [92] “Directorate General of Commercial Intelligence and Statistics (DGCI&S), Kolkata, https://nfsm.gov.in/BriefNote/BN_Jute.pdf.”
- [93] <http://www.fao.org/economic/futurefibres/fibres/sisal/en/> (accessed on 07/12/2018).
- [94] <http://www.londonsisalassociation.org/what-is-sisal.php#> (accessed on 07/12/2018).
- [95] [https://keys.lucidcentral.org/keys/v3/eafrinet/weeds/key/weeds/Media/Html/Agave_sisala_na_\(Sisal\).htm](https://keys.lucidcentral.org/keys/v3/eafrinet/weeds/key/weeds/Media/Html/Agave_sisala_na_(Sisal).htm) (accessed on 10/12/2018).

- [96] https://www.alibaba.com/product-detail/Sisal-fibre_142281629.html (accessed on 10/12/2018).
- [97] Sisal production guideline, <https://www.daff.gov.za/Daffweb3/Portals/0/Brochures%20and%20Production%20guidelines/Sisal%20Production%20Guideline.pdf>.
- [98] <http://www.mastersoflinen.com/fre/lin/4-benefices-lin> (accessed on 19/10/2018).
- [99] <http://www.mastersoflinen.com/fre/lin/3-ecosysteme-lin> (accessed on 19/10/2018).
- [100] L. Mercedes, L. Gil, E. Bernat-Maso, Mechanical performance of vegetal fabric reinforced cementitious matrix (FRCM) composites, *Construction and Building Materials* 175 (2018) 161-173.
- [101] J. Summerscale, N. P. J. Dissanayake, A. S. Virk, W. Hall, A review of bast fibres and their composites. Part 1 – Fibres as reinforcements, *Composites Part A: Applied Science and Manufacturing* 41 (2010) 1329-1335.
- [102] B. T. Truong, Formulation, performances mécaniques, et applications, d'un matériau TRC pour le renforcement et la réparation de structures en béton/ et béton armé: Approches expérimentale et numérique, PHD Thesis, Université de Lyon, 2016.
- [103] Glass fiber differences and properties, <https://www.princelund.com/glass-fiber.html> (accessed on 14 avril 2022).
- [104] SANECO. Prix moyen annuel (FOB) des fibres de lin teillées; 2015.
- [105] DB. Dittenber, HVS. GangaRao, Critical review of recent publications on use of natural composites in infrastructure, *Composite Part A: Applied Science and Manufacturing* 43 (2012) 1419-1429.
- [106] H. Ekstroem, The North American Pulpwood and Biomass Market This Quarter. *North Am Wood Fiber Rev*; 2012.
- [107] Institute N. Price index: hemp and flax technical short fibres; 2012.
- [108] F. Ardente, M. Beccali, M. Cellura, M. Mistretta, Building energy performance: a LCA case study of kenaf-fibres insulation board, *Energy and Buildings* 40 (2008) 1–10.
- [109] WWF. The impact of cotton on fresh water resources and ecosystems. A preliminary synthesis. World Wide Fund Nat. Gland, Swi; 1999.
- [110] A. Lefeuvre, A. Bourmaud, C. Morvan, C. Baley, Tensile properties of elementary fibres of flax and glass: analysis of reproducibility and scattering. *Materials Letters* 130 (2014) 289–291.

- [111] S. González-García, A. Hospido, G. Feijoo, M.T. Moreira, Life cycle assessment of raw materials for non-wood pulp mills: hemp and flax, *Resources, Conservation and Recycling* 54 (2010) 923–930.
- [112] M. George, D. C. Bressler, Comparative evaluation of the environmental impact of chemical methods used to enhance natural fibres for composite applications and glass fibre based composites, *Cleaner Production* 149 (2017) 491-501.
- [113] S.V. Joshia, L.T. Drzalb, A.K. Mohanty, S. Arora, Are natural fibres composites environmentally superior to glass fibre reinforced composites, *Composites Part A: Applied Science and Manufacturing* 35 (2004) 371-376.
- [114] A. Shahzad, Hemp fiber and its composites : A review. *Journal of Composite Materials*, 46 (8) (2011) 973-986.
- [115] F. Bensadoun, B. Vanderfeesten, K. Van Acker, I. Verpoest, AW. Van Vuure, End of life technologies for flax-thermoplastic composites and their effects on the environment. In: Fangueiro R, editor. 2nd international conference on natural fibers. Sao Miguel, Portugal; 2015.
- [116] N. Defoirdt, I. De Windt, J. Van Den Bulcke, J. Van Acker, Biological durability of natural fibre reinforced composites. In: 45th IRG annual meeting: international research group on wood protection (IRG); 2014.
- [117] L. Pil, F. Bensadoun, J. Pariset, I. Verpoest, Why are designers fascinated by flax and hemp fibre composites?, *Composites Part A: Applied Science and Manufacturing* 83 (2016) 193-205.
- [118] C. Scheffler, T. Forster, E. Mader, G. Heinrich, S. Hempel, V. Mechterine, Aging of alkali-resistant glass and basalt fibers in alkaline solutions: Evaluation of the failure stress by Weibull distribution function, *Journal of Non-Crystalline Solids* 355 (2009) 2588-2595.
- [119] M. Afroz, I. Patnaikuni, S. Venkatesan, Chemical durability and performance of modified basalt fiber in concrete medium, *Construction and Building Materials* 154 (2017) 191-203.
- [120] C. Jiang, K. Fan, F. Wu, D. Chen, Experimental study on the mechanical properties and microstructure of chopped basalt fibre reinforced concrete, *Materials and Design* 58 (2014) 187-193.
- [121] J. A. Melo Filho, F. A. Silva, R. D. Toledo Filho, Degradation kinetics and aging mechanisms on sisal fiber cement composite systems, *Cement and Concrete Composites* 40 (2013) 30-39.
- [122] D. W. Haas, B. F. Hrutfiord, K. V. Sarkanen, Kinetic study on the alkaline degradation of cotton hydrocellulose, *Applied Polymer Science* 11 (1967) 587-600.

- [123] L. R. Van loon, M. A. Glaus, Review of the kinetics of alkaline degradation of cellulose in view of its relevance for safety assessment of radioactive waste repositories, *Journal of Environmental Polymer Degradation* 5 (1997) 97-109.
- [124] J. Wei, Degradation behavior and kinetics of sisal fiber in pore solutions of sustainable cementitious composite containing metakaolin, *Polymer Degradation and Stability* 150 (2018) 1-12.
- [125] I. Pavasars, J. Hagberg, H. Boréen, B. Allard, Alkaline degradation of cellulose: mechanisms and kinetics, *Journal of Polymers and the Environment* 11 (2003) 39-47.
- [126] L. Boulos, M. R. Foruzanmehr, A. Tagnit-Hamou, M. Robert, The effect of a zirconium dioxide sol-gel treatment on the durability of flax reinforcements in cementitious composites, *Cement and Concrete Research* 115 (2019) 105-115.
- [127] J. Wei, C. Meyer, Degradation of natural fiber in ternary blended cement composites containing metakaolin and montmorillonite, *Corrosion Science* 120 (2017) 42-60.
- [128] J. Wei, S. Ma, D. G. Thomas, Correlation between hydration of cement and durability of natural fiber-reinforced cement composites, *Corrosion Science* 106 (2016) 1-15.
- [129] R. D. Toledo Filho, K. Ghavami, G. L. England, K. Scrivener, Development of vegetable fibre-mortar composites of improved durability, *Cement and Concrete Composites* 25 (2003) 185-196.
- [130] R. D. Toledo filho, F. A. Silva, E. M. R. Fairbairn, J. A. Melo Filho, Durability of compression molded sisal fiber reinforced mortar laminates, *Construction and Building Materials* 23 (2009) 2409-2420.
- [131] M. Butler, V. Mechterine, S. Hempel, Experimental investigations on the durability of fibre-matrix interfaces in textile-reinforced concrete, *Cement and Concrete Composites* 31 (2009) 221-231.
- [132] S. Chafei, F. Khadraoui, M. Boutouil, M. Gomina, Optimizing the formulation of flax fiber-reinforced cement composites, *Construction and Building Materials* 54 (2014) 659-664.
- [133] J. Claramunt, M. Ardanuy, J. A. Garcia-Hortal, R. D. Toledo Filho, The hornification of vegetable fibers to improve the durability of cement mortar composites, *Cement and Concrete Composites* 33 (2011) 586-595.
- [134] M. E. A. Fidelis, R. D. Toledo Filho, F. A. Silva, V. Mechtcherine, M. Butler, S. Hempel, The effect of accelerated aging on the interface of jute textile reinforced concrete, *Cement and Concrete Composites* 74 (2016) 7-15.

- [135] L. Boulos, M. R. Foruzanmehr, M. Robert, Evolution of the interfacial transition zone and the degradation mechanism of zirconia treated flax fabric reinforced cementitious composites, *Construction and Building Materials* 190 (2018) 120-130.
- [136] S. R. Ferreira, F. A. Silva, P. R. L. Lima, R. D. Toledo Filho, Effect of fiber treatments on the sisal fiber properties and fiber-matrix bond in cement based systems, *Construction and Building Materials* 101 (2015) 730-740.
- [137] A.E.F.S Almeida, G. H. D. Tonoli, S. F. Santos, H. Savastano Jr., Improved durability of vegetable fiber reinforced cement composite subject to accelerated carbonation at early stage, *Cement and Concrete Composites* 42 (2013) 49-58.
- [138] M. Fernandez Bertos, A. Muntean, S. J. R. Simons, C. D. Hills, P. J. Carey, A review of accelerated carbonation technology in the treatment of cement-based materials and sequestration of CO₂, *Hazardous Materials* 112 (2004) 193-205.
- [139] K. Charlet, S. Eve, J. P. Jernot, M. Gomina, J. Breard, Tensile deformation of a flax fiber, *Procedia Engineering* 1 (2009) 233-236.
- [140] M. Ramesh, K. Palanikumar, K. Hemachandra Reddy, Plant fiber based bio-composites: Sustainable and renewable green materials, *Renewable and Sustainable energy Reviews* 79 (2017) 558-584.
- [141] P. Larringa, C. Chastre, H. C. Biscaia, J. T. San-José, Experimental and numerical modeling of basalt tensile reinforced mortar behavior under uniaxial tensile stress, *Materials and design* 55 (2014) 66-74.
- [142] L. Ascione, G. De Felice, S. De Santis, A qualification method for externally bonded fibre reinforced cementitious matrix (FRCM) strengthening systems, *Composites Part B* 78 (2015) 497-506.
- [143] O.A. Cevallos, R. S. Olivito, effects of fabric parameters on the tensile behavior of sustainable cementitious composites, *Composites Part B: Engineering* 69 (2015) 256-266.
- [144] T. D'Antino, C. Papanicolaou, Mechanical characterization of textile reinforced inorganic-matrix composites, *Composites Part B: Engineering* 127 (2017) 78-91.
- [145] G. De Felice, S. De Santis, L. Garmendia, B. Ghiassi, P. Larrinaga, P. B. Lourenço, D. V. Oliveira, F. Paolacci, C. G. Papanicolaou, Mortar-based systems for externally bonded strengthening of masonry, *Materials and Structures* 47 (12) (2014) 2021-2037.
- [146] J. Claramunt, H. Ventura, L. J. Fernández-Carrasco, M. Ardanuy, Tensile and Flexural Properties of Cement Composites Reinforced with Flax Nonwoven Fabrics, *Materials (Basel Switzerland)* 10 (2) (2017) 215.

- [147] F. De Andrade Silva, B. Mobasher, R. D. Toledo Filho, Cracking mechanisms in durable sisal fiber reinforced cement composites, *Cement and Concrete Composites* 31 (2009) 721–730.
- [148] F. Micelli, M. A. Aiello, Residual tensile strength of dry and impregnated reinforcement fibres after exposure to alkaline environments, *Composites Part B: Engineering* 159 (2019) 490-501.
- [149] R. MacVicar, L. M. Matuana, J. J. Balatinez, Aging mechanisms in cellulose fiber reinforced cement composites, *Cement and Concrete Composites* 21 (1999) 189-196.
- [150] F. A. Silva, R. D. Toledo Filho, J. A. Melo Filho, E. M. R. Fairbairn, Physical and mechanical properties of durable sisal fiber-cement composites, *Construction and Building Materials* 24 (2010) 777-785.
- [151] J. Wei, C. Meyer, Degradation rate of natural fiber in cement composites exposed to various accelerated aging environment conditions, *Corrosion Science* 88 (2014) 118-132.
- [152] M. De Munck, M. El Kadi, E. Tsangouri, J. Vervolet, S. Verbruggen, J. Wastiels, T. Tysmans, O. Remy, Influence of environmental loading on the tensile and cracking behaviour of textile reinforced cementitious composites, *Construction and Building Materials* 181 (2018) 325-334.
- [153] L. K. Litherland, D. R. Oakley, B. A. Proctor, The use of accelerated ageing procedures to predict the long term strength of GRC composites, *Cement and Concrete Research* 11 (1981) 455-466.
- [154] J. Ambroise, M. Michel, Publication internationale WO 2015/146799 A1, “Materiau composite notamment pour la reparation de reservoir d’eau”, 22-10-2015.
- [155] Technical sheet Geocalce F Antisismico, https://products.kerakoll.com/yep-repository/kerakoll/media/GeoCalce_F_Antisismico_EN_2020.pdf (accessed on 03/01/2022).
- [156] NF EN 196-1. Methods of testing cement - Part 1: Determination of strength, September 2016.
- [157] NF EN 413-2. Masonry cement - Part 2: Test methods, March 2017.
- [158] NF EN 459-2. Building lime - Part 2: Test methods, August 2012.
- [159] NF EN 196-3. Methods of testing cement - Part 3 : determination of setting times and soundness, September 2017.
- [160] A. viretto and J. Galy, Development of Biobased Epoxy Matrices for the Preparation of Green Composite Materials for Civil Engineering Applications, *Macromolecular Materials Engineering* 303 (5) (2018).

- [161] CCFAT. (2017). Avis Technique 3/14-757*V2. Foreva® TFC (Ou TFC H), 45.
- [162] A. Viretto, & J. Galy. ANR MICRO Matériaux Innovants Composites pour la Réparation d’Ouvrages, rapport d’étude du Laboratoire IMP - INSA de Lyon, 2016.
- [163] M. Salvia, Résultats d’essais «caractérisation des matériaux en vue du choix du système bio », rapport du Laboratoire LTDS, Ecole Centrale de Lyon, 2017.
- [164] R. Chlela. Durabilité d’un système composite biosourcé (matrice epoxy-fibres de lin) pour applications de renforcement structural - approches expérimentale et fiabiliste. PhD thesis, Université PARIS-EST, 2019.
- [165] M.A.B. Promentilla, T. Sugiyama, T. Hitomi, N. Takeda, Quantification of tortuosity in hardened cement pastes using synchrotron-based X-ray computed microtomography, *Cement and Concrete Research* 39 (2009) 548–557.
- [166] L. Schoemana, P. Williamsa, A. Du Plessisb, M. Manleya, X-ray micro-computed tomography (μ CT) for non-destructive characterisation of food microstructure, *Trends in Food Science & Technology* 47 (2016) 10-24.
- [167] R. Moreno-Atanasio, R. A. Williams, X. Jia, Combining X-ray microtomography with computer simulation for analysis of granular and porous materials, *Particuology* 8 (2010) 81-99.
- [168] NF EN ISO 1889. Reinforcement yarns. Determination of linear density. 2009.
- [169] D. Ray, B.K. Sarkar, A.K. Rana, and N.R. Bose, Effect of alkali treated jute fibres on composite properties, *Bulletin of Materials Science* 24 (2001)129–135.
- [170] ISO 2062. Textiles - yarn from packages - determination of single-end breaking force and elongation at break using constant rate of extension (CRE) tester. International Organization for Standardization; 2009.
- [171] EN ISO 10618/2005. Carbon fibre_determination of tensile properties of resin-impregnated yarn. 2005.
- [172] M. Liua, A. Thygesena, J. Summerscales, A. S. Meyer, Targeted pre-treatment of hemp bast fibres for optimal performance in biocomposite materials: A review, *Industrial Crops and Products* 108 (2017) 660-683.
- [173] A.K. Bledzki, J. Gassan, Composites reinforced with cellulose based fibres, *Progress in Polymer Science* 24 (1999) 221–274.
- [174] L. Estevan, F. B. Varona, F. J. Baeza, B. Torres, D. Bru, Textile Reinforced Mortars (TRM) tensile behavior after high temperature exposure, *Construction and Building Materials* 328 (2022) 127116.

- [175] S. Jin and X. Gong, Study of mechanical properties and performance of aging hemp fibers, *World Journal of Engineering* 8(4) (2011) 325-330.
- [176] “C. Menna, D. Asprone, M. Durante, A. Zinno, A. Balsamo, Structural behavior of masonry panels strengthened with an innovative hemp fibre composite grid, *Construction and building materials* 100 (2015) 111-121.”
- [177] ACI 549.4R-13, Guide to Design and Construction of Externally Bonded Fabric-Reinforced Cementitious Matrix (FRCM) Systems for Repair and Strengthening Concrete and Masonry Structures, December 2013.
- [178] Technical sheet Eponal 380, Bostik, https://www.bostik.com/files/live/sites/shared_bostik/files/import-france/globalassets/products/eponal-380_france_fr/downloads/ft-eponal-380.pdf.
- [179] M. Zaydan, C. Caggegi, M. Michel, L. Curtil, Experimental analysis on tensile and bond properties of basalt-ettringite TRM for strengthening masonry structures, *European Journal of Environmental and Civil Engineering*, 2021. DOI: 10.1080/19648189.2021.1941266.
- [180] S. De Santis, F.G. Carozzi, G. de Felice, C. Poggi, Test methods for Textile Reinforced Mortar systems, *Composites Part B: Engineering* 127 (2017) 121–132.
- [181] C. Caggegi et al., “Experimental analysis on tensile and bond properties of PBO and aramid fabric reinforced cementitious matrix for strengthening masonry structures,” *Compos. Part B Eng.*, vol. 127, pp. 175–195, Oct. 2017, doi: 10.1016/j.compositesb.2017.05.048.
- [182] A. Dalalbashi, B. Ghiassi, D. V. Oliveira, Aging of lime-based TRM composites under natural environmental conditions, *Construction and Buildings Materials* 270 (2021) 121853.
- [183] G. de Felice, M. A. Aiello, C. Caggegi, F. Ceroni, S. De Santis, E. Garbin, N. Gattesco, Ł. Hojdys, P. Krajewski, A. Kwiecień, M. Leone, G. P. Lignola, C. Mazzotti, D. Oliveira, C. Papanicolaou, C. Poggi, T. Triantafillou, M. R. Valluzzi, and A. Viskovic, Recommendation of RILEM Technical Committee 250-CSM: Test method for Textile Reinforced Mortar to substrate bond characterization, *Materials and Structures* 51, 95 (2018). <https://doi.org/10.1617/s11527-018-1216-x>.
- [184] G. de Felice, M.A. Aiello, A. Bellini, F. Ceroni, S. De Santis, E. Garbin, M. Leone, G. P. Lignola, M. Malena, C. Mazzotti, M. Panizza, M. R. Valluzzi, Experimental characterization of composite-to-brick masonry shear bond. *Materials and Structures* 49 (2016) 2581–2596.
- [185] L. Ascione, G. de Felice, S. De Santis, A qualification method for externally bonded Fibre Reinforced Cementitious Matrix (FRCM) strengthening systems. *Composites Part B Engineering* 78 (2015) 497-506.

- [186] CNR-DT 215/2018, COMMISSIONE DI STUDIO PER LA PREDISPOSIZIONE E L'ANALISI DI NORME TECNICHE RELATIVE ALLE COSTRUZIONI, Istruzioni per la Progettazione, l'Esecuzione ed il Controllo di Interventi di Consolidamento Statico mediante l'utilizzo di Compositi Fibrorinforzati a Matrice Inorganica.
- [187] A. Bellini, A. Incerti, M. Bovo, C. Mazzotti, Effectiveness of FRCC reinforcement applied to masonry walls subjected to axial force and out-of-plane loads evaluated by experimental and numerical studies. *International Journal of Architectural Heritage* 12 (2018) 1-19.
- [188] S. De Santis, F. Ceroni, G. de Felice, M. Fagone, G. Ghiassi, A. Kwiecien, G. P. Lignola, M. Morganti, M. Santantandrea, M. R. Valluzzi, A. Viskovic, Round robin test on tensile and bond behavior of steel reinforced grout systems. *Composites Part B Engineering* 127 (2017) 100- 120.
- [189] F. Focacci, T. D'Antino, C. Carloni, L. H. Sneed, C. Pellegrino, An indirect method to calibrate the interfacial cohesive material law for FRCC-concrete joints. *Material and Design* 128 (2017) 206-217.
- [190] M. R. Valluzzi, F. da Porto, E. Garbin, M. Panizza, Out-of-plane behavior of infill masonry panels strengthened with composite materials. *Materials and Structures* 47 (12) (2014) 2131-2145.
- [191] L. Ascione, F. G. Carozzi, T. D'Antino, C. Poggi, New Italian Guidelines for design of externally bonded Fabric Reinforced Cementitious Matrix (FRCC) systems for repair and strengthening of masonry and concrete structures. *Procedia Structural Integrity* 11 (2018) 202-209.
- [192] ACI Committee 549, ACI 549.4R-13 – Guide to Design and construction of externally bonded fabric-reinforced cementitious matrix (FRCC) systems for repair and strengthening concrete and masonry structures; 2013.

Appendix A: Mechanical grip system of hemp and flax yarns

This appendix presents more details of the final geometry of the mechanical grip system developed to facilitate fixing the hemp and flax yarns in the testing machine and to avoid the stress concentration, which causes the failure of the yarn at the clamp.

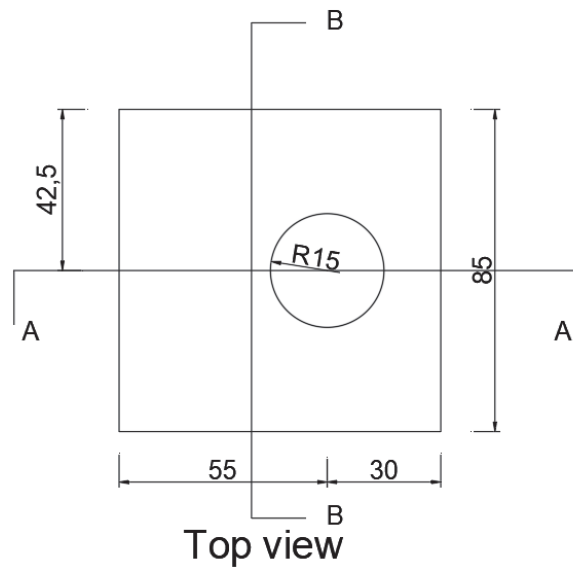


Figure A-1 : Top view of the mechanical grip system (dimensions are in mm).

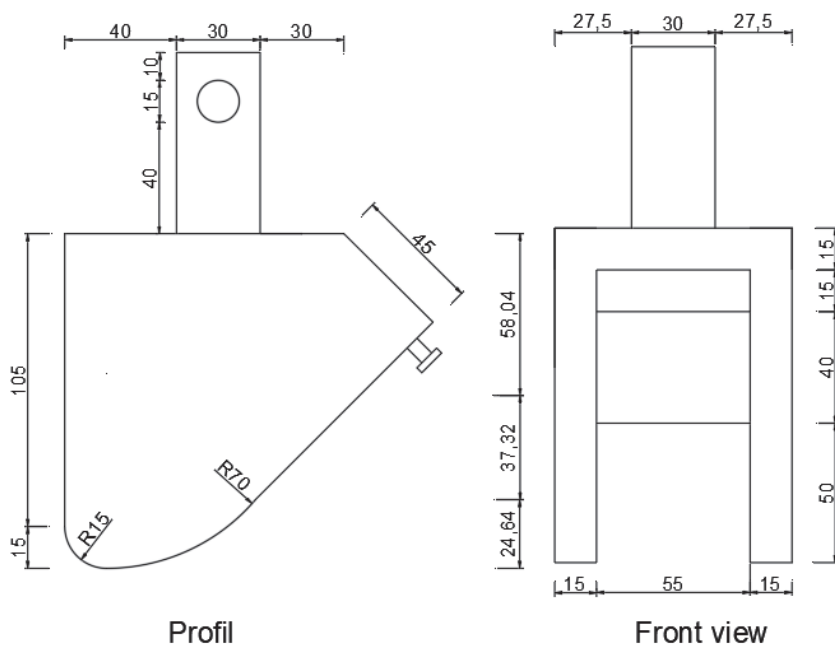


Figure A- 2 : Profile and Front view of the mechanical grip system (dimensions are in mm).

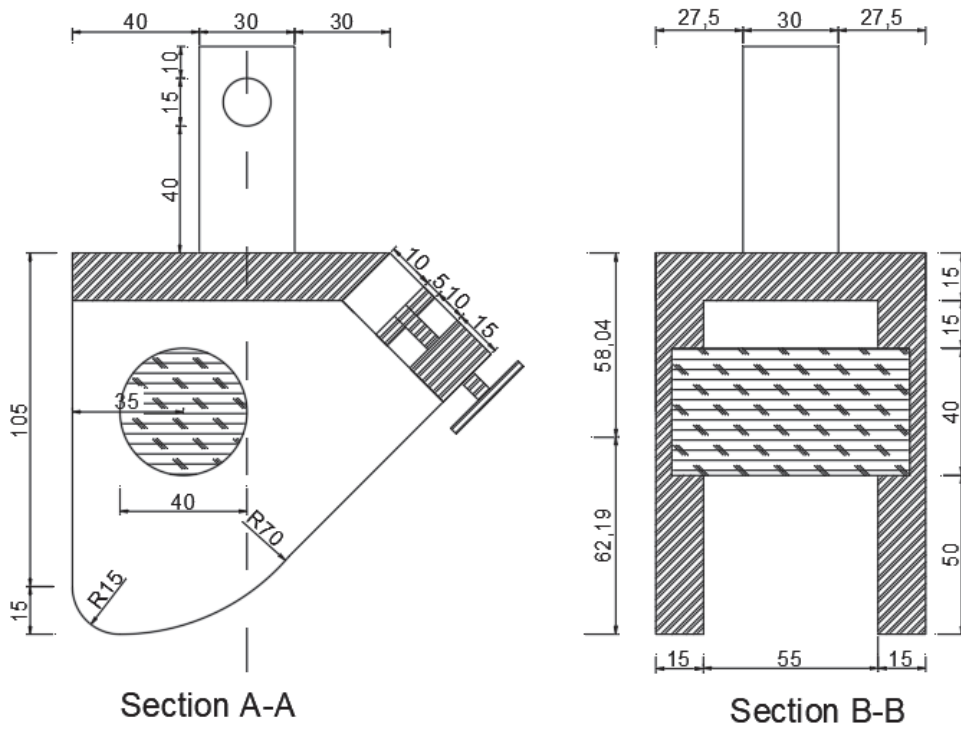


Figure A- 3 : Sections A-A and B-B of the mechanical grip system (dimensions are in mm).

Appendix B: Detailed results of all the tensile test series of hemp yarns (H)

a) In solution R-23

Table B- 1: Tensile properties of Hemp yarns after aging in solution H-R-23 for 7 days.

H-R-23-7d					
Specimen	F_{\max} (N)	σ_{\max} (MPa)	U_{\max} (mm)	ε (%)	E (GPa)
1	298.5	397.5	23.3	9.3	6.8
2	223.9	298.1	19.9	8.0	6.0
3	297.3	395.9	21.9	8.8	7.4
4	244.4	325.4	20.8	8.3	6.1
5	227.8	303.4	22.4	9.0	5.7
6	241.8	322.0	21.5	8.6	5.9
Average	255.6	340.4	21.7	8.7	6.3
st.dev	33.7	44.9	1.2	0.5	0.7
CoV (%)	13.2	13.2	5.5	5.5	10.3

Table B- 2: Tensile properties of Hemp yarns after aging in solution H-R-23 for 14 days.

H-R-23-14d					
Specimen	F_{\max} (N)	σ_{\max} (MPa)	U_{\max} (mm)	ε (%)	E (GPa)
1	303.6	404.3	21.3	8.5	7.4
2	297.0	395.5	22.9	9.1	6.1
3	252.5	336.2	20.3	8.1	6.2
4	254.9	339.5	18.9	7.6	6.5
5	300.3	399.8	20.9	8.4	7.7
6	270.2	359.8	20.8	8.3	6.6
Average	279.7	372.5	20.8	8.3	6.8
st.dev	23.4	31.2	1.3	0.5	0.7
CoV (%)	8.4	8.4	6.2	6.2	9.7

Table B- 3: Tensile properties of Hemp yarns after aging in solution H-R-23 for 28 days.

H-R-23-28d					
Specimen	F_{\max} (N)	σ_{\max} (MPa)	U_{\max} (mm)	ε (%)	E (GPa)
1	252.9	336.7	23.3	9.3	5.9
2	234.3	312.0	21.9	8.8	5.3
3	272.6	362.9	24.4	9.8	6.0
4	203.3	270.8	22.0	8.8	5.6
5	241.7	321.9	22.1	8.8	6.0
6	214.5	285.7	23.6	9.4	5.4
Average	236.6	315.0	22.9	9.1	5.7
St.dev	25.2	33.6	1.1	0.4	0.3
CoV (%)	10.7	10.7	4.6	4.6	5.4

Table B- 4: Tensile properties of Hemp yarns after aging in solution H-R-23 for 42 days.

H-R-23-42d					
Specimen	F_{\max} (N)	σ_{\max} (MPa)	U_{\max} (mm)	ε (%)	E (GPa)
1	217.5	289.6	21.6	8.6	5.6
2	214.6	285.7	23.7	9.5	5.5
3	210.4	280.2	23.7	9.5	5.6
4	256.5	341.5	24.7	9.9	5.9
5	223.6	297.7	25.3	10.1	5.3
6	233.3	310.6	24.8	9.9	5.6
Average	226.0	300.9	24.0	9.6	5.6
St.dev	16.9	22.5	1.3	0.5	0.2
CoV (%)	7.5	7.5	5.6	5.6	3.5

Table B- 5: Tensile properties of Hemp yarns after aging in solution H-R-23 for 60 days.

H-R-23-60d					
Specimen	F_{\max} (N)	σ_{\max} (MPa)	U_{\max} (mm)	ε (%)	E (GPa)
1	147.9	196.9	18.2	7.3	4.5
2	183.3	244.0	22.5	9.0	4.5
3	191.5	255.0	19.2	7.7	4.9
4	205.2	273.2	19.1	7.6	5.0
5	245.3	326.6	22.1	8.8	5.6
Average	194.6	259.1	20.2	8.1	4.9
St.dev	35.4	47.1	2.0	0.8	0.4
CoV (%)	18.2	18.2	9.7	9.7	9.0

Table B- 6: Tensile properties of Hemp yarns after aging in solution H-R-23 for 74 days.

H-R-23-74d					
Specimen	F_{\max} (N)	σ_{\max} (MPa)	U_{\max} (mm)	ε (%)	E (GPa)
1	175.8	234.0	21.2	8.5	4.5
2	110.4	147.0	16.8	6.7	3.7
3	113.7	151.4	15.9	6.4	3.8
4	160.5	213.7	16.9	6.8	4.6
5	90.8	121.0	15.0	6.0	3.1
Average	130.2	173.4	17.1	6.9	3.9
St.dev	36.1	48.1	2.4	1.0	0.6
CoV (%)	27.7	27.7	14.0	14.0	16.3

Table B- 7: Tensile properties of Hemp yarns after aging in solution H-R-23 for 90 days.

H-R-23-90d					
Specimen	F_{\max} (N)	σ_{\max} (MPa)	U_{\max} (mm)	ε (%)	E (GPa)
1	55.1	73.4	11.9	4.8	2.3
2	78.6	104.7	11.8	4.7	2.9
3	55.3	73.7	10.3	4.1	2.7
4	59.7	79.5	10.6	4.3	2.4
5	41.1	54.8	9.0	3.6	2.5
6	54.4	72.5	8.8	3.5	2.6
Average	57.4	76.4	10.4	4.2	2.6
st.dev	12.2	16.2	1.3	0.5	0.2
CoV (%)	21.2	21.2	12.9	12.9	7.8

b) In solution R-60

Table B- 8: Tensile properties of Hemp yarns after aging in solution H-R-60 for 7 days.

H-R-60-7d					
Specimen	F_{\max} (N)	σ_{\max} (MPa)	U_{\max} (mm)	ε (%)	E (GPa)
1	303.0	403.5	26.5	10.6	7.0
2	286.1	381.0	23.5	9.4	6.5
3	273.6	364.3	24.7	9.9	5.3
4	263.0	350.1	21.0	8.4	6.5
5	283.6	377.7	22.3	8.9	6.8
6	272.3	362.6	22.1	8.8	4.8
Average	280.3	373.2	23.4	9.3	6.1
stand, dev	13.9	18.6	2.0	0.8	0.9
CoV (%)	5.0	5.0	8.6	8.6	14.3

Table B- 9: Tensile properties of Hemp yarns after aging in solution H-R-60 for 14 days.

H-R-60-14d					
Specimen	F_{\max} (N)	σ_{\max} (MPa)	U_{\max} (mm)	ε (%)	E (GPa)
1	297.8	396.6	23.5	9.4	7.1
2	221.2	294.5	19.6	7.8	5.9
3	297.2	395.8	24.5	9.8	6.6
4	288.6	384.3	22.9	9.2	7.0
5	233.7	311.2	19.8	7.9	5.6
6	302.5	402.8	24.1	9.6	6.5
Average	273.5	364.2	22.4	8.9	6.5
St.dev	36.2	48.2	2.2	0.9	0.6
CoV (%)	13.2	13.2	9.7	9.7	9.2

Table B- 10: Tensile properties of Hemp yarns after aging in solution H-R-60 for 28 days.

H-R-60-28d					
Specimen	F_{\max} (N)	σ_{\max} (MPa)	U_{\max} (mm)	ε (%)	E (GPa)
1	273.7	364.5	26.9	10.8	5.6
2	241.6	321.8	24.4	9.8	5.5
3	262.9	350.1	25.9	10.4	5.9
4	296.3	394.6	26.0	10.4	6.8
5	279.7	372.4	26.1	10.4	6.1
6	306.8	408.5	27.8	11.1	6.3
Average	276.9	368.6	26.2	10.5	6.0
st.dev	23.4	31.1	1.1	0.5	0.5
CoV (%)	8.4	8.4	4.4	4.4	8.0

Table B- 11: Tensile properties of Hemp yarns after aging in solution H-R-60 for 42 days.

H-R-60-42d					
Specimen	F_{\max} (N)	σ_{\max} (MPa)	U_{\max} (mm)	ε (%)	E (GPa)
1	267.7	356.4	24.9	10.0	6.4
2	241.7	321.8	24.9	10.0	6.2
3	214.7	285.9	22.3	8.9	5.7
4	215.4	286.8	25.4	10.2	5.0
5	236.3	314.7	22.7	9.1	5.7
Average	235.2	313.1	24.0	9.6	5.8
st.dev	21.9	29.1	1.4	0.6	0.6
CoV (%)	9.3	9.3	6.0	6.0	9.7

Table B- 12: Tensile properties of Hemp yarns after aging in solution H-R-60 for 60 days.

H-R-60-60d					
Specimen	F_{\max} (N)	σ_{\max} (MPa)	U_{\max} (mm)	ε (%)	E (GPa)
1	166.7	221.9	17.8	7.1	4.7
2	231.7	308.5	25.2	10.1	5.6
3	245.4	326.8	26.1	10.4	5.4
4	225.7	300.6	25.9	10.4	4.7
5	205.6	273.8	22.2	8.9	5.2
Average	215.0	286.3	23.4	9.4	5.1
st.dev	30.6	40.8	3.5	1.4	0.4
CoV (%)	14.2	14.2	15.1	15.1	7.8

Table B- 13: Tensile properties of Hemp yarns after aging in solution H-R-60 for 74 days.

H-R-60-74d					
Specimen	F _{max} (N)	σ _{max} (MPa)	U _{max} (mm)	ε (%)	E (GPa)
1	185.1	246.5	21.7	8.7	4.6
2	180.2	239.9	22.8	9.1	4.7
3	200.8	267.4	22.1	8.9	4.9
4	182.9	243.6	20.1	8.0	4.9
5	204.3	272.0	23.3	9.3	5.2
6	186.2	247.9	19.7	7.9	4.6
Average	189.9	252.9	21.6	8.6	4.8
St.dev	10.1	13.4	1.4	0.6	0.2
CoV (%)	5.3	5.3	6.7	6.7	5.1

Table B- 14: Tensile properties of Hemp yarns after aging in solution H-R-60 for 90 days.

H-R-60-90d					
Specimen	F _{max} (N)	σ _{max} (MPa)	U _{max} (mm)	ε (%)	E (GPa)
1	168.7	224.7	19.5	7.8	5.1
2	143.0	190.4	19.7	7.9	4.2
3	137.0	182.5	18.4	7.4	4.3
4	141.0	187.7	14.7	5.9	4.9
5	139.2	185.3	19.1	7.7	4.0
6	184.8	246.1	18.2	7.3	5.4
Average	152.3	202.8	18.3	7.3	4.6
st.dev	19.7	26.3	1.9	0.7	0.6
CoV (%)	13.0	13.0	10.1	10.1	12.1

c) In solution E-23

Table B- 15: Tensile properties of Hemp yarns after aging in solution H-E-23 for 7 days.

H-E-23-7d					
Specimen	F_{\max} (N)	σ_{\max} (MPa)	U_{\max} (mm)	ε (%)	E (GPa)
1	223.7	297.9	24.1	9.7	4.0
2	283.4	377.4	25.4	10.2	4.3
3	198.3	264.0	26.0	10.4	3.7
4	223.6	297.7	26.3	10.5	3.7
5	265.1	353.0	32.0	12.8	3.6
6	305.3	406.5	32.5	13.0	4.4
Average	249.9	332.7	27.7	11.1	3.9
st.dev	41.2	54.8	3.6	1.4	3.3
CoV (%)	16.5	16.5	13.0	13.0	8.4

Table B- 16: Tensile properties of Hemp yarns after aging in solution H-E-23 for 14 days.

H-E-23-14d					
Specimen	F_{\max} (N)	σ_{\max} (MPa)	U_{\max} (mm)	ε (%)	E (GPa)
1	205.0	273.0	23.7	9.5	5.1
2	228.4	304.1	24.8	9.9	5.6
3	214.0	285.0	22.1	8.8	5.5
4	265.7	353.8	25.6	10.2	6.2
5	244.2	325.1	24.2	9.7	5.4
6	244.0	324.9	24.1	9.6	5.6
Average	233.6	311.0	24.1	9.6	5.6
st.dev	22.3	29.7	1.2	0.5	0.3
CoV (%)	9.5	9.5	4.9	4.9	6.1

Table B- 17: Tensile properties of Hemp yarns after aging in solution H-E-23 for 28 days.

H-E-23-28d					
Specimen	F _{max} (N)	σ _{max} (MPa)	U _{max} (mm)	ε (%)	E (GPa)
1	217.9	290.1	23.0	9.2	5.6
2	226.0	300.9	24.0	9.6	5.2
3	252.3	335.9	18.1	7.2	6.0
4	212.0	282.3	21.3	8.5	5.7
5	227.9	303.4	21.0	8.4	5.6
6	248.9	331.5	22.8	9.1	6.1
Average	230.8	307.3	21.7	8.7	5.7
st.dev	16.4	21.8	2.1	0.8	0.3
CoV (%)	7.1	7.1	9.7	9.7	5.9

Table B- 18: Tensile properties of Hemp yarns after aging in solution H-E-23 for 42 days.

H-E-23-42d					
Specimen	F _{max} (N)	σ _{max} (MPa)	U _{max} (mm)	ε (%)	E (GPa)
1	206.7	275.2	21.5	8.6	5.1
2	188.4	250.8	21.5	8.6	4.8
3	173.6	231.1	17.875	7.2	4.9
4	252.1	335.7	22.5	9.0	5.4
5	223.4	297.5	21.25	8.5	5.1
Average	208.8	278.1	20.9	8.4	5.1
st.dev	30.6	40.8	1.8	0.7	2.3
CoV (%)	14.7	14.7	8.5	8.5	4.5

Table B- 19: Tensile properties of Hemp yarns after aging in solution H-E-23 for 60 days.

H-E-23-60d					
Specimen	F_{\max} (N)	σ_{\max} (MPa)	U_{\max} (mm)	ε (%)	E (GPa)
1	209.9	279.5	24.8	9.9	5.0
2	279.0	371.5	25.7	10.3	6.1
3	206.7	275.2	20.3	8.1	5.3
4	217.7	289.9	19.7	7.9	5.7
5	275.0	366.1	22.9	9.2	6.2
6	228.4	304.2	19.9	8.0	6.0
Average	236.1	314.4	22.2	8.9	5.7
st.dev	32.6	43.4	2.6	1.1	0.5
CoV (%)	13.8	13.8	11.8	11.8	8.1

Table B- 20: Tensile properties of Hemp yarns after aging in solution H-E-23 for 74 days.

H-E-23-74d					
Specimen	F_{\max} (N)	σ_{\max} (MPa)	U_{\max} (mm)	ε (%)	E (GPa)
1	31.7	42.3	17.3	6.9	1.1
2	30.8	41.0	17.2	6.9	0.9
3	53.8	71.7	23.2	9.3	1.4
4	28.1	37.4	16.3	6.5	0.9
5	52.5	69.9	19.0	7.6	1.5
6	32.1	42.8	13.6	5.5	1.1
Average	38.2	50.8	17.8	7.1	1.1
st.dev	11.7	15.6	3.2	1.3	0.3
CoV (%)	30.6	30.6	18.0	17.9	23.51

Table B- 21: Tensile properties of Hemp yarns after aging in solution H-E-23 for 90 days.

H-E-23-90d					
Specimen	F_{\max} (N)	σ_{\max} (MPa)	U_{\max} (mm)	ε (%)	E (GPa)
1	Rupture of the specimen in the preload step				
2	16.5	22	7.1	2.8	1.0
3	Rupture of the specimen in the preload step				
4	7.1	9.5	3.8	1.5	0.5
5	3.9	5.1	2.2	0.9	0.4
6	14.4	19.2	5.7	2.3	1.0
Average	10.5	14.0	4.7	1.9	0.8
st.dev	6.0	8.0	2.2	0.9	0.3
CoV (%)	56.8	57.1	45.7	45.7	45.0

d) In solution E-40

Table B- 22: Tensile properties of Hemp yarns after aging in solution H-E-40 for 28 days.

H-E-40-28d					
Specimen	F_{\max} (N)	σ_{\max} (MPa)	U_{\max} (mm)	ε (%)	E (GPa)
1	92.9	123.7	12.8	5.1	3.4
2	108.4	144.3	13.2	5.3	3.9
3	76.2	101.5	10.6	4.2	2.9
Average	92.5	123.2	12.2	4.9	3.4
St.dev	16.1	21.4	1.4	0.6	0.5
CoV (%)	17.4	17.4	11.7	11.7	14.7

Table B- 23: Tensile properties of Hemp yarns after aging in solution H-E-40 for 60 days.

H-E-40-60d					
Specimen	F_{\max} (N)	σ_{\max} (MPa)	U_{\max} (mm)	ε (%)	E (GPa)
1	46.4	61.7	9.7	3.9	2.2
2	39.4	52.5	8.8	3.5	1.9
3	35.5	47.3	6.8	2.7	1.8
4	64.1	85.3	11.0	4.4	2.9
5	59.3	78.9	11.2	4.5	2.5
6	61.1	81.4	13.4	5.4	2.4
Average	51.0	67.9	10.1	4.1	2.3
st.dev	12.2	16.2	2.3	0.9	0.4
CoV (%)	23.8	23.8	22.2	22.2	18.2

Table B- 24: Tensile properties of Hemp yarns after aging in solution H-E-40 for 90 days.

H-E-40-90d					
Specimen	F_{\max} (N)	σ_{\max} (MPa)	U_{\max} (mm)	ε (%)	E (GPa)
1	18.1	24.2	3.9	1.6	1.4
2	37.3	49.6	11.5	4.6	1.3
3	31.5	41.9	6.6	2.6	1.7
4	22.8	30.4	5.3	2.1	1.5
5	19.5	25.9	4.3	1.7	1.4
6	31.6	42.1	8.5	3.4	2.2
Average	26.8	35.7	6.7	2.7	1.6
st.dev	7.7	10.3	2.9	1.2	0.3
CoV (%)	28.9	28.9	43.2	43.2	19.6

e) In solution E-60

Table B- 25: Tensile properties of Hemp yarns after aging in solution H-E-60 for 7 days.

H-E-60-7d					
Specimen	F_{\max} (N)	σ_{\max} (MPa)	U_{\max} (mm)	ε (%)	E (GPa)
1	274.8	366.0	26.1	10.5	5.4
2	241.7	321.9	26.3	10.5	5.3
3	256.8	341.9	26.4	10.6	5.3
4	246.2	327.8	25.1	10.0	5.3
5	246.0	327.5	25.8	10.3	5.1
6	248.7	331.1	25.8	10.3	5.3
Average	252.4	336.0	25.9	10.4	5.3
st.dev	12.1	16.1	0.5	0.2	1.1
CoV (%)	4.8	4.8	1.8	1.9	2.1

Table B- 26: Tensile properties of Hemp yarns after aging in solution H-E-60 for 14 days.

H-E-60-14d					
Specimen	F _{max} (N)	σ _{max} (MPa)	U _{max} (mm)	ε (%)	E (GPa)
1	231.5	308.2	24.3	9.7	5.6
2	204.0	271.7	27.1	10.9	4.6
3	252.6	336.4	28.6	11.5	5.2
4	218.3	290.7	25.0	10.0	5.1
5	226.8	302.0	24.2	9.7	5.6
Average	226.6	301.8	25.8	10.3	5.2
st.dev	17.9	23.8	2.0	0.8	0.4
CoV (%)	7.9	7.9	7.6	7.6	7.8

Table B- 27: Tensile properties of Hemp yarns after aging in solution H-E-60 for 28 days.

H-E-60-28d					
Specimen	F _{max} (N)	σ _{max} (MPa)	U _{max} (mm)	ε (%)	E (GPa)
1	192.4	256.2	23.0	9.2	4.2
2	222.6	296.5	21.0	8.4	5.5
3	174.9	232.9	18.8	7.5	4.4
4	259.8	345.9	21.0	8.4	5.9
5	175.0	233.0	19.0	7.6	4.7
6	201.2	268.0	23.0	9.2	4.8
Average	204.3	272.1	21.0	8.4	4.9
st.dev	32.5	43.3	1.9	0.7	0.7
CoV (%)	15.9	15.9	8.8	8.8	13.3

Table B- 28: Tensile properties of Hemp yarns after aging in solution H-E-60 for 42 days.

H-E-60-42d					
Specimen	F _{max} (N)	σ _{max} (MPa)	U _{max} (mm)	ε (%)	E (GPa)
1	204.0	271.6	23.5	9.4	4.9
2	211.9	282.1	23.3	9.3	4.7
3	127.7	170.0	19.6	7.8	3.4
4	178.3	237.4	23.6	9.4	4.0
5	211.3	281.4	21.8	8.7	4.9
6	170.0	226.4	16.6	6.6	4.7
Average	183.9	244.8	21.4	8.6	4.4
st.dev	32.6	43.5	2.8	1.1	0.6
CoV (%)	17.7	17.8	13.1	13.1	14.0

Table B- 29: Tensile properties of Hemp yarns after aging in solution H-E-60 for 60 days.

H-E-60-60d					
Specimen	F _{max} (N)	σ _{max} (MPa)	U _{max} (mm)	ε (%)	E (GPa)
1	83.5	111.2	14.0	5.6	2.9
2	52.4	69.7	14.1	5.7	2.1
4	74.7	99.5	12.5	5.0	2.8
5	69.8	92.9	11.7	4.7	2.8
6	72.6	96.7	13.5	5.4	2.9
Average	70.6	94.0	13.2	5.3	2.7
st.dev	11.4	15.2	1.1	0.4	0.3
CoV (%)	16.2	16.2	8.0	7.9	12.7

Table B- 30: Tensile properties of Hemp yarns after aging in solution H-E-60 for 74 days.

H-E-60-60d					
Specimen	F _{max} (N)	σ _{max} (MPa)	U _{max} (mm)	ε (%)	E (GPa)
1	44.9	59.8	16.9	6.8	1.4
2	73.7	98.1	25.8	10.3	1.9
3	56.1	74.8	20.8	8.3	1.6
4	59.6	79.4	22.0	8.8	1.6
Average	58.6	78.0	21.4	8.6	1.6
st.dev	11.9	15.8	3.7	1.5	0.2
CoV (%)	20.3	20.3	17.2	17.2	11.5

Table B- 31: Tensile properties of Hemp yarns after aging in solution H-E-60 for 90 days.

H-E-60-90d					
Specimen	F_{\max} (N)	σ_{\max} (MPa)	U_{\max} (mm)	ε (%)	E (GPa)
1	27.1	36.0	13.9	5.6	9.9
2	48.1	64.0	18.6	7.4	14.8
3	37.0	49.3	15.8	6.3	12.5
4	34.4	45.9	13.5	5.4	13.0
Average	36.6	48.8	15.4	6.2	12.5
st.dev	8.7	11.6	2.3	0.9	2.0
CoV (%)	23.7	23.7	15.0	15.0	16.2

f) In solution L-23

Table B- 32: Tensile properties of Hemp yarns after aging in solution H-L-23 for 7 days.

H-L-23-7d					
Specimen	F_{\max} (N)	σ_{\max} (MPa)	U_{\max} (mm)	ε (%)	E (GPa)
1	223.9	298.2	24.2	9.7	3.8
2	205.7	273.8	21.4	8.6	4.1
3	217.8	290.0	21.9	8.8	4.1
4	246.9	328.8	24.1	9.6	4.3
5	238.2	317.1	23.8	9.5	3.8
6	226.2	301.2	22.6	9.0	4.0
Average	226.4	301.5	23.0	9.2	4.0
st.dev	14.6	19.5	1.2	0.5	0.2
CoV (%)	6.5	6.5	5.3	5.2	4.3

Table B- 33: Tensile properties of Hemp yarns after aging in solution H- L-23 for 14 days.

H-L-23-14d					
Specimen	F_{\max} (N)	σ_{\max} (MPa)	U_{\max} (mm)	ε (%)	E (GPa)
1	265.5	353.6	26.0	10.4	5.1
2	231.1	307.7	23.8	9.5	4.9
3	257.6	343.0	28.2	11.3	4.8
4	286.9	382.0	29.3	11.7	4.6
5	252.5	336.2	24.5	10.6	4.9
6	236.8	315.3	25.2	10.1	4.8
Average	255.1	339.6	26.2	10.6	4.9
st.dev	20.2	26.9	2.2	0.8	0.2
CoV (%)	7.9	7.9	8.3	7.6	3.3

Table B- 34: Tensile properties of Hemp yarns after aging in solution H- L-23 for 28 days.

H-L-23-28d					
Specimen	F_{\max} (N)	σ_{\max} (MPa)	U_{\max} (mm)	ϵ (%)	E (GPa)
1	276.6	368.3	27.5	11.0	5.5
2	269.2	358.4	22.7	11.1	5.0
3	245.2	326.5	26.6	10.6	4.9
4	266.3	354.6	25.7	10.3	5.4
5	236.6	315.0	27.4	11.0	4.9
Average	258.8	344.6	26.0	10.8	5.2
st.dev	17.0	22.7	2.0	0.3	0.3
CoV (%)	6.6	6.6	7.7	3.1	5.5

Table B- 35: Tensile properties of Hemp yarns after aging in solution H- L-23 for 42 days.

H-L-23-42d					
Specimen	F_{\max} (N)	σ_{\max} (MPa)	U_{\max} (mm)	ϵ (%)	E (GPa)
1	150.4	200.2	16.3	6.5	4.4
2	131.3	174.8	14.8	5.9	4.1
3	177.6	236.5	16.5	6.6	4.6
4	189.0	251.7	18.8	7.5	4.5
5	212.6	283.1	19.8	7.9	5.2
6	204.9	272.9	18.8	7.5	5.2
7	131.1	174.6	14.0	5.6	4.2
Average	171.0	227.7	17.0	6.8	4.6
st.dev	33.8	45.0	2.2	0.9	0.4
CoV (%)	19.8	19.8	12.9	12.9	9.4

Table B- 36: Tensile properties of Hemp yarns after aging in solution H- L-23 for 60 days.

H-L-23-60d					
Specimen	F _{max} (N)	σ _{max} (MPa)	U _{max} (mm)	ε (%)	E (GPa)
1	121.7	162.0	11.3	4.5	4.2
2	145.1	193.2	15.2	6.1	4.2
3	113.3	150.9	14.0	5.6	3.6
4	148.6	197.9	16.3	6.5	4.3
5	138.0	183.8	14.2	5.7	4.2
Average	133.4	177.6	14.2	5.7	4.1
st.dev	15.2	20.3	1.9	0.8	0.3
CoV (%)	11.4	11.4	13.3	13.3	6.6

Table B- 37: Tensile properties of Hemp yarns after aging in solution H- L-23 for 74 days.

H-L-23-74d					
Specimen	F _{max} (N)	σ _{max} (MPa)	U _{max} (mm)	ε (%)	E (GPa)
1	30.3	40.4	17.1	6.8	1.0
2	30.8	41.1	15.2	6.1	1.0
3	31.7	42.2	16.8	6.7	1.1
4	37.2	49.5	18.5	7.4	1.2
5	36.2	48.2	16.1	6.5	1.2
Average	33.2	44.3	16.8	6.7	1.1
st.dev	3.2	4.3	1.2	0.5	0.1
CoV (%)	9.6	9.6	7.3	7.3	10.0

Table B- 38: Tensile properties of Hemp yarns after aging in solution H- L-23 for 90 days.

H-L-23-90d					
Specimen	F _{max} (N)	σ _{max} (MPa)	U _{max} (mm)	ε (%)	E (GPa)
1	9.9	13.2	5.3	2.1	0.7
2	1.9	2.6	0.5	0.2	0.6
3	2.0	2.7	0.9	0.4	0.4
4	6.8	9.1	3.2	1.3	0.5
5	4.0	5.3	2.1	0.8	0.5
Average	4.9	6.6	2.4	1.0	0.5
st.dev	3.4	4.5	1.9	0.8	0.1
CoV (%)	69.5	69.1	80.7	80.7	19.1

g) In solution L-40

Table B- 39: Tensile properties of Hemp yarns after aging in solution H- L-40 for 28 days.

H-L-40-28d					
Specimen	F_{\max} (N)	σ_{\max} (MPa)	U_{\max} (mm)	ε (%)	E (GPa)
1	221.4	294.8	18.2	7.3	5.6
2	202.5	269.7	15.0	6.0	5.8
3	224.8	299.3	22.5	9.0	5.4
4	231.9	308.8	23.8	9.5	5.9
5	286.6	381.6	25.1	10.0	6.7
6	259.5	345.6	24.3	9.7	6.3
Average	237.8	316.6	21.5	8.6	6.0
st.dev	30.2	40.2	4.0	1.6	0.5
CoV (%)	12.7	12.7	18.6	18.6	8.0

Table B- 40: Tensile properties of Hemp yarns after aging in solution H- L-40 for 60 days.

H-L-40-60d					
Specimen	F_{\max} (N)	σ_{\max} (MPa)	U_{\max} (mm)	ε (%)	E (GPa)
1	239.1	318.4	28.8	11.5	5.5
2	219.9	292.8	23.8	9.5	5.3
3	188.0	250.4	21.2	8.5	4.6
4	199.8	266.0	22.7	9.1	4.3
5	182.6	243.2	20.1	8.0	4.6
6	173.7	231.3	22.3	8.9	4.7
7	176.2	234.6	20.7	8.3	4.8
8	194.2	258.5	21.4	8.6	5.4
Average	196.7	261.9	22.6	9.0	4.9
st.dev	22.6	30.1	2.8	1.1	0.4
CoV (%)	11.5	11.5	12.3	12.3	8.6

Table B- 41: Tensile properties of Hemp yarns after aging in solution H- L-40 for 90 days.

H-L-40-90d					
Specimen	F_{\max} (N)	σ_{\max} (MPa)	U_{\max} (mm)	ε (%)	E (GPa)
1	179.9	239.5	20.0	8.0	4.9
2	200.3	266.7	22.4	9.0	5.1
3	232.6	309.8	21.9	8.8	5.9
4	211.8	282.0	19.6	7.8	5.5
5	186.8	248.7	20.4	8.2	5.1
6	210.8	280.8	22.4	9.0	5.5
7	186.1	247.9	20.0	8.0	4.8
Average	201.2	267.9	20.9	8.4	5.2
St.dev	18.6	24.8	1.2	0.5	0.4
CoV (%)	9.3	9.3	6.0	6.0	7.6

h) In solution L-60

Table B- 42: Tensile properties of Hemp yarns after aging in solution H-L-60 for 7 days.

H-L-60-7d					
Specimen	F_{\max} (N)	σ_{\max} (MPa)	U_{\max} (mm)	ε (%)	E (GPa)
1	176.6	235.2	20.5	8.2	4.4
2	201.6	268.4	27.5	11.0	4.2
3	199.0	264.9	25.0	10.0	4.2
4	222.5	296.2	26.1	10.4	4.9
5	198.9	264.5	24.6	9.9	4.9
Average	199.7	265.9	24.7	9.9	4.5
st.dev	16.2	21.6	2.6	1.0	0.3
CoV (%)	8.1	8.1	10.5	10.5	6.9

Table B- 43: Tensile properties of Hemp yarns after aging in solution H- L-60 for 14 days.

H-L-60-14d					
Specimen	F _{max} (N)	σ _{max} (MPa)	U _{max} (mm)	ε (%)	E (GPa)
1	290.8	387.2	27.8	11.1	6.0
2	292.7	389.8	30.2	12.1	5.9
3	275.4	366.8	27.4	11.0	5.7
4	204.9	272.7	25.9	10.4	4.8
5	235.8	314.0	27.1	10.9	5.3
6	205.2	273.2	24.0	9.6	5.0
Average	250.8	333.9	27.1	10.8	5.4
st.dev	40.9	54.5	2.1	0.8	0.5
CoV (%)	16.3	16.3	7.7	7.7	9.6

Table B- 44: Tensile properties of Hemp yarns after aging in solution H- L-60 for 28 days.

H-L-60-28d					
Specimen	F _{max} (N)	σ _{max} (MPa)	U _{max} (mm)	ε (%)	E (GPa)
1	260.6	347.1	29.0	11.6	5.1
2	191.7	255.2	23.0	9.2	4.8
3	266.6	355.0	25.3	10.1	5.9
4	190.6	253.8	21.0	8.4	4.7
5	269.4	358.8	25.0	10.0	5.9
6	173.3	230.8	20.5	8.2	4.8
Average	225.4	300.1	24.0	9.6	5.2
st.dev	44.6	59.4	3.2	1.3	0.6
CoV (%)	19.8	19.8	13.2	13.2	11.0

Table B- 45: Tensile properties of Hemp yarns after aging in solution H- L-60 for 42 days.

H-L-60-42d					
Specimen	F _{max} (N)	σ _{max} (MPa)	U _{max} (mm)	ε (%)	E (GPa)
1	167.7	223.3	16.1	6.5	5.3
2	168.4	224.2	17.3	6.9	4.8
3	169.9	226.2	15.9	6.4	5.2
4	181.6	241.9	16.8	6.7	5.2
5	198.9	264.9	19.7	7.9	5.6
6	175.5	233.8	16.6	6.6	4.9
Average	177.0	235.7	17.0	6.8	5.2
st.dev	12.0	15.9	1.4	0.6	0.3
CoV (%)	6.8	6.8	8.1	8.1	5.2

Table B- 46: Tensile properties of Hemp yarns after aging in solution H- L-60 for 60 days.

H-L-60-60d					
Specimen	F _{max} (N)	σ _{max} (MPa)	U _{max} (mm)	ε (%)	E (GPa)
1	157.1	209.2	15.9	6.4	4.7
2	178.4	237.6	18.7	7.5	5.0
3	136.0	181.1	15.2	6.1	4.2
4	171.6	228.5	16.7	6.7	5.1
5	169.1	225.1	19.8	7.9	4.9
6	161.0	214.4	17.0	6.8	5.0
Average	162.2	216.0	17.2	6.9	4.8
st.dev	14.9	19.9	1.7	0.7	0.3
CoV (%)	9.2	9.2	10.0	10.0	6.8

Table B- 47: Tensile properties of Hemp yarns after aging in solution H- L-60 for 74 days.

H-L-60-74d					
Specimen	F _{max} (N)	σ _{max} (MPa)	U _{max} (mm)	ε (%)	E (GPa)
1	149.4	198.9	16.0	6.4	4.7
2	166.3	221.5	17.4	7.0	5.0
3	192.4	256.2	18.1	7.3	5.5
4	127.1	169.2	15.5	6.2	4.3
5	195.8	260.7	17.2	6.9	5.4
Average	166.2	221.3	16.8	6.7	5.0
st.dev	29.1	38.7	1.1	0.4	0.5
CoV (%)	17.5	17.5	6.5	6.5	10.0

Table B- 48: Tensile properties of Hemp yarns after aging in solution H- L-60 for 90 days.

H-L-60-90d					
Specimen	F_{\max} (N)	σ_{\max} (MPa)	U_{\max} (mm)	ε (%)	E (GPa)
1	198.6	264.4	20.3	8.1	5.3
2	203.3	270.7	20.9	8.4	5.4
3	208.2	277.3	20.5	8.2	5.6
5	205.6	273.8	22.0	8.8	5.3
6	197.5	263.0	19.6	7.8	5.5
7	227.4	302.8	22.5	9.0	5.6
Average	206.8	275.3	21.0	8.4	5.5
st.dev	10.9	14.5	1.1	0.4	0.1
CoV (%)	5.3	5.3	5.2	5.2	2.5

Appendix C: Detailed results of all the tensile test series of Flax yarns (F)

a) In solution E-23

Table C- 1: Tensile properties of Flax yarns after aging in solution F-E-23 for 7 days.

F-E-23-7d					
Specimen	F_{\max} (N)	σ_{\max} (MPa)	U_{\max} (mm)	ε (%)	E (GPa)
1	50.2	58.3	4.9	2.0	3.2
2	60.2	70.0	4.6	1.9	4.3
3	41.5	48.2	3.8	1.5	3.7
4	43.2	50.1	3.3	1.3	4.3
5	52.8	61.3	3.8	1.5	4.2
6	52.7	61.2	3.4	1.4	4.5
Average	50.1	58.2	4.0	1.6	4.0
st.dev	6.9	8.0	0.7	0.3	0.5
CoV (%)	13.8	13.8	16.9	17.0	12.0

Table C- 2: Tensile properties of Flax yarns after aging in solution F-E-23 for 14 days.

F-E-23-14d					
Specimen	F_{\max} (N)	σ_{\max} (MPa)	U_{\max} (mm)	ε (%)	E (GPa)
1	53.9	62.5	6.2	2.5	3.0
2	58.9	68.4	5.2	2.1	3.6
3	71.8	83.4	6.2	2.5	4.0
4	70.2	81.5	6.4	2.6	3.6
5	51.1	59.3	4.8	1.9	3.4
6	56.9	66.0	4.6	1.9	3.7
Average	60.5	70.2	5.6	2.2	3.6
st.dev	8.6	10.0	0.8	0.3	0.3
CoV (%)	14.2	14.2	14.0	14.0	9.4

Table C- 3: Tensile properties of Flax yarns after aging in solution F-E-23 for 28 days.

F-E-23-28d					
Specimen	F_{\max} (N)	σ_{\max} (MPa)	U_{\max} (mm)	ε (%)	E (GPa)
1	73.8	85.8	5.0	2.0	4.9
2	75.4	87.6	5.8	2.3	4.3
3	51.3	59.6	3.8	1.5	4.1
4	72.3	83.9	4.8	1.9	5.0
5	47.6	55.2	4.5	1.8	3.5
Average	64.1	74.4	4.8	1.9	4.4
st.dev	13.5	15.7	0.7	0.3	0.6
CoV (%)	21.1	21.0	15.6	15.7	13.9

Table C- 4: Tensile properties of Flax yarns after aging in solution F-E-23 for 42 days.

F-E-23-42d					
Specimen	F_{\max} (N)	σ_{\max} (MPa)	U_{\max} (mm)	ε (%)	E (GPa)
1	69.2	80.3	6.6	2.6	4.4
2	82.0	95.2	6.8	2.7	4.4
3	74.1	86.0	5.2	2.1	4.5
4	51.3	59.6	4.8	1.9	3.2
5	61.3	71.2	5.1	2.1	3.7
Average	67.6	78.5	5.7	2.3	4.0
st.dev	11.8	13.7	0.9	0.3	0.6
CoV (%)	17.5	17.4	16.3	15.3	14.4

Table C- 5: Tensile properties of Flax yarns after aging in solution F-E-23 for 60 days.

F-E-23-60d					
Specimen	F_{\max} (N)	σ_{\max} (MPa)	U_{\max} (mm)	ε (%)	E (GPa)
1	91.5	106.2	6.9	2.8	4.7
2	81.2	94.3	5.2	2.1	4.5
3	87.1	101.1	7.8	3.1	3.9
4	99.8	115.9	8.1	3.3	4.6
5	79.8	92.7	6.5	2.6	2.5
6	71.0	82.4	5.2	2.1	4.2
7	73.6	85.4	5.3	2.1	4.7
8	58.6	68.1	5.8	2.3	3.3
Average	80.3	93.3	6.4	2.6	4.1
st.dev	12.8	14.9	1.2	0.5	0.8
CoV (%)	16.0	16.0	18.4	18.7	19.2

Table C- 6: Tensile properties of Flax yarns after aging in solution F-E-23 for 74 days.

F-E-23-74d					
Specimen	F_{\max} (N)	σ_{\max} (MPa)	U_{\max} (mm)	ε (%)	E (GPa)
1	67.1	77.9	4.3	1.7	4.5
2	64.5	75.0	5.0	2.0	3.7
3	62.1	72.1	5.0	2.0	4.0
4	81.4	94.6	5.4	2.2	4.2
5	53.7	62.3	5.3	2.1	3.2
6	76.7	89.1	6.4	2.6	4.4
Average	67.6	78.5	5.2	2.1	4.0
st.dev	10.1	11.7	0.7	0.3	0.5
CoV (%)	14.9	14.9	13.1	13.1	12.1

Table C- 7: Tensile properties of Flax yarns after aging in solution F-E-23 for 90 days.

F-E-23-90d					
Specimen	F_{\max} (N)	σ_{\max} (MPa)	U_{\max} (mm)	ε (%)	E (GPa)
1	64.4	74.8	5.3	2.1	3.8
2	63.0	73.2	4.9	2.0	4.1
3	42.7	49.6	3.3	1.3	3.6
4	56.1	65.2	3.9	1.6	4.2
5	39.8	46.3	3.1	1.2	3.9
6	51.8	60.1	4.7	1.9	3.1
8	41.9	48.7	3.3	1.3	3.7
Average	51.4	59.7	4.1	1.6	3.8
st.dev	10.2	11.9	0.9	0.4	0.4
CoV (%)	19.9	19.9	21.9	21.9	9.6

Table C- 8: Tensile properties of Flax yarns after aging in solution F-E-23 for 104 days.

F-E-23-104d					
Specimen	F_{\max} (N)	σ_{\max} (MPa)	U_{\max} (mm)	ε (%)	E (GPa)
1	63.8	74.1	5.4	2.2	4.7
2	52.6	61.1	4.8	1.9	4.3
3	64.3	74.7	5.2	2.1	4.5
4	60.1	69.8	5.2	2.1	4.5
5	60.0	69.7	5.1	2.0	4.2
6	60.4	70.1	6.0	2.4	3.9
Average	60.2	69.9	5.3	2.1	4.3
st.dev	4.2	4.9	0.4	0.2	0.3
CoV (%)	7.0	7.0	7.6	7.6	6.5

Table C- 9: Tensile properties of Flax yarns after aging in solution F-E-23 for 120 days.

F-E-23-120d					
Specimen	F _{max} (N)	σ _{max} (MPa)	U _{max} (mm)	ε (%)	E (GPa)
1	68.2	79.2	6.5	2.6	4.8
2	76.8	89.2	6.0	2.4	4.8
3	64.6	75.0	6.3	2.5	4.8
4	62.8	73.0	6.4	2.6	4.0
6	70.9	82.4	5.4	2.2	5.2
7	52.2	60.6	5.4	2.2	3.8
Average	65.9	76.5	6.0	2.4	4.6
st.dev	8.3	9.7	0.5	0.2	0.5
CoV (%)	12.6	12.7	8.1	8.0	11.5

Table C- 10: Tensile properties of Flax yarns after aging in solution F-E-23 for 150 days.

F-E-23-150d					
Specimen	F _{max} (N)	σ _{max} (MPa)	U _{max} (mm)	ε (%)	E (GPa)
1	42.5	49.3	4.3	1.7	3.2
2	59.2	68.7	5.4	2.2	4.4
3	49.9	57.9	4.5	1.8	3.9
4	57.4	66.7	5.5	2.2	4.7
5	62.3	72.3	5.9	2.4	4.0
6	48.8	56.7	5.1	2.1	3.4
Average	53.3	61.9	5.1	2.0	3.8
st.dev	7.5	8.7	0.6	0.2	0.4
CoV (%)	14.1	14.0	11.9	12.1	9.6

Table C- 11: Tensile properties of Flax yarns after aging in solution F-E-23 for 180 days.

F-E-23-180d					
Specimen	F _{max} (N)	σ _{max} (MPa)	U _{max} (mm)	ε (%)	E (GPa)
1	49.4	57.3	8.7	3.5	2.2
2	35.3	41.0	9.3	3.7	2.0
3	30.4	35.4	7.9	3.2	1.4
4	59.2	68.7	6.4	2.5	3.5
Average	43.6	50.6	8.1	3.2	2.2
st.dev	13.2	15.2	1.3	0.5	0.9
CoV (%)	30.2	30.1	15.5	16.3	39.5

Table C- 12: Tensile properties of Flax yarns after aging in solution F-E-23 for 210 days.

F-E-23-210d					
Specimen	F _{max} (N)	σ _{max} (MPa)	U _{max} (mm)	ε (%)	E (GPa)
1	41.7	48.4	6.1	2.4	2.6
2	37.0	42.9	6.0	2.4	2.5
3	51.4	59.7	7.5	3.0	2.9
4	49.4	57.4	5.9	2.4	3.2
5	32.9	38.2	5.1	2.0	2.6
6	54.1	62.8	5.4	2.2	4.0
Average	44.4	51.6	6.0	2.4	3.0
st.dev	8.5	9.9	0.8	0.3	0.6
CoV (%)	19.2	19.2	13.8	13.9	19.8

b) In solution E-60

Table C- 13: Tensile properties of Flax yarns after aging in solution F-E-60 for 7 days.

F-E-60-7d					
Specimen	F _{max} (N)	σ _{max} (MPa)	U _{max} (mm)	ε (%)	E (GPa)
1	60.1	69.7	3.6	1.5	4.9
2	33.8	39.3	2.8	1.1	3.5
3	41.2	47.8	3.3	1.3	4.0
4	32.9	38.2	3.1	1.2	3.7
5	53.2	61.8	3.5	1.4	4.5
6	46.1	53.5	2.9	1.2	5.2
7	38.5	44.7	3.8	1.5	3.7
Average	43.7	50.7	3.3	1.3	4.2
st.dev	10.1	11.7	0.4	0.2	0.7
CoV (%)	23.1	23.1	11.5	11.5	15.6

Table C- 14: Tensile properties of Flax yarns after aging in solution F-E-60 for 14 days.

F-E-60-14d					
Specimen	F_{\max} (N)	σ_{\max} (MPa)	U_{\max} (mm)	ε (%)	E (GPa)
1	55.7	64.7	4.6	1.9	4.6
2	48.3	56.1	3.7	1.5	4.0
3	54.5	63.3	5.0	2.0	3.7
4	62.2	72.2	4.5	1.8	4.9
5	44.7	51.9	4.0	1.6	3.8
Average	53.1	61.7	4.3	1.7	4.2
st.dev	6.8	7.9	0.5	0.2	0.5
CoV (%)	12.8	12.8	12.6	12.5	12.5

Table C- 15: Tensile properties of Flax yarns after aging in solution F-E-60 for 28 days.

F-E-60-28d					
Specimen	F_{\max} (N)	σ_{\max} (MPa)	U_{\max} (mm)	ε (%)	E (GPa)
1	30.1	35.0	4.5	1.8	2.0
2	44.7	51.9	4.3	1.7	3.1
Average	37.4	43.5	4.4	1.8	2.6
st.dev	10.3	12.0	0.2	0.1	0.8
CoV (%)	27.6	27.5	4.0	4.0	30.5

Table C- 16: Tensile properties of Flax yarns after aging in solution F-E-60 for 42 days.

F-E-60-42d					
Specimen	F_{\max} (N)	σ_{\max} (MPa)	U_{\max} (mm)	ε (%)	E (GPa)
1	39.6	46.0	4.5	1.8	2.9
2	42.6	49.4	4.5	1.8	3.1
3	38.8	45.0	4.5	1.8	2.9
4	29.9	34.7	3.5	1.4	3.0
5	30.2	35.0	3.1	1.2	3.0
6	29.9	34.8	3.3	1.3	2.6
Average	35.2	40.8	3.9	1.6	2.9
st.dev	5.8	6.7	0.7	0.3	0.2
CoV (%)	16.5	16.5	17.2	17.2	5.9

Table C- 17: Tensile properties of Flax yarns after aging in solution F-E-60 for 60 days.

F-E-60-60d					
Specimen	F_{\max} (N)	σ_{\max} (MPa)	U_{\max} (mm)	ε (%)	E (GPa)
1	21.5	25.0	4.4	1.8	1.5
2	23.0	26.7	3.7	1.5	1.2
3	30.1	34.9	5.9	2.4	1.1
4	23.0	26.7	4.5	1.8	1.6
Average	24.4	28.3	4.6	1.9	1.4
st.dev	3.8	4.5	0.9	0.4	0.2
CoV (%)	15.8	15.8	20.0	20.2	17.6

Table C- 18: Tensile properties of Flax yarns after aging in solution F-E-60 for 74 days.

F-E-60-74d					
Specimen	F_{\max} (N)	σ_{\max} (MPa)	U_{\max} (mm)	ε (%)	E (GPa)
1	36.3	42.1	7.5	3.0	2.0
2	25.3	29.3	8.9	3.5	1.1
3	37.7	43.8	7.4	3.0	2.2
4	33.8	39.2	6.7	2.7	1.9
5	32.9	38.2	7.3	2.9	1.8
6	23.0	26.7	6.4	2.6	1.3
Average	31.5	36.6	7.4	3.0	1.7
st.dev	6.0	6.9	0.8	0.3	0.4
CoV (%)	19.0	19.0	11.3	11.2	24.8

Table C- 19: Tensile properties of Flax yarns after aging in solution F-E-60 for 90 days.

F-E-60-90d					
Specimen	F_{\max} (N)	σ_{\max} (MPa)	U_{\max} (mm)	ε (%)	E (GPa)
1	16.9	19.6	4.5	1.8	1.5
2	14.4	16.7	3.7	1.5	1.2
3	18.1	21.0	4.2	1.7	1.5
4	19.9	23.1	4.3	1.7	1.8
5	11.9	13.8	3.0	1.2	1.3
Average	16.2	18.9	3.9	1.6	1.5
st.dev	3.2	3.7	0.6	0.2	0.2
CoV (%)	19.4	19.4	14.9	14.9	15.8

c) In solution L-23

Table C- 20: Tensile properties of Flax yarns after aging in solution F-L-23 for 7 days.

F-L-23-7d					
Specimen	F_{\max} (N)	σ_{\max} (MPa)	U_{\max} (mm)	ε (%)	E (GPa)
1	32.7	38.0	2.0	0.8	4.7
2	37.1	43.1	3.3	1.3	3.3
3	32.4	37.6	2.6	1.1	3.7
4	31.5	36.6	3.2	1.3	2.9
5	43.7	50.7	3.0	1.2	4.5
6	46.9	54.5	4.0	1.6	4.0
Average	37.4	43.4	3.0	1.2	3.8
st.dev	6.5	7.5	0.7	0.3	1.7
CoV (%)	17.4	17.4	22.4	22.4	44.6

Table C- 21: Tensile properties of Flax yarns after aging in solution F-L-23 for 14 days.

F-L-23-14d					
Specimen	F_{\max} (N)	σ_{\max} (MPa)	U_{\max} (mm)	ε (%)	E (GPa)
1	35.6	41.3	3.2	1.3	3.6
2	50.1	58.2	3.5	1.4	4.8
3	50.7	58.9	4.0	1.6	4.1
4	44.3	51.4	4.3	1.7	3.3
5	47.1	54.7	3.6	1.5	4.4
6	42.7	49.6	3.5	1.4	3.9
Average	45.1	52.3	3.7	1.5	4.0
st.dev	5.6	6.5	0.4	0.2	0.5
CoV (%)	12.4	12.4	11.3	11.3	13.5

Table C- 22: Tensile properties of Flax yarns after aging in solution F-L-23 for 28 days.

F-L-23-28d					
Specimen	F_{\max} (N)	σ_{\max} (MPa)	U_{\max} (mm)	ε (%)	E (GPa)
1	59.0	68.5	4.8	1.9	4.3
2	33.9	39.4	3.3	1.3	3.1
3	43.7	50.7	3.7	1.5	3.5
4	42.0	48.7	4.0	1.6	3.5
5	37.2	43.2	3.8	1.5	3.3
6	44.5	51.7	4.3	1.7	3.4
Average	43.4	50.4	4.0	1.6	3.5
st.dev	8.6	10.0	0.5	0.2	0.4
CoV (%)	19.9	19.9	13.4	13.3	11.7

Table C- 23: Tensile properties of Flax yarns after aging in solution F-L-23 for 42 days.

F-L-23-42d					
Specimen	F_{\max} (N)	σ_{\max} (MPa)	U_{\max} (mm)	ε (%)	E (GPa)
1	66.0	76.7	4.4	1.8	4.8
2	58.5	67.9	4.5	1.8	4.5
3	61.6	71.6	3.9	1.6	4.5
4	60.5	70.3	5.1	2.0	3.8
5	56.8	66.0	4.5	1.8	4.1
6	54.3	63.0	3.7	1.5	4.1
Average	59.6	69.3	4.4	1.8	4.3
st.dev	4.1	4.8	0.5	0.2	0.4
CoV (%)	6.8	6.9	11.4	10.1	8.4

Table C- 24: Tensile properties of Flax yarns after aging in solution F-L-23 for 60 days.

F-L-23-60d					
Specimen	F _{max} (N)	σ _{max} (MPa)	U _{max} (mm)	ε (%)	E (GPa)
1	76.9	89.3	6.0	2.4	5.1
2	59.2	68.8	4.7	1.9	3.9
3	51.5	59.8	4.7	1.9	3.6
4	62.0	72.0	5.6	2.2	4.0
5	75.0	87.1	5.8	2.3	4.9
6	56.9	66.1	4.0	1.6	4.0
Average	63.6	73.9	5.1	2.1	4.3
st.dev	10.2	11.8	0.8	0.3	1.9
CoV (%)	16.0	16.0	15.3	14.7	43.1

Table C- 25: Tensile properties of Flax yarns after aging in solution F-L-23 for 74 days.

F-L-23-74d					
Specimen	F _{max} (N)	σ _{max} (MPa)	U _{max} (mm)	ε (%)	E (GPa)
1	62.3	72.3	5.6	2.3	3.9
2	55.1	64.0	5.1	2.0	3.3
3	70.7	82.1	6.1	2.4	4.1
4	77.5	90.0	6.2	2.5	4.8
5	84.1	97.7	7.4	3.0	4.3
Average	69.9	81.2	6.1	2.4	4.1
st.dev	11.6	13.5	0.9	0.3	0.5
CoV (%)	16.6	16.6	14.1	14.1	13.5

Table C- 26: Tensile properties of Flax yarns after aging in solution F-L-23 for 90 days.

F-L-23-90d					
Specimen	F _{max} (N)	σ _{max} (MPa)	U _{max} (mm)	ε (%)	E (GPa)
1	53.4	62.0	7.4	3.0	3.0
2	50.8	59.0	6.2	2.5	3.3
3	54.5	63.3	6.0	2.4	3.6
4	50.6	58.7	6.2	2.5	3.3
5	42.1	48.9	6.5	2.6	2.7
Average	50.3	58.4	6.5	2.6	3.2
stand, dev	4.9	5.6	0.6	0.2	0.3
CoV (%)	9.7	9.7	8.6	8.6	10.8

Table C- 27: Tensile properties of Flax yarns after aging in solution F-L-23 for 104 days.

F-L-23-104d					
Specimen	F_{\max} (N)	σ_{\max} (MPa)	U_{\max} (mm)	ε (%)	E (GPa)
1	53.4	62.1	5.7	2.3	3.9
2	65.7	76.3	6.5	2.6	4.2
3	42.3	49.1	4.5	1.8	3.4
4	63.4	73.7	4.3	1.7	5.1
5	42.9	49.9	3.8	1.5	4.7
6	60.4	70.1	5.1	2.0	4.3
Average	54.7	63.5	5.0	2.0	4.3
st.dev	10.2	11.9	1.0	0.4	0.6
CoV (%)	18.7	18.7	19.9	19.9	14.0

Table C- 28: Tensile properties of Flax yarns after aging in solution F-L-23 for 120 days.

F-L-23-120d					
Specimen	F_{\max} (N)	σ_{\max} (MPa)	U_{\max} (mm)	ε (%)	E (GPa)
1	48.8	56.6	5.8	2.3	3.3
2	64.3	74.7	6.0	2.4	4.1
3	56.7	65.8	5.1	2.0	5.0
4	49.8	57.8	6.0	2.4	3.9
5	53.7	62.3	5.6	2.3	3.6
Average	54.6	63.4	5.7	2.3	4.0
st.dev	6.3	7.3	0.4	0.2	0.6
CoV (%)	11.5	11.5	6.7	6.7	16.2

Table C- 29: Tensile properties of Flax yarns after aging in solution F-L-23 for 150 days.

F-L-23-150d					
Specimen	F_{\max} (N)	σ_{\max} (MPa)	U_{\max} (mm)	ε (%)	E (GPa)
1	63.6	73.9	8.1	3.2	3.2
2	56.3	65.4	6.1	2.5	3.0
3	57.2	66.4	6.1	2.5	3.2
4	73.5	85.4	7.0	2.8	4.1
5	58.7	68.2	7.4	3.0	3.0
6	75.5	87.7	7.3	2.9	3.8
Average	64.1	74.5	7.0	2.8	3.4
st.dev	8.4	9.8	0.8	0.3	0.5
CoV (%)	13.2	13.2	11.0	11.0	13.5

Table C- 30: Tensile properties of Flax yarns after aging in solution F-L-23 for 180 days.

F-L-23-180d					
Specimen	F_{\max} (N)	σ_{\max} (MPa)	U_{\max} (mm)	ε (%)	E (GPa)
1	47.4	55.1	8.5	3.4	2.5
2	30.8	35.7	4.0	1.6	2.5
3	30.9	35.9	5.8	2.3	2.0
4	41.0	47.7	6.3	2.5	2.5
5	40.1	46.6	6.0	2.4	2.5
Average	38.0	44.2	6.1	2.4	2.4
st.dev	7.14	8.34	1.61	0.64	0.22
CoV (%)	18.77	18.86	26.34	26.34	9.32

Table C- 31: Tensile properties of Flax yarns after aging in solution F-L-23 for 210 days.

F-L-23-210d					
Specimen	F_{\max} (N)	σ_{\max} (MPa)	U_{\max} (mm)	ε (%)	E (GPa)
1	66.1	76.7	8.2	3.3	3.9
2	59.2	68.7	6.7	2.7	3.9
3	62.5	72.6	8.4	3.4	3.7
4	40.2	46.7	5.9	2.4	2.8
5	31.3	36.4	5.0	2.0	2.7
7	43.0	50.0	4.5	1.8	3.9
Average	50.4	58.5	6.5	2.6	3.5
stand, dev	14.1	16.3	1.6	0.7	0.6
CoV (%)	28.0	27.9	25.1	25.4	16.5

d) In solution L-60

Table C- 32: Tensile properties of Flax yarns after aging in solution F-L-60 for 7 days.

F-L-60-7d					
Specimen	F_{\max} (N)	σ_{\max} (MPa)	U_{\max} (mm)	ε (%)	E (GPa)
1	50.0	58.1	5.0	2.0	3.3
2	70.2	81.6	5.0	2.0	4.7
3	47.4	55.0	4.2	1.7	3.7
4	61.2	71.1	5.0	2.0	4.4
5	53.9	62.6	3.9	1.6	4.7
Average	56.6	65.7	4.6	1.9	4.2
st.dev	9.3	10.7	0.6	0.2	0.6
CoV (%)	16.4	16.4	12.2	12.2	15.2

Table C- 33: Tensile properties of Flax yarns after aging in solution F-L-60 for 14 days.

F-L-60-14d					
Specimen	F_{\max} (N)	σ_{\max} (MPa)	U_{\max} (mm)	ε (%)	E (GPa)
1	43.8	50.9	2.8	1.1	4.4
2	47.9	55.7	3.3	1.3	4.8
3	52.0	60.4	3.8	1.5	4.2
4	49.1	57.1	4.3	1.7	3.8
5	43.2	50.2	3.2	1.3	4.2
Average	47.2	54.8	3.5	1.4	4.3
st.dev	3.7	4.3	0.6	0.2	0.4
CoV (%)	7.9	7.9	17.4	17.3	8.5

Table C- 34: Tensile properties of Flax yarns after aging in solution F-L-60 for 28 days.

F-L-60-28d					
Specimen	F_{\max} (N)	σ_{\max} (MPa)	U_{\max} (mm)	ε (%)	E (GPa)
1	51.4	59.7	4.3	1.7	3.4
2	59.4	69.0	4.5	1.8	3.9
3	58.8	68.4	4.3	1.7	3.6
4	43.1	50.0	4.3	1.7	2.1
5	48.9	56.8	4.3	1.7	3.6
Average	52.3	60.8	4.3	1.7	3.3
St.dev	6.9	8.0	0.1	0.0	0.7
CoV (%)	13.2	13.2	2.6	2.6	21.2

Table C- 35: Tensile properties of Flax yarns after aging in solution F-L-60 for 42 days.

F-L-60-42d					
Specimen	F_{\max} (N)	σ_{\max} (MPa)	U_{\max} (mm)	ε (%)	E (GPa)
1	42.1	48.9	4.4	1.8	3.4
2	48.4	56.2	4.4	1.8	3.7
3	51.6	59.9	4.5	1.8	4.0
4	50.7	58.9	4.1	1.6	4.0
5	40.7	47.3	4.3	1.7	3.4
6	42.0	48.8	4.1	1.6	3.4
Average	45.9	53.3	4.3	1.7	3.7
st.dev	4.9	5.6	0.2	0.1	0.3
CoV (%)	10.6	10.6	3.9	3.9	8.1

Table C- 36: Tensile properties of Flax yarns after aging in solution F-L-60 for 60 days.

F-L-60-60d					
Specimen	F_{\max} (N)	σ_{\max} (MPa)	U_{\max} (mm)	ε (%)	E (GPa)
1	39.8	46.2	4.6	1.9	2.2
2	47.0	54.6	5.1	2.1	4.1
3	39.0	45.2	4.7	1.9	3.8
4	33.7	39.1	4.3	1.7	3.2
5	30.2	35.1	3.3	1.3	3.1
6	34.3	39.8	4.1	1.6	3.2
Average	37.3	43.3	4.3	1.7	3.3
st.dev	5.9	6.9	0.6	0.3	0.7
CoV (%)	15.9	15.9	14.8	14.8	20.1

Table C- 37: Tensile properties of Flax yarns after aging in solution F-L-60 for 74 days.

F-L-60-74d					
Specimen	F_{\max} (N)	σ_{\max} (MPa)	U_{\max} (mm)	ε (%)	E (GPa)
1	38.8	45.1	6.4	2.6	2.8
2	48.3	56.1	9.0	3.6	2.5
3	45.3	52.6	6.9	2.8	2.9
4	43.9	51.0	7.7	3.1	2.5
5	51.2	59.4	8.1	3.2	2.8
Average	45.5	52.9	7.6	3.0	2.7
st.dev	4.7	5.4	1.0	0.4	0.2
CoV (%)	10.3	10.3	13.3	13.3	6.9

Table C- 38: Tensile properties of Flax yarns after aging in solution F-L-60 for 90 days.

F-L-60-90d					
Specimen	F_{\max} (N)	σ_{\max} (MPa)	U_{\max} (mm)	ϵ (%)	E (GPa)
1	43.6	50.7	8.3	3.3	2.4
2	36.3	42.2	9.2	3.7	1.6
3	43.0	49.9	8.0	3.2	2.6
4	49.7	57.8	9.1	3.6	2.9
5	58.0	67.4	9.5	3.8	3.0
Average	46.1	53.6	8.8	3.5	2.5
st.dev	8.2	9.5	0.6	0.3	0.6
CoV (%)	17.7	17.7	7.4	7.4	22.3

Appendix D: Synthesis of the residual tensile properties of hemp (H) and flax (F) yarns after exposure to aging in different environments

Table D- 1 presents the residual tensile properties (tensile strength σ_{\max} , elastic modulus E and ultimate tensile strain ϵ_{\max}) of hemp yarns (H) after exposure to eight different aging environments at different periods. Similarly, Table D- 2 presents the residual tensile properties of flax yarns (F) after exposure to four different aging environments at different periods.

Table D- 1 : Residual tensile properties of Hemp yarns after aging in the eight different environments at different exposure periods.

Aging environment	Aging duration (days)	0	7	14	28	42	60	74	90
H-R-23	σ_{\max} (MPa)	269.3	330.4	372.5	315.0	300.9	259.1	173.4	76.4
	St.dev	43.6	44.9	31.2	33.6	22.5	47.1	48.1	16.2
	CoV%	16.2	13.2	8.4	10.7	7.5	18.2	27.7	21.2
	E (GPa)	4.2	6.3	6.8	5.7	5.6	4.9	3.9	2.6
	St.dev	0.4	0.7	0.7	0.3	0.2	0.4	0.6	0.2
	CoV%	9.2	10.3	9.7	5.4	3.5	9.0	16.3	7.8
	ϵ (%)	7.3	8.7	8.3	9.1	9.6	8.1	6.9	4.2
	St.dev	1.1	0.5	0.5	0.4	0.5	0.8	1.0	0.5
	CoV%	15.0	5.5	6.2	4.6	5.6	9.7	14.0	12.9
H-R-60	σ_{\max} (MPa)	269.3	373.2	364.2	368.6	313.1	286.3	252.9	202.8
	St.dev	43.6	18.6	48.2	31.1	29.1	40.8	13.4	26.3
	CoV%	16.2	5.0	13.2	8.4	9.3	14.2	5.3	13.0
	E (GPa)	4.2	6.1	6.5	6.0	5.8	5.1	4.8	4.6
	St.dev	0.4	0.9	0.6	0.5	0.5	0.4	0.2	0.6
	CoV%	9.2	14.3	9.2	8.0	9.4	7.8	5.1	12.1
	ϵ (%)	7.3	9.3	8.9	10.5	9.6	9.4	6.9	7.3
	St.dev	1.1	0.8	0.9	0.5	0.6	1.4	1.0	0.7
	CoV%	15.0	8.6	9.7	4.4	6.0	15.1	14.0	10.1
H-E-23	σ_{\max} (MPa)	269.3	332.7	311	307.3	278.1	314.4	50.8	14.0

	St.dev	43.6	54.8	29.7	21.8	40.8	43.4	15.6	8.0
	CoV%	16.2	16.5	9.5	7.1	14.7	13.8	30.6	57.1
	E (GPa)	4.2	3.9	5.6	5.7	5.1	5.7	1.1	0.3
	St.dev	0.4	0.3	0.3	0.3	0.2	0.5	0.3	0.3
	CoV%	9.2	8.4	6.1	5.9	4.5	8.1	23.5	45.0
	ε (%)	7.3	11.1	9.6	8.7	8.4	8.9	7.1	1.9
	St.dev	1.1	1.4	0.5	0.8	0.7	1.1	1.3	0.9
	CoV%	15.0	13.0	4.9	9.7	8.5	11.8	17.9	45.7
H-L-23	σ_{max} (MPa)	269.3	301.5	339.6	344.6	227.7	177.6	44.3	6.6
	St.dev	43.6	19.5	26.9	22.7	45.0	20.3	4.3	4.6
	CoV%	16.2	19.5	7.9	6.6	19.8	11.4	9.6	69.1
	E (GPa)	4.2	4.0	4.9	5.2	4.6	4.1	1.1	0.5
	St.dev	0.4	0.2	0.2	0.3	0.4	0.3	0.1	0.1
	CoV%	9.2	4.3	3.3	5.5	9.4	6.6	10.0	19.1
	ε (%)	7.3	9.2	10.6	10.8	6.8	5.7	6.7	1.0
	St.dev	1.1	0.5	0.8	0.3	0.9	0.8	0.5	0.8
	CoV%	15.0	5.2	7.6	3.1	12.9	13.3	7.3	80.7
H-E-40	σ_{max} (MPa)	269.3			123.2		67.9		35.7
	St.dev	43.6			21.4		16.2		10.3
	CoV%	16.2			17.4		23.8		28.9
	E (GPa)	4.2			3.4		2.3		1.6
	St.dev	0.4			0.5		0.4		0.3
	CoV%	9.2			14.7		18.2		19.6
	ε (%)	7.3			4.9		4.1		2.7
	St.dev	1.1			0.6		0.9		1.2
	CoV%	15.0			11.7		22.2		43.2
H-L-40	σ_{max} (MPa)	269.3			316.6		261.9		267.9
	St.dev	43.6			40.3		30.1		24.8
	(CoV%)	16.2			12.7		11.5		9.3
	E (GPa)	4.2			6.0		4.9		5.2

	St.dev	0.4			0.5		0.4		0.4
	CoV%	9.2			8.0		8.6		7.6
	ϵ (%)	7.3			8.6		9.0		8.4
	St.dev	1.1			1.6		1.1		0.5
	CoV%	15.0			18.6		12.3		6.0
H-E-60	σ_{\max} (MPa)	269.3	336.0	301.8	272.1	244.8	94.0	78.0	48.8
	St.dev	43.6	16.1	23.8	43.3	43.5	15.2	15.8	11.6
	CoV%	16.2	4.8	7.9	15.9	17.8	16.2	20.3	23.7
	E (GPa)	4.2	5.3	5.2	4.9	4.4	2.7	1.6	1.3
	St.dev	0.4	0.1	0.4	0.7	0.6	0.3	0.2	0.2
	CoV%	9.2	2.1	7.8	13.3	13.9	12.7	11.5	16.2
	ϵ (%)	7.3	10.4	10.3	8.4	8.6	5.3	8.6	6.2
	St.dev	1.1	0.2	0.8	0.7	1.1	0.4	1.5	0.9
	CoV%	15.0	1.9	7.6	8.8	13.1	7.9	17.2	15.0
H-L-60	σ_{\max} (MPa)	269.3	265.9	333.9	300.1	235.7	216.0	221.3	275.3
	St.dev	43.6	21.6	54.5	59.4	16.0	19.9	38.7	14.5
	(CoV%)	16.2	8.1	16.3	19.8	6.7	9.2	17.5	5.3
	E (GPa)	4.2	4.5	5.4	5.2	5.2	4.8	5.0	5.5
	St.dev	0.4	0.3	0.5	0.6	0.3	0.3	0.5	0.1
	CoV%	9.2	6.9	9.6	11.0	5.2	6.8	10.0	2.5
	ϵ (%)	7.3	9.9	10.8	9.6	6.8	6.9	6.7	8.4
	St.dev	1.1	1.0	0.8	1.3	0.6	0.7	0.4	0.4
	CoV%	15.0	10.5	7.7	13.2	8.1	10.0	6.5	5.2

Table D- 2 : Residual tensile properties of Flax yarns after aging in four different environments at different exposure periods.

Aging environment	Aging duration (days)	0	7	14	28	42	60	74	90	104	120	150	180	210
F-E-23	σ_{max} (MPa)	66.6	58.2	70.2	74.4	78.5	93.3	78.5	59.7	69.9	76.5	61.9	50.6	51.6
	St.dev	11.1	8.0	10.0	15.7	13.7	14.9	11.7	11.9	4.9	9.7	8.7	15.2	9.9
	CoV%	16.6	13.8	14.3	21.1	17.4	16.0	14.9	19.9	7.0	12.7	14.1	30.1	19.2
	E (GPa)	5.3	4.0	3.6	4.4	4.0	4.1	4.0	3.8	4.3	4.6	3.8	2.2	3.0
	St.dev	0.5	0.5	0.3	0.6	0.6	0.8	0.5	0.4	0.3	0.5	0.4	0.9	0.6
	CoV%	9.3	12.0	9.4	13.9	14.4	19.3	12.1	9.7	6.5	11.5	9.6	39.5	19.8
	ϵ (%)	1.4	1.6	2.2	1.9	2.3	2.6	2.1	1.6	2.1	2.4	2.0	3.2	2.4
	St.dev	0.2	0.3	0.3	0.3	0.4	0.5	0.3	0.4	0.2	0.2	0.3	0.5	0.3
	CoV%	10.6	17.0	14.0	15.7	15.3	18.8	13.1	21.9	7.6	8.0	12.1	16.3	13.9
	F-L-23	σ_{max} (MPa)	66.6	43.4	52.3	50.4	69.3	73.9	81.2	58.4	63.5	63.4	74.5	44.2
St.dev		11.1	7.6	6.5	10.0	4.8	11.8	13.8	5.7	11.9	7.3	9.8	8.3	16.3
CoV%		16.6	17.4	12.5	19.9	6.9	16.0	16.6	9.7	18.7	11.7	13.2	18.9	27.9
E (GPa)		5.3	3.9	4.0	3.5	4.3	4.3	4.1	3.2	4.2	4.0	3.4	2.4	3.5
St.dev		0.5	0.7	0.5	0.4	0.4	0.6	0.6	0.4	0.6	0.6	0.5	0.2	0.6
CoV%		9.3	6.7	13.4	11.9	8.6	13.3	13.5	11.0	13.9	16.1	13.7	9.4	16.1
ϵ (%)		1.4	1.2	1.5	1.6	1.8	2.1	2.4	2.6	2.0	2.3	2.8	2.4	2.6
St.dev		0.2	0.3	0.2	0.2	0.2	0.3	0.3	0.2	0.4	0.2	0.3	0.6	0.7
CoV%		10.6	22.4	11.3	13.3	10.1	14.7	14.1	8.6	19.9	6.7	11.0	26.3	25.4
F-E-60		σ_{max} (MPa)	66.6	50.7	61.7	43.5	40.8	28.3	36.6	18.9	-	-	-	-
	St.dev	11.1	11.7	7.9	11.3	6.7	4.5	7.0	3.7	-	-	-	-	-
	CoV%	16.6	23.1	12.8	27.5	16.5	15.8	19.0	19.4	-	-	-	-	-

	E (GPa)	5.3	4.2	4.2	2.6	2.9	1.4	1.7	1.5	-	-	-	-	-
	St.dev	0.5	0.7	0.5	0.8	0.2	0.2	0.4	0.2					
	CoV%	9.3	17.6	12.3	30.9	6.4	17.7	24.9	14.4					
	ε (%)	1.4	1.3	1.7	1.8	1.6	1.9	3.0	1.6	-	-	-	-	-
	St.dev	0.2	0.2	0.2	0.1	0.3	0.4	0.3	0.2					
	CoV%	10.6	11.5	12.6	4.0	17.2	20.2	11.2	14.9					
F-L-60	σ_{max} (MPa)	66.6	65.7	54.8	60.8	53.3	43.3	52.9	53.6	-	-	-	-	-
	St.dev	11.1	10.8	4.3	8.0	5.6	6.9	5.4	9.5					
	CoV%	16.6	16.4	7.9	13.2	10.6	15.9	10.3	17.7					
	E (GPa)	5.3	4.1	4.3	3.3	3.6	3.3	2.7	2.5	-	-	-	-	-
	St.dev	0.5	0.6	0.4	0.7	0.3	0.6	0.2	0.6					
	CoV%	9.3	14.6	8.1	21.8	8.5	19.7	6.1	22.4					
	ε (%)	1.4	1.9	1.4	1.7	1.7	1.7	3.0	3.5	-	-	-	-	-
	St.dev	0.2	0.2	0.2	0.0	0.1	0.3	0.4	0.3					
CoV%	10.6	12.2	17.3	2.6	3.9	14.8	13.3	7.4						

Appendix E: Force-displacement curves for all the tested specimens of the tensile test series of H-E and H-L hemp TRM

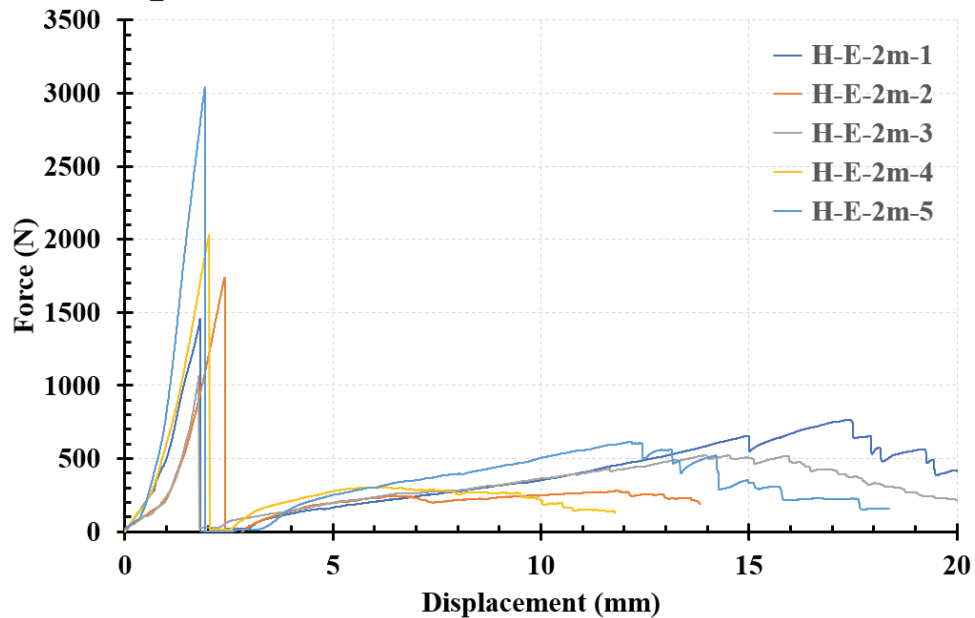


Figure E-1 : Force-displacement curves for the specimens of H-E-2m series.

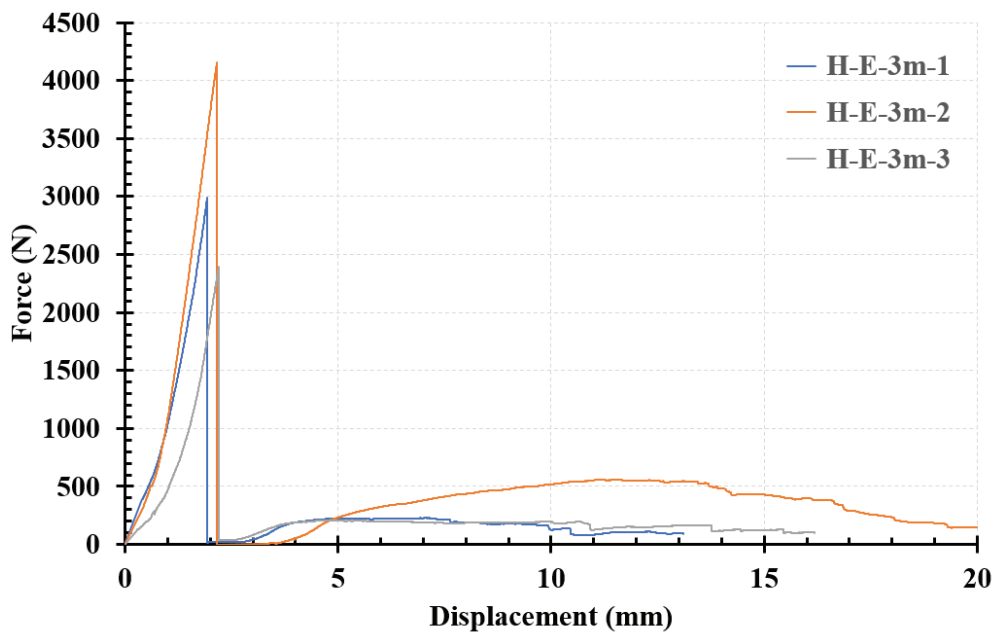


Figure E-2 : Force-displacement curves for the specimens of H-E-3m series.

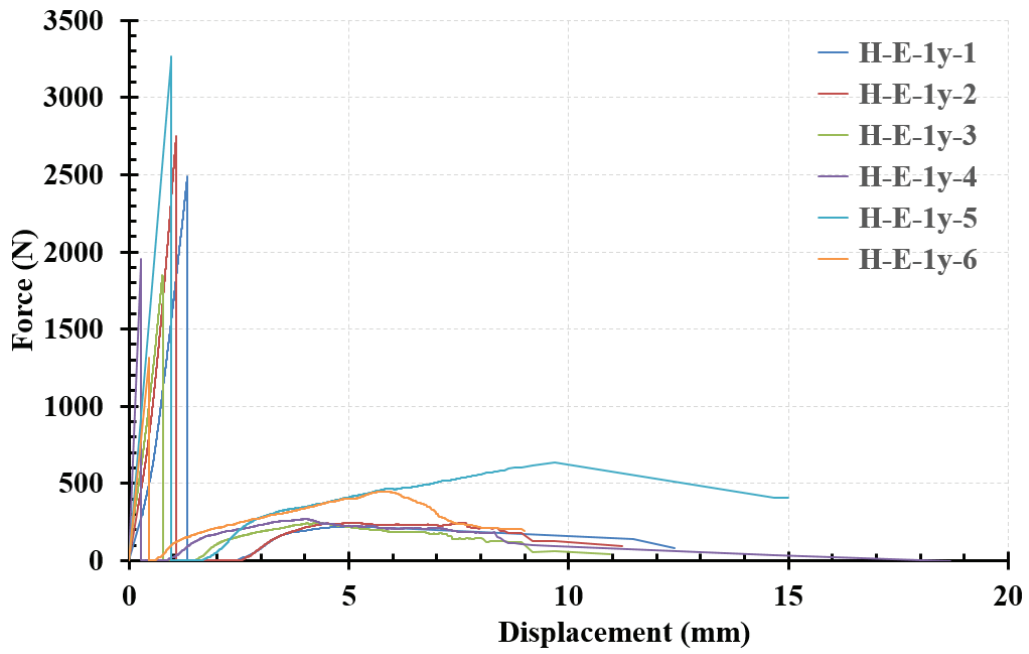


Figure E- 3 : Force-displacement curves for the specimens of H-E-1y series.

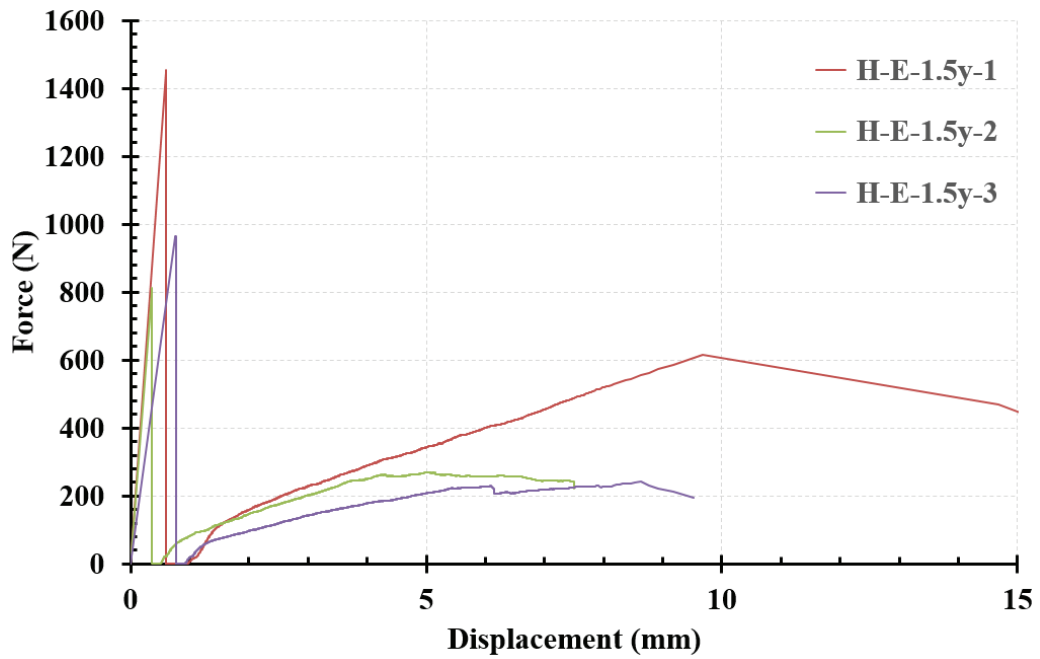


Figure E- 4 : Force-displacement curves for the specimens of H-E-1.5 y series.

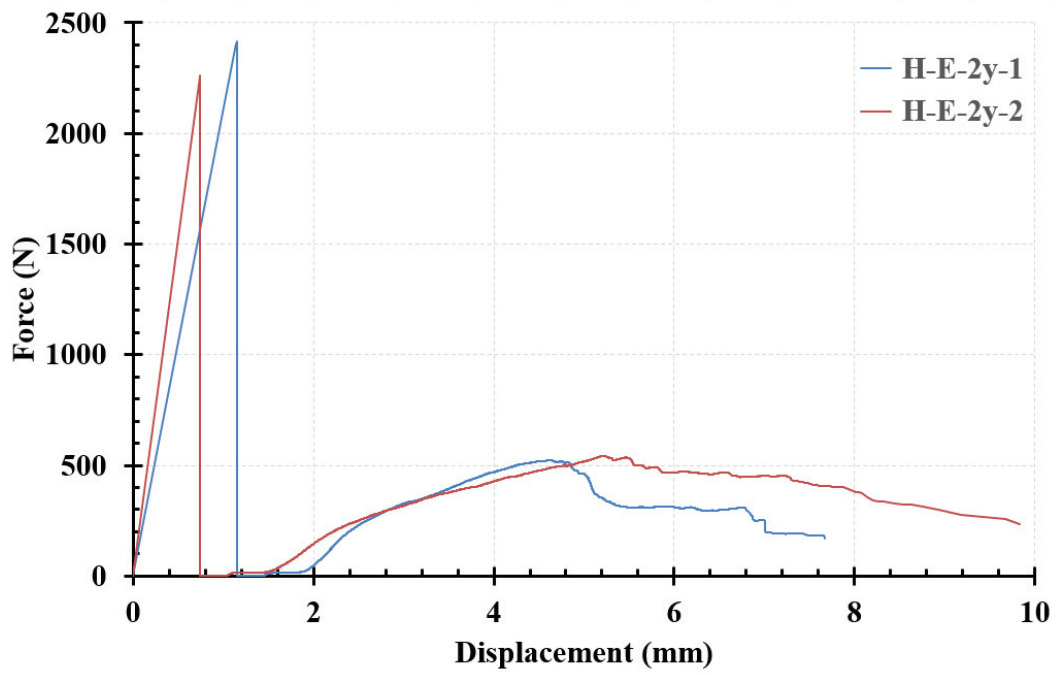


Figure E- 5 : Force-displacement curves for the specimens of H-E-2y series.

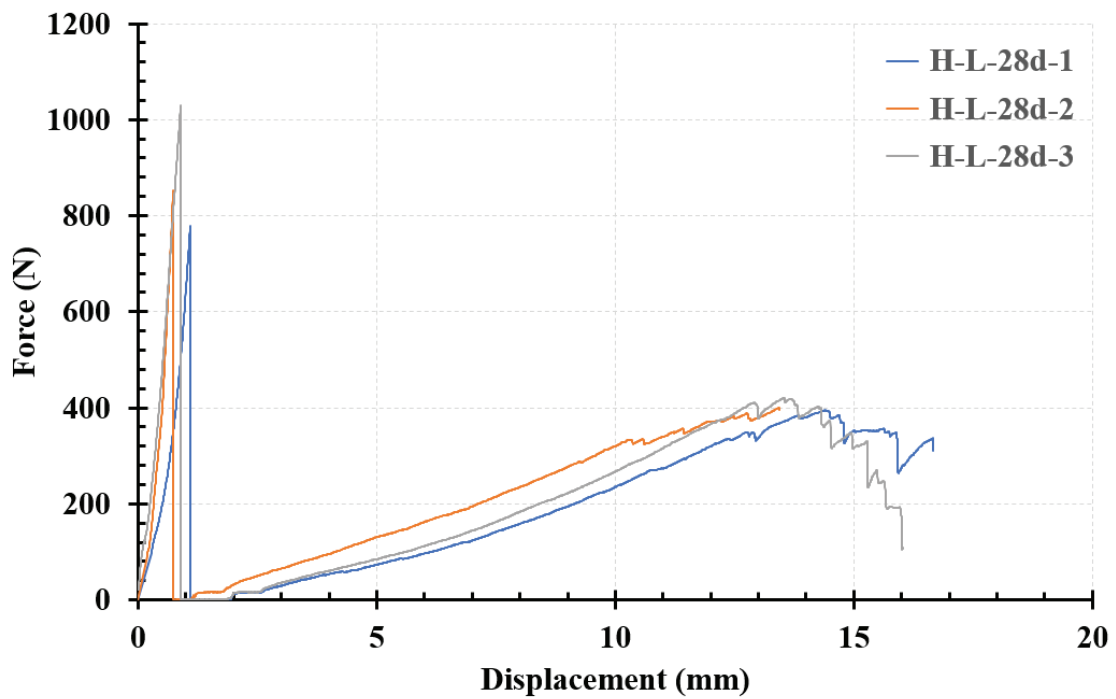


Figure E- 6 : Force-displacement curves for the specimens of H-L-28d series.

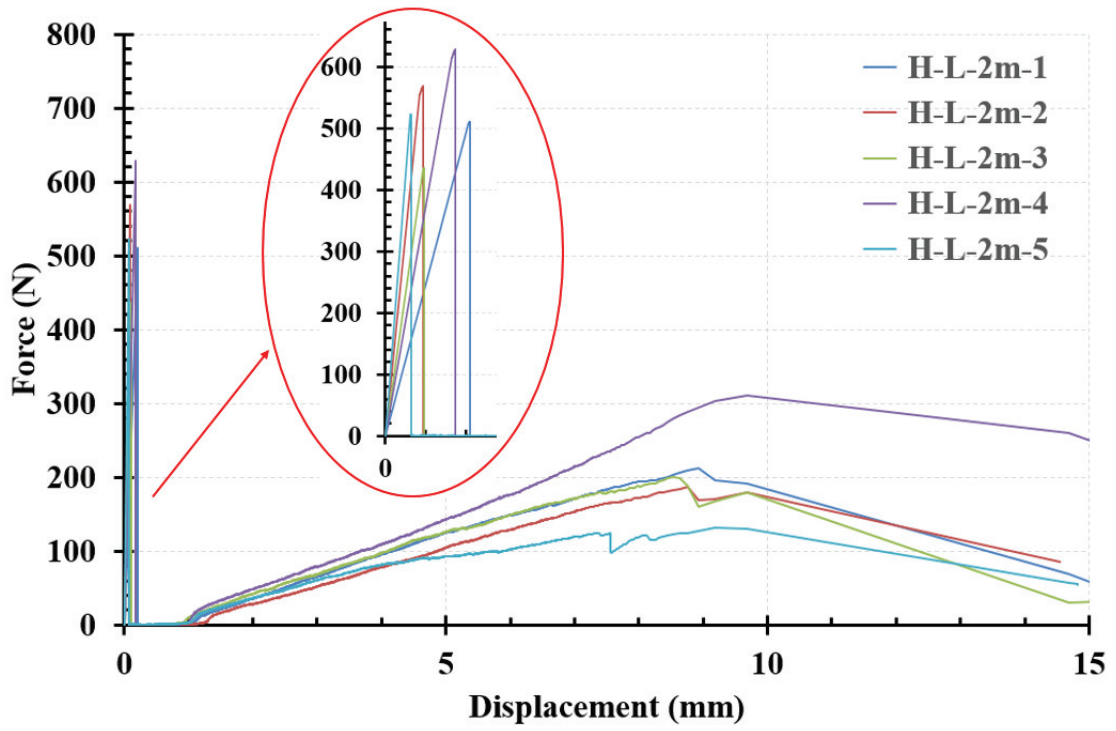


Figure E- 7 : Stress-strain curves for the specimens of H-L-2m series.

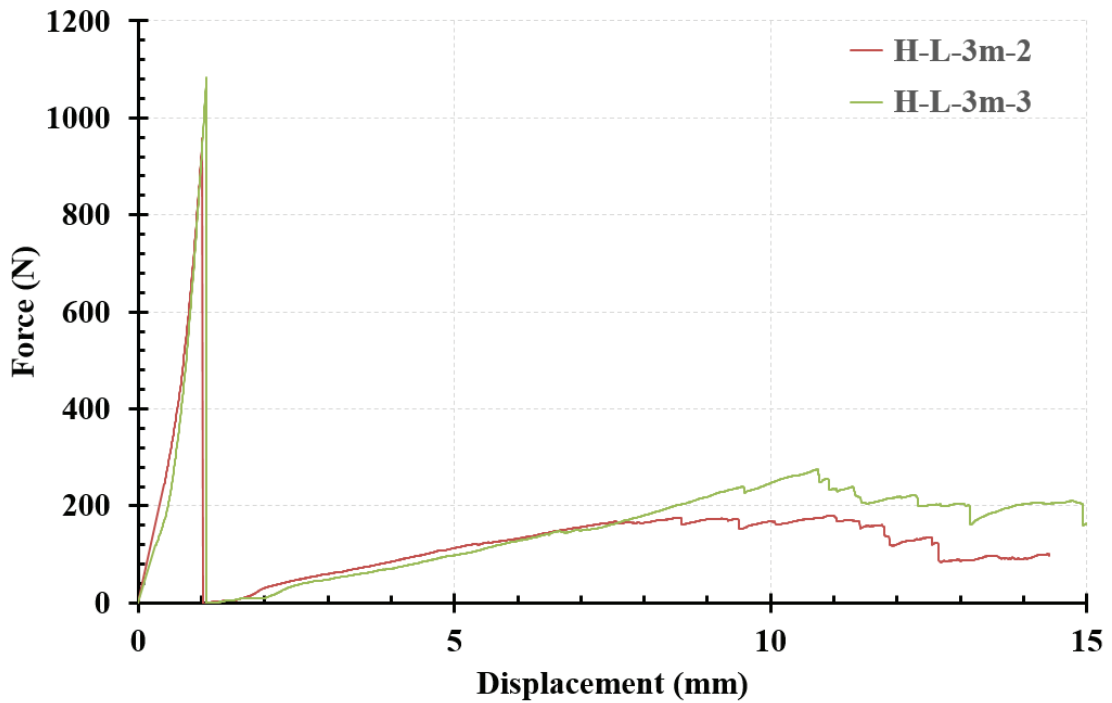


Figure E- 8 : Force-displacement curves for the specimens of H-L-3m series.

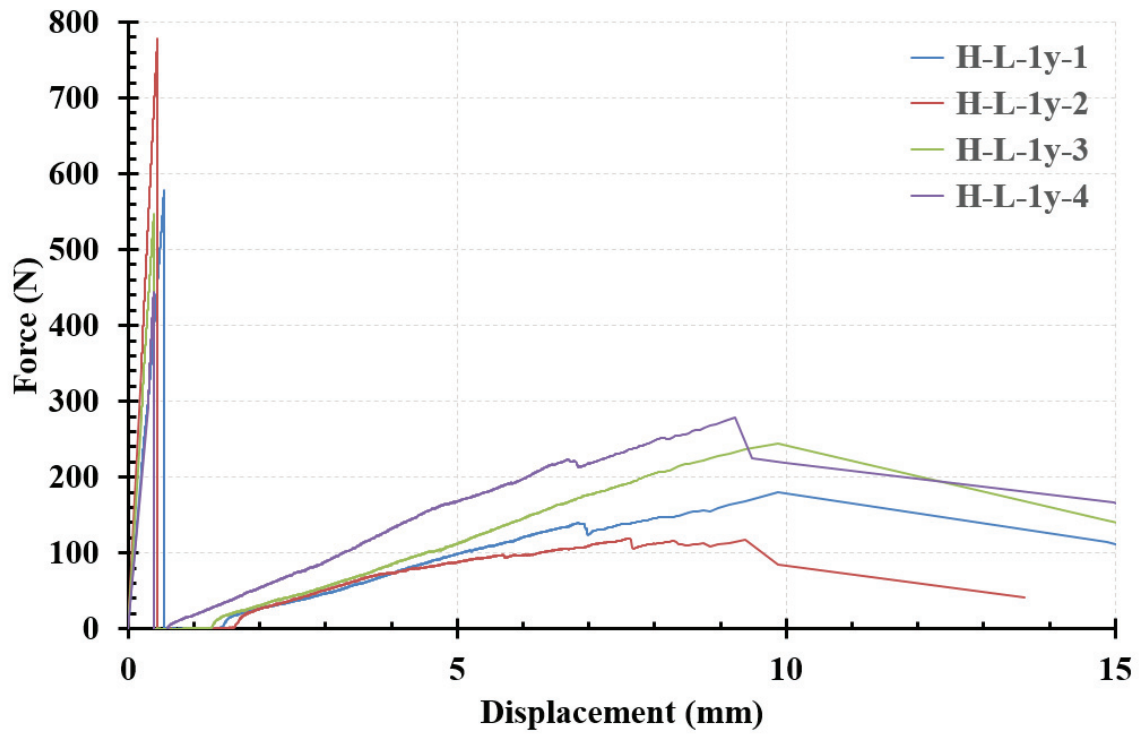


Figure E- 9 : Force-displacement curves for the specimens of H-L-1y series.

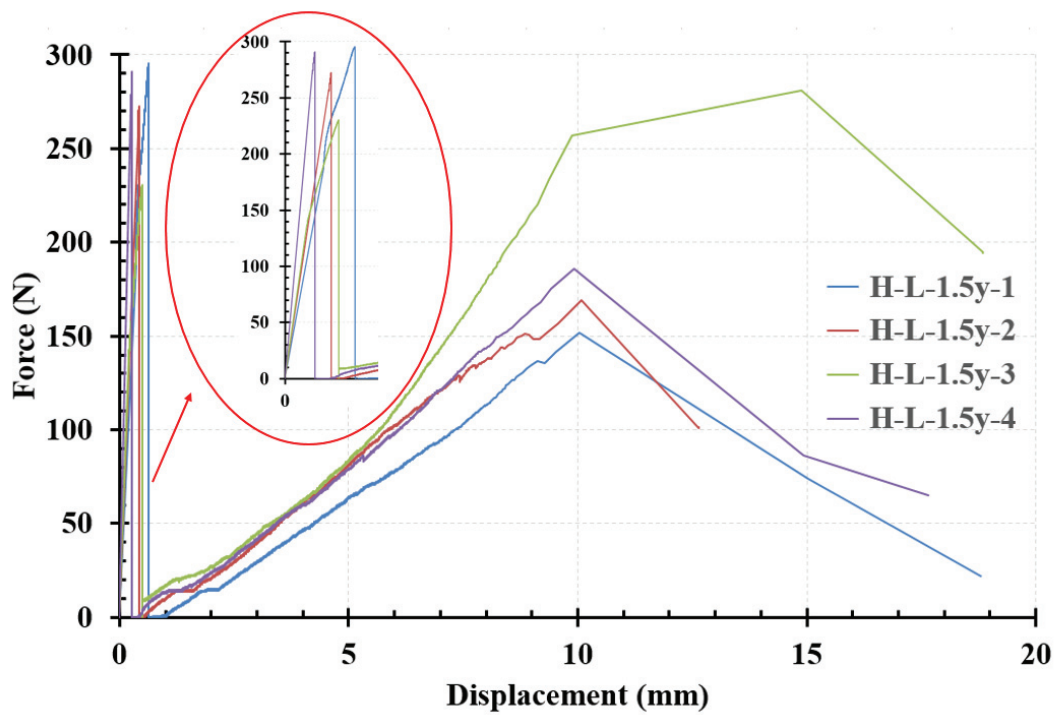


Figure E- 10 : Force-displacement curves for the specimens of H-L-1.5y series.

Appendix F: Detailed results of all the tensile test series of bio-resin-coated hemp yarns (HC)

a) In solution E-23

Table F- 1: Tensile properties of bio-resin-coated Hemp yarns after aging in solution HC-E-23 for 7 days.

HC-E-23-7d					
Specimen	F_{\max} (N)	σ_{\max} (MPa)	U_{\max} (mm)	ε (%)	E (GPa)
1	415.4	122.7	2.7	1.8	7.3
2	531.7	158.2	2.4	1.6	11.0
3	615.6	183.8	2.4	1.6	12.9
4	469.1	139.1	2.1	1.4	10.4
5	408.4	120.6	2.1	1.4	9.9
6	499.3	148.3	2.4	1.6	9.7
Average	489.9	145.5	2.3	1.6	10.2
st.dev	77.8	23.7	0.2	0.1	1.8
CoV (%)	15.9	16.3	9.3	9.3	18.0

Table F- 2: Tensile properties of bio-resin-coated Hemp yarns after aging in solution HC-E-23 for 14 days.

HC-E-23-14d					
Specimen	F_{\max} (N)	σ_{\max} (MPa)	U_{\max} (mm)	ε (%)	E (GPa)
1	516.7	149.3	3.4	2.3	9.1
2	445.7	127.7	2.6	1.7	9.5
3	609.7	177.7	2.5	1.6	12.6
4	407.1	115.9	2.6	1.7	8.2
5	405.4	115.4	2.3	1.6	9.0
6	458.7	131.6	2.8	1.9	8.4
Average	473.9	136.3	2.7	1.8	9.5
st.dev	78.0	23.8	0.4	0.3	1.6
CoV (%)	16.5	17.5	13.9	13.9	17.1

Table F- 3: Tensile properties of bio-resin-coated Hemp yarns after aging in solution HC-E-23 for 28 days.

HC-E-23-28d					
Specimen	F_{\max} (N)	σ_{\max} (MPa)	U_{\max} (mm)	ε (%)	E (GPa)
1	550.8	176.5	2.3	1.5	11.2
2	511.7	164.6	2.7	1.8	9.2
3	536.0	172.0	2.7	1.8	9.5
4	519.8	167.1	3.3	2.2	7.2
5	352.9	116.2	2.3	1.5	7.5
6	484.4	156.3	2.3	1.5	10.0
Average	492.6	158.8	2.6	1.7	9.1
st.dev	72.0	22.0	0.4	0.3	1.5
CoV (%)	14.6	13.8	15.6	15.6	16.6

Table F- 4: Tensile properties of bio-resin-coated Hemp yarns after aging in solution HC-E-23 for 42 days.

HC-E-23-42d					
Specimen	F_{\max} (N)	σ_{\max} (MPa)	U_{\max} (mm)	ε (%)	E (GPa)
1	474.0	132.8	3.0	2.0	7.7
2	350.5	95.1	4.3	2.9	6.5
3	570.7	162.3	3.4	2.3	8.2
4	517.3	146.0	2.5	1.7	11.0
5	490.8	137.9	3.0	2.0	8.4
6	385.1	105.7	3.4	2.3	5.9
Average	464.7	130.0	3.3	2.2	8.0
st.dev	82.6	25.2	0.6	0.4	1.8
CoV (%)	17.8	19.4	18.1	18.1	22.4

Table F- 5: Tensile properties of bio-resin-coated Hemp yarns after aging in solution HC-E-23 for 74 days.

HC-E-23-74d					
Specimen	F _{max} (N)	σ _{max} (MPa)	U _{max} (mm)	ε (%)	E (GPa)
1	573.4	174.9	3.9	2.6	8.4
2	503.9	153.7	3.4	2.3	9.3
3	515.9	157.4	4.3	2.9	8.4
4	402.3	122.7	3.0	2.0	7.6
5	462.3	141.0	3.1	2.1	8.7
6	508.0	155.0	3.4	2.2	8.8
Average	494.3	150.8	3.5	2.3	8.5
st.dev	57.4	17.5	0.5	0.3	0.5
CoV (%)	11.6	11.6	14.1	14.1	6.4

Table F- 6: Tensile properties of bio-resin-coated Hemp yarns after aging in solution HC-E-23 for 90 days.

HC-E-23-90d					
Specimen	F _{max} (N)	σ _{max} (MPa)	U _{max} (mm)	ε (%)	E (GPa)
1	464.1	141.6	2.7	1.8	9.2
2	365.1	111.4	2.4	1.6	7.9
3	411.9	125.7	2.7	1.8	8.1
4	377.8	115.3	2.5	1.7	8.2
5	455.1	138.8	2.9	1.9	8.4
6	436.1	133.0	2.7	1.8	8.8
Average	418.3	127.6	2.7	1.8	8.4
st.dev	40.7	12.4	0.2	0.1	0.5
CoV (%)	9.7	9.7	6.0	6.0	5.5

b) In solution E-40

Table F- 7: Tensile properties of bio-resin-coated Hemp yarns after aging in solution HC-E-40 for 28 days.

HC-E-40-28d					
Specimen	F_{\max} (N)	σ_{\max} (MPa)	U_{\max} (mm)	ε (%)	E (GPa)
1	425.6	151.9	3.5	2.3	6.6
2	339.3	121.1	3.4	2.2	5.5
3	448.7	160.2	3.3	2.2	7.9
4	383.2	136.8	3.1	2.1	6.8
5	404.0	144.2	3.9	2.6	5.9
6	415.2	148.2	3.4	2.3	6.8
Average	402.7	143.7	3.4	2.3	6.6
st.dev	38.0	13.6	0.3	0.2	0.8
CoV (%)	9.4	9.4	7.8	7.8	12.6

Table F- 8: Tensile properties of bio-resin-coated Hemp yarns after aging in solution HC-E-40 for 90 days.

HC-E-40-90d					
Specimen	F_{\max} (N)	σ_{\max} (MPa)	U_{\max} (mm)	ε (%)	E (GPa)
1	443.2	158.2	3.7	2.5	6.9
2	321.0	114.6	2.9	1.9	5.7
3	377.5	134.7	3.0	2.0	6.6
4	258.0	92.1	4.0	2.7	3.6
5	254.1	90.7	2.9	2.0	4.6
6	290.0	103.5	2.6	1.8	6.0
Average	324.0	115.6	3.2	2.1	5.6
st.dev	74.1	26.5	0.6	0.4	1.3
CoV (%)	22.9	22.9	17.3	17.3	22.7

c) In solution E-60

Table F- 9: Tensile properties of bio-resin-coated Hemp yarns after aging in solution HC-E-60 for 7 days.

HC-E-60-7d					
Specimen	F_{\max} (N)	σ_{\max} (MPa)	U_{\max} (mm)	ε (%)	E (GPa)
1	347.6	105.0	3.3	2.2	4.7
2	393.8	119.1	3.0	2.0	6.2
3	372.9	112.8	3.1	2.0	5.8
4	339.5	102.6	3.5	2.4	4.8
5	458.2	138.8	3.2	2.2	6.7
Average	382.4	115.7	3.2	2.1	5.7
st.dev	47.5	14.5	0.2	0.1	0.9
CoV (%)	12.4	12.5	6.9	6.9	15.7

Table F- 10: Tensile properties of bio-resin-coated Hemp yarns after aging in solution HC-E-60 for 14 days.

HC-E-60-14d					
Specimen	F_{\max} (N)	σ_{\max} (MPa)	U_{\max} (mm)	ε (%)	E (GPa)
1	396.0	120.8	3.3	2.2	5.8
2	435.8	132.9	3.2	2.2	5.8
3	361.9	110.4	2.6	1.7	6.3
4	373.8	114.0	2.8	1.8	6.2
5	463.0	141.2	3.5	2.4	5.9
6	408.9	124.7	3.7	2.5	5.8
Average	406.5	124.0	3.2	2.1	6.0
st.dev	38.0	11.6	0.4	0.3	0.2
CoV (%)	9.3	9.3	13.4	13.4	3.9

Table F- 11: Tensile properties of bio-resin-coated Hemp yarns after aging in solution HC-E-60 for 28 days.

HC-E-60-28d					
Specimen	F_{\max} (N)	σ_{\max} (MPa)	U_{\max} (mm)	ε (%)	E (GPa)
1	519.5	158.5	3.4	2.2	7.6
2	507.1	154.7	3.3	2.2	7.2
3	423.8	129.3	2.8	1.8	7.7
4	339.3	103.5	3.0	2.0	5.1
5	381.7	116.5	2.7	1.8	7.0
6	434.3	132.5	3.1	2.1	6.8
Average	434.3	132.5	3.0	2.0	6.9
st.dev	70.0	21.3	0.3	0.2	0.9
CoV (%)	16.1	16.1	9.5	9.5	13.7

Table F- 12: Tensile properties of bio-resin-coated Hemp yarns after aging in solution HC-E-60 for 42 days.

HC-E-60-42d					
Specimen	F_{\max} (N)	σ_{\max} (MPa)	U_{\max} (mm)	ε (%)	E (GPa)
1	495.5	151.2	3.5	2.3	7.9
2	427.8	130.5	4.2	2.8	5.1
3	469.9	143.4	3.6	2.4	6.6
4	405.5	123.7	4.5	3.0	4.2
5	437.4	133.4	3.1	2.1	7.6
6	387.8	118.3	3.4	2.3	5.5
Average	437.3	133.4	3.7	2.5	6.2
st.dev	40.0	12.2	0.5	0.3	1.4
CoV (%)	9.1	9.1	13.9	13.9	23.5

Table F- 13: Tensile properties of bio-resin-coated Hemp yarns after aging in solution HC-E-60 for 74 days.

HC-E-60-74d					
Specimen	F_{\max} (N)	σ_{\max} (MPa)	U_{\max} (mm)	ε (%)	E (GPa)
1	471.1	143.7	4.3	2.9	6.5
2	550.1	167.8	5.0	3.3	7.0
3	396.6	121.0	4.3	2.9	5.3
4	473.4	144.4	4.5	3.0	6.1
5	465.0	141.9	4.5	3.0	6.2
6	376.0	114.7	4.8	3.2	4.8
Average	455.4	138.9	4.6	3.1	6.0
st.dev	62.3	19.0	0.3	0.2	0.8
CoV (%)	13.7	13.7	5.8	5.8	13.2

Table F- 14: Tensile properties of bio-resin-coated Hemp yarns after aging in solution HC-E-60 for 90 days.

HC-E-60-90d					
Specimen	F_{\max} (N)	σ_{\max} (MPa)	U_{\max} (mm)	ε (%)	E (GPa)
1	415.4	126.7	4.5	3.0	5.0
2	463.7	141.5	5.1	3.4	5.0
3	499.9	152.5	3.8	2.6	7.2
4	437.3	133.4	4.0	2.7	5.8
5	406.8	124.1	3.3	2.2	6.4
6	343.3	104.7	3.4	2.2	5.3
Average	427.7	130.5	4.0	2.7	5.8
st.dev	53.5	16.3	0.7	0.5	0.9
CoV (%)	12.5	12.5	17.2	17.2	15.0

d) In solution L-23

Table F- 15: Tensile properties of bio-resin-coated Hemp yarns after aging in solution HC-L-23 for 7 days.

HC-L-23-7d					
Specimen	F_{\max} (N)	σ_{\max} (MPa)	U_{\max} (mm)	ε (%)	E (GPa)
1	486.7	148.5	2.4	1.6	10.0
2	591.5	180.4	2.5	1.7	11.6
3	531.8	162.2	2.3	1.6	11.1
4	562.4	171.6	2.7	1.8	9.7
5	460.8	140.6	2.2	1.4	11.0
6	550.2	167.8	2.6	1.8	11.4
Average	530.5	161.9	2.5	1.6	10.8
st.dev	48.8	14.9	0.2	0.1	0.8
CoV (%)	9.2	9.2	8.6	8.6	7.1

Table F- 16: Tensile properties bio-resin-coated Hemp yarns after aging in solution HC-L-23 for 14 days.

HC-L-23-14d					
Specimen	F_{\max} (N)	σ_{\max} (MPa)	U_{\max} (mm)	ε (%)	E (GPa)
1	356.7	123.1	2.5	1.6	8.1
2	481.1	161.1	2.6	1.7	10.0
3	532.7	176.8	2.3	1.5	11.8
4	573.5	189.2	2.8	1.8	10.9
5	450.9	151.9	2.7	1.8	8.7
6	380.3	130.3	2.5	1.7	8.5
Average	462.5	155.4	2.5	1.7	9.7
st.dev	84.5	25.8	0.2	0.1	1.5
CoV (%)	18.3	16.6	7.3	7.3	15.2

Table F- 17: Tensile properties of bio-resin-coated Hemp yarns after aging in solution HC-L-23 for 28 days.

HC-L-23-28d					
Specimen	F_{\max} (N)	σ_{\max} (MPa)	U_{\max} (mm)	ε (%)	E (GPa)
1	452.7	145.3	3.3	2.2	7.4
2	504.1	161.0	3.7	2.5	8.9
3	383.8	124.3	2.3	1.6	8.7
4	326.3	106.8	2.5	1.6	9.1
5	478.5	153.2	2.4	1.6	10.2
6	514.4	164.1	2.1	1.4	11.6
Average	443.3	142.4	2.7	1.8	9.3
st.dev	73.9	22.5	0.6	0.4	1.4
CoV (%)	16.7	15.8	22.9	22.9	15.4

Table F- 18: Tensile properties of bio-resin-coated Hemp yarns after aging in solution HC-L-23 for 74 days.

HC-L-23-74d					
Specimen	F_{\max} (N)	σ_{\max} (MPa)	U_{\max} (mm)	ε (%)	E (GPa)
1	402.3	130.7	3.4	2.3	6.9
2	474.9	152.9	3.0	2.0	9.3
3	513.2	164.5	3.8	2.5	8.0
4	608.3	193.6	3.3	2.2	10.5
5	548.6	175.3	3.6	2.4	8.7
6	651.5	206.7	3.7	2.4	10.2
Average	533.1	170.6	3.5	2.3	8.9
st.dev	90.3	27.6	0.3	0.2	1.4
CoV (%)	16.9	16.1	8.3	8.3	15.3

Table F- 19: Tensile properties of bio-resin-coated Hemp yarns after aging in solution HC-L-23 for 90 days.

HC-L-23-90d					
Specimen	F_{\max} (N)	σ_{\max} (MPa)	U_{\max} (mm)	ε (%)	E (GPa)
1	430.2	137.6	3.2	2.1	7.8
2	426.7	136.5	2.8	1.8	8.6
3	521.8	165.5	3.7	2.4	9.6
4	341.8	110.6	2.5	1.6	7.8
5	490.7	156.0	2.7	1.8	10.0
6	461.7	147.1	3.2	2.1	8.7
Average	445.5	142.2	3.0	2.0	8.7
st.dev	62.4	19.0	0.4	0.3	0.9
CoV (%)	14.0	13.4	14.5	14.5	10.5

e) In solution L-40

Table F- 20: Tensile properties of bio-resin-coated Hemp yarns after aging in solution HC-L-40 for 28 days.

HC-L-40-28d					
Specimen	F_{\max} (N)	σ_{\max} (MPa)	U_{\max} (mm)	ε (%)	E (GPa)
1	429.2	153.2	3.9	2.6	5.5
2	374.8	133.8	3.4	2.3	6.1
3	385.8	137.7	3.5	2.3	6.2
4	329.8	117.7	2.3	1.5	7.6
5	332.8	118.8	4.4	2.9	4.0
6	315.4	112.6	4.5	3.0	4.0
Average	361.3	129.0	3.7	2.4	5.6
st.dev	43.1	15.4	0.8	0.5	1.4
CoV (%)	11.9	11.9	21.7	21.7	24.9

Table F- 21: Tensile properties of bio-resin-coated Hemp yarns after aging in solution HC-L-40 for 90 days.

HC-L-40-90d					
Specimen	F _{max} (N)	σ _{max} (MPa)	U _{max} (mm)	ε (%)	E (GPa)
1	454.1	162.1	3.6	2.4	7.1
2	365.8	130.5	3.9	2.6	5.4
3	331.0	118.1	4.5	3.0	4.1
4	314.5	112.2	3.6	2.4	5.1
5	379.5	135.5	3.0	2.0	7.1
Average	369.0	131.7	3.7	2.5	5.7
st.dev	54.3	19.4	0.6	0.4	1.3
CoV (%)	14.7	14.7	14.8	14.8	22.7

f) In solution L-60

Table F- 22: Tensile properties of bio-resin-coated Hemp yarns after aging in solution HC-L-60 for 7 days.

HC-L-60-7d					
Specimen	F _{max} (N)	σ _{max} (MPa)	U _{max} (mm)	ε (%)	E (GPa)
1	354.7	114.4	2.9	1.9	5.4
2	479.1	152.4	2.9	1.9	7.5
3	309.7	100.7	2.8	1.8	5.2
4	505.3	160.3	3.6	2.4	6.9
5	400.6	128.4	2.8	1.8	6.9
6	427.7	136.7	2.8	1.9	7.4
Average	412.9	132.2	3.0	2.0	6.5
st.dev	73.9	22.5	0.3	0.2	1.0
CoV (%)	17.9	17.1	10.4	10.4	15.1

Table F- 23: Tensile properties of bio-resin-coated Hemp yarns after aging in solution HC-L-60 for 14 days.

HC-L-60-14d					
Specimen	F_{\max} (N)	σ_{\max} (MPa)	U_{\max} (mm)	ε (%)	E (GPa)
1	398.4	121.5	3.7	2.5	5.0
2	421.7	128.6	3.2	2.1	6.0
3	391.7	119.5	3.2	2.1	5.8
4	397.4	121.2	2.5	1.7	7.8
5	419.1	127.9	2.4	1.6	8.5
6	382.2	116.6	3.1	2.1	5.8
Average	401.8	122.6	3.0	2.0	6.5
st.dev	15.6	4.7	0.5	0.3	1.3
CoV (%)	3.9	3.9	16.6	16.6	20.8

Table F- 24: Tensile properties of bio-resin-coated Hemp yarns after aging in solution HC-L-60 for 28 days.

HC-L-60-28d					
Specimen	F_{\max} (N)	σ_{\max} (MPa)	U_{\max} (mm)	ε (%)	E (GPa)
1	442.9	134.6	3.6	2.4	4.9
2	466.2	141.7	3.0	2.0	5.9
3	436.2	132.6	3.0	2.0	5.7
4	441.9	134.3	2.3	1.6	7.7
5	463.6	140.9	2.2	1.5	8.4
6	426.7	129.7	2.9	2.0	5.7
Average	446.3	135.6	2.9	1.9	6.4
st.dev	15.6	4.7	0.5	0.3	1.3
CoV (%)	3.5	3.5	17.5	17.5	21.1

Table F- 25: Tensile properties of bio-resin-coated Hemp yarns after aging in solution HC-L-60 for 42 days.

HC-L-60-42d					
Specimen	F _{max} (N)	σ _{max} (MPa)	U _{max} (mm)	ε (%)	E (GPa)
1	368.7	112.5	4.5	3.0	5.2
2	389.3	118.8	4.3	2.9	5.5
3	332.1	101.3	4.0	2.7	5.0
4	383.5	117.0	3.8	2.6	6.1
5	447.9	136.7	3.1	2.0	9.2
6	418.2	127.6	4.0	2.6	6.4
Average	389.9	119.0	3.9	2.6	6.2
st.dev	40.0	12.2	0.5	0.3	1.5
CoV (%)	10.3	10.3	12.4	12.4	24.8

Table F- 26: Tensile properties of bio-resin-coated Hemp yarns after aging in solution HC-L-60 for 74 days.

HC-L-60-74d					
Specimen	F _{max} (N)	σ _{max} (MPa)	U _{max} (mm)	ε (%)	E (GPa)
1	373.3	123.2	3.0	2.0	7.1
2	256.3	87.5	3.3	2.2	5.0
3	306.4	102.8	3.6	2.4	5.5
4	307.9	103.2	2.6	1.8	6.8
5	364.5	120.5	3.7	2.5	6.0
6	235.6	81.2	2.8	1.9	5.3
Average	307.3	103.1	3.2	2.1	5.9
st.dev	55.4	16.9	0.4	0.3	0.8
CoV (%)	18.0	16.4	13.7	13.7	14.1

Table F- 27: Tensile properties of bio-resin-coated Hemp yarns after aging in solution HC-L-60 for 90 days.

HC-L-60-90d					
Specimen	F_{\max} (N)	σ_{\max} (MPa)	U_{\max} (mm)	ε (%)	E (GPa)
1	279.0	89.0	2.2	1.5	7.4
2	190.6	62.0	2.5	1.7	4.6
3	182.6	59.6	2.4	1.6	4.7
4	274.7	87.7	3.1	2.1	5.2
5	281.1	89.7	2.6	1.7	6.3
6	276.2	88.2	2.6	1.7	5.7
Average	247.4	79.4	2.6	1.7	5.7
st.dev	47.2	14.4	0.3	0.2	1.1
CoV (%)	19.1	18.1	11.2	11.2	18.9

Appendix G: Synthesis of the residual tensile properties of bio-resin-coated hemp yarns (HC) after exposure to aging in different environments

Table G- 1 presents the residual tensile properties (tensile strength σ_{\max} , elastic modulus E and ultimate tensile strain ε_{\max}) of bio-resin-coated hemp yarns (HC) after exposure to six different aging environments at different periods.

Table G- 1 : Residual tensile properties of bio-resin-coated hemp yarns (HC) after aging in the six different environments at different exposure periods.

Aging environment	Aging duration (days)	0	7	14	28	42	74	90
HC-E-23	σ_{\max} (MPa)	138.8	145.5	136.3	158.8	130.0	150.8	127.6
	St.dev	18.0	16.0	13.9	7.6	21.7	16.0	11.4
	CoV%	13.0	11.0	10.2	4.8	16.7	10.6	8.9
	E (GPa)	9.7	10.2	9.5	9.1	8.0	8.5	8.4
	St.dev	1.0	1.8	1.8	1.7	1.6	1.7	1.7
	CoV%	10.1	17.9	19.2	18.4	20.3	20.5	20.0
	ε (%)	1.4	1.6	1.8	1.7	2.2	2.3	1.8
	St.dev	0.1	0.1	0.3	0.3	0.4	0.3	0.1
	CoV%	3.8	9.3	13.9	15.6	18.1	14.1	6.0
HC-L-23	σ_{\max} (MPa)	138.8	161.8	155.4	142.4		170.6	142.2
	St.dev	18.0	15.0	16.6	15.9		19.4	11.1
	CoV%	13.0	9.2	10.7	11.2		11.4	7.8
	E (GPa)	9.7	10.8	9.7	9.3		8.9	8.7
	St.dev	1.0	0.8	1.6	0.2		1.6	1.5
	CoV%	10.1	7.4	16.5	2.1		18.0	17.5
	ε (%)	1.4	1.6	1.7	1.8		2.3	2.0
	St.dev	0.1	0.1	0.1	0.4		0.2	0.3
	CoV%	3.8	8.6	7.3	22.9		8.3	14.5

HC-E-40	σ_{\max} (MPa)	138.8	-	-	143.7	-	-	115.6
	St.dev	18.0			13.6			26.5
	CoV%	13.0			9.4			22.9
	E (GPa)	9.7	-	-	6.6	-	-	5.6
	St.dev	1.0			0.8			1.3
	CoV%	10.1			12.6			22.7
	ϵ (%)	1.4	-	-	2.3	-	-	2.1
	St.dev	0.1			0.2			0.4
CoV%	3.8			7.8			17.3	
HC-L-40	σ_{\max} (MPa)	138.8	-	-	129.0	-	-	131.7
	St.dev	18.0			15.4			19.4
	CoV%	13.0			11.9			14.7
	E (GPa)	9.7	-	-	5.6	-	-	5.7
	St.dev	1.0			1.4			1.3
	CoV%	10.1			24.9			22.7
	ϵ (%)	1.4	-	-	2.4	-	-	2.5
	St.dev	0.1			0.5			0.4
CoV%	1.8			21.7			14.8	
HC-E-60	σ_{\max} (MPa)	138.8	115.7	124.0	138.3	133.4	138.9	130.5
	St.dev	18.0	13.2	11.6	17.8	11.2	17.4	14.9
	CoV%	13.0	11.4	9.4	12.9	8.4	12.5	11.4
	E (GPa)	9.7	5.7	6.0	6.3	6.2	6.0	5.8
	St.dev	1.0	0.9	0.7	0.9	1.1	1.1	1.2
	CoV%	10.1	15.4	11.0	15.1	17.7	18.3	20.0
	ϵ (%)	1.4	2.1	2.1	2.0	2.5	3.1	2.7
	St.dev	0.1	0.1	0.1	0.2	0.3	0.2	0.5
CoV%	3.8	6.9	13.4	9.5	13.9	5.8	17.2	
HC-L-60	σ_{\max} (MPa)	138.8	132.3	122.7	135.6	119.0	103.1	79.4

	St.dev	18.0	18.4	5.3	14.8	11.2	9.5	10.6
	CoV%	13.0	13.9	4.3	10.9	9.4	9.2	13.4
	E (GPa)	9.7	6.5	6.5	6.4	6.2	5.9	5.7
	St.dev	1.0	1.0	1.1	1.2	1.3	1.4	1.4
	CoV%	10.1	15.7	16.9	18.2	21.2	23.5	24.1
	ϵ (%)	1.4	2.0	2.0	1.9	2.6	2.1	1.7
	St.dev	0.1	0.2	0.3	0.3	0.3	0.3	0.2
	CoV%	3.8	10.4	16.6	15.4	12.4	13.7	11.2